Chair of Designing Plastics and Composite Materials

# Doctoral Thesis

# On the formulation and numerical implementation of anisotropic elasto-plasticity with application to fibre-reinforced composites

## Swaroop Gaddikere Nagaraja, M.Sc.

October 2019

## AFFIDAVIT

I declare on oath that I wrote this thesis independently, did not use other than the specified sources and aids, and did not otherwise use any unauthorized aids.

I declare that I have read, understood, and complied with the guidelines of the senate of the Montanuniversität Leoben for "Good Scientific Practice".

Furthermore, I declare that the electronic and printed version of the submitted thesis are identical, both, formally and with regard to content.

Date  29.10.2019

_____

Signature Author
Swaroop, Gaddikere Nagaraja

This work is dedicated to the memory of Professor Christian Miehe (1956–2016) as a small token of appreciation for his contributions to computational mechanics.

# Abstract

The mechanics of highly anisotropic materials, such as composites, has raised many questions in solid mechanics which in turn have led to an improved understanding of the subject. For the effective use of such materials, it is important to have suitable and reliable mathematical models that describe their behaviour. In this context, the overall objective of this work is to develop physically motivated and sufficiently general constitutive equations that describe the non-linear material response of *fibre-reinforced composites* from the *continuum* perspective.

Macroscopically, a composite may be regarded as an anisotropic material which exhibits a highly direction-dependent mechanical response. These materials can be characterised by different symmetry groups based on their inherent micro-structure. If the material is reinforced by fibres in one direction, then the composite has only a single preferred direction and is characterised by the *transversely isotropic* system. Typical example is a unidirectional fibre-reinforced composite. It is also conceivable for a composite material to be reinforced by fibres in more than one direction. For example, a woven fabric has fibres aligned in two perpendicular directions. Such materials belong to the *orthorhombic* system and are characterised by the existence of two preferred directions.

While composite materials show a variety of mechanical responses, this thesis presents a framework for the description of elastic and plastic response. For the two selected symmetry groups, relatively general models of elastoplasticity are developed within the geometrically linear framework, and aspects of the finite element implementation are outlined. A key aspect is the formulation of anisotropic elastic and plastic constitutive response functions with the aid of general representation theorems, where additional (symmetric second-order) tensorial arguments which reflect the microstructural information on the macroscopic level are incorporated. A further core ingredient is the set-up of a canonical and non-conventional constitutive structure, with respect to associated and non-associated flow response, where the use of latter is motivated by the physical inconsistencies induced by the former under shear dominated loads. A rate-dependent approximation of the rate-independent setting is also outlined. The performance of the proposed models is evaluated qualitatively and quantitatively by means of representative numerical simulations.

# Zusammenfassung

Die Mechanik stark anisotroper Materialien, wie z.B. Verbundwerkstoffe, hat in der Festkörpermechanik viele Fragen aufgeworfen, die wiederum zu einem besseren Verständnis des Themas geführt haben. Für den effektiven Einsatz solcher Materialien ist es wichtig, über geeignete und zuverlässige mathematische Modelle zu verfügen, die ihr Verhalten beschreiben. In diesem Zusammenhang ist das übergeordnete Ziel dieser Arbeit, physikalisch motivierte und ausreichend allgemeine Konstitutivgleichungen zu entwickeln, die das nichtlineare Materialverhalten von faserverstärkten Verbundwerkstoffen aus der Kontinuumsperspektive beschreiben.

Auf der makroskopischen Ebene kann ein Verbundwerkstoff als anisotropes Material betrachtet werden, das ein richtungsabhängiges mechanisches Verhalten aufweist. Darüber hinaus können Verbundwerkstoffe aufgrund ihrer Mikrostruktur durch verschiedene Symmetriegruppen charakterisiert werden. Wenn das Material durch Fasern in einer Richtung verstärkt ist, hat der Verbundwerkstoff nur eine einzige Vorzugsrichtung und ist durch die Eigenschaften einer tranversal isotropen Symmetriegruppe gekennzeichnet. Typisches Beispiel dafür ist ein unidirektional faserverstärkter Verbundwerkstoff. Es ist auch denkbar, dass ein Verbundwerkstoff durch Fasern in mehr als einer Richtung verstärkt wird. So weist beispielsweise ein Gewebe Fasern auf, die in zwei aufeinander senkrechten Richtungen ausgerichtet sind. Solche Materialien gehören zum orthorhombischen System und zeichnen sich durch die Existenz von zwei Vorzugsrichtungen aus.

Obwohl Verbundwerkstoffe eine Vielzahl von mechanischen Reaktionen zeigen, stellt diese Arbeit einen Rahmen für die Beschreibung des anisotropen elastischen und plastischen Verhaltens dar. Für die beiden ausgewählten Symmetriegruppen werden relativ allgemeine Modelle der Elastoplastizität im Rahmen geometrisch lineare Theorie entwickelt und die Aspekte der Finite-Elemente-Implementierung skizziert. Wichtige Bestandteile sind die Formulierungen von anisotropen Konstitutivgleichungen mit Hilfe von Repräsentationstheoremen, bei denen zusätzliche tensorielle Argumente (symmetrisch, zweiter Stufe) einbezogen werden, die die mikrostrukturellen Informationen auf makroskopischer Ebene widerspiegeln. Ein weiterer Kernbestandteil ist der Aufbau einer kanonischen und nicht-konventionellen konstitutiven Struktur, d.h. assoziertes und nicht-assoziertes Fließverhalten, deren Verwendung physikalischen Inkonsistenzen motiviert ist, die bei schub-dominierter Belastung durch die kanonische Struktur verursacht werden. Eine ratenabhängigen Approximation der ratenunabhängigen Einstellung wird ebenfalls skizziert. Die Performance der vorgeschlagenen Modelle wird qualitativ und quantitativ mittels repräsentativer numerische Simulationen bewertet.

# Acknowledgements

# Contents

# List of symbols

**Greek symbols**

| | |
|---|---|
| $\alpha, \beta, \gamma$ | Grid angles |
| $\Im$ | Representative material parameter |
| $\eta$ | Penalty parameter characterizing time-dependent viscous flow |
| $\Theta$ | Absolute temperature of the material point |
| $\Theta_0$ | Reference temperature of the body |
| $\lambda, \Delta\lambda$ | Lagrange (plastic) multiplier and plastic increment, respectively |
| $\lambda_{\mathbb{Z}_i}$ | Eigenvalues |
| $\theta$ | Orientation of the fibres |
| $\mu_i, \vartheta_i, \varkappa_i, \zeta_i$ | Material parameters |
| $\nu_{ij}$ | Poisson's ratio |
| $\rho$ | Density |
| $\varrho, \varrho_p$ | Entropy and entropy production, respectively |
| $\psi, \chi, \phi$ | Helmholtz free energy, yield and plastic flow potential, respectively |
| $\boldsymbol{\epsilon}$ | RICCI permutation (third-order) tensor/Levi-Civita symbol |
| $\boldsymbol{\Upsilon}$ | Body force |
| $\boldsymbol{\varepsilon}$ | Symmetric second-order strain tensor |
| $\boldsymbol{\varepsilon}^e, \boldsymbol{\varepsilon}^p$ | Symmetric second-order elastic and plastic strain tensor, respectively |
| $\xi, \boldsymbol{\alpha}$ | Isotropic and kinematic hardening variable, respectively |
| $\boldsymbol{\sigma}$ | Cauchy stress tensor |
| $\kappa, \boldsymbol{\beta}$ | Driving forces dual to $\xi$ and $\boldsymbol{\alpha}$, respectively |
| $\boldsymbol{\Sigma}$ | Relative stress tensor |
| $\boldsymbol{\alpha}_t$ | Second-order tensor containing coefficients of thermal expansion |

**Coordinate systems**

| | |
|---|---|
| $\mathrm{x}, \mathrm{y}, \mathrm{z}$ | Global coordinate system |
| $1, 2, 3$ | Local coordinate system |

**Latin symbols**

| | |
|---|---|
| $a, b, c$ | Grid constants or lattice parameters |
| $e$ | Internal energy per unit mass |
| $k$ | Thermal conductivity |
| $m$ | Exponent associated with rate-dependency |
| $h, n$ | Hardening parameter and exponent associated with isotropic hardening, respectively |
| $p$ | Hydrostatic pressure |
| $t$ | Time |
| $u$ | Representative scalar |
| $w_l$ | Weights associated with numerical integration/average |
| $y_0$ | Initial threshold yield stress |
| $y_{ij}$ | Yield surface parameters |
| $E_i$ | Young's modulus |
| $G_{ij}$ | Shear modulus |
| $G_1, \ldots, G_n$ | Basic invariants |
| H | Isotropic hardening modulus |
| $I_1, \ldots, I_n$ | Invariants of the second-order strain and strain-like tensors |
| $J_1, \ldots, J_n$ | Invariants of the second-order stress and stress-like tensors |
| $\boldsymbol{a}, \boldsymbol{b}, \boldsymbol{c}$ | Grid vectors, preferred directions |
| $\boldsymbol{d}$ | Time-dependent translation vector |
| $\boldsymbol{m}_1, \boldsymbol{m}_2, \boldsymbol{m}_3$ | Structural tensors in the three principal directions |
| $\boldsymbol{n}, \tilde{\boldsymbol{n}}$ | Outward and unit normal vector, respectively |
| $\boldsymbol{t}$ | Traction vector |
| $\boldsymbol{u}, \boldsymbol{u}^+$ | Displacement and infinitesimal rigid body motion, respectively |
| $\boldsymbol{v}$ | Representative vector |
| $\boldsymbol{x}$ | Material point |
| $\boldsymbol{x}_0$ | Arbitrary basis position |
| $\boldsymbol{y}$ | Small neighbourhood of $\boldsymbol{x}$ |

| | |
|---|---|
| $\mathfrak{c}$ | Specific heat capacity |
| $\mathfrak{e}, \mathfrak{f}$ | Vector of internal variables and dual driving forces, respectively |
| $\mathfrak{h}, \mathfrak{q}$ | Heat flux and the corresponding vector, respectively |
| $\mathfrak{s}$ | Plasticity inducing stress tensor |
| $\mathfrak{m}_{\mathscr{B}_p}$ | Mass of the sub domain of the body of interest |
| $\mathfrak{x}$ | Isoparametric coordinate system |
| $\mathfrak{N}, \mathfrak{B}_{\varepsilon}$ | Shape functions and strain interpolation matrix, respectively |
| $\delta \boldsymbol{u}$ | Test function |
| $dA, \ dV$ | Area and volume element, respectively |
| $\boldsymbol{A}, \boldsymbol{U}_1, \ldots, \boldsymbol{U}_n$ | Symmetric second-order argument tensors |
| $\boldsymbol{V}_1, \ldots, \boldsymbol{V}_n$ | Skew-symmetric second-order argument tensors |
| $\boldsymbol{M}$ | Representative symmetric second-order structural tensor |
| $\mathbf{K}$ | Second-order thermal conductivity tensor |
| $\mathbf{T}$ | Second-order anisotropy tensor |
| $\mathbf{Y}, \overline{\mathbf{Y}}$ | Second-order yield strength tensors |
| $\boldsymbol{Q}$ | Orthogonal rotation |
| $\mathfrak{F}$ | Representative scalar-valued constitutive function |
| $\mathfrak{D}$ | Nodal displacement vector |
| $\mathfrak{P}$ | Point around which linearisation is carried out |
| $\mathfrak{R}, \mathfrak{R}(\mathfrak{P})_{,\mathfrak{P}}$ | Residual vector and necessary iteration tangent, respectively |
| $\mathcal{S}$ | Second-order stress-like tensor |
| $\mathcal{H}$ | Latent heat |
| $\mathcal{I}, \mathcal{K}$ | Minimum integrity basis for strain and strain-like tensors |
| $\mathcal{J}, \mathcal{L}$ | Minimum integrity basis for stress and stress-like tensors |
| $\mathscr{B}, \mathscr{B}_p$ | Body and sub domain of the body of interest of interest, respectively |
| $\partial \mathscr{B}$ | Boundary of the body of interest |
| $\mathscr{C}$ | Symmetry group of a material |
| $\mathscr{D}, \mathscr{D}_{\text{loc}}, \mathscr{D}_{\text{con}}, \mathscr{D}^{\text{red}}$ | Total, local, convective and reduced dissipation, respectively |

| | |
|---|---|
| $\mathscr{H}_{\mathscr{B}_p}, \mathscr{G}_{\mathscr{B}_p}, \widetilde{\mathscr{Q}}_{\mathscr{B}_p}$ | Entropy, entropy production and entropy power, respectively |
| $\mathscr{L}, \mathscr{P}$ | Lagrange and penalty functional, respectively |
| $\mathscr{U}_{\mathscr{B}_p}, \mathscr{K}_{\mathscr{B}_p}$ | Internal and kinetic energy, respectively |
| $\mathscr{N}_{\boldsymbol{x}}$ | Neighbourhood domain of $\boldsymbol{y}$ |
| $\mathscr{P}_{\mathscr{B}_p}, \mathscr{Q}_{\mathscr{B}_p}$ | External power associated with the mechanical and thermal problem, respectively |
| $\mathscr{R}$ | External heat source |
| $\mathscr{S}, \mathscr{Z}$ | Elastic and plastic flow potential domain, respectively |
| $\mathscr{T}$ | Time domain |
| $\partial\mathscr{S}, \partial\mathscr{Z}$ | Boundary of the elastic domain and plastic flow potential, respectively |
| $\boldsymbol{\mathscr{I}}_{\mathscr{B}_p}, \boldsymbol{\mathscr{F}}_{\mathscr{B}_p}$ | Linear momentum and the resultant mechanical force, respectively |
| $\boldsymbol{\mathscr{W}}^o_{\mathscr{B}_p}, \widetilde{\boldsymbol{\mathscr{F}}}^o_{\mathscr{B}_p}$ | Angular momentum and the resultant force defined w.r.t an origin $o$, respectively |
| $\mathbb{A}, \mathbb{B}$ | Fourth-order stress and strain transformation tensors, respectively |
| $\mathbb{C}$ | Fourth-order compliance tensor |
| $\mathbb{E}, \mathbb{E}^{\text{ep}}$ | Fourth-order elastic and elastic-plastic tangent modulus tensor, respectively |
| $\mathbb{F}$ | Representative fourth-order Hessian |
| $\mathbb{H}$ | Fourth-order kinematic hardening modulus tensor |
| $\mathbb{P}$ | Fourth-order projection tensor |
| $\mathbb{T}$ | Fourth-order anisotropy tensor |
| $\mathbb{X}, \mathbb{Y}$ | Fourth-order Hill-type tensors |

## Mathematical operators

| | |
|---|---|
| $\rightarrow, \mapsto$ | Mapping operators |
| $\in, \notin$ | Member and not a member, respectively |
| $\subseteq$ | Subset |
| $\backslash$ | Set difference |
| $\cup, \bigcup$ | Union of elements |

| | |
|---|---|
| $\forall$ | For all |
| $\implies$ | Material implication |
| $\geq$ | Greater than or equal to |
| $\leq$ | Less than or equal to |
| $\pm$ | Plus or minus |
| $\star$ | Rayleigh product |
| $\equiv, \iff$ | Material equivalence |
| $\angle$ | Angle |
| $\approx, \neq$ | Approximately equal and inequality, respectively |
| $\dot{(\ )}, (\ )_{,(\ )}$ | Time and partial derivative, respectively |
| $\|, \perp$ | Parallel with and perpendicular to, respectively |
| $\sum$ | Summation |
| $\emptyset$ | Empty set |
| $\prod$ | Assembly operator |
| $[(\ )^+]$ | Monotonically increasing ramp function |
| $|\ |, \|\ \|$ | Absolute value and euclidean norm, respectively |
| $\cos, \sin$ | Cosine and sine of an angle/function, respectively |
| $\Delta, \nabla$ | Increment and gradient operator, respectively |
| $\det$ | Determinant |
| $\mathrm{div}$ | Divergence operator |
| $\mathrm{Lin}$ | Linearisation |
| $\sup$ | Supremum |
| $\mathrm{tr}, \mathrm{dev}$ | Trace and deviator, respectively |
| $\ln$ | Natural logarithm |

**Number sets**

| | |
|---|---|
| $\mathbb{R}_+$ | Set of non-negative real numbers |
| $\mathbb{R}^d$ | $d$-dimensional Euclidean space |
| $\mathscr{A}$ | $\mathbb{R}^{1\times3\times6\times6}$-dimensional Euclidean space |
| $\mathcal{O}(3)$ | Orthogonal group |

## Mathematical symbols

$\boldsymbol{0}$                   Second-order zero tensor

$\boldsymbol{1}$                   Second-order identity tensor

$\mathbb{0}$                   Fourth-order zero tensor

## Vector and tensor operators

$\left\{ (*) \cdot (*) \right\}$          Dot product of two vectors

$\left\{ (*) \times (*) \right\}$          Cross product of two vectors

$\left\{ (*) \otimes (*) \right\}$          Outer product of two vectors

$\left\{ (\bullet) : (\bullet) \right\}$          Double contraction of two second-order tensors

$\left\{ (\bullet) \otimes (\bullet) \right\}_{ijkl}$          $(\bullet)_{ij}(\bullet)_{kl}$, Outer product of two second-order tensors

$\left\{ (\bullet) \oplus (\bullet) \right\}_{ijkl}$          $(\bullet)_{ik}(\bullet)_{jl}$, Outer product of two second-order tensors

$\left\{ (\bullet) \ominus (\bullet) \right\}_{ijkl}$          $(\bullet)_{il}(\bullet)_{jk}$, Outer product of two second-order tensors

# List of figures

# List of tables

# List of boxes

# 1. Introduction

The behaviour of fibre-reinforced composites with their excellent properties such as high strength and stiffness to weight ratios, lightweight, impact resistance and thermal stability which are different and superior compared to other conventional engineering materials, is governed by their micro-structure. The prediction of micro-structure and understanding its effect on the macroscopic behaviour is the key to reliable and physically motivated constitutive formulations which in turn provide a strong basis for an optimised design of such materials. In the present work, emphasis is placed on studying the overall material behaviour of composites, specifically the energetic and dissipative responses, and development of suitable thermodynamics-based material models that accurately predict the trends of experimentally observed behaviour.

## 1.1. Motivation and state of the art

The use of fibre-reinforced composites as a primary structural component in the automobile, civil, aerospace and other industries is increasingly popular due to interesting properties. In these structural applications, a failure analysis is required to study their material response for various loads. Owing to its heterogeneous nature with different constituents, the load response of composite materials is influenced by a number of physical mechanisms [3]. However, non-linearity prior to damage may lead to a redistribution of the stress state in a laminate, which eventually affects the failure onset. Therefore, the predictive modelling of the non-linear behaviour of composites has been a topic of intensive research over the last years.

The choice of a modelling scale to simulate the behaviour of composite materials is extremely important. Typically, three scales are available as shown in Fig. 2, namely (i) microscopic, (ii) mesoscopic and (iii) macroscopic, see also [2,4]. The microscopic scale is



| Civil engineering [1] | Aerospace [2] | Automobile [2] |

FIGURE 1: **Composite materials.** Applications where composite materials are used.
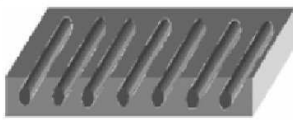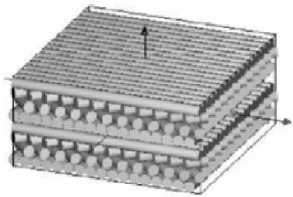


| Scale | Microscopic | Mesoscopic | Macroscopic |
|---|---|---|---|
| Constituents | Fibre, matrix | Ply/layer | Laminate |

FIGURE 2: **Modelling scales.** Different scales for modelling the material response [4].

not desired for large structures because of its complexities such as the need for multi-scale methods, a higher number of material constants and so on. On the other hand, there is loss of information on the macroscopic scale where individual layer positions cannot be taken into account due to the homogenisation of the laminate [4]. The choice of a meso-scopic scale that accounts for layer orientations and positions is thus a good compromise, and enables for an in-depth understanding of the energetic and dissipative effects.

From an experimental perspective, investigations pertaining to the non-linear behaviour of composites are documented in [5–8], among others. It has been observed that the material response of the composite to loading in the fibre direction remains essentially elastic up to failure, whereas that to shear and transverse directions is non-linear and inelastic. Due to the brittleness of matrix material, the non-linear inelastic behaviour is usually attributed to the brittle cracking inside the matrix material. Consequently, previous modelling efforts have focused on continuum damage mechanics [9, 10]. Recent research however implies that under shear dominated loads, considerable irreversible strains develop that cannot be explained by brittle mechanisms alone. It has been experimentally observed [11, 12] and computationally verified [13] that the non-linearity is due to plasticity in the matrix constituent. Therefore, precise constitutive relations that account for the elastic-plastic response of these materials are required to accurately predict the onset of damage and failure of composite materials [14].

Generally, the elastic-plastic behaviour of composite materials can be described using either a *micro-mechanical* or a *continuum* approach, see Fig. 3. Along the lines of a *micro-mechanical* approach, fibres and the matrix are modelled as individual phases. Fibres are assumed to be linear elastic anisotropic solids (as necessary for some fibres), whereas the matrix is modelled as an isotropic elastic-plastic solid. The overall composite behaviour is then deduced from a homogenisation procedure. Details regarding the constitutive framework and algorithmic implementation of micro-mechanics based models can be found in [17–20]. Most of the micro-mechanical models are based on the mean field theory, where the main aim is to determine stress and strain concentration tensors for fibres and the matrix. Within the elastic regime, these concentration tensors can be computed using for example Mori-Tanaka scheme [21]. However, the determination of concentration tensors in the plastic regime is much more complicated and requires the use of numerical evaluation techniques [22]. Though the micro-mechanics approach gives better comprehension of reasons behind the experimentally observed behaviour, this approach comes at a cost where higher number of material coefficients are required for the descrip-



Fibres            Matrix            $\mathcal{RVE}$                              Lamina

(a)                                                                    (b)
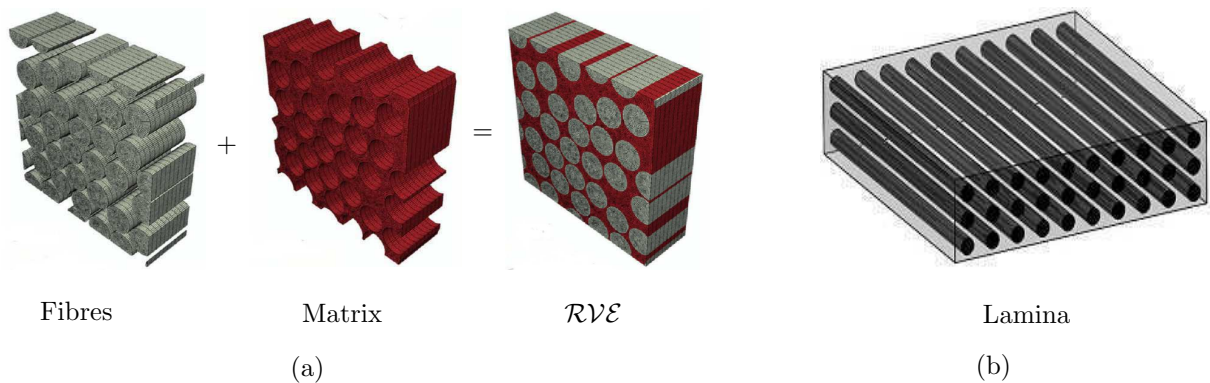
FIGURE 3: **Modelling approaches.** Representation of (a) micro-mechanical [15] and (b) continuum [16] based approaches.

tion of the material response. Although differing in detail with the micro-mechanical approach, a small number of anisotropic plasticity models based on the concept of space transformation have been proposed for fibre-reinforced composites, see [23, 24]. This theory assumes the existence of a fictitious isotropic space to which quantities from the real anisotropic space can be mapped, and a mapped problem can be solved. The real and fictitious spaces are related by means of linear fourth-order transformation tensors that are formulated based on the available information of strength in the respective spaces. The real anisotropic space is regarded as a homogenised composite material, while the fictitious isotropic space characterises the matrix material to which plasticity is usually restricted. As an advantage, standard isotropic response functions can be used and the numerical treatment is computationally inexpensive owing to the reduced setting.

A majority of relevant research has focused on the development and experimental validation of anisotropic yield criteria for *continuum* models. Hill [25] proposed one of the first yield functions for the description of orthotropy, which is a generalisation of the von Mises [26] isotropic yield criterion. The main limitation of this criterion is the impossibility of modelling materials that exhibit pressure sensitive behaviour, for example polymeric composite materials. Accordingly, there have been attempts to modify Hill's orthotropic yield criterion for use with composite materials [27–29], where the dissipative response is forced to be independent of fibre stress by imposing the direction of plastic flow in the fibre direction to be zero. For composites with metallic-type matrix constituents, there exist a considerable number of thermodynamically consistent models for the description of anisotropic elastic-plastic effects, see e.g. [30–35]. The review article of Chaboche [36] thoroughly treats the formulation and implementation aspects of elastoplasticity for metallic-type materials. However, the treatment of anisotropic plasticity for composites with polymeric matrix constituents is in most cases limited to a purely phenomenological approach [37–39], and modelling using the thermodynamics of irreversible processes has received less attention [40–43]. Additionally, none of the aforementioned works for polymer-matrix composites use functional forms of hardening (isotropic and kinematic) state variables or account for rate-dependency within a thermodynamically consistent formulation.

Motivated by these aspects, a relatively general, thermodynamically consistent formulation of anisotropic elastoplasticity is proposed for fibre-reinforced composites. The constitutive developments are based on the following main ideas [44]:

- *Restriction to geometrically linear framework:* The underlying objective of the proposed models is their application to modelling the mesoscopic response of composites, i.e. unidirectional plies in multi-directional laminates. In such materials, plasticity formulations are needed to accurately predict the constitutive response up to the initiation of damage, which typically occurs at rather small deformations (below 1%). In view of this objective, focus is restricted to the geometrically linear framework. Though numerical simulations are performed up to 5% strain, deviations are considered to be acceptable for the purposes of comparing various modelling techniques [18].

- *Representation in terms of isotropic tensor functions:* The methodology adopted here is to generate the constitutive functions representing the material response with the aid of representation theorems. This approach allows for the formulation of anisotropic constitutive functions in terms of isotropic counterparts by including

structural tensors as additional arguments [45–47]. In this context, new integrity bases are derived that yield a unique representation of the scalar energetic potential, stress and the elastic modulus tensor associated with the potential.

- *Non-evolving anisotropy:* A simplifying assumption made at the outset due to the restriction to geometrical linear framework is that the anisotropy does not evolve during the plastic deformation. Thus, focus is restricted to initial anisotropy only where the anisotropic variables are *a priori* given, and not plasticity-induced evolution of anisotropy where the variables develop during the course of plastic deformation and are governed by additional constitutive evolution equations. Details related to the modelling of an evolving anisotropy can be found in [48].

- *Exclusion of micro-mechanics:* Focusing on the continuum approach, micro-mechanics of the composite such as the interaction between individual fibre and the matrix is excluded. It is assumed that there is a perfect bonding between fibres and the matrix, as the effects associated with the failure of interface are usually observed at large deformations [49, 50].

## 1.2. Scope and outline of the thesis

The scope of the present work is to develop relatively general and thermodynamically consistent material models that describe the anisotropic response of fibre-reinforced composites at infinitesimal elastic and plastic deformations. A key aspect of these models is that the physical effects are reflected in the proposed mathematical structure. To this end, the significant contributions of this thesis are (i) formulation of *constitutive/governing equations* and derivation of *algorithmic treatment* for anisotropic dissipative solids, (ii) construction of *physically motivated* and *convex* dissipative response functions, and (iii) derivation of *canonical* and *non-conventional* constitutive structure. This thesis is organised as follows:

In **Chapter 2**, fundamental concepts of continuum mechanics, elasticity and plasticity are studied. The employed notations serve as the basis for subsequent developments. Starting with derivation of physical balance principles; the concept of stress, dissipation inequality and temperature evolution equation is introduced. Next, the notion of Bravais lattice and their classification is discussed, i.e. classification of solids based on the inherent symmetry of their micro-structure. In the following section, approaches to describe the anisotropic material response are outlined, and the constitutive equations representing the 13 mechanics symmetry groups, in addition to the isotropic group, are derived. This is followed by a discussion on a general theoretical framework of phenomenological elasticity, plasticity and viscoplasticity, their formulation and numerical implementation.

**Chapter 3** presents theory and numerics of anisotropic elasticity applicable to fibre-reinforced composites. The initial boundary value problem of elasticity, governed by the balance of linear momentum is presented. Specifically, focus is on the formulation of a scalar-valued energetic potential that yields a unique and decoupled representation of the stress and elastic modulus tensor for the selected symmetry groups.

In **Chapter 4**, two models that use isotropic yield/plastic flow potential functions are chosen from the literature, modified for use with unidirectional composites and presented to simulate the non-linearities exhibited by the composite. The underlying objective is to investigate in detail the effect of using isotropic plastic response functions in modelling

the anisotropic elastic-plastic response of fibre-reinforced composites, and draw special attention to the shortcomings and deficiencies of these models.

Based on the foregoing observations, **Chapter 5** presents a constitutive framework of anisotropic plasticity and viscoplasticity for fibre-reinforced composites. Starting with constitutive state variables and scalar-valued energetic potential, a mathematical structure of a combined non-linear hardening, applicable to the two selected symmetry groups is proposed. Plastic response functions for the selected symmetry groups are formulated in the following section. The formulation of plastic response functions is based on a physically motivated decomposition of the stress tensor, which ensures a linear elastic fibre response. Non-quadratic yield functions with a combined non-linear isotropic and kinematic hardening are proposed, with a simple representation in terms of the invariants of the stress tensor. Non-quadratic yield functions are chosen in order to maintain the same order of the stress invariants. It should be remarked here that though higher order yield functions are accurate, they require higher number of coefficients which must be obtained experimentally. The main advantage of the proposed yield functions is that they are governed by only a few coefficients, and they accurately predict the trends of the experimentally observed behaviour. Moreover, the conditions for the convexity of the proposed yield surfaces are simple to derive and impose, as seen subsequently. Next, a set of canonical and non-conventional evolution equations are derived for the associative and non-associative flow response, respectively. These evolution equations generally characterise non-linear kinematic hardening, but also recover linearity for a special choice of the associated parameters. To the knowledge of the author, this is derived here for the first time. Furthermore, a notably attractive feature of the framework is that it facilitates a straightforward extension of the rate-independent formulation to the rate-dependent setting, by a suitable penalisation procedure. The algorithmic treatment of the proposed models is prescribed in the following section, where the governing equations are solved using an elastic predictor-plastic corrector algorithm that imposes the constraint posed by the yield condition. Note that the models proposed for the transversely isotropic symmetric group in this work reduce to those in [44] for a special choice of the material parameters.

A detailed discussion on the methodology designed to calibrate plastic material parameters associated with the proposed models is provided in **Chapter 6**. The identification of material parameters associated with the constitutive equations is crucial for material models when trying to capture the experimentally observed behaviour accurately. To this end, a non-linear optimisation problem with least-squares-type functional is defined and the minimum is evaluated using a numerical method. Most of the plastic parameters associated with the proposed models are obtained using the said procedure.

In **Chapter 7**, the performance of models proposed in **Chapters 3–5** are analysed by means of selected numerical examples. At first, the implementation is verified using *homogeneous* boundary value problems. This is followed by a comprehensive evaluation (qualitative and quantitative) of the models by comparison to micro-mechanics simulations as well as to experimental data. Finally, *inhomogeneous* boundary value problems are analysed.

Concluding remarks appear in **Chapter 8**.

## 2.  Fundamental concepts of anisotropy, elasticity and plasticity

The aim of this chapter is to give a brief introduction to the concepts of anisotropy and the general modelling framework of elasticity and plasticity. This chapter is in no means comprehensive but intended to build the necessary background for subsequent developments.

In a first step, fundamentals of continuum mechanics are explained in detail. Essential aspects such as the kinematics, physical balance principles, and the concept of stress are discussed. For an in depth discussion of the pertinent topic, see [51–56].

This is followed by a discussion on the classification of solids based on the symmetry of their micro-structure. Materials are distinguished between solids having an amorphous and those having a crystalline micro-structure, where focus is restricted to the latter ones in the present work. The main objective of this section is to provide a sufficient theoretical background to the notion of Bravais lattices and their classification. An introduction to the theoretical treatment of the material symmetry has been suggested in [57]. For details of major developments in this field, the reader is referred to [58–60].

General constitutive developments related to the description of anisotropic material response are discussed in the following section. In this context, the classical approach and the coordinate free approach are studied, where focus is placed on the coordinate free approach. The methodology adopted here is to systematically generate anisotropic constitutive functions with the aid of representation theorems [46,51,61–64]. Several aspects of the invariants based theory are discussed which are indispensable for the description of anisotropic material behaviour. To this end, anisotropic equations characterising the 13 so-called mechanics symmetry groups, in addition to the isotropic group, are derived in this section.

Next, some basic aspects in modelling the elastic material response are discussed. Elasticity is an important partial ingredient for the description of dissipative material responses. It is also the most general case of material response characterised by a fully reversible and path-independent behaviour, where the material response depends solely on the current state of deformation [65].

Finally, a theoretical framework of phenomenological plasticity and viscoplasticity, its formulation and numerical implementation is discussed. To motivate the formulation of anisotropic plasticity that can be applied to composites, phenomenological plasticity is first considered here. In this context, the discussions in this section follows closely the monograph of Simo and Hughes [66]. A detailed discussion of the topic and relevant literature can also be found in [67–69].

### 2.1.  Geometrically linear continuum mechanics

In this section, a short introduction to continuum mechanics is given. The basic kinematic quantities used to describe the deformation of a solid at infinitesimal strains are studied.

### 2.1.1.  Basic kinematics of infinitesimal deformations

A starting point for the description of kinematics is the introduction of material body and the associated primary fields as explained below.

**2.1.1.1. Thermo-mechanical initial boundary value problem.** Let $\mathscr{B} \subseteq \mathbb{R}^3$ be the body of interest, assumed to be open and bound by a smooth boundary $\partial\mathscr{B}$. Then the

motion of the body is described by the primary fields

$$\boldsymbol{u} : \begin{cases} \mathscr{B} \times \mathscr{T} \to \mathbb{R}^3 \\ (\boldsymbol{x}, t) \mapsto \boldsymbol{u}(\boldsymbol{x}, t) \end{cases} \quad \text{and} \quad \Theta : \begin{cases} \mathscr{B} \times \mathscr{T} \to \mathbb{R}_+ \\ (\boldsymbol{x}, t) \mapsto \Theta(\boldsymbol{x}, t) \end{cases} , \tag{1}$$

where $\boldsymbol{u} \in \mathbb{R}^3$ and $\Theta \in \mathbb{R}_+$ denote the displacement and absolute temperature of the material point $\boldsymbol{x} \in \mathscr{B}$ at time $t \in \mathscr{T}$, respectively. The mechanical boundary $\partial\mathscr{B}$ of the body $\mathscr{B}$ under consideration is decomposed according to the primary fields such that

$$\partial\mathscr{B} = \partial\mathscr{B}_{\boldsymbol{u}} \cup \partial\mathscr{B}_{\boldsymbol{t}} \quad \text{and} \quad \partial\mathscr{B} = \partial\mathscr{B}_\Theta \cup \partial\mathscr{B}_{\mathfrak{h}} , \tag{2}$$

where, for a mechanical problem, the body is subjected to Dirichlet and Neumann (traction) boundary conditions as

$$\boldsymbol{u} = \bar{\boldsymbol{u}} \quad \text{on} \quad \partial\mathscr{B}_{\boldsymbol{u}} \quad \text{and} \quad \boldsymbol{t} = \bar{\boldsymbol{t}} \quad \text{on} \quad \partial\mathscr{B}_{\boldsymbol{t}} , \tag{3}$$

with $\boldsymbol{t}$ denoting the traction vector. Likewise, for a thermal problem, it follows that

$$\Theta = \bar{\Theta} \quad \text{on} \quad \partial\mathscr{B}_\Theta \quad \text{and} \quad \mathfrak{h} = \bar{\mathfrak{h}} \quad \text{on} \quad \partial\mathscr{B}_{\mathfrak{h}} , \tag{4}$$

where $\mathfrak{h}$ is the heat flux, see Fig. 4 for a geometrical interpretation. In a coupled thermo-mechanical setting, the two quantities $\boldsymbol{t}$ and $\mathfrak{h}$ are assumed to be governed by Cauchy-type theorems, namely that

$$\boldsymbol{t} := \boldsymbol{\sigma}\boldsymbol{n} \qquad \text{and} \qquad \mathfrak{h} := \mathbf{q} \cdot \boldsymbol{n} , \tag{5}$$

where $\boldsymbol{\sigma}(\boldsymbol{x}, t)$ is the Cauchy stress tensor, $\mathbf{q}(\boldsymbol{x}, t)$ is the Cauchy heat flux vector and $\boldsymbol{n}$ is the outward normal vector. The heat flux $\mathbf{q}$ is governed by Fourier's law, given by

$$\mathbf{q} := -k\nabla\Theta , \tag{6}$$

where $\nabla\Theta$ is the temperature gradient and $k$ is the thermal conductivity which must be positive ($k > 0$) to satisfy the thermodynamic restriction.

In a geometrically linear framework, the gradient of the displacement defines the symmetric second-order strain tensor as

$$\boldsymbol{\varepsilon} := \nabla_{\text{sym}}\boldsymbol{u} = \frac{1}{2}(\nabla\boldsymbol{u} + \nabla^T\boldsymbol{u}) , \tag{7}$$

which is the central quantity to describe the deformation in the small deformation theory.
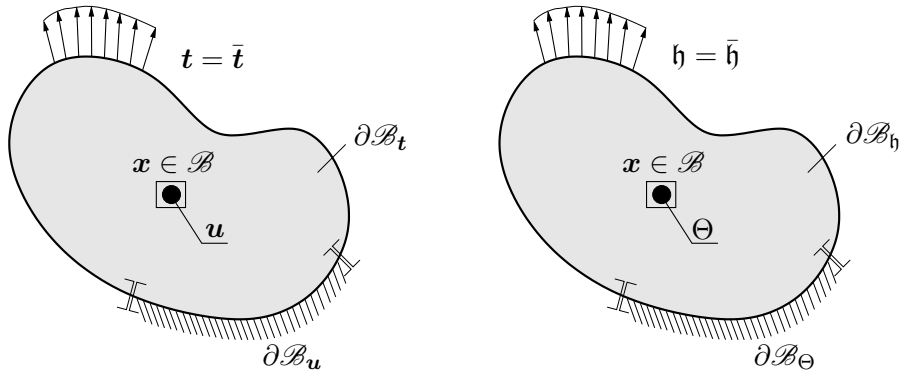


FIGURE 4: **Primary field variables.** The mechanical deformation process is governed by the *displacement field $\boldsymbol{u}$* and the thermal deformation process is governed by the *temperature field* $\Theta$. The boundary of the body $\mathscr{B}$ under consideration is split into $\partial\mathscr{B} = \partial\mathscr{B}_u \cup \partial\mathscr{B}_t$ and/or $\partial\mathscr{B} = \partial\mathscr{B}_\Theta \cup \partial\mathscr{B}_{\mathfrak{h}}$ where Dirichlet- and Neumann-type boundary conditions are prescribed.

### 2.1.2. Physical balance principles

The displacement $\boldsymbol{u}(\boldsymbol{x}, t)$ and temperature $\Theta(\boldsymbol{x}, t)$ are determined by governing balance equations (fundamental balance principles) which are discussed below. These principles are valid for all continuous bodies independent of their material response. To provide a starting point for the derivation of balance laws, consider a sub domain $\mathscr{B}_p \subseteq \mathscr{B}$ cut from the domain $\mathscr{B}$ (Fig. 5) and apply Euler's cut principle [70] to the sub domain $\mathscr{B}_p$. It follows that the mechanical and thermal action of the remaining body on the part $\mathscr{B}_p$ is given by the traction vector $\boldsymbol{t}$ and the heat flux $\mathfrak{h}$, defined in Eqn. (5) respectively.

**2.1.2.1. Balance of mass.** For a sub domain $\mathscr{B}_p \subseteq \mathscr{B}$ under consideration, the mass $\mathfrak{m}_{\mathscr{B}_p}$ is defined in terms of the time-dependent density $\rho = \rho(\boldsymbol{x}, t)$ as

$$\mathfrak{m}_{\mathscr{B}_p} = \int_{\mathscr{B}_p} \rho \, dV \ . \tag{8}$$

The local balance of mass states that the mass of any part of the body remains constant in time during the deformation process, i.e.

$$\frac{d}{dt} \mathfrak{m}_{\mathscr{B}_p} = 0 \ , \tag{9}$$

which can be equivalently written by taking into account Eqn. (8) as

$$\frac{d}{dt} \int_{\mathscr{B}_p} \rho \, dV = \int_{\mathscr{B}_p} \dot{\rho} \, dV = 0 \ . \tag{10}$$

Application of the localisation theorem[1] yields

$$\dot{\rho} = 0 \Rightarrow \rho = \text{constant} \ . \tag{11}$$

**2.1.2.2. Balance of linear momentum.** The linear momentum $\boldsymbol{\mathscr{I}}_{\mathscr{B}_p}$ and the resultant mechanical force $\boldsymbol{\mathscr{F}}_{\mathscr{B}_p}$ associated with the part $\mathscr{B}_p$ are defined as

$$\begin{aligned} \boldsymbol{\mathscr{I}}_{\mathscr{B}_p} &= \int_{\mathscr{B}_p} \rho \ddot{\boldsymbol{u}} \, dV \quad \text{and} \\ \boldsymbol{\mathscr{F}}_{\mathscr{B}_p} &= \int_{\mathscr{B}_p} \rho \boldsymbol{\Upsilon} \, dV + \int_{\partial \mathscr{B}_p} \boldsymbol{t} \, dA \end{aligned} \tag{12}$$
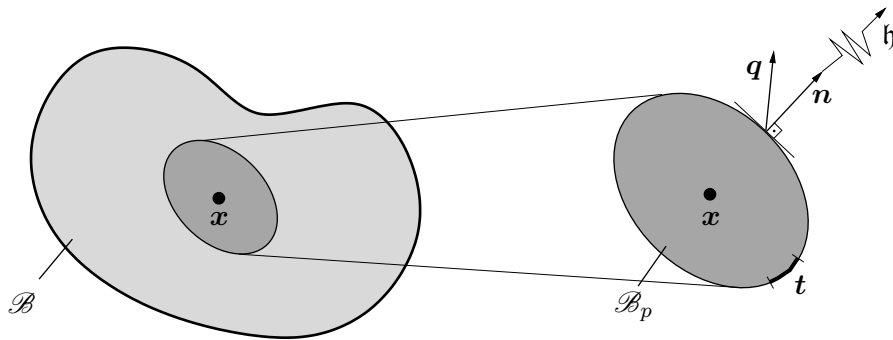


FIGURE 5: **Euler's cut principle.** The traction vector $\boldsymbol{t}(\boldsymbol{x}, t)$, and the heat flux $\mathfrak{h}$ representing the action of cut portion $\mathscr{B}_p \subseteq \mathscr{B}$ of the body.

---

[1]since Eqn. (10) has to hold for an arbitrary $\mathscr{B}_p$, and hence for $\mathscr{B}_p \to dV$, it can be localised to Eqn. (11).

in terms of the body force $\boldsymbol{\Upsilon} = \boldsymbol{\Upsilon}(\boldsymbol{x}, t)$ per unit mass. The balance of linear momentum states that the rate of change of linear momentum is equal to the resultant mechanical force that acts on the body, i.e.

$$\frac{d}{dt}\boldsymbol{\mathscr{I}}_{\mathscr{B}_p} := \boldsymbol{\mathscr{F}}_{\mathscr{B}_p} \ . \tag{13}$$

Appealing to the definition of $\boldsymbol{\mathscr{I}}_{\mathscr{B}_p}$ and $\boldsymbol{\mathscr{F}}_{\mathscr{B}_p}$ from Eqn. (12), Eqn. (13) reformulates to

$$\frac{d}{dt}\int_{\mathscr{B}_p} \rho\dot{\boldsymbol{u}}\,dV = \int_{\mathscr{B}_p} \rho\boldsymbol{\Upsilon}\,dV + \int_{\partial\mathscr{B}_p} \boldsymbol{t}\,dA \ . \tag{14}$$

Applying first the Cauchy-type theorem (Eqn. (5)) for traction, and next the Gauss theorem ($\int_{\mathscr{B}} \mathrm{div}[(\bullet)]\,dV = \int_{\partial\mathscr{B}}(\bullet)\cdot\boldsymbol{n}\,dA$) to the above equation gives

$$\int_{\mathscr{B}_p} \rho\ddot{\boldsymbol{u}}\,dV = \int_{\mathscr{B}_p} \mathrm{div}[\boldsymbol{\sigma}]\,dV + \int_{\mathscr{B}_p} \rho\boldsymbol{\Upsilon}\,dV \ . \tag{15}$$

Application of the localisation theorem results in the local form

$$\rho\ddot{\boldsymbol{u}} = \mathrm{div}[\boldsymbol{\sigma}] + \rho\boldsymbol{\Upsilon} \ . \tag{16}$$

**2.1.2.3. Balance of angular momentum.** The angular momentum $\boldsymbol{\mathscr{W}}^o_{\mathscr{B}_p}$ and the resultant moment $\widetilde{\boldsymbol{\mathscr{F}}}^o_{\mathscr{B}_p}$ associated with the part $\mathscr{B}_p$ are defined with respect to the origin "$o$" as

$$\begin{aligned} \boldsymbol{\mathscr{W}}^o_{\mathscr{B}_p} &= \int_{\mathscr{B}_p} \boldsymbol{x} \times \rho\ddot{\boldsymbol{u}}\,dV \quad \text{and} \\ \widetilde{\boldsymbol{\mathscr{F}}}^o_{\mathscr{B}_p} &= \int_{\mathscr{B}_p} \boldsymbol{x} \times \rho\boldsymbol{\Upsilon}\,dV + \int_{\partial\mathscr{B}_p} \boldsymbol{x} \times \boldsymbol{t}\,dA \end{aligned} \ , \tag{17}$$

The balance of angular momentum states that the rate of change of angular momentum is equal to the applied moment such that

$$\frac{d}{dt}\boldsymbol{\mathscr{W}}^o_{\mathscr{B}} := \widetilde{\boldsymbol{\mathscr{F}}}^o_{\mathscr{B}_p} \ . \tag{18}$$

Appealing to the respective definitions in Eqn. (17), Eqn. (18) reformulates to

$$\frac{d}{dt}\int_{\mathscr{B}_p} \boldsymbol{x} \times \rho\dot{\boldsymbol{u}}\,dV = \int_{\mathscr{B}_p} \boldsymbol{x} \times \rho\boldsymbol{\Upsilon}\,dV + \int_{\partial\mathscr{B}_p} \boldsymbol{x} \times \boldsymbol{t}\,dA \ . \tag{19}$$

After some straightforward transformations analogous to the balance of linear momentum, assuming a quasistatic loading case and taking into account the local mass balance equation (11), the local form of the balance of angular momentum reads

$$\boldsymbol{\sigma} = \boldsymbol{\sigma}^T \ , \tag{20}$$

which postulates the symmetry of the stress tensor.

**2.1.2.4. Balance of energy.** For the energy balance, the internal energy $\mathscr{U}_{\mathscr{B}_p}$ and the kinetic energy $\mathscr{K}_{\mathscr{B}_p}$ in the region $\mathscr{B}_p$ are given by

$$
\begin{aligned}
\mathscr{U}_{\mathscr{B}_p} &= \int_{\mathscr{B}_p} \rho e \, dV \\
\mathscr{K}_{\mathscr{B}_p} &= \int_{\mathscr{B}_p} \frac{1}{2} \rho \dot{\boldsymbol{u}} \cdot \dot{\boldsymbol{u}} \, dV
\end{aligned}
\quad ,
\tag{21}
$$

in terms of the internal energy $e = e(\boldsymbol{x}, t)$ per unit mass. The external powers $\mathscr{P}_{\mathscr{B}_p}$ and $\mathscr{Q}_{\mathscr{B}_p}$ associated with the mechanical and thermal problem respectively read

$$
\begin{aligned}
\mathscr{P}_{\mathscr{B}_p} &= \int_{\mathscr{B}_p} \rho \boldsymbol{\Upsilon} \cdot \dot{\boldsymbol{u}} \, dV + \int_{\partial \mathscr{B}_p} \boldsymbol{t} \cdot \dot{\boldsymbol{u}} \, dA \quad \text{and} \\
\mathscr{Q}_{\mathscr{B}_p} &= \int_{\mathscr{B}_p} \rho \mathscr{R} \, dV - \int_{\partial \mathscr{B}_p} \mathfrak{h} \, dA
\end{aligned}
\quad ,
\tag{22}
$$

where $\mathscr{R} = \mathscr{R}(\boldsymbol{x}, t)$ is the external heat source per unit mass. The balance of energy states that the rate of change in total energy is equal to the sum of mechanical and thermal power, i.e.

$$
\frac{d}{dt}[\mathscr{K}_{\mathscr{B}_p} + \mathscr{U}_{\mathscr{B}_p}] := \mathscr{P}_{\mathscr{B}_p} + \mathscr{Q}_{\mathscr{B}_p} \ ,
\tag{23}
$$

which may be equivalently expressed as

$$
\int_{\mathscr{B}_p} \rho \dot{\boldsymbol{u}} \cdot \ddot{\boldsymbol{u}} \, dV + \int_{\mathscr{B}_p} \rho \dot{e} \, dV = \int_{\mathscr{B}_p} \rho \boldsymbol{\Upsilon} \cdot \dot{\boldsymbol{u}} \, dV + \int_{\mathscr{B}_p} \boldsymbol{t} \cdot \dot{\boldsymbol{u}} \, dA + \int_{\mathscr{B}_p} \rho \mathscr{R} \, dV - \int_{\partial \mathscr{B}_p} \mathfrak{h} \, dA \ .
\tag{24}
$$

Applying the divergence theorem, and carrying out some straightforward, although lengthy transformations, Eqn. (24) reformulates to

$$
\int_{\mathscr{B}_p} \rho \dot{\boldsymbol{u}} \cdot \ddot{\boldsymbol{u}} \, dV + \int_{\mathscr{B}_p} \rho \dot{e} \, dV = \int_{\mathscr{B}_p} \rho \boldsymbol{\Upsilon} \cdot \dot{\boldsymbol{u}} \, dV + \int_{\mathscr{B}_p} \rho \mathscr{R} \, dV + \int_{\mathscr{B}_p} \mathrm{div}[\dot{\boldsymbol{u}} \cdot \boldsymbol{\sigma} - \mathbf{q}] \, dV \ .
\tag{25}
$$

Taking into account the identity

$$
\mathrm{div}[\boldsymbol{\sigma} \cdot \dot{\boldsymbol{u}}] = \dot{\boldsymbol{\varepsilon}} : \boldsymbol{\sigma} + \dot{\boldsymbol{u}} \cdot \mathrm{div}\, \boldsymbol{\sigma} \ ,
\tag{26}
$$

and applying the localisation theorem, Eqn. (26) leads to the definition of the local form of the energy balance as

$$
\rho \dot{e} = \boldsymbol{\sigma} : \dot{\boldsymbol{\varepsilon}} - \mathrm{div}[\mathbf{q}] + \rho \mathscr{R} \ ,
\tag{27}
$$

which is also known as the first law of thermodynamics.

**2.1.2.5. Balance of entropy.** The entropy $\mathscr{H}_{\mathscr{B}_p}$, its production $\mathscr{G}_{\mathscr{B}_p}$ and its power $\widetilde{\mathscr{Q}}_{\mathscr{B}_p}$ within the sub domain $\mathscr{B}_p \subseteq \mathscr{B}$ are defined by

$$
\begin{aligned}
\mathscr{H}_{\mathscr{B}_p} &= \int_{\mathscr{B}_p} \rho \varrho \, dV \ , \\
\mathscr{G}_{\mathscr{B}_p} &= \int_{\mathscr{B}_p} \rho \varrho_p \, dV \ , \\
\widetilde{\mathscr{Q}}_{\mathscr{B}_p} &= \int_{\mathscr{B}_p} \rho \frac{\mathscr{R}}{\Theta} \, dV - \int_{\partial \mathscr{B}_p} \frac{\mathfrak{h}}{\Theta} \, dA \ ,
\end{aligned}
\tag{28}
$$

where $\varrho = \varrho(\boldsymbol{x}, t)$ and $\varrho_p = \varrho_p(\boldsymbol{x}, t)$ denote the entropy and entropy production per unit mass. The balance of entropy postulates that the rate of entropy given by the sum of entropy production and entropy power, is always positive such that

$$\frac{d}{dt} \mathscr{H}_{\mathscr{B}_p} := \mathscr{G}_{\mathscr{B}_p} + \widetilde{\mathscr{Q}}_{\mathscr{B}_p} \geq 0 \ . \tag{29}$$

Inserting corresponding definitions and taking into account the balance of mass, Eqn. (29) leads to

$$\int_{\mathscr{B}_p} \rho \dot{\varrho} \, dV = \int_{\mathscr{B}_p} \rho \varrho_p \, dV + \int_{\mathscr{B}_p} \rho \frac{\mathscr{R}}{\Theta} \, dV - \int_{\partial \mathscr{B}} \frac{\mathfrak{h}}{\Theta} \, dA \geq 0 \ . \tag{30}$$

Substituting $\mathfrak{h}$ from Eqn. (5) and applying Gauss theorem to the above equation gives

$$\int_{\mathscr{B}_p} \rho \dot{\varrho} \, dV = \int_{\mathscr{B}_p} \rho \varrho_p \, dV + \int_{\mathscr{B}_p} \rho \frac{\mathscr{R}}{\Theta} \, dV - \int_{\mathscr{B}_p} \mathrm{div} \left[ \frac{\mathbf{q}}{\Theta} \right] dV \geq 0 \ , \tag{31}$$

where it can be trivially verified that

$$\mathrm{div} \left[ \frac{\mathbf{q}}{\Theta} \right] = \frac{1}{\Theta} \mathrm{div}[\mathbf{q}] - \frac{1}{\Theta^2} \nabla \Theta \cdot \mathbf{q} \geq 0 \ . \tag{32}$$

Insertion of Eqn. (32) into (31) and application of the localisation theorem gives

$$\rho \dot{\varrho} \, \Theta = \left[ - \mathrm{div}[\mathbf{q}] + \rho \mathscr{R} \right] + \rho \varrho_p \Theta + \frac{1}{\Theta} \nabla \Theta \cdot \mathbf{q} \geq 0 \ . \tag{33}$$

Using the energy balance to replace terms in the bracket with $[\rho \dot{e} - \boldsymbol{\sigma} : \dot{\boldsymbol{\varepsilon}}]$, and introducing the dissipation as $\mathscr{D} = \rho \Theta \varrho_p$ into the above equation yields the Clausius-Duhem inequality

$$\mathscr{D} = \rho \dot{\varrho} \Theta - [\rho \dot{e} - \boldsymbol{\sigma} : \dot{\boldsymbol{\varepsilon}}] - \frac{1}{\Theta} \nabla \Theta \cdot \mathbf{q} \geq 0 \ . \tag{34}$$

Finally, introducing the Helmholtz free energy density $e = \psi + \Theta \varrho$, with the rate

$$\dot{e} = \dot{\psi} + \dot{\varrho} \Theta + \varrho \dot{\Theta} \ , \tag{35}$$

into Eqn. (34) gives the local balance of entropy

$$\mathscr{D} = \boldsymbol{\sigma} : \dot{\boldsymbol{\varepsilon}} - \dot{\psi} - \varrho \dot{\Theta} - \frac{1}{\Theta} \nabla \Theta \cdot \mathbf{q} \geq 0 \ , \tag{36}$$

where the double contraction of the stress and strain rate tensor defines the stress power. Equation (36) is also referred to as the second law of thermodynamics which demands that the dissipation at all times be non-negative, thereby ensuring the thermodynamic consistency of the material. A summary of the balance equations is given in Box 1.

### 2.1.3. Dissipation postulate
As a further requirement of the formulation, the total dissipation (36) can be additively decomposed into a local and a convective part as

$$\mathscr{D} := \mathscr{D}_{\mathrm{loc}} + \mathscr{D}_{\mathrm{con}} \geq 0 \ . \tag{37}$$

Separately demanding non-negativity of Eqn. (37) yields the Clausius-Planck inequality $\mathscr{D}_{\mathrm{loc}}$ and the Fourier inequality $\mathscr{D}_{\mathrm{con}}$ as

$$\mathscr{D}_{\mathrm{loc}} := \boldsymbol{\sigma} : \dot{\boldsymbol{\varepsilon}} - \dot{\psi} - \varrho \dot{\Theta} \geq 0 \ ,$$

$$\mathscr{D}_{\mathrm{con}} := -\frac{1}{\Theta} \mathbf{q} \cdot \nabla \Theta \geq 0 \ . \tag{38}$$

Box 1: Summary of the physical balance principles.

$$
\begin{aligned}
&\text{1. Balance of mass} &&\dot{\rho} &&= 0 \\
&\text{2. Balance of linear momentum} &&\rho\ddot{\boldsymbol{u}} &&= \mathrm{div}[\boldsymbol{\sigma}] + \rho\boldsymbol{\Upsilon} \\
&\text{3. Balance of angular momentum} &&\boldsymbol{\sigma} &&= \boldsymbol{\sigma}^T \\
&\text{4. Balance of energy} &&\rho\dot{e} &&= \boldsymbol{\sigma}:\dot{\boldsymbol{\varepsilon}} - \mathrm{div}[\mathbf{q}] + \rho\mathscr{R}
\end{aligned}
$$

### 2.1.4. Requirement of the constitutive functions

The initial boundary value problem defined in Section 2.1.1.1 can be solved by the use of kinematics and balance equations. To this end, all the equations and unknowns are counted, where it follows from Box 1 that there are 8 equations, namely

$$
\left.\begin{aligned}
\dot{\rho} &= 0 &&\rightarrow 1 \text{ equation} \\
\rho\ddot{\boldsymbol{u}} &= \mathrm{div}[\boldsymbol{\sigma}] + \rho\boldsymbol{\Upsilon} &&\rightarrow 3 \text{ equations} \\
\boldsymbol{\sigma} &= \boldsymbol{\sigma}^T &&\rightarrow 3 \text{ equations} \\
\rho\dot{e} &= \boldsymbol{\sigma}:\dot{\boldsymbol{\varepsilon}} - \mathrm{div}[\mathbf{q}] + \rho\mathscr{R} &&\rightarrow 1 \text{ equation}
\end{aligned}\right\} \rightarrow 8 \text{ equations}. \tag{39}
$$

On the other hand, Eqn. (39) introduces 19 unknowns as listed below

$$
\left.\begin{aligned}
\text{density} \quad &\rho &&\rightarrow 1 \text{ unknown} \\
\text{displacement} \quad &\boldsymbol{u} &&\rightarrow 3 \text{ unknowns} \\
\text{stress} \quad &\boldsymbol{\sigma} &&\rightarrow 9 \text{ unknowns} \\
\text{energy} \quad &e &&\rightarrow 1 \text{ unknown} \\
\text{entropy} \quad &\varrho &&\rightarrow 1 \text{ unknown} \\
\text{temperature} \quad &\Theta &&\rightarrow 1 \text{ unknown} \\
\text{heat flux} \quad &\mathbf{q} &&\rightarrow 3 \text{ unknowns}
\end{aligned}\right\} \rightarrow 19 \text{ unknowns}, \tag{40}
$$

which are also known as the state variables since they represent the state of the material at every point. The missing $19-8 = 11$ equations, required for the solution of the boundary value problem are provided by the *constitutive relations* for the quantities

$$
\left.\begin{aligned}
\boldsymbol{\sigma}(\boldsymbol{x},t) &:= \boldsymbol{\sigma}(\cdots) \rightarrow 6 \text{ equations} \\
\psi(\boldsymbol{x},t) &:= \psi(\cdots) \rightarrow 1 \text{ equation} \\
\varrho(\boldsymbol{x},t) &:= \varrho(\cdots) \rightarrow 1 \text{ equation} \\
\mathbf{q}(\boldsymbol{x},t) &:= \mathbf{q}(\cdots) \rightarrow 3 \text{ equations}
\end{aligned}\right\} \rightarrow 11 \text{ additional equations}. \tag{41}
$$

In order to guarantee a thermodynamically consistent formulation, the dissipation inequality (38) also needs to be evaluated. The introduction of this inequality requires the specification of an additional constitutive relation for the free energy function $\psi$, which accounts for different material behaviour ranging from isotropic to anisotropic, elastic to inelastic, rate-independent to rate-dependent, etc. Additionally, the choice of constitutive relations (41) is not arbitrary but depends on the restrictions imposed by the balance laws and material symmetry, as discussed subsequently.

### 2.1.5. Restrictions on the constitutive functions

**2.1.5.1. Principle of determinism.**  It states that the value of all quantities in Eqn. (41) at a point $\boldsymbol{x} \in \mathscr{B}$ is fully determined by the history of displacement $\boldsymbol{u}$ and temperature $\Theta$ at all points $\boldsymbol{x} \in \mathscr{B}$ at time $t$, such that

$$
\begin{aligned}
\boldsymbol{\sigma}(\boldsymbol{x},t) &= \boldsymbol{\sigma}\Big[\boldsymbol{u}(\boldsymbol{x},t),\ \Theta(\boldsymbol{x},t),\ \cdot\ \cdot\Big] \\[4pt]
\psi(\boldsymbol{x},t) &= \psi\Big[\boldsymbol{u}(\boldsymbol{x},t),\ \Theta(\boldsymbol{x},t),\ \cdot\ \cdot\Big] \\[4pt]
\varrho(\boldsymbol{x},t) &= \varrho\Big[\boldsymbol{u}(\boldsymbol{x},t),\ \Theta(\boldsymbol{x},t),\ \cdot\ \cdot\Big] \\[4pt]
\mathfrak{q}(\boldsymbol{x},t) &= \mathfrak{q}\Big[\boldsymbol{u}(\boldsymbol{x},t),\ \Theta(\boldsymbol{x},t),\ \cdot\ \cdot\Big]
\end{aligned}
\tag{42}
$$

This rules out stochastic effects, but allows path dependent behaviour.

**2.1.5.2. Concept of internal variables.** Since it is difficult to calculate a quantity at every point based on full history of displacement $\boldsymbol{u}$ and temperature $\Theta$, a set of so-called internal variables $\boldsymbol{\mathfrak{e}}$ are introduced such that Eqn. (42) becomes

$$
\begin{aligned}
\boldsymbol{\sigma}(\boldsymbol{x},t) &= \boldsymbol{\sigma}\Big[\boldsymbol{u}(\boldsymbol{x},t),\ \Theta(\boldsymbol{x},t),\ \boldsymbol{\mathfrak{e}}(\boldsymbol{x},t),\ \cdot\Big] \\[4pt]
\psi(\boldsymbol{x},t) &= \psi\Big[\boldsymbol{u}(\boldsymbol{x},t),\ \Theta(\boldsymbol{x},t),\ \boldsymbol{\mathfrak{e}}(\boldsymbol{x},t),\ \cdot\Big] \\[4pt]
\varrho(\boldsymbol{x},t) &= \varrho\Big[\boldsymbol{u}(\boldsymbol{x},t),\ \Theta(\boldsymbol{x},t),\ \boldsymbol{\mathfrak{e}}(\boldsymbol{x},t),\ \cdot\Big] \\[4pt]
\mathfrak{q}(\boldsymbol{x},t) &= \mathfrak{q}\Big[\boldsymbol{u}(\boldsymbol{x},t),\ \Theta(\boldsymbol{x},t),\ \boldsymbol{\mathfrak{e}}(\boldsymbol{x},t),\ \cdot\Big]
\end{aligned}
\tag{43}
$$

The introduction of new unknowns $\boldsymbol{\mathfrak{e}} \in \mathbb{R}^d$ requires to specify $d$ initial conditions $\boldsymbol{\mathfrak{e}}(\boldsymbol{x}, t = 0) = \boldsymbol{\mathfrak{e}}_0(\boldsymbol{x})$ and additional evolution equations such that

$$
\dot{\boldsymbol{\mathfrak{e}}}(\boldsymbol{x},t) = \dot{\boldsymbol{\mathfrak{e}}}\Big[\boldsymbol{u}(\boldsymbol{x},t),\ \Theta(\boldsymbol{x},t),\ \boldsymbol{\mathfrak{e}}(\boldsymbol{x},t),\ \cdot\Big] ,
\tag{44}
$$

which are additional constitutive equations.

**2.1.5.3. Principle of local action.** In a small neighbourhood $\boldsymbol{y} \in \mathscr{N}_{\boldsymbol{x}} \subseteq \mathscr{B}$, the displacement, temperature and internal variables can be approximated as

$$
\begin{aligned}
\boldsymbol{u}(\boldsymbol{y} \in \mathscr{N}_{\boldsymbol{x}}) &\approx \boldsymbol{u}(\boldsymbol{x}) + \nabla u(\boldsymbol{x}) \cdot (\boldsymbol{y} - \boldsymbol{x}) \\[4pt]
\Theta(\boldsymbol{y} \in \mathscr{N}_{\boldsymbol{x}}) &\approx \Theta(\boldsymbol{x}) + \nabla\Theta(\boldsymbol{x}) \cdot (\boldsymbol{y} - \boldsymbol{x}) \\[4pt]
\boldsymbol{\mathfrak{e}}(\boldsymbol{y} \in \mathscr{N}_{\boldsymbol{x}}) &\approx \boldsymbol{\mathfrak{e}}(\boldsymbol{x}) + \nabla\boldsymbol{\mathfrak{e}}(\boldsymbol{x}) \cdot (\boldsymbol{y} - \boldsymbol{x})
\end{aligned}
\tag{45}
$$

**2.1.5.4. Principle of material objectivity.** The principle of material objectivity can be traced back to the work of Truesdell and Noll [51]. It demands that the constitutive equations be invariant to an infinitesimal rigid body motion superimposed to displacement. Consequently, if $\boldsymbol{u}(\boldsymbol{x},t)$ is a given displacement, it follows that

$$
\begin{aligned}
\psi(\boldsymbol{u}^+, \nabla\boldsymbol{u}^+, \Theta, \nabla\Theta, \boldsymbol{\mathfrak{e}}, \nabla\boldsymbol{\mathfrak{e}}) &:= \psi(\boldsymbol{u}, \nabla\boldsymbol{u}, \Theta, \nabla\Theta, \boldsymbol{\mathfrak{e}}, \nabla\boldsymbol{\mathfrak{e}}) \\[4pt]
\text{with} \quad \boldsymbol{u}^+(\boldsymbol{x},t) &:= \boldsymbol{u}(\boldsymbol{x},t) + \boldsymbol{d}(t) + \boldsymbol{Q}(t) \cdot \boldsymbol{x} \quad \forall \quad \boldsymbol{d}, \quad \boldsymbol{Q}\boldsymbol{Q}^T = \boldsymbol{1}
\end{aligned}
\tag{46}
$$

where $\boldsymbol{d}(t)$ is a time-dependent translation and $\boldsymbol{Q}(t)$ defines a small orthogonal time-dependent rotation. These two together define an infinitesimal rigid body motion. Equation (46) can only be generally fulfilled if $\psi$ is not a function of $\boldsymbol{u}$ directly and $\psi$ only depends on $\nabla_{\mathrm{sym}}\boldsymbol{u}$. This yields

$$
\begin{aligned}
\boldsymbol{\sigma} &= \boldsymbol{\sigma}(\boldsymbol{\varepsilon}, \Theta, \nabla\Theta, \boldsymbol{\mathfrak{e}}, \nabla\boldsymbol{\mathfrak{e}}) \\
\psi &= \psi(\boldsymbol{\varepsilon}, \Theta, \nabla\Theta, \boldsymbol{\mathfrak{e}}, \nabla\boldsymbol{\mathfrak{e}}) \\
\varrho &= \varrho(\boldsymbol{\varepsilon}, \Theta, \nabla\Theta, \boldsymbol{\mathfrak{e}}, \nabla\boldsymbol{\mathfrak{e}}) \quad . \\
\mathbf{q} &= \mathbf{q}(\boldsymbol{\varepsilon}, \Theta, \nabla\Theta, \boldsymbol{\mathfrak{e}}, \nabla\boldsymbol{\mathfrak{e}}) \\
\dot{\boldsymbol{\mathfrak{e}}} &= \dot{\boldsymbol{\mathfrak{e}}}(\boldsymbol{\varepsilon}, \Theta, \nabla\Theta, \boldsymbol{\mathfrak{e}}, \nabla\boldsymbol{\mathfrak{e}})
\end{aligned}
\tag{47}
$$

**2.1.5.5. Principle of material symmetry.** Consider a free energy function having a functional dependence on the strain tensor. Then, the amount of stored energy will not only depend on the applied deformation but also on the orientation of the material. As an example, consider two materials with different micro-structural orientations $\boldsymbol{a}$ and $\tilde{\boldsymbol{a}}$, and assume that these orientations are linked with an orthogonal transformation, i.e. $\tilde{\boldsymbol{a}} = \boldsymbol{Q}^T\boldsymbol{a}$. Additionally, assume that in both these cases, the material is subjected to the same deformation state. Then, the stored free energies are given by

$$
\psi = \psi(\boldsymbol{\varepsilon}) \quad \text{and} \quad \tilde{\psi} = \psi(\boldsymbol{Q}\boldsymbol{\varepsilon}\boldsymbol{Q}^T) \; . \tag{48}
$$

In general, both these function values will differ such that $\psi \neq \tilde{\psi}$. The set of all transformations $\boldsymbol{Q}$, yielding $\psi = \tilde{\psi}$, is known as the material symmetry group, and the principle of material symmetry strongly restricts the constitutive functions to be invariant to the material symmetry group.

With Eqn. $(47)_2$, the rate of the energetic potential can be evaluated as

$$
\dot{\psi} = \psi_{,\boldsymbol{\varepsilon}} : \dot{\boldsymbol{\varepsilon}} + \psi_{,\Theta}\,\dot{\Theta} + \psi_{,\nabla\Theta} \cdot \nabla\dot{\Theta} + \psi_{,\boldsymbol{\mathfrak{e}}} \cdot \dot{\boldsymbol{\mathfrak{e}}} + \psi_{,\nabla\boldsymbol{\mathfrak{e}}} \cdot \nabla\dot{\boldsymbol{\mathfrak{e}}} \; . \tag{49}
$$

Substituting Eqns. (49) and (47) into Eqn. (37) and taking into account Eqn. (38), gives the expression

$$
\mathscr{D} = [\boldsymbol{\sigma} - \psi_{,\boldsymbol{\varepsilon}}] : \dot{\boldsymbol{\varepsilon}} - [\varrho + \psi_{,\Theta}]\dot{\Theta} - \psi_{,\nabla\Theta} \cdot \nabla\dot{\Theta} - \psi_{,\boldsymbol{\mathfrak{e}}} \cdot \dot{\boldsymbol{\mathfrak{e}}} - \psi_{,\nabla\boldsymbol{\mathfrak{e}}} \cdot \nabla\dot{\boldsymbol{\mathfrak{e}}} - \frac{1}{\Theta}\nabla\Theta \cdot \mathbf{q} \geq 0 \; . \tag{50}
$$

The requirement for Eqn. (50) to be true for any rates $\dot{\boldsymbol{\varepsilon}}$, $\dot{\Theta}$ and $\nabla\dot{\Theta}$, usually known as the Coleman-Noll argument [67, 71] leads to the definition of two constitutive relations

$$
\boxed{\boldsymbol{\sigma} := \psi_{,\boldsymbol{\varepsilon}} \quad \text{and} \quad \varrho := -\psi_{,\Theta}} \; , \tag{51}
$$

together with the condition

$$
\psi_{,\nabla\Theta} = \boldsymbol{0} \; , \tag{52}
$$

where $\boldsymbol{0}$ is the second-order zero tensor, and the reduced dissipation inequality

$$
\boxed{\mathscr{D}^{\mathrm{red}} = -\psi_{,\boldsymbol{\mathfrak{e}}} \cdot \dot{\boldsymbol{\mathfrak{e}}} - \psi_{,\nabla\boldsymbol{\mathfrak{e}}} \cdot \nabla\dot{\boldsymbol{\mathfrak{e}}} - \frac{1}{\Theta}\nabla\Theta \cdot \mathbf{q} \geq 0} \; , \tag{53}
$$

which can be additively decomposed as

$$\mathscr{D}^{\mathrm{red}} = \mathscr{D}^{\mathrm{red}}_{\mathrm{loc}} + \mathscr{D}^{\mathrm{red}}_{\mathrm{con}} \geq 0$$

$$\text{with}\quad \mathscr{D}^{\mathrm{red}}_{\mathrm{loc}} = -\psi,_{\mathfrak{c}} \cdot \dot{\mathfrak{c}} - \psi,_{\nabla\mathfrak{c}} \cdot \nabla\dot{\mathfrak{c}} \geq 0 \quad\text{and}\quad \mathscr{D}^{\mathrm{red}}_{\mathrm{con}} = -\frac{1}{\Theta}\nabla\Theta \cdot \mathbf{q} \geq 0 \qquad (54)$$

These conditions allow for the reformulation of the constitutive relations as

$$\boxed{\begin{aligned} \psi &= \psi(\boldsymbol{\varepsilon}, \Theta, \mathfrak{c}, \nabla\mathfrak{c}) \\ \mathbf{q} &= \mathbf{q}(\boldsymbol{\varepsilon}, \Theta, \nabla\Theta, \mathfrak{c}, \nabla\mathfrak{c}) \\ \dot{\mathfrak{c}} &= \dot{\mathfrak{c}}(\boldsymbol{\varepsilon}, \Theta, \nabla\Theta, \mathfrak{c}, \nabla\mathfrak{c}) \end{aligned}} \,, \qquad (55)$$

for which functional forms need to be prescribed. With Eqn. (55), all the constitutive functions necessary for the closure of the boundary value problem are specified. Before proceeding further, the governing balance equation of temperature field $\Theta(\boldsymbol{x}, t)$ is reformulated as explained subsequently. Recall here the energy balance

$$\rho\dot{e} = \boldsymbol{\sigma} : \dot{\boldsymbol{\varepsilon}} - \mathrm{div}[\mathbf{q}] + \rho\mathscr{R} \,, \qquad (56)$$

which can be equivalently expressed using Eqn. (35) as

$$\dot{\psi} + \dot{\varrho}\Theta + \varrho\dot{\Theta} = \boldsymbol{\sigma} : \dot{\boldsymbol{\varepsilon}} - \mathrm{div}[\mathbf{q}] + \mathscr{R} \,, \qquad (57)$$

where the density $\rho$ has been dropped for brevity. Taking into account the expression

$$\dot{\varrho} = -\frac{d}{dt}\psi,_{\Theta} = -\psi,_{\boldsymbol{\varepsilon}\Theta} : \dot{\boldsymbol{\varepsilon}} - \psi,_{\Theta\Theta}\dot{\Theta} - \psi,_{\mathfrak{c}\Theta} \cdot \dot{\mathfrak{c}} - \psi,_{\nabla\mathfrak{c}\Theta} \cdot \nabla\dot{\mathfrak{c}} \,, \qquad (58)$$

and appealing to Eqn. (49), Eqn. (57) reformulates to

$$\begin{aligned} \boldsymbol{\sigma} : \dot{\boldsymbol{\varepsilon}} &- \varrho\dot{\Theta} + \psi,_{\mathfrak{c}} \cdot \dot{\mathfrak{c}} + \psi,_{\nabla\mathfrak{c}} \cdot \nabla\dot{\mathfrak{c}} + \varrho\dot{\Theta} \\ &- \psi,_{\boldsymbol{\varepsilon}\Theta} : \dot{\boldsymbol{\varepsilon}} - \psi,_{\Theta\Theta}\dot{\Theta} - \psi,_{\mathfrak{c}\Theta} \cdot \dot{\mathfrak{c}} - \psi,_{\nabla\mathfrak{c}\Theta} \cdot \nabla\dot{\mathfrak{c}} = \boldsymbol{\sigma} : \dot{\boldsymbol{\varepsilon}} - \mathrm{div}[\mathbf{q}] + \mathscr{R} \end{aligned} \qquad (59)$$

Furthermore, setting $\mathfrak{c} = -\Theta\psi,_{\Theta\Theta}$ and taking into account Eqn. (54), it follows that the governing balance equation of temperature can be expressed as

$$\boxed{\mathfrak{c}\dot{\Theta} = \mathscr{D}^{\mathrm{red}}_{\mathrm{loc}} + \mathcal{H} - \mathrm{div}[\mathbf{q}] + \mathscr{R}} \,, \qquad (60)$$

where

$$\mathcal{H} = \Theta\{\psi,_{\boldsymbol{\varepsilon}\Theta} : \dot{\boldsymbol{\varepsilon}} - \psi,_{\mathfrak{c}\Theta} \cdot \dot{\mathfrak{c}} - \psi,_{\nabla\mathfrak{c}\Theta} \cdot \nabla\dot{\mathfrak{c}}\} = \Theta\psi,_{\Theta}\{\boldsymbol{\sigma} : \dot{\boldsymbol{\varepsilon}} + \mathscr{D}^{\mathrm{red}}_{\mathrm{loc}}\} \,, \qquad (61)$$

denotes the latent heat which is the thermoelastic counterpart of the thermoplastic dissipation, see also [72, 73]. Note that $\mathfrak{c} = \psi,_{\Theta\Theta}$ is generally a material parameter denoting specific heat capacity, and follows from the choice of the functional form of the thermal contribution of scalar energetic potential.

## 2.2. Classification of solids

In this section, basics of the crystal structure are discussed. Crystal structure is defined by the spatial arrangement of atoms or molecules inside the material. Based on the arrangement of atoms, solids can be classified into two groups namely *crystalline solids* where atoms are periodically arranged with a definite repetitive pattern inside the material and *amorphous solids* where atoms are randomly arranged [74]. The periodicity of atoms in crystalline solids can be described by a network of points in the space called *crystal lattice*. The most simple form of a crystal lattice can be constructed following the principles of a three-dimensional mathematical point grid as

$$\mathbb{R}^3 : \left\{ \boldsymbol{x} = \boldsymbol{x}_0 + i\boldsymbol{a} + j\boldsymbol{b} + k\boldsymbol{c} \mid i, j, k \in \mathbb{R} \right\}, \tag{62}$$
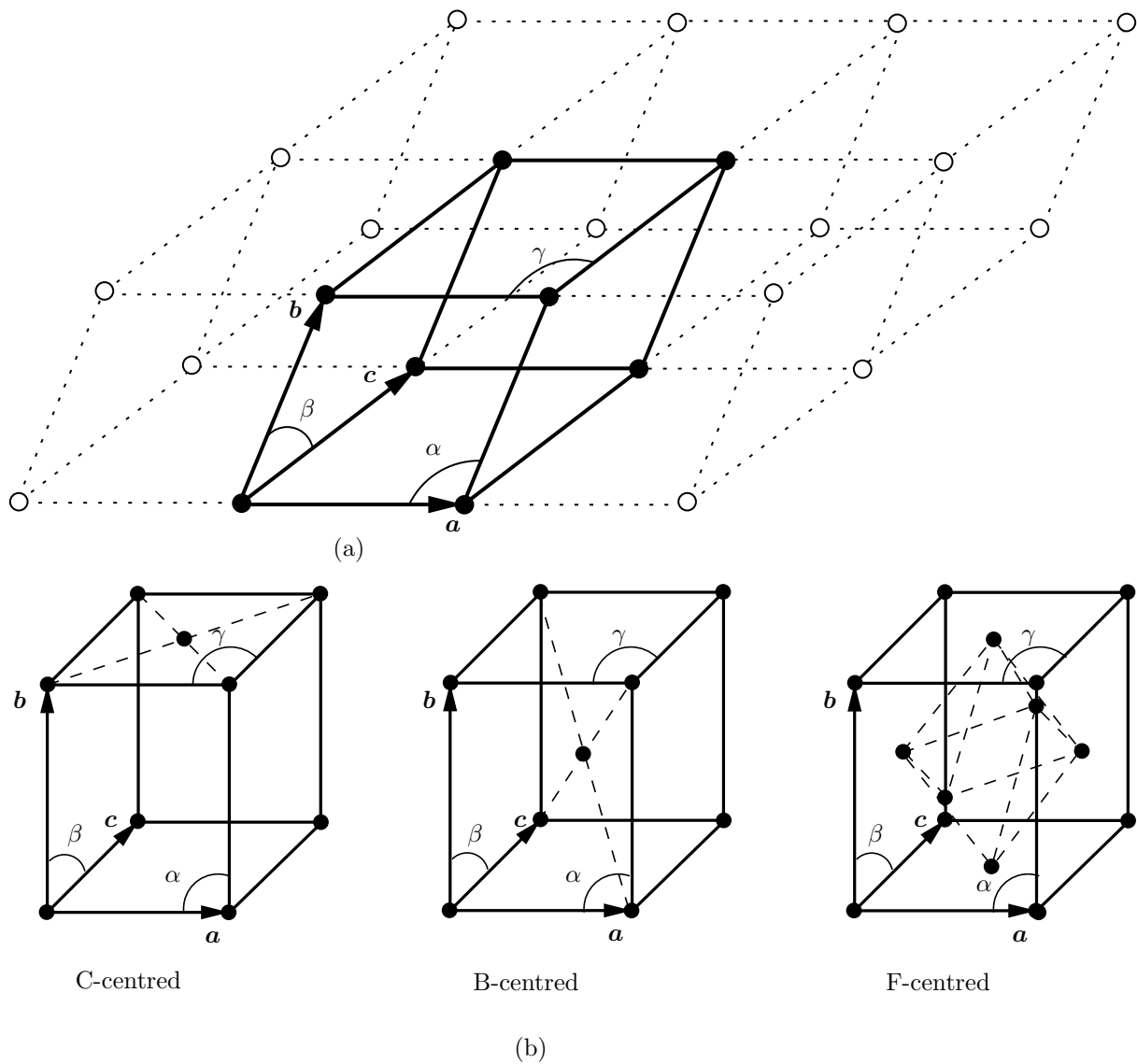


FIGURE 6: **Construction of a grid.** The grids are spanned by the grid vectors $\boldsymbol{a}, \boldsymbol{b}$ and $\boldsymbol{c}$ and the corresponding grid angles $\alpha, \beta$ and $\gamma$. Angles and lengths of the unit-cell form the *metric* of the grid. (a) Primitive unit-cell containing one grid point inside. (b) Non-primitive unit-cells namely C-centred, B-centred and F-centred unit-cell having more than one grid point inside.

where $\boldsymbol{x}_0$ is an arbitrary basis position and $\{\boldsymbol{a}, \boldsymbol{b}, \boldsymbol{c}\} \in \mathbb{R}^3$ are the lattice vectors or grid vectors, see also [75]. Any lattice that can be described by Eqn. (62) is called a *Bravais lattice*. Further, for any two points $\boldsymbol{x}_0$ and $\boldsymbol{x}_i$ from which the atomic arrangement looks the same, the vectors $\boldsymbol{a}, \boldsymbol{b}$ and $\boldsymbol{c}$ are said to be *primitive* and hence define a primitive unit-cell[2] [76], if they satisfy Eqn. (62). Alternatively, a primitive unit-cell can also be described by the grid constants or lattice parameters

$$a = \|\boldsymbol{a}\|, \quad b = \|\boldsymbol{b}\| \quad \text{and} \quad c = \|\boldsymbol{c}\| \ , \tag{63}$$

where $\|\bullet\|$ denotes the Euclidean norm, and their corresponding angles

$$\alpha = \angle(\boldsymbol{ab}), \quad \beta = \angle(\boldsymbol{bc}) \quad \text{and} \quad \gamma = \angle(\boldsymbol{ac}) \ . \tag{64}$$

Angles and lengths of the unit-cell constitute the *metric* of the grid. The unit-cell as seen in Fig. 6 a), contains one (one-eighth times eight) grid point and is therefore primitive. Non-primitive unit-cells are characterised by having more than one grid point inside, e.g. C-centred, B-centred or F-centred unit-cell, see Fig. 6 b). An infinite number of primitive and non-primitive unit-cells can be chosen for defining the grid. Overall there exists 14 space lattices named after the physicist Auguste Bravais.

### 2.2.1. Symmetry transformations

The symmetry transformation of a lattice, consisting of rotations and rotation-inversions, is an operation which maps the lattice onto itself[3]. Rotations and rotation-inversions can be described with orthogonal tensors. To this end, let $\alpha$ be an arbitrary rotation angle around an axis $\boldsymbol{a}$, with $\|\boldsymbol{a}\| = 1$. Then the rotation tensor can be defined by the standard Euler-Rodrigues formula

$$\boldsymbol{Q} := \cos\alpha \boldsymbol{1} + (1 - \cos\alpha)\boldsymbol{a} \otimes \boldsymbol{a} + \sin\alpha \boldsymbol{\epsilon a} \ , \tag{65}$$

where $\boldsymbol{1}$ denotes the second-order identity tensor and $\boldsymbol{\epsilon}$ is the RICCI permutation (third-order) tensor. Rotation-inversions can be described using the central inversion with the rotation tensor as $-\boldsymbol{Q} = (-\boldsymbol{1})\boldsymbol{Q}$, see [75, 77]. The set of allowed rotations $\mathscr{C} \subseteq \mathcal{O}(3)$ for which the constitutive response remains unchanged is called the symmetry group of the material, and $\mathcal{O}(3)$ is the orthogonal group with the properties

$$\mathcal{O}(3) := \{\boldsymbol{Q} | \boldsymbol{Q}^T \boldsymbol{Q} = \boldsymbol{1} \quad \text{and} \quad \det[\boldsymbol{Q}] = +1\} \ . \tag{66}$$

**Remark 1.** Some properties of the symmetric group

- if $\boldsymbol{Q}_1 \in \mathscr{C}$ and $\boldsymbol{Q}_2 \in \mathscr{C}$, then $\boldsymbol{Q}_1\boldsymbol{Q}_2 \in \mathscr{C}$

- multiplicative associativity holds true, i.e. $(\boldsymbol{Q}_1\boldsymbol{Q}_2)\boldsymbol{Q}_3 = \boldsymbol{Q}_1(\boldsymbol{Q}_2\boldsymbol{Q}_3)$

- the symmetry group $\mathscr{C}$ contains the identity $\boldsymbol{1}$, such that $\boldsymbol{1Q} = \boldsymbol{Q1} = \boldsymbol{Q}$

- if there exists $\boldsymbol{Q} \in \mathscr{C}$, then there also exists $\boldsymbol{Q}^{-1} \in \mathscr{C}$, such that $\boldsymbol{Q}\boldsymbol{Q}^{-1} = \boldsymbol{1}$

---

[2]A unit-cell is the basic building block of the crystal structure, which defines the crystal structure with positions of the atom.

[3]Only such symmetry transformations are considered in the present work.

### 2.2.2. Classification of Bravais lattices

Based on their inherent symmetry (shape of the unit-cell), Bravais lattices can be distinguished into 14 different types belonging to the seven different crystal systems. Starting with the lowest symmetry (fully anisotropic case) where all the grid constants and angles are different, symmetry operations transforming the grid onto itself are studied.

**2.2.2.1. Triclinic symmetry.** The most general form of a Bravais lattice is that of the triclinic symmetry. The only possible symmetry operations are the *identity* and *inversion*. The three grid constants $a, b$ and $c$, and their corresponding angles $\alpha, \beta$ and $\gamma$ satisfy

$$a \neq b \neq c \quad \text{and} \quad \alpha \neq \beta \neq \gamma \,, \tag{67}$$

which indicates crystals that belong to the triclinic system have three unequal axes and all of them intersect at oblique angles, see also Fig. 7. Triclinic crystals have no symmetry and no mirrored planes.

**2.2.2.2. Monoclinic symmetry.** A monoclinic system is characterised by the existence of a single plane of mirror symmetry. If the plane of symmetry is parallel to $\boldsymbol{a}$, then the metric of the grid are given by

$$a \neq b \neq c \quad \text{and} \quad \alpha = \gamma = 90° \neq \beta \,. \tag{68}$$

The restrictions change accordingly if the plane of symmetry is parallel to $\boldsymbol{b}$ or $\boldsymbol{c}$. The name "monoclinic" indicates that only one angle is inclined, as seen from Eqn. (68). Additionally, it also follows from Eqn. (68) that the crystals in the monoclinic system have three unequal axes. The $\boldsymbol{a}$ and $\boldsymbol{c}$ axes are inclined toward each other at an oblique angle, see Fig. 8 a) and the $\boldsymbol{b}$ axis is perpendicular to $\boldsymbol{a}$ and $\boldsymbol{c}$. Alternatively, instead of the primitive unit-cell, a C-centred non-primitive unit-cell can also be used to characterise this symmetry group because of its standard monoclinic metric, see Fig. 8 b).

**2.2.2.3. Orthorhombic symmetry.** An orthorhombic system is characterised by the existence of three mutually perpendicular planes of mirror symmetry. Its grid parameters and their corresponding angles constitutes a standard orthotropic shape such that

$$a \neq b \neq c \quad \text{and} \quad \alpha = \beta = \gamma = 90° \,, \tag{69}$$

see Fig. 9. Orthorhombic crystals have three unequal axes mutually perpendicular to each other. The primitive orthorhombic unit-cell can be obtained by introducing two additional planes of mirror symmetry into the monoclinic unit-cell. Instead of the primitive unit-cell, the orthorhombic symmetry can also be identified by non-primitive unit-cells such as C-centred, B-centred or F-centred unit-cell as explained in [60].
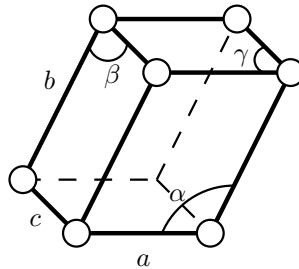


FIGURE 7: **Triclinic unit-cell.** The grid constants $a, b$ and $c$, and their corresponding angles $\alpha, \beta$ and $\gamma$ are arbitrary.

**2.2.2.4. Tetragonal symmetry.** A tetragonal system is characterised by a unit-cell with two equal edges, where the crystal has same dimensions for the bottom and top face. However, edges representing the front, back and side faces are comparatively taller. The introduced symmetry operations so far only affected the angles of the unit-cells and not the ratio of the edges. This changes for a primitive tetragonal unit-cell, with restrictions

$$a = b \neq c \quad \text{and} \quad \alpha = \beta = \gamma = 90° \;, \tag{70}$$

see Fig. 10. In addition to a primitive unit-cell, a non-primitive B-centred unit-cell can also describe a tetragonal crystal.

**2.2.2.5. Trigonal symmetry.** A trigonal system is characterised by the following restrictions on the metric

$$a = b = c \quad \text{and} \quad \alpha = \beta = \gamma \neq 90° \;, \tag{71}$$

for the primitive unit-cell as depicted in Fig. 11. A trigonal crystal is similar to a cube, except that its faces are rhombii. It resembles a cube that has been compressed to one side.
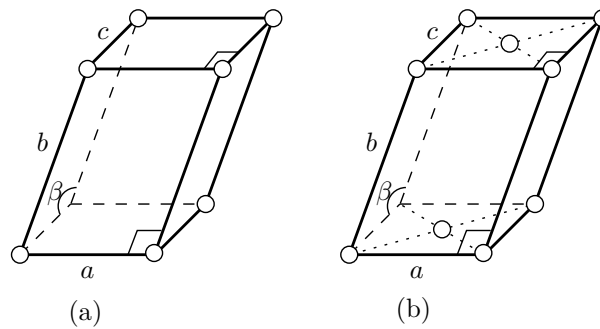


FIGURE 8: **Monoclinic unit-cell.** The grid constants $a, b$ and $c$ are arbitrary with $a \neq b \neq c$, whereas the corresponding angles are satisfy the symmetry $\alpha = \gamma = 90° \neq \beta$. (a) Primitive unit-cell and (b) C-centred unit-cell.
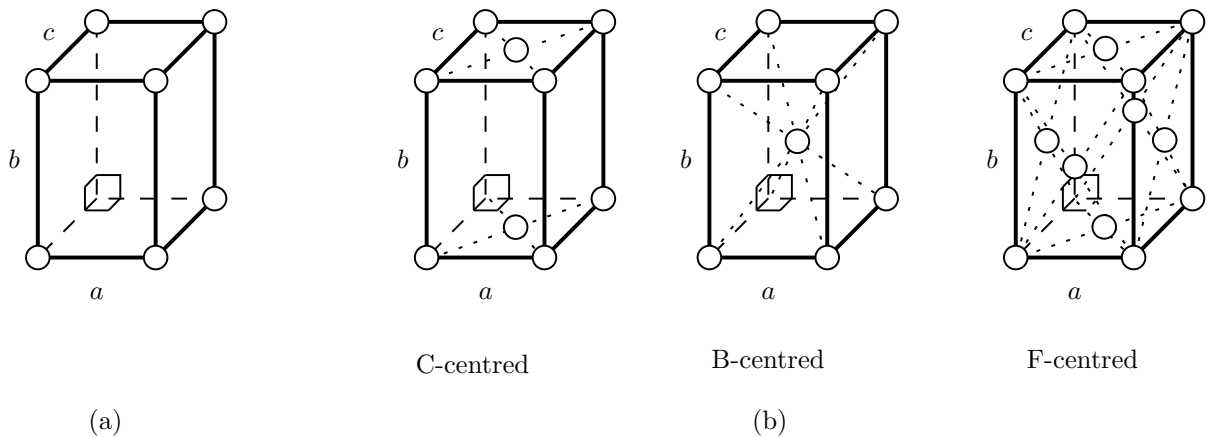


FIGURE 9: **Orthorhombic unit-cell.** The grid constants $a, b$ and $c$ are arbitrary with $a \neq b \neq c$, whereas the corresponding angles are orthogonal with $\alpha = \beta = \gamma = 90°$. Its metric constitutes a standard orthotropic shape. (a) Primitive-unit cell and (b) Non-primitive unit-cells namely C-centred, B-centred and F-centred unit-cell.

**2.2.2.6. Hexagonal symmetry.** A primitive hexagonal unit-cell is obtained from a primitive monoclinic unit-cell by setting the grid parameters and their corresponding angles to satisfy

$$a = b \neq c \quad \text{and} \quad \alpha = \beta = 90°, \gamma = 120° \ . \tag{72}$$

The hexagonal symmetry can only be observed in stacks of unit-cells as as visualised in Fig. 12.



B-centred

(a)                                    (b)
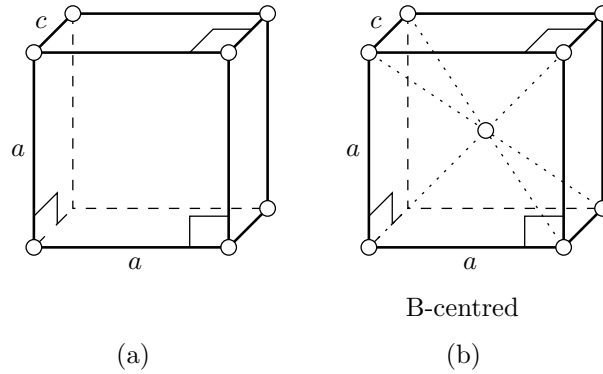
FIGURE 10: **Tetragonal unit-cell.** The grid constants are now restricted according to $a = b \neq c$ and the corresponding angles are orthogonal with $\alpha = \beta = \gamma = 90°$. (a) Primitive tetragonal unit-cell which can be thought of as a modified orthorhombic unit-cell, and (b) Non-primitive B-centred unit-cell.
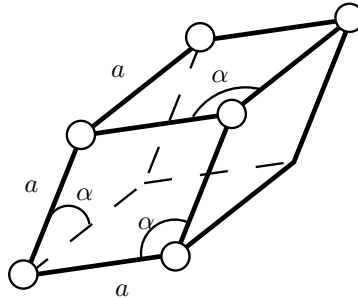


FIGURE 11: **Trigonal unit-cell.** The grid constants are now restricted according to $a = b = c$, whereas the corresponding angles are equal but not orthogonal, i.e. $\alpha = \beta = \gamma \neq 90°$.
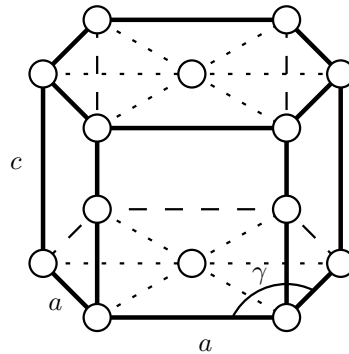


FIGURE 12: **Hexagonal unit-cell.** The grid constants are now restricted according to $a = b \neq c$ and the corresponding angles satisfy $\alpha = \beta = 90°, \gamma = 120°$.

TABLE 1: Classification of the crystal systems.

| No. | Crystal system | Lattice parameters | Corresponding angles |
|---|---|---|---|
| 1. | triclinic | $a \neq b \neq c$ | $\alpha \neq \beta \neq \gamma$ |
| 2. | monoclinic | $a \neq b \neq c$ | $\alpha = \gamma = 90° \neq \beta$ |
| 3. | orthorhombic | $a \neq b \neq c$ | $\alpha = \beta = \gamma = 90°$ |
| 4. | tetragonal | $a = b \neq c$ | $\alpha = \beta = \gamma = 90°$ |
| 5. | trigonal | $a = b = c$ | $\alpha = \beta = \gamma \neq 90°$ |
| 6. | hexagonal | $a = b \neq c$ | $\alpha = \beta = 90°, \gamma = 120°$ |
| 7. | cubic | $a = b = c$ | $\alpha = \beta = \gamma = 90°$ |

**2.2.2.7. Cubic symmetry.** To derive the Bravais cells for the cubic symmetry, one can introduce four three-fold axes along the body diagonals into an orthorhombic system. Consequently, all the faces will be squares and the edges will have the same length. Hence, the restrictions are given by

$$a = b = c \quad \text{and} \quad \alpha = \beta = \gamma = 90° \ . \tag{73}$$

The cubic crystal system, also known as the isometric system, is characterised by its total symmetry. It has three equal crystallographic axes which are mutually perpendicular to each other, see Fig. 13. Unit-cells having higher symmetry than that of the cubic system do not exist. The seven crystal systems along with their corresponding metric are summarised in Table 1.

### 2.2.3. Classification into 13 types of anisotropy

So far, the restrictions on the unit-cell to describe a space lattice were outlined. The symmetry groups of 14 Bravais lattices can be subdivided into proper subgroups which results in the formation of 32 crystal classes. Taking into account materials with fibrous micro-structure like *composites* or biological materials such as soft tissues, further symmetry operations have to be considered. For these materials, rotations around an axis or multiple axes along with the corresponding rotation-inversions are possible, resulting in five additional transversely isotropic symmetric groups. To this end, let $\{\boldsymbol{a}, \boldsymbol{b}, \boldsymbol{c}\}$ denote
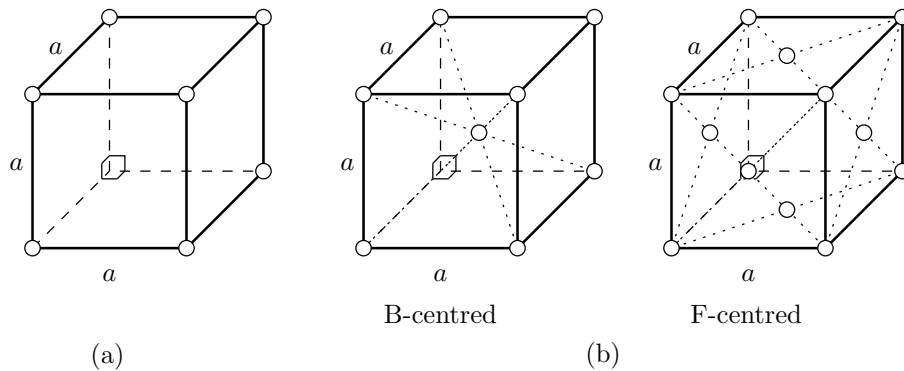


FIGURE 13: **Cubic unit-cell.** All the edges have the same length $a = b = c$, and the corresponding angles satisfy $\alpha = \beta = \gamma = 90°$. (a) Primitive-unit cell and (b) Non-primitive unit-cells namely B-centred and F-centred unit-cells.

TABLE 2: Classification of material symmetry groups.

| No. | Symbol | Symmetry group | Generators |
|-----|--------|----------------|------------|
| 1. | $\mathscr{C}_1$ | triclinic | $\boldsymbol{1}$ |
| 2. | $\mathscr{C}_2$ | monoclinic | $\boldsymbol{Q}_c^\pi$ |
| 3. | $\mathscr{C}_3$ | orthorhombic | $\boldsymbol{Q}_a^\pi, \boldsymbol{Q}_b^\pi$ |
| 4. | $\mathscr{C}_4$ | tetragonal | $\boldsymbol{Q}_c^{\frac{\pi}{2}}$ |
| 5. | $\mathscr{C}_5$ | tetragonal | $\boldsymbol{Q}_c^{\frac{\pi}{2}}, \boldsymbol{Q}_a^\pi$ |
| 6. | $\mathscr{C}_6$ | trigonal | $\boldsymbol{Q}_c^{\frac{2\pi}{3}}$ |
| 7. | $\mathscr{C}_7$ | trigonal | $\boldsymbol{Q}_c^{\frac{2\pi}{3}}, \boldsymbol{Q}_a^\pi$ |
| 8. | $\mathscr{C}_8$ | hexagonal | $\boldsymbol{Q}_a^{\frac{\pi}{3}}$ |
| 9. | $\mathscr{C}_9$ | hexagonal | $\boldsymbol{Q}_c^{\frac{\pi}{3}}, \boldsymbol{Q}_a^\pi$ |
| 10. | $\mathscr{C}_{10}$ | cubic | $\boldsymbol{Q}_a^\pi, \boldsymbol{Q}_b^\pi, \boldsymbol{Q}_d^\pi$ [x] |
| 11. | $\mathscr{C}_{11}$ | cubic | $\boldsymbol{Q}_a^{\frac{\pi}{2}}, \boldsymbol{Q}_b^{\frac{\pi}{2}}, \boldsymbol{Q}_c^{\frac{\pi}{2}}$ |
| 12. | $\mathscr{C}_{12}$ | transversely isotropic | $\boldsymbol{Q}_a^\alpha$ |
| 13. | $\mathscr{C}_{13}$ | transversely isotropic | $\boldsymbol{Q}_c^\alpha, \boldsymbol{Q}_a^\pi$ |
| 14. | $\mathscr{C}_{14}$ | isotropic | $\mathcal{O}(3)$ |

$^x\boldsymbol{d} = \sqrt{\frac{1}{3}}(\boldsymbol{a} + \boldsymbol{b} + \boldsymbol{c})$

a positively oriented orthonormal vector triad attached to a material point, such that rotations and reflections relative to these vectors fully describe the material symmetry group. The 32 crystal symmetry groups and the five transversely isotropic symmetric groups contain the central inversion as a common factor, namely that $-\boldsymbol{1} \in \mathscr{C}$. With this restriction, all the constitutive relations are centrosymmetric, which reduces the 32 crystal symmetry groups and the five transversely isotropic symmetric groups to a combined total of 13 so-called mechanics symmetry groups, in addition to the isotropic group. These groups are classified in [64, 78] as summarised in Table 2.

## 2.3. Description of anisotropic material behaviour

Anisotropic material response (elastic or inelastic) considers the response of materials with micro-structures at lower scales, e.g. crystals or composite materials. For materials as such, the micro-structure induces a direction dependent macroscopic material response. A micro-structure is defined on the macroscopic level by a symmetry group $\mathscr{C}$, which represents all the rotations $\boldsymbol{Q}$ that map the material structure onto itself. Then, it is clear that these rotations belong to the symmetry group, i.e. $\boldsymbol{Q} \in \mathscr{C}$. Fundamentally, the anisotropic material response can be described by a *classical approach* or a *coordinate-free* approach. After a brief introduction to the classical approach, emphasis is placed on the coordinate-free approach where anisotropic functions are generated with the aid of general representation theorems [45].

### 2.3.1. Classical approach to anisotropy

To mathematically motivate the classical approach to anisotropy, consider a domain $\mathscr{A}$ consisting of a scalar $u$, vector $\boldsymbol{v}$, symmetric second-order tensor $\boldsymbol{U}$ and skew-symmetric

second-order tensor $\boldsymbol{V}^4$ such that

$$\mathscr{A} := \mathbb{R} \times \mathbb{R}^3 \times \mathbb{R}^6 \times \mathbb{R}^6 \ , \tag{74}$$

where $\mathbb{R}, \mathbb{R}^3$ and $\mathbb{R}^6$ denote the scalar, Euclidean vector and tensor spaces, respectively. For brevity, let $\mathfrak{F}$ represent a scalar-valued constitutive function which depends explicitly on $u, \boldsymbol{v}, \boldsymbol{U}$ and $\boldsymbol{V}$ such that

$$\mathfrak{F} = \mathfrak{F}(u, \boldsymbol{v}, \boldsymbol{U}, \boldsymbol{V}) \ . \tag{75}$$

The function $\mathfrak{F}$ is classified according to its transformation properties under the action of the orthogonal group $\mathcal{O}(3)$ or the symmetry groups $\mathscr{C} \subseteq \mathcal{O}(3)$. Then, an anisotropic response is defined by the constitutive function $\mathfrak{F}$ that is invariant to the rotations of the considered symmetry group such that

$$\mathfrak{F}(\boldsymbol{Q} \star u, \boldsymbol{Q} \star \boldsymbol{v}, \boldsymbol{Q} \star \boldsymbol{U}, \boldsymbol{Q} \star \boldsymbol{V}) = \boldsymbol{Q} \star \mathfrak{F}(u, \boldsymbol{v}, \boldsymbol{U}, \boldsymbol{V}) \quad \forall \quad \boldsymbol{Q} \in \mathscr{C} \subseteq \mathcal{O}(3) \ , \tag{76}$$

which is known as the invariance condition. Here, a Rayleigh product has been used in line with [75] as

$$\star : \mathcal{O}(3) : \begin{cases} \boldsymbol{Q} \star u := u \ , \\ \boldsymbol{Q} \star \boldsymbol{v} := Q_{ij}v_j \ , \\ \boldsymbol{Q} \star \boldsymbol{U} := U_{ij}Q_{ia}Q_{jb} \quad \text{and} \\ \boldsymbol{Q} \star \boldsymbol{V} := V_{ij}Q_{ia}Q_{jb} \ . \end{cases} \tag{77}$$

where $\boldsymbol{Q} \in \mathcal{O}(3)$. From Eqn. (76), it can be immediately deduced that if $\mathscr{C} \equiv \mathcal{O}(3)$, then the function $\mathfrak{F}(u, \boldsymbol{v}, \boldsymbol{U}, \boldsymbol{V})$ is an *isotropic* function, else, with respect to particular symmetry group $\mathscr{C}$, it is a $\mathscr{C}$-invariant function.

### 2.3.2. Coordinate-free approach to anisotropy

The underlying idea of a coordinate-free approach is to generate anisotropic tensor functions in terms of equivalent isotropic tensor functions with the help of representation theorems. The key aspect is to systematically generate the tensor functions that are invariant for a given material symmetry group $\mathscr{C}$. This can be achieved by extending the set of arguments to include *structural tensors* as additional arguments. A second-order tensor $\boldsymbol{M}$ is a structural tensor for an anisotropic material characterised by a symmetry group $\mathscr{C}$, if

$$\boldsymbol{Q} \star \boldsymbol{M} = \boldsymbol{M} \quad \forall \quad \boldsymbol{Q} \in \mathscr{C} \ . \tag{78}$$

From Eqn. (78) it follows that any $\mathscr{C}$-invariant function $\mathfrak{F}(\boldsymbol{x})$ with $\boldsymbol{x}$ as a set of arguments, can be expressed equivalently as an isotropic function with structural tensors as additional arguments. Therefore, the invariance condition (76) reformulates to the isotropic form

$$\mathfrak{F}(\boldsymbol{Q} \star u, \boldsymbol{Q} \star \boldsymbol{v}, \boldsymbol{Q} \star \boldsymbol{U}, \boldsymbol{Q} \star \boldsymbol{V}, \boldsymbol{Q} \star \boldsymbol{M}) = \mathfrak{F}(u, \boldsymbol{v}, \boldsymbol{U}, \boldsymbol{V}, \boldsymbol{M}) \quad \forall \quad \boldsymbol{Q} \in \mathcal{O}(3) \ . \tag{79}$$

Substituting Eqn. (78) into Eqn. (79), the desired anisotropic behaviour is observed

$$\mathfrak{F}(\boldsymbol{Q} \star u, \boldsymbol{Q} \star \boldsymbol{v}, \boldsymbol{Q} \star \boldsymbol{U}, \boldsymbol{Q} \star \boldsymbol{V}, \boldsymbol{M}) = \mathfrak{F}(u, \boldsymbol{v}, \boldsymbol{U}, \boldsymbol{V}, \boldsymbol{M}) \quad \forall \quad \boldsymbol{Q} \in \mathscr{C} \subseteq \mathcal{O}(3) \ . \tag{80}$$

The key observation from the equation above is that the material symmetry group of the structural tensor solely characterises the type of anisotropy. This extension method with

---

[4]in the sense that $\boldsymbol{V} = -\boldsymbol{V}^T$.

frozen structural tensors[5] is referred to as the *isotropicization* theorem [45, 46]. The construction of structural tensors for the mechanics symmetry groups has been thoroughly treated in [47, 79]. Furthermore, the reviewarticle of Zheng [64] accounts for a detailed discussion of the representation theorems for anisotropic scalar- and tensor-valued functions. The representation theorem of general isotropic tensor functions is based on the concept of *integrity bases* which define a minimum number of invariants for a particular set of argument tensors. An integrity basis consists of the traces of the argument tensors (their products and the powers of their products). They can be divided in two main groups namely the *principal invariants* which contain the invariants of the arguments tensor alone or the structural tensor alone, and the *mixed invariants* which contain invariants comprising both the arguments and the structural tensor.

To this end, let $\mathfrak{F}(\boldsymbol{A}) \in \mathbb{R}$ be a scalar-valued function of a set $\boldsymbol{A} \in \mathbb{R}^6$ of a symmetric second-order tensor. Then, the isotropy condition (79) reads

$$\mathfrak{F}(\boldsymbol{Q} \star \boldsymbol{A}) = \mathfrak{F}(\boldsymbol{A}) \quad \forall \quad \boldsymbol{Q} \in \mathcal{O}(3) \ . \tag{81}$$

The principal invariants of $\boldsymbol{A}$ are defined as the coefficients of the characteristic polynomial, also known as the Cayley-Hamilton polynomial. For a symmetric second-order tensor $\boldsymbol{A}$, the polynomial is the equation corresponding to the eigenvalue problem, i.e.

$$\det \left[ \lambda_{\mathbb{Z}} \boldsymbol{1} - \boldsymbol{A} \right] = 0 \ , \tag{82}$$

where $\lambda_{\mathbb{Z}}$ are the eigenvalues. Equation (82) gives the well-known characteristic equation

$$\lambda_{\mathbb{Z}}^3 - I_1 \lambda_{\mathbb{Z}}^2 + I_2 \lambda_{\mathbb{Z}} - I_3 = 0 \ , \tag{83}$$

in terms of the principal invariants

$$I_1 = \mathrm{tr}[\boldsymbol{A}], \ \ I_2 = \tfrac{1}{2}\left[ \mathrm{tr}^{\,2}[\boldsymbol{A}] - \mathrm{tr}[\boldsymbol{A}^2] \right] \ \ \text{and} \ \ I_3 = \tfrac{1}{6}\left[ \mathrm{tr}^{\,3}[\boldsymbol{A}] + 2\,\mathrm{tr}[\boldsymbol{A}^3] - 3\,\mathrm{tr}[\boldsymbol{A}^2]\,\mathrm{tr}[\boldsymbol{A}] \right] \ , \tag{84}$$

which can be equivalently expressed in terms of the *basic invariants*

$$G_1 = I_1 = \mathrm{tr}[\boldsymbol{A}], \ \ G_2 = I_1^2 - 2I_2 = \mathrm{tr}[\boldsymbol{A}^2] \ \ \text{and} \ \ G_3 = I_1^3 - 3I_1 I_2 + 3I_3 = \mathrm{tr}[\boldsymbol{A}^3] \ , \tag{85}$$

as functions of the traces of the powers of $\boldsymbol{A}$. For a given symmetry group $\mathscr{C}$, it is possible to express the scalar-valued function $\mathfrak{F}$ as

$$\mathfrak{F} = \mathfrak{F}(\boldsymbol{A}) = \mathfrak{F}(I_1(\boldsymbol{A}), \ldots, I_n(\boldsymbol{A})) \ , \tag{86}$$

in terms of quantities $I_1(\boldsymbol{A}), \ldots, I_n(\boldsymbol{A})$, which are invariant under the action of $\mathscr{C}$. The set of invariants $I_1(\boldsymbol{A}), \ldots, I_n(\boldsymbol{A})$ is called the *functional basis*. If the potential $\mathfrak{F}(I_1(\boldsymbol{A}), \ldots, I_n(\boldsymbol{A}))$ is chosen to be a polynomial in terms of $\boldsymbol{A}$, then it is noted that the functional basis $I_1(\boldsymbol{A}), \ldots, I_n(\boldsymbol{A})$ turns out to be a set of polynomial scalar functions, and is therefore called the *polynomial basis* or the *integrity basis*. Besides, an integrity basis is said to be irreducible or minimal if none of its elements can be expressed in terms of the remaining ones [80, 81].

**Remark 2.** The orthogonal group $\mathcal{O}(3)$ has an infinite number of subgroups associated with non-crystalline solids, some of which are discussed in Section 2.2. With application to fibre-reinforced composites, focus is restricted only to the orthorhombic $\mathscr{C}_3$ and transversely isotropic $\mathscr{C}_{13}$ symmetry groups in the ensuing developments. Corresponding expressions for the groups $\mathscr{C}_{1-14}$ from Table 2 are recorded in Appendix A for the sake of completeness.

---

[5] in the sense Eqn. (78).

## 2.4. Phenomenological elasticity

This section addresses general developments in modelling the linear elastic response of materials based on concepts discussed in the previous section. Generally, *elasticity* is the ability of a material to *store* the work done by an applied external force during the loading process, and *gain* the stored work without loss while unloading. Additionally, an elastic material response is non-dissipative ($\mathscr{D} = 0$), i.e. the stress power is identical to the evolution of the energetic potential thereby ruling out hysteretic effects.

### 2.4.1. Underlying assumptions

- Restriction to the theory of grade one, where the constitutive functions are assumed to depend on primary variables and their first gradient only.

- Quasi static loading is considered, where the forces related to inertial effects are neglected.

- Isothermal conditions are considered such that $\Theta = \text{constant}$, $\dot{\Theta} = 0$ and $\nabla\Theta = \boldsymbol{0}$, within the body $\mathscr{B}$ under consideration.

### 2.4.2. General developments

With reference to the theory of elasticity, it can be immediately deduced that the set of internal variables in Eqn. (43) is essentially empty, i.e. $\mathfrak{c} = \emptyset$, as the elastic material response is fully reversible and depends only on the current deformation state.

### 2.4.3. Formulation of governing equations

With the assumption of isothermal and quasi static conditions, the governing balance equations of elasticity are the balance of mass, linear momentum and angular momentum in their local form, namely that

$$
\begin{aligned}
\dot{\rho} &= 0 \\
\boldsymbol{0} &= \text{div}[\boldsymbol{\sigma}] + \boldsymbol{\Upsilon} \quad , \\
\boldsymbol{\sigma} &= \boldsymbol{\sigma}^T
\end{aligned}
\tag{87}
$$

where $\boldsymbol{0}$ denotes the second-order zero tensor. From Eqns. (51) and (55), it can be inferred that the only constitutive relation needed for the closure of Eqn. (87) is the scalar-valued energetic potential $\psi$. The general developments stated above leads to the reduced definition of the scalar-valued energetic potential (55) as

$$
\psi = \psi(\boldsymbol{\varepsilon}) \; .
\tag{88}
$$

It follows from Eqn. (51) that the stress tensor is obtained from the scalar-valued energetic potential in Eqn. (88) as

$$
\boldsymbol{\sigma} = \psi(\boldsymbol{\varepsilon})_{,\boldsymbol{\varepsilon}} \; .
\tag{89}
$$

A further derivative of Eqn. (88) with respect to the strain tensor $\boldsymbol{\varepsilon}$ yields the fourth-order elasticity tensor (equivalent to the Hessian) as

$$
\mathbb{E} = \psi(\boldsymbol{\varepsilon})_{,\boldsymbol{\varepsilon}\boldsymbol{\varepsilon}} \; .
\tag{90}
$$

From a numerical implementation perspective, the second-order stress tensor $\boldsymbol{\sigma}$ and the fourth-order elasticity tensor $\mathbb{E}$ are the only quantities to be specified in the material subroutine, owing to the fact that the stress power is equal to the rate of the scalar energetic potential.

## 2.5. Phenomenological plasticity and viscoplasticity

In this section, a modelling framework for phenomenological plasticity and viscoplasticity at small strains is provided along with a finite element oriented algorithmic treatment.

### 2.5.1. Underlying assumptions

- Restriction to the theory of grade one, where the constitutive functions are assumed to depend on primary variables and their first gradient only.

- Quasi static loading is considered, where the forces related to inertial effects are neglected.

- Isothermal conditions are considered such that $\Theta = \text{constant}$, $\dot{\Theta} = 0$ and $\nabla\Theta = \boldsymbol{0}$, within the body $\mathscr{B}$ under consideration.

- A purely local dependence of the constitutive equations on the internal variables is assumed.

### 2.5.2. General developments

The infinitesimal plasticity theory allows for an additive decomposition of the total strain $\boldsymbol{\varepsilon}$ into a reversible *elastic part* $\boldsymbol{\varepsilon}^e$ and an irreversible *plastic part* $\boldsymbol{\varepsilon}^p$, such that

$$\boldsymbol{\varepsilon} := \boldsymbol{\varepsilon}^e + \boldsymbol{\varepsilon}^p \Longrightarrow \boldsymbol{\varepsilon}^e := \boldsymbol{\varepsilon} - \boldsymbol{\varepsilon}^p \ , \tag{91}$$

where $\boldsymbol{\varepsilon}^p$ is the symmetric second-order plastic strain tensor. Recall here that in the infinitesimal theory, plastic strain can be experimentally deduced by unloading the specimen to a stress-free state. Further, as $\boldsymbol{\varepsilon}$ is already an argument of constitutive relations, it is sufficient to introduce $\boldsymbol{\varepsilon}^p$ as an internal variable.

Plasticity is an extremely non-linear process which on initial loading leads to a purely elastic behaviour until a threshold value, termed as the yield stress, is reached. From this point on, any further loading leads to an irreversible plastic deformation. To incorporate these two features into modelling, an elastic domain $\mathscr{S}$ is introduced in the stress space. For all the stress states $\boldsymbol{\sigma} \in \mathscr{S}$, an elastic behaviour is observed. Plastic behaviour can only be observed on the boundary $\partial\mathscr{S}$, of the domain $\mathscr{S}$, i.e. $\boldsymbol{\sigma} \in \partial\mathscr{S}$. Experimentally, it is observed that most materials are not perfectly plastic (no increase in stress during the plastic deformation), but they exhibit some kind of hardening. In the present work, two kinds of hardening phenomena are distinguished.

*Isotropic hardening* is characterised by an increase of the yield stress in tension connected to an increase of the yield stress in compression. To describe the isotropic hardening phenomenon, an internal variable $\xi$ is introduced which is a scalar measure of the cumulative amount of the plastic strain and is therefore known as the equivalent plastic strain.

*Kinematic hardening* is characterised by an increase of the yield stress in tension connected to the decrease of the yield stress in compression. Analogous to the previous case, to describe the kinematic hardening phenomenon, an internal variable $\boldsymbol{\alpha}$ is introduced. In contrast to the isotropic hardening variable, this symmetric tensor shifts the centre of the elastic domain from the origin. For the sake of completeness, mixed isotropic and kinematic hardening is considered in the present work.

### 2.5.3. Formulation of governing equations

**2.5.3.1. Energetic potential.** It follows from the discussion in the previous subsection that a suitable set of internal variables are given by

$$\mathbf{c} = \{\boldsymbol{\varepsilon}^p, \xi, \boldsymbol{\alpha}\} \in \mathbb{R}^6 \times \mathbb{R} \times \mathbb{R}^6 \ . \tag{92}$$

To ensure the non-negativity of the work done by any external load in a closed strain cycle, the existence of a scalar energetic potential is necessary. The scalar energetic potential which has an explicit functional dependence on Eqn. (92), can generally be specified as

$$\psi = \psi(\boldsymbol{\varepsilon}, \mathbf{c}) = \psi(\boldsymbol{\varepsilon}, \boldsymbol{\varepsilon}^p, \xi, \boldsymbol{\alpha}) = \psi(\boldsymbol{\varepsilon} - \boldsymbol{\varepsilon}^p, \boldsymbol{\varepsilon}^p, \xi, \boldsymbol{\alpha}) = \psi(\boldsymbol{\varepsilon} - \boldsymbol{\varepsilon}^p, \xi, \boldsymbol{\alpha}) \ . \tag{93}$$

A simplifying assumption made at the outset is that the energetic potential can be additively decomposed into elastic and plastic parts as

$$\psi(\boldsymbol{\varepsilon} - \boldsymbol{\varepsilon}^p, \xi, \boldsymbol{\alpha}) = \psi^e(\boldsymbol{\varepsilon} - \boldsymbol{\varepsilon}^p) + \psi^p(\xi, \boldsymbol{\alpha}) = \psi^e(\boldsymbol{\varepsilon} - \boldsymbol{\varepsilon}^p) + \psi^p_{\text{iso}}(\xi) + \psi^p_{\text{kin}}(\boldsymbol{\alpha}) \ . \tag{94}$$

It should be remarked here that the stored elastic energy $\psi^e$ depends only the reversible part of the strain $(\boldsymbol{\varepsilon} - \boldsymbol{\varepsilon}^p)$. While a quadratic form is suitable to describe the stored elastic energy $\psi^e$, the plastic (hardening) parts $\psi^p_{\text{iso}}(\xi)$ and $\psi^p_{\text{kin}}(\boldsymbol{\alpha})$ should be formulated such that they reflect experimental observations. Commonly used functional forms include the linear, exponential and power hardening law.

**2.5.3.2. Thermodynamic restriction.** Taking into account the representation (94), the dissipation postulate (53) can be evaluated for isothermal conditions as

$$\mathscr{D}^{\text{red}} = -\psi,_{\mathbf{c}} \cdot \dot{\mathbf{c}} = -\psi,_{\boldsymbol{\varepsilon}^p} : \dot{\boldsymbol{\varepsilon}}^p - \psi,_\xi \dot{\xi} - \psi,_{\boldsymbol{\alpha}} : \dot{\boldsymbol{\alpha}} \geq 0 \ , \tag{95}$$

which leads to the definition of the stress tensor and driving forces associated with the potential (94) as

$$\begin{aligned}
\boldsymbol{\sigma} &= +\psi^e(\boldsymbol{\varepsilon} - \boldsymbol{\varepsilon}^p),_{(\boldsymbol{\varepsilon} - \boldsymbol{\varepsilon}^p)} = -\psi^e(\boldsymbol{\varepsilon} - \boldsymbol{\varepsilon}^p),_{\boldsymbol{\varepsilon}^p} = \boldsymbol{\sigma}^p \ , \\
\kappa &= -\psi^p_{\text{iso}}(\xi),_\xi \ , \\
\boldsymbol{\beta} &= -\psi^p_{\text{kin}}(\boldsymbol{\alpha}),_{\boldsymbol{\alpha}} \ .
\end{aligned} \tag{96}$$

Equation $(96)_1$ is a consequence of the definition of elastic strain measure within the framework of geometrically linear theory. For brevity, let $\mathfrak{f} = -\psi,_{\mathbf{c}} = \{\boldsymbol{\sigma}, \kappa, \boldsymbol{\beta}\} \in \mathbb{R}^6 \times \mathbb{R} \times \mathbb{R}^6$, denote the set of conjugate thermodynamic driving forces which are dual to the introduced set of internal variables in Eqn. (92). Then, Eqn. (95) can be expressed in a compact form taking into account Eqn. (96) as

$$\mathscr{D}^{\text{red}} = \mathfrak{f} \cdot \dot{\mathbf{c}} = \boldsymbol{\sigma} : \dot{\boldsymbol{\varepsilon}}^p + \kappa \dot{\xi} + \boldsymbol{\beta} : \dot{\boldsymbol{\alpha}} \geq 0 \ , \tag{97}$$

where the reduced dissipation is expressed as an inner product of the conjugate thermodynamic driving forces and internal variables in the space $\mathbb{R}^6 \times \mathbb{R} \times \mathbb{R}^6$.

**2.5.3.3. Evolution of the internal variables.** Besides the free energy function $\psi$, the evolution of internal variables $\mathbf{c} = \{\boldsymbol{\varepsilon}^p, \xi, \boldsymbol{\alpha}\}$ should also be constitutively prescribed in line with the restriction (95). This is accomplished using two ingredients, namely (i) a yield function that specifies the elastic domain $\mathscr{S}$, and its boundary $\partial\mathscr{S}$, to decide when the plastic flow takes place, and (ii) a description of how the plastic flow takes place, i.e. how exactly the internal variables $\mathbf{c} = \{\boldsymbol{\varepsilon}^p, \xi, \boldsymbol{\alpha}\}$ evolve during the plastic deformation. This is achieved by the flow rule.

**2.5.3.3.1. Yield function.** To mathematically specify the elastic domain $\mathscr{S}$, the following form is utilised

$$\mathscr{S} = \{(\boldsymbol{\sigma}, \kappa, \boldsymbol{\beta}) \in \mathbb{R}^6 \times \mathbb{R} \times \mathbb{R}^6 | \chi(\boldsymbol{\sigma}, \kappa, \boldsymbol{\beta}) \leq 0\} \ . \tag{98}$$

The boundary $\partial\mathscr{S}$ of the elastic domain is called the yield surface and it takes the form

$$\partial\mathscr{S} = \{(\boldsymbol{\sigma}, \kappa, \boldsymbol{\beta}) \in \mathbb{R}^6 \times \mathbb{R} \times \mathbb{R}^6 | \chi(\boldsymbol{\sigma}, \kappa, \boldsymbol{\beta}) = 0\} \ , \tag{99}$$

where $\chi = \chi(\mathfrak{f}) = \chi(\boldsymbol{\sigma}, \kappa, \boldsymbol{\beta})$ is the yield function in the space of admissible thermodynamic forces. The functional form of $\chi$ defines the size and shape of the elastic domain $\mathscr{S}$ and thus the yield surface. Additionally, for the inequality (95) to hold true, the yield function should satisfy the following constraints:

- convexity

$$\chi(\Im\mathfrak{f}_1 + (1 - \Im)\mathfrak{f}_2) \leq \Im\chi(\mathfrak{f}_1) + (1 - \Im)\chi(\mathfrak{f}_2) \quad \forall \quad \{\mathfrak{f}_1, \mathfrak{f}_2\} \in \mathscr{S}, \ \Im \in [0, 1] \ , \tag{100}$$

- degree-one homogeneity

$$\chi(\Im\mathfrak{f}) = \Im\chi(\mathfrak{f}) \quad \text{for} \quad \Im > 0 \ . \tag{101}$$

Convexity of the yield function is a necessary requirement for minimisation problems in order to have a unique solution [82]. It ensures the dissipation to remain positive for all admissible thermodynamic processes, which is the central idea of the second axiom of thermodynamics. Mathematically, the convexity of the yield surface $\chi$ is demonstrated if it can be shown that the Hessian matrix $\mathbb{F}$ of this function is positive semi-definite, i.e. its eigenvalues are all positive or zero, see [33].

**2.5.3.3.2. Principle of maximum dissipation.** From Eqn. (95), it can be seen that the evolution of internal variables $\mathfrak{e} = \{\boldsymbol{\varepsilon}^p, \xi, \boldsymbol{\alpha}\}$ depends on the conjugate thermodynamic driving forces $\mathfrak{f} = \{\boldsymbol{\sigma}, \kappa, \boldsymbol{\beta}\}$. To completely define the evolution of the internal variables, the *principle of maximum dissipation* is used. This principle, often credited to von Mises [25, pp. 60] and subsequently considered by several authors [69, 83], is central in the mathematical formulation of plasticity theory and plays a crucial role in the variational formulation of such dissipative processes [73, 84].

The principle of maximum dissipation states that, for a given flux $\mathfrak{e}$ among all admissible thermodynamic forces $\mathfrak{f}^* \in \mathscr{S}$ satisfying the yield criterion, plastic dissipation is given by

$$\mathscr{D}^{\mathrm{red}^*}(\mathfrak{f}^*, \mathfrak{e}) = \mathfrak{f}^* \cdot \dot{\mathfrak{e}} = \boldsymbol{\sigma}^* : \dot{\boldsymbol{\varepsilon}}^p + \kappa^* \dot{\xi} + \boldsymbol{\beta}^* : \dot{\boldsymbol{\alpha}} \ . \tag{102}$$

Then, the actual thermodynamic forces $\mathfrak{f} \in \mathscr{S}$ are the arguments of the principle

$$\mathscr{D}^{\mathrm{red}}(\mathfrak{f}, \mathfrak{e}) = \sup_{\mathfrak{f}^* \in \mathscr{S}} \left[ \mathscr{D}^{\mathrm{red}^*}(\mathfrak{f}^*, \mathfrak{e}) \right] \ . \tag{103}$$

This principle is used here in a more general context by application to all the thermodynamic forces [48].

**Proposition 2.5.1.** *The principle of maximum dissipation implies the following*

*(i) associative flow rule in the stress space, often called the normality rules,*

*(ii) Karush-Kuhn-Tucker-type loading/unloading conditions, and*

*(iii) convexity of the elastic domain $\mathscr{S}$.*

*Proof.* The propositions (i) and (ii) can be proved by using the method of Lagrange multipliers. At first, the maximisation principle (102) is transformed into a minimisation principle merely by changing the sign. Next, the constrained minimisation problem is transformed into an unconstrained saddle point problem with the introduction of Lagrange multiplier $\lambda$ and considering the Lagrange functional $\mathscr{L} : \mathbb{R}^{6+1+6} \times \mathbb{R} \times \mathbb{R}^{6+1+6}$ as

$$\mathscr{L}(\mathfrak{f}^*, \lambda, \dot{\mathfrak{e}}) = -\mathfrak{f}^* \cdot \dot{\mathfrak{e}} + \lambda \chi(\mathfrak{f}^*) = -\boldsymbol{\sigma}^* : \dot{\boldsymbol{\varepsilon}}^p - \kappa^* \dot{\xi} - \boldsymbol{\beta}^* : \dot{\boldsymbol{\alpha}} + \lambda \chi(\mathfrak{f}^*) \ . \tag{104}$$

The solution to the problem (103) is then given by the point $(\mathfrak{f}, \lambda)$, satisfying the classical Karush-Kuhn-Tucker conditions,

$$\boxed{\begin{array}{c} \mathscr{L}_{,\mathfrak{f}} \equiv \pm\dot{\mathfrak{e}} + \lambda \chi_{,\mathfrak{f}} = \boldsymbol{0} \\[4pt] \lambda \geq 0, \quad \chi \leq 0 \quad \text{and} \quad \lambda\chi \equiv 0 \end{array}} \ , \tag{105}$$

see Simo and Hughes [66, Chapter 2, Section 2.6, Subsection 2.6.2, pp. 99]. These equations represent precisely the statement of normality rules and the loading/unloading conditions, respectively. To prove that the convexity condition on the elastic domain also follows from the principle of maximum dissipation, it suffices to show that the yield function $\chi(\mathfrak{f})$ is convex, in the sense of Eqn. (100). $\qquad\square$

Based on Eqn. $(105)_1$, evolution equations for the internal variables are given by

$$\boxed{\begin{array}{rcl} \dot{\boldsymbol{\varepsilon}}^p & = & \dot{\boldsymbol{\varepsilon}}^p(\lambda, \boldsymbol{\sigma}, \kappa, \boldsymbol{\beta}) = \lambda \chi_{,\boldsymbol{\sigma}} \\[4pt] \dot{\xi} & = & \dot{\xi}(\lambda, \boldsymbol{\sigma}, \kappa, \boldsymbol{\beta}) \ = \lambda \chi_{,\kappa} \\[4pt] \dot{\boldsymbol{\alpha}} & = & \dot{\boldsymbol{\alpha}}(\lambda, \boldsymbol{\sigma}, \kappa, \boldsymbol{\beta}) \ = \lambda \chi_{,\boldsymbol{\beta}} \end{array}} \ . \tag{106}$$

The Lagrange multiplier $\lambda \geq 0$ can be characterised as the "plastic multiplier" that acts as a switch for the plastic behaviour, i.e. $\lambda = 0 \Rightarrow$ elastic and $\lambda > 0 \Rightarrow$ plastic. It is determined from the consistency condition $\chi(\boldsymbol{\sigma}, \kappa, \boldsymbol{\beta}) = 0$ and $\dot{\chi}(\boldsymbol{\sigma}, \kappa, \boldsymbol{\beta}) = 0$ during the plastic flow. With $\chi = \chi(\boldsymbol{\sigma}, \kappa, \boldsymbol{\beta})$, the rate of the yield function can be evaluated as

$$\dot{\chi} = \chi_{,\boldsymbol{\sigma}} : \dot{\boldsymbol{\sigma}} + \chi_{,\kappa} \dot{\kappa} + \chi_{,\boldsymbol{\beta}} : \dot{\boldsymbol{\beta}} \ , \tag{107}$$

along with the definitions

$$\begin{aligned} \dot{\boldsymbol{\sigma}} & = \frac{d}{dt}[-\psi^e(\boldsymbol{\varepsilon} - \boldsymbol{\varepsilon}^p)_{,(\boldsymbol{\varepsilon}-\boldsymbol{\varepsilon}^p)}] = \psi^e(\boldsymbol{\varepsilon} - \boldsymbol{\varepsilon}^p)_{,(\boldsymbol{\varepsilon}-\boldsymbol{\varepsilon}^p)(\boldsymbol{\varepsilon}-\boldsymbol{\varepsilon}^p)} : (\dot{\boldsymbol{\varepsilon}} - \dot{\boldsymbol{\varepsilon}}^p) \\[4pt] \dot{\kappa} & = \frac{d}{dt}[-\psi^p_{\text{iso}}(\xi)_{,\xi}] = -\psi^p_{\text{iso}}(\xi)_{,\xi\xi} \dot{\xi} \\[4pt] \dot{\boldsymbol{\beta}} & = \frac{d}{dt}[-\psi^p_{\text{kin}}(\boldsymbol{\alpha})_{,\boldsymbol{\alpha}}] = -\psi^p_{\text{kin}}(\boldsymbol{\alpha})_{,\boldsymbol{\alpha}\boldsymbol{\alpha}} : \dot{\boldsymbol{\alpha}} \end{aligned} \tag{108}$$

Setting

$$\mathbb{E} = \psi^e(\boldsymbol{\varepsilon} - \boldsymbol{\varepsilon}^p)_{,(\boldsymbol{\varepsilon}-\boldsymbol{\varepsilon}^p)(\boldsymbol{\varepsilon}-\boldsymbol{\varepsilon}^p)} \ , \quad \mathrm{H} = \psi^p_{\text{iso}}(\xi)_{,\xi\xi} \quad \text{and} \quad \mathbb{H} = \psi^p_{\text{kin}}(\boldsymbol{\alpha})_{,\boldsymbol{\alpha}\boldsymbol{\alpha}} \ , \tag{109}$$

and taking into account Eqn. (106), Eqn. (108) reformulates to

$$\begin{aligned}
\dot{\boldsymbol{\sigma}} &= \mathbb{E} : [\dot{\boldsymbol{\varepsilon}} - \lambda \chi_{,\boldsymbol{\sigma}}] \\
\dot{\kappa} &= -\lambda \mathrm{H} \chi_{,\kappa} \\
\dot{\boldsymbol{\beta}} &= -\lambda \mathbb{H} : \chi_{,\boldsymbol{\beta}}
\end{aligned} \qquad . \tag{110}$$

With Eqn. (110) at hand, the yield rate (107) takes the form

$$\dot{\chi} = \chi_{,\boldsymbol{\sigma}} : \mathbb{E} : [\dot{\boldsymbol{\varepsilon}} - \lambda \chi_{,\boldsymbol{\sigma}}] + \chi_{,\kappa} [-\lambda \mathrm{H} \chi_{,\kappa}] + \chi_{,\boldsymbol{\beta}} : [-\lambda \mathbb{H} : \chi_{,\boldsymbol{\beta}}] , \tag{111}$$

where it can be seen that during elastic behaviour ($\lambda = 0$), the yield rate simplifies to

$$\dot{\chi}(\lambda = 0, \dot{\boldsymbol{\varepsilon}}, \boldsymbol{\sigma}, \kappa, \boldsymbol{\beta}) = \chi_{,\boldsymbol{\sigma}} : \mathbb{E} : \dot{\boldsymbol{\varepsilon}} , \tag{112}$$

which can be thought of as an elastic trial value for $\dot{\chi}$. With $\chi(\boldsymbol{\sigma}, \kappa, \boldsymbol{\beta})$ and $\dot{\chi}(\lambda, \dot{\boldsymbol{\varepsilon}}, \boldsymbol{\sigma}, \kappa, \boldsymbol{\beta})$ at hand, the value of the plastic multiplier $\lambda$ can be computed with the so-called "loading cases", which are identified, illustrated in Fig. 14, as follows:

$$\left.\begin{aligned}
\chi < 0 & & \Longleftrightarrow \text{ elastic loading} \\
\chi = 0 \quad \text{and} \quad \dot{\chi} < 0 & & \Longleftrightarrow \text{ elastic unloading} \\
\chi = 0 \quad \text{and} \quad \dot{\chi} = 0 & & \Longleftrightarrow \text{ neutral loading} \\
\chi = 0 \quad \text{and} \quad \dot{\chi} > 0 & & \Longleftrightarrow \text{ plastic loading}^6
\end{aligned}\right\} \quad . \tag{113}$$

If $\chi < 0$, it is known that $\boldsymbol{\sigma} \in \mathscr{S}(\kappa, \boldsymbol{\beta}) \setminus \partial\mathscr{S}$ and thus an elastic loading is identified with Eqn. (113)$_1$. If $\dot{\chi} > 0$, the stress state is outside of the elastic domain $\boldsymbol{\sigma} \notin \mathscr{S}(\kappa, \boldsymbol{\beta})$, which is not permitted. Therefore, a plastic flow is needed, as seen from Eqn. (113)$_4$. Furthermore, if the case is plastic, the amount ($\lambda > 0$) of the plastic flow is obtained from the consistency condition which follows from Eqn. (111) as

$$\chi_{,\boldsymbol{\sigma}} : \mathbb{E} : \dot{\boldsymbol{\varepsilon}} = \lambda \chi_{,\boldsymbol{\sigma}} : \mathbb{E} : \chi_{,\boldsymbol{\sigma}} + \lambda \chi_{,\kappa} \, \mathrm{H} \chi_{,\kappa} + \lambda \chi_{,\boldsymbol{\beta}} : \mathbb{H} : \chi_{,\boldsymbol{\beta}} , \tag{114}$$



| Elastic loading | Elastic unloading | Neutral loading | Plastic loading |
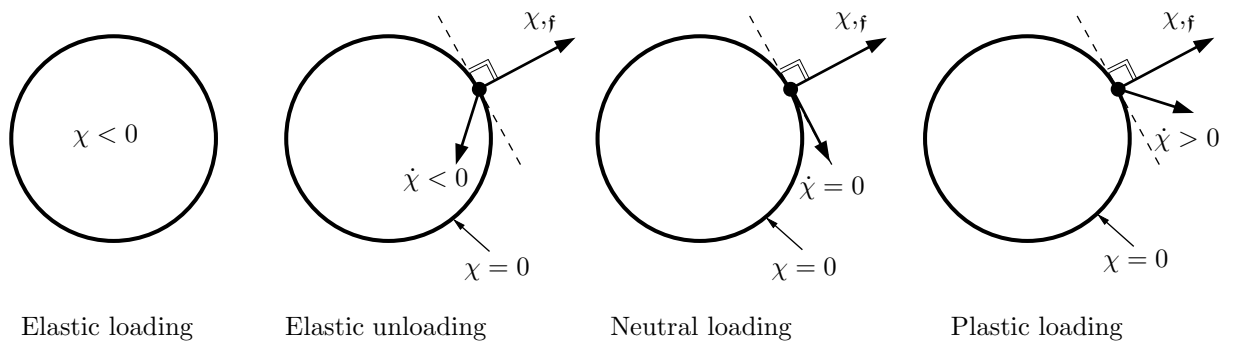
FIGURE 14: **Loading cases in the space of admissible thermodynamic forces.** If $\chi < 0$, an elastic loading is identified where $\boldsymbol{\sigma} \in \mathscr{S}(\kappa, \boldsymbol{\beta}) \setminus \partial\mathscr{S}$, whereas if $\chi = 0$, it is understood that $\boldsymbol{\sigma} \in \partial\mathscr{S}(\kappa, \boldsymbol{\beta})$ and a plastic flow is possible. To evaluate this possibility, the rate of the yield function $\dot{\chi}$ needs to be considered. It follows that if $\dot{\chi} < 0$, an elastic unloading step is observed. For $\chi < 0$ and $\dot{\chi} = 0$, a neutral loading step is identified. Finally, for $\chi = 0$ and $\dot{\chi} > 0$, a plastic flow is observed where further loading leads to values outside the elastic domain as a result of which plastic flow sets in. The final loading step is however observed only in a rate-dependent setting.

---

[6]only possible in a rate-dependent setting.

resulting in the standard form

$$\lambda = \boxed{\frac{\chi_{,\boldsymbol{\sigma}} : \mathbb{E} : \dot{\boldsymbol{\varepsilon}}}{\chi_{,\boldsymbol{\sigma}} : \mathbb{E} : \chi_{,\boldsymbol{\sigma}} + \chi_{,\kappa} \, \mathrm{H} \chi_{,\kappa} + \chi_{,\boldsymbol{\beta}} : \mathbb{H} : \chi_{,\boldsymbol{\beta}}}} \ . \tag{115}$$

The plastic multiplier $\lambda$ ensures the fulfilment of the consistency condition during the plastic flow. Evolution laws of type (106) are termed as *associated flow* rules and are characterised by the fact that the rates of the internal variables are normal to the yield surface $(\chi = 0)$.

For some materials where the canonical normal directions of the evolution equations (106) do not characterise the real material response, e.g. polymers, soils, concrete among others, the constitutive response is modified by introducing an additional constitutive function $\phi$, henceforth known as the plastic flow potential. It is assumed to depend on the same variables as the yield function such that

$$\phi = \phi(\boldsymbol{\sigma}, \kappa, \boldsymbol{\beta}) \ , \tag{116}$$

based on which the evolution equations for the internal variables take the form

$$\boxed{\begin{aligned} \dot{\boldsymbol{\varepsilon}}^p &= \dot{\boldsymbol{\varepsilon}}^p(\lambda, \boldsymbol{\sigma}, \kappa, \boldsymbol{\beta}) = \lambda \phi_{,\boldsymbol{\sigma}} \\ \dot{\xi} &= \dot{\xi}(\lambda, \boldsymbol{\sigma}, \kappa, \boldsymbol{\beta}) = \lambda \phi_{,\kappa} \\ \dot{\boldsymbol{\alpha}} &= \dot{\boldsymbol{\alpha}}(\lambda, \boldsymbol{\sigma}, \kappa, \boldsymbol{\beta}) = \lambda \phi_{,\boldsymbol{\beta}} \end{aligned}} \ . \tag{117}$$

Evolution laws of type (117) are termed as *non-associative flow* rules, which replace the normality rules in Eqn. (106) though the plastic loading conditions remain unchanged. The plastic multiplier $\lambda$ is determined from the consistency condition similar to the case of associative flow rule. In particular, with Eqn. (117) at hand, Eqns. (107)–(111) can be evaluated for the non-associative flow response, and the resulting form of consistency condition reads

$$\chi_{,\boldsymbol{\sigma}} : \mathbb{E} : \dot{\boldsymbol{\varepsilon}} = \lambda \phi_{,\boldsymbol{\sigma}} : \mathbb{E} : \phi_{,\boldsymbol{\sigma}} + \lambda \phi_{,\kappa} \, \mathrm{H} \phi_{,\kappa} + \lambda \phi_{,\boldsymbol{\beta}} : \mathbb{H} : \phi_{,\boldsymbol{\beta}} \ , \tag{118}$$

yielding the plastic multiplier in the standard form

$$\lambda = \boxed{\frac{\chi_{,\boldsymbol{\sigma}} : \mathbb{E} : \dot{\boldsymbol{\varepsilon}}}{\chi_{,\boldsymbol{\sigma}} : \mathbb{E} : \phi_{,\boldsymbol{\sigma}} + \chi_{,\kappa} \, \mathrm{H} \phi_{,\kappa} + \chi_{,\boldsymbol{\beta}} : \mathbb{H} : \phi_{,\boldsymbol{\beta}}}} \ . \tag{119}$$

A geometrical interpretation of the associative and non-associative flow response is shown in Fig. 15, and a summary of the modelling framework for associative and non-associative flow response is outlined in Box 2.

**Remark 3.** Owing to experimental investigations, it is sometimes necessary to relax the *principle of maximum dissipation* for certain materials (e.g. polymeric composites) with the assumption of a plastic flow potential that is different from the yield function, thereby framing the model within non-associative plasticity [85]. However, relaxing the principle of maximum dissipation should not violate the second law of thermodynamics and therefore the choice of the plastic flow potential is generally similar to the functional form of the yield function, but with a different choice of governing parameters.

**2.5.3.4. Continuum elastic-plastic tangent modulus.** The goal of this subsection is to compute the fourth-order elastic-plastic tangent modulus also known as the generalised Prandtl-Reuss tensors. They connect the rate of stress tensor with the rate of total strain. Starting with the case of an *associative flow* response, consider the rate equation for the stress tensor which is given by

$$\dot{\boldsymbol{\sigma}} = \mathbb{E} : [\dot{\boldsymbol{\varepsilon}} - \dot{\boldsymbol{\varepsilon}}^p] = \mathbb{E} : [\dot{\boldsymbol{\varepsilon}} - \lambda \chi_{,\boldsymbol{\sigma}}] . \tag{120}$$

Substituting $\lambda$ from Eqn. (115), it follows that the rate equation can be reformulated as

$$\dot{\boldsymbol{\sigma}} = \mathbb{E}^{\text{ep}} : \dot{\boldsymbol{\varepsilon}} \quad \text{with} \quad \mathbb{E}^{\text{ep}} = \left[ \mathbb{E} - \frac{\mathbb{E} : \chi_{,\boldsymbol{\sigma}} \otimes \chi_{,\boldsymbol{\sigma}} : \mathbb{E}}{\chi_{,\boldsymbol{\sigma}} : \mathbb{E} : \chi_{,\boldsymbol{\sigma}} + \chi_{,\kappa} \, \mathrm{H} \chi_{,\kappa} + \chi_{,\boldsymbol{\beta}} : \mathbb{H} : \chi_{,\boldsymbol{\beta}}} \right], \tag{121}$$

where $\mathbb{E}^{\text{ep}}$ is the fourth-order elastic-plastic tangent modulus tensor. Likewise, for the case of *non-associative flow* response, the rate equation is given by

$$\dot{\boldsymbol{\sigma}} = \mathbb{E} : [\dot{\boldsymbol{\varepsilon}} - \dot{\boldsymbol{\varepsilon}}^p] = \mathbb{E} : [\dot{\boldsymbol{\varepsilon}} - \lambda \phi_{,\boldsymbol{\sigma}}] . \tag{122}$$

Substituting $\lambda$ from Eqn. (119) it follows that the rate equation can be expressed as

$$\dot{\boldsymbol{\sigma}} = \mathbb{E}^{\text{ep}} : \dot{\boldsymbol{\varepsilon}} \quad \text{with} \quad \mathbb{E}^{\text{ep}} = \left[ \mathbb{E} - \frac{\mathbb{E} : \chi_{,\boldsymbol{\sigma}} \otimes \phi_{,\boldsymbol{\sigma}} : \mathbb{E}}{\chi_{,\boldsymbol{\sigma}} : \mathbb{E} : \phi_{,\boldsymbol{\sigma}} + \chi_{,\kappa} \, \mathrm{H} \phi_{,\kappa} + \chi_{,\boldsymbol{\beta}} : \mathbb{H} : \phi_{,\boldsymbol{\beta}}} \right] . \tag{123}$$
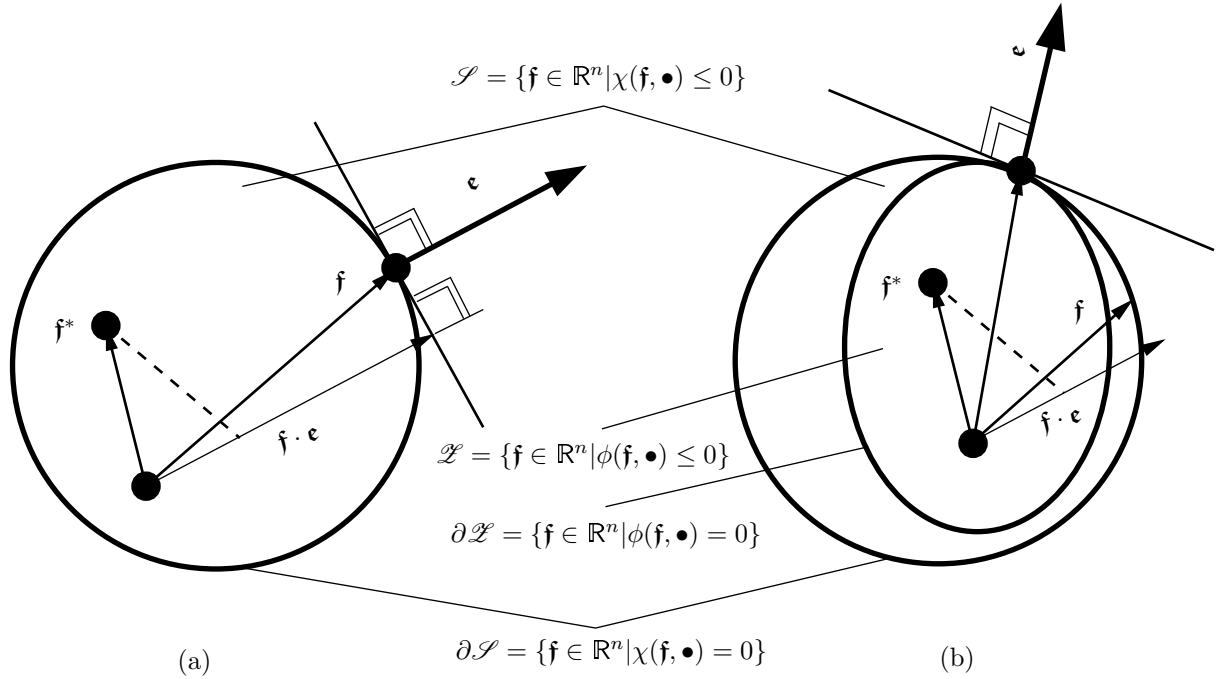


FIGURE 15: **Associative and Non-associative flow response.** Let $\mathscr{S}$ be a convex elastic domain in the space of admissible thermodynamic forces $\mathfrak{f}$, characterised by a flow hyper surface $\chi(\mathfrak{f}; \bullet) = 0$. (a) Associative flow. The principle of maximum dissipation forces the thermodynamic flux vector $\mathfrak{e}$ to be normal to the hyper surface $\chi(\mathfrak{f}; \bullet) = 0$. For smooth and differentiable functions $\chi$, the flux $\mathfrak{e}$ is proportional to the gradient $\chi_{,\mathfrak{f}}$. (b) Non-associative flow. Often, the evolution of thermodynamic fluxes $\mathfrak{e}$ can be expressed in terms of a plastic flow potential $\phi(\mathfrak{f}; \bullet)$ that differs from the flow hyper surface $\chi(\mathfrak{f}; \bullet) = 0$, i.e. $\phi \neq \chi$. In such cases, the principle of maximum dissipation can be often relaxed, while the second law of thermodynamics should still be satisfied with an appropriate choice of $\phi(\mathfrak{f}; \bullet)$. Then, for smooth and differentiable functions $\phi$, the flux $\mathfrak{e}$ is now proportional to the gradient $\phi_{,\mathfrak{f}}$.

Box 2: Rate-independent setting–summary of the modelling framework.

---

1. Kinematics :                       $\boldsymbol{\varepsilon} = \boldsymbol{\varepsilon}^e + \boldsymbol{\varepsilon}^p$

2. Internal variables :               $\mathfrak{e} = \{\boldsymbol{\varepsilon}^p, \xi, \boldsymbol{\alpha}\}$

3. Energetic potential :              $\psi = \psi^e(\boldsymbol{\varepsilon} - \boldsymbol{\varepsilon}^p) + \psi^p_{\mathrm{iso}}(\xi) + \psi^p_{\mathrm{kin}}(\boldsymbol{\alpha})$

4. Stress tensor :                    $\boldsymbol{\sigma} = \psi^e(\boldsymbol{\varepsilon} - \boldsymbol{\varepsilon}^p)_{,\boldsymbol{\varepsilon}}$

5. Driving forces :                   $\kappa = -\psi^p_{\mathrm{iso}}(\xi)_{,\xi}$

                                       $\boldsymbol{\beta} = -\psi^p_{\mathrm{kin}}(\boldsymbol{\alpha})_{,\boldsymbol{\alpha}}$

6. Yield function :                   $\chi = \chi(\boldsymbol{\sigma}, \kappa, \boldsymbol{\beta})$

7. Plastic flow potential :           $\phi = \phi(\boldsymbol{\sigma}, \kappa, \boldsymbol{\beta})$

8. Evolution equations :

   Associative

                                       $\dot{\boldsymbol{\varepsilon}}^p = \lambda \chi(\boldsymbol{\sigma}, \kappa, \boldsymbol{\beta})_{,\boldsymbol{\sigma}}$

                                       $\dot{\xi} = \lambda \chi(\boldsymbol{\sigma}, \kappa, \boldsymbol{\beta})_{,\kappa}$

                                       $\dot{\boldsymbol{\alpha}} = \lambda \chi(\boldsymbol{\sigma}, \kappa, \boldsymbol{\beta})_{,\boldsymbol{\beta}}$

   Non-associative

                                       $\dot{\boldsymbol{\varepsilon}}^p = \lambda \phi(\boldsymbol{\sigma}, \kappa, \boldsymbol{\beta})_{,\boldsymbol{\sigma}}$

                                       $\dot{\xi} = \lambda \phi(\boldsymbol{\sigma}, \kappa, \boldsymbol{\beta})_{,\kappa}$

                                       $\dot{\boldsymbol{\alpha}} = \lambda \phi(\boldsymbol{\sigma}, \kappa, \boldsymbol{\beta})_{,\boldsymbol{\beta}}$

9. Karush-Kuhn-Tucker conditions : $\lambda \geq 0, \quad \chi \leq 0 \quad$ and $\quad \lambda\chi \equiv 0$

---

It can be seen from Eqns. (121) and (123) that the elastic-plastic tangent modulus is a symmetric and non-symmetric fourth-order tensor for the associative and non-associative flow response, respectively.

### 2.5.4.  Extension to viscoplasticity

The general framework of phenomenological plasticity outlined so far, assumes a *rate-independent* setting, such that the material behaviour will not qualitatively change for varying load rates $\dot{\boldsymbol{\varepsilon}}$. In what follows, the classical rate-independent formulation is extended to a classical *rate-dependent* formulation of Perzyna-type [86, 87].

Analogous to the rate-independent setting, the maximisation principle (102) is transformed into an minimisation principle by reversing the sign. Next, the constrained minimisation problem is transformed into an unconstrained problem by appending a *penalisation function*. In other words, the Lagrange functional (104) is replaced by a penalty functional $\mathscr{P} : \mathbb{R}^{6+1+6} \times \mathbb{R}^{6+1+6}$ of the type

$$
\begin{aligned}
\mathscr{P}(\mathfrak{f}^*, \dot{\mathfrak{e}}) &= -\mathfrak{f}^* \cdot \dot{\mathfrak{e}} + \frac{1}{\eta(m+1)}[\chi(\mathfrak{f}^*)^+]^{(m+1)} \\
&= -\boldsymbol{\sigma}^* : \dot{\boldsymbol{\varepsilon}}^p - \kappa^* \dot{\xi} - \boldsymbol{\beta}^* : \dot{\boldsymbol{\alpha}} + \frac{1}{\eta(m+1)}[\chi(\mathfrak{f}^*)^+]^{(m+1)}
\end{aligned}
, \tag{124}
$$

see [48,88,89]. Here, $\eta \in (0,\infty)$ is called the *penalty parameter* which characterises time-dependent viscous plastic flow and the function $[\chi(\mathfrak{f}^*)^+]$ is a monotonically increasing ramp function such that

$$[\chi(\mathfrak{f}^*)^+] := \frac{1}{2}\big[\chi(\mathfrak{f}^*) + |\chi(\mathfrak{f}^*)|\,\big] \tag{125}$$

see also [84]. The material parameter $m > 0$ in Eqn. (124) should be chosen such that $[\chi(\mathfrak{f}^*)^+]$ is a $\mathcal{C}^1$ function[7]. Based on Eqn. (124), the evolution equations for internal variables take the generalised form analogous to Eqn. (106) as

$$
\boxed{
\begin{aligned}
\dot{\boldsymbol{\varepsilon}}^p &= \dot{\boldsymbol{\varepsilon}}^p(\boldsymbol{\sigma}, \kappa, \boldsymbol{\beta}) = \frac{1}{\eta}[\chi(\mathfrak{f})^+]^m \chi_{,\boldsymbol{\sigma}} \\[2mm]
\dot{\xi} &= \dot{\xi}(\boldsymbol{\sigma}, \kappa, \boldsymbol{\beta}) = \frac{1}{\eta}[\chi(\mathfrak{f})^+]^m \chi_{,\kappa} \\[2mm]
\dot{\boldsymbol{\alpha}} &= \dot{\boldsymbol{\alpha}}(\boldsymbol{\sigma}, \kappa, \boldsymbol{\beta}) = \frac{1}{\eta}[\chi(\mathfrak{f})^+]^m \chi_{,\boldsymbol{\beta}}
\end{aligned}
}
\tag{126}
$$

Comparing Eqn. (126) with Eqn. (106), it can be seen that the only difference to the case of rate-independent plasticity is that the plastic multiplier $\lambda$ is now determined by the constitutive expression

$$\lambda = \frac{1}{\eta}[\chi(\mathfrak{f})^+]^m \ . \tag{127}$$

Equation (127) is known as the *pseudo-consistency condition* which yields the rate-dependent $\lambda$ in terms of viscosity $\eta$ and the ramp function $(\chi^+)^m$. In contrast to the rate-independent setting, the thermodynamic driving forces are not bound and can take values outside the elastic domain $\mathscr{S}$. The amount $\lambda$ depends on the viscous over-stress function $(\chi^+)^m$, thereby implying that the higher the over-stress, the faster the development of plastic strain. The framework of associative rate-dependent plasticity described by Eqns. (124)–(127), can be extended in a straightforward manner to describe non-associative rate-dependent plasticity, see Box 3. With the preceding definitions, the generalised Prandtl-Reuss tensors for a rate-dependent setting can be computed analogous to those of the rate-independent setting.

For general finite element computations, the continuum elastic-plastic tangent modulus obtained with the rate equations will not lead to quadratic convergence when a Newton-Raphson iterative procedure is used on a global level [90,91]. In the following subsection, algorithmic elastic-plastic tangent modulus consistent with the Newton-Raphson method is derived using an integration algorithm based on the general return method [76,92].

### 2.5.5. Algorithmic treatment

The *algorithmic treatment* is a crucial aspect of computational plasticity, as it is concerned with determining new updated values of state variables by integrating the corresponding governing equations for given initial conditions. In the present work, the algorithmic treatment is derived in three steps as follows

- At first, a *time discretisation* of the balance and evolution equations is carried out.

- Next, the time discrete governing balance equations are recast into their *weak form*.

- Finally, a *space discretisation* is carried out by the use of the finite element method.

---

[7]in the sense that Eqn. (125) is satisfied.

Box 3: Rate-dependent setting–summary of the modelling framework.

---

1. Kinematics : $\quad\quad\quad \boldsymbol{\varepsilon} = \boldsymbol{\varepsilon}^e + \boldsymbol{\varepsilon}^p$

2. Internal variables : $\quad \boldsymbol{\mathfrak{e}} = \{\boldsymbol{\varepsilon}^p, \xi, \boldsymbol{\alpha}\}$

3. Energetic potential : $\quad \psi = \psi^e(\boldsymbol{\varepsilon} - \boldsymbol{\varepsilon}^p) + \psi^p_{\text{iso}}(\xi) + \psi^p_{\text{kin}}(\boldsymbol{\alpha})$

4. Stress tensor : $\quad\quad \boldsymbol{\sigma} = \psi^e(\boldsymbol{\varepsilon} - \boldsymbol{\varepsilon}^p),_{\boldsymbol{\varepsilon}}$

5. Driving forces : $\quad\quad \kappa = -\psi^p_{\text{iso}}(\xi),_{\xi}$

$\quad\quad\quad\quad\quad\quad\quad\quad \boldsymbol{\beta} = -\psi^p_{\text{kin}}(\boldsymbol{\alpha}),_{\boldsymbol{\alpha}}$

6. Yield function : $\quad\quad \chi = \chi(\boldsymbol{\sigma}, \kappa, \boldsymbol{\beta})$

7. Plastic flow potential : $\phi = \phi(\boldsymbol{\sigma}, \kappa, \boldsymbol{\beta})$

8. Evolution equations :

Associative

$$\dot{\boldsymbol{\varepsilon}}^p = \lambda \chi(\boldsymbol{\sigma}, \kappa, \boldsymbol{\beta}),_{\boldsymbol{\sigma}}$$

$$\dot{\xi} = \lambda \chi(\boldsymbol{\sigma}, \kappa, \boldsymbol{\beta}),_{\kappa}$$

$$\dot{\boldsymbol{\alpha}} = \lambda \chi(\boldsymbol{\sigma}, \kappa, \boldsymbol{\beta}),_{\boldsymbol{\beta}}$$

with $\quad\quad \lambda = \dfrac{1}{\eta}[\chi^+]^m \quad \text{and} \quad [\chi^+] = \dfrac{1}{2}\big[\chi + |\chi|\big]$

Non-associative

$$\dot{\boldsymbol{\varepsilon}}^p = \lambda \phi(\boldsymbol{\sigma}, \kappa, \boldsymbol{\beta}),_{\boldsymbol{\sigma}}$$

$$\dot{\xi} = \lambda \phi(\boldsymbol{\sigma}, \kappa, \boldsymbol{\beta}),_{\kappa}$$

$$\dot{\boldsymbol{\alpha}} = \lambda \phi(\boldsymbol{\sigma}, \kappa, \boldsymbol{\beta}),_{\boldsymbol{\beta}}$$

with $\quad\quad \lambda = \dfrac{1}{\eta}[\phi^+]^m \quad \text{and} \quad [\phi^+] = \dfrac{1}{2}\big[\phi + |\phi|\big]$

---

**2.5.5.1. Time discretisation.** In order to predict the material behaviour in a time interval $[0, T] \subseteq \mathbb{R}_+$, the time interval is discretised by a discrete set of points. Hence, one can write $[0, T] \subseteq \mathbb{R}_+ \to [0, T]^{\Delta t} = \{\cdot, \cdot, t_n, t_{n+1}, \cdot, \cdot\} \subseteq [0, T]$, where the space between discrete points is the same. Consider a finite time step $[t_{n+1}, t_n]$ and set $\Delta t_{n+1} = t_{n+1} - t_n$. All the quantities at the time $t_n$ are assumed to be known and the goal is to determine them at time $t_{n+1}$.

**2.5.5.1.1. Elastic domain and trial yield state.** As for the time continuous setting, it has to be ensured that any stress state stays inside the elastic domain $\boldsymbol{\sigma}_{n+1} \in \mathscr{S}(\kappa_{n+1}, \boldsymbol{\beta}_{n+1})$, which can be expressed in terms of the yield function $\chi$ as

$$\boxed{\chi(\boldsymbol{\sigma}_{n+1}, \kappa_{n+1}, \boldsymbol{\beta}_{n+1}) \leq 0} \,, \tag{128}$$

which has to be valid at all times.

**2.5.5.1.2. Algorithmic flow rule.** With the time discretisation at hand, the associative flow rule given by Eqn. (106) can be numerically integrated using a backwards Cauchy-

Euler scheme as

$$
\left.
\begin{aligned}
\dot{\boldsymbol{\varepsilon}}^p &= \frac{1}{\Delta t}(\boldsymbol{\varepsilon}^p_{n+1} - \boldsymbol{\varepsilon}^p_n) = \lambda_{n+1}\chi_{,\boldsymbol{\sigma}_{n+1}} \\
\dot{\xi} &= \frac{1}{\Delta t}(\xi_{n+1} - \xi_n) = \lambda_{n+1}\chi_{,\kappa_{n+1}} \\
\dot{\boldsymbol{\alpha}} &= \frac{1}{\Delta t}(\boldsymbol{\alpha}_{n+1} - \boldsymbol{\alpha}_n) = \lambda_{n+1}\chi_{,\boldsymbol{\beta}_{n+1}}
\end{aligned}
\right\} \quad .
\tag{129}
$$

Likewise, for the non-associative flow rule it follows that

$$
\left.
\begin{aligned}
\dot{\boldsymbol{\varepsilon}}^p &= \frac{1}{\Delta t}(\boldsymbol{\varepsilon}^p_{n+1} - \boldsymbol{\varepsilon}^p_n) = \lambda_{n+1}\phi_{,\boldsymbol{\sigma}_{n+1}} \\
\dot{\xi} &= \frac{1}{\Delta t}(\xi_{n+1} - \xi_n) = \lambda_{n+1}\phi_{,\kappa_{n+1}} \\
\dot{\boldsymbol{\alpha}} &= \frac{1}{\Delta t}(\boldsymbol{\alpha}_{n+1} - \boldsymbol{\alpha}_n) = \lambda_{n+1}\phi_{,\boldsymbol{\beta}_{n+1}}
\end{aligned}
\right\} \quad .
\tag{130}
$$

Setting $\Delta\lambda_{n+1} = \Delta t\lambda_{n+1}$, which is henceforth known as the plastic increment, Eqns. (129) and (130) can be rewritten as

$$
\boxed{
\begin{aligned}
\boldsymbol{\varepsilon}^p_{n+1} &= \boldsymbol{\varepsilon}^p_n + \Delta\lambda_{n+1}\chi_{,\boldsymbol{\sigma}_{n+1}} \\
\xi_{n+1} &= \xi_n + \Delta\lambda_{n+1}\chi_{,\kappa_{n+1}} \\
\boldsymbol{\alpha}_{n+1} &= \boldsymbol{\alpha}_n + \Delta\lambda_{n+1}\chi_{,\boldsymbol{\beta}_{n+1}}
\end{aligned}
}
\quad ,
\tag{131}
$$

and likewise, for the non-associative flow rule it follows

$$
\boxed{
\begin{aligned}
\boldsymbol{\varepsilon}^p_{n+1} &= \boldsymbol{\varepsilon}^p_n + \Delta\lambda_{n+1}\phi_{,\boldsymbol{\sigma}_{n+1}} \\
\xi_{n+1} &= \xi_n + \Delta\lambda_{n+1}\phi_{,\kappa_{n+1}} \\
\boldsymbol{\alpha}_{n+1} &= \boldsymbol{\alpha}_n + \Delta\lambda_{n+1}\phi_{,\boldsymbol{\beta}_{n+1}}
\end{aligned}
}
\quad ,
\tag{132}
$$

where $\Delta\lambda_{n+1} \geq 0$. Recalling Eqn. (96), it can be seen that Eqn. (131) allows the statement of relations for the driving forces $\mathfrak{f}_{n+1} = \{\boldsymbol{\sigma}_{n+1}, \kappa_{n+1}, \boldsymbol{\beta}_{n+1}\}$ as

$$
\begin{aligned}
\boldsymbol{\sigma}_{n+1} &= +\psi^e(\boldsymbol{\varepsilon}_{n+1} - \boldsymbol{\varepsilon}^p_{n+1})_{,(\varepsilon-\varepsilon^p)} = +\psi^e\big(\boldsymbol{\varepsilon}_{n+1} - \boldsymbol{\varepsilon}^p_n - \Delta\lambda_{n+1}\chi_{,\boldsymbol{\sigma}}\big)_{,(\varepsilon-\varepsilon^p)} \\
\kappa_{n+1} &= -\psi^p_{\text{iso}}(\xi_{n+1})_{,\xi} && = -\psi^p_{\text{iso}}\big(\xi_n + \Delta\lambda_{n+1}\chi_{,\kappa}\big)_{,\xi} \\
\boldsymbol{\beta}_{n+1} &= -\psi^p_{\text{kin}}(\boldsymbol{\alpha}_{n+1})_{,\boldsymbol{\alpha}} && = -\psi^p_{\text{kin}}\big(\boldsymbol{\alpha}_n + \Delta\lambda_{n+1}\chi_{,\boldsymbol{\beta}}\big)_{,\boldsymbol{\alpha}}
\end{aligned}
\quad ,
\tag{133}
$$

for the associative flow response, and

$$
\begin{aligned}
\boldsymbol{\sigma}_{n+1} &= +\psi^e(\boldsymbol{\varepsilon}_{n+1} - \boldsymbol{\varepsilon}^p_{n+1})_{,(\varepsilon-\varepsilon^p)} = +\psi^e\big(\boldsymbol{\varepsilon}_{n+1} - \boldsymbol{\varepsilon}^p_n - \Delta\lambda_{n+1}\phi_{,\boldsymbol{\sigma}}\big)_{,(\varepsilon-\varepsilon^p)} \\
\kappa_{n+1} &= -\psi^p_{\text{iso}}(\xi_{n+1})_{,\xi} && = -\psi^p_{\text{iso}}\big(\xi_n + \Delta\lambda_{n+1}\phi_{,\kappa}\big)_{,\xi} \\
\boldsymbol{\beta}_{n+1} &= -\psi^p_{\text{kin}}(\boldsymbol{\alpha}_{n+1})_{,\boldsymbol{\alpha}} && = -\psi^p_{\text{kin}}\big(\boldsymbol{\alpha}_n + \Delta\lambda_{n+1}\phi_{,\boldsymbol{\beta}}\big)_{,\boldsymbol{\alpha}}
\end{aligned}
\quad ,
\tag{134}
$$

for the non-associative flow response. The idea is now to compute elastic trial values $\mathfrak{f}^{\text{trial}}_{n+1} = \{\boldsymbol{\sigma}^{\text{trial}}_{n+1}, \kappa^{\text{trial}}_{n+1}, \boldsymbol{\beta}^{\text{trial}}_{n+1}\}$ of the driving forces by assuming an elastic step between $t_n$ and $t_{n+1}$ and further setting $\Delta\lambda_{n+1} = 0$ in Eqns. (133) and (134), i.e.

$$
\boldsymbol{\sigma}^{\text{trial}}_{n+1} = \psi^e(\boldsymbol{\varepsilon}_{n+1} - \boldsymbol{\varepsilon}^p_n)_{,(\varepsilon-\varepsilon^p)} \ , \quad \kappa^{\text{trial}}_{n+1} = -\psi^p_{\text{iso}}(\xi_n)_{,\xi} \quad \text{and} \quad \boldsymbol{\beta}^{\text{trial}}_{n+1} = -\psi^p_{\text{kin}}(\boldsymbol{\alpha}_n)_{,\boldsymbol{\alpha}} \ , \tag{135}
$$

which allow for the expression of the yield function in a trial state as

$$\chi^{\text{trial}} = \chi^{\text{trial}}(\mathfrak{f}_{n+1}^{\text{trial}}) = \chi(\boldsymbol{\sigma}_{n+1}^{\text{trial}}, \kappa_{n+1}^{\text{trial}}, \boldsymbol{\beta}_{n+1}^{\text{trial}}) \ . \tag{136}$$

The computation of $\{\boldsymbol{\epsilon}_{n+1}, \boldsymbol{\sigma}_{n+1}, \mathbb{E}_{n+1}^{\text{ep}}\}$ now depends on the trial state of yield function (136), based on which the load cases can again be distinguished as

$$\left.\begin{array}{llll} \chi^{\text{trial}} < 0 & \text{and} & \Delta\lambda_{n+1} = 0 \iff \text{elastic step} \\ \chi^{\text{trial}} > 0 & \text{and} & \Delta\lambda_{n+1} > 0 \iff \text{plastic step} \end{array}\right\} \ . \tag{137}$$

For an elastic step given by Eqn. (137)$_1$, the evolution of plastic variables are given by

$$\boldsymbol{\varepsilon}_{n+1}^{p} = \boldsymbol{\varepsilon}_{n}^{p}, \quad \xi_{n+1} = \xi_n \quad \text{and} \quad \boldsymbol{\alpha}_{n+1} = \boldsymbol{\alpha}_n \ . \tag{138}$$

The updated stress and the algorithmically consistent elastic-plastic tangent modulus are the same as the trial values, i.e.

$$\boldsymbol{\sigma}_{n+1} = \boldsymbol{\sigma}_{n+1}^{\text{trial}} \quad \text{and} \quad \mathbb{E}_{n+1}^{\text{ep}} = \psi^e(\boldsymbol{\varepsilon} - \boldsymbol{\varepsilon}_n^p)_{,(\varepsilon-\varepsilon^p)(\varepsilon-\varepsilon^p)} \ , \tag{139}$$

whereas if $\chi^{\text{trial}} > 0$, the assumption of an elastic step is wrong and a plastic step has to be carried out to ensure consistency with Eqn. (128). From Eqns. (129) and (130), it is clear that in order to carry out a plastic step, the values of $\boldsymbol{\sigma}_{n+1}$, $\kappa_{n+1}$, $\boldsymbol{\beta}_{n+1}$ and $\Delta\lambda_{n+1}$ need to be determined. Taking into account Eqns. (133) and (134), and recalling the consistency condition $\dot{\chi}(\boldsymbol{\sigma}_{n+1}, \kappa_{n+1}, \boldsymbol{\beta}_{n+1}) = 0$ during plastic flow, the related non-linear system of equations can be identified as

$$\mathfrak{R} = \begin{bmatrix} \mathfrak{R}_{\boldsymbol{\sigma}} \\ \mathfrak{R}_{\kappa} \\ \mathfrak{R}_{\boldsymbol{\beta}} \\ \mathfrak{R}_{\chi} \end{bmatrix} = \begin{bmatrix} \boldsymbol{\sigma}_{n+1} - \psi^e\big(\boldsymbol{\varepsilon}_{n+1} - \boldsymbol{\varepsilon}_n^p - \Delta\lambda_{n+1}\chi_{,\boldsymbol{\sigma}}\big)_{,(\varepsilon-\varepsilon^p)} \\ \kappa_{n+1} + \psi_{\text{iso}}^p\big(\xi_n + \Delta\lambda_{n+1}\chi_{,\kappa}\big)_{,\xi} \\ \boldsymbol{\beta}_{n+1} + \psi_{\text{kin}}^p\big(\boldsymbol{\alpha}_n + \Delta\lambda_{n+1}\chi_{,\boldsymbol{\beta}}\big)_{,\boldsymbol{\alpha}} \\ \chi(\boldsymbol{\sigma}_{n+1}, \kappa_{n+1}, \boldsymbol{\beta}_{n+1}) \end{bmatrix} = \boldsymbol{0} \ , \tag{140}$$

for the associative flow response, and

$$\mathfrak{R} = \begin{bmatrix} \mathfrak{R}_{\boldsymbol{\sigma}} \\ \mathfrak{R}_{\kappa} \\ \mathfrak{R}_{\boldsymbol{\beta}} \\ \mathfrak{R}_{\chi} \end{bmatrix} = \begin{bmatrix} \boldsymbol{\sigma}_{n+1} - \psi^e\big(\boldsymbol{\varepsilon}_{n+1} - \boldsymbol{\varepsilon}_n^p - \Delta\lambda_{n+1}\phi_{,\boldsymbol{\sigma}}\big)_{,(\varepsilon-\varepsilon^p)} \\ \kappa_{n+1} + \psi_{\text{iso}}^p\big(\xi_n + \Delta\lambda_{n+1}\phi_{,\kappa}\big)_{,\xi} \\ \boldsymbol{\beta}_{n+1} + \psi_{\text{kin}}^p\big(\boldsymbol{\alpha}_n + \Delta\lambda_{n+1}\phi_{,\boldsymbol{\beta}}\big)_{,\boldsymbol{\alpha}} \\ \chi(\boldsymbol{\sigma}_{n+1}, \kappa_{n+1}, \boldsymbol{\beta}_{n+1}) \end{bmatrix} = \boldsymbol{0} \ , \tag{141}$$

for the non-associative flow response. For a general non linear case, Eqns. (140) and (141) should be solved by a Newton-Raphson scheme based on the linearisation of $\mathfrak{R}$ around a point $\mathfrak{P}_{n+1}^i = \{\boldsymbol{\sigma}_{n+1}^i, \kappa_{n+1}^i, \boldsymbol{\beta}_{n+1}^i, \Delta\lambda_{n+1}^i\}$, as

$$\text{Lin}\big[\mathfrak{R}\big]_{\mathfrak{P}_{n+1}^i} = \mathfrak{R}(\mathfrak{P}_{n+1}^i) + \mathfrak{R}(\mathfrak{P}_{n+1}^i)_{,\mathfrak{P}} \cdot \Delta\mathfrak{P}_{n+1}^i = \boldsymbol{0} \ , \tag{142}$$

which yields the update algorithm

$$\boxed{\mathfrak{P}_{n+1}^{i+1} = \mathfrak{P}_{n+1}^i + \Delta\mathfrak{P}_{n+1}^i, \quad \Delta\mathfrak{P}_{n+1}^i = -\big[\mathfrak{R}(\mathfrak{P}_{n+1}^i)_{,\mathfrak{P}}\big]^{-1}\mathfrak{R}(\mathfrak{P}_{n+1}^i)} \ , \tag{143}$$

where $i$ denotes the iteration index. The linearisation is carried out until $\left\|\mathfrak{R}(\mathfrak{P}_{n+1}^i)\right\| <$ TOL, and the explicit form of $\mathfrak{R}(\mathfrak{P}_{n+1}^i),_{\mathfrak{P}}$ can be determined based on Eqn. (140) as

$$
\mathfrak{R}(\mathfrak{P}_{n+1}^i),_{\mathfrak{P}} = \begin{bmatrix} (\boldsymbol{1} \oplus \boldsymbol{1}) + \Delta\lambda\mathbb{E} : \chi,_{\boldsymbol{\sigma\sigma}} & \Delta\lambda\mathbb{E} : \chi,_{\boldsymbol{\sigma}\kappa} & \Delta\lambda\mathbb{E} : \chi,_{\boldsymbol{\sigma\beta}} & \mathbb{E} : \chi,_{\boldsymbol{\sigma}} \\ \Delta\lambda\mathrm{H}\chi,_{\kappa\boldsymbol{\sigma}} & 1 + \Delta\lambda\mathrm{H}\chi,_{\kappa\kappa} & \Delta\lambda\mathrm{H}\chi,_{\kappa\boldsymbol{\beta}} & \mathrm{H}\chi,_{\kappa} \\ \Delta\lambda\mathbb{H} : \chi,_{\boldsymbol{\beta\sigma}} & \Delta\lambda\mathbb{H} : \chi,_{\boldsymbol{\beta}\kappa} & (\boldsymbol{1} \oplus \boldsymbol{1}) + \Delta\lambda\mathbb{H} : \chi,_{\boldsymbol{\beta\beta}} & \mathbb{H} : \chi,_{\boldsymbol{\beta}} \\ \chi,_{\boldsymbol{\sigma}} & \chi,_{\kappa} & \chi,_{\boldsymbol{\beta}} & \chi,_{\Delta\lambda} \end{bmatrix} ,
$$
(144)

for the associative flow response, and

$$
\mathfrak{R}(\mathfrak{P}_{n+1}^i),_{\mathfrak{P}} = \begin{bmatrix} (\boldsymbol{1} \oplus \boldsymbol{1}) + \Delta\lambda\mathbb{E} : \phi,_{\boldsymbol{\sigma\sigma}} & \Delta\lambda\mathbb{E} : \phi,_{\boldsymbol{\sigma}\kappa} & \Delta\lambda\mathbb{E} : \phi,_{\boldsymbol{\sigma\beta}} & \mathbb{E} : \phi,_{\boldsymbol{\sigma}} \\ \Delta\lambda\mathrm{H}\phi,_{\kappa\boldsymbol{\sigma}} & 1 + \Delta\lambda\mathrm{H}\phi,_{\kappa\kappa} & \Delta\lambda\mathrm{H}\phi,_{\kappa\boldsymbol{\beta}} & \mathrm{H}\phi,_{\kappa} \\ \Delta\lambda\mathbb{H} : \phi,_{\boldsymbol{\beta\sigma}} & \Delta\lambda\mathbb{H} : \phi,_{\boldsymbol{\beta}\kappa} & (\boldsymbol{1} \oplus \boldsymbol{1}) + \Delta\lambda\mathbb{H} : \phi,_{\boldsymbol{\beta\beta}} & \mathbb{H} : \phi,_{\boldsymbol{\beta}} \\ \chi,_{\boldsymbol{\sigma}} & \chi,_{\kappa} & \chi,_{\boldsymbol{\beta}} & \chi,_{\Delta\lambda} \end{bmatrix} ,
$$
(145)

for the non-associative flow response. The converged solution of Eqn. (142) contains the consistent values of the driving forces $\mathfrak{f}_{n+1} = \{\boldsymbol{\sigma}_{n+1}, \kappa_{n+1}, \boldsymbol{\beta}_{n+1}\}$. Insertion of $\mathfrak{P}_{n+1}$ into Eqn. (129) and (130) yields the consistent update of the internal variables $\mathfrak{e}_{n+1} = \{\boldsymbol{\varepsilon}_{n+1}^p, \xi_{n+1}, \boldsymbol{\alpha}_{n+1}\}$ for the associative and non-associative flow response, respectively. The only quantity to be determined is the algorithmic elastic-plastic tangent modulus consistent with Newton's method. This can be obtained by taking the variation of the residual equations with respect to the strain. A direct calculation from Eqn. (143) shows that

$$
\begin{bmatrix} \boldsymbol{\sigma}^{i+1} - \boldsymbol{\sigma}^i \\ \kappa^{i+1} - \kappa^i \\ \boldsymbol{\beta}^{i+1} - \boldsymbol{\beta}^i \\ \Delta\lambda^{i+1} - \Delta\lambda^i \end{bmatrix} = - \begin{bmatrix} \mathfrak{C}_{\boldsymbol{\sigma\sigma}} & \mathfrak{C}_{\boldsymbol{\sigma}\kappa} & \mathfrak{C}_{\boldsymbol{\sigma\beta}} & \mathfrak{C}_{\boldsymbol{\sigma}\chi} \\ \mathfrak{C}_{\boldsymbol{\beta\sigma}} & \mathfrak{C}_{\boldsymbol{\beta}\kappa} & \mathfrak{C}_{\boldsymbol{\beta\beta}} & \mathfrak{C}_{\boldsymbol{\beta}\chi} \\ \mathfrak{C}_{\kappa\boldsymbol{\sigma}} & \mathfrak{C}_{\kappa\kappa} & \mathfrak{C}_{\kappa\boldsymbol{\beta}} & \mathfrak{C}_{\kappa\chi} \\ \mathfrak{C}_{\chi\boldsymbol{\sigma}} & \mathfrak{C}_{\chi\kappa} & \mathfrak{C}_{\chi\boldsymbol{\beta}} & \mathfrak{C}_{\chi\chi} \end{bmatrix} \begin{bmatrix} \mathfrak{R}_{\boldsymbol{\sigma}} \\ \mathfrak{R}_{\kappa} \\ \mathfrak{R}_{\boldsymbol{\beta}} \\ \mathfrak{R}_{\chi} \end{bmatrix} ,
$$
(146)

where $\mathfrak{C}_{\boldsymbol{\sigma\sigma}}, \mathfrak{C}_{\boldsymbol{\sigma\beta}}, \mathfrak{C}_{\boldsymbol{\sigma}\kappa}, \mathfrak{C}_{\boldsymbol{\sigma}\chi}, \cdots$, are the sub-matrices of $\mathfrak{C} = \left[\mathfrak{R}(\mathfrak{P}_{n+1}^i),_{\mathfrak{P}}\right]^{-1}$. The desired consistent tangent operator is obtained by a straightforward derivation of the first row of Eqn. (146) with respect to $\boldsymbol{\varepsilon}$, taking into account Eqns. (140) and (141) as

$$
\mathbb{E}^{\mathrm{ep}} := \boldsymbol{\sigma},_{\boldsymbol{\varepsilon}} = (\boldsymbol{\sigma}^{i+1} - \boldsymbol{\sigma}^i),_{\boldsymbol{\varepsilon}} = \mathfrak{C}_{\boldsymbol{\sigma\sigma}} : \mathbb{E} .
$$
(147)

Note that the algorithmic treatment of general fully non linear phenomenological plasticity summarised so far, often drastically simplifies for specific modelling choices of hardening energies $\psi_{\mathrm{iso}}^p$ and $\psi_{\mathrm{kin}}^p$, the yield function $\chi$, and the flow potential $\phi$. In many cases, the system of equations is linear and can be solved without an iterative procedure.

**Remark 4.** For the rate-dependent setting, recall the pseudo-consistency condition (127)

$$
\lambda = \frac{1}{\eta}[\chi(\mathfrak{f})^+]^m ,
$$
(148)

which can be treated for a plastic step $\chi > 0$, by employing a backwards Cauchy-Euler time integration scheme as

$$
\frac{\lambda_{n+1} - \lambda_{n+1}}{\Delta t} = \frac{\Delta\lambda_{n+1}}{\Delta t} = \frac{1}{\eta}[\chi(\mathfrak{f}_{n+1})^+]^m ,
$$
(149)

which may be equivalently written as

$$[\chi(\mathfrak{f}_{n+1})^+]^m - \frac{\eta}{\Delta t}\Delta\lambda_{n+1} = 0 \; , \tag{150}$$

where $\Delta\lambda_{n+1} = \lambda_{n+1}-\lambda_n$. In contrast to the rate-independent setting, the yield function is not zero for the plastic flow but restricted by Eqn. (150), which replaces the consistency condition in Eqn. $(140)_4$ and Eqn. $(141)_4$. A key aspect is that the rate-independent setting is recovered for $\eta = 0$. Note that a time regularisation of the rate-independent model always stabilises the algorithmic setting [65].

**2.5.5.2. Weak form of the balance equations.** In this step, the time discrete strong form of the balance equations are recast as a time discrete weak form using the *test functions*. This reformulation provides a starting point for the space discretisation of phenomenological plasticity using the finite element method. With the updated stress $\boldsymbol{\sigma}_{n+1}$ at hand, the governing balance equation for the motion of the body, i.e. the balance of linear momentum (16) can be reformulated to a time discrete strong form as

$$\mathrm{div}[\boldsymbol{\sigma}_{n+1}] + \boldsymbol{\Upsilon}_{n+1} = \boldsymbol{0} \; , \tag{151}$$

If Eqn. (151) is to hold everywhere in $\mathscr{B}$, then at any point $\boldsymbol{x} \in \mathscr{B}$, it is possible to write

$$\delta\boldsymbol{u} \cdot \big\{ - \mathrm{div}[\boldsymbol{\sigma}_{n+1}] - \boldsymbol{\Upsilon}_{n+1}\big\} = \boldsymbol{0}, \quad \forall \quad \delta\boldsymbol{u} \in \mathbb{R}^3 \; , \tag{152}$$

where $\delta\boldsymbol{u} = \delta\boldsymbol{u}(\boldsymbol{x})$ is a test function that guarantees certain differentiability as well as boundary conditions. These aspects are not relevant for further considerations. Since Eqn. (152) has to be fulfilled everywhere in the body $\mathscr{B}$, one can write

$$\int_{\mathscr{B}} \delta\boldsymbol{u} \cdot \big\{ - \mathrm{div}[\boldsymbol{\sigma}_{n+1}] - \boldsymbol{\Upsilon}_{n+1}\big\} \, dV = \boldsymbol{0} \; . \tag{153}$$

Recalling here the identity

$$\mathrm{div}[\delta\boldsymbol{u} \cdot \boldsymbol{\sigma}] = \nabla\delta\boldsymbol{u} : \boldsymbol{\sigma} + \delta\boldsymbol{u} \cdot \mathrm{div}[\boldsymbol{\sigma}] \; , \tag{154}$$

and inserting the above into Eqn. (153), it follows that

$$-\int_{\mathscr{B}} \mathrm{div}[\delta\boldsymbol{u} \cdot \boldsymbol{\sigma}_{n+1}] \, dV + \int_{\mathscr{B}} \nabla\delta\boldsymbol{u} : \boldsymbol{\sigma}_{n+1} \, dV - \int_{\mathscr{B}} \delta\boldsymbol{u} \cdot \boldsymbol{\Upsilon}_{n+1} \, dV = \boldsymbol{0} \; . \tag{155}$$

Due to the restriction to geometrically linear theory, the following expression holds true

$$\nabla\delta\boldsymbol{u} : \boldsymbol{\sigma}_{n+1} = \nabla_{\mathrm{sym}}\boldsymbol{u} : \boldsymbol{\sigma}_{n+1} = \delta\boldsymbol{\varepsilon} : \boldsymbol{\sigma}_{n+1} \; . \tag{156}$$

Substitution of Eqn. (156) into (155) and application of the Gauss theorem leads to the reformulation of Eqn. (155) as

$$\boxed{-\int_{\partial\mathscr{B}} \delta\boldsymbol{u} \cdot \boldsymbol{t}_{n+1} \, dA - \int_{\mathscr{B}} \delta\boldsymbol{u} \cdot \boldsymbol{\Upsilon}_{n+1} \, dV + \int_{\mathscr{B}} \delta\boldsymbol{\varepsilon} : \boldsymbol{\sigma}_{n+1} \, dV = \boldsymbol{0}} \; . \tag{157}$$

Equation (157) is the time discrete weak form of Eqn. (151), which now allows for the space discretisation using finite elements.

**2.5.5.3. Space discretisation using finite elements.** The displacement $\boldsymbol{u}_{n+1}(\boldsymbol{x})$ in Eqn. (157) is still an infinite dimensional unknown. The idea of space discretisation is to reduce the dimension of the unknowns to a finite number [93]. To do so, first introduce an approximation of the domain $\mathscr{B}$ by an union of $N^e$ so-called finite element domains $\mathscr{B}^e$, that are defined by

$$\mathscr{B} \approx \mathscr{B}^h = \bigcup_{e=1}^{N^e} \mathscr{B}^e \ , \tag{158}$$

see Fig. 16. Next, introduce $\mathfrak{N}^I = \mathfrak{N}^I(\boldsymbol{x})$ shape functions associated with the $\mathfrak{N}^I$ nodes $\boldsymbol{x}^I$ such that

$$\mathfrak{N}_I(\boldsymbol{x}^j) := \delta_{ij} \ , \tag{159}$$

where $\delta_{ij}$ is the Kronecker delta. Starting with the standard Q1 formulation[8], the unknown displacement field $\boldsymbol{u}_{n+1}(\boldsymbol{x})$ can be approximated using a set of nodal values such that

$$\boldsymbol{u}_{n+1} \approx \boldsymbol{u}_{n+1}^h = \sum_{I=1}^{N^I} \mathfrak{N}_I \cdot \boldsymbol{u}_{n+1}^I \ . \tag{160}$$

Likewise, the test function $\delta\boldsymbol{u}$ associated with the weak form (157) can also be approximated as

$$\delta\boldsymbol{u}_{n+1} \approx \delta\boldsymbol{u}_{n+1}^h = \sum_{I=1}^{N^I} \mathfrak{N}_I \cdot \delta\boldsymbol{u}_{n+1}^I \ . \tag{161}$$

For a standard three-dimensional brick-like Q1 element with eight nodes, trilinear shape functions of the following form are used

$$\mathfrak{N}_I(\mathfrak{x}) = \frac{1}{8}(1 + \mathfrak{x}_1\mathfrak{x}_1^I)(1 + \mathfrak{x}_2\mathfrak{x}_2^I)(1 + \mathfrak{x}_3\mathfrak{x}_3^I) \ , \tag{162}$$

where $\mathfrak{x} = \{\mathfrak{x}| -1 \le \mathfrak{x}_I \le +1\}$ denotes the isoparametric coordinate system [94]. To this end, combining all the nodal displacements into a single vector as

$$\boldsymbol{\mathfrak{D}}_{n+1} = \left[u_{x_{n+1}}^1, u_{y_{n+1}}^1, u_{z_{n+1}}^1, \cdots, u_{x_{n+1}}^{\mathfrak{N}^I}, u_{y_{n+1}}^{\mathfrak{N}^I}, u_{z_{n+1}}^{\mathfrak{N}^I}\right]^T \ , \tag{163}$$
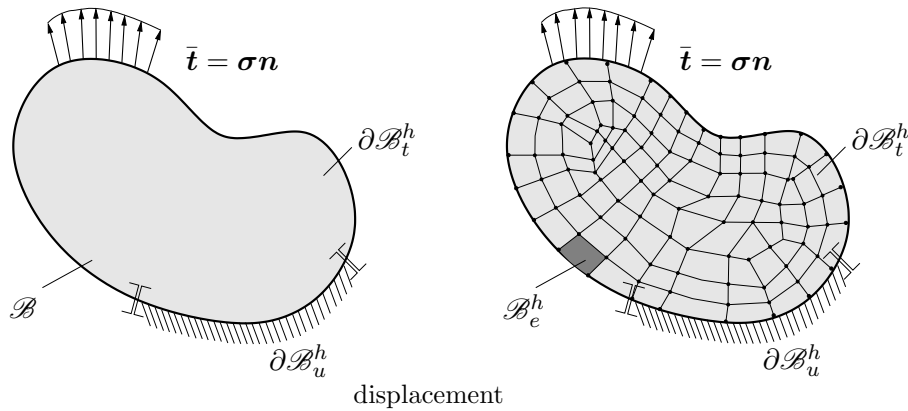


FIGURE 16: **Finite element discretisation.** The domain $\mathscr{B}$ is approximated by the union of finite elements $\mathscr{B}_e^h$. This allows for the approximation of the infinite dimensional unknown $\boldsymbol{u}$ by a finite number of piecewise polynomial functions.

---

[8]all the primary variables are discretised using $C^0$ continuous interpolations.

Eqn. (160) can be reformulated as

$$\boldsymbol{u}^h_{n+1} = \mathfrak{N}_{\boldsymbol{u}} \cdot \mathfrak{D}_{n+1} \ , \tag{164}$$

where $\mathfrak{N}_{\boldsymbol{u}}$ is the global interpolation matrix for $\boldsymbol{u}$, defined as

$$\left[\mathfrak{N}_{\boldsymbol{u}}\right] = \begin{bmatrix} \mathfrak{N}_1 & 0 & 0 & \cdots & \mathfrak{N}_I & 0 & 0 & \cdots & \mathfrak{N}_{N^I} & 0 & 0 \\ 0 & \mathfrak{N}_1 & 0 & \cdots & 0 & \mathfrak{N}_I & 0 & \cdots & 0 & \mathfrak{N}_{N^I} & 0 \\ 0 & 0 & \mathfrak{N}_1 & \cdots & 0 & 0 & \mathfrak{N}_I & \cdots & 0 & 0 & \mathfrak{N}_{N^I} \end{bmatrix} \ . \tag{165}$$

It follows from Eqns. (164) and (165) that the displacement field $\boldsymbol{u}_{n+1}$ depends solely on the shape functions. It can be seen from the weak form (157) that the spatial gradient $\boldsymbol{\varepsilon}$ of the primary field $\boldsymbol{u}$, also needs to be discretised. This is done using spatial derivatives of the shape functions as they are space dependent. Taking into account Eqn. (163), these gradients can be approximated as

$$\boldsymbol{\varepsilon}_{n+1} \approx \boldsymbol{\varepsilon}^h_{n+1} = \nabla \boldsymbol{u}^h_{n+1} = \nabla \mathfrak{N}_{\boldsymbol{u}} \cdot \mathfrak{D}_{n+1} = \mathfrak{B}_{\boldsymbol{\varepsilon}} \cdot \mathfrak{D}_{n+1} \ , \tag{166}$$

where $\mathfrak{B}_{\boldsymbol{\varepsilon}}$ denotes the strain interpolation matrix, defined as

$$\left[\mathfrak{B}_{\boldsymbol{\varepsilon}}\right] = \begin{bmatrix} \mathfrak{N}_{1,1} & \mathfrak{N}_{1,2} & \mathfrak{N}_{1,3} & 0 & 0 & 0 & 0 & 0 & 0 & 0 & 0 & 0 & 0 \\ 0 & 0 & 0 & \mathfrak{N}_{1,1} & \mathfrak{N}_{1,2} & \mathfrak{N}_{1,3} & 0 & 0 & 0 & 0 & 0 & 0 & 0 \\ 0 & 0 & 0 & 0 & 0 & 0 & \mathfrak{N}_{1,1} & \mathfrak{N}_{1,2} & \mathfrak{N}_{1,3} & 0 & 0 & 0 & 0 \\ 0 & 0 & 0 & 0 & 0 & 0 & 0 & 0 & 0 & \mathfrak{N}_1 & \mathfrak{N}_{1,1} & \mathfrak{N}_{1,2} & \mathfrak{N}_{1,3} \\ & & & & & & \vdots \\ \mathfrak{N}_{I,1} & \mathfrak{N}_{I,2} & \mathfrak{N}_{I,3} & 0 & 0 & 0 & 0 & 0 & 0 & 0 & 0 & 0 & 0 \\ 0 & 0 & 0 & \mathfrak{N}_{I,1} & \mathfrak{N}_{I,2} & \mathfrak{N}_{I,3} & 0 & 0 & 0 & 0 & 0 & 0 & 0 \\ 0 & 0 & 0 & 0 & 0 & 0 & \mathfrak{N}_{I,1} & \mathfrak{N}_{I,2} & \mathfrak{N}_{I,3} & 0 & 0 & 0 & 0 \\ 0 & 0 & 0 & 0 & 0 & 0 & 0 & 0 & 0 & \mathfrak{N}_I & \mathfrak{N}_{I,1} & \mathfrak{N}_{I,2} & \mathfrak{N}_{I,3} \\ & & & & & & \vdots \\ \mathfrak{N}_{N^I,1} & \mathfrak{N}_{N^I,2} & \mathfrak{N}_{N^I,3} & 0 & 0 & 0 & 0 & 0 & 0 & 0 & 0 & 0 & 0 \\ 0 & 0 & 0 & \mathfrak{N}_{N^I,1} & \mathfrak{N}_{N^I,2} & \mathfrak{N}_{N^I,3} & 0 & 0 & 0 & 0 & 0 & 0 & 0 \\ 0 & 0 & 0 & 0 & 0 & 0 & \mathfrak{N}_{N^I,1} & \mathfrak{N}_{N^I,2} & \mathfrak{N}_{N^I,3} & 0 & 0 & 0 & 0 \\ 0 & 0 & 0 & 0 & 0 & 0 & 0 & 0 & 0 & \mathfrak{N}_{N^I} & \mathfrak{N}_{N^I,1} & \mathfrak{N}_{N^I,2} & \mathfrak{N}_{N^I,3} \end{bmatrix}^T \ . \tag{167}$$

Finally, setting

$$\delta\mathfrak{D}_{n+1} = \left[\delta u^1_{x_{n+1}}, \delta u^1_{y_{n+1}}, \delta u^1_{z_{n+1}}, \cdots, \delta u^{\mathfrak{N}^I}_{x_{n+1}}, \delta u^{\mathfrak{N}^I}_{y_{n+1}}, \delta u^{\mathfrak{N}^I}_{z_{n+1}}\right]^T \ , \tag{168}$$

analogous to Eqn. (163), and

$$\delta\boldsymbol{\varepsilon}^h_{n+1} = \mathfrak{B}_{\boldsymbol{\varepsilon}} \cdot \delta\mathfrak{D}_{n+1} \ , \tag{169}$$

analogous to Eqn. (161), the weak form (157) can be approximated as

$$-\int_{\partial\mathscr{B}} (\mathfrak{N}_u \cdot \delta\mathfrak{D}) \cdot \boldsymbol{t}_{n+1} \, dA - \int_{\mathscr{B}} (\mathfrak{N}_u \cdot \delta\mathfrak{D}) \cdot \boldsymbol{\Upsilon}_{n+1} \, dV + \int_{\mathscr{B}} (\mathfrak{B}_{\boldsymbol{\varepsilon}} \cdot \delta\mathfrak{D}) : \boldsymbol{\sigma}_{n+1} \, dV = \boldsymbol{0} \ . \tag{170}$$

Using the Voigt notation $\delta\boldsymbol{\varepsilon} : \boldsymbol{\sigma} = \delta\boldsymbol{\varepsilon}^T \cdot \boldsymbol{\sigma}$, Eqn. (170) can be equivalently expressed as

$$-\int_{\partial\mathscr{B}} \delta\mathfrak{D}^T \mathfrak{N}_u^T \cdot \boldsymbol{t}_{n+1} \, dA - \int_{\mathscr{B}} \delta\mathfrak{D}^T \mathfrak{N}_u^T \cdot \boldsymbol{\Upsilon}_{n+1} \, dV + \int_{\mathscr{B}} \delta\mathfrak{D}^T \mathfrak{B}_{\boldsymbol{\varepsilon}}^T \cdot \boldsymbol{\sigma}_{n+1} \, dV = \boldsymbol{0} \ . \tag{171}$$

Box 4**:** Summary of the algorithmic treatment.

1. Given are the history variables $\mathbf{\varepsilon}_n = \{\boldsymbol{\varepsilon}_n^p, \xi_n, \boldsymbol{\alpha}_n\}$ and the current strain $\boldsymbol{\varepsilon}_{n+1}$

2. Compute the trial values

$$\boldsymbol{\sigma}_{n+1}^{\text{trial}} = \psi^e(\boldsymbol{\varepsilon}_{n+1} - \boldsymbol{\varepsilon}_n^p)_{,(\varepsilon-\varepsilon^p)} \ , \quad \kappa_{n+1}^{\text{trial}} = -\psi_{\text{iso}}^p(\xi_n)_{,\xi} \quad \text{and} \quad \boldsymbol{\beta}_{n+1}^{\text{trial}} = -\psi_{\text{kin}}^p(\boldsymbol{\alpha}_n)_{,\boldsymbol{\alpha}}$$

3. Compute the trial yield criterion $\chi^{\text{trial}} = \chi(\boldsymbol{\sigma}_{n+1}^{\text{trial}}, \kappa_{n+1}^{\text{trial}}, \boldsymbol{\beta}_{n+1}^{\text{trial}})$

4. IF $\chi^{\text{trial}} \leq 0$ THEN

   - Elastic step:
       set
       $$\boldsymbol{\varepsilon}_{n+1}^p = \boldsymbol{\varepsilon}_n^p, \quad \xi_{n+1} = \xi_n, \quad \boldsymbol{\alpha}_{n+1} = \boldsymbol{\alpha}_n \ ,$$
       $$\boldsymbol{\sigma}_{n+1} = \boldsymbol{\sigma}_{n+1}^{\text{trial}} \quad \text{and} \quad \mathbb{E}_{n+1}^{\text{ep}} = \psi^e(\boldsymbol{\varepsilon} - \boldsymbol{\varepsilon}_n^p)_{,(\varepsilon-\varepsilon^p)(\varepsilon-\varepsilon_n^p)}$$

5. ELSE

   - Plastic step:
       determine $\mathbf{\mathfrak{P}}_{n+1}^i = \{\boldsymbol{\sigma}_{n+1}^i, \kappa_{n+1}^i, \boldsymbol{\beta}_{n+1}^i, \Delta\lambda_{n+1}^i\}$ iteratively

       $$\mathbf{\mathfrak{P}}_{n+1}^{i+1} = \mathbf{\mathfrak{P}}_{n+1}^i + \Delta\mathbf{\mathfrak{P}}_{n+1}^i, \quad \Delta\mathbf{\mathfrak{P}}_{n+1}^i = -\left[\mathfrak{R}(\mathbf{\mathfrak{P}}_{n+1}^i)_{,\mathfrak{P}}\right]^{-1}\mathfrak{R}(\mathbf{\mathfrak{P}}_{n+1}^i)$$

       update the internal variables using Eqns. (131), (132)
       compute the algorithmically consistent tangent modulus using Eqn. (147)

6. ENDIF

7. Reformulate time discrete governing balance equations to time discrete weak form, Eqns. (151)–(157)

8. Solve for the infinite dimensional unknown $\boldsymbol{u}_{n+1}(\boldsymbol{x})$, using the finite element method, Eqns. (158)–(180)

The term $\delta\boldsymbol{D}$ can be removed from the integral such that

$$\delta\mathbf{\mathfrak{D}}^T \cdot \left\{ \int_{\mathscr{B}} \mathbf{\mathfrak{B}}_{\boldsymbol{\varepsilon}}^T \cdot \boldsymbol{\sigma}_{n+1} \, dV - \int_{\partial\mathscr{B}} \mathbf{\mathfrak{N}}_u^T \cdot \boldsymbol{t}_{n+1} \, dA - \int_{\mathscr{B}} \mathbf{\mathfrak{N}}_u^T \cdot \boldsymbol{\Upsilon}_{n+1} \, dV \right\} = \boldsymbol{0} \ , \qquad (172)$$

where it follows that if Eqn. (172) has to hold for all $\delta\mathbf{\mathfrak{D}}$, then

$$\int_{\mathscr{B}} \mathbf{\mathfrak{B}}_{\boldsymbol{\varepsilon}}^T \cdot \boldsymbol{\sigma}_{n+1} \, dV - \int_{\partial\mathscr{B}} \mathbf{\mathfrak{N}}_u^T \cdot \boldsymbol{t}_{n+1} \, dA - \int_{\mathscr{B}} \mathbf{\mathfrak{N}}_u^T \cdot \boldsymbol{\Upsilon}_{n+1} \, dV = \boldsymbol{0} \ . \qquad (173)$$

To this end, define

$$\mathbf{\mathfrak{R}}_{\text{int}}(\mathbf{\mathfrak{D}}_{n+1}) = \int_{\mathscr{B}} \mathbf{\mathfrak{B}}_{\boldsymbol{\varepsilon}}^T \cdot \boldsymbol{\sigma}_{n+1} \, dV \quad \text{and} \quad \mathbf{\mathfrak{R}}_{\text{ext}} = \int_{\partial\mathscr{B}} \mathbf{\mathfrak{N}}_u^T \cdot \boldsymbol{t}_{n+1} \, dA + \int_{\mathscr{B}} \mathbf{\mathfrak{N}}_u^T \cdot \boldsymbol{\Upsilon}_{n+1} \, dV \ ,$$

$$(174)$$

to be the vector of internal and external forces, respectively. Then, the non-linear equation (173) can be solved using Newton-Raphson iteration scheme based on the linearisation

$$\text{Lin} \left[ \mathfrak{R}_{\text{int}}(\mathfrak{D}_{n+1}^k) - \mathfrak{R}_{\text{ext}} \right] = \mathfrak{R}_{\text{int}}(\mathfrak{D}_{n+1}^k) - \mathfrak{R}_{\text{ext}} + \left[ \mathfrak{R}_{\text{int}}(\mathfrak{D}_{n+1}^k),_{\mathfrak{D}} \right]_{\mathfrak{D}_{n+1}^k} \cdot [\mathfrak{D}_{n+1}^{k+1} - \mathfrak{D}_{n+1}^k] = \boldsymbol{0} \; ,$$
$$(175)$$

which yields the update algorithm

$$\mathfrak{D}_{n+1}^{k+1} = \mathfrak{D}_{n+1}^k - \left[ \mathfrak{R}_{\text{int}}(\mathfrak{D}_{n+1}^k),_{\mathfrak{D}} \right]^{-1} \mathfrak{R}_{\text{int}}(\mathfrak{D}_{n+1}^k) \; , \tag{176}$$

where $k$ denotes the iteration index, see also [95]. The linearisation is carried out until $\left\| \mathfrak{R}_{\text{int}}(\mathfrak{D}_{n+1}^{k+1}) \right\| < \textbf{TOL}$. The two material dependent terms in Eqn. (176) are $\mathfrak{R}_{\text{int}}(\mathfrak{D}_{n+1})$ and $\mathfrak{R}_{\text{int}}(\mathfrak{D}_{n+1}),_{\mathfrak{D}}$. Recall from Eqn. (172), the definition $\mathfrak{R}_{\text{int}}(\mathfrak{D}_{n+1})$

$$\mathfrak{R}_{\text{int}}(\mathfrak{D}_{n+1}) = \int_{\mathscr{B}} \mathfrak{B}_{\boldsymbol{\varepsilon}}^T \cdot \boldsymbol{\sigma}_{n+1} \, dV = \boldsymbol{0} \; , \tag{177}$$

where $\boldsymbol{\sigma}_{n+1}$ is the stress tensor derived in Eqn. (142). Likewise, the necessary iteration tangent $\mathfrak{R}_{\text{int}}(\mathfrak{D}_{n+1}),_{\mathfrak{D}}$ can be expressed as

$$\mathfrak{R}_{\text{int}}(\mathfrak{D}_{n+1}),_{\mathfrak{D}} = \int_{\mathscr{B}} \mathfrak{B}_{\boldsymbol{\varepsilon}}^T \cdot \boldsymbol{\sigma}_{n+1,\boldsymbol{\varepsilon}} \cdot \boldsymbol{\varepsilon},_{\mathfrak{D}} \, dV = \int_{\mathscr{B}} \mathfrak{B}_{\boldsymbol{\varepsilon}}^T \cdot \mathbb{E}_{n+1}^{\text{ep}} \cdot \mathfrak{B}_{\boldsymbol{\varepsilon}} \, dV \; , \tag{178}$$

where $\mathbb{E}^{\text{ep}}$ is the algorithmic elastic-plastic tangent modulus tensor derived in Eqn. (147). From a computational perspective, $\boldsymbol{\sigma}_{n+1}$ and $\mathbb{E}_{n+1}^{\text{ep}}$ are the two quantities that need to be specified in the material routine, in addition to the update of internal variables.

Generally, $\mathfrak{R}_{\text{int}}$ and $\mathfrak{R}_{\text{int},\mathfrak{D}}$ are computed element-wise by integration over the element domain. The overall $N^e$ element force vectors and tangent matrices are then suitably assembled to $\mathfrak{R}_{\text{int}}$ and $\mathfrak{R}_{\text{int},\mathfrak{D}}$ such that

$$\mathfrak{R}_{\text{int}}(\mathfrak{D}_{n+1}^k) = \prod_{e=1}^{N^e} \int_{\mathscr{B}} \mathfrak{B}_{\boldsymbol{\varepsilon}}^{eT} \cdot \boldsymbol{\sigma}_{n+1} \, dV \quad \text{and} \quad \mathfrak{R}_{\text{int}}(\mathfrak{D}_{n+1}^k),_{\mathfrak{D}} = \prod_{e=1}^{N^e} \int_{\mathscr{B}} \mathfrak{B}_{\boldsymbol{\varepsilon}}^{eT} \cdot \mathbb{E}_{n+1}^{\text{ep}} \cdot \mathfrak{B}_{\boldsymbol{\varepsilon}}^e \, dV \; ,$$
$$(179)$$

where $\prod_{e=1}^{N^e}$ is the assembly operator that suitably assembles the element quantities to the global quantities based on the mapping between the elements and the global nodes. Equation (179) is numerically integrated using Gauss integration where the integrands are evaluated at specific Gauss points $\boldsymbol{x}_l^e \in \mathscr{B}^e$ and a weighted sum with weights $w_l^e$ as

$$\mathfrak{R}_{\text{int}}^e = \sum_{l=1}^{n_{gauss}} w_l^e \mathfrak{B}_{\boldsymbol{\varepsilon}}^{eT} \cdot \boldsymbol{\sigma}_{n+1} \, dV \quad \text{and} \quad \mathfrak{R}_{\text{int},\mathfrak{D}}^e = \sum_{l=1}^{n_{gauss}} w_l^e \mathfrak{B}_{\boldsymbol{\varepsilon}}^{eT} \cdot \mathbb{E}_{n+1}^{\text{ep}} \cdot \mathfrak{B}_{\boldsymbol{\varepsilon}}^e \, dV \; . \tag{180}$$

It should be remarked here that since $\boldsymbol{\sigma}_{n+1}$ has a functional dependence on the set of internal variables $\boldsymbol{\mathfrak{e}}_{n+1}$, the values of $\boldsymbol{\mathfrak{e}}_{n+1}$ and $\boldsymbol{\mathfrak{e}}_n$ are exclusively needed at the Gauss points. As a consequence, the variables $[\boldsymbol{\mathfrak{e}}_{n+1}^k]_l^e$ and $[\boldsymbol{\mathfrak{e}}_n^k]_l^e$ are stored as *local history variables* at each time step at $N^e \times n_{gauss}$ Gauss points. A summary of the algorithmic treatment discussed so far is outlined in Box 4.

# 3. Anisotropic elasticity

In this chapter, theory and numerics of anisotropic elasticity applicable to fibre-reinforced composites are studied. In particular, an explicit form of the scalar-valued energetic potential is proposed for the orthorhombic group $\mathscr{C}_3$ and the transversely isotropic group $\mathscr{C}_{13}$, based on the concepts discussed in **Chapter 2**, Sections 2.3 and 2.4. For brevity, attention is restricted only to the coordinate-free approach. A simplifying assumption made at the outset is that fibres are systematically arranged inside the matrix, so that mesoscopically the composite can be regarded as an anisotropic material. Additionally fibres are assumed to be continuously distributed in the material, which enables the application of continuum theories. A thorough discussion of the constitutive formulation and numerical implementation of elasticity with a strong focus on fibre-reinforced composites can be found in [96–100]. Different approaches for the constitutive description of anisotropic elasticity at geometrically non-linear deformations are outlined in [101–103]. A detailed discussion of the pertinent topic and the relevant literature can also be found in the monograph of Spencer [104]. Before proceeding to the subsequent developments, the identities

$$
\begin{aligned}
\left\{(\bullet) \otimes (\bullet)\right\}_{ijkl} &= (\bullet)_{ij}(\bullet)_{kl} \ , \\
\left\{(\bullet) \oplus (\bullet)\right\}_{ijkl} &= (\bullet)_{ik}(\bullet)_{jl} \ , \\
\left\{(\bullet) \ominus (\bullet)\right\}_{ijkl} &= (\bullet)_{il}(\bullet)_{jk} \ ,
\end{aligned}
\tag{181}
$$

are introduced to better comprehend the constitutive equations.

## 3.1. Orthorhombic symmetry group

As outlined in Section 2.3, the orthotropic symmetry group $\mathscr{C}_3$ is characterised by

$$
\mathscr{C}_3 = \{\boldsymbol{Q}_{\boldsymbol{a}}^{\pi}, \boldsymbol{Q}_{\boldsymbol{b}}^{\pi}\} \ ,
\tag{182}
$$

in terms of two orthogonal rotation tensors $\boldsymbol{Q}_{\boldsymbol{a}}^{\pi}$ and $\boldsymbol{Q}_{\boldsymbol{b}}^{\pi}$ which correspond to 180° rotations around the axes $\boldsymbol{a}$ and $\boldsymbol{b}$, respectively. In view of a coordinate-free formulation, it has been proven in Section 2.3.2 that an anisotropic constitutive function can be expressed equivalently as an isotropic function with an extended set of arguments denoted as *structural tensors*. Recall here that the orthotropic symmetry group is fully characterised by a single second-order structural tensor $\boldsymbol{M}$ [64], written as

$$
\boldsymbol{M} = \boldsymbol{a} \otimes \boldsymbol{a} - \boldsymbol{b} \otimes \boldsymbol{b} \quad \text{with} \quad \boldsymbol{Q} \star \boldsymbol{M} = \boldsymbol{M} \quad \forall \quad \boldsymbol{Q} \in \mathscr{C}_3 \ ,
\tag{183}
$$

which, together with the argument tensor $\boldsymbol{\varepsilon}$, allows for the definition of a possible complete and irreducible integrity basis. The representation theorem of general isotropic tensor functions of several arguments is based on the concept of integrity basis, which defines a minimum number of invariants for a particular set of arguments of the energy storage function. In the present case, for two symmetric second-order tensors $\boldsymbol{\varepsilon}$ and $\boldsymbol{M}$, an irreducible integrity basis is given by

$$
\mathcal{I}_{\mathscr{C}_3} = \{\mathrm{tr}[\boldsymbol{\varepsilon}], \mathrm{tr}[\boldsymbol{\varepsilon}^2], \mathrm{tr}[\boldsymbol{\varepsilon}^3], \mathrm{tr}[\boldsymbol{M}\boldsymbol{\varepsilon}], \mathrm{tr}[\boldsymbol{M}^2\boldsymbol{\varepsilon}], \mathrm{tr}[\boldsymbol{M}\boldsymbol{\varepsilon}^2], \mathrm{tr}[\boldsymbol{M}^2\boldsymbol{\varepsilon}^2]\} \ ,
\tag{184}
$$

see [45]. Equation (184) can be transformed to the well known alternative integrity basis for the orthotropic symmetry group, in terms of two structural tensors $\boldsymbol{m}_1$ and $\boldsymbol{m}_2$ as

$$
\hat{\mathcal{I}}_{\mathscr{C}_3} = \{\mathrm{tr}[\boldsymbol{\varepsilon}], \mathrm{tr}[\boldsymbol{\varepsilon}^2], \mathrm{tr}[\boldsymbol{\varepsilon}^3], \mathrm{tr}[\boldsymbol{m}_1\boldsymbol{\varepsilon}], \mathrm{tr}[\boldsymbol{m}_2\boldsymbol{\varepsilon}], \mathrm{tr}[\boldsymbol{m}_1\boldsymbol{\varepsilon}^2], \mathrm{tr}[\boldsymbol{m}_2\boldsymbol{\varepsilon}^2]\} \ ,
\tag{185}
$$

where $\boldsymbol{m}_{1-2}$ are obtained by the dyadic product of direction vectors with themselves such that

$$
\left.\begin{array}{l}
\boldsymbol{m}_1 = \boldsymbol{a} \otimes \boldsymbol{a} \quad \text{with} \quad \boldsymbol{Q} \star \boldsymbol{m}_1 = \boldsymbol{m}_1 \\[4pt]
\boldsymbol{m}_2 = \boldsymbol{b} \otimes \boldsymbol{b} \quad \text{with} \quad \boldsymbol{Q} \star \boldsymbol{m}_1 = \boldsymbol{m}_2
\end{array}\right\} \quad \forall \quad \boldsymbol{Q} \in \mathscr{C}_3 \;.
\tag{186}
$$

As it is well known that the direction vectors form an orthonormal basis, it follows that the third directional vector can be linearly expressed in terms of the other two such that $\boldsymbol{a}_3 = \boldsymbol{a}_1 \times \boldsymbol{a}_2$. Consequently, the third second-order structural tensor $\boldsymbol{m}_3$ can be expressed in terms of the other two as $\boldsymbol{m}_3 = \boldsymbol{1} - \boldsymbol{m}_1 - \boldsymbol{m}_2$, where

$$
\boldsymbol{m}_3 = \boldsymbol{a}_3 \otimes \boldsymbol{a}_3 \quad \text{with} \quad \boldsymbol{Q} \star \boldsymbol{m}_3 = \boldsymbol{m}_3 \quad \forall \quad \boldsymbol{Q} \in \mathscr{C}_3 \;.
\tag{187}
$$

Equations (186) and (187) facilitate for the definition of an isotropic scalar energetic function as

$$
\psi(\boldsymbol{Q} \star \boldsymbol{\varepsilon}, \boldsymbol{Q} \star \boldsymbol{m}_1, \boldsymbol{Q} \star \boldsymbol{m}_2, \boldsymbol{Q} \star \boldsymbol{m}_3) = \psi(\boldsymbol{\varepsilon}, \boldsymbol{m}_1, \boldsymbol{m}_2, \boldsymbol{m}_3) \quad \forall \quad \boldsymbol{Q} \in \mathcal{O}\mathit{(3)} \;.
\tag{188}
$$

Using Eqns. (185) and (187), a new integrity basis is developed following [84], which yields a unique and transparent representation of the scalar-valued energetic potential (188), the associated stress and elasticity tensor. This basis is obtained by first reformulating the basic invariants of the strain tensor as

$$
\begin{aligned}
\text{tr}[\boldsymbol{\varepsilon}] &= \text{tr}[\boldsymbol{m}_1 \boldsymbol{\varepsilon}] + \text{tr}[\boldsymbol{m}_2 \boldsymbol{\varepsilon}] + \text{tr}[\boldsymbol{m}_3 \boldsymbol{\varepsilon}] \quad \text{and} \\
\text{tr}[\boldsymbol{\varepsilon}^2] &= \text{tr}[\boldsymbol{m}_1 \boldsymbol{\varepsilon}^2] + \text{tr}[\boldsymbol{m}_2 \boldsymbol{\varepsilon}^2] + \text{tr}[\boldsymbol{m}_3 \boldsymbol{\varepsilon}^2]
\end{aligned}
\tag{189}
$$

Secondly, the cubic invariant $\text{tr}[\boldsymbol{\varepsilon}^3]$ is replaced by $\det[\boldsymbol{\varepsilon}]$ using the Cayley-Hamilton's theorem [75]. Finally, setting

$$
\boldsymbol{m}_{12} = (\boldsymbol{a} \otimes \boldsymbol{b} + \boldsymbol{b} \otimes \boldsymbol{a}), \quad \boldsymbol{m}_{13} = (\boldsymbol{a} \otimes \boldsymbol{c} + \boldsymbol{c} \otimes \boldsymbol{a}) \quad \text{and} \quad \boldsymbol{m}_{23} = (\boldsymbol{b} \otimes \boldsymbol{c} + \boldsymbol{c} \otimes \boldsymbol{b}) \;,
\tag{190}
$$

and following the argument in [84] where the identity

$$
\text{tr}[\boldsymbol{m}_i \boldsymbol{\varepsilon}^2] - \text{tr}^{\,2}[\boldsymbol{m}_i \boldsymbol{\varepsilon}] = \text{tr}^{\,2}[\boldsymbol{m}_{ij} \boldsymbol{\varepsilon}] + \text{tr}^{\,2}[\boldsymbol{m}_{ik} \boldsymbol{\varepsilon}] \;,
\tag{191}
$$

is valid for every even and odd permutation of $(i, j, k)$, the new integrity basis is obtained by insertion of Eqns. (189) and (190) into Eqn. (185), while taking into account (191) as

$$
\tilde{\mathcal{I}}_{\mathscr{C}_3} = \{ \text{tr}[\boldsymbol{m}_1 \boldsymbol{\varepsilon}], \text{tr}[\boldsymbol{m}_2 \boldsymbol{\varepsilon}], \text{tr}[\boldsymbol{m}_3 \boldsymbol{\varepsilon}], \text{tr}^{\,2}[\boldsymbol{m}_{12} \boldsymbol{\varepsilon}], \text{tr}^{\,2}[\boldsymbol{m}_{13} \boldsymbol{\varepsilon}], \text{tr}^{\,2}[\boldsymbol{m}_{23} \boldsymbol{\varepsilon}], \det[\boldsymbol{\varepsilon}] \} \;.
\tag{192}
$$

Scalar-valued functions can be constructed by taking combinations of the invariants defined above. In particular, a quadratic form of the energetic function can be readily written with the aid of Eqn. (192) as

$$
\psi = \frac{\mu_1}{2} I_1^2 + \frac{\mu_2}{2} I_2^2 + \frac{\mu_3}{2} I_3^2 + \mu_4 I_1 I_2 + \mu_5 I_1 I_3 + \mu_6 I_2 I_3 + \frac{\mu_7}{2} I_4 + \frac{\mu_8}{2} I_5 + \frac{\mu_9}{2} I_6 \;,
\tag{193}
$$

where $I_{1-6}$ are the elements of the integrity basis $\tilde{\mathcal{I}}_{\mathscr{C}_3}$. Given the potential (193), the second-order stress tensor $\boldsymbol{\sigma}$ associated with the potential is given by the chain rule as

$$
\boldsymbol{\sigma} = \psi_{,\boldsymbol{\varepsilon}} = \sum_{i=1}^{6} \psi_{,I_i} \, I_{i;\boldsymbol{\varepsilon}} \;,
\tag{194}
$$

where the derivatives $\psi_{,I_i}$ read

$$\psi_{,I_1} = \mu_1 I_1 + \mu_4 I_2 + \mu_5 I_3 \ , \quad \psi_{,I_2} = \mu_2 I_2 + \mu_4 I_1 + \mu_6 I_3 \ , \quad \psi_{,I_3} = \mu_3 I_3 + \mu_5 I_1 + \mu_6 I_2 \ ,$$

$$\psi_{,I_4} = \frac{\mu_7}{2} \ , \quad \psi_{,I_5} = \frac{\mu_8}{2} \quad \text{and} \quad \psi_{,I_6} = \frac{\mu_9}{2} \ ,$$

(195)

and the tensor generators $I_{(1-6),\varepsilon}$ are given by

$$I_{1,\varepsilon} = \boldsymbol{m}_1 \ , \quad I_{2,\varepsilon} = \boldsymbol{m}_2 \ , \quad I_{3,\varepsilon} = \boldsymbol{m}_3 \ ,$$

$$I_{4,\varepsilon} = 2\operatorname{tr}[\boldsymbol{m}_{12}\boldsymbol{\varepsilon}]\boldsymbol{m}_{12} \ , \quad I_{5,\varepsilon} = 2\operatorname{tr}[\boldsymbol{m}_{13}\boldsymbol{\varepsilon}]\boldsymbol{m}_{13} \quad \text{and} \quad I_{6,\varepsilon} = 2\operatorname{tr}[\boldsymbol{m}_{23}\boldsymbol{\varepsilon}]\boldsymbol{m}_{23} \ .$$

(196)

Insertion of Eqns. (195) and (196) into Eqn. (194) yields the stress tensor as

$$\boldsymbol{\sigma} = \mu_1 I_1 \boldsymbol{m}_1 + \mu_2 I_2 \boldsymbol{m}_2 + \mu_3 I_3 \boldsymbol{m}_3$$
$$+ (\mu_4 I_2 + \mu_5 I_3)\boldsymbol{m}_1 + (\mu_4 I_1 + \mu_6 I_3)\boldsymbol{m}_2 + (\mu_5 I_1 + \mu_6 I_2)\boldsymbol{m}_3 \quad .$$
$$+ \mu_7 \operatorname{tr}[\boldsymbol{m}_{12}\boldsymbol{\varepsilon}]\boldsymbol{m}_{12} + \mu_8 \operatorname{tr}[\boldsymbol{m}_{13}\boldsymbol{\varepsilon}]\boldsymbol{m}_{13} + \mu_9 \operatorname{tr}[\boldsymbol{m}_{23}\boldsymbol{\varepsilon}]\boldsymbol{m}_{23}$$

(197)

The fourth-order elasticity tensor can be expressed with the aid of Eqn. (90) as

$$\mathbb{E} = \psi_{,\varepsilon\varepsilon} = \sum_{i=1}^{6}\sum_{j=1}^{6} \psi_{,I_i} I_{i,\varepsilon\varepsilon} + \psi_{,I_i I_j} I_{i,\varepsilon} \otimes I_{j,\varepsilon} \ ,$$

(198)

where the first derivatives in the above equation namely $\psi_{,I_i}$ and $I_{i,\varepsilon}$ are already defined in Eqns. (195) and (196). The non-zero second derivatives of the energetic potential read

$$\psi_{,I_1 I_1} = \mu_1 \ , \qquad \psi_{,I_1 I_2} = \mu_4 \ , \qquad \psi_{,I_1 I_3} = \mu_5 \ ,$$

$$\psi_{,I_2 I_1} = \mu_4 \ , \qquad \psi_{,I_2 I_2} = \mu_2 \ , \qquad \psi_{,I_2 I_3} = \mu_6 \ ,$$

$$\psi_{,I_3 I_1} = \mu_5 \ , \qquad \psi_{,I_3 I_2} = \mu_6 \ , \qquad \psi_{,I_3 I_3} = \mu_3 \ .$$

(199)

Likewise, the non-zero second derivatives of the tensor generators read

$$I_{4,\varepsilon\varepsilon} = 2\boldsymbol{m}_{12} \otimes \boldsymbol{m}_{12} \ , \qquad I_{5,\varepsilon\varepsilon} = 2\boldsymbol{m}_{13} \otimes \boldsymbol{m}_{13} \ , \qquad I_{6,\varepsilon\varepsilon} = 2\boldsymbol{m}_{23} \otimes \boldsymbol{m}_{23} \ .$$

(200)

Substitution of Eqns. (199), (200) and (195) into Eqn. (198) yields the closed form expression of the elasticity tensor as

$$\mathbb{E} = \mu_1 \boldsymbol{m}_1 \otimes \boldsymbol{m}_1 + \mu_2 \boldsymbol{m}_2 \otimes \boldsymbol{m}_2 + \mu_3 \boldsymbol{m}_3 \otimes \boldsymbol{m}_3 + \mu_4(\boldsymbol{m}_1 \otimes \boldsymbol{m}_2 + \boldsymbol{m}_2 \otimes \boldsymbol{m}_1)$$

$$+ \mu_5(\boldsymbol{m}_1 \otimes \boldsymbol{m}_3 + \boldsymbol{m}_3 \otimes \boldsymbol{m}_1) + \mu_6(\boldsymbol{m}_2 \otimes \boldsymbol{m}_3 + \boldsymbol{m}_3 \otimes \boldsymbol{m}_2) \qquad ,$$

$$+ \mu_7 \boldsymbol{m}_{12} \otimes \boldsymbol{m}_{12} + \mu_8 \boldsymbol{m}_{13} \otimes \boldsymbol{m}_{13} + \mu_9 \boldsymbol{m}_{23} \otimes \boldsymbol{m}_{23}$$

(201)

where, if a coordinate system is chosen such that it is aligned to the principal axes of orthotropy $\{\boldsymbol{a}, \boldsymbol{b}, \boldsymbol{c}\}$, namely that $\boldsymbol{a} = [1,0,0]^T$, $\boldsymbol{b} = [0,1,0]^T$ and $\boldsymbol{c} = [0,0,1]^T$, the fourth-order tensor $\mathbb{E}$ appears in a simple coordinate form

$$[\mathbb{E}] = \begin{bmatrix} \mu_1 & \mu_4 & \mu_5 & 0 & 0 & 0 \\ & \mu_2 & \mu_6 & 0 & 0 & 0 \\ & & \mu_3 & 0 & 0 & 0 \\ & & & \mu_7 & 0 & 0 \\ & \text{sym.} & & & \mu_8 & 0 \\ & & & & & \mu_9 \end{bmatrix} \ ,$$

(202)

in terms of nine material parameters $\mu_{1-9}$. Alternatively, the elasticity tensor of an orthotropic material can also be defined as the inverse of the compliance tensor, in terms of so-called the engineering constants. Following [105–107], the fourth-order elasticity tensor of an orthotropic material reads

$$\mathbb{E} = \mathbb{C}^{-1} \quad \text{with} \quad [\mathbb{C}] = \begin{bmatrix} \dfrac{1}{E_1} & -\dfrac{\nu_{12}}{E_1} & -\dfrac{\nu_{13}}{E_1} & 0 & 0 & 0 \\[2mm] & \dfrac{1}{E_2} & -\dfrac{\nu_{23}}{E_2} & 0 & 0 & 0 \\[2mm] & & \dfrac{1}{E_3} & 0 & 0 & 0 \\[2mm] & & & \dfrac{1}{G_{12}} & 0 & 0 \\[2mm] & \text{sym.} & & & \dfrac{1}{G_{13}} & 0 \\[2mm] & & & & & \dfrac{1}{G_{23}} \end{bmatrix}, \qquad (203)$$

where $E_i$ denotes the Young's modulus along the axis $i$, $G_{ij}$ denotes the shear modulus in the direction $j$ whose normal is in the direction $i$, and $\nu_{ij}$ is the Poisson's ratio that corresponds to a contraction in the direction $j$ for an applied extension in the direction $i$. To this end, inversion of the compliance matrix in Eqn. (203) and comparison of the resulting $\mathbb{C}^{-1}$ with the elasticity tensor in Eqn. (202) yields the nine material parameters $\mu_{1-9}$ in terms of the engineering constants as

$$\mu_1 = \frac{E_1^2(E_3\nu_{23}^2 - E_2)}{E_1 E_3 \nu_{23}^2 + E_2 E_3(2\nu_{12}\nu_{13}\nu_{23} + \nu_{13}^2) + \nu_{12}^2 E_2^2 - E_1 E_2},$$

$$\mu_2 = \frac{E_2^2(E_3\nu_{13}^2 - E_1)}{E_1 E_3 \nu_{23}^2 + E_2 E_3(2\nu_{12}\nu_{13}\nu_{23} + \nu_{13}^2) + \nu_{12}^2 E_2^2 - E_1 E_2},$$

$$\mu_3 = \frac{E_2 E_3(E_2\nu_{12}^2 - E_1)}{E_1 E_3 \nu_{23}^2 + E_2 E_3(2\nu_{12}\nu_{13}\nu_{23} + \nu_{13}^2) + \nu_{12}^2 E_2^2 - E_1 E_2},$$

$$\mu_4 = -\frac{E_1 E_2(E_2\nu_{12} + E_3\nu_{13}\nu_{23})}{E_1 E_3 \nu_{23}^2 + E_2 E_3(2\nu_{12}\nu_{13}\nu_{23} + \nu_{13}^2) + \nu_{12}^2 E_2^2 - E_1 E_2}, \qquad (204)$$

$$\mu_5 = -\frac{E_1 E_2 E_3(\nu_{13} + \nu_{12}\nu_{23})}{E_1 E_3 \nu_{23}^2 + E_2 E_3(2\nu_{12}\nu_{13}\nu_{23} + \nu_{13}^2) + \nu_{12}^2 E_2^2 - E_1 E_2},$$

$$\mu_6 = -\frac{E_2 E_3(E_1\nu_{23} + E_2\nu_{12}\nu_{13})}{E_1 E_3 \nu_{23}^2 + E_2 E_3(2\nu_{12}\nu_{13}\nu_{23} + \nu_{13}^2) + \nu_{12}^2 E_2^2 - E_1 E_2},$$

$$\mu_7 = G_{12}, \quad \mu_8 = G_{13} \quad \text{and} \quad \mu_9 = G_{23}.$$

The framework of coordinate free approach to orthotropic elasticity outlined so far is summarised in Box 5.

## 3.2. Transversely isotropic symmetry group

This subsection is devoted to the coordinate-free representation of transversely isotropic elasticity. Common examples of transversely isotropic materials are biological tissues,

Box 5: Orthotropic elasticity–coordinate free approach.

1. Given is the strain tensor $\boldsymbol{\varepsilon}$, and the structural tensors $\boldsymbol{m}_1 = \boldsymbol{a} \otimes \boldsymbol{a}$, $\boldsymbol{m}_2 = \boldsymbol{b} \otimes \boldsymbol{b}$

2. Determine $\boldsymbol{m}_3 = \boldsymbol{c} \otimes \boldsymbol{c}$ with $\boldsymbol{c} = \boldsymbol{a} \times \boldsymbol{b}$

3. Compute

$$\boldsymbol{m}_{12} = (\boldsymbol{a} \otimes \boldsymbol{b} + \boldsymbol{b} \otimes \boldsymbol{a}), \quad \boldsymbol{m}_{13} = (\boldsymbol{a} \otimes \boldsymbol{c} + \boldsymbol{c} \otimes \boldsymbol{a}) \quad \text{and} \quad \boldsymbol{m}_{23} = (\boldsymbol{b} \otimes \boldsymbol{c} + \boldsymbol{c} \otimes \boldsymbol{b})$$

4. Compute the invariants

$$I_1 = \operatorname{tr}[\boldsymbol{m}_1 \boldsymbol{\varepsilon}] \ , \quad I_2 = \operatorname{tr}[\boldsymbol{m}_2 \boldsymbol{\varepsilon}] \ , \quad I_3 = \operatorname{tr}[\boldsymbol{m}_3 \boldsymbol{\varepsilon}] \ ,$$
$$I_4 = \operatorname{tr}^2[\boldsymbol{m}_{12} \boldsymbol{\varepsilon}] \ , \quad I_5 = \operatorname{tr}^2[\boldsymbol{m}_{13} \boldsymbol{\varepsilon}] \ , \quad I_6 = \operatorname{tr}^2[\boldsymbol{m}_{23} \boldsymbol{\varepsilon}] \quad \text{and} \quad I_7 = \det[\boldsymbol{\varepsilon}]$$

5. Compute the stress tensor

$$\boldsymbol{\sigma} = \sum_{i=1}^{6} \psi_{,I_i} \, I_{i,\boldsymbol{\varepsilon}}$$

6. Compute the elasticity tensor

$$\mathbb{E} = \sum_{i=1}^{6} \sum_{j=1}^{6} \psi_{,I_i} \, I_{i,\boldsymbol{\varepsilon}\boldsymbol{\varepsilon}} + \psi_{,I_i I_j} \, I_{i,\boldsymbol{\varepsilon}} \otimes I_{j,\boldsymbol{\varepsilon}}$$

carbon nano tubes and *unidirectional fibre-reinforced composites*, to name a few. A unidirectional fibre-reinforced composite is characterised by a material reinforced by fibres in only one direction, e.g. polymer matrix reinforced with carbon/glass fibres, metal matrix reinforced with boron fibres. The micro-structure of a transversely isotropic material possesses a single well-defined preferred direction denoted by the unit vector $\boldsymbol{a}$, such that $\|\boldsymbol{a}\| = 1$. This is the key information that helps to construct the symmetry group of a transversely isotropic material. As outlined in Section 2.3, the symmetry group of a transversely isotropic material is given by

$$\mathscr{C}_{13} = \{\boldsymbol{Q}_{\boldsymbol{c}}^{\alpha}, \boldsymbol{Q}_{\boldsymbol{a}}^{\pi}\} \quad \text{with} \quad 0 \leq \alpha \leq 2\pi \ , \tag{205}$$

which can be equivalently expressed following [48] as

$$\mathscr{C}_{13} = \{\boldsymbol{Q}_{\|\boldsymbol{a}}, \boldsymbol{Q}_{\perp\boldsymbol{a}}^{\pi}\} \ , \tag{206}$$

where $\boldsymbol{Q}_{\|\boldsymbol{a}}$ are arbitrary rotations relative to the vector $\boldsymbol{a}$ and $\boldsymbol{Q}_{\perp\boldsymbol{a}}^{\pi}$ are rotations about a vector perpendicular to $\boldsymbol{a}$ by an angle $\pi$. As mentioned in the previous subsection, the key idea of coordinate-free representation of anisotropic materials is to introduce isotropic tensor functions with an extended set of arguments (structural tensors), such that they remain invariant under arbitrary rotations $\boldsymbol{Q} \in \mathcal{O}(3)$. For the case of transverse isotropy, there exists a single second-order structural tensor

$$\boldsymbol{m} = \boldsymbol{a} \otimes \boldsymbol{a} \quad \text{with} \quad \boldsymbol{Q} \star \boldsymbol{m} = \boldsymbol{m} \quad \forall \quad \boldsymbol{Q} \in \mathscr{C}_{13} \ , \tag{207}$$

which allows to express any transversely isotropic scalar potential equivalently as an isotropic function as

$$\psi(\boldsymbol{Q} \star \boldsymbol{\varepsilon}, \boldsymbol{Q} \star \boldsymbol{m}) = \psi(\boldsymbol{\varepsilon}, \boldsymbol{m}) \quad \forall \quad \boldsymbol{Q} \in \mathcal{O}(3) \ . \tag{208}$$

Analogous to the previous case, for two symmetric second-order tensors $\boldsymbol{\varepsilon}$ and $\boldsymbol{m}$, an irreducible integrity basis is given by

$$\mathcal{I}_{\mathscr{C}_{13}} = \{\mathrm{tr}[\boldsymbol{\varepsilon}], \mathrm{tr}[\boldsymbol{\varepsilon}^2], \mathrm{tr}[\boldsymbol{\varepsilon}^3], \mathrm{tr}[\boldsymbol{m}], \mathrm{tr}[\boldsymbol{m}^2], \mathrm{tr}[\boldsymbol{m}^3], \mathrm{tr}[\boldsymbol{m}\boldsymbol{\varepsilon}], \mathrm{tr}[\boldsymbol{m}\boldsymbol{\varepsilon}^2], \mathrm{tr}[\boldsymbol{m}^2\boldsymbol{\varepsilon}], \mathrm{tr}[\boldsymbol{m}^2\boldsymbol{\varepsilon}^2]\} \ , \tag{209}$$

see [62,63]. Considering the fact that the first-order structural vector $\boldsymbol{a}$ is of unit length, it follows that every power of the structural tensor is itself ($\boldsymbol{m}^3 = \boldsymbol{m}^2 = \boldsymbol{m}$), yielding

$$\mathrm{tr}[\boldsymbol{m}^3] = \mathrm{tr}[\boldsymbol{m}^2] = \mathrm{tr}[\boldsymbol{m}] \ . \tag{210}$$

Further, the following equalities hold true since $\boldsymbol{m}$ is a constant

$$\mathrm{tr}[\boldsymbol{m}^2\boldsymbol{\varepsilon}] = \mathrm{tr}[\boldsymbol{m}\boldsymbol{\varepsilon}] \quad \text{and} \quad \mathrm{tr}[\boldsymbol{m}^2\boldsymbol{\varepsilon}^2] = \mathrm{tr}[\boldsymbol{m}\boldsymbol{\varepsilon}^2] \ . \tag{211}$$

Thus, from the ten invariants in Eqn. (209), only five are needed for the representation of transverse isotropy as a result of Eqns. (210)–(211). Consequently, the irreducible integrity basis (209) reformulates to

$$\hat{\mathcal{I}}_{\mathscr{C}_{13}} = \{\mathrm{tr}[\boldsymbol{\varepsilon}], \mathrm{tr}[\boldsymbol{\varepsilon}^2], \mathrm{tr}[\boldsymbol{\varepsilon}^3], \mathrm{tr}[\boldsymbol{m}\boldsymbol{\varepsilon}], \mathrm{tr}[\boldsymbol{m}\boldsymbol{\varepsilon}^2]\} \ . \tag{212}$$

Similar to Eqn. (189), the basic invariants of the strain tensor $\boldsymbol{\varepsilon}$ are reformulated as

$$\mathrm{tr}[\boldsymbol{\varepsilon}] = \mathrm{tr}[\boldsymbol{m}\boldsymbol{\varepsilon}] + \mathrm{tr}[(\boldsymbol{1} - \boldsymbol{m})\boldsymbol{\varepsilon}] \quad \text{and} \quad \frac{1}{2}\mathrm{tr}[\boldsymbol{\varepsilon}^2] = \mathrm{tr}[\boldsymbol{m}\boldsymbol{\varepsilon}^2] + \mathrm{tr}[(\frac{1}{2}\boldsymbol{1} - \boldsymbol{m})\boldsymbol{\varepsilon}^2] \ . \tag{213}$$

Substituting Eqn. (213) in (212) and replacing $\mathrm{tr}[\boldsymbol{\varepsilon}^3]$ by $\det[\boldsymbol{\varepsilon}]$ using the Cayley-Hamilton's theorem, the new integrity basis reads

$$\tilde{\mathcal{I}}_{\mathscr{C}_{13}} = \{\mathrm{tr}[\boldsymbol{m}\boldsymbol{\varepsilon}], \mathrm{tr}[(\boldsymbol{1} - \boldsymbol{m})\boldsymbol{\varepsilon}], \mathrm{tr}[\boldsymbol{m}\boldsymbol{\varepsilon}^2], \mathrm{tr}[(\frac{1}{2}\boldsymbol{1} - \boldsymbol{m})\boldsymbol{\varepsilon}^2], \det[\boldsymbol{\varepsilon}]\} \ . \tag{214}$$

The scalar energetic potential can now be constructed using combinations of the invariants defined above. In particular, one may write

$$\psi = \frac{\mu_1}{2}I_1^2 + \frac{\mu_2}{2}I_2^2 + \mu_3 I_1 I_2 + 2\mu_4 I_3 + 2\mu_5 I_4 \ , \tag{215}$$

where $\mu_{1-5}$ are five independent Lamé parameters required to describe the transversely isotropic response and $I_{1-4}$ denote the elements of the integrity basis $\tilde{\mathcal{I}}_{\mathscr{C}_{13}}$. The stress associated with the potential $\psi$ is defined analogous to Eqn. (194) as

$$\boldsymbol{\sigma} = \psi_{,\boldsymbol{\varepsilon}} = \sum_{i=1}^{4} \psi_{,I_i} I_{i,\boldsymbol{\varepsilon}} \ . \tag{216}$$

The derivatives of $\psi$ with respect to $I_{1-4}$ read

$$\psi_{,I_1} = \mu_1 I_1 + \mu_3 I_2 \ , \quad \psi_{,I_2} = \mu_2 I_2 + \mu_3 I_1 \ , \quad \psi_{,I_3} = 2\mu_4 \quad \text{and} \quad \psi_{,I_4} = 2\mu_5 \ . \tag{217}$$

Likewise, the tensor generators $I_{(1-4),\varepsilon}$ are given by

$$I_{1,\varepsilon} = \boldsymbol{m} \;, \quad I_{2,\varepsilon} = \boldsymbol{1} - \boldsymbol{m} \;, \quad I_{3,\varepsilon} = \boldsymbol{m}\varepsilon + \varepsilon\boldsymbol{m} \quad \text{and} \quad I_{4,\varepsilon} = \varepsilon - (\boldsymbol{m}\varepsilon + \varepsilon\boldsymbol{m}) \;. \quad (218)$$

Insertion of Eqns. (217) and (218) into Eqn. (216) yields the stress tensor as

$$\boldsymbol{\sigma} = (\mu_1 I_1 + \mu_3 I_2)\boldsymbol{m} + (\mu_2 I_2 + \mu_3 I_1)(\boldsymbol{1} - \boldsymbol{m}) + 2\mu_4\{\boldsymbol{m}\varepsilon + \varepsilon\boldsymbol{m}\} + 2\mu_5\{\varepsilon - [\boldsymbol{m}\varepsilon + \varepsilon\boldsymbol{m}]\} \;. \quad (219)$$

The fourth-order elasticity tensor can be expressed as

$$\mathbb{E} = \psi_{,\varepsilon\varepsilon} = \sum_{i=1}^{4}\sum_{j=1}^{4} \psi_{,I_i}\, I_{i,\varepsilon\varepsilon} + \psi_{,I_i I_j}\, I_{i,\varepsilon} \otimes I_{j,\varepsilon} \;. \quad (220)$$

The non-zero second derivatives of the energetic potential in Eqn. (220) read

$$\psi_{,I_1 I_1} = \mu_1 \;, \quad \psi_{,I_1 I_2} = \mu_3 \;, \quad \psi_{,I_2 I_1} = \mu_3 \quad \text{and} \quad \psi_{,I_2 I_2} = \mu_2 \;, \quad (221)$$

and the non-zero second derivatives of the tensor generators take the form

$$\begin{aligned}
I_{3,\varepsilon\varepsilon} &= \big\{ (\boldsymbol{1} \oplus \boldsymbol{m}) + (\boldsymbol{1} \ominus \boldsymbol{m}) + (\boldsymbol{m} \oplus \boldsymbol{1}) + (\boldsymbol{m} \ominus \boldsymbol{1}) \big\} \;, \\
I_{4,\varepsilon\varepsilon} &= \big\{ (\boldsymbol{1} \oplus \boldsymbol{1}) + (\boldsymbol{1} \ominus \boldsymbol{1}) - (\boldsymbol{1} \oplus \boldsymbol{m}) - (\boldsymbol{1} \ominus \boldsymbol{m}) - (\boldsymbol{m} \oplus \boldsymbol{1}) - (\boldsymbol{m} \ominus \boldsymbol{1}) \big\} \;.
\end{aligned} \quad (222)$$

Substitution of Eqns. (221), (222) and (217) into Eqn. (220) yields the closed form expression of the elasticity tensor as

$$\begin{aligned}
\mathbb{E} =\; & \mu_1 \boldsymbol{m} \otimes \boldsymbol{m} + \mu_2 (\boldsymbol{1} - \boldsymbol{m}) \otimes (\boldsymbol{1} - \boldsymbol{m}) \\
& + \mu_3 \big\{ \boldsymbol{m} \otimes (\boldsymbol{1} - \boldsymbol{m}) + (\boldsymbol{1} - \boldsymbol{m}) \otimes \boldsymbol{m} \big\} \\
& + \mu_4 \big\{ (\boldsymbol{1} \oplus \boldsymbol{m}) + (\boldsymbol{1} \ominus \boldsymbol{m}) + (\boldsymbol{m} \oplus \boldsymbol{1}) + (\boldsymbol{m} \ominus \boldsymbol{1}) \big\} \\
& + \mu_5 \big\{ (\boldsymbol{1} \oplus \boldsymbol{1}) + (\boldsymbol{1} \ominus \boldsymbol{1}) - (\boldsymbol{1} \oplus \boldsymbol{m}) - (\boldsymbol{1} \ominus \boldsymbol{m}) - (\boldsymbol{m} \oplus \boldsymbol{1}) - (\boldsymbol{m} \ominus \boldsymbol{1}) \big\}
\end{aligned} \quad , \quad (223)$$

where, if the preferred direction $\boldsymbol{a}$ is chosen such that $\boldsymbol{a} = [1,0,0]^T$, the fourth-order tensor $\mathbb{E}$ appears in a simple coordinate form

$$[\mathbb{E}] = \begin{bmatrix}
\mu_1 + 4\mu_4 - 2\mu_5 & \mu_3 & \mu_3 & 0 & 0 & 0 \\
 & \mu_2 + 2\mu_5 & \mu_2 & 0 & 0 & 0 \\
 & & \mu_2 + 2\mu_5 & 0 & 0 & 0 \\
 & & & \mu_4 & 0 & 0 \\
 & \text{sym.} & & & \mu_4 & 0 \\
 & & & & & \mu_5
\end{bmatrix} \;, \quad (224)$$

in terms of five material parameters $\mu_{1-5}$. Analogous to the case of orthotropic elasticity, the Lamé parameters can be expressed in terms of engineering constants as

$$\begin{aligned}
\mu_1 &= -\frac{E_1^2 (4G_{23} - E_2)}{E_1 E_2 + 4G_{23}(\nu_{12}^2 E_2 - E_1)} - 4G_{12} + 2G_{23} \;, \\[2mm]
\mu_2 &= -\frac{2E_1 E_2 G_{23} + 4G_{23}^2 (\nu_{12}^2 E_2 - E_1)}{E_1 E_2 + 4G_{23}(\nu_{12}^2 E_2 - E_1)} \;, \\[2mm]
\mu_3 &= -\frac{2\nu_{12} E_1 E_2 G_{23}}{E_1 E_2 + 4G_{23}(\nu_{12}^2 E_2 - E_1)} \;, \\[2mm]
\mu_4 &= G_{12} \;, \quad \mu_5 = G_{23} \;.
\end{aligned} \quad (225)$$

Box 6: Transversely isotropic elasticity–coordinate free approach.

1. Given is the strain tensor $\boldsymbol{\varepsilon}$, and the structural tensor $\boldsymbol{m} = \boldsymbol{a} \otimes \boldsymbol{a}$

2. Compute the invariants

$$I_1 = \text{tr}[\boldsymbol{m}\boldsymbol{\varepsilon}] , \quad I_2 = \text{tr}[(\boldsymbol{1} - \boldsymbol{m})\boldsymbol{\varepsilon}] , \quad I_3 = \text{tr}[\boldsymbol{m}\boldsymbol{\varepsilon}^2] ,$$

$$I_4 = \text{tr}[(\frac{1}{2}\boldsymbol{1} - \boldsymbol{m})\boldsymbol{\varepsilon}^2] \quad \text{and} \quad I_5 = \det[\boldsymbol{\varepsilon}]$$

3. Compute the stress tensor

$$\boldsymbol{\sigma} = \sum_{i=1}^{4} \psi_{,I_i} \, I_{i,\boldsymbol{\varepsilon}}$$

4. Compute the elasticity tensor

$$\mathbb{E} = \sum_{i=1}^{4} \sum_{j=1}^{4} \psi_{,I_i} \, I_{i,\boldsymbol{\varepsilon}\boldsymbol{\varepsilon}} + \psi_{,I_i I_j} \, I_{i,\boldsymbol{\varepsilon}} \otimes I_{j,\boldsymbol{\varepsilon}}$$

where the equalities

$$
\begin{aligned}
E_3 &= E_2 \\
G_{13} &= G_{12} \\
\nu_{13} &= \nu_{12} \\
\nu_{23} &= \frac{E_2}{2G_{23}} - 1
\end{aligned}
\qquad , \tag{226}
$$

which hold true for a transversely isotropic material are taken into account in Eqn. (203). A summary of the modelling framework for transversely isotropic elasticity is given in Box 6.

## 4.  Anisotropic plasticity. Isotropic dissipative response functions

The objective of this chapter is to investigate in detail the effect of using isotropic plastic response functions in modelling the non-linear behaviour of fibre-reinforced composites on the meso level. Based on the elements of infinitesimal plasticity theory introduced in **Chapter 2**, two models chosen from the literature are presented to simulate the non-linearities exhibited by the composite. The first model is a modified Drucker-Prager (MDPR) model, formulated following [27], in which the classical Drucker-Prager-type pressure-dependent isotropic yield criterion is modified for use with fibre-reinforced composites. This is followed by a second model, which is a modified version of the model proposed by Car, Oller and Oñate [23, 24] (MCOO). It assumes the existence of a fictitious isotropic space where a mapped problem is solved. The numerical implementation of both the models is briefly discussed next. A key aspect is the qualitative and quantitative investigation of the aforementioned models by comparison to experimental data, which provides valuable insight towards the constitutive formulation of anisotropic plasticity that appears in the following chapter. The shortcomings of these models are also discussed in detail by representative numerical simulations in **Chapter 7**.

**Remark 5.** Discussions in this chapter are restricted only to the transversely isotropic symmetry group.

Starting from Eqns. (93) and (94), an explicit form of the decoupled scalar energetic potential reads

$$\psi(\boldsymbol{\varepsilon} - \boldsymbol{\varepsilon}^p, \xi, \boldsymbol{\alpha}) = \frac{1}{2} \left\| \boldsymbol{\varepsilon} - \boldsymbol{\varepsilon}^p \right\|_{\mathbb{E}}^2 + \frac{h}{n+1} (\bar{\xi} + \xi)^{n+1} + \frac{1}{2} \left\| \boldsymbol{\alpha} \right\|_{\mathbb{H}}^2 \ , \qquad (227)$$

where $\left\| \boldsymbol{\varepsilon} - \boldsymbol{\varepsilon}^p \right\|_{\mathbb{E}}^2 = (\boldsymbol{\varepsilon} - \boldsymbol{\varepsilon}^p) : \mathbb{E} : (\boldsymbol{\varepsilon} - \boldsymbol{\varepsilon}^p)$ is the norm of the elastic strain $(\boldsymbol{\varepsilon} - \boldsymbol{\varepsilon}^p)$ with respect to a symmetric and anisotropic fourth-order elasticity tensor $\mathbb{E}$ of the form (224). The parameter $h$ denotes the hardening modulus, $n > 0$ is the hardening exponent and $\bar{\xi}$ is a parameter describing prestrain, which is necessary for numerical reasons and is set to a very low value such that it has negligible effect on the results. The expression $\left\| \boldsymbol{\alpha} \right\|_{\mathbb{H}}^2 = \boldsymbol{\alpha} : \mathbb{H} : \boldsymbol{\alpha}$, denotes the norm of the kinematic hardening variable $\boldsymbol{\alpha}$ with respect to a symmetric and anisotropic fourth-order kinematic hardening tensor $\mathbb{H}$ of the form similar to (224). The stress tensor and driving forces associated with the potential $\psi$ read

$$\begin{aligned}
\boldsymbol{\sigma} &= +\psi_{,(\boldsymbol{\varepsilon} - \boldsymbol{\varepsilon}^p)} = \mathbb{E} : (\boldsymbol{\varepsilon} - \boldsymbol{\varepsilon}^p) \ , \\
\kappa &= -\psi^p_{\text{iso}}(\xi)_{,\xi} = -h(\bar{\xi} + \xi)^n \ , \\
\boldsymbol{\beta} &= -\psi^p_{\text{kin}}(\boldsymbol{\alpha})_{,\boldsymbol{\alpha}} = -\mathbb{H} : \boldsymbol{\alpha} \ .
\end{aligned} \qquad (228)$$

As a main characteristic of elastoplastic material response, an elastic domain $\mathscr{S}$ is assumed which is defined by

$$\mathscr{S} = \{ (\boldsymbol{\sigma}, \kappa, \boldsymbol{\beta}) \in \mathbb{R}^6 \times \mathbb{R} \times \mathbb{R}^6 | \chi(\boldsymbol{\sigma}, \kappa, \boldsymbol{\beta}) \leq 0 \} \ , \qquad (229)$$

where $\chi = \chi(\boldsymbol{\sigma}, \kappa, \boldsymbol{\beta})$ is a yield function of the generalised Drucker-Prager-type given by

$$\chi = \varkappa p + \left\| \boldsymbol{\Sigma} \right\|_{\mathbb{X}} - \sqrt{\frac{2}{3}}[y_0 - \kappa] + \frac{\zeta}{2} \left\| \boldsymbol{\beta} \right\|_{\mathbb{X}}^2 \quad \text{with} \quad \boldsymbol{\Sigma} = \boldsymbol{\sigma} + \boldsymbol{\beta} \ , \qquad (230)$$

where $\varkappa$ is the coefficient of the hydrostatic pressure, $p = \frac{1}{3} \text{tr}[\boldsymbol{\Sigma}]$ is the hydrostatic pressure, $\left\| \boldsymbol{\Sigma} \right\|_{\mathbb{X}} = \sqrt{\boldsymbol{\Sigma} : \mathbb{X} : \boldsymbol{\Sigma}}$ is the norm of the relative stress tensor $\boldsymbol{\Sigma}$ with respect to a symmetric, anisotropic and deviatoric fourth-order Hill-type tensor $\mathbb{X}$, and $y_0$ is the initial threshold yield stress. The parameter $\zeta$ controls the non-linearity of kinematic hardening.

## 4.1. Modified Drucker-Prager model

In this section, the plastic response functions for the associative and non-associative MDPR model are outlined. The yield function and the plastic flow potential formulated subsequently, are based on the definition of a plasticity inducing stress which is obtained in an additive format from the overall stress, hydrostatic pressure and the deviatoric fibre stress for a given fibre direction $\boldsymbol{m}$, see [31, 32, 108]. This is specified to the present model by setting the fourth-order Hill-type tensor $\mathbb{X}$ in Eqn. (230) as

$$\widetilde{\mathbb{X}} = (\boldsymbol{1} \oplus \boldsymbol{1}) + (\boldsymbol{1} \ominus \boldsymbol{1}) - \frac{1}{3}(\boldsymbol{1} \otimes \boldsymbol{1}) - \frac{3}{2}(\boldsymbol{m}' \otimes \boldsymbol{m}') \quad \text{with} \quad \boldsymbol{m}' = \boldsymbol{m} - \frac{1}{3}\boldsymbol{1} \; , \quad (231)$$

with the following characteristics

$$\widetilde{\mathbb{X}} : \boldsymbol{1} = \boldsymbol{0} \quad \text{and} \quad \widetilde{\mathbb{X}} : \boldsymbol{m} = \boldsymbol{0} \; , \quad (232)$$

see [84] for details. Additionally, let $\widetilde{p}$ denote the hydrostatic pressure such that

$$\widetilde{p} = \frac{1}{3} \operatorname{tr}[(\boldsymbol{1} - \boldsymbol{m})\boldsymbol{\Sigma}] \; . \quad (233)$$

Appealing to Eqns. (231) and (233), the yield function (230) reformulates to

$$\chi = \varkappa\widetilde{p} + \|\boldsymbol{\Sigma}\|_{\widetilde{\mathbb{X}}} - \sqrt{\frac{2}{3}}[y_0 - \kappa] + \frac{\zeta}{2}\|\boldsymbol{\beta}\|_{\widetilde{\mathbb{X}}}^2 \; . \quad (234)$$

Taking into account Eqns. (106) and (234), the flow rule takes the form

$$\dot{\boldsymbol{\varepsilon}}^p = \lambda \left\{ \frac{\varkappa}{3}(\boldsymbol{1} - \boldsymbol{m}) + \frac{\widetilde{\mathbb{X}} : \boldsymbol{\Sigma}}{\|\boldsymbol{\Sigma}\|_{\widetilde{\mathbb{X}}}} \right\} = \lambda \left\{ \frac{\varkappa}{3}(\boldsymbol{1} - \boldsymbol{m}) + \widetilde{\mathfrak{n}} \right\} \; , \quad (235)$$

where $\widetilde{\mathfrak{n}}$ is the direction of the plastic flow. It follows that the rate equations for $\xi$ and $\boldsymbol{\alpha}$ are given by

$$\dot{\xi} = \lambda \sqrt{\frac{2}{3}} \quad \text{and} \quad \dot{\boldsymbol{\alpha}} = \lambda \left\{ \frac{\varkappa}{3}(\boldsymbol{1} - \boldsymbol{m}) + \widetilde{\mathfrak{n}} + \zeta\widetilde{\mathbb{X}} : \boldsymbol{\beta} \right\} \; . \quad (236)$$

For the case of non-associative plasticity, the corresponding flow rule and rate equations for the hardening variables can be obtained in a similar manner. In particular, a deviatoric flow potential can be defined following [109] as

$$\phi = \|\boldsymbol{\Sigma}\|_{\widetilde{\mathbb{X}}} - \sqrt{\frac{2}{3}}[y_0 - \kappa] + \frac{\zeta}{2}\|\boldsymbol{\beta}\|_{\widetilde{\mathbb{X}}}^2 \; , \quad (237)$$

based on which the evolution equations take the form

$$\dot{\boldsymbol{\varepsilon}}^p = \lambda \frac{\widetilde{\mathbb{X}} : \boldsymbol{\Sigma}}{\|\boldsymbol{\Sigma}\|_{\widetilde{\mathbb{X}}}} = \lambda\widetilde{\mathfrak{n}} \; , \quad (238)$$

and

$$\dot{\xi} = \lambda \sqrt{\frac{2}{3}} \quad \text{and} \quad \dot{\boldsymbol{\alpha}} = \lambda\{\widetilde{\mathfrak{n}} + \zeta\widetilde{\mathbb{X}} : \boldsymbol{\beta}\} \; . \quad (239)$$

The next computational aspect is the integration of rate equations (235)–(236) and (238)–(239), subject to the constraint posed by the yield condition. The general return method outlined in **Chapter 2** is used here.

## 4.2. Modified Car, Oller and Oñate model

This is a material model for fibre-reinforced composites based on the work of Car, Oller and Oñate [23, 24]. It assumes the existence of a fictitious isotropic space where a mapped problem is solved. The real and fictitious spaces are related by means of fourth-order transformation tensors which are formulated based on the available information of strengths in the respective spaces. The real anisotropic space is regarded as a homogenised composite material, while the fictitious isotropic space characterises the matrix material to which plasticity is usually restricted.

### 4.2.1. Space transformation: real anisotropic to fictitious isotropic

Let $\mathbf{Y}$ and $\overline{\mathbf{Y}}$ each represent a second-order yield strength tensor for the real anisotropic space and so-called the fictitious isotropic space, respectively. To this end, a fourth-order space transformation tensor for the stress is proposed as

$$\mathbb{A} = \frac{1}{2}\big\{(\overline{\mathbf{Y}} \oplus \mathbf{Y}^{-1}) + (\mathbf{Y}^{-1} \oplus \overline{\mathbf{Y}})\big\} \, , \tag{240}$$

which satisfies the major and minor symmetries

$$\mathbb{A}_{ijkl} = \mathbb{A}_{jikl} = \mathbb{A}_{ijlk} = \mathbb{A}_{klij} \, . \tag{241}$$

The fourth-order tensor $\mathbb{A}$ relates the stress tensor and the back-stress tensor in the real and fictitious spaces as

$$\overline{\boldsymbol{\sigma}} = \mathbb{A} : \boldsymbol{\sigma} \quad \text{and} \quad \overline{\boldsymbol{\beta}} = \mathbb{A} : \boldsymbol{\beta} \, , \tag{242}$$

with $\boldsymbol{\sigma}$ denoting the stress tensor in the real anisotropic space, defined in Eqn. (219). It should be noted here that Car, Oller and Oñate [23, 24] defined the transformation tensor as $\mathbb{A} = \overline{\mathbf{Y}} \otimes \mathbf{Y}^{-1}$, but it is slightly modified in the present work to get a compact representation of the transformation tensor. In what follows, the quantities $(\cdot)$ and $\overline{(\cdot)}$ relate to the real anisotropic and the fictitious isotropic space, respectively. Analogous to Eqn. (242), the relationship between the elastic strain in both spaces is defined by

$$(\overline{\boldsymbol{\varepsilon}} - \overline{\boldsymbol{\varepsilon}}^p) = \mathbb{B} : (\boldsymbol{\varepsilon} - \boldsymbol{\varepsilon}^p) \, , \tag{243}$$

which implies the non-uniqueness of elastic strain during space transformation. The fourth-order strain transformation tensor $\mathbb{B}$ is obtained with the aid of Eqn. (242) as

$$\mathbb{B} = \overline{\mathbb{E}}^{-1} : \mathbb{A} : \mathbb{E} \, , \tag{244}$$

where $\mathbb{E}$ and $\overline{\mathbb{E}}$ are the elastic modulus tensors in the real anisotropic and fictitious isotropic spaces, respectively. The fourth-order tensor $\mathbb{E}$ includes the actual properties of the material (i.e. Eqn. (224)), whereas the choice of $\overline{\mathbb{E}}$ can be arbitrary [23, 24].

In the following subsection, the governing constitutive equations of the plastic deformation process are specified in the fictitious isotropic space. Note that it is equivalent to formulate the model in either of the two spaces because of the invariance of the dissipation postulate [23]. Due to the advantages of the existing algorithms for isotropy, modelling in the fictitious isotropic space is considered.

### 4.2.2. Dissipative response functions

Starting from Eqn. (230), the yield function in the fictitious isotropic space is given by

$$\chi = \varkappa \overline{p} + \left\| \overline{\boldsymbol{\Sigma}} \right\|_{\overline{\mathbb{X}}} - \sqrt{\frac{2}{3}} [y_0 - \kappa] + \frac{\zeta}{2} \left\| \boldsymbol{\beta} \right\|_{\overline{\mathbb{X}}}^2 \quad \text{with} \quad \overline{\boldsymbol{\Sigma}} = \overline{\boldsymbol{\sigma}} + \overline{\boldsymbol{\beta}} \; , \tag{245}$$

where $\overline{p} = \frac{1}{3} \mathrm{tr}[\overline{\boldsymbol{\Sigma}}]$ is the hydrostatic pressure, and $\overline{\mathbb{X}}$ is the symmetric and isotropic fourth-order deviatoric projection tensor given by

$$\overline{\mathbb{X}} = (\boldsymbol{1} \oplus \boldsymbol{1}) + (\boldsymbol{1} \ominus \boldsymbol{1}) - \frac{1}{3} (\boldsymbol{1} \otimes \boldsymbol{1}) \; . \tag{246}$$

The flow rule and rate equations of the hardening variables within the isotropic space are specified analogous to Eqn. (235) as

$$\dot{\overline{\boldsymbol{\varepsilon}}}^p = \lambda \left\{ \frac{\varkappa}{3} \boldsymbol{1} + \frac{\overline{\mathbb{X}} : \overline{\boldsymbol{\Sigma}}}{\left\| \overline{\boldsymbol{\Sigma}} \right\|_{\overline{\mathbb{X}}}} \right\} = \lambda \left\{ \frac{\varkappa}{3} \boldsymbol{1} + \overline{\mathfrak{n}} \right\} \; , \tag{247}$$

and

$$\dot{\xi} = \lambda \sqrt{\frac{2}{3}} \quad \text{and} \quad \dot{\overline{\boldsymbol{\alpha}}} = \lambda \left\{ \frac{\varkappa}{3} \boldsymbol{1} + \overline{\mathfrak{n}} + \zeta \overline{\mathbb{X}} : \overline{\boldsymbol{\beta}} \right\} \; . \tag{248}$$

Furthermore, a separate deviatoric flow potential that governs the evolution of plastic variables within the framework of non-associative plasticity is defined as

$$\phi = \left\| \overline{\boldsymbol{\Sigma}} \right\|_{\overline{\mathbb{X}}} - \sqrt{\frac{2}{3}} [y_0 - \kappa] + \frac{\zeta}{2} \left\| \overline{\boldsymbol{\beta}} \right\|_{\overline{\mathbb{X}}}^2 \; , \tag{249}$$

based on which the evolution equations (247) and (248) reformulate respectively to

$$\dot{\overline{\boldsymbol{\varepsilon}}}^p = \lambda \overline{\mathfrak{n}} \; , \tag{250}$$

and

$$\dot{\xi} = \lambda \sqrt{\frac{2}{3}} \quad \text{and} \quad \dot{\overline{\boldsymbol{\alpha}}} = \lambda \{ \overline{\mathfrak{n}} + \zeta \overline{\mathbb{X}} : \overline{\boldsymbol{\beta}} \} \; , \tag{251}$$

for the non-associative flow response. The set of equations (245)–(251) are solved by a general elastic predictor-plastic corrector algorithm described in [66, 92], also in **Chapter 2**, which gives the consistent update of the stress tensor, plastic strain tensor, hardening variables and the algorithmically consistent elastic-plastic tangent modulus.

### 4.2.3. Space transformation: fictitious isotropic to real anisotropic

With the elastic-plastic stress tensor and tangent modulus in the fictitious isotropic space at hand, the corresponding real anisotropic counterparts are obtained by a straightforward transformation as follows

$$\boldsymbol{\sigma}^{\mathrm{ep}} = \mathbb{A}^{-1} : \overline{\boldsymbol{\sigma}}^{\mathrm{ep}} \quad \text{and} \quad \mathbb{E}^{\mathrm{ep}} = \mathbb{A}^{-1} : \overline{\mathbb{E}}^{\mathrm{ep}} : \mathbb{B} \; . \tag{252}$$

To describe the elastic-plastic deformation of unidirectional fibre-reinforced composite materials, the model proposed in [23, 24] requires the following material properties in the respective spaces:

TABLE 3: Material parameters for the MDPR models.

| No. | Name | Par. | Value | Unit |
|-----|------|------|-------|------|
| 1. | Longitudinal Young's modulus | $E_1$ | 130000 | [MPa] |
| 2. | Transverse Young's modulus | $E_2$ | 11000 | [MPa] |
| 3. | Longitudinal shear modulus | $G_{12}$ | 5800 | [MPa] |
| 4. | Transverse shear modulus | $G_{23}$ | 3720 | [MPa] |
| 5. | Poisson's ratio | $\nu_{12}$ | 0.306 | [−] |
| 6. | Coefficient of hydrostatic pressure | $\varkappa$ | $\begin{cases} 0.9497^a \\ 1.105^b \end{cases}$ | [−] |
| 7. | Initial yield stress | $y_0$ | 10.6 | [MPa] |
| 8. | Hardening modulus | $h$ | 237.9 | [MPa] |
| 10. | Pre-strain | $\bar{\xi}$ | $1\times10^{-12}$ | [−] |
| 11. | Hardening exponent | $n$ | 0.249 | [−] |

[a]Associative flow
[b]Non-associative flow

TABLE 4: Material parameters for the MCOO models.

| No. | Name | Par. | | Value | | Unit |
|-----|------|------|------|-------|------|------|
| 1. | Longitudinal Young's modulus | $E_1$ | | 130000 | | [MPa] |
| 2. | Transverse Young's modulus | $E_2$ | | 11000 | | [MPa] |
| 3. | Longitudinal shear modulus | $G_{12}$ | | 5800 | | [MPa] |
| 4. | Transverse shear modulus | $G_{23}$ | | 3720 | | [MPa] |
| 5. | Poisson's ratio | $\nu_{12}$ | | 0.306 | | [−] |
| 6. | Anisotropic space yield strengths | $\begin{cases} y_{11} \\ y_{22} \end{cases}$ | | $\begin{cases} \approx \infty \\ 158.6 \end{cases}$ | | [MPa] |
| 7. | Isotropic space yield strength | $y_{iso}$ | | 158.6 | | [MPa] |
| 8. | Coefficient of hydrostatic pressure | $\varkappa$ | | $\begin{cases} 1.931^a \\ 1.917^b \end{cases}$ | | [−] |
| 9. | Initial yield stress | $y_0$ | | 20.5 | | [MPa] |
| 10. | Hardening modulus | $h$ | | 415.7 | | [MPa] |
| 11. | Pre-strain | $\bar{\xi}$ | | $1\times10^{-12}$ | | [−] |
| 12. | Hardening exponent | $n$ | | 0.241 | | [−] |

[a]Associative flow
[b]Non-associative flow

- Real anisotropic space:

  - elastic parameters $\mu_{1-5}$,
  - yield strength tensor $\mathbf{Y}$.

- Fictitious isotropic space:

  - plastic parameters $\varkappa$, $y_0$, $h$, $\overline{\alpha}$ and $n$,
  - yield strength tensor $\overline{\mathbf{Y}}$.

Following [109], three different constitutive laws for the MDPR and MCOO models are implemented, namely

1. MDPR-a/MCOO-a: pressure-independent model, represented by Eqns. (227) and $\left[ (234)/(245) \right]\big|_{\varkappa=0}$ ,

2. MDPR-b/MCOO-b: associative pressure-dependent model, obtained by Eqns. (227) and (234)/(245) ,

3. MDPR-c/MCOO-c: non-associative pressure-dependent model, given by Eqns. (227), (234)/(245) and (237)/(249) .

## 4.3. Discussion

To illustrate the predictive capability of these models, the inelastic behaviour of a certain composite which has carbon fibres reinforced in a polymer matrix (AS4/PEEK) is considered. The pertinent experimental investigations are documented in [7]. The material parameters used in the numerical simulations are listed in Tables 3–4, and the elastic material parameters of the fictitious isotropic space are chosen to be $E = 4100$ MPa and $\nu_{12} = 0.356$. At first, predictions of the two aforementioned meso models are compared
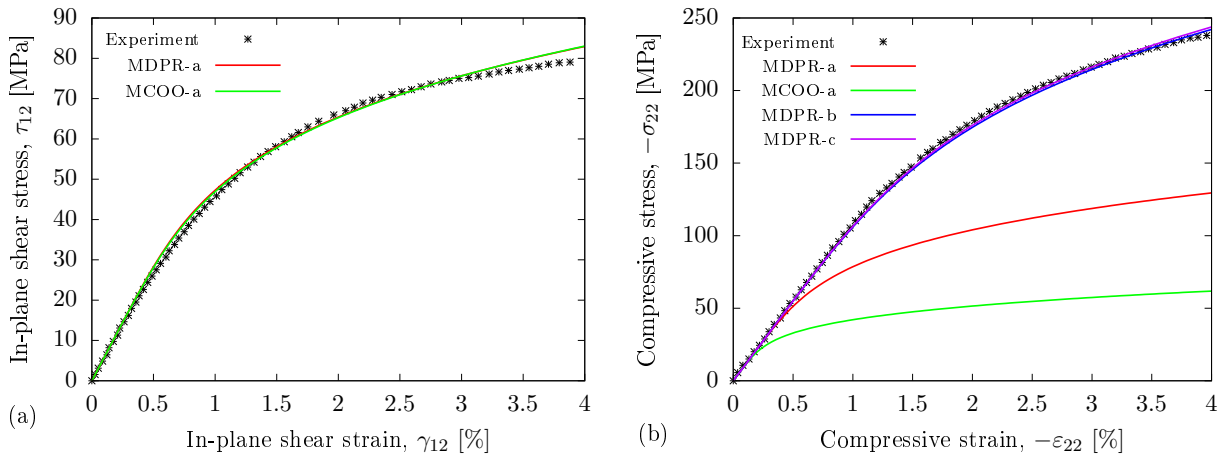


FIGURE 17: **Predictions for standard load cases.** Comparison of the experimental [7], and the two meso models responses for (a) in-plane shear and (b) transverse compression load.
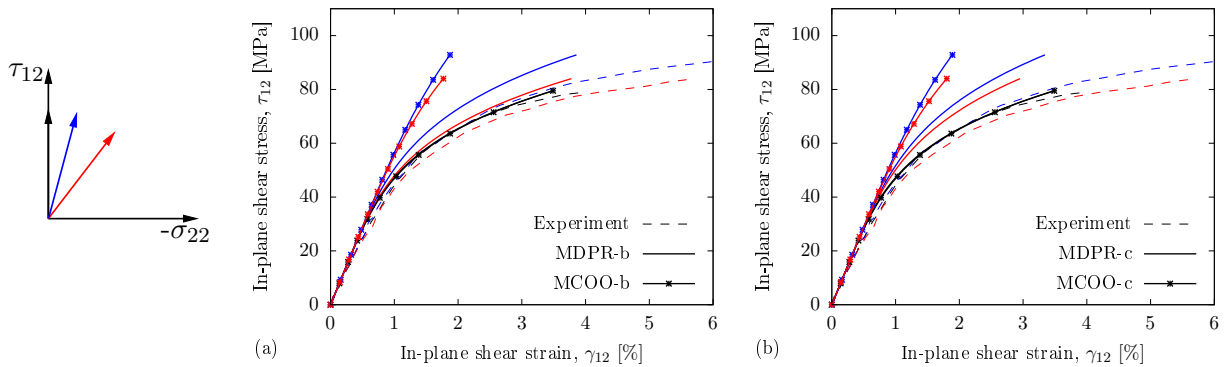


FIGURE 18: **Predictions for combined loads.** Comparison of the experimental [7], and the two meso models for combined shear-compression loads with (a) associative flow response and (b) non-associative flow response.

with that of the experiment [7] for the two standard test cases, namely the in-plane and transverse compression test case, as shown in Fig. 17. Though both the models reproduce the shear response accurately, as seen in Fig. 17 (a), the pressure-independent versions of these models underestimate the transverse compressive stress. It is clear that to overcome this deficiency, the constitutive formulation should be pressure-dependent, evident by the pressure-dependent models predictions in Fig. 17 (b).

Figures 18 (a) and (b) show a comparison of the associative and non-associative model predictions with that of the experimental results [7] respectively, for proportional loading where compression and shear stress are applied in proportion with each other. Three different proportionality factors are considered for the analyses such that $-\sigma_{22}/\tau_{12} = \{0, 0.98, 1, 96\}$. It can be seen that there is an observable deviation between models predictions and the biaxial experimental response. Additionally, the experimental results show that the overall material response first stiffens and then subsequently softens for increasing proportionality factors. This trend is also not reproduced by the two models.

The experimental investigations are affirmative to the fact that to realistically predict the non-linear behaviour of composite materials for different load combinations, the constitutive response must be pressure sensitive. Additionally, plastic response functions that are pressure-dependent but isotropic, need to be either mathematically manipulated [110,111] or extended to anisotropic forms to reproduce the experimentally observed biaxial response. Clearly, the stress tensor should be decomposed not just into volumetric and deviatoric components, but also into the respective normal and shear modes associated with the symmetry group. Only then can the experimental biaxial response be captured accurately on the meso scale. Furthermore, an argument in [112] suggests that a non-associative flow rule must be considered in order to eliminate the physical inconsistency caused by the associative flow rule under shear dominated loads. This aspect is examined in detail with the aid of representative numerical simulations appearing in **Chapter 7**. Recent studies have also shown that polymeric composites are rate sensitive [7], and exhibit kinematic hardening [113] for cyclic loads.

Based on these observations, a constitutive formulation of anisotropic plasticity is developed in the next chapter that overcomes the observed deficiencies of using isotropic dissipative response functions.

# 5. Anisotropic plasticity. Anisotropic dissipative response functions

This chapter is concerned with the formulation and numerical implementation of plasticity and viscoplasticity for fibre-reinforced composites from a continuum perspective. In this context, physically motivated, explicit forms of the energetic and dissipative response functions are proposed for the orthorhombic $\mathscr{C}_3$ and transversely isotropic $\mathscr{C}_{13}$ symmetry groups, based on the concepts discussed in **Chapters 2–3**. The proposed formulations account for anisotropic behaviour in the stress response, yield condition, flow rules and the hardening laws.

This chapter is organised as follows: energetic response functions for the $\mathscr{C}_3$ and $\mathscr{C}_{13}$ symmetry groups are formulated in Section 5.1. The mathematical structure of a combined non-linear hardening applicable to these symmetry groups is discussed. These material symmetry groups impose certain restrictions on the material response, which are taken into account by choosing a simple tensor basis to generate the constitutive equations. Although developments are restricted to $\mathscr{C}_3$ and $\mathscr{C}_{13}$ symmetry groups, they can be applied to other selected symmetry groups in a straightforward manner. Dissipative response functions for the aforementioned symmetry groups are formulated in the following section. A decoupled representation of the stress tensor in terms of hydrostatic pressure, fibre stress and the shear stress, originally introduced by Spencer [32], facilitates physically motivated modelling in this work. Additionally, non-quadratic yield functions are chosen so that the invariants are of the same order. A rate-independent setting is first considered and the models are constitutively framed within the associative and non-associative plasticity. The framework is eventually extended for a rate-dependent setting following conceptually [48,84]. Finally in Section 5.4, a finite element oriented algorithmic treatment of the models is provided where the resulting differential/algebraic equations are solved using an integration scheme. Specifically, the governing equations are solved using a predictor-corrector algorithm which imposes the constraint posed by the yield condition [66, 76].

At the outset, it is assumed that the anisotropy does not evolve during the course of plastic deformation. This assumption greatly simplifies the constitutive developments and is reasonably adequate for the geometrically linear framework as there is no change in the orientation of the individual grains (fibres) at small deformations. Furthermore, material properties in the two principal directions are assumed to be identical for the $\mathscr{C}_3$ symmetry group.

## 5.1. Energetic response functions

Recall here from Eqn. (91) the additive decomposition of the overall strain tensor

$$\boldsymbol{\varepsilon} = \boldsymbol{\varepsilon}^e + \boldsymbol{\varepsilon}^p \ , \tag{253}$$

into elastic and plastic parts respectively, where the latter one remains post stress relaxation [114]. With reference to Eqns. (92)–(94), define

$$\psi = \psi(\boldsymbol{\varepsilon} - \boldsymbol{\varepsilon}^p, \xi, \boldsymbol{\alpha}) \ , \tag{254}$$

to be a general form of the scalar energetic potential which has functional dependence on a suitable set $\boldsymbol{\mathfrak{c}} = \{\boldsymbol{\varepsilon}^p, \xi, \boldsymbol{\alpha}\}$ of internal variables. One of the underlying objectives of

this chapter is to formulate an explicit form of Eqn. (254) as an isotropic scalar-valued function by extending the set of arguments such that

$$\psi(\boldsymbol{Q} \star (\boldsymbol{\varepsilon} - \boldsymbol{\varepsilon}^p), \boldsymbol{Q} \star \xi, \boldsymbol{Q} \star \boldsymbol{\alpha}, \boldsymbol{Q} \star \boldsymbol{M}) = \psi(\boldsymbol{\varepsilon} - \boldsymbol{\varepsilon}^p, \xi, \boldsymbol{\alpha}, \boldsymbol{M}) \quad \forall \quad \boldsymbol{Q} \in \mathcal{O}(3) , \quad (255)$$

where the invariance of the structural tensor for a given symmetry group is already assumed, i.e. $\boldsymbol{Q} \star \boldsymbol{M} = \boldsymbol{M} \quad \forall \quad \boldsymbol{Q} \in \mathcal{C}$. Thus, a particular class of anisotropy is solely determined by the material symmetry group of the structural tensors.

### 5.1.1. Orthorhombic symmetry group

Appealing to **Chapter 3**, the integrity basis to describe the elastic stored energy is defined analogous to Eqn. (192) as

$$\tilde{\mathcal{I}}_{\mathcal{C}_3} = \{\operatorname{tr}[\boldsymbol{m}_1(\boldsymbol{\varepsilon} - \boldsymbol{\varepsilon}^p)], \operatorname{tr}[\boldsymbol{m}_2(\boldsymbol{\varepsilon} - \boldsymbol{\varepsilon}^p)], \operatorname{tr}[\boldsymbol{m}_3(\boldsymbol{\varepsilon} - \boldsymbol{\varepsilon}^p)], \operatorname{tr}^2[\boldsymbol{m}_{12}(\boldsymbol{\varepsilon} - \boldsymbol{\varepsilon}^p)],$$
$$\operatorname{tr}^2[\boldsymbol{m}_{13}(\boldsymbol{\varepsilon} - \boldsymbol{\varepsilon}^p)], \operatorname{tr}^2[\boldsymbol{m}_{23}(\boldsymbol{\varepsilon} - \boldsymbol{\varepsilon}^p)], \det[(\boldsymbol{\varepsilon} - \boldsymbol{\varepsilon}^p)]\} . \quad (256)$$

Due to the assumption of a decoupled energetic potential, the integrity basis to describe the plastic part of the stored energy can be defined analogous to Eqn. (256) as

$$\tilde{\mathcal{K}}_{\mathcal{C}_3} = \{\operatorname{tr}[\boldsymbol{m}_1\boldsymbol{\alpha}], \operatorname{tr}[\boldsymbol{m}_2\boldsymbol{\alpha}], \operatorname{tr}[\boldsymbol{m}_3\boldsymbol{\alpha}], \operatorname{tr}^2[\boldsymbol{m}_{12}\boldsymbol{\alpha}], \operatorname{tr}^2[\boldsymbol{m}_{13}\boldsymbol{\alpha}], \operatorname{tr}^2[\boldsymbol{m}_{23}\boldsymbol{\alpha}], \det[\boldsymbol{\alpha}]\} . \quad (257)$$

With Eqns. (256)–(257) at hand, a decoupled form of the scalar energetic potential (94) is given by

$$\psi(\boldsymbol{\varepsilon} - \boldsymbol{\varepsilon}^p, \xi, \boldsymbol{\alpha}, \boldsymbol{m}_1, \boldsymbol{m}_2, \boldsymbol{m}_3) = \psi^e(\boldsymbol{\varepsilon} - \boldsymbol{\varepsilon}^p, \boldsymbol{m}_1, \boldsymbol{m}_2, \boldsymbol{m}_3) + \psi^p_{\mathrm{iso}}(\xi) + \psi^p_{\mathrm{kin}}(\boldsymbol{\alpha}, \boldsymbol{m}_1, \boldsymbol{m}_2, \boldsymbol{m}_3)$$
$$= \psi^e(I_1, \cdots, I_6) + \psi^p_{\mathrm{iso}}(\xi) + \psi^p_{\mathrm{kin}}(K_1, \cdots, K_6) \quad , \quad (258)$$

where $I_{1-6}$ and $K_{1-6}$ are the first six elements of the integrity bases $\tilde{\mathcal{I}}_{\mathcal{C}_3}$ and $\tilde{\mathcal{K}}_{\mathcal{C}_3}$, respectively. The individual energetic contributions take the explicit form

$$\psi^e(I_1, \cdots, I_6) = \frac{\mu_1}{2}I_1^2 + \frac{\mu_2}{2}I_2^2 + \frac{\mu_3}{2}I_3^2 + \mu_4 I_1 I_2 + \mu_5 I_1 I_3 + \mu_6 I_2 I_3$$
$$+ \frac{\mu_7}{2}I_4 + \frac{\mu_8}{2}I_5 + \frac{\mu_9}{2}I_6$$

$$\psi^p_{\mathrm{iso}}(\xi) = \frac{h}{n+1}(\bar{\xi} + \xi)^{n+1} \quad , \quad (259)$$

$$\psi^p_{\mathrm{kin}}(K_1, \cdots, K_6) = \frac{\vartheta_1}{2}K_1^2 + \frac{\vartheta_2}{2}K_2^2 + \frac{\vartheta_3}{2}K_3^2 + \vartheta_4 K_1 K_2 + \vartheta_5 K_1 K_3 + \vartheta_6 K_2 K_3$$
$$+ \frac{\vartheta_7}{2}K_4 + \frac{\vartheta_8}{2}K_5 + \frac{\vartheta_9}{2}K_6$$

where a quadratic and linear relation is used to describe the elastic and kinematic hardening parts of the energetic potentials. Power law based hardening represents the nonlinearity in the isotropic hardening part of the energetic potential. Note that the nonlinearity in kinematic hardening is taken into account by plastic response functions, as seen subsequently. The material parameters $\vartheta_{1-9}$ are associated with kinematic hardening. Taking into account the representation (259), the reduced dissipation inequality can be evaluated in line with Eqn. (95) as

$$\mathscr{D}^{\mathrm{red}} = -\psi_{,\boldsymbol{\varepsilon}} \cdot \dot{\boldsymbol{\varepsilon}} = -\psi_{,\boldsymbol{\varepsilon}^p} : \dot{\boldsymbol{\varepsilon}}^p - \psi_{,\xi} \dot{\xi} - \psi_{,\boldsymbol{\alpha}} : \dot{\boldsymbol{\alpha}} \geq 0 , \quad (260)$$

which leads to the definition of the stress tensor and driving forces associated with the potential (259) as

$$
\begin{aligned}
\boldsymbol{\sigma} &= +\psi^e(I_1, \cdots, I_6)_{,(\varepsilon-\varepsilon^p)} = \sum_{i=1}^{6} \psi^e(I_1, \cdots, I_6)_{,I_i}\, I_{i,(\varepsilon-\varepsilon^p)} \\
\kappa &= -\psi_{\mathrm{iso}}^p(\xi)_{,\xi} \\
\boldsymbol{\beta} &= -\psi_{\mathrm{kin}}^p(K_1, \cdots, K_6)_{,\boldsymbol{\alpha}} = -\sum_{i=1}^{6} \psi_{\mathrm{kin}}^p(K_1, \cdots, K_6)_{,K_i}\, K_{i,\boldsymbol{\alpha}}
\end{aligned}
\qquad, \qquad (261)
$$

where the individual terms can be explicitly expressed based on Eqns. (195)–(196) as

$$
\begin{aligned}
\boldsymbol{\sigma} =\ & \mu_1 I_1 \boldsymbol{m}_1 + \mu_2 I_2 \boldsymbol{m}_2 + \mu_3 I_3 \boldsymbol{m}_3 \\
& + (\mu_4 I_2 + \mu_5 I_3)\boldsymbol{m}_1 + (\mu_4 I_1 + \mu_6 I_3)\boldsymbol{m}_2 + (\mu_5 I_1 + \mu_6 I_2)\boldsymbol{m}_3 \\
& + \mu_7 \operatorname{tr}[\boldsymbol{m}_{12}(\boldsymbol{\varepsilon} - \boldsymbol{\varepsilon}^p)]\boldsymbol{m}_{12} + \mu_8 \operatorname{tr}[\boldsymbol{m}_{13}(\boldsymbol{\varepsilon} - \boldsymbol{\varepsilon}^p)]\boldsymbol{m}_{13} + \mu_9 \operatorname{tr}[\boldsymbol{m}_{23}(\boldsymbol{\varepsilon} - \boldsymbol{\varepsilon}^p)]\boldsymbol{m}_{23} \\[4pt]
\kappa =\ & -h(\bar{\xi} + \xi)^n \\[4pt]
\boldsymbol{\beta} =\ & -\{\vartheta_1 K_1 \boldsymbol{m}_1 + \vartheta_2 K_2 \boldsymbol{m}_2 + \vartheta_3 K_3 \boldsymbol{m}_3 \\
& + (\vartheta_4 K_2 + \vartheta_5 K_3)\boldsymbol{m}_1 + (\vartheta_4 K_1 + \vartheta_6 K_3)\boldsymbol{m}_2 + (\vartheta_5 K_1 + \vartheta_6 K_2)\boldsymbol{m}_3 \\
& + \vartheta_7 \operatorname{tr}[\boldsymbol{m}_{12}\boldsymbol{\alpha}]\boldsymbol{m}_{12} + \vartheta_8 \operatorname{tr}[\boldsymbol{m}_{13}\boldsymbol{\alpha}]\boldsymbol{m}_{13} + \vartheta_9 \operatorname{tr}[\boldsymbol{m}_{23}\boldsymbol{\alpha}]\boldsymbol{m}_{23}\}
\end{aligned}
\qquad. \qquad (262)
$$

Letting $\mathfrak{f} = -\psi_{,\mathfrak{e}} = \{\boldsymbol{\sigma}, \kappa, \boldsymbol{\beta}\}$ be the set of conjugate thermodynamic driving forces which are dual to the set of internal variables, Eqn. (260) can be expressed in a compact form analogous to Eqn. (97).

The fourth-order elasticity tensor, isotropic hardening modulus and the fourth-order kinematic hardening tensor, which are necessary for further developments can be expressed with the aid of Eqn. (198) as

$$
\begin{aligned}
\mathbb{E} &= \psi^e_{,(\varepsilon-\varepsilon^p)(\varepsilon-\varepsilon^p)} = \sum_{i=1}^{6}\sum_{j=1}^{6} \psi^e_{,I_i}\, I_{i,(\varepsilon-\varepsilon^p)(\varepsilon-\varepsilon^p)} + \psi^e_{,I_i I_j}\, I_{i,(\varepsilon-\varepsilon^p)} \otimes I_{j,(\varepsilon-\varepsilon^p)} \\
\mathrm{H} &= -\psi_{\mathrm{iso}}^p{}_{,\xi\xi} \\
\mathbb{H} &= -\psi_{\mathrm{kin}}^p{}_{,\boldsymbol{\alpha}\boldsymbol{\alpha}} = -\sum_{i=1}^{6}\sum_{j=1}^{6} \psi_{\mathrm{kin}}^p{}_{,K_i}\, K_{i,\boldsymbol{\alpha}\boldsymbol{\alpha}} + \psi_{\mathrm{kin}}^p{}_{,K_i K_j}\, K_{i,\boldsymbol{\alpha}} \otimes K_{j,\boldsymbol{\alpha}}
\end{aligned}
\qquad. \qquad (263)
$$

The first and second derivatives in the above equation are similar to those in Eqns. (195)–

(200), based on which the individual terms in Eqn. (263) take the explicit form

$$
\begin{aligned}
\mathbb{E}=&\mu_1 \boldsymbol{m}_1 \otimes \boldsymbol{m}_1 + \mu_2 \boldsymbol{m}_2 \otimes \boldsymbol{m}_2 + \mu_3 \boldsymbol{m}_3 \otimes \boldsymbol{m}_3 + \mu_4(\boldsymbol{m}_1 \otimes \boldsymbol{m}_2 + \boldsymbol{m}_2 \otimes \boldsymbol{m}_1) \\
&+\mu_5(\boldsymbol{m}_1 \otimes \boldsymbol{m}_3 + \boldsymbol{m}_3 \otimes \boldsymbol{m}_1) + \mu_6(\boldsymbol{m}_2 \otimes \boldsymbol{m}_3 + \boldsymbol{m}_3 \otimes \boldsymbol{m}_2) \\
&+\mu_7 \boldsymbol{m}_{12} \otimes \boldsymbol{m}_{12} + \mu_8 \boldsymbol{m}_{13} \otimes \boldsymbol{m}_{13} + \mu_9 \boldsymbol{m}_{23} \otimes \boldsymbol{m}_{23} \\
\mathrm{H}=&-nh(\bar{\xi} + \xi)^{n-1} \\
\mathbb{H}=&-\{\vartheta_1 \boldsymbol{m}_1 \otimes \boldsymbol{m}_1 + \vartheta_2 \boldsymbol{m}_2 \otimes \boldsymbol{m}_2 + \vartheta_3 \boldsymbol{m}_3 \otimes \boldsymbol{m}_3 + \vartheta_4(\boldsymbol{m}_1 \otimes \boldsymbol{m}_2 + \boldsymbol{m}_2 \otimes \boldsymbol{m}_1) \\
&+\vartheta_5(\boldsymbol{m}_1 \otimes \boldsymbol{m}_3 + \boldsymbol{m}_3 \otimes \boldsymbol{m}_1) + \vartheta_6(\boldsymbol{m}_2 \otimes \boldsymbol{m}_3 + \boldsymbol{m}_3 \otimes \boldsymbol{m}_2) \\
&+\vartheta_7 \boldsymbol{m}_{12} \otimes \boldsymbol{m}_{12} + \vartheta_8 \boldsymbol{m}_{13} \otimes \boldsymbol{m}_{13} + \vartheta_9 \boldsymbol{m}_{23} \otimes \boldsymbol{m}_{23}\}
\end{aligned}
\tag{264}
$$

### 5.1.2. Transversely isotropic symmetry group

For the transversely isotropic symmetry group, the integrity basis to describe the elastic stored energy is defined analogous to Eqn. (214) as

$$
\begin{aligned}
\tilde{\mathcal{I}}_{\mathscr{C}_{13}} = \{&\mathrm{tr}[\boldsymbol{m}(\boldsymbol{\varepsilon} - \boldsymbol{\varepsilon}^p)], \mathrm{tr}[(\boldsymbol{1} - \boldsymbol{m})(\boldsymbol{\varepsilon} - \boldsymbol{\varepsilon}^p)], \mathrm{tr}[\boldsymbol{m}(\boldsymbol{\varepsilon} - \boldsymbol{\varepsilon}^p)^2], \\
&\mathrm{tr}[(\frac{1}{2}\boldsymbol{1} - \boldsymbol{m})(\boldsymbol{\varepsilon} - \boldsymbol{\varepsilon}^p)^2], \det[(\boldsymbol{\varepsilon} - \boldsymbol{\varepsilon}^p)]\} .
\end{aligned}
\tag{265}
$$

Likewise, the integrity basis to describe the plastic stored energy can be defined as

$$
\tilde{\mathcal{K}}_{\mathscr{C}_{13}} = \{\mathrm{tr}[\boldsymbol{m}\boldsymbol{\alpha}], \mathrm{tr}[(\boldsymbol{1} - \boldsymbol{m})\boldsymbol{\alpha}], \mathrm{tr}[\boldsymbol{m}\boldsymbol{\alpha}^2], \mathrm{tr}[(\frac{1}{2}\boldsymbol{1} - \boldsymbol{m})\boldsymbol{\alpha}^2], \det[\boldsymbol{\alpha}]\} .
\tag{266}
$$

With Eqns. (265)–(266) at hand, a decoupled scalar energetic potential (94) is given by

$$
\begin{aligned}
\psi(\boldsymbol{\varepsilon} - \boldsymbol{\varepsilon}^p, \xi, \boldsymbol{\alpha}, \boldsymbol{m})=&\psi^e(\boldsymbol{\varepsilon} - \boldsymbol{\varepsilon}^p, \boldsymbol{m}) + \psi_{\mathrm{iso}}^p(\xi) + \psi_{\mathrm{kin}}^p(\boldsymbol{\alpha}, \boldsymbol{m}) \\
=&\psi^e(I_1, \cdots, I_4) + \psi_{\mathrm{iso}}^p(\xi) + \psi_{\mathrm{kin}}^p(K_1, \cdots, K_4)
\end{aligned}
\tag{267}
$$

where $I_{1-4}$ and $K_{1-4}$ are the first four elements of the integrity bases $\tilde{\mathcal{I}}_{\mathscr{C}_{13}}$ and $\tilde{\mathcal{K}}_{\mathscr{C}_{13}}$, respectively. The individual energetic contributions are assumed to be

$$
\begin{aligned}
\psi^e(I_1, \cdots, I_4)=&\frac{\mu_1}{2}I_1^2 + \frac{\mu_2}{2}I_2^2 + \mu_3 I_1 I_2 + 2\mu_4 I_3 + 2\mu_5 I_4 \\
\psi_{\mathrm{iso}}^p(\xi)=&\frac{h}{n+1}(\bar{\xi} + \xi)^{n+1} \\
\psi_{\mathrm{kin}}^p(K_1, \cdots, K_4)=&\frac{\vartheta_1}{2}K_1^2 + \frac{\vartheta_2}{2}K_2^2 + \vartheta_3 K_1 K_2 + 2\vartheta_4 K_3 + 2\vartheta_5 K_4
\end{aligned}
\tag{268}
$$

With these definitions, the rate of the scalar energetic potential can be evaluated as

$$
\dot{\psi} = \frac{d}{dt}\psi = \psi_{,(\boldsymbol{\varepsilon} - \boldsymbol{\varepsilon}^p)} : (\dot{\boldsymbol{\varepsilon}} - \dot{\boldsymbol{\varepsilon}}^p) + \psi_{,\xi}\,\dot{\xi} + \psi_{,\boldsymbol{\alpha}} : \dot{\boldsymbol{\alpha}} ,
\tag{269}
$$

which contains the stress tensor and driving forces, namely

$$\boldsymbol{\sigma} = +\psi_{,(\varepsilon-\varepsilon^p)} = +\psi^e(I_1,\cdots,I_4)_{,(\varepsilon-\varepsilon^p)} = \sum_{i=1}^{4} \psi^e(I_1,\cdots,I_4)_{,I_i} I_{i,(\varepsilon-\varepsilon^p)}$$

$$\kappa = -\psi_{,\xi} = -\psi^p_{\text{iso}}(\xi)_{,\xi}$$

$$\boldsymbol{\beta} = -\psi_{,\boldsymbol{\alpha}} = -\psi^p_{\text{kin}}(K_1,\cdots,K_4)_{,\boldsymbol{\alpha}} = -\sum_{i=1}^{4} \psi^p_{\text{kin}}(K_1,\cdots,K_4)_{,K_i} K_{i,\boldsymbol{\alpha}}$$

$$. \qquad (270)$$

The closed form expressions of the individual terms in the above equation are given by

$$
\boxed{
\begin{aligned}
\boldsymbol{\sigma} &= (\mu_1 I_1 + \mu_3 I_2)\boldsymbol{m} + (\mu_2 I_2 + \mu_3 I_1)(\boldsymbol{1} - \boldsymbol{m}) \\
&\quad + 2\mu_4\{\boldsymbol{m}(\varepsilon - \varepsilon^p) + (\varepsilon - \varepsilon^p)\boldsymbol{m}\} + 2\mu_5\{(\varepsilon - \varepsilon^p) - [\boldsymbol{m}(\varepsilon - \varepsilon^p) + (\varepsilon - \varepsilon^p)\boldsymbol{m}]\} \\
\kappa &= -h(\bar{\xi} + \xi)^n \\
\boldsymbol{\beta} &= -\big\{(\vartheta_1 K_1 + \vartheta_3 K_2)\boldsymbol{m} + (\vartheta_2 K_2 + \vartheta_3 K_1)(\boldsymbol{1} - \boldsymbol{m}) \\
&\qquad + 2\vartheta_4\{\boldsymbol{m}\boldsymbol{\alpha} + \boldsymbol{\alpha}\boldsymbol{m}\} + 2\vartheta_5\{\boldsymbol{\alpha} - [\boldsymbol{m}\boldsymbol{\alpha} + \boldsymbol{\alpha}\boldsymbol{m}]\}\big\}
\end{aligned}
}
\qquad .
$$

$$(271)$$

The fourth-order elasticicty tensor, isotropic hardening modulus and the fourth-order kinematic hardening tensor can be expressed similar to the previous case as

$$
\boxed{
\begin{aligned}
\mathbb{E} &= \mu_1 \boldsymbol{m} \otimes \boldsymbol{m} + \mu_2(\boldsymbol{1} - \boldsymbol{m}) \otimes (\boldsymbol{1} - \boldsymbol{m}) \\
&\quad + \mu_3\big\{\boldsymbol{m} \otimes (\boldsymbol{1} - \boldsymbol{m}) + (\boldsymbol{1} - \boldsymbol{m}) \otimes \boldsymbol{m}\big\} \\
&\quad + \mu_4\big\{(\boldsymbol{1} \oplus \boldsymbol{m}) + (\boldsymbol{1} \ominus \boldsymbol{m}) + (\boldsymbol{m} \oplus \boldsymbol{1}) + (\boldsymbol{m} \ominus \boldsymbol{1})\big\} \\
&\quad + \mu_5\big\{(\boldsymbol{1} \oplus \boldsymbol{1}) + (\boldsymbol{1} \ominus \boldsymbol{1}) - (\boldsymbol{1} \oplus \boldsymbol{m}) - (\boldsymbol{1} \ominus \boldsymbol{m}) - (\boldsymbol{m} \oplus \boldsymbol{1}) - (\boldsymbol{m} \ominus \boldsymbol{1})\big\} \\
\mathrm{H} &= -nh(\bar{\xi} + \xi)^{n-1} \\
\mathbb{H} &= -\Big\{\vartheta_1 \boldsymbol{m} \otimes \boldsymbol{m} + \vartheta_2(\boldsymbol{1} - \boldsymbol{m}) \otimes (\boldsymbol{1} - \boldsymbol{m}) \\
&\qquad + \vartheta_3\big\{\boldsymbol{m} \otimes (\boldsymbol{1} - \boldsymbol{m}) + (\boldsymbol{1} - \boldsymbol{m}) \otimes \boldsymbol{m}\big\} \\
&\qquad + \vartheta_4\big\{(\boldsymbol{1} \oplus \boldsymbol{m}) + (\boldsymbol{1} \ominus \boldsymbol{m}) + (\boldsymbol{m} \oplus \boldsymbol{1}) + (\boldsymbol{m} \ominus \boldsymbol{1})\big\} \\
&\qquad + \vartheta_5\big\{(\boldsymbol{1} \oplus \boldsymbol{1}) + (\boldsymbol{1} \ominus \boldsymbol{1}) - (\boldsymbol{1} \oplus \boldsymbol{m}) - (\boldsymbol{1} \ominus \boldsymbol{m}) - (\boldsymbol{m} \oplus \boldsymbol{1}) - (\boldsymbol{m} \ominus \boldsymbol{1})\big\}\Big\}
\end{aligned}
}
\qquad .
$$

$$(272)$$

## 5.2. Dissipative response functions

As discussed in **Chapter 2**, the evolution of internal variables should also be constitutively prescribed in line with Eqn. (260), besides the scalar energetic function. This can be achieved with the help of plastic response functions, which in the present work are based on a physically motivated decomposition of the stress tensor [32]. This additive split ensures a precise formulation of the plastic response functions for composite materials based on the following essential features:

1. For fibre-reinforced composite materials, the plastic response is independent of stress in the fibre directions [32, 43, 115].

2. The yield behaviour of some composites is significantly affected by the hydrostatic pressure [116]. Therefore, pressure-dependent plastic response functions are formulated which can also reproduce the pressure-independent behaviour for a particular choice of the governing coefficients.

3. Plastic yielding should be governed by limited number of coefficients.

In what follows, explicit forms of the dissipative response functions, namely the non-quadratic yield function, flow and hardening rules are derived for the two selected symmetry groups. Although higher order yield functions are accurate, they require higher number of coefficients that must be obtained experimentally [117].

### 5.2.1. Orthorhombic symmetry group

The dissipative response functions for the $\mathscr{C}_3$ symmetry group are formulated based on the definition of a plasticity inducing stress tensor $\mathfrak{s}$, which is *deviatoric* and *stress free in the preferred directions* such that

$$\mathrm{tr}[\mathfrak{s}] = 0, \quad \mathrm{tr}[\boldsymbol{m}_1 \mathfrak{s}] = 0 \quad \text{and} \quad \mathrm{tr}[\boldsymbol{m}_2 \mathfrak{s}] = 0 \implies \mathrm{tr}[\boldsymbol{m}_3 \mathfrak{s}] = 0 \ . \tag{273}$$

These conditions lead to the definition of $\mathfrak{s}$ in terms of the relative stress tensor $\boldsymbol{\Sigma} = \boldsymbol{\sigma} + \boldsymbol{\beta}$, for given $\boldsymbol{m}_{1-3}$ as

$$\mathfrak{s} = \boldsymbol{\Sigma} - \mathrm{tr}[\boldsymbol{m}_3 \boldsymbol{\Sigma}]\boldsymbol{1} + \mathrm{tr}[(\boldsymbol{m}_3 - \boldsymbol{m}_1)\boldsymbol{\Sigma}]\boldsymbol{m}_1 + \mathrm{tr}[(\boldsymbol{m}_3 - \boldsymbol{m}_2)\boldsymbol{\Sigma}]\boldsymbol{m}_2 \ , \tag{274}$$

see also [32]. In line with Eqn. (188), an isotropic yield function can be defined as

$$\chi(\boldsymbol{Q} \star \boldsymbol{\Sigma}, \boldsymbol{Q} \star \boldsymbol{m}_1, \boldsymbol{Q} \star \boldsymbol{m}_2, \boldsymbol{Q} \star \boldsymbol{m}_3, \kappa) = \chi(\boldsymbol{\Sigma}, \boldsymbol{m}_1, \boldsymbol{m}_2, \boldsymbol{m}_3, \kappa) \quad \forall \quad \boldsymbol{Q} \in \mathcal{O}(3) \ . \tag{275}$$

To specify the yield function, an integrity basis similar to Eqn. (256) or (257) is necessary. Taking into account Eqn. (273), the integrity basis can be specified as

$$\hat{\mathcal{J}}_{\mathscr{C}_3} = \{\mathrm{tr}[\boldsymbol{m}_1 \boldsymbol{\Sigma}], \mathrm{tr}[\boldsymbol{m}_2 \boldsymbol{\Sigma}], \mathrm{tr}[\boldsymbol{m}_3 \boldsymbol{\Sigma}], \mathrm{tr}^2[\boldsymbol{m}_{12}\mathfrak{s}], \mathrm{tr}^2[\boldsymbol{m}_{13}\mathfrak{s}], \mathrm{tr}^2[\boldsymbol{m}_{23}\mathfrak{s}], \det[\mathfrak{s}]\} \ , \tag{276}$$

where $\boldsymbol{m}_{12}, \boldsymbol{m}_{13}$ and $\boldsymbol{m}_{23}$ are introduced in Eqn. (190). The linear invariants in the above set characterise the normal modes, while the quadratic invariants represent the shear modes. To incorporate the aforementioned features, the integrity basis (276) is reformulated as

$$\widetilde{\mathcal{J}}_{\mathscr{C}_3} = \{\mathrm{tr}[\boldsymbol{m}_3 \boldsymbol{\Sigma}], \frac{9}{4} \mathrm{tr}^2[\boldsymbol{m}_3' \boldsymbol{\Sigma}], \mathrm{tr}^2[\boldsymbol{m}_{12}\mathfrak{s}], \mathrm{tr}^2[\boldsymbol{m}_{13}\mathfrak{s}], \mathrm{tr}^2[\boldsymbol{m}_{23}\mathfrak{s}], \det[\mathfrak{s}]\} \ , \tag{277}$$

with $\boldsymbol{m}_3' = \boldsymbol{m}_3 - \frac{1}{3}\boldsymbol{1}$. The first two invariants in the equation above represent the volumetric and deviatoric components of the relative stress tensor respectively, in the third principal direction. Recall here that the invariant representing a deviatoric component of the relative stress tensor $\boldsymbol{\Sigma}$ in the direction $\boldsymbol{m}_3$ is given by

$$\tilde{J}_2 = \frac{3}{2} \mathrm{tr}[\boldsymbol{m}_3 \mathrm{dev}[\boldsymbol{\Sigma}]] = \frac{3}{2} \mathrm{tr}[\boldsymbol{m}_3' \boldsymbol{\Sigma}] \quad \text{with} \quad \mathrm{dev}[\boldsymbol{\Sigma}] = \boldsymbol{\Sigma} - \frac{1}{3} \mathrm{tr}[\boldsymbol{\Sigma}]\boldsymbol{1} \ . \tag{278}$$

The square of this invariant, given by the second element in (277), is usually considered in the formulation of scalar potentials with a decoupled volumetric-deviatoric split [109].

**5.2.1.1.  Yield function.** With the preceding definitions at hand, a pressure-dependent yield function for the $\mathscr{C}_3$ symmetry group is proposed in the stress space as

$$\chi = \left[ \varkappa_1 \tilde{J}_1 + \left\{ \varkappa_2 \tilde{J}_2 + \frac{\varkappa_3}{2} \tilde{J}_3 + \frac{\varkappa_4}{2} \tilde{J}_4 + \frac{\varkappa_5}{2} \tilde{J}_5 \right\}^{1/2} - \left( 1 - \frac{\kappa}{y_{12}} \right) \right. $$

$$\left. + \zeta_1 \tilde{J}_2 |_{\sigma=o} + \frac{\zeta_2}{2} \tilde{J}_3 |_{\sigma=o} + \frac{\zeta_3}{2} \tilde{J}_4 |_{\sigma=o} + \frac{\zeta_4}{2} \tilde{J}_5 |_{\sigma=o} \right] \leq 0 \tag{279}$$

where $\varkappa_{1-5}, \zeta_{1-5}$ and $y_{12}$ are material parameters, and $\tilde{J}_{1-5}$ are the elements of the integrity basis (276), respectively. It can be seen that the orthotropic pressure-dependent plastic yielding is governed by five material parameters $\varkappa_{1-5}$. These parameters are related to initial threshold yield stress $y_{ij}$, associated with the principal directions of the orthotropy. Further, they are determined by two normal and three shear tests at fixed orientations $\boldsymbol{a}_1 = [1, 0, 0]^T$ and $\boldsymbol{a}_2 = [0, 1, 0]^T$, with $\kappa = 0$ and $\boldsymbol{\beta} = \boldsymbol{0}$ as follows:
<u>uniaxial tension test in 3-direction</u>

$$\boldsymbol{\sigma} = \begin{bmatrix} 0 & 0 & 0 \\ & 0 & 0 \\ \text{sym.} & & y_{33} \end{bmatrix} \implies \left. \begin{array}{l} \tilde{J}_1 = y_{33} \\ \tilde{J}_2 = y_{33}^2 \\ \tilde{J}_3 = 0 \\ \tilde{J}_4 = 0 \\ \tilde{J}_5 = 0 \end{array} \right\} , \tag{280}$$

<u>uniaxial compression test in 3-direction</u>

$$\boldsymbol{\sigma} = \begin{bmatrix} 0 & 0 & 0 \\ & 0 & 0 \\ \text{sym.} & & -y_{33} \end{bmatrix} \implies \left. \begin{array}{l} \tilde{J}_1 = -y_{33} \\ \tilde{J}_2 = y_{33}^2 \\ \tilde{J}_3 = 0 \\ \tilde{J}_4 = 0 \\ \tilde{J}_5 = 0 \end{array} \right\} , \tag{281}$$

<u>shear test in 12-plane</u>

$$\boldsymbol{\sigma} = \begin{bmatrix} 0 & y_{12} & 0 \\ & 0 & 0 \\ \text{sym.} & & 0 \end{bmatrix} \implies \left. \begin{array}{l} \tilde{J}_1 = 0 \\ \tilde{J}_2 = 0 \\ \tilde{J}_3 = 4y_{12}^2 \\ \tilde{J}_4 = 0 \\ \tilde{J}_5 = 0 \end{array} \right\} , \tag{282}$$

<u>shear test in 13-plane</u>

$$\boldsymbol{\sigma} = \begin{bmatrix} 0 & 0 & y_{13} \\ & 0 & 0 \\ \text{sym.} & & 0 \end{bmatrix} \implies \left. \begin{array}{l} \tilde{J}_1 = 0 \\ \tilde{J}_2 = 0 \\ \tilde{J}_3 = 0 \\ \tilde{J}_4 = 4y_{13}^2 \\ \tilde{J}_5 = 0 \end{array} \right\} , \tag{283}$$

shear test in 23-plane

$$\boldsymbol{\sigma} = \begin{bmatrix} 0 & 0 & 0 \\ & 0 & 0 \\ \text{sym}. & & y_{23} \end{bmatrix} \quad \Longrightarrow \quad \left.\begin{array}{l} \tilde{J}_1 = 0 \\ \tilde{J}_2 = 0 \\ \tilde{J}_3 = 0 \\ \tilde{J}_4 = 0 \\ \tilde{J}_5 = 4y_{23}^2 \end{array}\right\} . \quad (284)$$

Evaluation of the yield criterion (279) for the choice $\boldsymbol{a}_1 = [1, 0, 0]^T$, $\boldsymbol{a}_2 = [0, 1, 0]^T$, $\kappa = 0$ and $\boldsymbol{\beta} = \boldsymbol{0}$ leads to the following definitions of the parameters

$$\varkappa_1 = \frac{-1}{y_{33}} , \qquad \varkappa_2 = \frac{1}{4y_{33}^2} ,$$

$$\varkappa_3 = \frac{1}{2y_{12}^2} , \qquad \varkappa_4 = \frac{1}{2y_{13}^2} \quad \text{and} \quad \varkappa_5 = \frac{1}{2y_{23}^2} . \quad (285)$$

Note that the chosen tests serve only as examples of a possible set of tests. Indeed, they can be replaced by other tests based on the available data. A comparison of the yield function in Eqn. (279) to Hill's orthotropic yield function [25] is provided in Appendix B.

**5.2.1.2. Convexity of the yield surface.** In what follows, convexity of the yield surface (279) is demonstrated in line with the ideas outlined in **Chapter 2**. Mathematically it is proved that the Hessian matrix $\mathbb{F}$ of this function is positive semi-definite, i.e. its eigenvalues are all positive or zero, thereby implying the non-negativity of plastic dissipation [118]. To this end, rewrite the yield function (279) in component form with $\kappa = 0$ and $\boldsymbol{\beta} = \boldsymbol{0}$ as

$$\chi = \varkappa_1 \sigma_{33} + \left[ \varkappa_2 \frac{(2\sigma_{33} - \sigma_{22} - \sigma_{11})^2}{4} + 2\varkappa_3 \sigma_{12}^2 + 2\varkappa_4 \sigma_{13}^2 + 2\varkappa_5 \sigma_{23}^2 \right]^{1/2} - 1 \leq 0 . \quad (286)$$

To determine if the equation above is convex, recall here that if $n$-functions $f_1, \dots, f_n$ are convex, then any weighted combination $\sum_{i=1}^n w_i f_i$ is also convex for $w_i > 0$. Starting with the first term in Eqn. (286), namely $\varkappa_1 \sigma_{33}$, it can be immediately deduced that the Hessian of this term is positive semi-definite which implies that this term is a convex function. To prove that the bracketed term is convex, it is first equivalently expressed as

$$\left[ \varkappa_2 \frac{(2\sigma_{33} - \sigma_{22} - \sigma_{11})^2}{4} + 2\varkappa_3 \sigma_{12}^2 + 2\varkappa_4 \sigma_{13}^2 + 2\varkappa_5 \sigma_{23}^2 \right]^{1/2}$$

$$= \left\| \left[ \sqrt{\varkappa_2} \frac{(2\sigma_{33} - \sigma_{22} - \sigma_{11})}{2}, \sqrt{\frac{\varkappa_3}{2}}(2\sigma_{12}), \sqrt{\frac{\varkappa_4}{2}}(2\sigma_{13}), \sqrt{\frac{\varkappa_5}{2}}(2\sigma_{23}) \right]^T \right\|_2 , \quad (287)$$

where $\left\| [\cdot, \cdot, \cdot, \cdot]^T \right\|_2$ is a composition of 2-norm with an affine transformation[9]. Taking into account the fact that (a) norm is convex and (b) composition of a norm with an affine

---

[9]An affine transformation is a map $f : \mathbb{R}^n \mapsto \mathbb{R}^n$ such that

$$f(\mathbf{X}) = \mathbb{A} : \mathbf{X} + \mathbf{Q} \quad \forall \quad \mathbf{X} \in \mathbb{R}^n$$

where $\mathbb{A}$ denotes a linear transformation

transformation is convex [119], the requirement for convexity of the bracketed term is given by $\varkappa_{2-5} > 0$ which ensures that the norm is non-negative. Thus, it can be safely stated that the composition is convex.

### 5.2.1.3. Evolution equations.
**5.2.1.3.1. Model-X-$\mathcal{RI}$: Rate-independent setting.** For a rate-independent setting, the evolution equations of plastic variables $\mathfrak{c} = \{\boldsymbol{\varepsilon}^p, \xi, \boldsymbol{\alpha}\}$ can be formally derived in terms of the energetic driving forces $\mathfrak{f} = \{\boldsymbol{\sigma}, \kappa, \boldsymbol{\beta}\}$ using the principle of maximum dissipation. With Eqn. (279) at hand, a constrained minimisation problem can be formulated analogous to Eqn. (104) as

$$\mathscr{L}(\boldsymbol{\sigma}, \kappa, \boldsymbol{\beta}, \lambda, \dot{\boldsymbol{\varepsilon}}^p, \dot{\xi}, \dot{\boldsymbol{\alpha}}) = -\boldsymbol{\sigma} : \dot{\boldsymbol{\varepsilon}}^p - \kappa\dot{\xi} - \boldsymbol{\beta} : \dot{\boldsymbol{\alpha}} + \lambda\chi \Longrightarrow \text{STATIONARY} . \tag{288}$$

The necessary conditions of the above constrained problem gives the evolution equations in line with Eqns. (105) and (106) as

$$\begin{aligned}
&1. \quad \mathscr{L},_{\boldsymbol{\sigma}} \equiv -\dot{\boldsymbol{\varepsilon}}^p + \lambda\chi,_{\boldsymbol{\sigma}} = \dot{\boldsymbol{\varepsilon}}^p - \lambda\chi,_{\boldsymbol{\sigma}} = \boldsymbol{0} , \\
&2. \quad \mathscr{L},_{\kappa} \equiv -\dot{\xi} \; + \lambda\chi,_{\kappa} = \dot{\xi} \; - \lambda\chi,_{\kappa} = 0 , \\
&3. \quad \mathscr{L},_{\boldsymbol{\beta}} \equiv -\dot{\boldsymbol{\alpha}} \; + \lambda\chi,_{\boldsymbol{\beta}} = \dot{\boldsymbol{\alpha}} \; - \lambda\chi,_{\boldsymbol{\beta}} = \boldsymbol{0} ,
\end{aligned} \tag{289}$$

along with the plastic loading/unloading conditions

$$\lambda \geq 0, \quad \chi \leq 0 \quad \text{and} \quad \lambda\chi \equiv 0 , \tag{290}$$

where $\lambda$ denotes the amount of the plastic flow. The terms $\chi,_{\boldsymbol{\sigma}}, \chi,_{\kappa}$ and $\chi,_{\boldsymbol{\beta}}$ are the normals to the yield function (279), and are derived to have the following forms

$$\chi,_{\boldsymbol{\sigma}} = \sum_{i=1}^{5} \chi,_{\tilde{J}_i} \tilde{J}_i,_{\boldsymbol{\sigma}} = \sum_{i=1}^{2} \chi,_{\tilde{J}_i} \tilde{J}_i,_{\boldsymbol{\sigma}} + \sum_{i=3}^{5} \chi,_{\tilde{J}_i} \tilde{J}_i,_{\mathfrak{s}} : \mathfrak{s}_{\boldsymbol{\sigma}}$$

$$= \varkappa_1 \boldsymbol{m}_3 + \frac{\dfrac{9\varkappa_2}{2} \text{tr}[\boldsymbol{m}_3'\boldsymbol{\Sigma}]\boldsymbol{m}_3' + \left\{\varkappa_3 \text{tr}[\boldsymbol{m}_{12}\mathfrak{s}]\boldsymbol{m}_{12} + \varkappa_4 \text{tr}[\boldsymbol{m}_{13}\mathfrak{s}]\boldsymbol{m}_{13} + \varkappa_5 \text{tr}[\boldsymbol{m}_{23}\mathfrak{s}]\boldsymbol{m}_{23}\right\} : \mathbb{P}}{2\left[\varkappa_2 \tilde{J}_2 + \dfrac{\varkappa_3}{2}\tilde{J}_3 + \dfrac{\varkappa_4}{2}\tilde{J}_4 + \dfrac{\varkappa_5}{2}\tilde{J}_5\right]^{1/2}} ,$$

$$\chi,_{\kappa} = \{1/y_{12}\}$$

$$\chi,_{\boldsymbol{\beta}} = \chi,_{\boldsymbol{\sigma}} + \frac{9\zeta_1}{2} \text{tr}[\boldsymbol{m}_3'\boldsymbol{\beta}]\boldsymbol{m}_3' + \zeta_2 \text{tr}[\boldsymbol{m}_{12}\boldsymbol{\beta}]\boldsymbol{m}_{12} + \zeta_3 \text{tr}[\boldsymbol{m}_{13}\boldsymbol{\beta}]\boldsymbol{m}_{13} + \zeta_4 \text{tr}[\boldsymbol{m}_{23}\boldsymbol{\beta}]\boldsymbol{m}_{23}$$

$$\tag{291}$$

where the fourth-order projection tensor $\mathbb{P}$ can be expressed with Eqn. (274) as

$$\mathbb{P} = \mathfrak{s},_{\boldsymbol{\sigma}} = (\boldsymbol{1} \oplus \boldsymbol{1}) - (\boldsymbol{m}_3 \otimes \boldsymbol{1}) + \left[(\boldsymbol{m}_3 - \boldsymbol{m}_1) \otimes \boldsymbol{m}_1\right] + \left[(\boldsymbol{m}_3 - \boldsymbol{m}_2) \otimes \boldsymbol{m}_2\right] . \tag{292}$$

Setting

$$\bar{\mathfrak{n}} = \frac{\dfrac{9\varkappa_2}{2} \text{tr}[\boldsymbol{m}_3'\boldsymbol{\Sigma}]\boldsymbol{m}_3' + \left\{\varkappa_3 \text{tr}[\boldsymbol{m}_{12}\mathfrak{s}]\boldsymbol{m}_{12} + \varkappa_4 \text{tr}[\boldsymbol{m}_{13}\mathfrak{s}]\boldsymbol{m}_{13} + \varkappa_5 \text{tr}[\boldsymbol{m}_{23}\mathfrak{s}]\boldsymbol{m}_{23}\right\} : \mathbb{P}}{2\left[\varkappa_2 \tilde{J}_2 + \dfrac{\varkappa_3}{2}\tilde{J}_3 + \dfrac{\varkappa_4}{2}\tilde{J}_4 + \dfrac{\varkappa_5}{2}\tilde{J}_5\right]^{1/2}} \quad \text{and}$$

$$\hat{\mathfrak{n}} = \bar{\mathfrak{n}} + \frac{9\zeta_1}{2} \text{tr}[\boldsymbol{m}_3'\boldsymbol{\beta}]\boldsymbol{m}_3' + \zeta_2 \text{tr}[\boldsymbol{m}_{12}\boldsymbol{\beta}]\boldsymbol{m}_{12} + \zeta_3 \text{tr}[\boldsymbol{m}_{13}\boldsymbol{\beta}]\boldsymbol{m}_{13} + \zeta_4 \text{tr}[\boldsymbol{m}_{23}\boldsymbol{\beta}]\boldsymbol{m}_{23}$$

$$\tag{293}$$

which satisfy

$$\mathrm{tr}[\bar{\mathbf{n}}] = 0, \quad \bar{\mathbf{n}} : \mathbb{P} = \bar{\mathbf{n}}, \quad \hat{\mathbf{n}} : \mathbb{P} = \hat{\mathbf{n}} \quad \text{and} \quad \mathrm{tr}[\hat{\mathbf{n}}] = 0 \ , \tag{294}$$

Eqn. (291) reformulates to

$$\chi,_{\boldsymbol{\sigma}} = \{\varkappa_1 \boldsymbol{m}_3 + \bar{\mathbf{n}}\}$$

$$\chi,_{\kappa} = \{1/y_{12}\} \qquad \qquad . \tag{295}$$

$$\chi,_{\boldsymbol{\beta}} = \{\varkappa_1 \boldsymbol{m}_3 + \hat{\mathbf{n}}\}$$

Substituting Eqn. (295) into Eqn. (289) yields the closed form expressions of the evolution equations as

$$\begin{aligned}
1. \quad & \mathscr{L},_{\boldsymbol{\sigma}} \equiv -\dot{\boldsymbol{\varepsilon}}^p + \lambda \chi,_{\boldsymbol{\sigma}} = \dot{\boldsymbol{\varepsilon}}^p - \lambda\{\varkappa_1 \boldsymbol{m}_3 + \bar{\mathbf{n}}\} = \mathbf{0} \ , \\
2. \quad & \mathscr{L},_{\kappa} \equiv -\dot{\xi} \ + \lambda \chi,_{\kappa} = \dot{\xi} \ - \lambda\{1/y_{12}\} = 0 \ , \\
3. \quad & \mathscr{L},_{\boldsymbol{\beta}} \equiv -\dot{\boldsymbol{\alpha}} \ + \lambda \chi,_{\boldsymbol{\beta}} = \dot{\boldsymbol{\alpha}} \ - \lambda\{\varkappa_1 \boldsymbol{m}_3 + \hat{\mathbf{n}}\} = \mathbf{0} \ .
\end{aligned} \tag{296}$$

Furthermore, substituting Eqns. (291) into Eqn. (296), the evolution equations can be reformulated as

$$\dot{\boldsymbol{\varepsilon}}^p = \lambda\left\{\varkappa_1 \boldsymbol{m}_3 + \frac{\frac{9\varkappa_2}{2}\mathrm{tr}[\boldsymbol{m}_3'\boldsymbol{\Sigma}]\boldsymbol{m}_3' + \left\{\varkappa_3 \mathrm{tr}[\boldsymbol{m}_{12}\mathfrak{s}]\boldsymbol{m}_{12} + \varkappa_4 \mathrm{tr}[\boldsymbol{m}_{13}\mathfrak{s}]\boldsymbol{m}_{13} + \varkappa_5 \mathrm{tr}[\boldsymbol{m}_{23}\mathfrak{s}]\boldsymbol{m}_{23}\right\} : \mathbb{P}}{2\left[\varkappa_2 \tilde{J}_2 + \frac{\varkappa_3}{2}\tilde{J}_3 + \frac{\varkappa_4}{2}\tilde{J}_4 + \frac{\varkappa_5}{2}\tilde{J}_5\right]^{1/2}}\right\}$$

$$\dot{\xi} = \lambda\{1/y_{12}\}$$

$$\begin{aligned}
\dot{\boldsymbol{\alpha}} = \lambda\Bigg\{ & \varkappa_1 \boldsymbol{m}_3 + \frac{\frac{9\varkappa_2}{2}\mathrm{tr}[\boldsymbol{m}_3'\boldsymbol{\Sigma}]\boldsymbol{m}_3' + \left\{\varkappa_3 \mathrm{tr}[\boldsymbol{m}_{12}\mathfrak{s}]\boldsymbol{m}_{12} + \varkappa_4 \mathrm{tr}[\boldsymbol{m}_{13}\mathfrak{s}]\boldsymbol{m}_{13} + \varkappa_5 \mathrm{tr}[\boldsymbol{m}_{23}\mathfrak{s}]\boldsymbol{m}_{23}\right\} : \mathbb{P}}{2\left[\varkappa_2 \tilde{J}_2 + \frac{\varkappa_3}{2}\tilde{J}_3 + \frac{\varkappa_4}{2}\tilde{J}_4 + \frac{\varkappa_5}{2}\tilde{J}_5\right]^{1/2}} \\
& + \frac{9\zeta_1}{2}\mathrm{tr}[\boldsymbol{m}_3'\boldsymbol{\beta}]\boldsymbol{m}_3' + \zeta_2 \mathrm{tr}[\boldsymbol{m}_{12}\boldsymbol{\beta}]\boldsymbol{m}_{12} + \zeta_3 \mathrm{tr}[\boldsymbol{m}_{13}\boldsymbol{\beta}]\boldsymbol{m}_{13} + \zeta_4 \mathrm{tr}[\boldsymbol{m}_{23}\boldsymbol{\beta}]\boldsymbol{m}_{23}\Bigg\}
\end{aligned} \tag{297}$$

These evolution equations characterise Armstrong-Fredrick-type non-linear kinematic hardening [120], generalised to the present case. For the choice $\zeta_1 = \zeta_2 = \zeta_3 = \zeta_4 = 0$, the model reduces to the well known Melan-Prager-type kinematic hardening [121], where $\boldsymbol{\alpha}$ is linear and homogeneous in $\dot{\boldsymbol{\varepsilon}}^p$ [78, 84].

With the normals to the yield function, namely $\chi,_{\boldsymbol{\sigma}}$, $\chi,_{\kappa}$ and $\chi,_{\boldsymbol{\beta}}$ at hand, the plastic multiplier $\lambda$ can be computed using Eqns. (107)-(115) as

$$\boxed{\lambda = \frac{(\varkappa_1 \boldsymbol{m}_3 + \bar{\mathbf{n}}) : \mathbb{E} : \dot{\boldsymbol{\varepsilon}}}{(\varkappa_1 \boldsymbol{m}_3 + \bar{\mathbf{n}}) : \mathbb{E} : (\varkappa_1 \boldsymbol{m}_3 + \bar{\mathbf{n}}) + \mathrm{H}\{1/y_{12}^2\} + (\varkappa_1 \boldsymbol{m}_3 + \hat{\mathbf{n}}) : \mathbb{H} : (\varkappa_1 \boldsymbol{m}_3 + \hat{\mathbf{n}})}} , \tag{298}$$

which leads to the definition of the fourth-order continuum elastic-plastic tangent stiffness tensor analogous to Eqn. (121) as

$$\mathbb{E}^{\mathrm{ep}} = \left[\mathbb{E} - \frac{\mathbb{E} : (\varkappa_1 \boldsymbol{m}_3 + \bar{\mathbf{n}}) \otimes (\varkappa_1 \boldsymbol{m}_3 + \bar{\mathbf{n}}) : \mathbb{E}}{(\varkappa_1 \boldsymbol{m}_3 + \bar{\mathbf{n}}) : \mathbb{E} : (\varkappa_1 \boldsymbol{m}_3 + \bar{\mathbf{n}}) + \mathrm{H}\{1/y_{12}^2\} + (\varkappa_1 \boldsymbol{m}_3 + \hat{\mathbf{n}}) : \mathbb{H} : (\varkappa_1 \boldsymbol{m}_3 + \hat{\mathbf{n}})}\right] . \tag{299}$$

Clearly, $\mathbb{E}^{ep}$ in Eqn. (299) is symmetric, owing to the constitutive assumptions. Evolution equations of type (296) and (297) are known as *associated flow* rules where the rates of the internal variables are normal to the yield surface ($\chi = 0$).

For a *non-associated flow* response where the canonical normals to the yield function (291) do not characterise the real material response, a separate plastic flow potential $\phi$ is introduced such that it has a functional dependence on the same variables as that of the yield function, i.e.

$$\phi = \phi(\boldsymbol{\Sigma}, \kappa) \ , \tag{300}$$

which can be also be expressed as an isotropic function similar to Eqn. (275) as

$$\phi(\boldsymbol{Q} \star \boldsymbol{\Sigma}, \boldsymbol{Q} \star \boldsymbol{m}_1, \boldsymbol{Q} \star \boldsymbol{m}_2, \boldsymbol{Q} \star \boldsymbol{m}_3, \kappa) = \phi(\boldsymbol{\Sigma}, \boldsymbol{m}_1, \boldsymbol{m}_2, \boldsymbol{m}_3, \kappa) \quad \forall \quad \boldsymbol{Q} \in \mathcal{O}(3) \ . \tag{301}$$

Following conceptually [18,44,109], the plastic flow potential is assumed to be of the form

$$\phi = \chi|_{\varkappa_1 = 0} = \left[ \left\{ \varkappa_2 \tilde{J}_2 + \frac{\varkappa_3}{2} \tilde{J}_3 + \frac{\varkappa_4}{2} \tilde{J}_4 + \frac{\varkappa_5}{2} \tilde{J}_5 \right\}^{1/2} - \left( 1 - \frac{\kappa}{y_{12}} \right) \right. $$
$$\left. + \zeta_1 \tilde{J}_2|_{\sigma=0} + \frac{\zeta_2}{2} \tilde{J}_3|_{\sigma=0} + \frac{\zeta_3}{2} \tilde{J}_4|_{\sigma=0} + \frac{\zeta_4}{2} \tilde{J}_5|_{\sigma=0} \right] \ , \tag{302}$$

based on which the evolution equations for the internal variables take the form

$$\begin{aligned}
&1. \quad \dot{\boldsymbol{\varepsilon}}^p - \lambda \phi_{,\boldsymbol{\sigma}} = \dot{\boldsymbol{\varepsilon}}^p - \lambda \bar{\mathbf{n}} = \boldsymbol{0} \ , \\
&2. \quad \dot{\xi} \ - \lambda \phi_{,\kappa} = \dot{\xi} \ - \lambda \{1/y_{12}\} = 0 \ , \\
&3. \quad \dot{\boldsymbol{\alpha}} - \lambda \phi_{,\boldsymbol{\beta}} = \dot{\boldsymbol{\alpha}} - \lambda \hat{\mathbf{n}} = \boldsymbol{0} \ .
\end{aligned} \tag{303}$$

It can be inferred from the equation above that the evolution equations are deviatoric and independent of the stress in the preferred directions. Note that $\bar{\mathbf{n}}$ and $\hat{\mathbf{n}}$ are the same as those in Eqn. (291), and satisfy the properties in Eqn. (294). Additionally, the fourth-order projection tensor $\mathbb{P}$ also remains the same as in Eqn. (292). The set of equations (303) replaces the normality rules in Eqn. (296) though the plastic loading/unloading conditions in Eqn. (290) remain unchanged. The scalar plastic multiplier $\lambda$ and the fourth-order elastic-plastic tangent stiffness tensor $\mathbb{E}^{ep}$ can be derived similar to Eqns. (298) and (299) respectively, with the aid of Eqns. (118)-(123) as

$$\boxed{\lambda = \frac{(\varkappa_1 \boldsymbol{m}_3 + \bar{\mathbf{n}}) : \mathbb{E} : \dot{\boldsymbol{\varepsilon}}}{(\varkappa_1 \boldsymbol{m}_3 + \bar{\mathbf{n}}) : \mathbb{E} : \bar{\mathbf{n}} + \mathrm{H}\{1/y_{12}^2\} + (\varkappa_1 \boldsymbol{m}_3 + \hat{\mathbf{n}}) : \mathbb{H} : \hat{\mathbf{n}}}} \ , \tag{304}$$

and

$$\mathbb{E}^{ep} = \left[ \mathbb{E} - \frac{\mathbb{E} : (\varkappa_1 \boldsymbol{m}_3 + \bar{\mathbf{n}}) \otimes \bar{\mathbf{n}} : \mathbb{E}}{(\varkappa_1 \boldsymbol{m}_3 + \bar{\mathbf{n}}) : \mathbb{E} : \bar{\mathbf{n}} + \mathrm{H}\{1/y_{12}^2\} + (\varkappa_1 \boldsymbol{m}_3 + \hat{\mathbf{n}}) : \mathbb{H} : \hat{\mathbf{n}}} \right] \ , \tag{305}$$

where it can be seen that $\mathbb{E}^{ep}$ is a non-symmetric fourth-order tensor for the non-associative flow response. A summary of the modelling framework for a rate-independent setting is given in Box 7.

Box 7: Rate-independent setting–summary of the modelling framework for the orthorhombic symmetry group.

<div style="border:1px solid black; padding:1em;">

1. Kinematics : $\quad\quad\quad\quad\quad\quad\boldsymbol{\varepsilon} = \boldsymbol{\varepsilon}^e + \boldsymbol{\varepsilon}^p$

2. Internal variables : $\quad\quad\quad\quad\mathfrak{e} = \{\boldsymbol{\varepsilon}^p, \xi, \boldsymbol{\alpha}\}$

3. Energetic potential : $\quad\quad\quad\psi = \psi^e(\boldsymbol{\varepsilon} - \boldsymbol{\varepsilon}^p, \boldsymbol{m}_1, \boldsymbol{m}_2, \boldsymbol{m}_3)$
$$\quad\quad\quad\quad\quad\quad\quad\quad\quad +\psi^p_{\mathrm{iso}}(\xi) + \psi^p_{\mathrm{kin}}(\boldsymbol{\alpha}, \boldsymbol{m}_1, \boldsymbol{m}_2, \boldsymbol{m}_3)$$

4. Stress tensor : $\quad\quad\quad\quad\quad\boldsymbol{\sigma} = \psi^e(\boldsymbol{\varepsilon} - \boldsymbol{\varepsilon}^p, \boldsymbol{m}_1, \boldsymbol{m}_2, \boldsymbol{m}_3)_{,\boldsymbol{\varepsilon}}$

5. Driving forces : $\quad\quad\quad\quad\quad\kappa = -\psi^p_{\mathrm{iso}}(\xi)_{,\xi}$
$$\quad\quad\quad\quad\quad\quad\quad\quad\quad \boldsymbol{\beta} = -\psi^p_{\mathrm{kin}}(\boldsymbol{\alpha}, \boldsymbol{m}_1, \boldsymbol{m}_2, \boldsymbol{m}_3)_{,\boldsymbol{\alpha}}$$

5. Relative stress tensor : $\quad\quad\boldsymbol{\Sigma} = \boldsymbol{\sigma} + \boldsymbol{\beta}$

6. Plasticity inducing stress tensor : $\mathfrak{s} = \mathfrak{s}(\boldsymbol{\Sigma})$

7. Yield function : $\quad\quad\quad\quad\quad\chi = \chi(\boldsymbol{\Sigma}, \boldsymbol{m}_1, \boldsymbol{m}_2, \boldsymbol{m}_3, \kappa)$

8. Plastic flow potential : $\quad\quad\phi = \phi(\mathfrak{s}, \boldsymbol{m}_1, \boldsymbol{m}_2, \boldsymbol{m}_3, \kappa)$

9. Evolution equations :

    Associative
$$\dot{\boldsymbol{\varepsilon}}^p = \lambda\chi_{,\boldsymbol{\sigma}} = \lambda\{\varkappa_1\boldsymbol{m}_3 + \bar{\mathfrak{n}}\}$$
$$\dot{\xi} = \lambda\chi_{,\kappa}$$
$$\dot{\boldsymbol{\alpha}} = \lambda\chi_{,\boldsymbol{\beta}} = \lambda\{\varkappa_1\boldsymbol{m}_3 + \hat{\mathfrak{n}}\}$$

    Non-associative
$$\dot{\boldsymbol{\varepsilon}}^p = \lambda\phi_{,\boldsymbol{\sigma}} = \lambda\bar{\mathfrak{n}}$$
$$\dot{\xi} = \lambda\phi_{,\kappa}$$
$$\dot{\boldsymbol{\alpha}} = \lambda\phi_{,\boldsymbol{\beta}} = \lambda\hat{\mathfrak{n}}$$

10. Karush-Kuhn-Tucker conditions : $\lambda \geq 0, \quad \chi \leq 0 \quad \text{and} \quad \lambda\chi \equiv 0$

</div>

**5.2.1.3.2. Model-X-$\mathcal{RD}$: Rate-dependent setting.** For a rate-dependent setting where the material behaviour changes for varying strain rates, the constrained minimisation problem is transformed into an unconstrained optimisation problem using a *penalisation function* as explained in **Chapter 2**. Thus, the Lagrange functional (288) reformulates to a penalty functional $\mathscr{P}$ of the form

$$\mathscr{P}(\boldsymbol{\sigma}, \kappa, \boldsymbol{\beta}, \dot{\boldsymbol{\varepsilon}}^p, \dot{\xi}, \dot{\boldsymbol{\alpha}}) = -\boldsymbol{\sigma} : \dot{\boldsymbol{\varepsilon}}^p - \kappa\dot{\xi} - \boldsymbol{\beta} : \dot{\boldsymbol{\alpha}} + \frac{1}{\eta(m+1)}[\chi^+]^{(m+1)} \implies \text{STATIONARY},$$
(306)

in terms of the penalty parameter $\eta \in (0, \infty)$, and a monotonically increasing ramp function $[\chi^+]$ with the properties

$$[\chi^+] := \frac{1}{2}[\chi + |\chi|]$$
(307)

where $\chi$ is the yield function defined in Eqn. (279). Based on Eqn. (306), explicit forms of the evolution equations for the internal variables are given analogous to Eqn. (296) as

$$
\begin{aligned}
&1. \quad \mathscr{P}_{,\boldsymbol{\sigma}} \equiv -\dot{\boldsymbol{\varepsilon}}^p + \frac{1}{\eta}[\chi^+]^m \, \chi_{,\boldsymbol{\sigma}} = \dot{\boldsymbol{\varepsilon}}^p - \frac{1}{\eta}[\chi^+]^m \, \{\varkappa_1 \boldsymbol{m}_3 + \bar{\mathfrak{n}}\} = \boldsymbol{0} \ , \\[2mm]
&2. \quad \mathscr{P}_{,\kappa} \equiv -\dot{\xi} \; + \frac{1}{\eta}[\chi^+]^m \, \chi_{,\kappa} = \dot{\xi} \; - \frac{1}{\eta}[\chi^+]^m \, \{1/y_{12}\} = 0 \ , \\[2mm]
&3. \quad \mathscr{P}_{,\boldsymbol{\beta}} \equiv -\dot{\boldsymbol{\alpha}} \; + \frac{1}{\eta}[\chi^+]^m \, \chi_{,\boldsymbol{\beta}} = \dot{\boldsymbol{\alpha}} \; - \frac{1}{\eta}[\chi^+]^m \, \{\varkappa_1 \boldsymbol{m}_3 + \hat{\mathfrak{n}}\} = \boldsymbol{0} \ .
\end{aligned}
\tag{308}
$$

In contrast to the rate-independent setting, the amount of the plastic flow $\lambda$ is given by the pseudo-consistency condition

$$
\lambda = \frac{1}{\eta}[\chi^+]^m \ ,
\tag{309}
$$

which gives the rate-dependent $\lambda$ in terms of viscosity $\eta$ and the ramp function $(\chi^+)^m$. Likewise, for a non-associative flow response, it follows that the evolution equations (308) reformulate, respectively, to

$$
\begin{aligned}
&1. \quad \dot{\boldsymbol{\varepsilon}}^p - \frac{1}{\eta}[\phi^+]^m \, \phi_{,\boldsymbol{\sigma}} = \dot{\boldsymbol{\varepsilon}}^p - \frac{1}{\eta}[\phi^+]^m \, \bar{\mathfrak{n}} = \boldsymbol{0} \ , \\[2mm]
&2. \quad \dot{\xi} \; - \frac{1}{\eta}[\phi^+]^m \, \phi_{,\kappa} = \dot{\xi} \; - \frac{1}{\eta}[\phi^+]^m \, \{1/y_{12}\} = 0 \ , \\[2mm]
&3. \quad \dot{\boldsymbol{\alpha}} \; - \frac{1}{\eta}[\phi^+]^m \, \phi_{,\boldsymbol{\beta}} = \dot{\boldsymbol{\alpha}} \; - \frac{1}{\eta}[\phi^+]^m \, \hat{\mathfrak{n}} = \boldsymbol{0} \ ,
\end{aligned}
\tag{310}
$$

in terms of the monotonically increasing ramp function $[\phi^+]$ with the properties

$$
[\phi^+] := \frac{1}{2}\big[\phi + |\phi|\,\big]
\tag{311}
$$

where $\phi$ is the plastic flow potential defined in Eqn. (302). With the preceding definitions, the fourth-order continuum elastic-plastic tangent modulus tensor for the associative and non-associative plasticity within a rate-dependent setting can be computed analogous to Eqns. (299) and (305), respectively. The rate-dependent plasticity model for the $\mathscr{C}_3$ group is summarised in Box 8.

### 5.2.2. Transversely isotropic symmetry group

For the $\mathscr{C}_{13}$ symmetry group, the properties of the plasticity inducing stress tensor $\mathfrak{s}$ in Eqn. (273) read

$$
\mathrm{tr}[\mathfrak{s}] = 0 \quad \text{and} \quad \mathrm{tr}[\boldsymbol{m}\mathfrak{s}] = 0 \ ,
\tag{312}
$$

owing to the fact that the $\mathscr{C}_{13}$ group is characterised by the existence of a single symmetric second-order structural tensor $\boldsymbol{m}$. Therefore, for a given $\boldsymbol{m}$, Eqn. (274) reformulates to

$$
\mathfrak{s} = \boldsymbol{\Sigma} - \frac{1}{3}\,\mathrm{tr}[\boldsymbol{\Sigma}]\boldsymbol{1} - \frac{3}{2}\,\mathrm{tr}[\boldsymbol{m}'\boldsymbol{\Sigma}]\boldsymbol{m}' \quad \text{with} \quad \boldsymbol{m}' = \boldsymbol{m} - \frac{1}{3}\boldsymbol{1} \ ,
\tag{313}
$$

see also [108]. The yield function can also be expressed as an isotropic scalar function such that

$$
\chi(\boldsymbol{Q}\star\boldsymbol{\Sigma}, \boldsymbol{Q}\star\boldsymbol{m}, \kappa) = \chi(\boldsymbol{\Sigma}, \boldsymbol{m}, \kappa) \quad \forall \quad \boldsymbol{Q} \in \mathcal{O}(3) \ .
\tag{314}
$$

Box 8: Rate-dependent setting–summary of the modelling framework for the orthorhombic symmetry group.

---

1. Kinematics :                  $\boldsymbol{\varepsilon} = \boldsymbol{\varepsilon}^e + \boldsymbol{\varepsilon}^p$

2. Internal variables :        $\boldsymbol{\mathfrak{e}} = \{\boldsymbol{\varepsilon}^p, \xi, \boldsymbol{\alpha}\}$

3. Energetic potential :       $\psi = \psi^e(\boldsymbol{\varepsilon} - \boldsymbol{\varepsilon}^p, \boldsymbol{m}_1, \boldsymbol{m}_2, \boldsymbol{m}_3)$

                                         $+\psi_{\mathrm{iso}}^p(\xi) + \psi_{\mathrm{kin}}^p(\boldsymbol{\alpha}, \boldsymbol{m}_1, \boldsymbol{m}_2, \boldsymbol{m}_3)$

4. Stress tensor :            $\boldsymbol{\sigma} = \psi^e(\boldsymbol{\varepsilon} - \boldsymbol{\varepsilon}^p, \boldsymbol{m}_1, \boldsymbol{m}_2, \boldsymbol{m}_3)_{,\boldsymbol{\varepsilon}}$

5. Driving forces :           $\kappa = -\psi_{\mathrm{iso}}^p(\xi)_{,\xi}$

                             $\boldsymbol{\beta} = -\psi_{\mathrm{kin}}^p(\boldsymbol{\alpha}, \boldsymbol{m}_1, \boldsymbol{m}_2, \boldsymbol{m}_3)_{,\boldsymbol{\alpha}}$

5. Relative stress tensor :    $\boldsymbol{\Sigma} = \boldsymbol{\sigma} + \boldsymbol{\beta}$

6. Plasticity inducing stress tensor : $\boldsymbol{\mathfrak{s}} = \boldsymbol{\mathfrak{s}}(\boldsymbol{\Sigma})$

7. Yield function :            $\chi = \chi(\boldsymbol{\Sigma}, \boldsymbol{m}_1, \boldsymbol{m}_2, \boldsymbol{m}_3, \kappa)$

8. Plastic flow potential :     $\phi = \phi(\boldsymbol{\mathfrak{s}}, \boldsymbol{m}_1, \boldsymbol{m}_2, \boldsymbol{m}_3, \kappa)$

9. Evolution equations :

     Associative

$$\dot{\boldsymbol{\varepsilon}}^p = \lambda \chi_{,\boldsymbol{\sigma}} = \lambda\{\varkappa_1 \boldsymbol{m}_3 + \bar{\mathfrak{n}}\}$$

$$\dot{\xi} = \lambda \chi_{,\kappa}$$

$$\dot{\boldsymbol{\alpha}} = \lambda \chi_{,\boldsymbol{\beta}} = \lambda\{\varkappa_1 \boldsymbol{m}_3 + \hat{\mathfrak{n}}\}$$

     with                  $\lambda = \dfrac{1}{\eta}[\chi^+]^m$    and    $[\chi^+] = \dfrac{1}{2}[\chi + |\chi|]$

     Non-associative

$$\dot{\boldsymbol{\varepsilon}}^p = \lambda \phi_{,\boldsymbol{\sigma}} = \lambda \bar{\mathfrak{n}}$$

$$\dot{\xi} = \lambda \phi_{,\kappa}$$

$$\dot{\boldsymbol{\alpha}} = \lambda \phi_{,\boldsymbol{\beta}} = \lambda \hat{\mathfrak{n}}$$

     with                  $\lambda = \dfrac{1}{\eta}[\phi^+]^m$    and    $[\phi^+] = \dfrac{1}{2}[\phi + |\phi|]$

---

With Eqn. (313) at hand, two threshold-type pressure-dependent yield functions are proposed that are suitable for fibre-reinforced composites. The underlying difference is the condition for their convexity which is elaborated subsequently.

Taking into account Eqn. (312), an integrity basis for the scalar yield function is given analogous to Eqn. (212) as

$$\hat{\mathcal{J}}_{\mathscr{C}_{13}} = \{\mathrm{tr}[\boldsymbol{\Sigma}], \mathrm{tr}[\boldsymbol{\mathfrak{s}}^2], \mathrm{tr}[\boldsymbol{\mathfrak{s}}^3], \mathrm{tr}[\boldsymbol{m}\boldsymbol{\Sigma}], \mathrm{tr}[\boldsymbol{m}\boldsymbol{\mathfrak{s}}^2]\} \ . \tag{315}$$

Following [44], the linear and quadratic isotropic invariants in Eqn. (315) can be refor-

mulated as

$$\begin{aligned}
\mathrm{tr}[\boldsymbol{\Sigma}] &= \mathrm{tr}[\boldsymbol{m}\boldsymbol{\Sigma}] + \mathrm{tr}[(\boldsymbol{1} - \boldsymbol{m})\boldsymbol{\Sigma}] \quad \text{and} \\
\mathrm{tr}[\mathfrak{s}^2] &= \mathrm{tr}[\boldsymbol{m}\mathfrak{s}^2 + \mathfrak{s}^2\boldsymbol{m}] + \mathrm{tr}[\mathfrak{s}^2 - (\boldsymbol{m}\mathfrak{s}^2 + \mathfrak{s}^2\boldsymbol{m})]
\end{aligned} \tag{316}$$

Substituting Eqn. (316) into Eqn. (315) and replacing $\mathrm{tr}[\mathfrak{s}^3]$ by $\det[\mathfrak{s}]$ using the Cayley-Hamilton's theorem, the new integrity basis for the yield function reads

$$\widetilde{\mathcal{J}}_{\mathscr{C}_{13}} = \{\mathrm{tr}[(\boldsymbol{1} - \boldsymbol{m})\boldsymbol{\Sigma}], \mathrm{tr}[\boldsymbol{m}\mathfrak{s}^2 + \mathfrak{s}^2\boldsymbol{m}], \mathrm{tr}[\mathfrak{s}^2 - (\boldsymbol{m}\mathfrak{s}^2 + \mathfrak{s}^2\boldsymbol{m})], \mathrm{tr}[\boldsymbol{m}\boldsymbol{\Sigma}], \det[\mathfrak{s}]\} . \tag{317}$$

Note that the reformulation of quadratic invariants in Eqn. $(316)_2$ is different from that in Eqn. $(213)_2$. It has been suggested and verified in [44] that a plastic response function formulated using this particular form of quadratic invariants is found to capture the experimental behaviour quite well, as seen in **Chapter 7**.

**5.2.2.1.  Yield function: Model-I.** With the basis (317) at hand, a pressure-dependent yield function for the $\mathscr{C}_{13}$ group is proposed in the stress space as

$$\chi = \varkappa_1 \tilde{J}_1 + \left[\varkappa_2 \tilde{J}_2 + \varkappa_3 \tilde{J}_3\right]^{1/2} - \left(1 - \frac{\kappa}{y_{12}}\right) + \frac{\zeta_1}{2}\tilde{J}_2|_{\sigma=0} + \frac{\zeta_2}{2}\tilde{J}_3|_{\sigma=0} \leq 0 , \tag{318}$$

where $\varkappa_{1-3}$ are material parameters governing the transversely isotropic plastic yielding. These parameters are related to initial threshold yield stress $y_{ij}$, associated with one compression mode and two shear modes which are characterised by the $\mathscr{C}_{13}$ group. They are determined analogous to those of the $\mathscr{C}_3$ group as follows

shear test in 12-plane

$$\boldsymbol{\sigma} = \begin{bmatrix} 0 & y_{12} & 0 \\ & 0 & 0 \\ \mathrm{sym.} & & 0 \end{bmatrix} \qquad \Longrightarrow \qquad \left.\begin{array}{l} \tilde{J}_1 = 0 \\ \tilde{J}_2 = 2y_{12}^2 \\ \tilde{J}_3 = 0 \end{array}\right\} , \tag{319}$$

shear test in 23-plane

$$\boldsymbol{\sigma} = \begin{bmatrix} 0 & 0 & 0 \\ & 0 & 0 \\ \mathrm{sym.} & & y_{23} \end{bmatrix} \qquad \Longrightarrow \qquad \left.\begin{array}{l} \tilde{J}_1 = 0 \\ \tilde{J}_2 = 0 \\ \tilde{J}_3 = 2y_{23}^2 \end{array}\right\} , \tag{320}$$

uniaxial compression in 2-direction

$$\boldsymbol{\sigma} = \begin{bmatrix} 0 & 0 & 0 \\ & -y_{22c} & 0 \\ \mathrm{sym.} & & 0 \end{bmatrix} \qquad \Longrightarrow \qquad \left.\begin{array}{l} \tilde{J}_1 = -y_{22c} \\ \tilde{J}_2 = 0 \\ \tilde{J}_3 = y_{22c}^2/2 \end{array}\right\} . \tag{321}$$

Evaluation of the yield criterion (318) for the the three aforementioned tests with the choice $\boldsymbol{a} = [1, 0, 0]^T$, $\kappa = 0$ and $\boldsymbol{\beta} = \boldsymbol{0}$ leads to the following definitions of the parameters

$$\varkappa_1 = \frac{1}{2y_{23}} - \frac{1}{y_{22c}}, \quad \varkappa_2 = \frac{1}{2y_{12}^2} \quad \text{and} \quad \varkappa_3 = \frac{1}{2y_{23}^2} . \tag{322}$$

The material parameters $\zeta_1$ and $\zeta_2$ in Eqn. (318) govern the non-linearity of kinematic hardening.

**5.2.2.2. Convexity of the yield surface: Model-I.** In this subsection, a proof of convexity of the yield surface (318) is shown. For the particular model at hand, recall the yield function

$$\chi = \varkappa_1 \tilde{J}_1 + \left[\varkappa_2 \tilde{J}_2 + \varkappa_3 \tilde{J}_3\right]^{1/2} - \left(1 - \frac{\kappa}{y_{12}}\right) + \frac{\zeta_1}{2}\tilde{J}_2|_{\sigma=0} + \frac{\zeta_2}{2}\tilde{J}_3|_{\sigma=0} \leq 0 \ . \tag{323}$$

The Hessian $\mathbb{Z}$ for the function (323) is given by

$$\mathbb{Z} = \chi_{,\boldsymbol{\sigma}\boldsymbol{\sigma}} = \frac{\varkappa_3 \mathbb{P} + (\varkappa_2 - \varkappa_3)\mathbb{P}_a}{\left[\varkappa_2 \tilde{J}_2 + \varkappa_3 \tilde{J}_3\right]^{1/2}} - \frac{\varkappa_3^2 \mathbb{J} + \varkappa_3(\varkappa_2 - \varkappa_3)\{\mathbb{K} + \mathbb{L}\} + (\varkappa_2 - \varkappa_3)^2 \mathbb{M}}{\left[\varkappa_2 \tilde{J}_2 + \varkappa_3 \tilde{J}_3\right]^{3/2}} \ , \tag{324}$$

together with the corresponding definitions

$$\begin{aligned}
\mathbb{P} &= (\boldsymbol{1} \oplus \boldsymbol{1}) - \frac{1}{3}(\boldsymbol{1} \otimes \boldsymbol{1}) - \frac{3}{2}(\boldsymbol{m}' \otimes \boldsymbol{m}') \\
\mathbb{P}_a &= \boldsymbol{m}\mathbb{P} + \mathbb{P}\boldsymbol{m} \\
\mathbb{J} &= \mathfrak{s} \otimes \mathfrak{s} \\
\mathbb{K} &= \mathfrak{s} \otimes \{\boldsymbol{m}\mathfrak{s} + \mathfrak{s}\boldsymbol{m}\} \\
\mathbb{L} &= \{\boldsymbol{m}\mathfrak{s} + \mathfrak{s}\boldsymbol{m}\} \otimes \mathfrak{s} \\
\mathbb{M} &= \{\boldsymbol{m}\mathfrak{s} + \mathfrak{s}\boldsymbol{m}\} \otimes \{\boldsymbol{m}\mathfrak{s} + \mathfrak{s}\boldsymbol{m}\}
\end{aligned} \tag{325}$$

The six eigenvalues of Eqn. (324) are given in terms of stress components by

$$\lambda_{\mathbb{Z}} = \begin{bmatrix} 0 \\[4pt] 0 \\[4pt] 0 \\[4pt] \dfrac{\varkappa_2}{\sqrt{2}\sqrt{4\varkappa_2(\sigma_{12}^2 + \sigma_{13}^2) + 4\varkappa_3\sigma_{23}^2 + \varkappa_3(\sigma_{22} - \sigma_{33})^2}} \\[14pt] \dfrac{4\varkappa_2\varkappa_3(3\sigma_{12}^2 + 3\sigma_{13}^2 + \sigma_{23}^2) + \varkappa_3(\varkappa_2 + \varkappa_3)(\sigma_{22} - \sigma_{33})^2 + 8\varkappa_3^2\sigma_{23}^2 - \aleph}{2\sqrt{2}\left(\sqrt{4\varkappa_2(\sigma_{12}^2 + \sigma_{13}^2) + 4\varkappa_3\sigma_{23}^2 + \varkappa_3(\sigma_{22} - \sigma_{33})^2}\right)^3} \\[14pt] \dfrac{4\varkappa_2\varkappa_3(3\sigma_{12}^2 + 3\sigma_{13}^2 + \sigma_{23}^2) + \varkappa_3(\varkappa_2 + \varkappa_3)(\sigma_{22} - \sigma_{33})^2 + 8\varkappa_3^2\sigma_{23}^2 + \aleph}{2\sqrt{2}\left(\sqrt{4\varkappa_2(\sigma_{12}^2 + \sigma_{13}^2) + 4\varkappa_3\sigma_{23}^2 + \varkappa_3(\sigma_{22} - \sigma_{33})^2}\right)^3} \end{bmatrix} \ , \tag{326}$$

with

$$\aleph = \Big\{\left[4\varkappa_2\varkappa_3(\sigma_{12}^2 + \sigma_{13}^2 - \sigma_{23}^2) + \varkappa_3(\varkappa_2 - \varkappa_3)(\sigma_{22} - \sigma_{33})^2 + 8\varkappa_3^2\sigma_{23}^2\right]^2 \\ + 16\varkappa_3^2\sigma_{23}^2(\sigma_{22} - \sigma_{33})^2\left[2\varkappa_3^2 - 3\varkappa_2\varkappa_3 + \varkappa_2^2\right]\Big\}^{1/2} \ . \tag{327}$$

Mathematically, the only condition that is imposed on the parameters $\varkappa_2$ and $\varkappa_3$ is that they both must be greater than zero, as they represent the magnitudes of yield strengths. This condition is also satisfied in their computation, as seen in Eqn. (322). Hence, without any loss of generality, it can be safely stated that $\varkappa_{2,3} > 0$. Furthermore, it is directly

seen from Eqn. (326) that the first four eigenvalues $\lambda_{\mathbb{Z}(1)}$, $\lambda_{\mathbb{Z}(2)}$, $\lambda_{\mathbb{Z}(3)}$ and $\lambda_{\mathbb{Z}(4)}$ are all $\geq$ 0. For $\lambda_{\mathbb{Z}(5)}$ to be $\geq 0$, the following condition should be true

$$\frac{4\varkappa_2\varkappa_3(3\sigma_{12}^2 + 3\sigma_{13}^2 + \sigma_{23}^2) + \varkappa_3(\varkappa_2 + \varkappa_3)(\sigma_{22} - \sigma_{33})^2 + 8\varkappa_3^2\sigma_{23}^2}{2\sqrt{2}\left(\sqrt{4\varkappa_2(\sigma_{12}^2 + \sigma_{13}^2) + 4\varkappa_3\sigma_{23}^2 + \varkappa_3(\sigma_{22} - \sigma_{33})^2}\right)^3} \geq \frac{\aleph}{2\sqrt{2}\left(\sqrt{4\varkappa_2(\sigma_{12}^2 + \sigma_{13}^2) + 4\varkappa_3\sigma_{23}^2 + \varkappa_3(\sigma_{22} - \sigma_{33})^2}\right)^3} . \tag{328}$$

Squaring both sides and rearranging the expression gives

$$\begin{aligned} &\left[4\varkappa_2\varkappa_3(3\sigma_{12}^2 + 3\sigma_{13}^2 + \sigma_{23}^2) + \varkappa_3(\varkappa_2 + \varkappa_3)(\sigma_{22} - \sigma_{33})^2 + 8\varkappa_3^2\sigma_{23}^2\right]^2 \geq \\ &\left[4\varkappa_2\varkappa_3(\sigma_{12}^2 + \sigma_{13}^2 - \sigma_{23}^2) + \varkappa_3(\varkappa_2 - \varkappa_3)(\sigma_{22} - \sigma_{33})^2 + 8\varkappa_3^2\sigma_{23}^2\right]^2 \\ &+ 16\varkappa_3^2\sigma_{23}^2(\sigma_{22} - \sigma_{33})^2\left[2\varkappa_3^2 - 3\varkappa_2\varkappa_3 + \varkappa_2^2\right] \end{aligned} . \tag{329}$$

After some straightforward, howbeit lengthy algebraic simplifications, it is observed that the expression on the LHS is positive whereas that on the RHS is negative, implying $\lambda_{\mathbb{Z}(5)}$ is $\geq 0$. For $\lambda_{\mathbb{Z}(6)}$ to be $\geq 0$, it needs to be shown that

$$\frac{\aleph}{2\sqrt{2}\left(\sqrt{4\varkappa_2(\sigma_{12}^2 + \sigma_{13}^2) + 4\varkappa_3\sigma_{23}^2 + \varkappa_3(\sigma_{22} - \sigma_{33})^2}\right)^3} \geq 0 , \tag{330}$$

which is a priori true for

$$16\varkappa_3^2\sigma_{23}^2(\sigma_{22} - \sigma_{33})^2\left[2\varkappa_3^2 - 3\varkappa_2\varkappa_3 + \varkappa_2^2\right] \geq 0 \implies \varkappa_3 \geq \varkappa_2 \implies y_{12} \geq y_{23} . \tag{331}$$

The above inequality is the necessary condition for the yield surface to be convex in the stress space, cf. [44].

**5.2.2.3. Yield function: Model-II.** To circumvent the restriction imposed by the convexity condition of Model-I, use can be made of the Euclidean norm in context of defining the second yield function. To do so, consider a further decomposition of $\mathfrak{s}$ in Eqn. (313) as

$$\mathfrak{s}_2 = \boldsymbol{m}\mathfrak{s} + \mathfrak{s}\boldsymbol{m} \quad \text{and} \quad \mathfrak{s}_3 = \mathfrak{s} - (\boldsymbol{m}\mathfrak{s} + \mathfrak{s}\boldsymbol{m}) . \tag{332}$$

The decomposition above is an extension of the additive stress split into two distinct shear modes associated with the $\mathscr{C}_{13}$ group, namely the in-plane and transverse shear. Further, let $p$ denote the hydrostatic pressure such that

$$p = \text{tr}[(\boldsymbol{1} - \boldsymbol{m})\boldsymbol{\Sigma}] . \tag{333}$$

Appealing to Eqns. (332) and (333), a Drucker Prager-type pressure-dependent yield function is proposed in the stress space as

$$\chi = \varkappa_1 p + \left[\varkappa_2 \|\mathfrak{s}_2\|^2 + \varkappa_3 \|\mathfrak{s}_3\|^2\right]^{1/2} - \left(1 - \frac{\kappa}{y_{12}}\right) + \frac{\zeta_1}{2}\|\mathfrak{s}_2\|_{\sigma=0}\|^2 + \frac{\zeta_2}{2}\|\mathfrak{s}_3\|_{\sigma=0}\|^2 \leq 0 , \tag{334}$$

see also [78, 122]. In line with Eqns. (319)–(322), the governing coefficients of the yield surface are evaluated to be

$$\varkappa_1 = \frac{1}{\sqrt{2}y_{23}} - \frac{1}{y_{22c}}, \quad \varkappa_2 = \frac{1}{y_{12}^2} \quad \text{and} \quad \varkappa_3 = \frac{1}{y_{23}^2} . \tag{335}$$

**5.2.2.4. Convexity of the yield surface: Model-II.** Considering the fact that the Hessian of the squared Euclidean norm is the identity matrix which is axiomatically positive definite, the requirement for convexity of the yield surface (334) is given by $\varkappa_{2,3} \geq 0$, see also Naghdi-Trapp inequality [123–125], which is generally fulfilled by Eqn. (335).

**5.2.2.5. Evolution equations.**

**5.2.2.5.1. Model-I-$\mathcal{RI}$: Rate-independent setting.** The evolution equations of the plastic variables can be specified analogous to Eqns. (288) and (296), with the aid of Eqn. (318), as

$$
\begin{aligned}
&1. \quad \mathscr{L},_{\boldsymbol{\sigma}} \equiv -\dot{\boldsymbol{\varepsilon}}^p + \lambda\chi,_{\boldsymbol{\sigma}} = \dot{\boldsymbol{\varepsilon}}^p - \lambda\{\varkappa_1(\boldsymbol{1} - \boldsymbol{m}) + \bar{\mathfrak{n}}\} = \boldsymbol{0} \;, \\
&2. \quad \mathscr{L},_{\kappa} \equiv -\dot{\xi} \;\; + \lambda\chi,_{\kappa} = \dot{\xi} \;\; - \lambda\{1/y_{12}\} = 0 \;, \\
&3. \quad \mathscr{L},_{\boldsymbol{\beta}} \equiv -\dot{\boldsymbol{\alpha}} \;\; + \lambda\chi,_{\boldsymbol{\beta}} = \dot{\boldsymbol{\alpha}} \;\; - \lambda\{\varkappa_1(\boldsymbol{1} - \boldsymbol{m}) + \hat{\mathfrak{n}}\} = \boldsymbol{0} \;,
\end{aligned}
\tag{336}
$$

along with the plastic loading/unloading conditions

$$
\lambda \geq 0, \quad \chi \leq 0 \quad \text{and} \quad \lambda\chi \equiv 0 \;.
\tag{337}
$$

For the particular choice of Model-II, the terms $\bar{\mathfrak{n}}$ and $\hat{\mathfrak{n}}$ are derived to have the following explicit forms

$$
\bar{\mathfrak{n}} = \sum_{i=2}^{3} \chi,_{\tilde{J}_i} \tilde{J}_{i,\,\mathfrak{s}} = \frac{\varkappa_3 \mathfrak{s} + (\varkappa_2 - \varkappa_3)(\boldsymbol{m}\mathfrak{s} + \mathfrak{s}\boldsymbol{m})}{\left[\varkappa_2 \tilde{J}_2 + \varkappa_3 \tilde{J}_3\right]^{1/2}} \;.
\tag{338}
$$

$$
\hat{\mathfrak{n}} = \bar{\mathfrak{n}} + \zeta_2 \mathfrak{s} + (\zeta_2 - \zeta_3)(\boldsymbol{m}\mathfrak{s} + \mathfrak{s}\boldsymbol{m})
$$

It follows from Eqn. (313) that the fourth-order projection tensor can be expressed as

$$
\mathbb{P} = \mathfrak{s},_{\boldsymbol{\sigma}} = (\boldsymbol{1} \oplus \boldsymbol{1}) - \frac{1}{3}(\boldsymbol{1} \otimes \boldsymbol{1}) - \frac{3}{2}(\boldsymbol{m}' \otimes \boldsymbol{m}') \;.
\tag{339}
$$

The canonical form of the evolution equations given by Eqn. (336) is a straightforward consequence of invoking the principle of maximum dissipation, which frames the model within *associative plasticity.*

For *non-associative plasticity*, a plastic flow potential $\phi$ is chosen such that it has similar functional form as that of the yield function; and the only difference is that $\phi$ is deviatoric, that is

$$
\phi = \chi|_{\varkappa_1 = 0} = \left[\varkappa_2 \tilde{J}_2 + \varkappa_3 \tilde{J}_3\right]^{1/2} - \left(1 - \frac{\kappa}{y_{12}}\right) + \frac{\zeta_1}{2}\tilde{J}_2|_{\boldsymbol{\sigma}=\boldsymbol{0}} + \frac{\zeta_2}{2}\tilde{J}_3|_{\boldsymbol{\sigma}=\boldsymbol{0}} \;,
\tag{340}
$$

which allows for the definition of deviatoric evolution equations as

$$
\begin{aligned}
&1. \quad \dot{\boldsymbol{\varepsilon}}^p - \lambda\chi,_{\boldsymbol{\sigma}} = \dot{\boldsymbol{\varepsilon}}^p - \lambda\bar{\mathfrak{n}} = \boldsymbol{0} \;, \\
&2. \quad \dot{\xi} \;\; - \lambda\chi,_{\kappa} = \dot{\xi} \;\; - \lambda\{1/y_{12}\} = 0 \;, \\
&3. \quad \dot{\boldsymbol{\alpha}} \;\; - \lambda\chi,_{\boldsymbol{\beta}} = \dot{\boldsymbol{\alpha}} \;\; - \lambda\hat{\mathfrak{n}} = \boldsymbol{0} \;.
\end{aligned}
\tag{341}
$$

The set of equations $(341)_{1-3}$ is a consequence of relaxing the principle of maximum dissipation, which frames the model within non-associative plasticity. This is sometimes referred to as *non-conventional* constitutive structure.

Box 9: Rate-independent setting–summary of the modelling framework for the transversely isotropic symmetry group.

1. Kinematics : $\qquad \boldsymbol{\varepsilon} = \boldsymbol{\varepsilon}^e + \boldsymbol{\varepsilon}^p$

2. Internal variables : $\qquad \mathfrak{e} = \{\boldsymbol{\varepsilon}^p, \xi, \boldsymbol{\alpha}\}$

3. Energetic potential : $\qquad \psi = \psi^e(\boldsymbol{\varepsilon} - \boldsymbol{\varepsilon}^p, \boldsymbol{m}) + \psi_{\mathrm{iso}}^p(\xi) + \psi_{\mathrm{kin}}^p(\boldsymbol{\alpha}, \boldsymbol{m})$

4. Stress tensor : $\qquad \boldsymbol{\sigma} = \psi^e(\boldsymbol{\varepsilon} - \boldsymbol{\varepsilon}^p, \boldsymbol{m})_{,\boldsymbol{\varepsilon}}$

5. Driving forces : $\qquad \kappa = -\psi_{\mathrm{iso}}^p(\xi)_{,\xi}$

$\qquad\qquad\qquad\qquad\qquad\quad \boldsymbol{\beta} = -\psi_{\mathrm{kin}}^p(\boldsymbol{\alpha}, \boldsymbol{m})_{,\boldsymbol{\alpha}}$

5. Relative stress tensor : $\qquad \boldsymbol{\Sigma} = \boldsymbol{\sigma} + \boldsymbol{\beta}$

6. Plasticity inducing stress tensor : $\mathfrak{s} = \mathfrak{s}(\boldsymbol{\Sigma})$

7. Yield function : $\qquad \chi = \chi(\boldsymbol{\Sigma}, \boldsymbol{m}, \kappa)$

8. Plastic flow potential : $\qquad \phi = \phi(\mathfrak{s}, \boldsymbol{m}, \kappa)$

9. Evolution equations :

    Associative

$$\dot{\boldsymbol{\varepsilon}}^p = \lambda \chi_{,\boldsymbol{\sigma}} = \lambda\{\varkappa_1(\boldsymbol{1} - \boldsymbol{m}) + \bar{\mathfrak{n}}\}$$

$$\dot{\xi} = \lambda \chi_{,\kappa}$$

$$\dot{\boldsymbol{\alpha}} = \lambda \chi_{,\boldsymbol{\beta}} = \lambda\{\varkappa_1(\boldsymbol{1} - \boldsymbol{m}) + \hat{\mathfrak{n}}\}$$

    Non-associative

$$\dot{\boldsymbol{\varepsilon}}^p = \lambda \phi_{,\boldsymbol{\sigma}} = \lambda \bar{\mathfrak{n}}$$

$$\dot{\xi} = \lambda \phi_{,\kappa}$$

$$\dot{\boldsymbol{\alpha}} = \lambda \phi_{,\boldsymbol{\beta}} = \lambda \hat{\mathfrak{n}}$$

10. Karush-Kuhn-Tucker conditions : $\lambda \geq 0, \quad \chi \leq 0 \quad \text{and} \quad \lambda\chi \equiv 0$

**5.2.2.5.2. Model-II-$\mathcal{RI}$: Rate-independent setting.** For the particular choice of Model-II, the evolution of plastic variables can be prescribed based on Eqn. (334) as

$$
\begin{aligned}
&1. \;\; \mathscr{L}_{,\boldsymbol{\sigma}} \equiv -\dot{\boldsymbol{\varepsilon}}^p + \lambda \chi_{,\boldsymbol{\sigma}} = \dot{\boldsymbol{\varepsilon}}^p - \lambda\{\varkappa_1(\boldsymbol{1} - \boldsymbol{m}) + \bar{\mathfrak{n}}\} = \boldsymbol{0} \;, \\
&2. \;\; \mathscr{L}_{,\kappa} \equiv -\dot{\xi} + \lambda \chi_{,\kappa} = \dot{\xi} - \lambda\{1/y_{12}\} = 0 \;, \\
&3. \;\; \mathscr{L}_{,\boldsymbol{\beta}} \equiv -\dot{\boldsymbol{\alpha}} + \lambda \chi_{,\boldsymbol{\beta}} = \dot{\boldsymbol{\alpha}} - \lambda\{\varkappa_1(\boldsymbol{1} - \boldsymbol{m}) + \hat{\mathfrak{n}}\} = \boldsymbol{0} \;,
\end{aligned}
\tag{342}
$$

along with the plastic loading/unloading conditions

$$\lambda \geq 0, \quad \chi \leq 0 \quad \text{and} \quad \lambda\chi \equiv 0 \;. \tag{343}$$

The terms $\bar{\mathbf{n}}$ and $\hat{\mathbf{n}}$ are derived to have the following explicit forms with respect to the choice of Model-II,

$$\bar{\mathbf{n}} = \frac{\varkappa_3 \mathfrak{s} + (\varkappa_2 - \varkappa_3)(\boldsymbol{m}\mathfrak{s} + \mathfrak{s}\boldsymbol{m})}{\left[\varkappa_2 \left\| \mathfrak{s}_2 \right\|^2 + \varkappa_3 \left\| \mathfrak{s}_3 \right\|^2 \right]^{1/2}} \quad . \tag{344}$$

$$\hat{\mathbf{n}} = \bar{\mathbf{n}} + \zeta_2 \mathfrak{s} + (\zeta_2 - \zeta_3)(\boldsymbol{m}\mathfrak{s} + \mathfrak{s}\boldsymbol{m})$$

Evolution equations of type (342) are referred to as the *associative flow rules*. To formally prescribe the *non-associative flow rules*, the plastic flow potential is chosen to be of the form

$$\phi = \chi|_{\varkappa_1 = 0} = \left[\varkappa_2 \left\| \mathfrak{s}_2 \right\|^2 + \varkappa_3 \left\| \mathfrak{s}_3 \right\|^2 \right]^{1/2} - \left(1 - \frac{\kappa}{y_{12}}\right) + \frac{\zeta_1}{2} \left\| \mathfrak{s}_2|_{\sigma=0} \right\|^2 + \frac{\zeta_2}{2} \left\| \mathfrak{s}_3|_{\sigma=0} \right\|^2 \ , \tag{345}$$

based on which Eqn. (342) reformulates to

$$\begin{aligned}
&1. \quad \dot{\boldsymbol{\varepsilon}}^p - \lambda\chi_{,\boldsymbol{\sigma}} = \dot{\boldsymbol{\varepsilon}}^p - \lambda\bar{\mathbf{n}} = \boldsymbol{0} \ , \\
&2. \quad \dot{\xi} \ - \lambda\chi_{,\kappa} = \dot{\xi} \ - \lambda\{1/y_{12}\} = 0 \ , \\
&3. \quad \dot{\boldsymbol{\alpha}} - \lambda\chi_{,\boldsymbol{\beta}} = \dot{\boldsymbol{\alpha}} - \lambda\hat{\mathbf{n}} = \boldsymbol{0} \ .
\end{aligned} \tag{346}$$

The rate-independent framework of transversely isotropic plasticity outlined so far, and completely defined by **Model-I-$\mathcal{RI}$** and **Model-II-$\mathcal{RI}$**, is summarised in Box 9.

**5.2.2.5.3. Model-I-$\mathcal{RD}$: Rate-dependent setting.** Within a rate-dependent setting, the canonical evolution equations (*associative flow rules*) of **Model-I-$\mathcal{RI}$** which are given by Eqn. (336) reformulate to

$$\begin{aligned}
&1. \quad \mathscr{P}_{,\boldsymbol{\sigma}} \equiv -\dot{\boldsymbol{\varepsilon}}^p + \frac{1}{\eta}[\chi^+]^m \ \chi_{,\boldsymbol{\sigma}} = \dot{\boldsymbol{\varepsilon}}^p - \frac{1}{\eta}[\chi^+]^m \ \{\varkappa_1(\boldsymbol{1} - \boldsymbol{m}) + \bar{\mathbf{n}}\} = \boldsymbol{0} \ , \\[2mm]
&2. \quad \mathscr{P}_{,\kappa} \equiv -\dot{\xi} \ + \frac{1}{\eta}[\chi^+]^m \ \chi_{,\kappa} = \dot{\xi} \ - \frac{1}{\eta}[\chi^+]^m \ \{1/y_{12}\} = 0 \ , \\[2mm]
&3. \quad \mathscr{P}_{,\boldsymbol{\beta}} \equiv -\dot{\boldsymbol{\alpha}} + \frac{1}{\eta}[\chi^+]^m \ \chi_{,\boldsymbol{\beta}} = \dot{\boldsymbol{\alpha}} - \frac{1}{\eta}[\chi^+]^m \ \{\varkappa_1(\boldsymbol{1} - \boldsymbol{m}) + \hat{\mathbf{n}}\} = \boldsymbol{0} \ ,
\end{aligned} \tag{347}$$

where $\mathscr{P}$ is the penalty functional of the type (306) with $\chi$ defined in Eqn. (318), and the quantities $\bar{\mathbf{n}}$ and $\hat{\mathbf{n}}$ defined in Eqn. (338).

For a *non-associative flow* response, the evolution equations (347) reformulate, respectively, to

$$\begin{aligned}
&1. \quad \dot{\boldsymbol{\varepsilon}}^p - \frac{1}{\eta}[\phi^+]^m \ \phi_{,\boldsymbol{\sigma}} = \dot{\boldsymbol{\varepsilon}}^p - \frac{1}{\eta}[\phi^+]^m \ \bar{\mathbf{n}} = \boldsymbol{0} \ , \\[2mm]
&2. \quad \dot{\xi} \ - \frac{1}{\eta}[\phi^+]^m \ \phi_{,\kappa} = \dot{\xi} \ - \frac{1}{\eta}[\phi^+]^m \ \{1/y_{12}\} = 0 \ , \\[2mm]
&3. \quad \dot{\boldsymbol{\alpha}} - \frac{1}{\eta}[\phi^+]^m \ \phi_{,\boldsymbol{\beta}} = \dot{\boldsymbol{\alpha}} - \frac{1}{\eta}[\phi^+]^m \ \hat{\mathbf{n}} = \boldsymbol{0} \ ,
\end{aligned} \tag{348}$$

where $[\phi^+]$ is of the form defined in (311) with respect to the plastic flow potential $\phi$ given by Eqn. (340). The quantities $\bar{\mathbf{n}}$ and $\hat{\mathbf{n}}$ defined in Eqn. (338).

**5.2.2.5.4. Model-II-$\mathcal{RD}$: Rate-dependent setting.** In complete analogy to **Model-I-$\mathcal{RD}$**, the *associative* and *non-associative* flow rules for a rate-dependent setting for the choice of Eqns. (334) and (345) are given, respectively, by

$$1. \quad \mathscr{P}_{,\boldsymbol{\sigma}} \equiv -\dot{\boldsymbol{\varepsilon}}^p + \frac{1}{\eta}[\chi^+]^m \, \chi_{,\boldsymbol{\sigma}} = \dot{\boldsymbol{\varepsilon}}^p - \frac{1}{\eta}[\chi^+]^m \, \{\varkappa_1(\boldsymbol{1} - \boldsymbol{m}) + \bar{\mathfrak{n}}\} = \boldsymbol{0} \; ,$$

$$2. \quad \mathscr{P}_{,\kappa} \equiv -\dot{\xi} \; + \frac{1}{\eta}[\chi^+]^m \, \chi_{,\kappa} = \dot{\xi} \; - \frac{1}{\eta}[\chi^+]^m \, \{1/y_{12}\} = 0 \; , \qquad (349)$$

$$3. \quad \mathscr{P}_{,\boldsymbol{\beta}} \equiv -\dot{\boldsymbol{\alpha}} + \frac{1}{\eta}[\chi^+]^m \, \chi_{,\boldsymbol{\beta}} = \dot{\boldsymbol{\alpha}} - \frac{1}{\eta}[\chi^+]^m \, \{\varkappa_1(\boldsymbol{1} - \boldsymbol{m}) + \hat{\mathfrak{n}}\} = \boldsymbol{0} \; ,$$

and

$$1. \quad \dot{\boldsymbol{\varepsilon}}^p - \frac{1}{\eta}[\phi^+]^m \, \phi_{,\boldsymbol{\sigma}} = \dot{\boldsymbol{\varepsilon}}^p - \frac{1}{\eta}[\phi^+]^m \, \bar{\mathfrak{n}} = \boldsymbol{0} \; ,$$

$$2. \quad \dot{\xi} \; - \frac{1}{\eta}[\phi^+]^m \, \phi_{,\kappa} = \dot{\xi} \; - \frac{1}{\eta}[\phi^+]^m \, \{1/y_{12}\} = 0 \; , \qquad (350)$$

$$3. \quad \dot{\boldsymbol{\alpha}} \; - \frac{1}{\eta}[\phi^+]^m \, \phi_{,\boldsymbol{\beta}} = \dot{\boldsymbol{\alpha}} \; - \frac{1}{\eta}[\phi^+]^m \, \hat{\mathfrak{n}} = \boldsymbol{0} \; ,$$

where the threshold-type yield function and the plastic flow potential are defined in Eqns. (334) and (345) respectively, while $\bar{\mathfrak{n}}$ and $\hat{\mathfrak{n}}$ are defined in Eqn. (344). To this end, a summary of the rate-dependent framework of transversely isotropic plasticity, defined by Eqns. (347)–(350), is given in Box 10.

**Remark 6.** With reference to the *rate-dependent* theory of Perzyna-type viscoplasticity [86,87], it is well known that the plastic multiplier $\lambda$ is governed by the *pseudo-consistency condition*, i.e.

$$\lambda = \frac{1}{\eta}[\chi(\mathfrak{f})^+]^m \geq 0 \; . \qquad (351)$$

To this end, consider a generalised yield function

$$\chi(\mathfrak{f}) = \|\mathfrak{f}\| - y_0 \leq 0 \; , \qquad (352)$$

based on which a set of canonical evolution equations read

$$\dot{\mathfrak{e}} = \lambda \chi_{,\mathfrak{f}} \; . \qquad (353)$$

Recall here the generalised reduced plastic dissipation such that

$$\mathscr{D}^{\mathrm{red}}(\mathfrak{f}, \mathfrak{e}) = \mathfrak{f} \cdot \dot{\mathfrak{e}} \geq 0 \; . \qquad (354)$$

Substituting Eqns. (353) and (351) into Eqn. (354), and noting that $\mathfrak{f} \cdot \chi(\mathfrak{f})_{,\mathfrak{f}} = \|\mathfrak{f}\|$ yields the representation

$$\mathscr{D}^{\mathrm{red}} = \lambda(\chi + y_0) = \frac{[\chi(\mathfrak{f})^+]^m(\chi + y_0)}{\eta} \geq 0 \; , \qquad (355)$$

for the rate-dependent case, and similarly

$$\mathscr{D}^{\mathrm{red}} = \lambda y_0 \geq 0 \; , \qquad (356)$$

for the rate-independent setting. With these observations (non-negative dissipation), the constitutive framework of plasticity is said to be thermodynamically consistent [66,84].

Box 10: Rate-dependent setting–summary of the modelling framework for the transversely isotropic symmetry group.

---

1. Kinematics : $\quad \boldsymbol{\varepsilon} = \boldsymbol{\varepsilon}^e + \boldsymbol{\varepsilon}^p$

2. Internal variables : $\quad \boldsymbol{\mathfrak{e}} = \{\boldsymbol{\varepsilon}^p, \xi, \boldsymbol{\alpha}\}$

3. Energetic potential : $\quad \psi = \psi^e(\boldsymbol{\varepsilon} - \boldsymbol{\varepsilon}^p, \boldsymbol{m}) + \psi_{\text{iso}}^p(\xi) + \psi_{\text{kin}}^p(\boldsymbol{\alpha}, \boldsymbol{m})$

4. Stress tensor : $\quad \boldsymbol{\sigma} = \psi^e(\boldsymbol{\varepsilon} - \boldsymbol{\varepsilon}^p, \boldsymbol{m})_{,\boldsymbol{\varepsilon}}$

5. Driving forces : $\quad \kappa = -\psi_{\text{iso}}^p(\xi)_{,\xi}$

$\quad \boldsymbol{\beta} = -\psi_{\text{kin}}^p(\boldsymbol{\alpha}, \boldsymbol{m})_{,\boldsymbol{\alpha}}$

5. Relative stress tensor : $\quad \boldsymbol{\Sigma} = \boldsymbol{\sigma} + \boldsymbol{\beta}$

6. Plasticity inducing stress tensor : $\boldsymbol{\mathfrak{s}} = \boldsymbol{\mathfrak{s}}(\boldsymbol{\Sigma})$

7. Yield function : $\quad \chi = \chi(\boldsymbol{\Sigma}, \boldsymbol{m}, \kappa)$

8. Plastic flow potential : $\quad \phi = \phi(\boldsymbol{\mathfrak{s}}, \boldsymbol{m}, \kappa)$

9. Evolution equations :

Associative

$$\dot{\boldsymbol{\varepsilon}}^p = \lambda \chi_{,\boldsymbol{\sigma}} = \lambda\{\varkappa_1(\boldsymbol{1} - \boldsymbol{m}) + \bar{\boldsymbol{\mathfrak{n}}}\}$$

$$\dot{\xi} = \lambda \chi_{,\kappa}$$

$$\dot{\boldsymbol{\alpha}} = \lambda \chi_{,\boldsymbol{\beta}} = \lambda\{\varkappa_1(\boldsymbol{1} - \boldsymbol{m}) + \hat{\boldsymbol{\mathfrak{n}}}\}$$

with $\quad \lambda = \dfrac{1}{\eta}[\chi^+]^m \quad \text{and} \quad [\chi^+] = \dfrac{1}{2}\big[\chi + |\chi|\big]$

Non-associative

$$\dot{\boldsymbol{\varepsilon}}^p = \lambda \phi_{,\boldsymbol{\sigma}} = \lambda \bar{\boldsymbol{\mathfrak{n}}}$$

$$\dot{\xi} = \lambda \phi_{,\kappa}$$

$$\dot{\boldsymbol{\alpha}} = \lambda \phi_{,\boldsymbol{\beta}} = \lambda \hat{\boldsymbol{\mathfrak{n}}}$$

with $\quad \lambda = \dfrac{1}{\eta}[\phi^+]^m \quad \text{and} \quad [\phi^+] = \dfrac{1}{2}\big[\phi + |\phi|\big]$

---

## 5.3. Alternative formulations of non-associative plasticity

The proposed framework of non-associative plasticity for the $\mathscr{C}_3$ and $\mathscr{C}_{13}$ symmetry groups, governed mainly by the plastic flow potentials (302) and (340)/(345) respectively, do not account for dilatation which affects the plastic volume change of the material. This can be attributed to the corresponding definitions of the plasticity inducing stress tensor, which ensure a volume-preserving plastic material response. To incorporate the volume changes, the plastic flow potentials for the two selected symmetry groups are modified according to the arguments in [85] as explained below.

**Remark 7.** The alternative formulations are suggested but not yet implemented.

Starting with the $\mathscr{C}_3$ symmetry group, the plastic flow potential given by Eqn. (302) is modified to have the following form

$$
\phi = \left[ \bar{\varkappa}_1 \tilde{J}_1 + \left\{ \bar{\varkappa}_2 \tilde{J}_2 + \frac{\bar{\varkappa}_3}{2} \tilde{J}_3 + \frac{\bar{\varkappa}_4}{2} \tilde{J}_4 + \frac{\bar{\varkappa}_5}{2} \tilde{J}_5 \right\}^{1/2} - \left( 1 - \frac{\kappa}{\bar{y}_{12}} \right) \right.
$$
$$
\left. + \bar{\zeta}_1 \tilde{J}_2|_{\sigma=0} + \frac{\bar{\zeta}_2}{2} \tilde{J}_3|_{\sigma=0} + \frac{\bar{\zeta}_3}{2} \tilde{J}_4|_{\sigma=0} + \frac{\bar{\zeta}_4}{2} \tilde{J}_5|_{\sigma=0} \right] \leq 0 \qquad (357)
$$

where $\bar{\varkappa}_{1-5} \neq \varkappa_{1-5}$ are the material parameters governing the pressure-dependent plastic flow potential which are determined analogous to Eqns. (280)–(285). Additionally, the inequality $\bar{\varkappa}_i > 0$, $i = 2-5$, should be satisfied for the plastic flow potential to be convex. Taking into account Eqns. (357) and (303), the evolution of plastic variables is given by

$$
\begin{aligned}
&1. \quad \dot{\varepsilon}^p - \lambda \phi,_{\boldsymbol{\sigma}} = \dot{\varepsilon}^p - \lambda \{ \bar{\varkappa}_1 \boldsymbol{m}_3 + \bar{\boldsymbol{N}} \} = \boldsymbol{0} \ , \\
&2. \quad \dot{\xi} \ - \lambda \phi,_{\kappa} = \dot{\xi} \ - \lambda \{ 1/\bar{y}_{12} \} = 0 \ , \\
&3. \quad \dot{\boldsymbol{\alpha}} - \lambda \phi,_{\boldsymbol{\beta}} = \dot{\boldsymbol{\alpha}} - \lambda \{ \bar{\varkappa}_1 \boldsymbol{m}_3 + \hat{\boldsymbol{N}} \} = \boldsymbol{0} \ ,
\end{aligned} \qquad (358)
$$

with

$$
\bar{\boldsymbol{N}} = \sum_{i=2}^{5} \phi,_{\tilde{J}_i} \tilde{J}_i,_{\boldsymbol{\sigma}} = \phi,_{\tilde{J}_2} \tilde{J}_2,_{\boldsymbol{\sigma}} + \sum_{i=3}^{5} \phi,_{\tilde{J}_i} \tilde{J}_i,_{\mathfrak{s}} : \mathfrak{s},_{\boldsymbol{\sigma}}
$$

$$
= \frac{\dfrac{9\bar{\varkappa}_2}{2} \operatorname{tr}[\boldsymbol{m}_3' \boldsymbol{\Sigma}] \boldsymbol{m}_3' + \left\{ \bar{\varkappa}_3 \operatorname{tr}[\boldsymbol{m}_{12}\mathfrak{s}] \boldsymbol{m}_{12} + \bar{\varkappa}_4 \operatorname{tr}[\boldsymbol{m}_{13}\mathfrak{s}] \boldsymbol{m}_{13} + \bar{\varkappa}_5 \operatorname{tr}[\boldsymbol{m}_{23}\mathfrak{s}] \boldsymbol{m}_{23} \right\} : \mathbb{P}}{2 \left[ \bar{\varkappa}_2 \tilde{J}_2 + \dfrac{\bar{\varkappa}_3}{2} \tilde{J}_3 + \dfrac{\bar{\varkappa}_4}{2} \tilde{J}_4 + \dfrac{\bar{\varkappa}_5}{2} \tilde{J}_5 \right]^{1/2}} \ ,
$$

$$
\hat{\boldsymbol{N}} = \bar{\boldsymbol{N}} + \frac{9\bar{\zeta}_1}{2} \operatorname{tr}[\boldsymbol{m}_3' \boldsymbol{\beta}] \boldsymbol{m}_3' + \bar{\zeta}_2 \operatorname{tr}[\boldsymbol{m}_{12}\boldsymbol{\beta}] \boldsymbol{m}_{12} + \bar{\zeta}_3 \operatorname{tr}[\boldsymbol{m}_{13}\boldsymbol{\beta}] \boldsymbol{m}_{13} + \bar{\zeta}_4 \operatorname{tr}[\boldsymbol{m}_{23}\boldsymbol{\beta}] \boldsymbol{m}_{23}
$$

$$(359)$$

where $\mathbb{P}$ is defined in Eqn. (292). Analogous to Eqn. (294), it follows

$$
\operatorname{tr}[\bar{\boldsymbol{N}}] = 0, \quad \bar{\boldsymbol{N}} : \mathbb{P} = \bar{\boldsymbol{N}}, \quad \hat{\boldsymbol{N}} : \mathbb{P} = \hat{\boldsymbol{N}} \quad \text{and} \quad \operatorname{tr}[\hat{\boldsymbol{N}}] = 0 \ . \qquad (360)
$$

Note that the plastic flow potential $\phi$ is of the same functional form as the yield function $\chi$, but with a different choice of material parameters that govern the plastic flow direction. In contrast to Eqn. (302), the plastic flow potential is now pressure-dependent, and the plastic volume change of the material is accounted in the formulation with Eqn. (358).

For the $\mathscr{C}_{13}$ symmetry group, the plastic flow potential corresponding to Model-I, given by Eqn. (340), is modified as

$$
\phi = \bar{\varkappa}_1 \tilde{J}_1 + \left[ \bar{\varkappa}_2 \tilde{J}_2 + \bar{\varkappa}_3 \tilde{J}_3 \right]^{1/2} - \left( 1 - \frac{\kappa}{\bar{y}_{12}} \right) + \frac{\bar{\zeta}_1}{2} \tilde{J}_2|_{\sigma=0} + \frac{\bar{\zeta}_2}{2} \tilde{J}_3|_{\sigma=0} \ , \qquad (361)
$$

where $\bar{\varkappa}_{1-3} \neq \varkappa_{1-3}$ are the material parameters governing the pressure-dependent plastic flow which are determined similar to Eqn. (322). Further, the inequality $\bar{\varkappa}_3 \geq \bar{\varkappa}_2$ is

assumed to ensure the convexity of the plastic flow potential, as implied by Eqns. (323)–(331). In line with Eqn. (341), the evolution equations take the form

$$
\begin{aligned}
&1. \quad \dot{\boldsymbol{\varepsilon}}^p - \lambda \phi_{,\boldsymbol{\sigma}} = \dot{\boldsymbol{\varepsilon}}^p - \lambda \{ \bar{\varkappa}_1 (\mathbf{1} - \boldsymbol{m}) + \bar{\mathbf{N}} \} = \boldsymbol{0} \ , \\
&2. \quad \dot{\xi} \ - \lambda \phi_{,\kappa} = \dot{\xi} \ - \lambda \{ 1/\bar{y}_{12} \} = 0 \ , \\
&3. \quad \dot{\boldsymbol{\alpha}} \ - \lambda \phi_{,\boldsymbol{\beta}} = \dot{\boldsymbol{\alpha}} \ - \lambda \{ \bar{\varkappa}_1 (\mathbf{1} - \boldsymbol{m}) + \hat{\mathbf{N}} \} = \boldsymbol{0} \ ,
\end{aligned}
\tag{362}
$$

with

$$
\bar{\mathbf{N}} = \sum_{i=2}^{3} \phi_{,\tilde{J}_i} \, \tilde{J}_{i,\,\mathfrak{s}} = \left\{ \frac{\bar{\varkappa}_3 \mathfrak{s} + (\bar{\varkappa}_2 - \bar{\varkappa}_3)(\boldsymbol{m}\mathfrak{s} + \mathfrak{s}\boldsymbol{m})}{\left[ \bar{\varkappa}_2 \tilde{J}_2 + \bar{\varkappa}_3 \tilde{J}_3 \right]^{1/2}} \right\} : \mathbb{P} \ .
\tag{363}
$$

$$
\hat{\mathbf{N}} = \bar{\mathbf{N}} + \bar{\zeta}_2 \mathfrak{s} + (\bar{\zeta}_2 - \bar{\zeta}_3)(\boldsymbol{m}\mathfrak{s} + \mathfrak{s}\boldsymbol{m})
$$

Likewise, for Model-II, it follows that the plastic flow potential (345) can be modified as

$$
\chi = \bar{\varkappa}_1 p + \left[ \bar{\varkappa}_2 \left\| \mathfrak{s}_2 \right\|^2 + \bar{\varkappa}_3 \left\| \mathfrak{s}_3 \right\|^2 \right]^{1/2} - \left( 1 - \frac{\kappa}{\bar{y}_{12}} \right) + \frac{\bar{\zeta}_1}{2} \left\| \mathfrak{s}_2 \right\|_{\boldsymbol{\sigma}=\boldsymbol{o}}^2 + \frac{\bar{\zeta}_2}{2} \left\| \mathfrak{s}_3 \right\|_{\boldsymbol{\sigma}=\boldsymbol{o}}^2 \ \leq \ 0 \ ,
\tag{364}
$$

allowing for the closed-form expressions of the evolution equations as

$$
\begin{aligned}
&1. \quad \dot{\boldsymbol{\varepsilon}}^p - \lambda \phi_{,\boldsymbol{\sigma}} = \dot{\boldsymbol{\varepsilon}}^p - \lambda \{ \bar{\varkappa}_1 (\mathbf{1} - \boldsymbol{m}) + \bar{\mathbf{N}} \} = \boldsymbol{0} \ , \\
&2. \quad \dot{\xi} \ - \lambda \phi_{,\kappa} = \dot{\xi} \ - \lambda \{ 1/\bar{y}_{12} \} = 0 \ , \\
&3. \quad \dot{\boldsymbol{\alpha}} \ - \lambda \phi_{,\boldsymbol{\beta}} = \dot{\boldsymbol{\alpha}} \ - \lambda \{ \bar{\varkappa}_1 (\mathbf{1} - \boldsymbol{m}) + \hat{\mathbf{N}} \} = \boldsymbol{0} \ ,
\end{aligned}
\tag{365}
$$

with

$$
\bar{\mathbf{N}} = \left\{ \frac{\bar{\varkappa}_3 \mathfrak{s} + (\bar{\varkappa}_2 - \bar{\varkappa}_3)(\boldsymbol{m}\mathfrak{s} + \mathfrak{s}\boldsymbol{m})}{\left[ \bar{\varkappa}_2 \left\| \mathfrak{s}_2 \right\|^2 + \bar{\varkappa}_3 \left\| \mathfrak{s}_3 \right\|^2 \right]^{1/2}} \right\} : \mathbb{P} \ .
\tag{366}
$$

$$
\hat{\mathbf{N}} = \bar{\mathbf{N}} + \bar{\zeta}_2 \mathfrak{s} + (\bar{\zeta}_2 - \bar{\zeta}_3)(\boldsymbol{m}\mathfrak{s} + \mathfrak{s}\boldsymbol{m})
$$

Note that, while the parameters $\kappa_i, \bar{\kappa}_i$ and $y_{12}, \bar{y}_{12}$ are obtained from the experimental curves, the choice of $\zeta_i, \bar{\zeta}_i$ is arbitrary in the present work. A prescription for the identification of material parameters associated with kinematic hardening is given in [34]. With these set of equations, the plastic multiplier $\lambda$ and the fourth-order Prandtl-Reuss tensors of the non-associative plasticity can be computed analogous to Eqn. (299). Generally, the continuum elastic-plastic tangent modulus, given for example by Eqn. (299), will not lead to quadratic convergence when an iterative procedure is used on a global level for the solution of equilibrium equations. For a proper quadratic convergence, the choice of the tangent must be consistent with the iterative procedure. Therefore, in the following subsection, an algorithmic elastic-plastic tangent modulus which is consistent with the Newton-Raphson-type iteration procedure is derived. This is achieved using an integration algorithm based on the general return method [76, 92].

### 5.4. Algorithmic treatment

In this section, aspects of the algorithmic implementation of the proposed plasticity models are discussed in detail. In particular, emphasis is placed on the numerical integration of the set of constitutive equations developed in Section 5.2. Precisely, the algorithmic treatment is concerned with solving the governing equations using a predictor-corrector-type

algorithm [66] which imposes the constraint posed by the yield condition, as discussed in **Chapter 2**, Section 2.5.5. Such algorithms are widely used for implicit simulations. In the present work, the algorithmic developments are identical for the two selected symmetry groups, however, the first and second derivatives appearing in the developments (for example in Eqns. (140)–(145)) differ significantly, and they are highlighted in this section.

### 5.4.1. Time discrete strong form of the governing equations

The first step of the algorithmic treatment is to integrate the governing equations in the time domain. Following [126], a fully implicit backward Euler time integration scheme is used for the integration of the balance and evolution equations of all the models. This integration scheme is fully implicit[10] in the plastic multiplier, internal variables and direction of the plastic flow. The choice of an implicit time integration scheme is motivated by the stability analysis of the numerical solution methods, where it is well-known that an implicit time integration scheme always results in an unconditionally stable solution [127].

Consider a finite time step $[t_{n+1}, t_n]$ and set $\Delta t = t_{n+1} - t_n$. Within this time continuous setting, it has to be ensured that any stress state stays inside the elastic domain, i.e. Eqn. (128) has to be valid at all times.

#### 5.4.1.1. Orthorhombic symmetry group.
##### 5.4.1.1.1. Model-X-$\mathcal{RI}$: Rate-independent setting.   Starting with a rate-independent setting, the associative flow rule given by Eqn. (296) can be numerically integrated analogous to Eqns. (129) and (131) as

$$
\begin{aligned}
\boldsymbol{\varepsilon}^p_{n+1} &= \boldsymbol{\varepsilon}^p_n + \Delta\lambda_{n+1}\{\varkappa_1\boldsymbol{m}_3 + \bar{\mathbf{n}}_{n+1}\} \ , \\
\xi_{n+1} &= \xi_n + \Delta\lambda_{n+1}\{1/y_{12}\} \ , \\
\boldsymbol{\alpha}_{n+1} &= \boldsymbol{\alpha}_n + \Delta\lambda_{n+1}\{\varkappa_1\boldsymbol{m}_3 + \hat{\mathbf{n}}_{n+1}\} \ ,
\end{aligned}
\tag{367}
$$

where $\Delta\lambda_{n+1} = \Delta t\lambda_{n+1} \geq 0$ denotes the plastic increment, and $\bar{\mathbf{n}}$ and $\hat{\mathbf{n}}$ are defined in Eqn. (291), respectively. Likewise, for the non-associative plasticity rule it follows that the evolution equations (303) can be integrated as

$$
\begin{aligned}
\boldsymbol{\varepsilon}^p_{n+1} &= \boldsymbol{\varepsilon}^p_n + \Delta\lambda_{n+1}\bar{\mathbf{n}}_{n+1} \ , \\
\xi_{n+1} &= \xi_n + \Delta\lambda_{n+1}\{1/y_{12}\} \ , \\
\boldsymbol{\alpha}_{n+1} &= \boldsymbol{\alpha}_n + \Delta\lambda_{n+1}\hat{\mathbf{n}}_{n+1} \ .
\end{aligned}
\tag{368}
$$

These two equations allow the statement of relations for the driving forces $\mathfrak{f}_{n+1} = \{\boldsymbol{\sigma}_{n+1}, \kappa_{n+1}, \boldsymbol{\beta}_{n+1}\}$, with the aid of Eqn. (262), as

$$
\begin{aligned}
\boldsymbol{\sigma}_{n+1} &= \mathbb{E} : (\boldsymbol{\varepsilon}_{n+1} - \boldsymbol{\varepsilon}^p_{n+1}) = \mathbb{E} : (\boldsymbol{\varepsilon}_{n+1} - \boldsymbol{\varepsilon}^p_n - \Delta\lambda_{n+1}\{\varkappa_1\boldsymbol{m}_3 + \bar{\mathbf{n}}_{n+1}\}) \\
\kappa_{n+1} &= -h(\bar{\xi} + \xi_{n+1})^n &= -h(\bar{\xi} + \xi_n + \Delta\lambda_{n+1}\{1/y_{12}\})^n \\
\boldsymbol{\beta}_{n+1} &= -\mathbb{H} : \boldsymbol{\alpha}_{n+1} &= -\mathbb{H} : (\boldsymbol{\alpha}_n + \Delta\lambda_{n+1}\{\varkappa_1\boldsymbol{m}_3 + \hat{\mathbf{n}}_{n+1}\})
\end{aligned}
\tag{369}
$$

for the associative flow response, and

$$
\begin{aligned}
\boldsymbol{\sigma}_{n+1} &= \mathbb{E} : (\boldsymbol{\varepsilon}_{n+1} - \boldsymbol{\varepsilon}^p_{n+1}) = \mathbb{E} : (\boldsymbol{\varepsilon}_{n+1} - \boldsymbol{\varepsilon}^p_n - \Delta\lambda_{n+1}\bar{\mathbf{n}}_{n+1}) \\
\kappa_{n+1} &= -h(\bar{\xi} + \xi_{n+1})^n &= -h(\bar{\xi} + \xi_n + \Delta\lambda_{n+1}\{1/y_{12}\})^n \ , \\
\boldsymbol{\beta}_{n+1} &= -\mathbb{H} : \boldsymbol{\alpha}_{n+1} &= -\mathbb{H} : (\boldsymbol{\alpha}_n + \Delta\lambda_{n+1}\hat{\mathbf{n}}_{n+1})
\end{aligned}
\tag{370}
$$

---

[10]Evaluated at the current time step

for the non-associative flow response, where $\mathbb{E}$ and $\mathbb{H}$ are defined in Eqn. (264). Setting $\Delta\lambda_{n+1} = 0$ in Eqns. (369) and (370) and assuming an elastic step between $t_n$ and $t_{n+1}$, it follows that the trial values $\mathfrak{f}_{n+1}^{\text{trial}} = \{\boldsymbol{\sigma}_{n+1}^{\text{trial}}, \kappa_{n+1}^{\text{trial}}, \boldsymbol{\beta}_{n+1}^{\text{trial}}\}$ of the driving forces can be computed as

$$\boldsymbol{\sigma}_{n+1}^{\text{trial}} = \mathbb{E} : (\boldsymbol{\varepsilon}_{n+1} - \boldsymbol{\varepsilon}_n^p) , \quad \kappa_{n+1}^{\text{trial}} = -h(\bar{\xi} + \xi_n) \quad \text{and} \quad \boldsymbol{\beta}_{n+1}^{\text{trial}} = -\mathbb{H} : \boldsymbol{\alpha}_n , \tag{371}$$

which allow for the definition of a trial yield function as

$$\chi^{\text{trial}} = \chi^{\text{trial}}(\mathfrak{f}_{n+1}^{\text{trial}}) = \chi(\boldsymbol{\sigma}_{n+1}^{\text{trial}}, \kappa_{n+1}^{\text{trial}}, \boldsymbol{\beta}_{n+1}^{\text{trial}}) , \tag{372}$$

based on which the loading cases can be distinguished as

$$\left.\begin{array}{lll} \chi^{\text{trial}} < 0 & \text{and} & \Delta\lambda_{n+1} = 0 \Longleftrightarrow \text{elastic step} \\ \chi^{\text{trial}} > 0 & \text{and} & \Delta\lambda_{n+1} > 0 \Longleftrightarrow \text{plastic step} \end{array}\right\} . \tag{373}$$

For an elastic step, the updated values are same as the trial values such that

$$\boldsymbol{\varepsilon}_{n+1}^p = \boldsymbol{\varepsilon}_n^p, \quad \xi_{n+1} = \xi_n, \quad \boldsymbol{\alpha}_{n+1} = \boldsymbol{\alpha}_n, \quad \boldsymbol{\sigma}_{n+1} = \boldsymbol{\sigma}_{n+1}^{\text{trial}} \quad \text{and} \quad \mathbb{E}_{n+1}^{\text{ep}} = \mathbb{E} . \tag{374}$$

For $\chi^{\text{trial}} > 0$, a plastic step has to be carried out to ensure consistency with Eqn. (372). In line with Eqns. (140) and (141), the related non-linear system of equations can be grouped into a residual vector $\mathfrak{R}$, taking into account Eqns. (369), (370), (371) and recalling the consistency condition, as

$$\mathfrak{R} = \begin{bmatrix} \mathfrak{R}_{\boldsymbol{\sigma}} \\ \mathfrak{R}_{\kappa} \\ \mathfrak{R}_{\boldsymbol{\beta}} \\ \mathfrak{R}_{\chi} \end{bmatrix} = \begin{bmatrix} \boldsymbol{\sigma}_{n+1} - \boldsymbol{\sigma}_{n+1}^{\text{trial}} + \Delta\lambda_{n+1}\mathbb{E} : \{\varkappa_1 \boldsymbol{m}_3 + \bar{\mathbf{n}}_{n+1}\} \\ \kappa_{n+1} + h(\bar{\xi} + \xi_n + \Delta\lambda_{n+1}\{1/y_{12}\})^n \\ \boldsymbol{\beta}_{n+1} - \boldsymbol{\beta}_{n+1}^{\text{trial}} + \Delta\lambda_{n+1}\mathbb{H} : \{\varkappa_1 \boldsymbol{m}_3 + \hat{\mathbf{n}}_{n+1}\} \\ \chi \end{bmatrix} = \boldsymbol{0} , \tag{375}$$

for the associative flow response, and

$$\mathfrak{R} = \begin{bmatrix} \mathfrak{R}_{\boldsymbol{\sigma}} \\ \mathfrak{R}_{\kappa} \\ \mathfrak{R}_{\boldsymbol{\beta}} \\ \mathfrak{R}_{\chi} \end{bmatrix} = \begin{bmatrix} \boldsymbol{\sigma}_{n+1} - \boldsymbol{\sigma}_{n+1}^{\text{trial}} + \Delta\lambda_{n+1}\mathbb{E} : \bar{\mathbf{n}}_{n+1} \\ \kappa_{n+1} + h(\bar{\xi} + \xi_n + \Delta\lambda_{n+1}\{1/y_{12}\})^n \\ \boldsymbol{\beta}_{n+1} - \boldsymbol{\beta}_{n+1}^{\text{trial}} + \Delta\lambda_{n+1}\mathbb{H} : \hat{\mathbf{n}}_{n+1} \\ \chi \end{bmatrix} = \boldsymbol{0} , \tag{376}$$

for the non-associative flow response, where $\chi$ is the yield function defined in Eqn. (279). The algebraic solution to general non-linear functions (375) and (376) is complicated, and they often must be numerically solved using some basic concepts of calculus. The commonly used technique is the Newton-Raphson method which yields the solution iteratively considering the function, its gradient and an initial value. If the unknowns are stored in a vector $\mathfrak{P}_{n+1}^i = \{\boldsymbol{\sigma}_{n+1}^i, \kappa_{n+1}^i, \boldsymbol{\beta}_{n+1}^i, \Delta\lambda_{n+1}^i\}$, then the solution to Eqns. (375) and (376) is obtained by the linearisation of $\mathfrak{R}$ around the point $\mathfrak{P}^i$, i.e.

$$\text{Lin}\left[\mathfrak{R}\right]_{\mathfrak{P}_{n+1}^i} = \mathfrak{R}(\mathfrak{P}_{n+1}^i) + \mathfrak{R}(\mathfrak{P}_{n+1}^i),_{\mathfrak{P}} \cdot \Delta\mathfrak{P}_{n+1}^i = \boldsymbol{0} , \tag{377}$$

which gives the update algorithm

$$\boldsymbol{\mathfrak{P}}_{n+1}^{i+1} = \boldsymbol{\mathfrak{P}}_{n+1}^{i} + \Delta\boldsymbol{\mathfrak{P}}_{n+1}^{i}, \quad \Delta\boldsymbol{\mathfrak{P}}_{n+1}^{i} = -\left[\mathfrak{R}(\boldsymbol{\mathfrak{P}}_{n+1}^{i})_{,\boldsymbol{\mathfrak{P}}}\right]^{-1}\mathfrak{R}(\boldsymbol{\mathfrak{P}}_{n+1}^{i}) . \tag{378}$$

In Eqns. (377) and (378), the explicit form of the necessary iteration tangent $\mathfrak{R}(\boldsymbol{\mathfrak{P}}_{n+1}^{i})_{,\boldsymbol{\mathfrak{P}}}$ can be determined based on the residual vectors (375) and (376), with the aid of Eqns. (144) and (145) as

$$\mathfrak{R}(\boldsymbol{\mathfrak{P}}_{n+1}^{i})_{,\boldsymbol{\mathfrak{P}}} = \begin{bmatrix} (\boldsymbol{1} \oplus \boldsymbol{1}) & \boldsymbol{0} & \mathbb{0} & \mathbb{E} : \{\varkappa_1 \boldsymbol{m}_3 + \bar{\boldsymbol{\mathfrak{n}}}_{n+1}\} \\ \boldsymbol{0} & 1 & \boldsymbol{0} & \dfrac{nh}{y_{12}}(\bar{\xi} + \xi_n + \Delta\lambda_{n+1}/y_{12})^{n-1} \\ \mathbb{0} & \boldsymbol{0} & (\boldsymbol{1} \oplus \boldsymbol{1}) & \mathbb{H} : \{\varkappa_1 \boldsymbol{m}_3 + \hat{\boldsymbol{\mathfrak{n}}}_{n+1}\} \\ \{\varkappa_1 \boldsymbol{m}_3 + \bar{\boldsymbol{\mathfrak{n}}}_{n+1}\} & \{1/y_{12}\} & \{\varkappa_1 \boldsymbol{m}_3 + \hat{\boldsymbol{\mathfrak{n}}}_{n+1}\} & 0 \end{bmatrix}, \tag{379}$$

for the associative flow response, and

$$\mathfrak{R}(\boldsymbol{\mathfrak{P}}_{n+1}^{i})_{,\boldsymbol{\mathfrak{P}}} = \begin{bmatrix} (\boldsymbol{1} \oplus \boldsymbol{1}) & \boldsymbol{0} & \mathbb{0} & \mathbb{E} : \bar{\boldsymbol{\mathfrak{n}}}_{n+1} \\ \boldsymbol{0} & 1 & \boldsymbol{0} & \dfrac{nh}{y_{12}}(\bar{\xi} + \xi_n + \Delta\lambda_{n+1}/y_{12})^{n-1} \\ \mathbb{0} & \boldsymbol{0} & (\boldsymbol{1} \oplus \boldsymbol{1}) & \mathbb{H} : \hat{\boldsymbol{\mathfrak{n}}}_{n+1} \\ \{\varkappa_1 \boldsymbol{m}_3 + \bar{\boldsymbol{\mathfrak{n}}}_{n+1}\} & \{1/y_{12}\} & \{\varkappa_1 \boldsymbol{m}_3 + \hat{\boldsymbol{\mathfrak{n}}}_{n+1}\} & 0 \end{bmatrix}, \tag{380}$$

for the non-associative flow response, respectively, where $\mathbb{0}$ is the fourth-order zero tensor. With these quantities, Eqn. (377) can be solved, and its converged solution gives the consistent update of the unknowns $\boldsymbol{\mathfrak{P}}_{n+1} = \{\boldsymbol{\sigma}_{n+1}, \kappa_{n+1}, \boldsymbol{\beta}_{n+1}, \Delta\lambda_{n+1}\}$. Insertion of $\boldsymbol{\mathfrak{P}}_{n+1}$ into Eqns. (367) and (368) yields the consistent update of the internal variables $\boldsymbol{\mathfrak{e}}_{n+1} = \{\boldsymbol{\varepsilon}_{n+1}^{p}, \xi_{n+1}, \boldsymbol{\alpha}_{n+1}\}$. The algorithmic elastic-plastic tangent modulus which is consistent with the Newton-Raphson method can be obtained by taking the variation of the residual equations with respect to the strain. Accordingly, it follows from Eqn. (378) that

$$\begin{bmatrix} \boldsymbol{\sigma}^{i+1} - \boldsymbol{\sigma}^{i} \\ \kappa^{i+1} - \kappa^{i} \\ \boldsymbol{\beta}^{i+1} - \boldsymbol{\beta}^{i} \\ \Delta\lambda^{i+1} - \Delta\lambda^{i} \end{bmatrix} = -\begin{bmatrix} \boldsymbol{\mathfrak{C}}_{\sigma\sigma} & \boldsymbol{\mathfrak{C}}_{\sigma\kappa} & \boldsymbol{\mathfrak{C}}_{\sigma\beta} & \boldsymbol{\mathfrak{C}}_{\sigma\chi} \\ \boldsymbol{\mathfrak{C}}_{\beta\sigma} & \boldsymbol{\mathfrak{C}}_{\beta\kappa} & \boldsymbol{\mathfrak{C}}_{\beta\beta} & \boldsymbol{\mathfrak{C}}_{\beta\chi} \\ \boldsymbol{\mathfrak{C}}_{\kappa\sigma} & \boldsymbol{\mathfrak{C}}_{\kappa\kappa} & \boldsymbol{\mathfrak{C}}_{\kappa\beta} & \boldsymbol{\mathfrak{C}}_{\kappa\chi} \\ \boldsymbol{\mathfrak{C}}_{\chi\sigma} & \boldsymbol{\mathfrak{C}}_{\chi\kappa} & \boldsymbol{\mathfrak{C}}_{\chi\beta} & \boldsymbol{\mathfrak{C}}_{\chi\chi} \end{bmatrix} \begin{bmatrix} \mathfrak{R}_{\sigma} \\ \mathfrak{R}_{\kappa} \\ \mathfrak{R}_{\beta} \\ \mathfrak{R}_{\chi} \end{bmatrix}, \tag{381}$$

with $\boldsymbol{\mathfrak{C}} = \left[\mathfrak{R}(\boldsymbol{\mathfrak{P}}_{n+1}^{i})_{,\boldsymbol{\mathfrak{P}}}\right]^{-1}$. A straightforward derivation of the first row of Eqn. (381) with respect to $\boldsymbol{\varepsilon}$ while taking into account Eqns. (375) and (376) gives the desired consistent tangent operator as

$$\mathbb{E}^{\mathrm{ep}} := \boldsymbol{\sigma}_{,\boldsymbol{\varepsilon}} = (\boldsymbol{\sigma}^{i+1} - \boldsymbol{\sigma}^{i})_{,\boldsymbol{\varepsilon}} = \boldsymbol{\mathfrak{C}}_{\sigma\sigma} : \mathbb{E} , \tag{382}$$

where it should be noted that $\boldsymbol{\mathfrak{C}} = \left[\mathfrak{R}(\boldsymbol{\mathfrak{P}}_{n+1}^{i})_{,\boldsymbol{\mathfrak{P}}}\right]^{-1}$ changes for the associative and non-associative flow based on Eqns. (379) and (380), respectively.

**5.4.1.1.2. Model-X-$\mathcal{RD}$: Rate-dependent setting.** Within a rate-dependent setting, the residual vectors (375) and (376) for the associative and non-associative plasticity reformulate, respectively, for the choice $m = 1$ to

$$\mathfrak{R} = \begin{bmatrix} \mathfrak{R}_{\boldsymbol{\sigma}} \\ \mathfrak{R}_{\kappa} \\ \mathfrak{R}_{\boldsymbol{\beta}} \\ \mathfrak{R}_{\chi} \end{bmatrix} = \begin{bmatrix} \boldsymbol{\sigma}_{n+1} - \boldsymbol{\sigma}_{n+1}^{\text{trial}} + \Delta\lambda_{n+1}\mathbb{E} : \{\varkappa_1\boldsymbol{m}_3 + \bar{\mathbf{n}}_{n+1}\} \\ \kappa_{n+1} + h(\bar{\xi} + \xi_n + \Delta\lambda_{n+1}\{1/y_{12}\})^n \\ \boldsymbol{\beta}_{n+1} - \boldsymbol{\beta}_{n+1}^{\text{trial}} + \Delta\lambda_{n+1}\mathbb{H} : \{\varkappa_1\boldsymbol{m}_3 + \hat{\mathbf{n}}_{n+1}\} \\ \chi^+ - \dfrac{\eta}{\Delta t}\Delta\lambda_{n+1} \end{bmatrix} = \boldsymbol{0} \quad, \qquad (383)$$

and

$$\mathfrak{R} = \begin{bmatrix} \mathfrak{R}_{\boldsymbol{\sigma}} \\ \mathfrak{R}_{\kappa} \\ \mathfrak{R}_{\boldsymbol{\beta}} \\ \mathfrak{R}_{\chi} \end{bmatrix} = \begin{bmatrix} \boldsymbol{\sigma}_{n+1} - \boldsymbol{\sigma}_{n+1}^{\text{trial}} + \Delta\lambda_{n+1}\mathbb{E} : \bar{\mathbf{n}}_{n+1} \\ \kappa_{n+1} + h(\bar{\xi} + \xi_n + \Delta\lambda_{n+1}\{1/y_{12}\})^n \\ \boldsymbol{\beta}_{n+1} - \boldsymbol{\beta}_{n+1}^{\text{trial}} + \Delta\lambda_{n+1}\mathbb{H} : \hat{\mathbf{n}}_{n+1} \\ \chi^+ - \dfrac{\eta}{\Delta t}\Delta\lambda_{n+1} \end{bmatrix} = \boldsymbol{0} \quad, \qquad (384)$$

where the pseudo-consistency condition given by (309)/(150) replaces the consistency condition, in a rate-dependent setting. Likewise, the necessary iteration tangent (379) and (380) for the associative and non-associative plasticity reformulate, respectively, for the choice $m = 1$ to

$$\mathfrak{R}(\mathfrak{P}_{n+1}^i)_{,\mathfrak{P}} = \begin{bmatrix} (\boldsymbol{1} \oplus \boldsymbol{1}) & \boldsymbol{0} & \mathbb{0} & \mathbb{E} : \{\varkappa_1\boldsymbol{m}_3 + \bar{\mathbf{n}}_{n+1}\} \\ \boldsymbol{0} & 1 & \boldsymbol{0} & \dfrac{nh}{y_{12}}(\bar{\xi} + \xi_n + \Delta\lambda_{n+1}/y_{12})^{n-1} \\ \mathbb{0} & \boldsymbol{0} & (\boldsymbol{1} \oplus \boldsymbol{1}) & \mathbb{H} : \{\varkappa_1\boldsymbol{m}_3 + \hat{\mathbf{n}}_{n+1}\} \\ \{\varkappa_1\boldsymbol{m}_3 + \bar{\mathbf{n}}_{n+1}\} & \{1/y_{12}\} & \{\varkappa_1\boldsymbol{m}_3 + \hat{\mathbf{n}}_{n+1}\} & -\dfrac{\eta}{\Delta t} \end{bmatrix},$$
$$(385)$$

and

$$\mathfrak{R}(\mathfrak{P}_{n+1}^i)_{,\mathfrak{P}} = \begin{bmatrix} (\boldsymbol{1} \oplus \boldsymbol{1}) & \boldsymbol{0} & \mathbb{0} & \mathbb{E} : \bar{\mathbf{n}}_{n+1} \\ \boldsymbol{0} & 1 & \boldsymbol{0} & \dfrac{nh}{y_{12}}(\bar{\xi} + \xi_n + \Delta\lambda_{n+1}/y_{12})^{n-1} \\ \mathbb{0} & \boldsymbol{0} & (\boldsymbol{1} \oplus \boldsymbol{1}) & \mathbb{H} : \hat{\mathbf{n}}_{n+1} \\ \{\varkappa_1\boldsymbol{m}_3 + \bar{\mathbf{n}}_{n+1}\} & \{1/y_{12}\} & \{\varkappa_1\boldsymbol{m}_3 + \hat{\mathbf{n}}_{n+1}\} & -\dfrac{\eta}{\Delta t} \end{bmatrix},$$
$$(386)$$

where $\chi$ is given by Eqn. (279). Clearly, for $\eta = 0$, a rate-independent setting is recovered. The elastic-plastic tangent modulus which is algorithmically consistent can be computed using Eqn. (382), with the corresponding definitions.

### 5.4.1.2. Transversely isotropic symmetry group.

**5.4.1.2.1. Model-I-$\mathcal{RI}$: Rate-independent setting.** The evolution equations of this model within the frame of associative plasticity, given by Eqn. (336), can be numerically integrated using a fully implicit backward Euler time integration scheme as

$$
\begin{aligned}
\boldsymbol{\varepsilon}_{n+1}^p &= \boldsymbol{\varepsilon}_n^p + \Delta\lambda_{n+1}\{\varkappa_1(\boldsymbol{1}-\boldsymbol{m}) + \bar{\mathbf{n}}_{n+1}\} \,, \\
\xi_{n+1} &= \xi_n + \Delta\lambda_{n+1}\{1/y_{12}\} \,, \\
\boldsymbol{\alpha}_{n+1} &= \boldsymbol{\alpha}_n + \Delta\lambda_{n+1}\{\varkappa_1(\boldsymbol{1}-\boldsymbol{m}) + \hat{\mathbf{n}}_{n+1}\} \,.
\end{aligned}
\tag{387}
$$

Similarly, the evolution equations within the frame of non-associative plasticity, given by Eqn. (341) can be expressed in the time discrete form as

$$
\begin{aligned}
\boldsymbol{\varepsilon}_{n+1}^p &= \boldsymbol{\varepsilon}_n^p + \Delta\lambda_{n+1}\bar{\mathbf{n}}_{n+1} \,, \\
\xi_{n+1} &= \xi_n + \Delta\lambda_{n+1}\{1/y_{12}\} \,, \\
\boldsymbol{\alpha}_{n+1} &= \boldsymbol{\alpha}_n + \Delta\lambda_{n+1}\hat{\mathbf{n}}_{n+1} \,,
\end{aligned}
\tag{388}
$$

in terms of the expressions $\bar{\mathbf{n}}$ and $\hat{\mathbf{n}}$ defined in Eqn. (338). Analogous to subsection 5.4.1.1, the residual vectors can be defined as

$$
\mathfrak{R} = \begin{bmatrix} \mathfrak{R}_{\sigma} \\ \mathfrak{R}_{\kappa} \\ \mathfrak{R}_{\beta} \\ \mathfrak{R}_{\chi} \end{bmatrix} = \begin{bmatrix} \boldsymbol{\sigma}_{n+1} - \boldsymbol{\sigma}_{n+1}^{\text{trial}} + \Delta\lambda_{n+1}\mathbb{E} : \{\varkappa_1(\boldsymbol{1}-\boldsymbol{m}) + \bar{\mathbf{n}}_{n+1}\} \\ \kappa_{n+1} + h(\bar{\xi} + \xi_n + \Delta\lambda_{n+1}\{1/y_{12}\})^n \\ \boldsymbol{\beta}_{n+1} - \boldsymbol{\beta}_{n+1}^{\text{trial}} + \Delta\lambda_{n+1}\mathbb{H} : \{\varkappa_1(\boldsymbol{1}-\boldsymbol{m}) + \hat{\mathbf{n}}_{n+1}\} \\ \chi \end{bmatrix} = \boldsymbol{0} \,,
\tag{389}
$$

for the associative flow response, and

$$
\mathfrak{R} = \begin{bmatrix} \mathfrak{R}_{\sigma} \\ \mathfrak{R}_{\kappa} \\ \mathfrak{R}_{\beta} \\ \mathfrak{R}_{\chi} \end{bmatrix} = \begin{bmatrix} \boldsymbol{\sigma}_{n+1} - \boldsymbol{\sigma}_{n+1}^{\text{trial}} + \Delta\lambda_{n+1}\mathbb{E} : \bar{\mathbf{n}}_{n+1} \\ \kappa_{n+1} + h(\bar{\xi} + \xi_n + \Delta\lambda_{n+1}\{1/y_{12}\})^n \\ \boldsymbol{\beta}_{n+1} - \boldsymbol{\beta}_{n+1}^{\text{trial}} + \Delta\lambda_{n+1}\mathbb{H} : \hat{\mathbf{n}}_{n+1} \\ \chi \end{bmatrix} = \boldsymbol{0} \,,
\tag{390}
$$

for the non-associative flow response, where $\chi$ is the yield function defined in Eqn. (318). Based on Eqns. (389) and (389), the necessary iteration tangent for the associative and non-associative flow response read

$$
\mathfrak{R}(\mathfrak{P}_{n+1}^i)_{,\mathfrak{P}} = \begin{bmatrix} (\boldsymbol{1}\oplus\boldsymbol{1}) & \boldsymbol{0} & \mathbb{0} & \mathbb{E} : \{\varkappa_1(\boldsymbol{1}-\boldsymbol{m}) + \bar{\mathbf{n}}_{n+1}\} \\ \boldsymbol{0} & 1 & \boldsymbol{0} & \dfrac{nh}{y_{12}}(\bar{\xi} + \xi_n + \Delta\lambda_{n+1}/y_{12})^{n-1} \\ \mathbb{0} & \boldsymbol{0} & (\boldsymbol{1}\oplus\boldsymbol{1}) & \mathbb{H} : \{\varkappa_1(\boldsymbol{1}-\boldsymbol{m}) + \hat{\mathbf{n}}_{n+1}\} \\ \{\varkappa_1(\boldsymbol{1}-\boldsymbol{m}) + \bar{\mathbf{n}}_{n+1}\} & \{1/y_{12}\} & \{\varkappa_1(\boldsymbol{1}-\boldsymbol{m}) + \hat{\mathbf{n}}_{n+1}\} & 0 \end{bmatrix} \,,
\tag{391}
$$

and

$$
\Re(\mathfrak{P}_{n+1}^i),_{\mathfrak{P}} =
\begin{bmatrix}
(\boldsymbol{1} \oplus \boldsymbol{1}) & \boldsymbol{0} & \mathbb{0} & \mathbb{E} : \bar{\mathfrak{n}}_{n+1} \\[2mm]
\boldsymbol{0} & 1 & \boldsymbol{0} & \dfrac{nh}{y_{12}}(\bar{\xi} + \xi_n + \Delta\lambda_{n+1}/y_{12})^{n-1} \\[2mm]
\mathbb{0} & \boldsymbol{0} & (\boldsymbol{1} \oplus \boldsymbol{1}) & \mathbb{H} : \hat{\mathfrak{n}}_{n+1} \\[2mm]
\{\varkappa_1(\boldsymbol{1} - \boldsymbol{m}) + \bar{\mathfrak{n}}_{n+1}\} & \{1/y_{12}\} & \{\varkappa_1(\boldsymbol{1} - \boldsymbol{m}) + \hat{\mathfrak{n}}_{n+1}\} & 0
\end{bmatrix} ,
\tag{392}
$$

respectively, which allow for the computation of algorithmically consistent elastic-plastic tangent modulus using Eqn. (382).

**5.4.1.2.2. Model-I-$\mathcal{RD}$: Rate-dependent setting.** For a rate-dependent setting, Eqns. (389) and (390) reformulate for the choice of $m = 1$ in Eqn. (347) to

$$
\mathfrak{R} =
\begin{bmatrix}
\mathfrak{R}_{\boldsymbol{\sigma}} \\[1mm]
\mathfrak{R}_{\kappa} \\[1mm]
\mathfrak{R}_{\boldsymbol{\beta}} \\[1mm]
\mathfrak{R}_{\chi}
\end{bmatrix}
=
\begin{bmatrix}
\boldsymbol{\sigma}_{n+1} - \boldsymbol{\sigma}_{n+1}^{\text{trial}} + \Delta\lambda_{n+1}\mathbb{E} : \{\varkappa_1(\boldsymbol{1} - \boldsymbol{m}) + \bar{\mathfrak{n}}_{n+1}\} \\[1mm]
\kappa_{n+1} + h(\bar{\xi} + \xi_n + \Delta\lambda_{n+1}\{1/y_{12}\})^n \\[1mm]
\boldsymbol{\beta}_{n+1} - \boldsymbol{\beta}_{n+1}^{\text{trial}} + \Delta\lambda_{n+1}\mathbb{H} : \{\varkappa_1(\boldsymbol{1} - \boldsymbol{m}) + \hat{\mathfrak{n}}_{n+1}\} \\[1mm]
\chi^+ - \dfrac{\eta}{\Delta t}\Delta\lambda_{n+1}
\end{bmatrix}
= \boldsymbol{0} \quad ,
\tag{393}
$$

for the associative flow response, and

$$
\mathfrak{R} =
\begin{bmatrix}
\mathfrak{R}_{\boldsymbol{\sigma}} \\[1mm]
\mathfrak{R}_{\kappa} \\[1mm]
\mathfrak{R}_{\boldsymbol{\beta}} \\[1mm]
\mathfrak{R}_{\chi}
\end{bmatrix}
=
\begin{bmatrix}
\boldsymbol{\sigma}_{n+1} - \boldsymbol{\sigma}_{n+1}^{\text{trial}} + \Delta\lambda_{n+1}\mathbb{E} : \bar{\mathfrak{n}}_{n+1} \\[1mm]
\kappa_{n+1} + h(\bar{\xi} + \xi_n + \Delta\lambda_{n+1}\{1/y_{12}\})^n \\[1mm]
\boldsymbol{\beta}_{n+1} - \boldsymbol{\beta}_{n+1}^{\text{trial}} + \Delta\lambda_{n+1}\mathbb{H} : \hat{\mathfrak{n}}_{n+1} \\[1mm]
\chi^+ - \dfrac{\eta}{\Delta t}\Delta\lambda_{n+1}
\end{bmatrix}
= \boldsymbol{0} \quad ,
\tag{394}
$$

for the non-associative flow response, respectively, where $\chi$ is given by Eqn. (318). The necessary iteration tangent for the associative and non-associative flow response, respectively, is of the form

$$
\Re(\mathfrak{P}_{n+1}^i),_{\mathfrak{P}} =
\begin{bmatrix}
(\boldsymbol{1} \oplus \boldsymbol{1}) & \boldsymbol{0} & \mathbb{0} & \mathbb{E} : \{\varkappa_1(\boldsymbol{1} - \boldsymbol{m}) + \bar{\mathfrak{n}}_{n+1}\} \\[2mm]
\boldsymbol{0} & 1 & \boldsymbol{0} & \dfrac{nh}{y_{12}}(\bar{\xi} + \xi_n + \Delta\lambda_{n+1}/y_{12})^{n-1} \\[2mm]
\mathbb{0} & \boldsymbol{0} & (\boldsymbol{1} \oplus \boldsymbol{1}) & \mathbb{H} : \{\varkappa_1(\boldsymbol{1} - \boldsymbol{m}) + \hat{\mathfrak{n}}_{n+1}\} \\[2mm]
\{\varkappa_1(\boldsymbol{1} - \boldsymbol{m}) + \bar{\mathfrak{n}}_{n+1}\} & \{1/y_{12}\} & \{\varkappa_1(\boldsymbol{1} - \boldsymbol{m}) + \hat{\mathfrak{n}}_{n+1}\} & -\dfrac{\eta}{\Delta t}
\end{bmatrix} ,
\tag{395}
$$

and

$$
\Re(\mathfrak{P}_{n+1}^i),_{\mathfrak{P}} =
\begin{bmatrix}
(\boldsymbol{1} \oplus \boldsymbol{1}) & \boldsymbol{0} & \mathbb{0} & \mathbb{E} : \bar{\mathfrak{n}}_{n+1} \\[2mm]
\boldsymbol{0} & 1 & \boldsymbol{0} & \dfrac{nh}{y_{12}}(\bar{\xi} + \xi_n + \Delta\lambda_{n+1}/y_{12})^{n-1} \\[2mm]
\mathbb{0} & \boldsymbol{0} & (\boldsymbol{1} \oplus \boldsymbol{1}) & \mathbb{H} : \hat{\mathfrak{n}}_{n+1} \\[2mm]
\{\varkappa_1(\boldsymbol{1} - \boldsymbol{m}) + \bar{\mathfrak{n}}_{n+1}\} & \{1/y_{12}\} & \{\varkappa_1(\boldsymbol{1} - \boldsymbol{m}) + \hat{\mathfrak{n}}_{n+1}\} & -\dfrac{\eta}{\Delta t}
\end{bmatrix} .
\tag{396}
$$

**5.4.1.2.3. Model-II-$\mathcal{RI}$: Rate-independent setting.** The corresponding equations of **Model-II-$\mathcal{RI}$** are same as that of **Model-I-$\mathcal{RI}$** for the choice of $\chi$ and $\phi$ defined in Eqns. (334) and (345), and the terms $\bar{\mathfrak{n}}$ and $\hat{\mathfrak{n}}$ defined in Eqn. (344).

**5.4.1.2.4. Model-II-$\mathcal{RD}$: Rate-dependent setting.** In this setting, the corresponding equations are obtained from those of **Model-I-$\mathcal{RD}$** by choosing $\chi$ and $\phi$ in Eqns. (334) and (345), and $\bar{\mathfrak{n}}, \hat{\mathfrak{n}}$ in Eqn. (344).

### 5.4.2. Time discrete weak form of the governing equations

In what follows, the time discrete governing equations (for both symmetry groups) obtained from the previous step recast into their weak form. It should be emphasised here that the plastic variables $\mathfrak{c}_{n+1} = \{\boldsymbol{\varepsilon}_{n+1}^p, \xi_{n+1}, \boldsymbol{\alpha}_{n+1}\}$ are solved locally at the end of the previous step, using for example Eqn. (367) which defines the local update algorithm for these variables. Consequently, the reduced global boundary value problem in its time discrete strong form reads

$$\text{div}[\boldsymbol{\sigma}_{n+1}] + \boldsymbol{\Upsilon}_{n+1} = \boldsymbol{0} \ , \tag{397}$$

where $\boldsymbol{\sigma}_{n+1}$ is obtained from the previous step. Appealing to the standard arguments of variational calculus, i.e. Eqns. (151)–(157), the desired weak form is obtained as

$$\boxed{\int_{\mathscr{B}} \delta\boldsymbol{\varepsilon} : \boldsymbol{\sigma}_{n+1} \, dV - \int_{\partial\mathscr{B}} \delta\boldsymbol{u} \cdot \boldsymbol{t}_{n+1} \, dA - \int_{\mathscr{B}} \delta\boldsymbol{u} \cdot \boldsymbol{\Upsilon}_{n+1} \, dV = \boldsymbol{0}} \ , \tag{398}$$

which provides the starting point for the space discretisation using finite elements.

### 5.4.3. Space discretisation

With reference to the non-linear equation (398), it follows that the displacement $\boldsymbol{u}_{n+1}(\boldsymbol{x})$ is still an infinite dimensional unknown. It can be solved using the finite element method, which requires an exact linearisation of the time discrete weak form (398). The spatial discretisation with finite elements is analogous to that outlined in **Chapter 2**, Eqns. (158)–(180), where standard approximations $\boldsymbol{u}_{n+1} = \sum_{I=1}^{N^I} \mathfrak{N}_I \boldsymbol{u}_{n+1}^I$ and $\delta\boldsymbol{u}_{n+1} = \sum_{I=1}^{N^I} \mathfrak{N}_I \delta\boldsymbol{u}_{n+1}^I$ of the actual and virtual displacement fields, respectively, are considered. The primary field $\boldsymbol{u}_{n+1}(\boldsymbol{x})$ is discretised using $C^0$ continuous interpolations. This will eventually lead to a set of algebraic equations that can be solved for the displacement field $\boldsymbol{u}$. To this end, a summary of the rate-independent algorithmic treatment for $\mathscr{C}_3$ and $\mathscr{C}_{13}$ symmetry groups is given in Box 11 and Box 12, respectively, which can be extended for a rate-dependent setting in a straightforward manner. Additionally, for alternate non-associative plasticity models outlined in Section 5.3, the algorithmic treatment is completely analogous to that of the other models in this section and is therefore overlooked.

Analogous to **Chapter 4**, three different constitutive laws are implemented for each model of the two selected symmetry groups. Starting with the $\mathscr{C}_3$ symmetry group, they are defined by

1. Model-X-RI-a/Model-X-RD-a: associative pressure-independent model, represented by Eqns. (259) and $\left[(279)\right]\big|_{\varkappa_1=0}$ ,

2. Model-X-RI-b/Model-X-RD-b: associative pressure-dependent model, obtained by Eqns. (259) and (279) ,

Box 11: Summary of the algorithmic treatment for the $\mathscr{C}_3$ symmetry group.

1. Given are the history variables $\boldsymbol{\mathfrak{e}}_n = \{\boldsymbol{\varepsilon}_n^p, \xi_n, \boldsymbol{\alpha}_n\}$ and the current strain $\boldsymbol{\varepsilon}_{n+1}$

2. Compute the trial values

$$\boldsymbol{\sigma}_{n+1}^{\text{trial}} = \psi^e(\boldsymbol{\varepsilon}_{n+1} - \boldsymbol{\varepsilon}_n^p)_{,(\varepsilon-\varepsilon^p)} \ , \quad \kappa_{n+1}^{\text{trial}} = -\psi_{\text{iso}}^p(\xi_n)_{,\xi} \quad \text{and} \quad \boldsymbol{\beta}_{n+1}^{\text{trial}} = -\psi_{\text{kin}}^p(\boldsymbol{\alpha}_n)_{,\alpha}$$

3. Compute the trial plasticity inducing stress tensor in terms of $\boldsymbol{\Sigma}_{n+1}^{\text{trial}} = \boldsymbol{\sigma}_{n+1}^{\text{trial}} + \boldsymbol{\beta}_{n+1}^{\text{trial}}$

$$\mathfrak{s}_{n+1}^{\text{trial}} = \boldsymbol{\Sigma}_{n+1}^{\text{trial}} - \text{tr}[\boldsymbol{m}_3\boldsymbol{\Sigma}_{n+1}^{\text{trial}}]\mathbf{1} + \text{tr}[(\boldsymbol{m}_3 - \boldsymbol{m}_1)\boldsymbol{\Sigma}_{n+1}^{\text{trial}}]\boldsymbol{m}_1 + \text{tr}[(\boldsymbol{m}_3 - \boldsymbol{m}_2)\boldsymbol{\Sigma}_{n+1}^{\text{trial}}]\boldsymbol{m}_2$$

4. Compute the trial yield criterion $\chi^{\text{trial}} = \chi(\boldsymbol{\Sigma}_{n+1}^{\text{trial}}, \mathfrak{s}_{n+1}^{\text{trial}}, \kappa_{n+1}^{\text{trial}})$

5. IF $\chi^{\text{trial}} \leq 0$ THEN

   - Elastic step:
     set
     $$\boldsymbol{\varepsilon}_{n+1}^p = \boldsymbol{\varepsilon}_n^p, \quad \xi_{n+1} = \xi_n, \quad \boldsymbol{\alpha}_{n+1} = \boldsymbol{\alpha}_n \ ,$$
     $$\boldsymbol{\sigma}_{n+1} = \boldsymbol{\sigma}_{n+1}^{\text{trial}} \quad \text{and} \quad \mathbb{E}_{n+1}^{\text{ep}} = \psi^e(\boldsymbol{\varepsilon} - \boldsymbol{\varepsilon}_n^p)_{,(\varepsilon-\varepsilon^p)(\varepsilon-\varepsilon_n^p)}$$

6. ELSE

   - Plastic step:
     determine $\boldsymbol{\mathfrak{P}}_{n+1}^i = \{\boldsymbol{\sigma}_{n+1}^i, \kappa_{n+1}^i, \boldsymbol{\beta}_{n+1}^i, \Delta\lambda_{n+1}^i\}$ using Eqns. (375)–(381)

     $$\boldsymbol{\mathfrak{P}}_{n+1}^{i+1} = \boldsymbol{\mathfrak{P}}_{n+1}^i + \Delta\boldsymbol{\mathfrak{P}}_{n+1}^i, \quad \Delta\boldsymbol{\mathfrak{P}}_{n+1}^i = -\left[\mathfrak{R}(\boldsymbol{\mathfrak{P}}_{n+1}^i)_{,\mathfrak{P}}\right]^{-1}\mathfrak{R}(\boldsymbol{\mathfrak{P}}_{n+1}^i)$$

     update the internal variables using Eqns. (367), (368)
     compute the algorithmically consistent tangent modulus using Eqn. (382)

7. ENDIF

8. Reformulate time discrete governing balance equations to time discrete weak form

9. Solve for the infinite dimensional unknown $\boldsymbol{u}_{n+1}(\boldsymbol{x})$ using the finite element method

3. Model-X-RI-c/Model-X-RD-c: non-associative pressure-dependent model, given by Eqns. (259), (279) and (302) .

Likewise, with respect to the two plastic response functions defined for the $\mathscr{C}_{13}$ symmetry group, the three constitutive laws are defined by

1. Model-I-RI-a/Model-I-RD-a: associative pressure-independent model, represented by Eqns. (268) and $\left[(318)\right]\big|_{\varkappa_1=0}$ ,

2. Model-I-RI-b/Model-I-RD-b: associative pressure-dependent model, obtained by Eqns. (268) and (318) ,

Box 12: Summary of the algorithmic treatment for the $\mathscr{C}_{13}$ symmetry group.

---

1. Given are the history variables $\boldsymbol{\mathfrak{e}}_n = \{\boldsymbol{\varepsilon}_n^p, \xi_n, \boldsymbol{\alpha}_n\}$ and the current strain $\boldsymbol{\varepsilon}_{n+1}$

2. Compute the trial values

$$\boldsymbol{\sigma}_{n+1}^{\text{trial}} = \psi^e(\boldsymbol{\varepsilon}_{n+1} - \boldsymbol{\varepsilon}_n^p)_{,(\varepsilon - \varepsilon^p)} \quad , \quad \kappa_{n+1}^{\text{trial}} = -\psi_{\text{iso}}^p(\xi_n)_{,\xi} \quad \text{and} \quad \boldsymbol{\beta}_{n+1}^{\text{trial}} = -\psi_{\text{kin}}^p(\boldsymbol{\alpha}_n)_{,\boldsymbol{\alpha}}$$

3. Compute the trial plasticity inducing stress tensor in terms of $\boldsymbol{\Sigma}_{n+1}^{\text{trial}} = \boldsymbol{\sigma}_{n+1}^{\text{trial}} + \boldsymbol{\beta}_{n+1}^{\text{trial}}$

$$\boldsymbol{\mathfrak{s}}_{n+1}^{\text{trial}} = \boldsymbol{\Sigma}_{n+1}^{\text{trial}} - \frac{1}{3}\text{tr}[\boldsymbol{\Sigma}_{n+1}^{\text{trial}}]\boldsymbol{1} - \frac{3}{2}\text{tr}[\boldsymbol{m}'\boldsymbol{\Sigma}_{n+1}^{\text{trial}}]\boldsymbol{m}'$$

4. Compute the trial yield criterion $\chi^{\text{trial}} = \chi(\boldsymbol{\Sigma}_{n+1}^{\text{trial}}, \boldsymbol{\mathfrak{s}}_{n+1}^{\text{trial}}, \kappa_{n+1}^{\text{trial}})$

5. IF $\chi^{\text{trial}} \leq 0$ THEN

   - Elastic step:

     set
     $$\boldsymbol{\varepsilon}_{n+1}^p = \boldsymbol{\varepsilon}_n^p, \quad \xi_{n+1} = \xi_n, \quad \boldsymbol{\alpha}_{n+1} = \boldsymbol{\alpha}_n \ ,$$
     $$\boldsymbol{\sigma}_{n+1} = \boldsymbol{\sigma}_{n+1}^{\text{trial}} \quad \text{and} \quad \mathbb{E}_{n+1}^{\text{ep}} = \psi^e(\boldsymbol{\varepsilon} - \boldsymbol{\varepsilon}_n^p)_{,(\varepsilon - \varepsilon^p)(\varepsilon - \varepsilon_n^p)}$$

6. ELSE

   - Plastic step:

     determine $\boldsymbol{\mathfrak{P}}_{n+1}^i = \{\boldsymbol{\sigma}_{n+1}^i, \kappa_{n+1}^i, \boldsymbol{\beta}_{n+1}^i, \Delta\lambda_{n+1}^i\}$ using Eqns. (389)–(392)

     $$\boldsymbol{\mathfrak{P}}_{n+1}^{i+1} = \boldsymbol{\mathfrak{P}}_{n+1}^i + \Delta\boldsymbol{\mathfrak{P}}_{n+1}^i, \quad \Delta\boldsymbol{\mathfrak{P}}_{n+1}^i = -\left[\boldsymbol{\mathfrak{R}}(\boldsymbol{\mathfrak{P}}_{n+1}^i)_{,\boldsymbol{\mathfrak{P}}}\right]^{-1}\boldsymbol{\mathfrak{R}}(\boldsymbol{\mathfrak{P}}_{n+1}^i)$$

     update the internal variables using Eqns. (387), (388)
     compute the algorithmically consistent tangent modulus using Eqn. (382)

7. ENDIF

8. Reformulate time discrete governing balance equations to time discrete weak form

9. Solve for the infinite dimensional unknown $\boldsymbol{u}_{n+1}(\boldsymbol{x})$ using the finite element method

---

3. Model-I-RI-c/Model-I-RD-c: non-associative pressure-dependent model, given by Eqns. (268), (318) and (340) ,

and

1. Model-II-RI-a/Model-II-RD-a: associative pressure-independent model, represented by Eqns. (268) and $[(334)]\big|_{\varkappa_1 = 0}$ ,

2. Model-II-RI-b/Model-II-RD-b: associative pressure-dependent model, obtained by Eqns. (268) and (334) ,

3. Model-II-RI-c/Model-II-RD-c: non-associative pressure-dependent model, given by Eqns. (268), (334) and (345) ,

respectively.

# 6. Parameter identification

In this section, a methodology designed to calibrate the models developed in the previous section is described. The identification of material parameters associated with the constitutive equations is crucial for material models, as the reliability on these models for non-linear inelastic simulations not only depends on the underlying physical assumptions and accuracy of the numerical solution, but also on the accurate deduction of the material parameters from the experimental data. The parameter identification problem can be expressed mathematically as a non-linear optimisation problem subjected to inequality constraints [128]. The solution of this problem using various optimisation techniques [129–131] yields optimal parameters for a given set of algebraic/differential equations associated with the model, initial and loading conditions, available experimental data and the simulated material response.

**Remark 8.** Discussions in this chapter are restricted only to the transversely isotropic system due to the lack of experimental data for the orthorhombic symmetry group. Thus, constitutive equations appearing only in subsections 5.1.2 and 5.2.2 are of interest here.

## 6.1. Transversely isotropic symmetric group

For the parameter calibration, elastic parameters are taken directly from [7, 18], and parameters describing the plastic response in Eqns. (268) and (318)/(334) are obtained by an optimisation procedure [132]. The experimental data for the present study is taken from [7, 18], which provides the in-plane shear stress curve (Fig. 3(a) from [18]) and the transverse compression curve (Fig. 4(b) at $\dot{\varepsilon}_0 = 1.5 \times 10^{-4}$ from [18]). To this end, the parameters $y_{12}$, $h$ and $n$ are calibrated from the non-linear in-plane shear stress-strain curve, $y_{23}$ is calibrated from the transverse shear stress-strain curve and $y_{22c}$ is calibrated from the transverse compression data. Due to the lack of experimental data for the transverse shear response, *micro-mechanical* models are used to generate missing data. Two types of micro-mechanical models are used in the present study, namely a
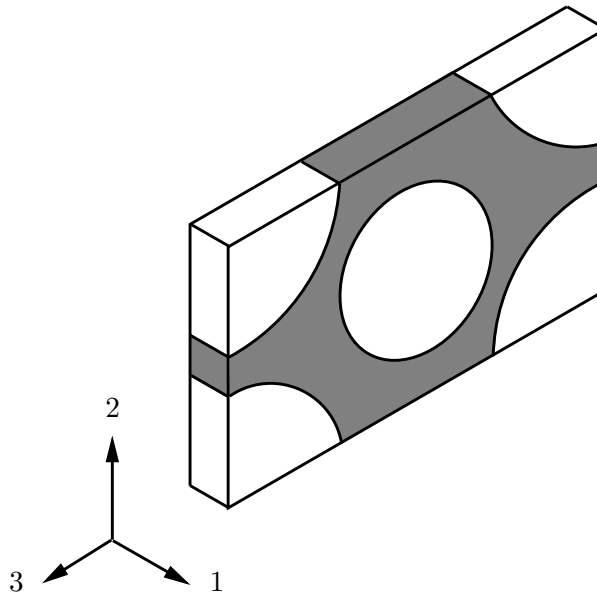


FIGURE 19: **Micro-mechanical models.** Geometrical set up of the unit cell (UCA).

TABLE 5: Material parameters for the micro-mechanical models

| No. | Name | Par. | Value | Unit |
|-----|------|------|-------|------|
| | | | DIG/UCA | |
| | **Fibre** | | | |
| 1. | Young's modulus 1-axis | $E_{1f}$ | 214000 | [MPa] |
| 2. | Young's modulus 2-axis | $E_{2f}$ | 26000 | [MPa] |
| 3. | Shear modulus 12-plane | $G_{12f}$ | 112000 | [MPa] |
| 4. | Shear modulus 23-plane | $G_{23f}$ | 8996.3 | [MPa] |
| 5. | Poisson's ratio | $\nu_{12f}$ | 0.28 | [−] |
| | **Matrix** | | | |
| 6. | Young's modulus | $E_m$ | 4100 | [MPa] |
| 7. | Poisson's ratio | $\nu_m$ | 0.356 | [−] |
| 8. | Initial yield stress | $\sigma_y^0$ | 13.05/12.99 | [MPa] |
| 9. | Hardening modulus | $h$ | 187/220.05 | [MPa] |
| 10. | Hardening exponent | $n$ | 0.269/0.228 | [−] |

unit cell analysis (UCA) with hexagonal arrangement[11], see Fig. 19, and an incremental Mori-Tanaka approach using DIGIMAT (DIG) [133]. For a detailed discussion on the incremental Mori-Tanaka approach, cf. [17, 19, 20]. Furthermore, fibres are assumed to be linear elastic and transversely isotropic with a fibre volume fraction of 60% as given in [18], and the matrix is assumed to be an isotropic elastic-plastic solid. A rate- and pressure-independent plasticity formulation using power law hardening is chosen for both the micro-mechanical models. Due to the availability in the software packages, a standard $J_2$-plasticity is used in the case of the DIGIMAT model and the *Johnson-Cook* material model provided by ABAQUS [134] is chosen for the UCA. Note that the rate- and temperature-dependency in the Johnson-Cook model are not considered. Consequently, the yield stress $\sigma_y$ is governed by the Ludwig equation of the form

$$\sigma_y = \sigma_y^0 + h\xi^n \ . \tag{399}$$

The elastic properties of fibres and the matrix are given in [18] and listed in Table 5, whereas the plastic parameters are calibrated from the experimental data based on the $\tau_{12} - \gamma_{12}$ curve using the calibration procedure explained subsequently.

Note that all the models use periodic boundary conditions and are discretised using hexahedral 3D continuum elements (C3D8) with linear interpolation. For the UCA, the unit cell is discretised into 122 C3D8 elements. A convergence study of UCA showed no change in the overall stress-strain response for increasing mesh resolutions. For the simulations of the DIG and the models proposed in **Chapter 5**, a single C3D8 element is used.

### 6.1.1. Calibration procedure

The plastic parameters of the two micro-mechanical models and the two meso models associated with the group, are calculated by a least squares minimisation of the function

$$f(\boldsymbol{x}) = \frac{1}{k} \sum_{k=1}^{n} \left\| \bar{\boldsymbol{\delta}}_k - \boldsymbol{\delta}_k(\boldsymbol{x}) \right\| \ \rightarrow \ \min \ , \tag{400}$$

---

[11]hexagonal arrangement is a better representation of the reality according to [18]

Table 6: Material parameters for transversely isotropic plasticity

| No. | Name | Par. | Value | Unit |
|-----|------|------|-------|------|
| 1. | Young's modulus 1-axis | $E_1$ | 130000 | [MPa] |
| 2. | Young's modulus 2-axis | $E_2$ | 11000 | [MPa] |
| 3. | Shear modulus 12-plane | $G_{12}$ | 5800 | [MPa] |
| 4. | Poisson's ratio | $\nu_{12}$ | 0.306 | [−] |
| 5. | Poisson's ratio | $\nu_{23}$ | 0.44 | [−] |
| 6. | Transverse compressive yield stress | $y_{22c}$ | $\begin{cases} 45.9/24.6^a \\ 50.01/27.4^b \end{cases}$ | [MPa] |
| 7. | In-plane shear yield stress | $y_{12}$ | 17.9/9.41 | [MPa] |
| 8. | Transverse shear yield stress | $y_{23}$ | 15.9/10.66 | [MPa] |
| 9. | Hardening modulus | $h$ | 192.3/177.5 | [MPa] |
| 10. | Pre-strain | $\bar{\alpha}$ | $1\times10^{-12}$ | [−] |
| 11. | Hardening exponent | $n$ | 0.296/0.246 | [−] |

[a]Model-I-RI-b/-II-RI-b
[b]Model-I-RI-c/-II-RI-c

where $\bar{\boldsymbol{\delta}}_k$ and $\boldsymbol{\delta}_k(\boldsymbol{x})$ represent target and computed values, respectively. The points $k = \{1, \cdots, n\}$ denote the identification points at which target and computed values are to be compared, and $\boldsymbol{x}$ is an array of fitting parameters, i.e. $\boldsymbol{x} = \{\sigma_y^0, h, n\}|_{12}$ for the micro-mechanical models calibration, $\boldsymbol{x} = \{y_{12}, h, n\}|_{12}$ and $\boldsymbol{x} = \{y_{23}\}|_{23}$ for the pressure-independent models and additionally $\boldsymbol{x} = \{y_{22c}\}|_{22}$ for the two pressure-dependent models calibration. A simplex Nelder-Mead algorithm [129, 135] is used for the minimisation of Eqn. (400).

At first, the calibration procedure is used to obtain the plastic parameters of the micro-mechanical models. As pressure dependency is not considered in these models, only the experimental $\tau_{12} - \gamma_{12}$ curve is needed to calibrate the associated parameters $\sigma_y^0$, $h$ and $n$. With the calibrated micro-mechanical models, the transverse compression and transverse shear predictions can be obtained.

**Remark 9.** For the micro-mechanics simulations, only phase averaged stresses show zero hydrostatic pressure under transverse shear loading. Due to the stress concentrations in the matrix, the UCA locally shows a hydrostatic component which may affect the overall plastic response. It has been found that this effect is rather low compared to variations caused by other factors, for example fibre arrangement, and is therefore neglected. The transverse compression curve, which also does not include pressure sensitivity of the matrix, is used for the additional verification of the meso models and not for calibration. By considering the pressure-independent models under transverse compression it is possible to distinguish between the effects of anisotropy (due to the micro-structure) and pressure dependency of the matrix, which cannot be inferred from experimental data [44].

To calibrate the plastic parameters of meso models, the calibration procedure is first used to obtain $y_{12}$, $h$ and $n$ of Model-I-RI-a/-II-RI-a by fitting to the experimental data of the in-plane shear response. Keeping these parameters fixed, $y_{23}$ values for Model-I-RI-a and Model-II-RI-a are obtained from the curves of the calibrated micro-mechanical models.

Finally, $y_{22c}$ values for Model-I-RI-b/-II-RI-b and Model-I-RI-c/-II-RI-c are obtained from the experimental $\sigma_{22} - \varepsilon_{22}$ curve. The calibrated plastic parameters for all the micromechanical and meso models are reported in Tables 5–6.

### 6.1.2. Calibration results

Figure 20 shows results of the calibration comparing the experimental data and various models for the three calibration load cases. It can be seen that all models reproduce the experimental shear $(\tau_{12} - \gamma_{12})$ response very well. Further, the numerical results in Fig. 20 (a) and (b) show that the transverse shear response is stiffer than the in-plane shear response for UCA, whereas the transverse shear response is softer than the in-plane shear response for DIG. The difference between the predicted responses can be attributed to the fact that mean field methods, such as the incremental Mori-Tanaka approach used by DIG, are based on analytical solution of phase averaged stresses that do not take stress concentrations and details of the fibre arrangement into account. As a result, such incremental Mori-Tanaka schemes are less accurate than discrete unit-cell predictions. With reference to subsection 5.2.2.2, Eqn. (331), this readily implies that the convexity requirement for Model-I-RI-a is not fulfilled for calibration to UCA. Hence, Model-I-RI-a is calibrated to DIG and Model-II-RI-a is calibrated to UCA. Note that calibrating $y_{23}$ for Model-II-RI-a to DIG would be admissible as well, however this comparison did not
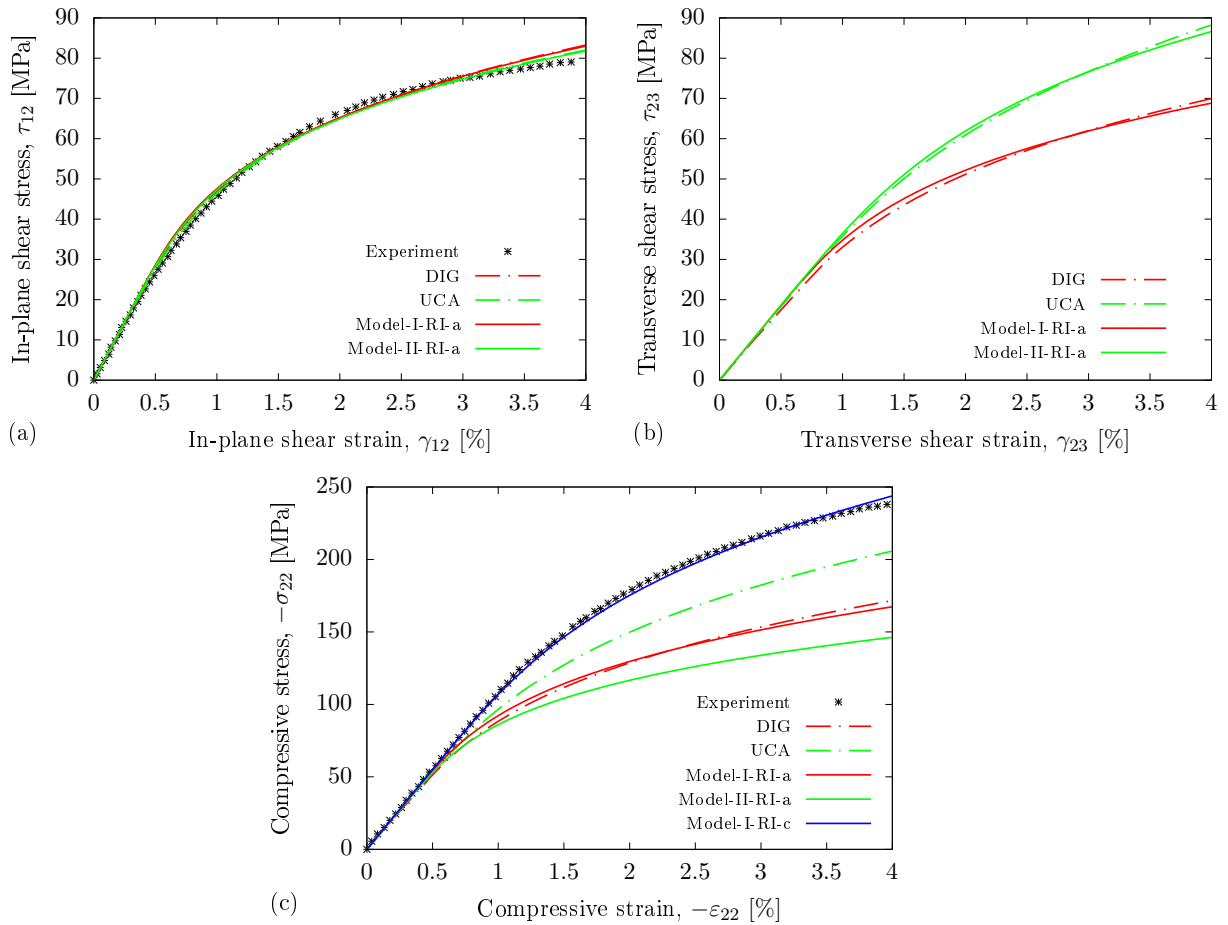


FIGURE 20: **Calibration results.** Comparison of experimental, micro-mechanical and meso models responses for (a) in-plane shear, (b) transverse shear and (c) transverse compression load.

yield any significant insights and is therefore not discussed further.

Figure 20 (c) shows the comparison of micro-mechanical and meso models to the experimental response, for a transverse compression load. It can be seen that the compressive response of Model-I-RI-a fits the DIG model very well whereas Model-II-RI-a is significantly less stiff than UCA in the non-linear compression regime. As stated and computationally verified in [18, 44], this behaviour can be corrected by taking into account the influence of hydrostatic pressure in the formulation of plastic response functions. Therefore, Model-I-RI-b/-II-RI-b and Model-I-RI-c/-II-RI-c are used to capture the experimental transverse compression $(\sigma_{22} - \varepsilon_{22})$ data by calibrating $y_{22c}$. The resulting good agreement between the experimental data and Model-I-RI-c is shown in Fig. 20 (c). Likewise, Model-I-RI-b/-II-RI-b and Model-II-RI-c can be calibrated for $y_{22c}$, which essentially yields the same compressive response as Model-I-RI-c. It should, however, be noted that, in order to reproduce the compression test curve, the coefficient of hydrostatic pressure is comparatively higher for Model-II-RI-b/-RI-c than that of Model-I-RI-b/-RI-c. Furthermore, $y_{22c}$ values also differ slightly between associative (b) and non-associative (c) models.

# 7. Selected numerical examples

The applicability and predictive capacity of models discussed in **Chapters 3–5** is now demonstrated by means of representative numerical simulations. All the proposed models are numerically implemented as user subroutines (UMAT) in ABAQUS, a general purpose non-linear finite element program documented in [134]. These numerical examples highlight the basic constitutive characteristics of the framework of anisotropic elasticity and plasticity, with respect to the two selected symmetry groups. At first, numerical simulations for *homogeneous* deformations are performed to verify the correctness of the implementation. Subsequently *inhomogeneous* boundary value problems are considered.

## 7.1. Anisotropic elasticity

In this section, homogeneous uni-axial deformation is considered in order to highlight the constitutive characteristics of the framework of elasticity, for instance the effect of fibre orientation on the overall material response.

### 7.1.1. Single element test for the orthorhombic symmetry group

Starting with the $\mathscr{C}_3$ symmetric group, predictions of the model (Eqns. (182)–(204)) for various fibre orientations $\theta$, for an applied uni-axial deformation are studied. The geometrical set up and loading conditions are shown in Fig. 21, while the material properties used in the simulation are listed in Table 7. The simulation is performed in a displacement driven context with an axial deformation of $\bar{u} = 0.05$ mm applied as shown in Fig. 21. At y = 0, the vertical movement of the bottom surface is constrained by imposing $u_y = 0$. Likewise, at x = 0 and z = 0, the constraints $u_x = 0$ and $u_z = 0$, respectively, are imposed.

Figure 22 (a) shows the stress-strain curve for six different fibre orientations. Recall here that a woven fabric, which is a typical example for the orthorhombic symmetry group, has two fibre orientations perpendicular to each other and these fibre directions denote the principal material directions. For such a material, stiffness in the loading direction decreases when fibre orientations are changed with respect to loading direction, as seen in Fig. 22 (a). The orientations of fibres with respect to the loading direction are pivotal
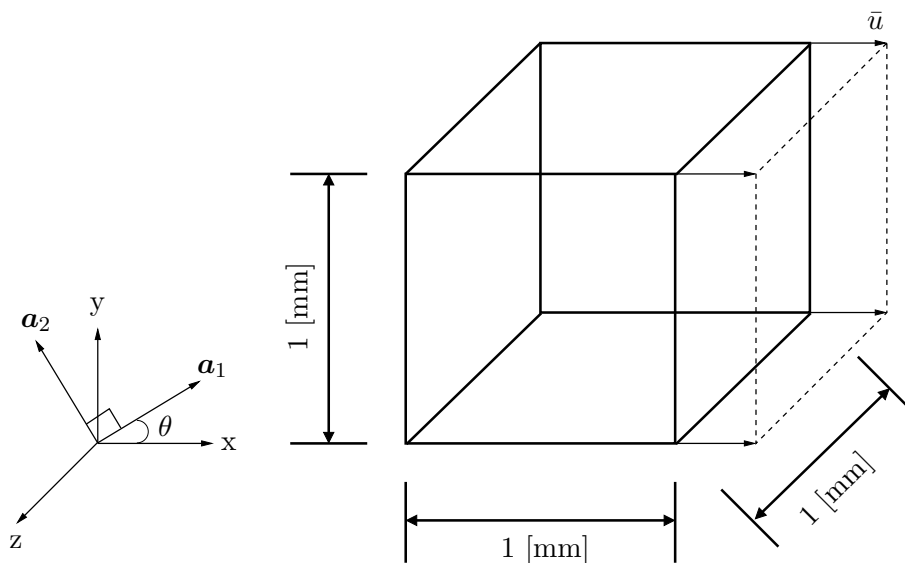


FIGURE 21: **Single element test for the orthorhombic symmetry group.** Geometrical set up and the loading conditions.

TABLE 7: Material parameters for the single element test–$\mathscr{C}_3$ symmetric group

| No. | Name | Par. | Value | Unit |
|-----|------|------|-------|------|
| 1. | Young's modulus 1-axis | $E_1$ | 61340 | [MPa] |
| 2. | Young's modulus 2-axis | $E_2$ | $0.5 \times E_1$ | [MPa] |
| 3. | Young's modulus 3-axis | $E_3$ | $0.75 \times E_1$ | [MPa] |
| 4. | Shear modulus 12-plane | $G_{12}$ | 19500 | [MPa] |
| 5. | Shear modulus 13-plane | $G_{13}$ | $0.5 \times G_{12}$ | [MPa] |
| 6. | Shear modulus 23-plane | $G_{23}$ | $0.75 \times G_{12}$ | [MPa] |
| 7. | Poisson's ratio | $\nu_{12}$ | 0.3 | [−] |
| 8. | Poisson's ratio | $\nu_{13}$ | $0.5 \times \nu_{12}$ | [−] |
| 9. | Poisson's ratio | $\nu_{23}$ | $0.75 \times \nu_{12}$ | [−] |

parameters affecting the mechanical properties of the composite [105]. Thus, the variation of elastic moduli with the fibre orientation angle $\theta$ is illustrated in Fig. 22 (b). It is seen that the modulus $E_{\mathrm{x}}$ is highest for $\theta = 0°$ (loading along x-axis) and lowest for $\theta = 90°$. In contrast, the modulus $E_{\mathrm{y}}$ is highest for $\theta = 90°$ and lowest for $\theta = 0°$. Furthermore, an U-shaped dependency of $E_{\mathrm{x}}$ and $E_{\mathrm{y}}$ on the fibre orientation is seen [136]. The shear modulus $G_{\mathrm{xy}}$ is relatively constant for different fibre orientations. This is a direct consequence of the choice of $G_{13}$ and $G_{23}$, which are nearly identical, see also [106, 107] for a detailed discussion. Meanwhile, the moduli $G_{\mathrm{xz}}$ and $G_{\mathrm{yz}}$ follow same trend as that of $E_{\mathrm{y}}$ and $E_{\mathrm{x}}$, respectively, but at lower magnitudes.

### 7.1.2.  Single element test for the transversely isotropic symmetry group

With respect to the $\mathscr{C}_{13}$ symmetric group, the performance of the model described by Eqns. (206)–(225) is now analysed by means of numerical simulations. The geometrical set up, boundary and loading conditions are identical to the previous case, except that $\mathscr{C}_{13}$ symmetric group is characterised by the existence of a single preferred direction $\boldsymbol{a}$ (Fig. 23). The material parameters used for the simulation are given in Table 8.
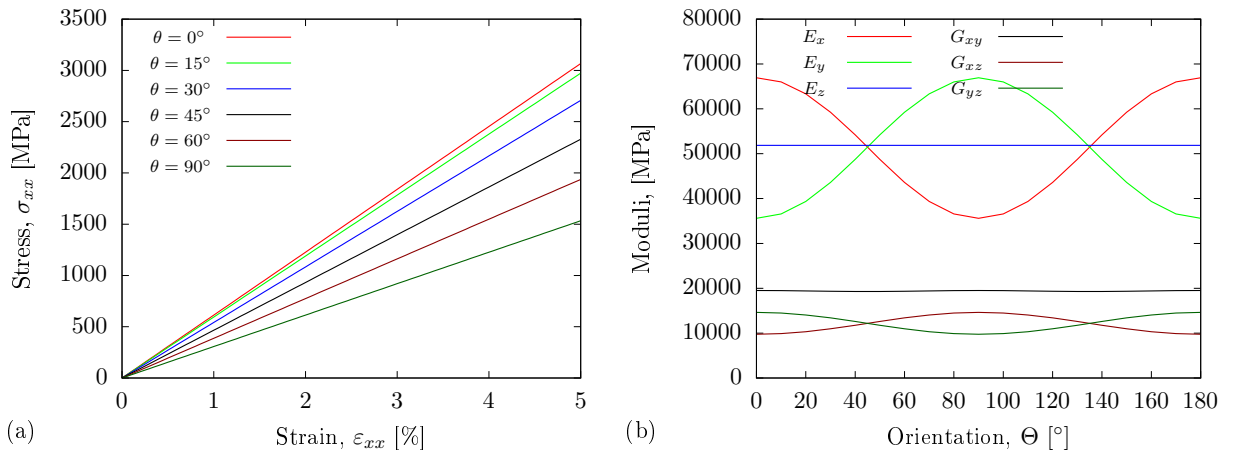


FIGURE 22: **Single element test for the orthorhombic symmetry group.** (a) Stress-strain curves for varying orientations $\theta$ of the fibres, and (b) variation of elastic moduli for various fibre orientations.

TABLE 8: Material parameters for the single element test–$\mathscr{C}_{13}$ symmetric group

| No. | Name | Par. | Value | Unit |
|-----|------|------|-------|------|
| 1. | Young's modulus 1-axis | $E_1$ | 121000 | [MPa] |
| 2. | Young's modulus 2-axis | $E_2$ | 8600 | [MPa] |
| 3. | Shear modulus 12-plane | $G_{12}$ | 4700 | [MPa] |
| 4. | Poisson's ratio | $\nu_{12}$ | 0.27 | [−] |
| 5. | Poisson's ratio | $\nu_{23}$ | 0.4 | [−] |

Figure 24 (a) shows the stress-strain curve for varying fibre orientations. In line with the expectations, it is seen that the material response is stiffer for smaller fibre orientations. The variation of elastic moduli with fibre orientation is illustrated in Fig. 24 (b), for a
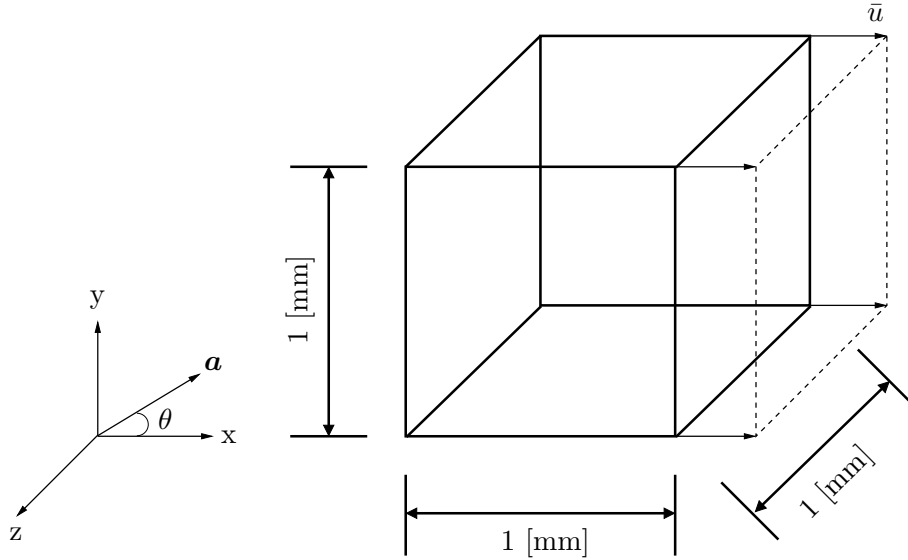


FIGURE 23: **Single element test for the transversely isotropic symmetry group.** Geometrical set up and the loading conditions.
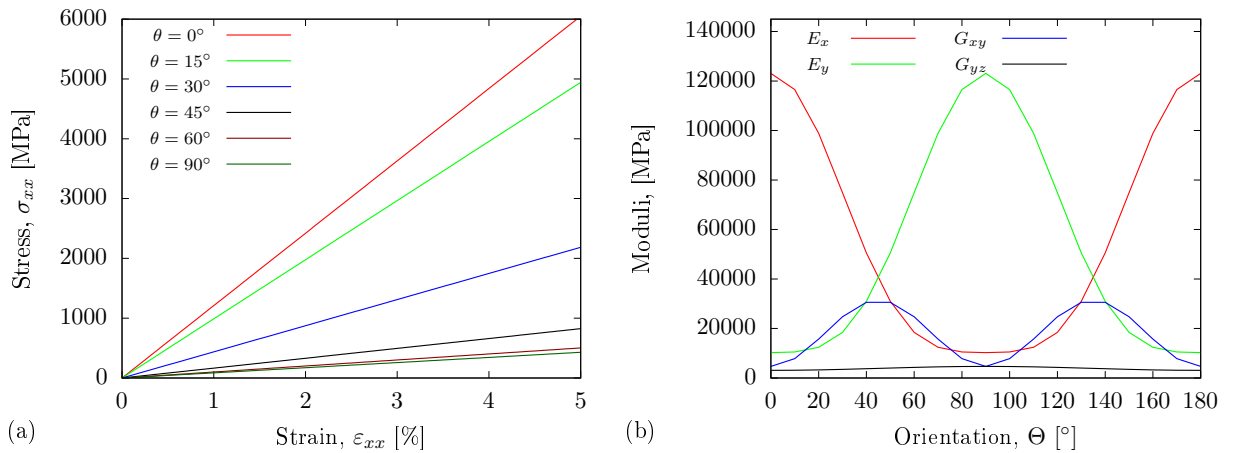


FIGURE 24: **Single element test for the transversely isotropic symmetry group.** (a) Stress-strain curves for varying orientations $\theta$ of the fibres, and (b) variation of elastic moduli for various fibre orientations.

TABLE 9: Summary of the load paths

| Load path | No. | $\tau_{12}^*$ | $-\sigma_{22}^*$ | $-\sigma_{22}^f$ | $\tau_{12}^f$ | $\lambda = -\sigma_{22}^f/\tau_{12}^f$ | Unit |
|---|---|---|---|---|---|---|---|
| $\tau_{12} \to -\varepsilon_{22}$ | ① | 43.1 | – | – | – | – | [MPa] |
| | ② | 56.2 | – | – | – | – | [MPa] |
| | ③ | 66.9 | – | – | – | – | [MPa] |
| | ④ | 79.5 | 0 | – | – | – | [MPa] |
| $-\sigma_{22} \to \gamma_{12}$ | ⑤ | – | 50.2 | – | – | – | [MPa] |
| | ⑥ | – | 84.83 | – | – | – | [MPa] |
| | ⑦ | – | 124.1 | – | – | – | [MPa] |
| | ⑧ | – | 164.5 | – | – | – | [MPa] |
| | ⑨ | 0 | 242.6 | – | – | – | [MPa] |
| radial load | ⑩ | – | – | 215.6 | 30.2 | 7.17 | [–] |
| | ⑪ | – | – | 192.1 | 65.5 | 2.94 | [–] |
| | ⑫ | – | – | 164.7 | 84.3 | 1.96 | [–] |
| | ⑬ | – | – | 91 | 93 | 0.98 | [–] |

typical carbon epoxy unidirectional material. Analogous to the $\mathscr{C}_3$ symmetric group, $E_\mathrm{x}$ is highest for $\theta = 0°$ and decreases monotonically to reach its minimum value at $\theta = 90°$. The shear modulus $G_\mathrm{xy}$ is maximum at $\theta = 45°$ and minimum at $\theta = 0°$. Indeed, it can be seen that the form of the variation of elastic moduli depends on the relative magnitudes of the elastic constants defined with respect to the principal material coordinates [106].

## 7.2. Anisotropic plasticity. Isotropic dissipative response functions

In this section, the predictions of the two models described in **Chapter 4** are compared with experimental results from the literature [7], for a set of biaxial loads. Note that MDPR-a and MCOO-a are not considered as it is seen that they are deficient in predicting transverse compression. The geometrical set up is the same as Fig. 23, except that periodic boundary conditions are imposed. The material parameters used for the numerical analysis are listed in Tables 3–4.

### 7.2.1. Single element test. Predictions for biaxial loads

Thirteen different load paths given in [7] are considered which are summarised in Table 9. For the first load path, referred to as the $\tau_{12} \to -\varepsilon_{22}$ path, the specimen is first sheared to a predetermined stress level $(\tau_{12}^*)$ and it is then compressed under displacement control while the shear stress is kept constant. The shear stress values are taken directly from [7] and the final value of compressive strain is chosen to be $-\varepsilon_{22} = 4\%$. Along the same lines, in the second load path, referred to as the $-\sigma_{22} \to \gamma_{12}$ path, the specimen is first compressed to a desired stress level $(-\sigma_{22}^*)$ and then sheared with $\gamma_{12} = 4\%$ while keeping the transverse compressive stress constant. Finally, for the radial load path, a proportional increase of compressive and shear stress is considered with four different proportionality factors. Note that for this particular load path, final stress values $(-\sigma_{22}^f$ and $\tau_{12}^f)$ from the experiments are applied in numerical simulations.
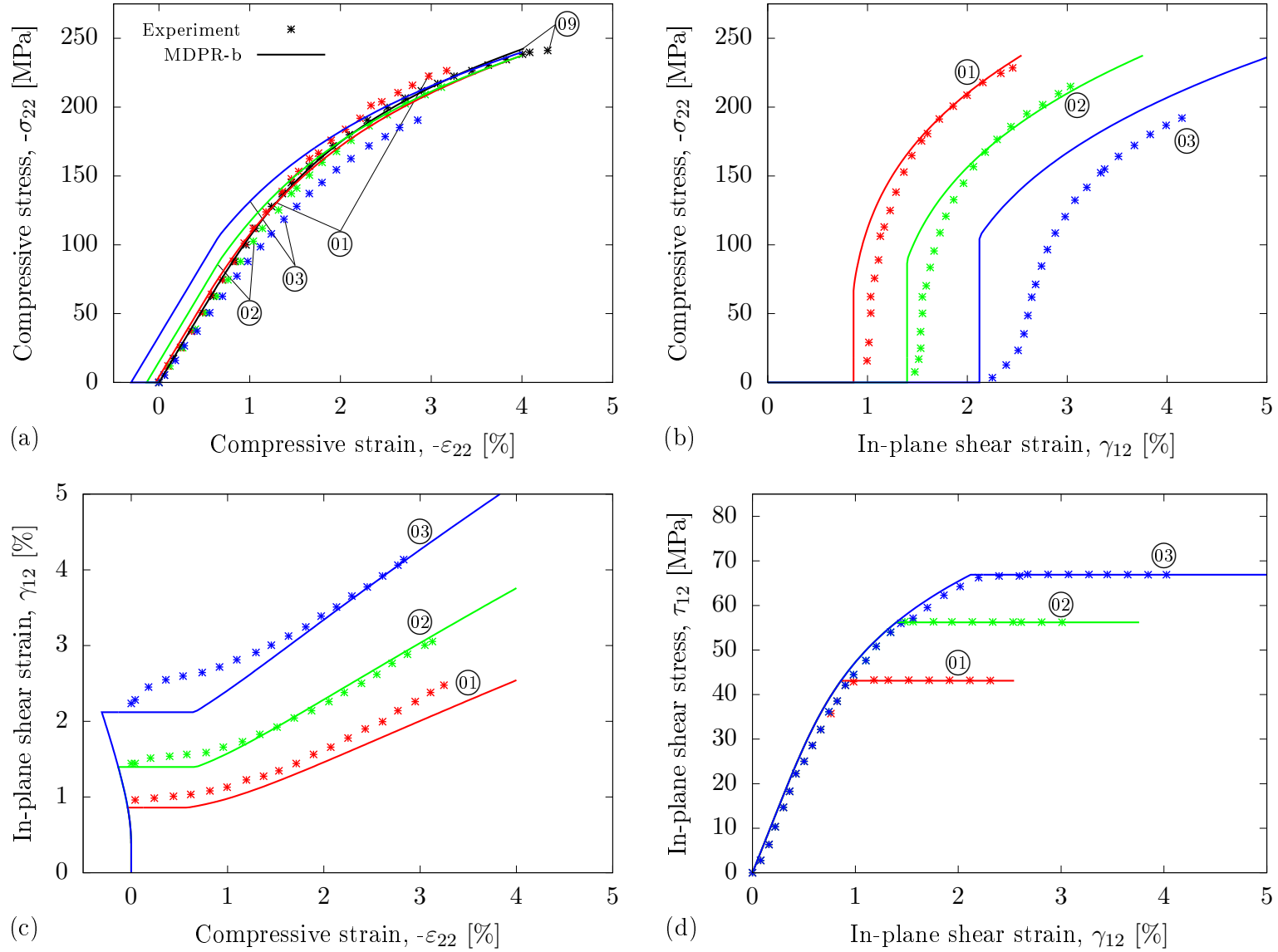
FIGURE 25: **Predictions for biaxial loads.** Comparison of experimental and MDPR-b model responses for the $\tau_{12} \rightarrow -\varepsilon_{22}$ loading path.
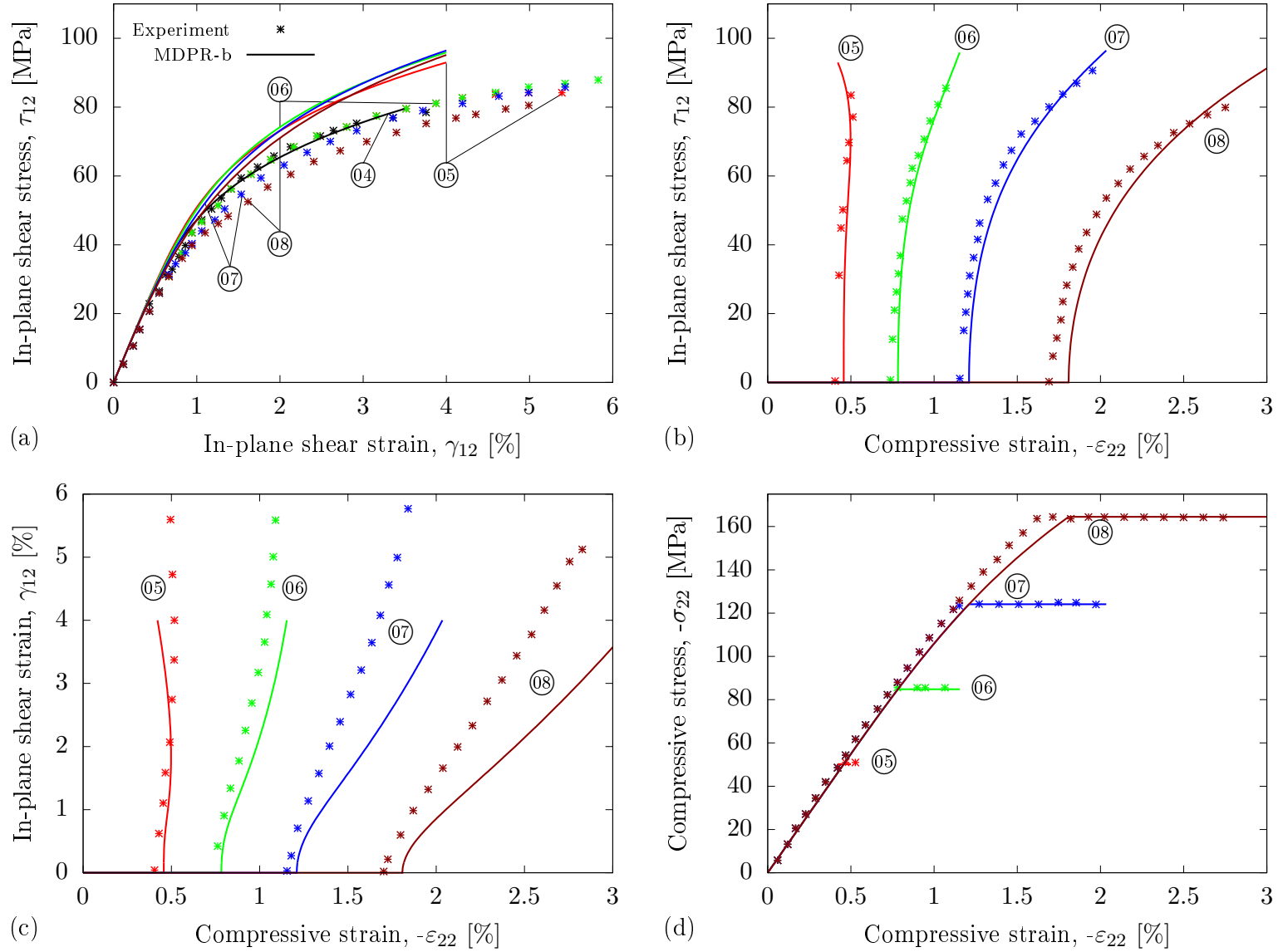
FIGURE 26: **Predictions for biaxial loads.** Comparison of experimental and MDPR-b model responses for the $-\sigma_{22} \to \gamma_{12}$ loading path.
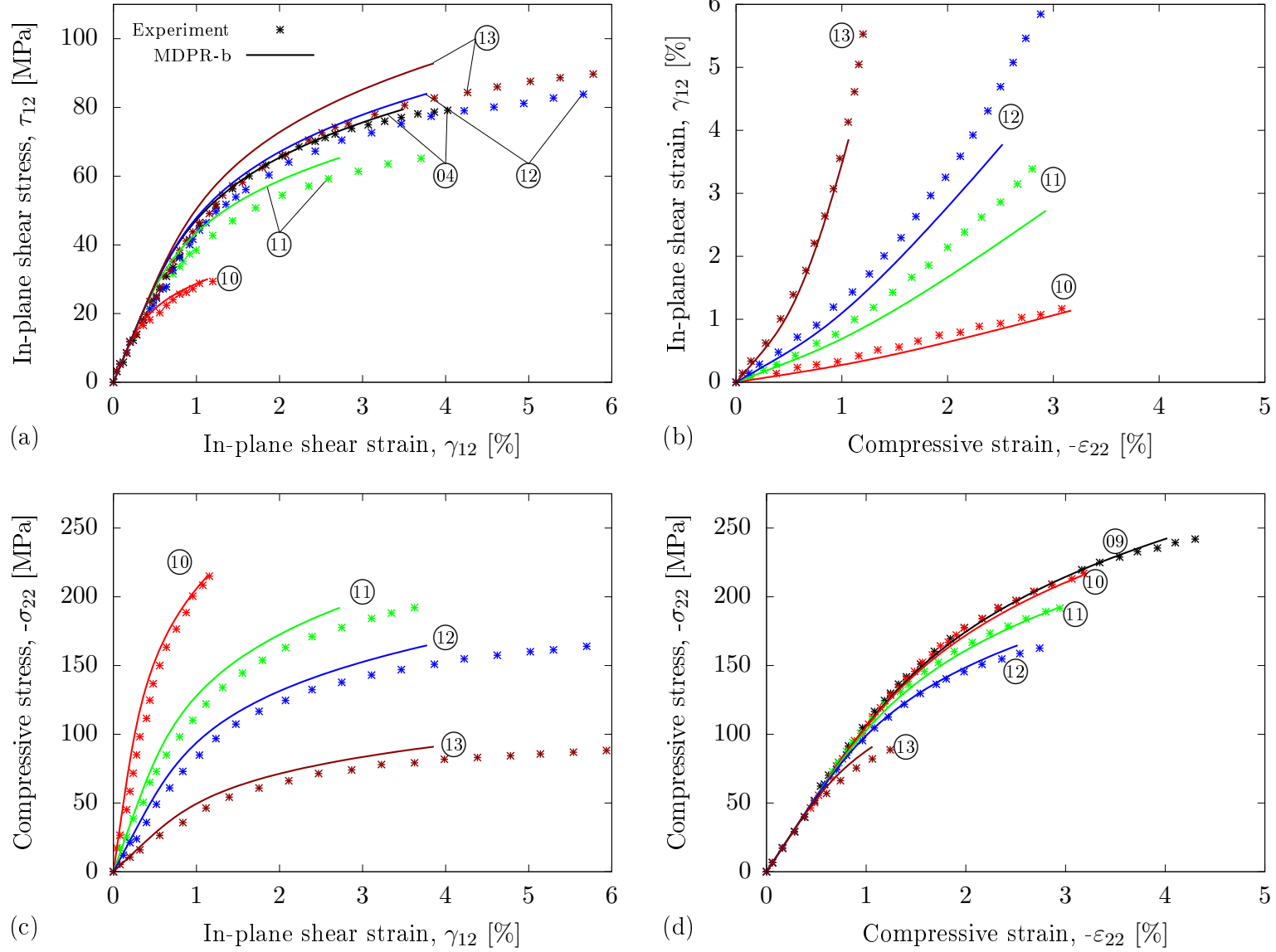
FIGURE 27: **Predictions for biaxial loads.** Comparison of experimental and MDPR-b model responses for the radial loading path.
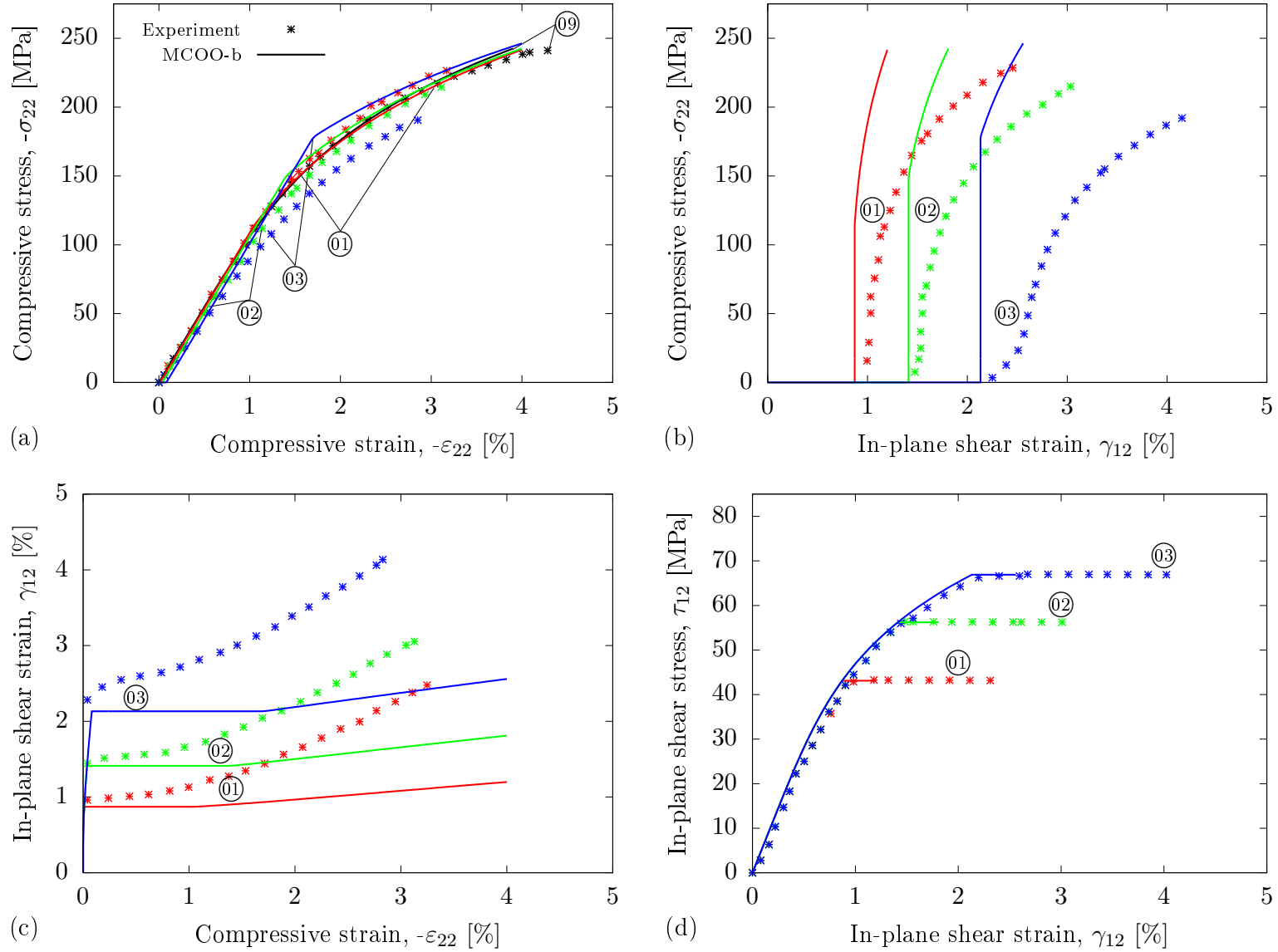
FIGURE 28: **Predictions for biaxial loads.** Comparison of experimental and MCOO-b model responses for the $\tau_{12} \to -\varepsilon_{22}$ loading path.
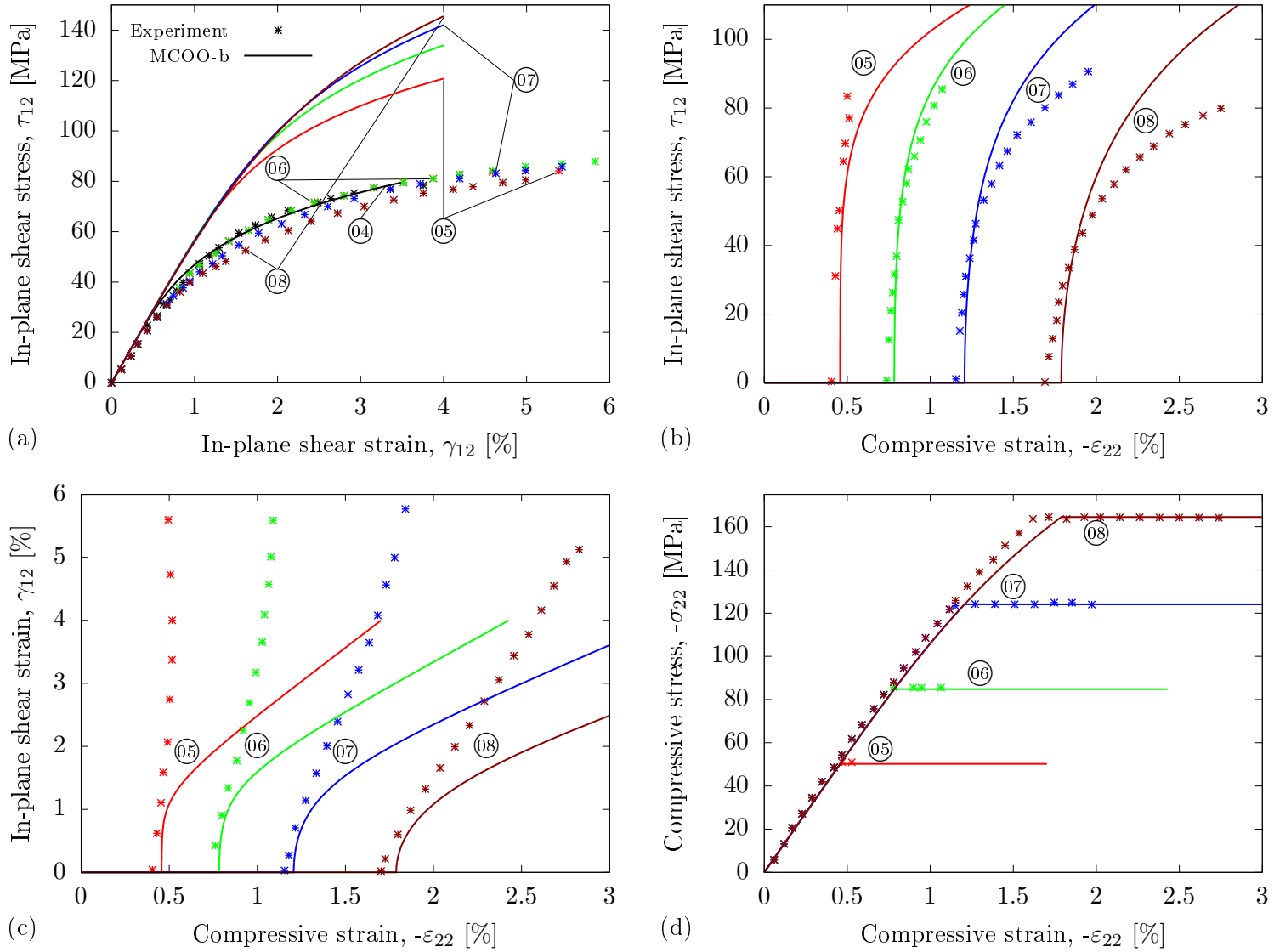
FIGURE 29: **Predictions for biaxial loads.** Comparison of experimental and MCOO-b model responses for the $-\sigma_{22} \rightarrow \gamma_{12}$ loading path.
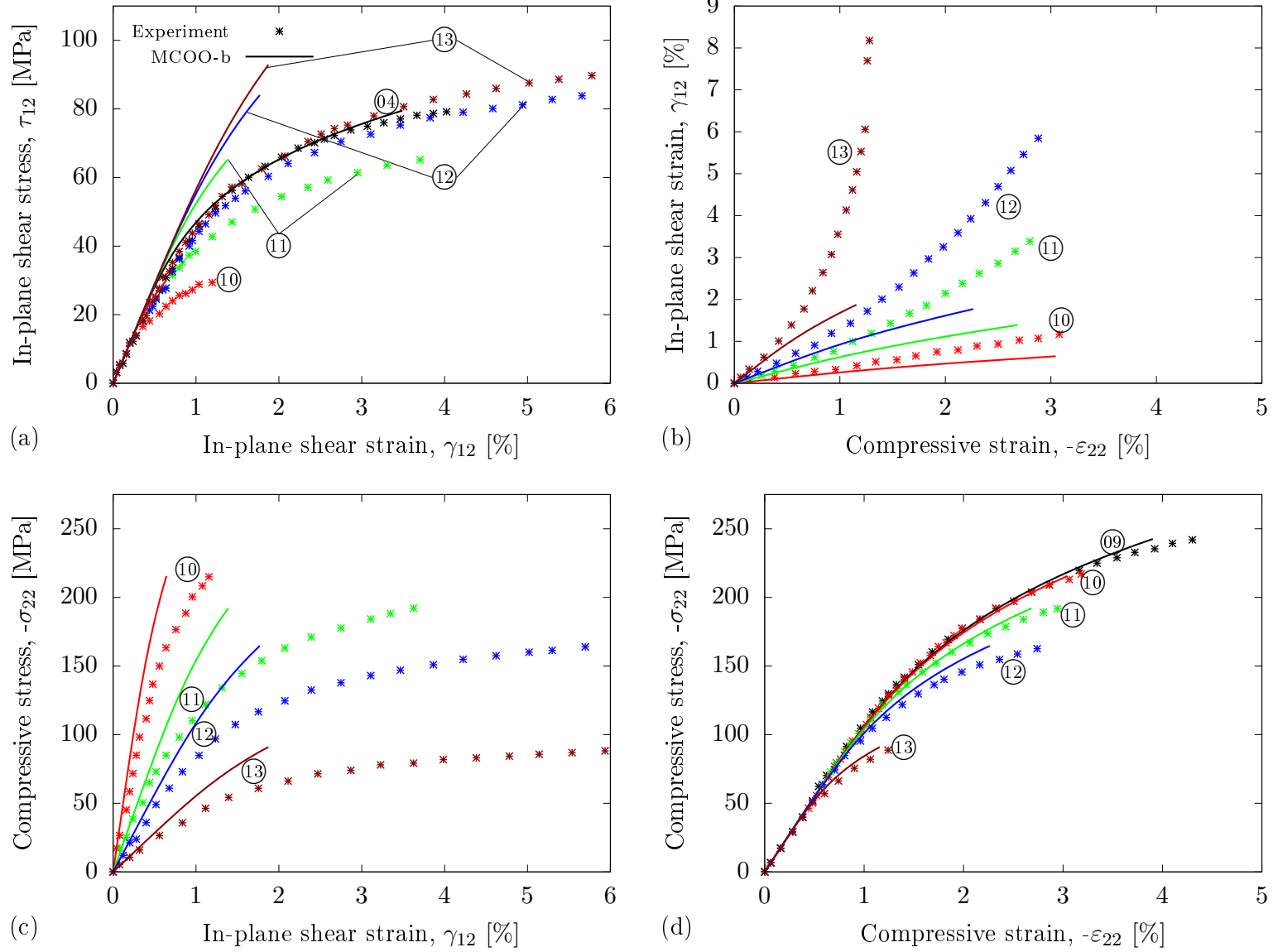
FIGURE 30: **Predictions for biaxial loads.** Comparison of experimental and MCOO-b model responses for the radial loading path.
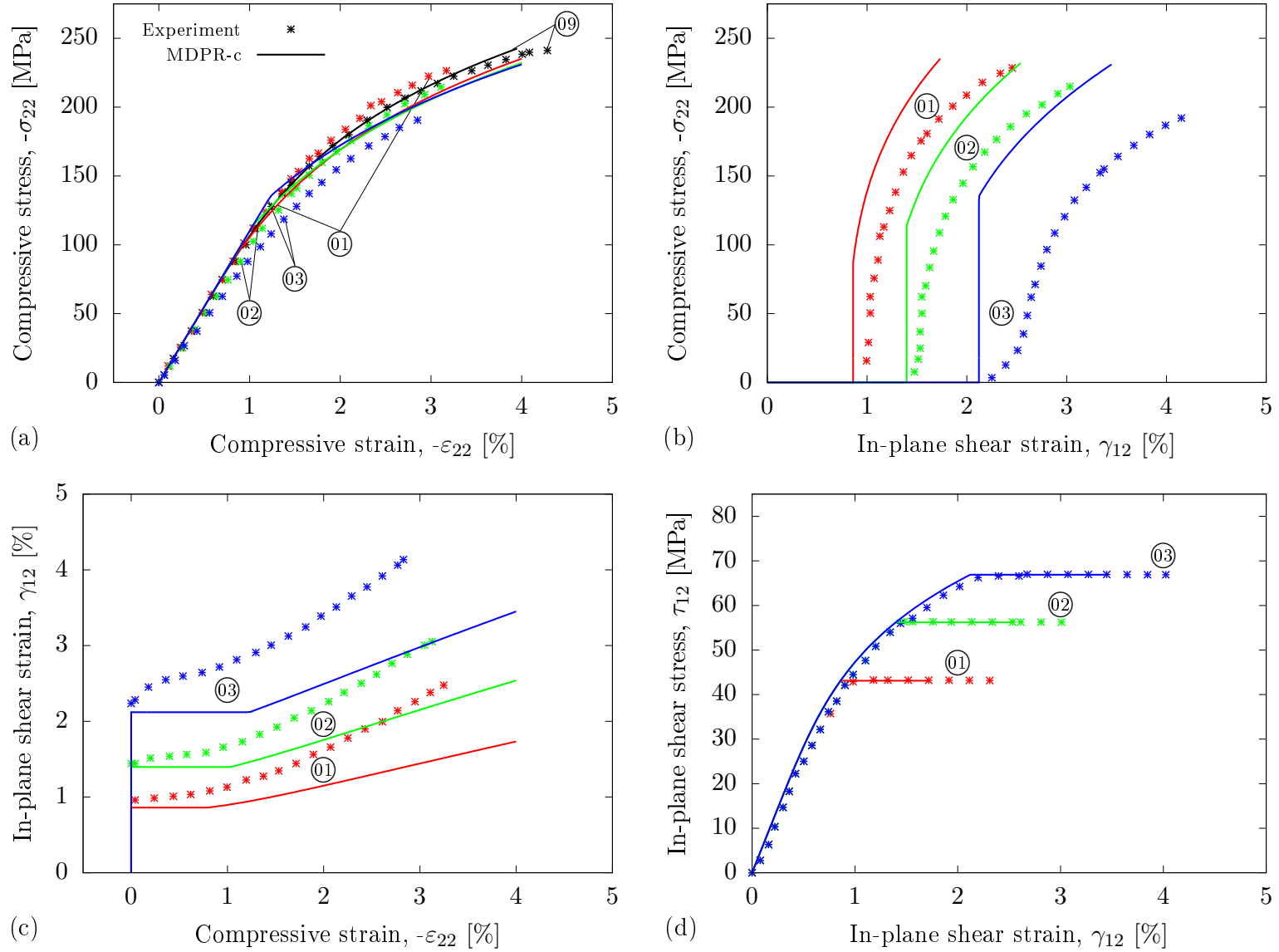
FIGURE 31: **Predictions for biaxial loads.** Comparison of experimental and MDPR-c model responses for the $\tau_{12} \rightarrow -\varepsilon_{22}$ loading path.
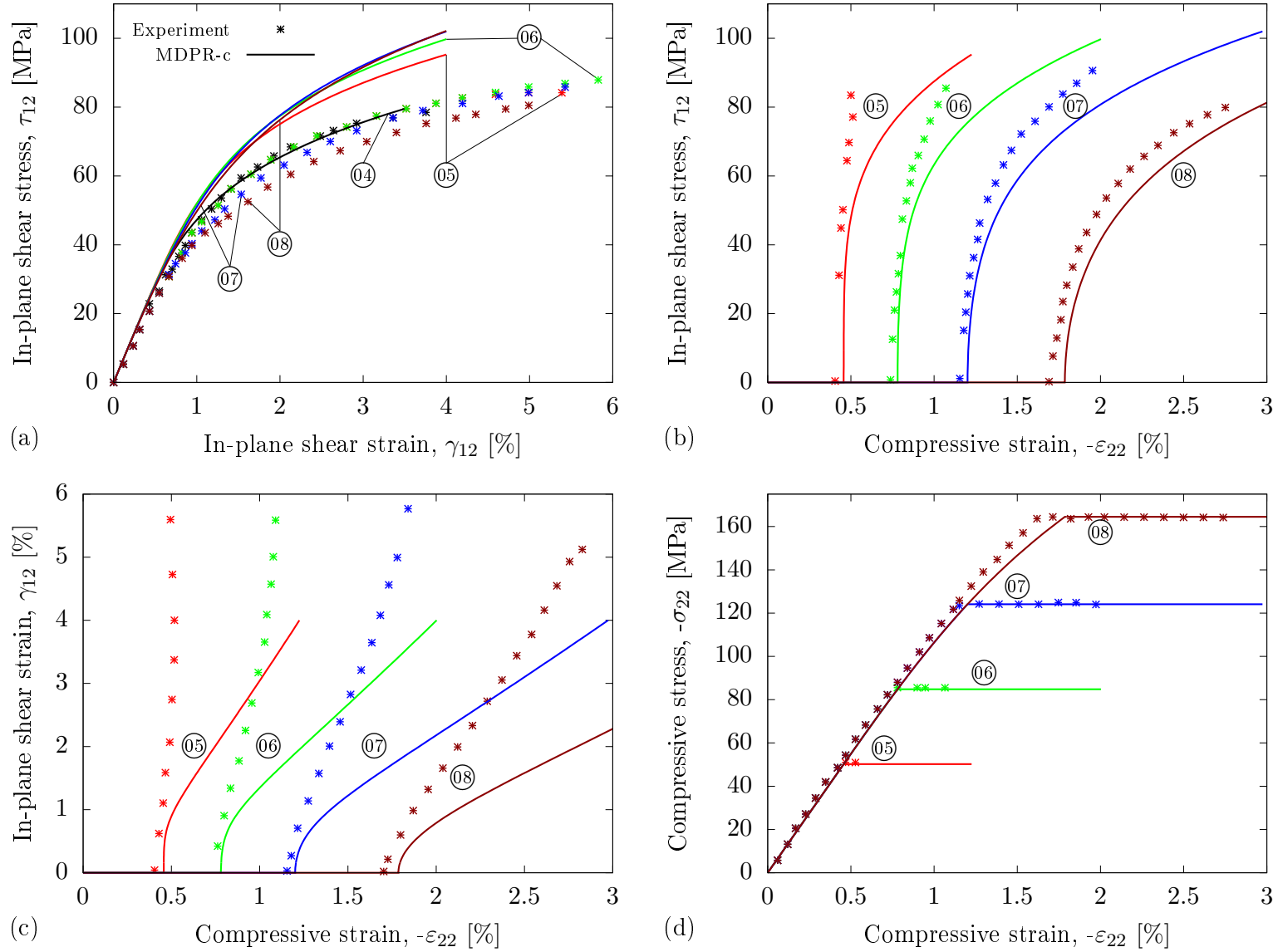
FIGURE 32: **Predictions for biaxial loads.** Comparison of experimental and MDPR-c model responses for the $-\sigma_{22} \to \gamma_{12}$ loading path.
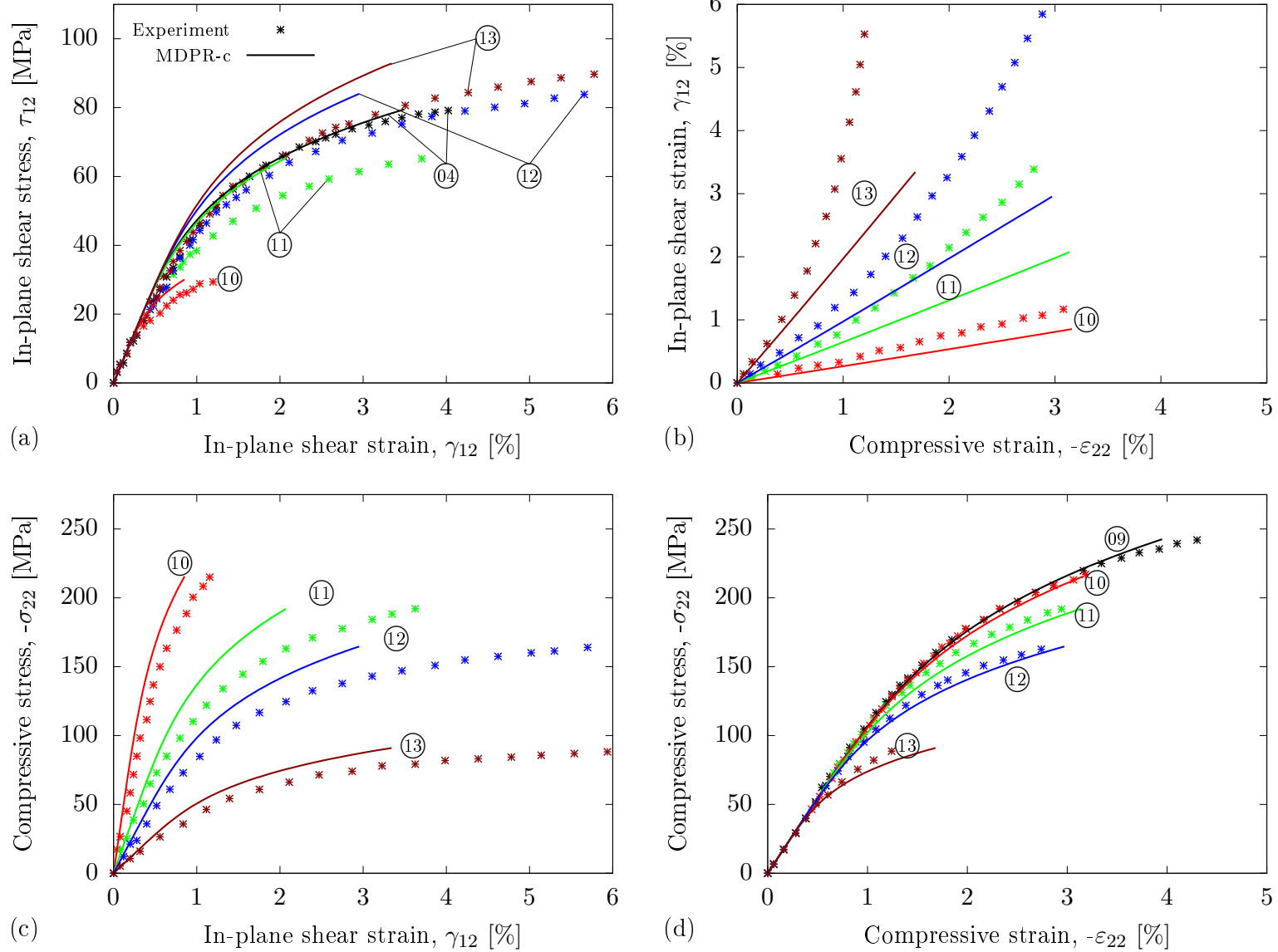
FIGURE 33: **Predictions for biaxial loads.** Comparison of experimental and MDPR-c model responses for the radial loading path.
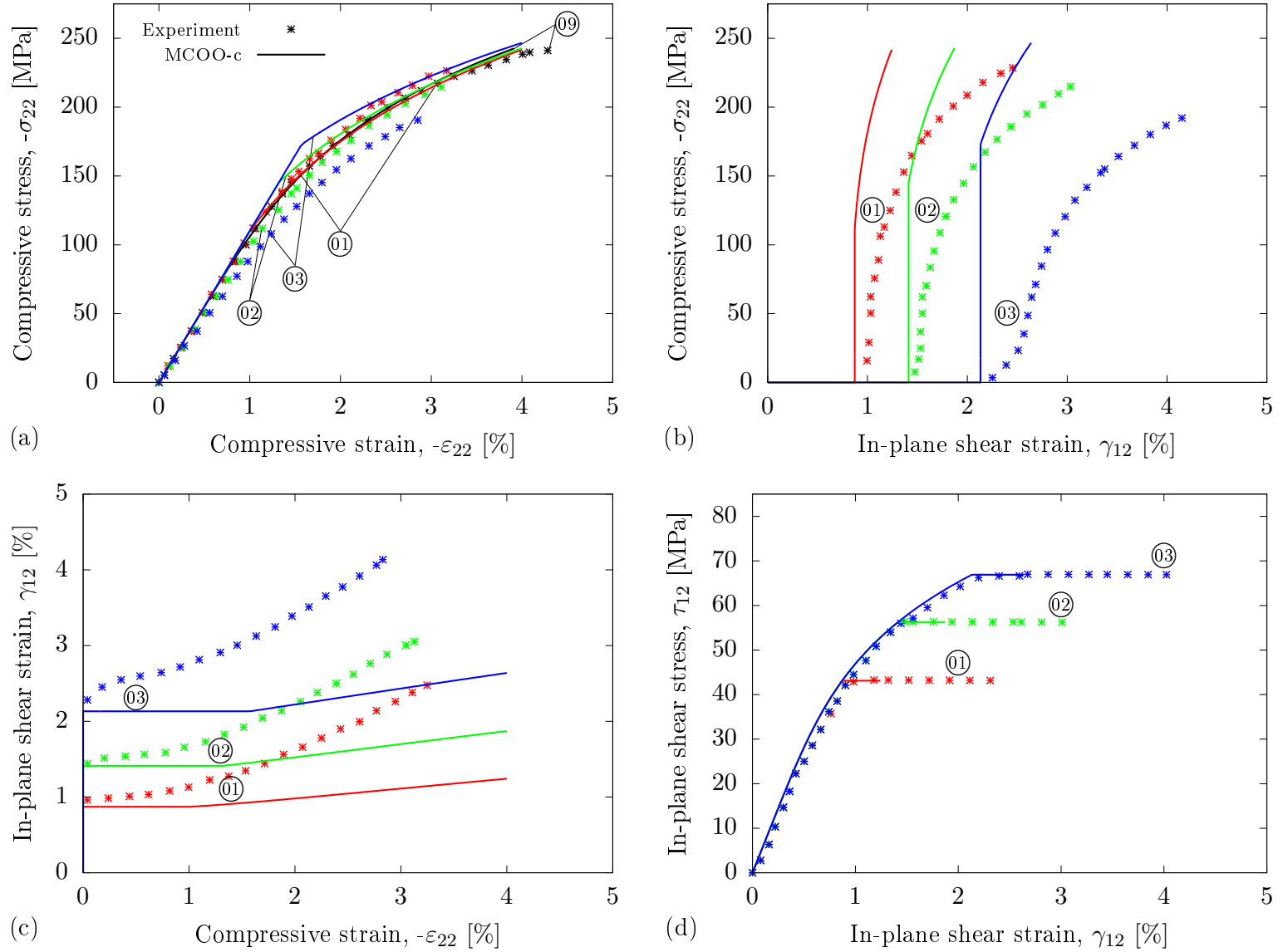
FIGURE 34: **Predictions for biaxial loads.** Comparison of experimental and MCOO-c model responses for the $\tau_{12} \to -\varepsilon_{22}$ loading path.
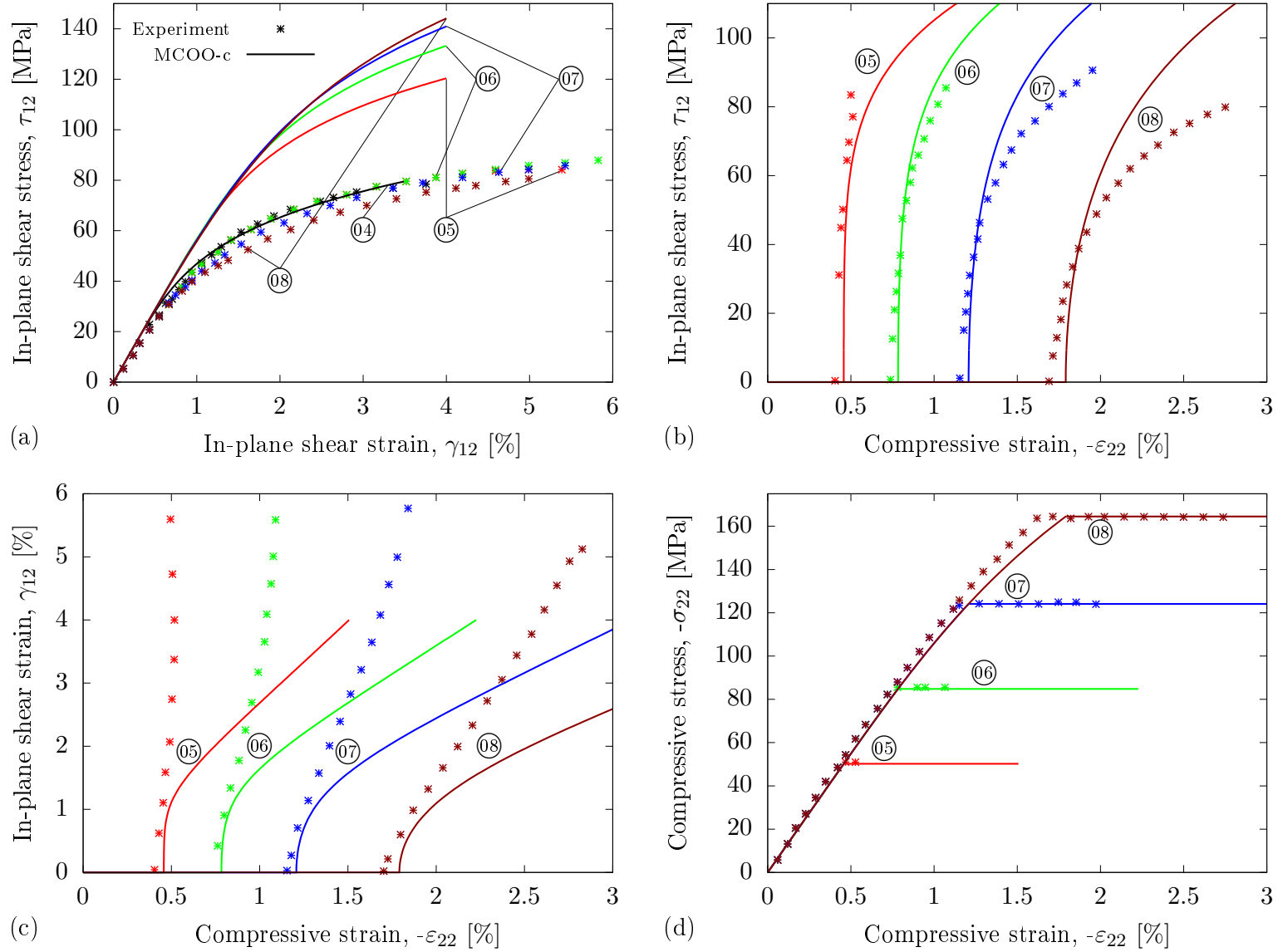
FIGURE 35: **Predictions for biaxial loads.** Comparison of experimental and MCOO-c model responses for the $-\sigma_{22} \to \gamma_{12}$ loading path.
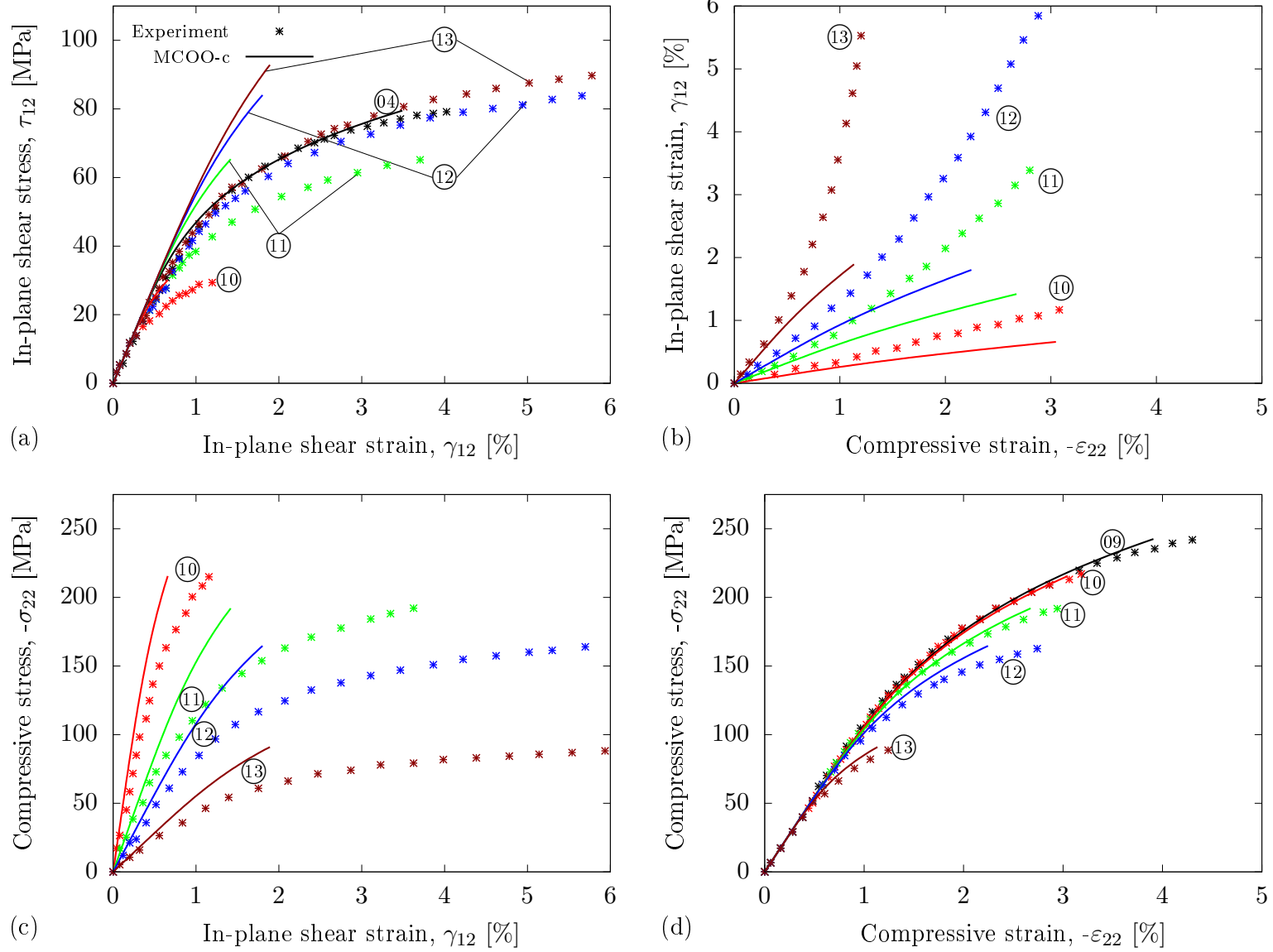
FIGURE 36: **Predictions for biaxial loads.** Comparison of experimental and MCOO-c model responses for the radial loading path.

**7.2.1.1. Predictions of MDPR-b.** Starting with the $\tau_{12} \to -\varepsilon_{22}$ load path, Fig. 25 shows a comparison of the MDPR-b model predictions with the experimental results. Compressive responses predicted by the model along with a pure compression case (load path ⑨) are shown in Fig. 25 (a). The experimental results show that the material response first softens and then subsequently stiffens for increasing shear preloads. This general behaviour is not captured by the model. Additionally, for shear dominated stress states (load paths ①–③), erroneous predictions of the model can be seen where tensile rather than compressive strain is predicted. Good qualitative agreement with the experimental response is seen in Figs. 25 (b) and (c), with the predicted shear strains being rather high. The shear response is captured quite well by the model, see Fig. 25 (d), where the model predicts the increase in shear strain during compressive loading as seen in the experiments.

For the $-\sigma_{22} \to \gamma_{12}$ load path, the predicted shear responses of the model do not agree well with experiments as seen in Fig. 26 (a). Owing to pressure-dependent plastic response functions, the application of transverse compression load hinders the onset of yielding and thus results in the reduced plastic flow [18]. Consequently, the shear response in presence of compression is overpredicted. Excellent agreement with experiments can be seen in Fig. 26 (b), whereas qualitative agreement with experiments is observed in Fig. 26 (c) with the predicted compressive strains being quite low. The transverse compressive behaviour is well reproduced by the model as seen in Fig. 26 (d).

Results of the radial load path are compared in Fig. 27. Though the predicted shear response is reasonable and the predicted shear strains are quite low, the model partly reproduces the experimentally observed trends where the material response first shifts up (from ④ to ⑬) before shifting down, as seen in Fig. 27 (a). However, the response of load path ⑫ is overestimated. The predicted compressive responses, as seen in Fig. 27 (d), are in excellent agreement with the experimental responses.

**7.2.1.2. Predictions of MCOO-b.** Figure 28 shows a comparison of MCOO-b model predictions and experimental results for the $\tau_{12} \to -\varepsilon_{22}$ load path. Though there are no erroneous predictions for shear dominated loads, the general trends of experimentally observed behaviour are not captured by the model, see Fig. 28 (a). For the load path ③, there is an observable overprediction by the model. In comparison with the MDPR model, the agreement with the experimental response is not satisfactory, as seen in Figs. 28 (b) and (c). It can be inferred from Fig. 28 (d) that the shear response agrees reasonably well with the experimental response, although the predicted shear strains are noticeably low.

Analogous to MDPR-b model, the shear response in presence of compression is overpredicted by the MCOO-b model in the $-\sigma_{22} \to \gamma_{12}$ load path, as seen in Fig. 29 (a). Good qualitative agreement is seen with the experimental response in Fig. 29 (b), while the predicted compressive strains in Fig. 29 (c) are much higher and the qualitative agreement is also not good. Meanwhile, the predicted transverse compressive responses agree well with the experiment as seen in Fig. 29 (d), again with the predicted $-\varepsilon_{22}$ much greater than those observed experimentally.

The material responses for radial load paths are also not reproduced well by the MCOO-b model, which is evident from Figs. 30 (a)–(c). However, compressive responses predicted by the model is in good agreement with experiments as seen in Fig. 30 (d).

**7.2.1.3. Predictions of MDPR-c.** Figure 31 shows a comparison of MDPR-c model predictions and experimental responses for the $\tau_{12} \to -\varepsilon_{22}$ load path. The non-associative

flow rule corrects the physically inconsistent material response exhibited by the associative flow rule under shear dominated loads, as seen in Fig. 31 (a). A good qualitative agreement with experiments is seen for the compressive response. In comparison with MDPR-b, the predicted shear strains are much lower, and significant deviations are observed for load paths ①–③ which is visible from Figs. 31 (b) and (c). The shear response is captured well by the model as seen in Fig. 31 (d).

Figure 32 shows MDPR-c model predictions for the $-\sigma_{22} \to \gamma_{12}$ load path. Similar to the associated flow response, the shear response in presence of compression is overpredicted by the MDPR-c model as seen in Fig. 32 (a). The compressive strains are overpredicted for load paths ⑤–⑧, and rather high deviations can be seen in Fig. 32 (c). The overall compressive response for this load path is captured well by the model, with a slightly overpredicted compressive strain as seen in Fig. 32 (d).

For the radial load path, material responses are again overpredicted by the model, see Figs. 33 (a)–(c). Under shear dominated stress states (lower proportionality factors), the agreement with experimental results is not good. In Fig. 33 (b), a rather linear relationship between the shear and compressive strain is observed for load paths ⑪–⑬. Nevertheless, the compressive response is captured quite well as seen in Fig. 33 (d).

**7.2.1.4. Predictions of MCOO-c.** Figures 34–36 show the MCOO-c model predictions for the thirteen load paths. Predictions of the non-associative model are largely similar to that of the associative model (MCOO-b). Overall, the MCOO-c model reproduces the shear and compressive response accurately for the non-proportional loading paths. However, predictions are not good for the radial load path where deviations are strong.

From a theoretical standpoint, while the use of pressure-dependent plastic response functions corrects the underpredictions of transverse stress, an excessive hardening is induced in the shear response for combined compressive/shear loads. This can mainly be attributed to the cone shaped Drucker-Prager-type yield surface used by these models, an effect which is also observed in [18]. Moreover, the MCOO model does not ensure a linear elastic fibre response owing to singularity problems of the transformation tensor. Thus, the use of isotropic plastic response functions is not desirable on the meso scale since they do not reproduce the full complexity of the problem. The lack of a decoupled stress response results in significant deviations under biaxial loads.

**7.3. Anisotropic plasticity. Anisotropic dissipative response functions**

Restricting to the $\mathscr{C}_{13}$ symmetry group, the performance of the six respective models developed in **Chapter 5** are now analysed by homogeneous and inhomogeneous boundary value problems. The material parameters used in the numerical simulations are listed in Table 6.

**7.3.1. Single element test. Rate dependency and homogeneous strain cycling**

To demonstrate the effect of rate dependency and anisotropic plastic response, the analysis of a single element test is considered. The geometrical set up is same as that in Fig. 23. Figure 37 (a) shows stress-strain curves of Model-I-RD-a (without kinematic hardening) for the in-plane shear response, for increasing viscosity parameters. In line with the expectations, it can be seen that as $\eta \to 0$, the material response is rate-independent. On the other hand, a linear elastic material response is expected as $\eta \to \infty$. Between these limits, the material response is expected to be stiffer for increasing viscosity parameters, which can be clearly inferred from Fig. 37 (a).

TABLE 10: Kinematic hardening parameters for the $\mathscr{C}_{13}$ symmetric group

| No. | Par. | Value | Unit |
|-----|------|-------|------|
| 1. | $\vartheta_1$ | $0.015 \times E_2$ | [MPa] |
| 2. | $\vartheta_2$ | $0.025 \times E_2$ | [MPa] |
| 3. | $\vartheta_3$ | $0.035 \times E_2$ | [MPa] |
| 4. | $\vartheta_4$ | $0.045 \times E_2$ | [MPa] |
| 5. | $\vartheta_5$ | $0.055 \times E_2$ | [MPa] |
| 6. | $\zeta_2$ | 0.004 | [−] |
| 7. | $\zeta_3$ | 0.003 | [−] |

Figure 37 (b) shows the stress-strain curves of a single element subjected to longitudinal cyclic load, for three different fibre orientations. The kinematic hardening parameters used in the simulation are listed in Table 10. The response of 0° fibre orientation is linear elastic as expected. For 45° fibre orientation, the initial elastic response is stiffer than that of 90°. However, in the plastic regime, the response of 90° fibre orientation is stiffer as significant plastic strains that develop during shear deformation softens the material response.

### 7.3.2. Single element test. Tension–compression asymmetry

The six meso models are now applied to the analysis of a single element test for a uni-axial strain cycle to verify the implementation. The geometrical set up is identical to the previous case. In addition to the material parameters in Table 6, the kinematic hardening parameters are chosen to be same as those in the previous example, as listed in Table 10. It should be noted here that for comparison purposes, in this particular example, the same transverse compressive yield stresses are used for associative and non-associative pressure-dependent models, i.e. $y_{22c} = 50.01$ MPa for Model-I-RI-b/-c, and $y_{22c} = 27.4$ MPa for Model-II-RI-b/-c, such that differences in the predicted response can purely be attributed to the respective model formulations.

The first test case is a uni-axial cyclic test where the specimen is loaded in the transverse
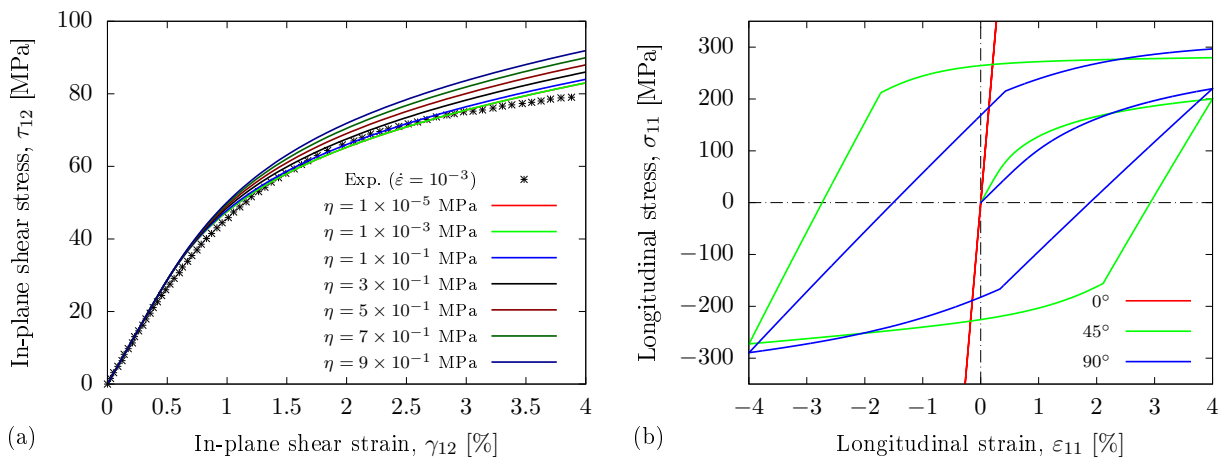


FIGURE 37: **Single element test.** Stress-strain curves of Model-I-RD-a. (a) In-plane shear behaviour for different viscosity parameters and (b) longitudinal strain cycling for three different fibre orientations, with a constant viscosity parameter $\eta = 1 \times 10^{-5}$ MPa.

direction up to a magnitude of $\varepsilon_{22} = \pm 5\%$. The results of the finite element analyses for one loading/unloading/reloading cycle are shown in Fig. 38 (a) for Model-I-RI and Fig. 38 (c) for Model-II-RI. It can be seen that the stress in the direction of straining behaves symmetrically in the tension and compression regime for the pressure-independent models. In contrast, the two pressure-dependent models exhibit the well-known tension-compression asymmetry, where a difference between the yield limits in tension and the compression regime is observed. Also, hardening effects are more dominant in the compression regime.

As a subsequent example, a combined compression-shear test is analysed. Recall here that the associative pressure-independent model and non-associative pressure-dependent model yield identical results for a simple shear load. Therefore, a full shear loading cycle is superimposed by additional transverse strain. To this end, a transverse compressive strain of magnitude $\varepsilon_{22} = -1.5\%$ is first applied. While $\varepsilon_{22}$ is kept fixed, the specimen is sheared upto a shear strain of magnitude $\gamma_{12} = 5\%$. The computed results for one loading/unloading/reloading cycle are summarised in Fig. 38 (b) and (d). Since the hardening parameters are identical for the pressure-independent and pressure-dependent models, it is expected that the predicted response of the non-associative pressure-dependent model be bound by the associative pressure-independent and associative pressure-dependent mod-
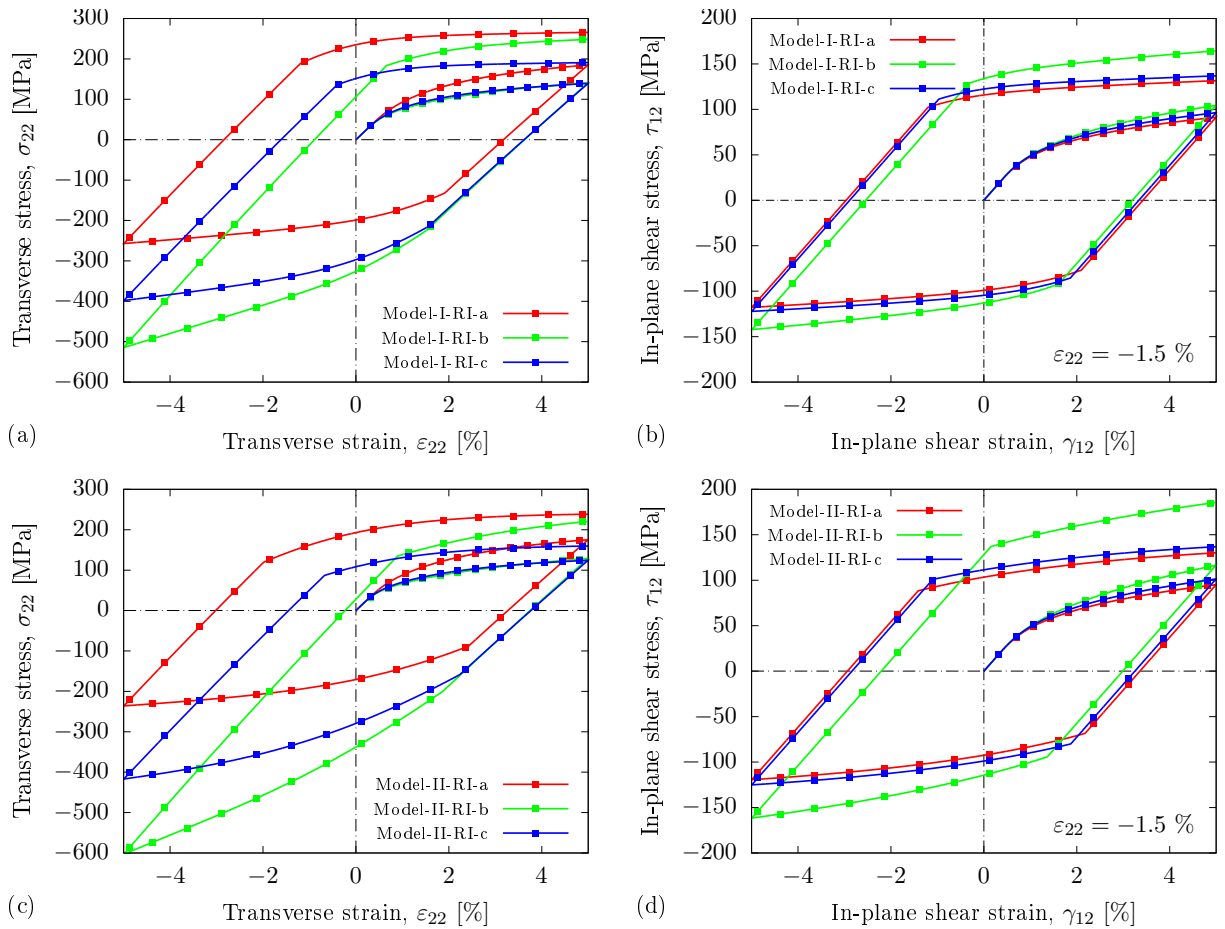


FIGURE 38: **Single element test. Tension-compression asymmetry**. Stress-strain curves of a single element test for (a),(c) transverse and (b),(d) in-plane shear behaviour of **Model-I-$\mathcal{RI}$** and **Model-II-$\mathcal{RI}$**, respectively, for one loading/unloading/reloading cycle.

els. The numerical results in Fig. 38 (a)–(d) are in agreement with this expectation. These results are similar to predictions reported in [109] in their work on finite strain plasticity.

### 7.3.3. Single element test. Predictions for biaxial loads

In this section, predictions of the six (rate-independent) models developed in **Chapter 5** are compared with micro-mechanics simulations and experimental results for the set of biaxial loads listed in Table 9. Note that the pressure-independent models Model-I-RI-a and Model-II-RI-a are still considered even though they are deficient in predicting transverse compression. Their predictions are compared against DIG and UCA respectively, to get a broader evaluation of their performance. The geometrical set up is same as that in Fig. 23, and periodic boundary conditions are imposed.

**7.3.3.1. Comparison of Model-I-RI-a and DIG models predictions.** Figure 39 compares the Model-I-RI-a and DIG predictions for the $\tau_{12} \rightarrow -\varepsilon_{22}$ load path. The compressive response predicted by Model-I-RI-a agree well with that of DIG as seen in Fig. 39 (a). There is a slight underprediction of the shear stress for load paths ①–③. However, the shear strains are reasonably overpredicted in Figs. 31 (b) and (c), though the shape of these curves is similar to that of DIG. An excellent agreement is seen with DIG in the predicted shear response which is evident from Fig. 39 (d).

Predictions of Model-I-RI-a and DIG for the $-\sigma_{22} \rightarrow \gamma_{12}$ load path is shown in Fig. 40. The in-plane shear response is slightly underpredicted by Model-I-RI-a in comparison with DIG, mainly for load paths ⑦ and ⑧ as seen in Fig. 40 (a). The predicted compressive strains are in good agreement for load paths ⑤ and ⑥, but large deviations are seen for load paths ⑦ and ⑧ in Figs. 40 (b) and (c). This can be attributed to the pressure-independent formulation of these models, which causes the deficiency in transverse compression. The predicted transverse compressive response as seen in Fig. 40 (d), is in excellent agreement with DIG model predictions.

Of all three load paths, the best agreement of Model-I-RI-a with DIG is for the radial loading as seen in Fig. 41. The predicted shear response is in excellent agreement with DIG, which is clear from Fig. 41 (a). Figures 41 (b) and (c) also show very good agreement. The predicted compressive responses by Model-I-RI-a are substantially the same as that predicted by DIG, which is clearly evident in Fig. 41 (d).
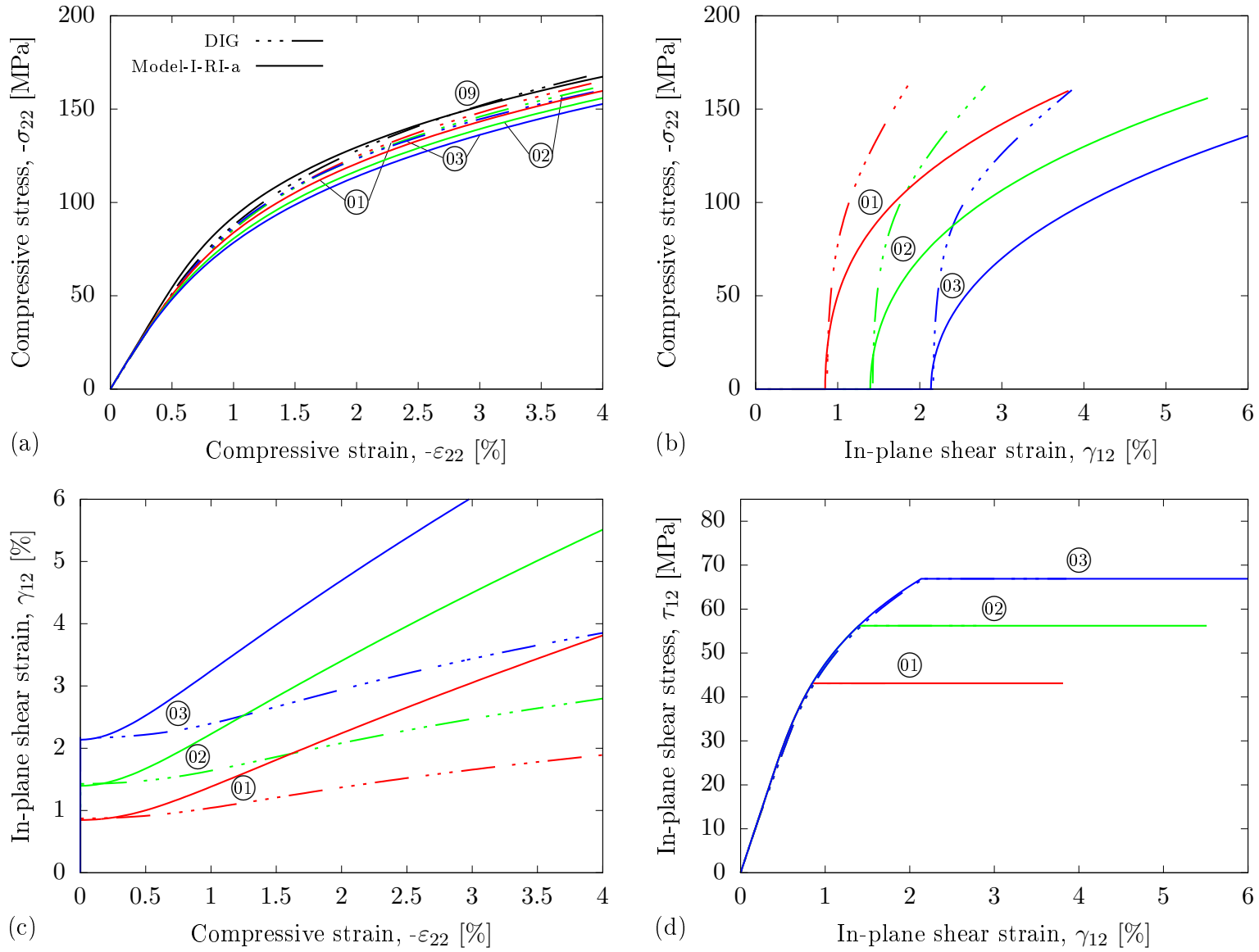
FIGURE 39: **Predictions for biaxial loads.** Comparison of DIG and Model-I-RI-a responses for the $\tau_{12} \rightarrow -\varepsilon_{22}$ loading path.

FIGURE 40: **Predictions for biaxial loads.** Comparison of DIG and Model-I-RI-a responses for the $-\sigma_{22} \to \gamma_{12}$ loading path.

FIGURE 41: **Predictions for biaxial loads.** Comparison of DIG and Model-I-RI-a responses for the radial loading path.

FIGURE 42: **Predictions for biaxial loads.** Comparison of UCA and Model-II-RI-a responses for the $\tau_{12} \to -\varepsilon_{22}$ loading path.

FIGURE 43: **Predictions for biaxial loads.** Comparison of UCA and Model-II-RI-a responses for the $-\sigma_{22} \rightarrow \gamma_{12}$ loading path.

FIGURE 44: **Predictions for biaxial loads.** Comparison of UCA and Model-II-RI-a responses for the radial loading path.

**7.3.3.2. Comparison of Model-II-RI-a and UCA models predictions.** Predictions of Model-II-RI-a are now compared with that of UCA for the thirteen load paths. Figure 42 shows the comparison for the $\tau_{12} \to -\varepsilon_{22}$ load path. The predicted compressive response by Model-II-RI-a is significantly less stiff than that of UCA for load paths ①–③ and ⑨, as seen in Fig. 42 (a). This effect can also be seen in Fig. 42 (b) though the model predictions qualitatively agree with those of UCA. The shear response predicted by the model agrees with that of UCA quite well as seen in Figs. 42 (c) and (d).

Plots depicting Model-II-RI-a and UCA predictions for the $-\sigma_{22} \to \gamma_{12}$ load path is shown in Fig. 43. The shear response predicted by the model agrees fairly well with that of UCA, see Fig. 43 (a). Only high compression preloads (load paths ⑦ and ⑧) cause noticeable underpredictions in the shear response. Furthermore, the predicted compressive strains are much higher for load paths ⑦ and ⑧ as seen in Figs. 43 (b) and (c), again owing to the pressure-independent plastic response functions. The predicted compressive response by the model agrees well with that of UCA for the load paths ⑤ and ⑥ as seen in Fig. 43 (d). Notable deviations are observed for high compression preloads (⑦ and ⑧).

Predictions of Model-II-RI-a for the radial load path are reported in Fig. 44. The shear response predicted by the model, as seen in Fig. 44 (a), is less stiff than that of UCA for increasing proportionality factors $\lambda$. Good qualitative agreement is seen in Figs. 44 (b) and (c), with the compressive and shear strains overpredicted for increasing proportionality factors. In line with the discussions in **Chapter 6**, the compressive response is significantly underpredicted for all the load paths as seen in Fig. 44 (d).

In summary, the main deficiency of the pressure-independent models is that they underpredict the transverse compressive stress in the non-linear regime. Additionally they exhibit an insensitivity to initial shear/compression preloads – an effect observed in experiments where the material response first softens and then subsequently stiffens for increasing shear/compression preloads [7, 18]. Nevertheless, good qualitative agreement can be seen with the micro-mechanical models predictions. Recall here that the convexity requirement for Model-I-RI-a is not fulfilled for calibration to UCA. Hence, Model-I-RI-a is compared with DIG and Model-II-RI-a is compared with UCA.

**7.3.3.3. Predictions of Model-I-RI-b.** Figure 45 shows the comparison of Model-I-RI-b predictions and the experimental response for $\tau_{12} \to -\varepsilon_{22}$ load path. The use of associative flow rule induces physical inconsistencies in the material response where tensile rather than compressive transverse strains are predicted for shear dominated stress states (load paths ② and ③). The predicted compressive response by the model agrees well with experiments, as seen in Fig. 45 (a). Only for the highest shear preload (load path ③), the response is slightly overpredicted. The general trend of the experimental behaviour where the material response first shifts up and then down for increasing shear preloads is also not captured by the model, though the effect is minimal. The predicted shear and compressive strains agree well with the experimental response (Figs. 45 (b) and (c)), except for load path ③. The increase in shear strain caused by compression is captured well by the model in Fig. 45 (d) with minor over predictions.

Predictions of the model for the $-\sigma_{22} \to \gamma_{12}$ load path is shown in Fig. 46. Figure 46 (a) depicts a comparison of the model predictions and experimental shear response in presence of compression. The agreement with experiments is good although the experimental shear response for load paths ⑤–⑦ are almost same as that of load path ④, see [7] for a detailed discussion. The predicted compressive strains are in excellent agreement with

experiments as seen in Fig. 46 (b). The transverse predictions by the model qualitatively and quantitatively agree with the experimental response as seen in Fig. 46 (d).

Plots depicting the model predictions for the radial load path are shown in Figs. 47 (a)–(d). It is seen that the predicted shear and compressive response are in very good agreement with the experimental results.

**7.3.3.4. Predictions of Model-II-RI-b.** Figures 48–50 show the predictions of Model-II-RI-b for all the thirteen different load paths. The predictions of this model are to a large extent similar to that of Model-I-RI-b. Only for radial loads, it is seen from Fig. 50 (a) that the predicted material response for load paths Ⓞ₄ and ⑫ is essentially the same, albeit not much change is observed in the experimental response as well.

An assessment of the predictions from Figs. 45–50 reveals that pressure dependency is needed in order to reproduce the trends of experimentally observed behaviour. It is also reported that whilst using an associated flow rule, the predictions are in excellent agreement with the experimental results. For the two non-radial load paths, the compressive response with shear preload and shear response with compression preload is overpredicted by both models, only at the highest value of the respective preload. It has been reported in [7] that the presence of shear preload does not affect the compressive response significantly. Likewise, the shear response is almost insensitive to the presence of compression preload. These aspects are also reflected in the models predictions as seen in Figs. 45 (a), 46 (a), 48 (a) and 49 (a). However, for the two non-radial load paths, the associated flow rule exhibits non-physical constitutive response under shear dominated combined stress states. This aspect is discussed in detail in the following subsection. Of all the three load paths, predictions for radial load path are the best. An increase in the strain induced by a proportional increase in the stress is captured excellently by both models.
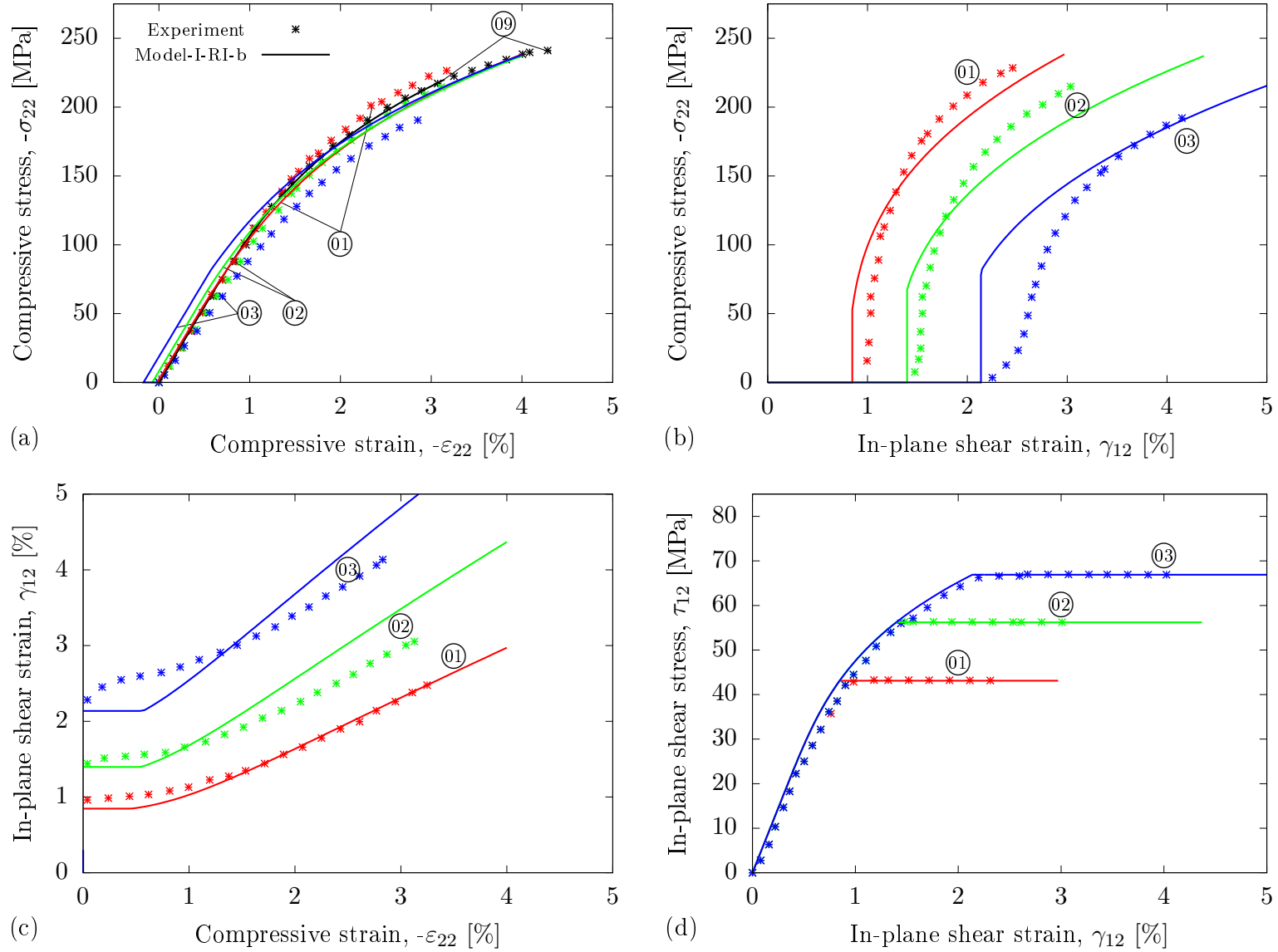
FIGURE 45: **Predictions for biaxial loads.** Comparison of experimental and Model-I-RI-b responses for the $\tau_{12} \to -\varepsilon_{22}$ loading path.
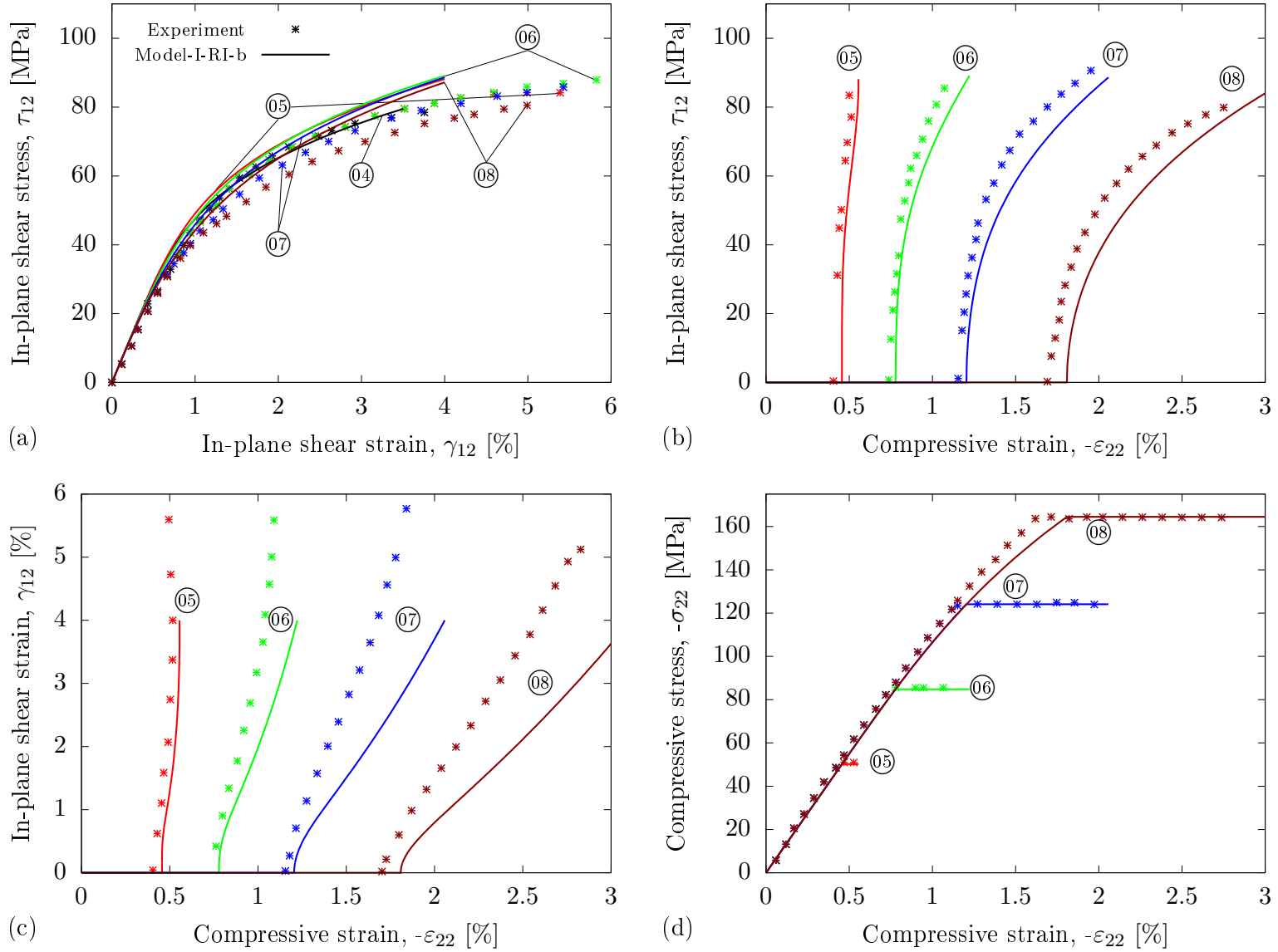
FIGURE 46: **Predictions for biaxial loads.** Comparison of experimental and Model-I-RI-b responses for the $-\sigma_{22} \rightarrow \gamma_{12}$ loading path.
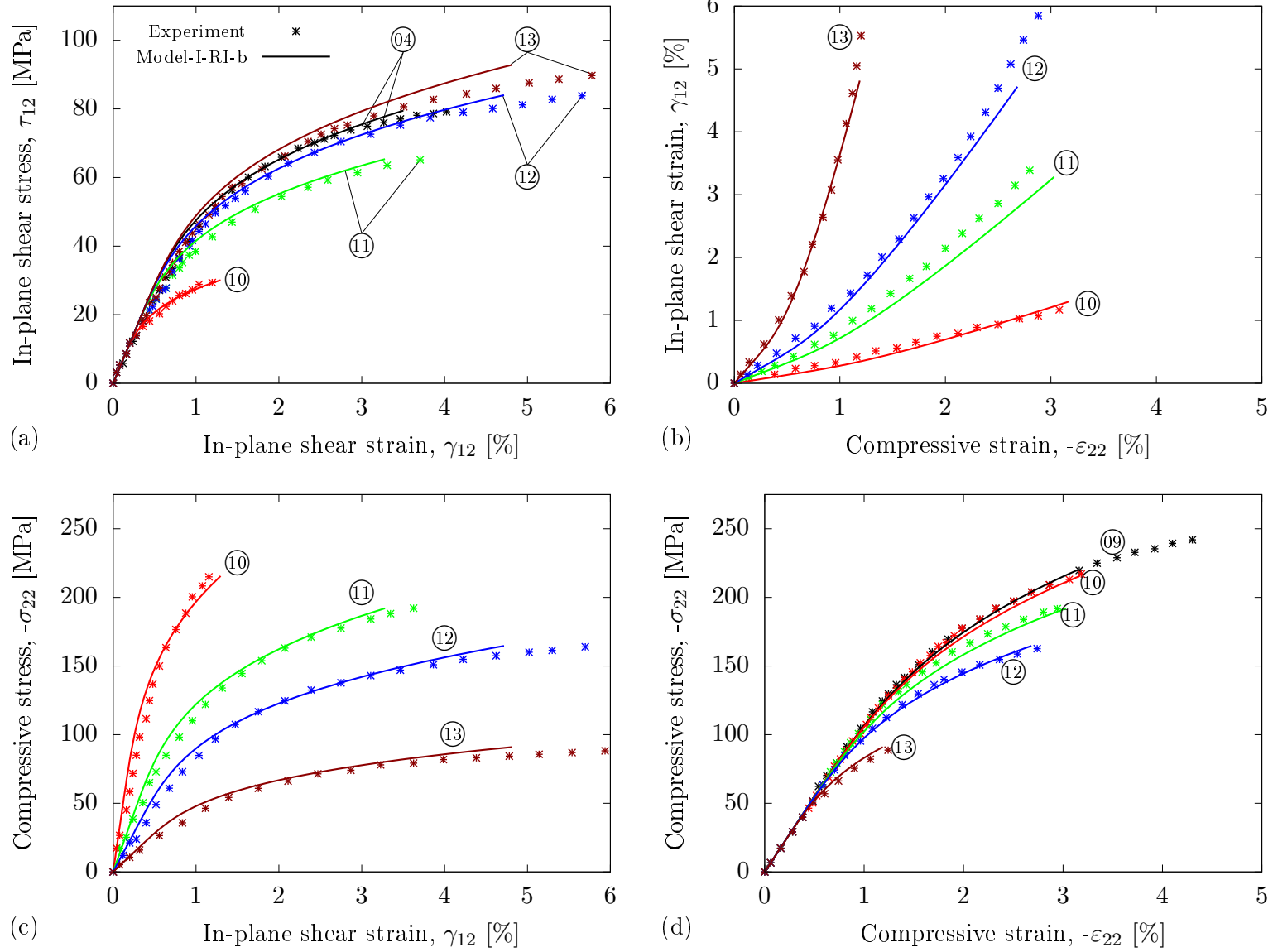
FIGURE 47: **Predictions for biaxial loads.** Comparison of experimental and Model-I-RI-b responses for the radial loading path.
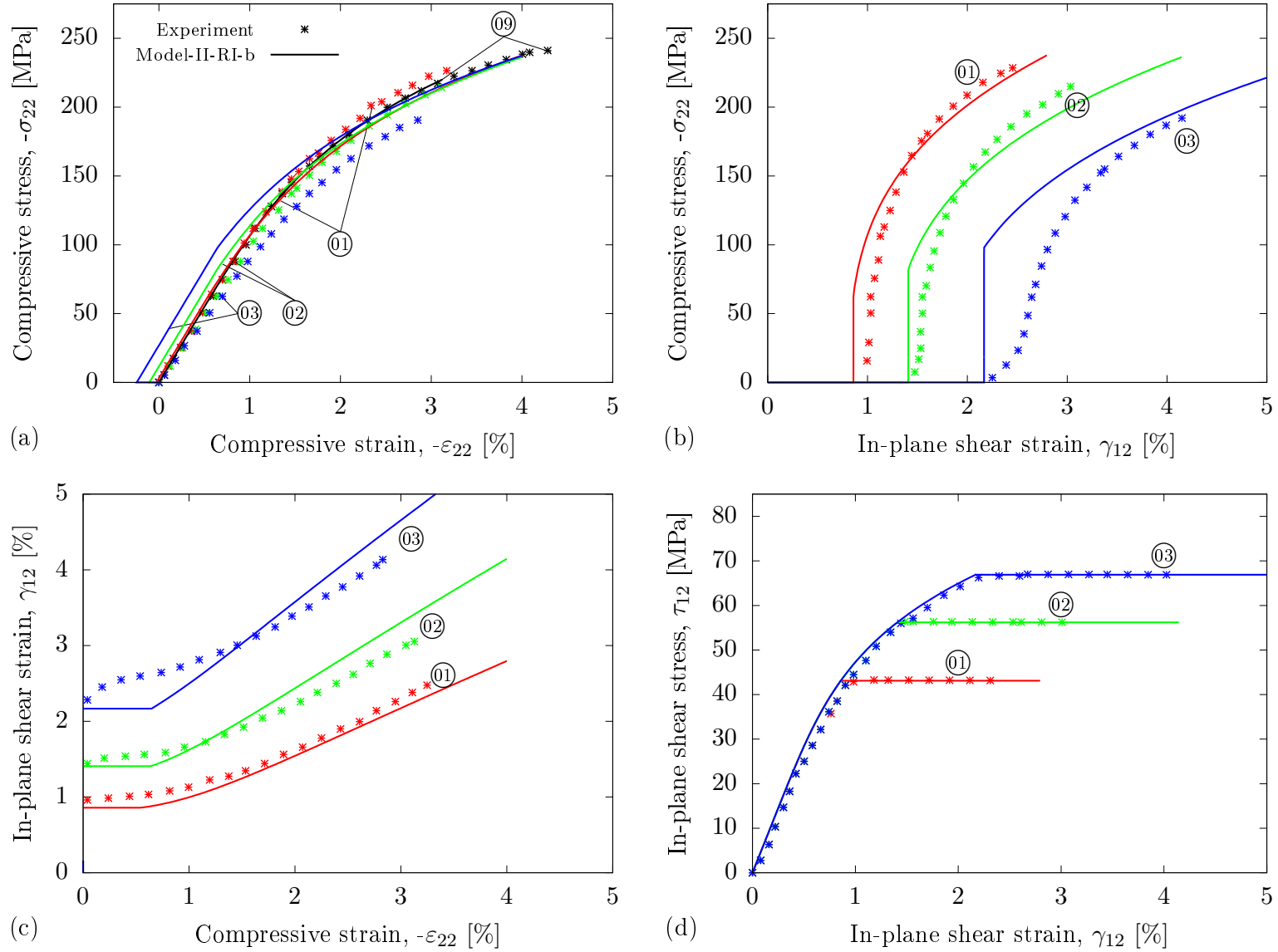
FIGURE 48: **Predictions for biaxial loads.** Comparison of experimental and Model-II-RI-b responses for the $\tau_{12} \rightarrow -\varepsilon_{22}$ loading path.
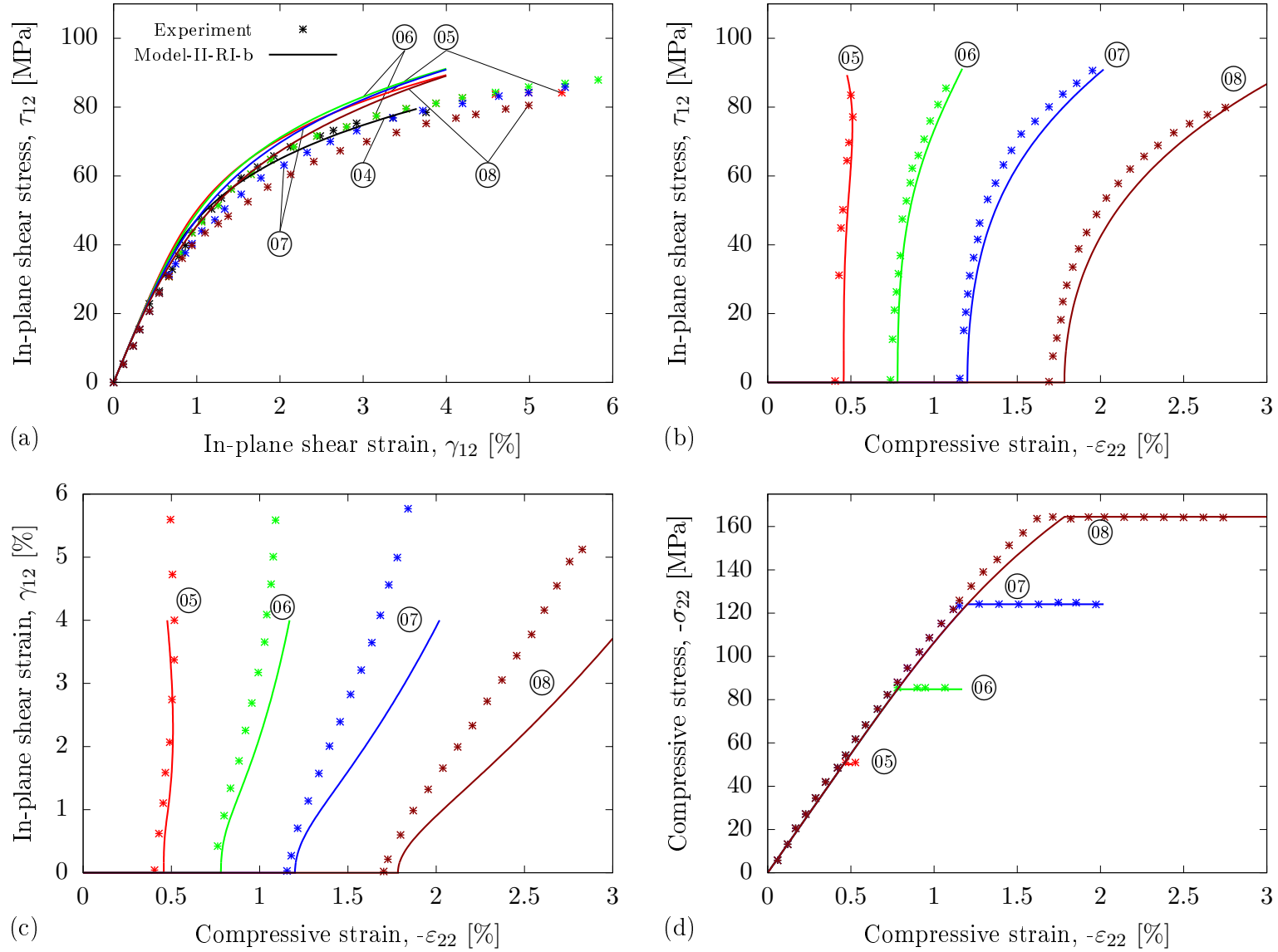
FIGURE 49: **Predictions for biaxial loads.** Comparison of experimental and Model-II-RI-b responses for the $-\sigma_{22} \to \gamma_{12}$ loading path.
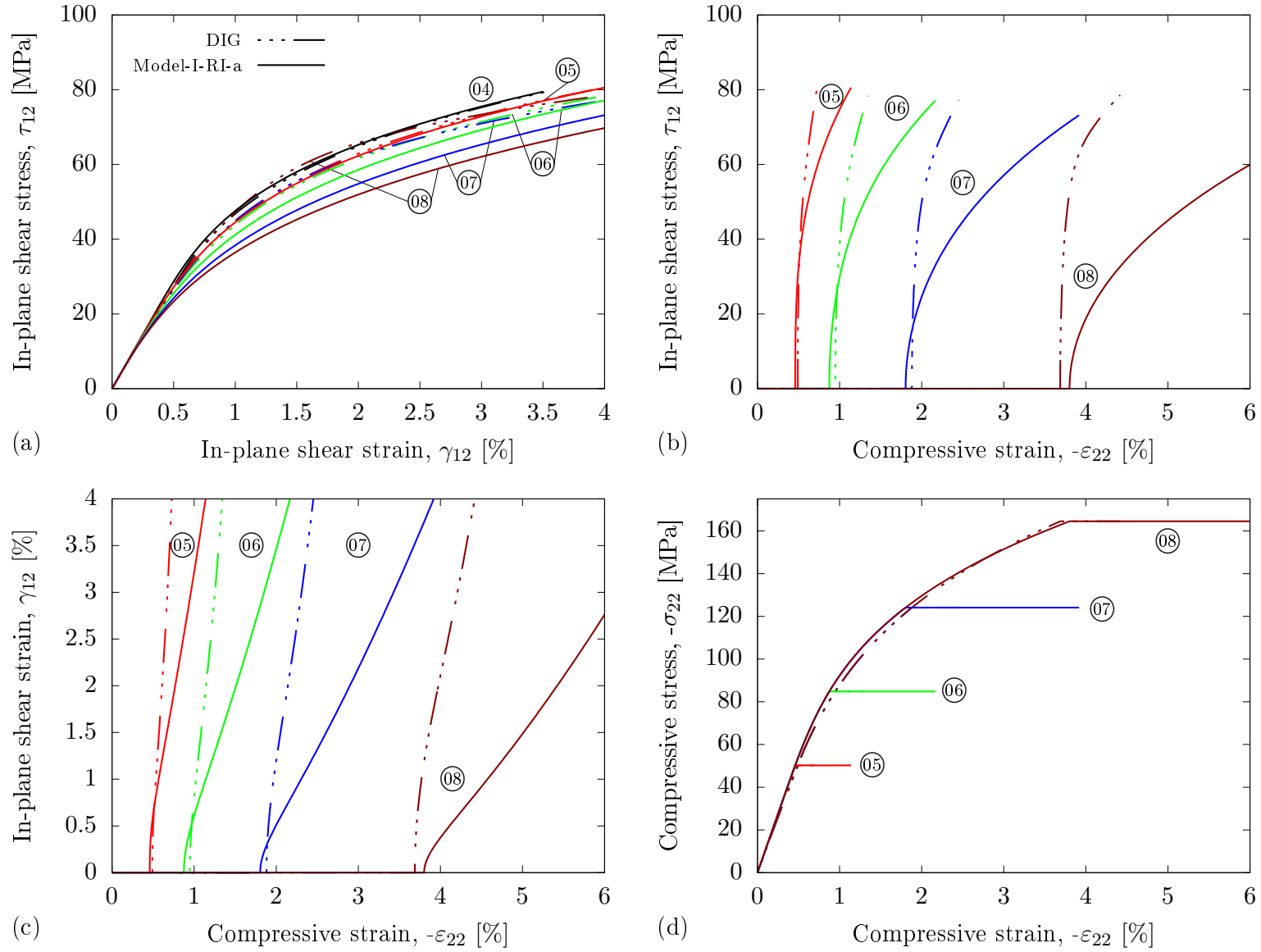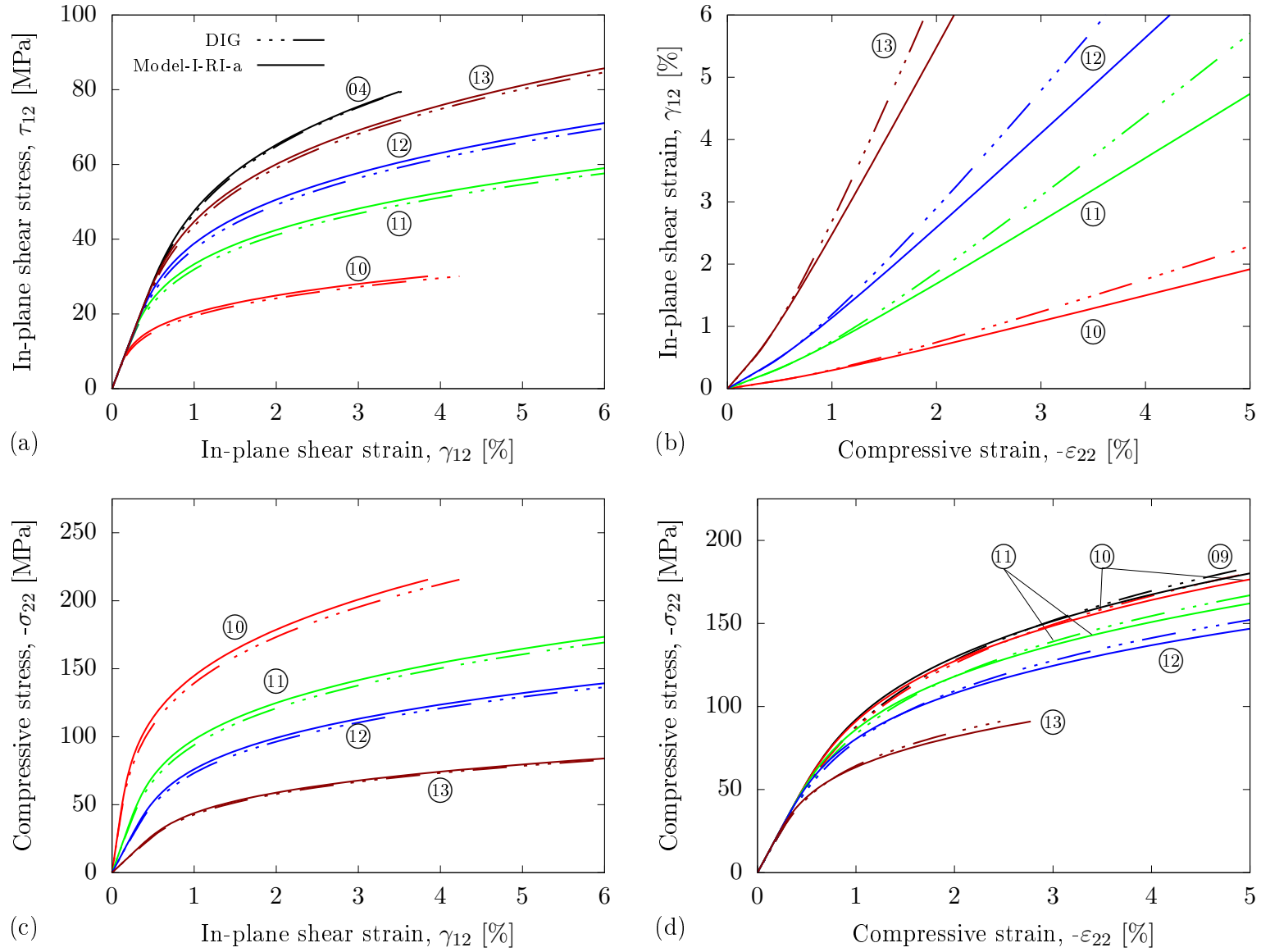
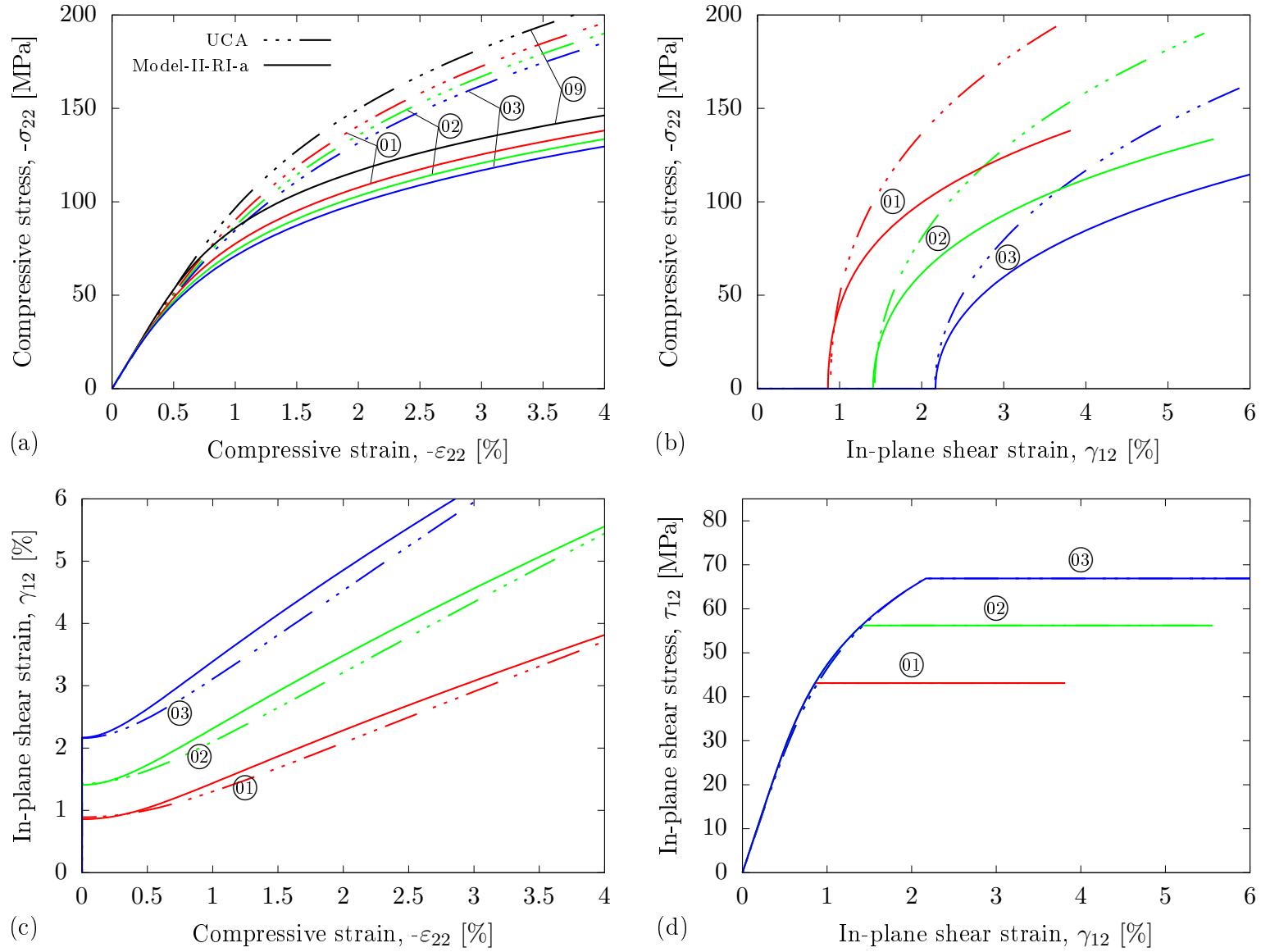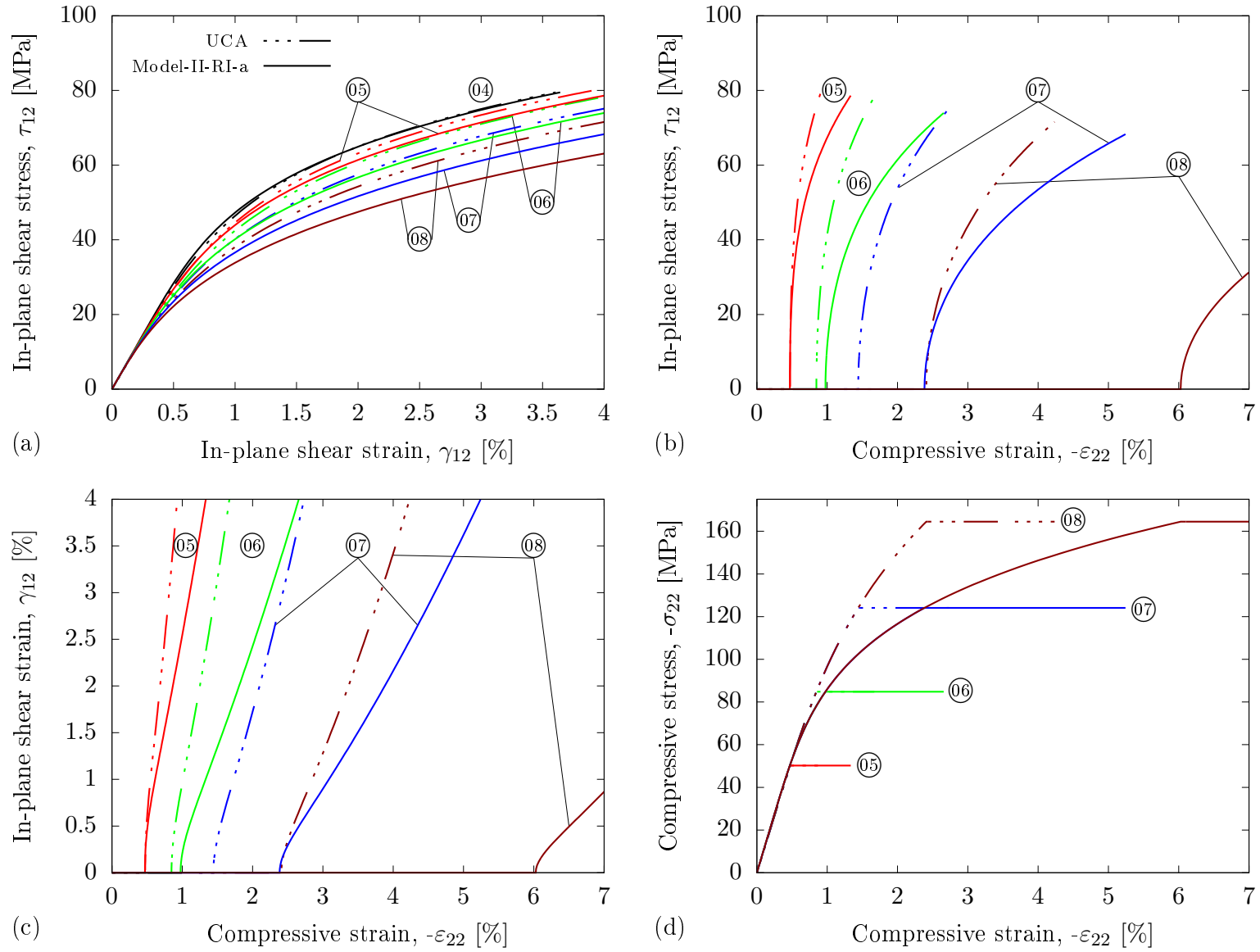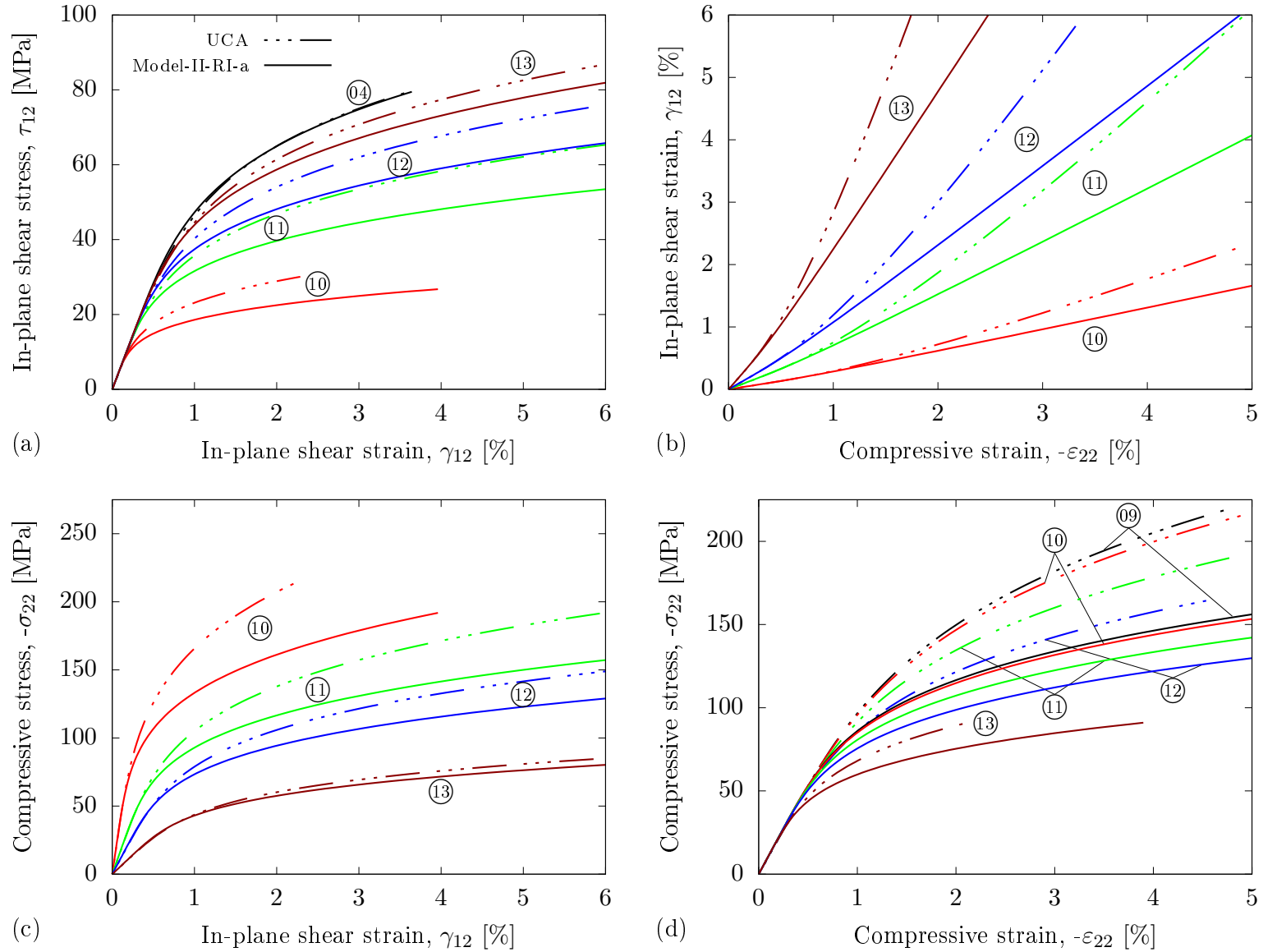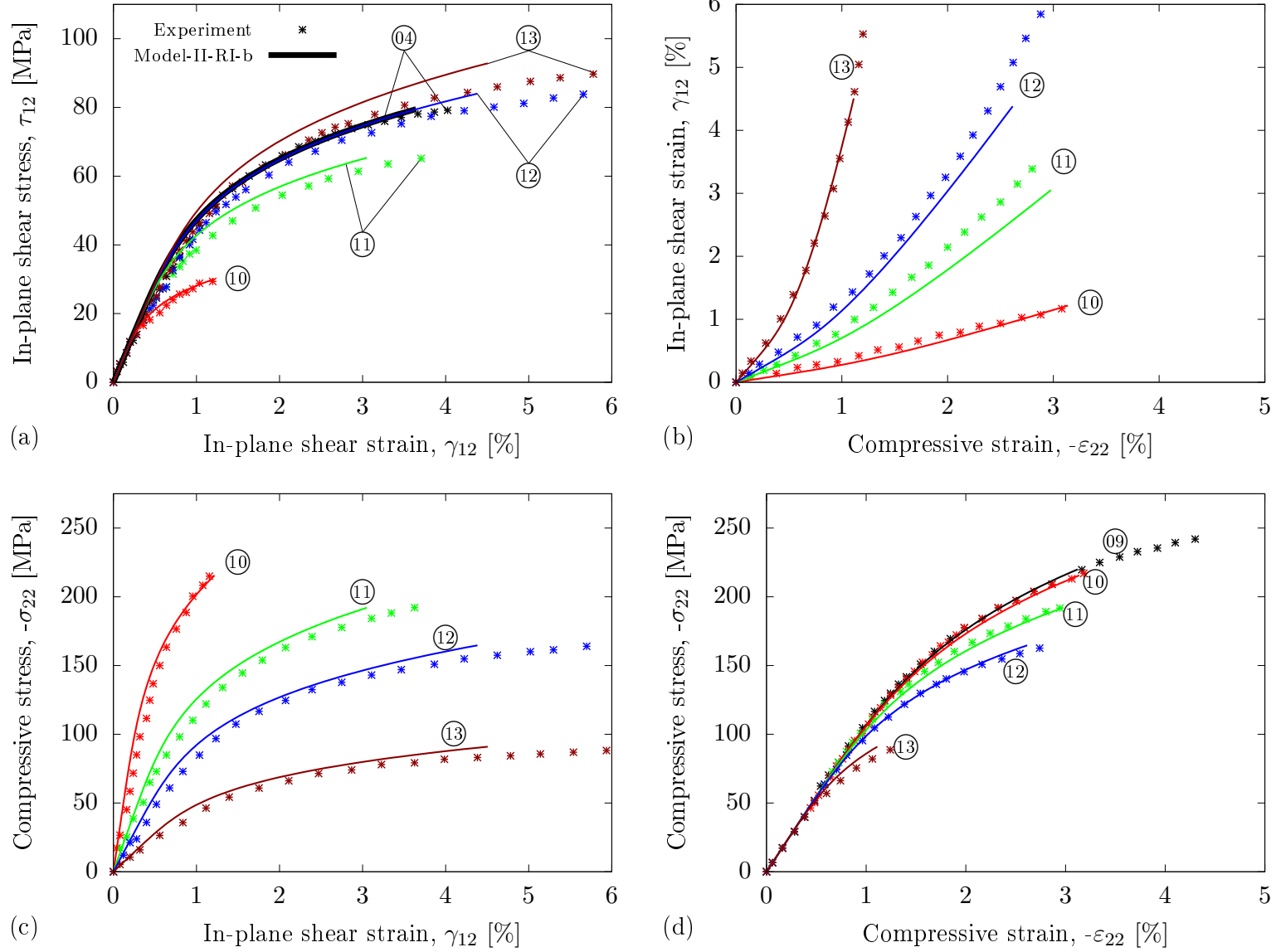FIGURE 50: **Predictions for biaxial loads.** Comparison of experimental and Model-II-RI-b responses for the radial loading path.

**7.3.3.5. Erroneous predictions of the associated flow response.** To illustrate the erroneous predictions of an associated flow response for a pressure sensitive fibre-reinforced composite, the $\tau_{12} \rightarrow -\varepsilon_{22}$ load path is considered. Figure 51 shows MDPR-b, Model-I-RI-b and Model-II-RI-b predictions for the load paths ①–④. The assessment of the plastic flow direction is apparent in these $\gamma_{12}$ vs. $-\varepsilon_{22}$ strain plots. For a pure shear stress state (load path ④), positive transverse strain is induced which is not expected (Figs. 51 (a)–(c)). The same phenomenon is observed for shear dominated combined stress states (load paths ①–③) where unexpected transverse tensile strain is predicted rather than expected compressive strain. This aspect is also demonstrated in [18] for load paths ⑤–⑧ where the pressure-dependent model with an associative flow rule predicts a decrease in the transverse strain for an increasing shear strain, a trend opposite to the experimental results reported in [7]. Similarly, the non-physical behaviour of associated flow response is also discussed in the recent work [112], with respect to compressive off-axis tests on a carbon-epoxy material. Again, it is seen that tensile rather than compressive transverse strain is predicted for 15° and 45° off-axis angles. This non-physical behaviour is a consequence of the negative slope of the Drucker-Prager-type yield surfaces used by these models, for pure shear and shear dominated combined stress states.

The corrected material response using a non-associative flow rule is shown in Figs. 52 (a)–(c). In line with the expectations, it is seen that the direction of plastic flow is aligned to the vertical axis for pure shear stress state. Additionally, the predicted transverse strains are compressive for shear dominated combined compression/shear stress states. In what follows, predictions of the pressure-dependent models with a non-associative flow rule are reported and discussed based on the foregoing observations.

**7.3.3.6. Predictions of Model-I-RI-c.** Figure 53 shows a comparison of Model-I-RI-c predictions and the experimental results for the $\tau_{12} \rightarrow -\varepsilon_{22}$ load path. The predicted compressive response by the model is in good agreement with experiments, as seen in Fig. 53 (a). The predicted transverse strains are compressive for the load paths ①–④, thereby eliminating the inconsistencies exhibited by Model-I-RI-b. Additionally, there is no overprediction of transverse stress for load path ③. Good agreement with the experimental response is seen in Figs. 53 (b) and (c). The shear response in presence of compression is captured by the model rather accurately as seen in Fig. 53 (d).

Plots depicting the model predictions and experimental results for the $-\sigma_{22} \rightarrow \gamma_{12}$ load path are shown in Fig. 54. The shear response in presence of compression is slightly overpredicted by the model as seen in Fig. 54 (a). This is a direct consequence of a higher value of the governing coefficient of hydrostatic pressure, as higher transverse stress leads to excessive stiffening in the shear response [18]. The parameter $\varkappa_1$ in Eqn. (318) should be rather low based on the experimental results where shear responses of the load paths ④–⑦ are almost the same, see [7]. The predicted $-\varepsilon_{22}$ agrees well with the experimental results as seen in Fig. 54 (b) with slight over estimation for load path ⑧. Figure 54 (c) shows the predicted $-\varepsilon_{22}$ for an applied shear strain $\gamma_{12} = 4\%$, for the load paths ⑤–⑧. The predicted transverse strains are much higher than the experimental ones, mainly because of the pressure-independent flow rule. The compressive response predicted by the model is in excellent agreement with the experimental results as seen in Fig. 54 (d).

The predictions of the model for the radial load path are compared with the experimental response in Fig. 55. The shear response is captured quite well by the model as seen in Fig. 55 (a). The assessment of the plastic flow direction is shown in the $\gamma_{12} - (-\varepsilon_{22})$ strain plot in Fig. 55 (b), where notable deviations from the experimental results are observed for

shear dominated loads (decreasing proportionality factors). The predicted shear strains are in excellent agreement with the experimental results (Fig. 55 (b)); only for load paths ⑫ and ⑬ is there a significant underprediction. The transverse predictions of the model are accurate as seen in Fig. 55 (d).

**7.3.3.7. Predictions of Model-II-RI-c.** Figures 56–58 show a comparison of Model-II-RI-c predictions and experimental response for the thirteen different load paths. It is seen that the model essentially predicts the same response as that of Model-I-RI-c. The only noticeable change is for the radial load path where the predicted material response for load paths ⑭ and ⑫ is now different (Fig. 58 (a)), in contrast to that of Model-I-RI-c (Fig. 50 (a)) where the material response is indistinguishable for these two load paths.

In summary, the non-associated flow response circumvents the physical inconsistencies induced by the associated flow response under shear dominated combined stress states, and yields the expected behaviour. However, notable deviations are observed for non-radial load paths where the shear response in presence of compression is overestimated. This can be attributed to the choice of a pressure-independent plastic flow potential and thereby a pressure-independent flow rule, as a result of which the predicted transverse strains are much higher than those observed experimentally. In view of these characteristics, the proposed alternative formulations of non-associative plasticity in **Chapter 5** can be used to overcome these deviations.
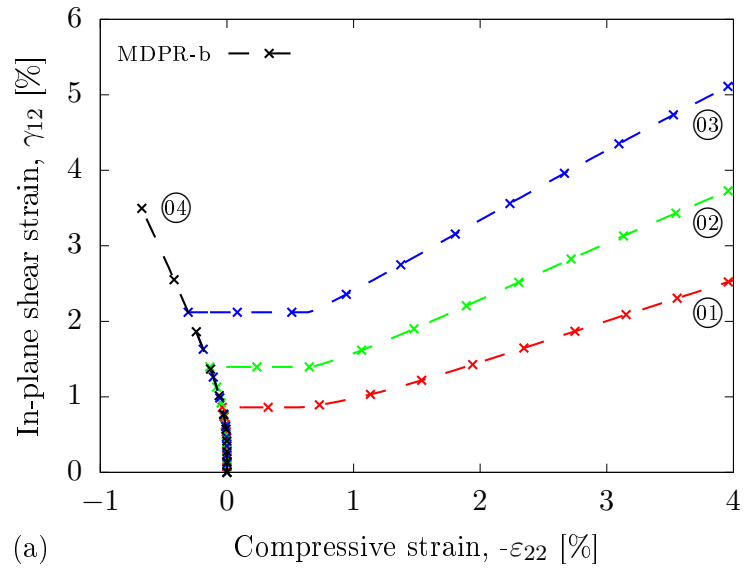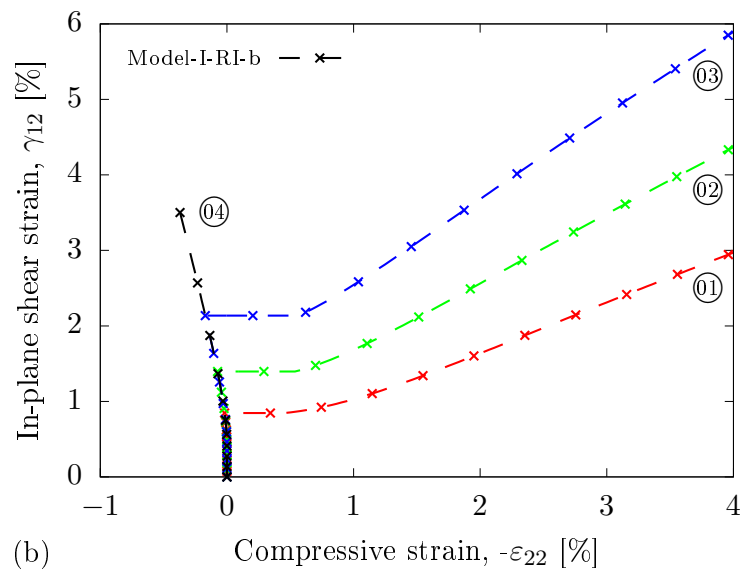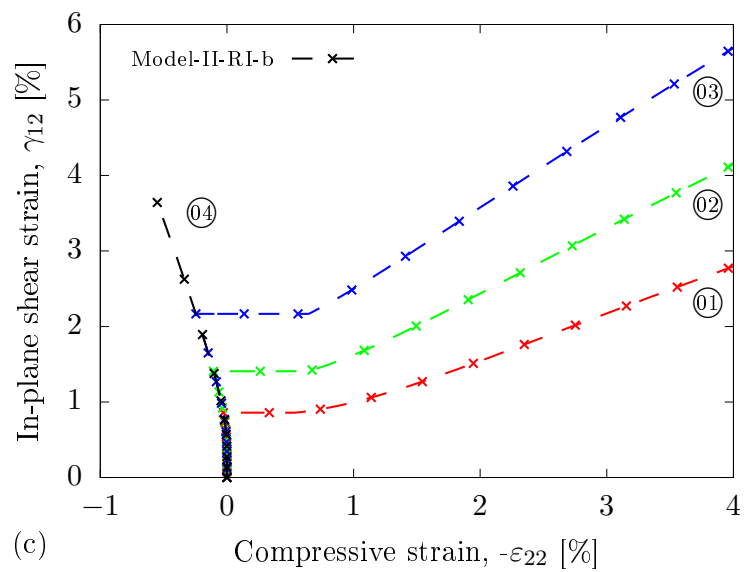
FIGURE 51: **Predicitions for biaxial loads.** Erroneous predictions of the associated flow response for shear dominated loads.
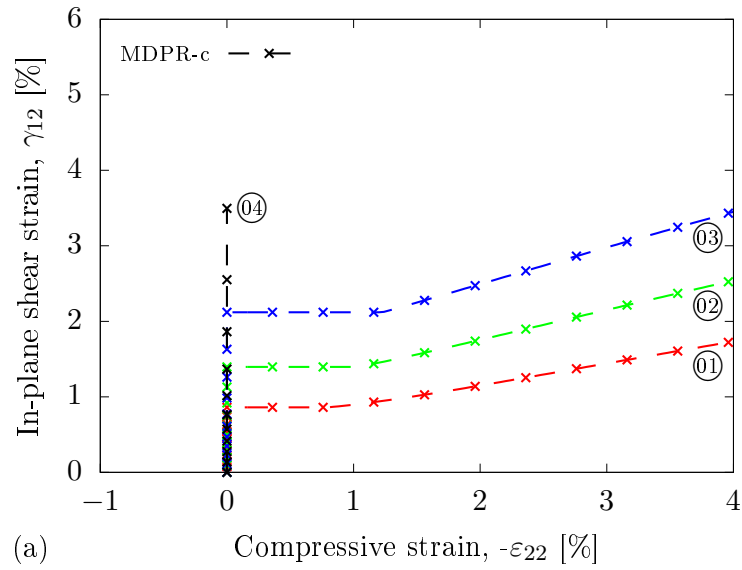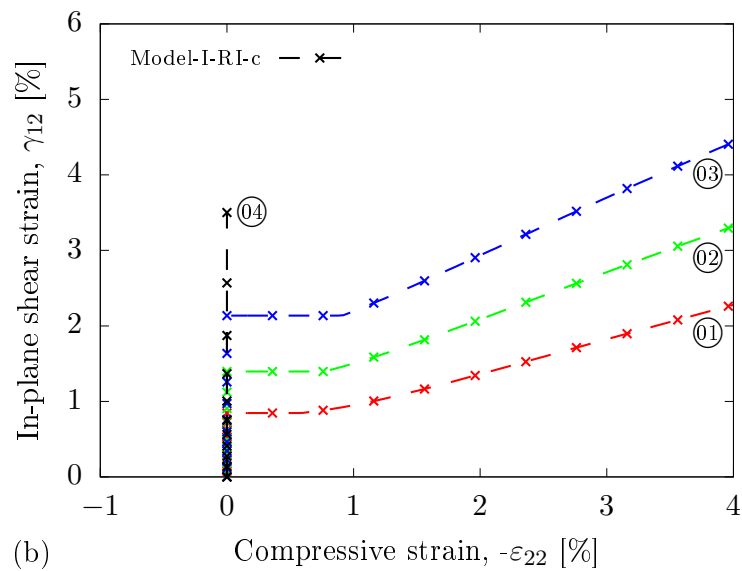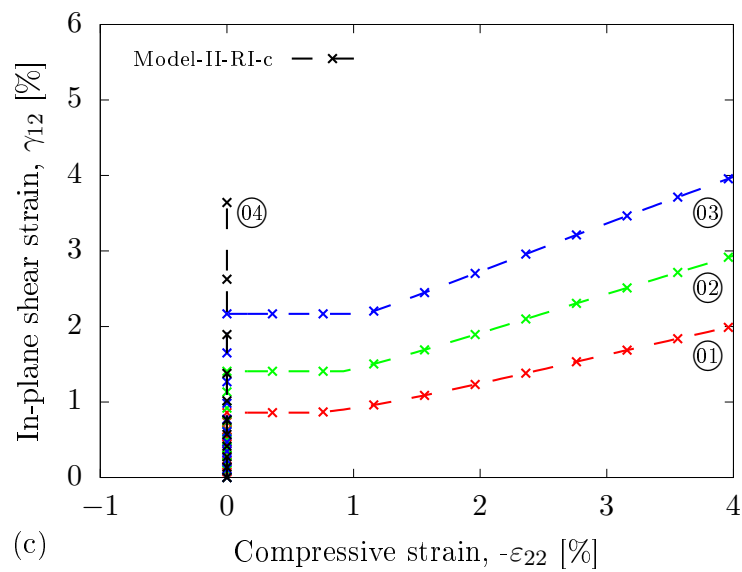
FIGURE 52: **Predictions for biaxial loads.** Corrected material response by the non-associative flow rule for shear dominated loads.
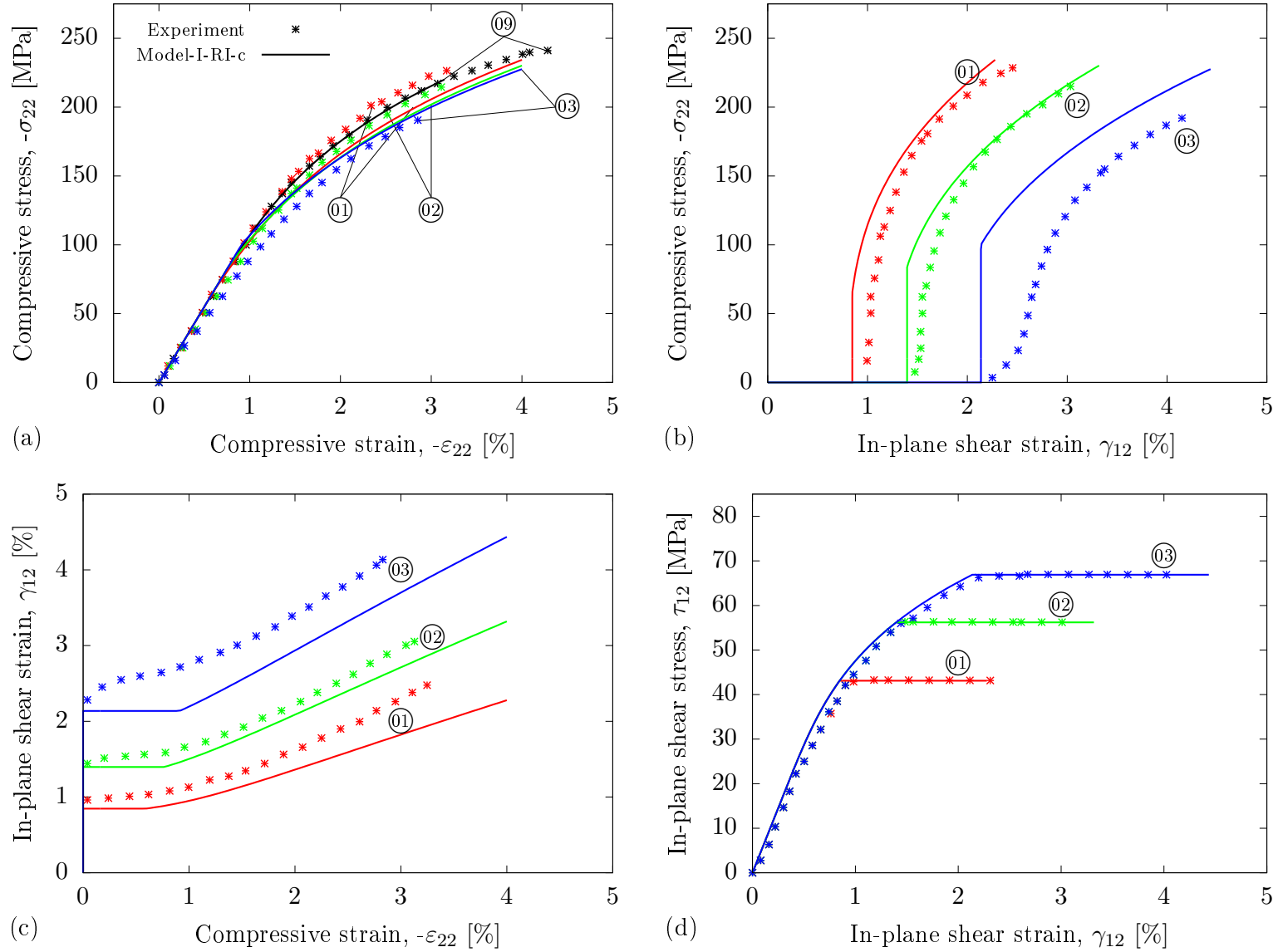
FIGURE 53: **Predictions for biaxial loads.** Comparison of experimental and Model-I-RI-c responses for the $\tau_{12} \to -\varepsilon_{22}$ loading path.
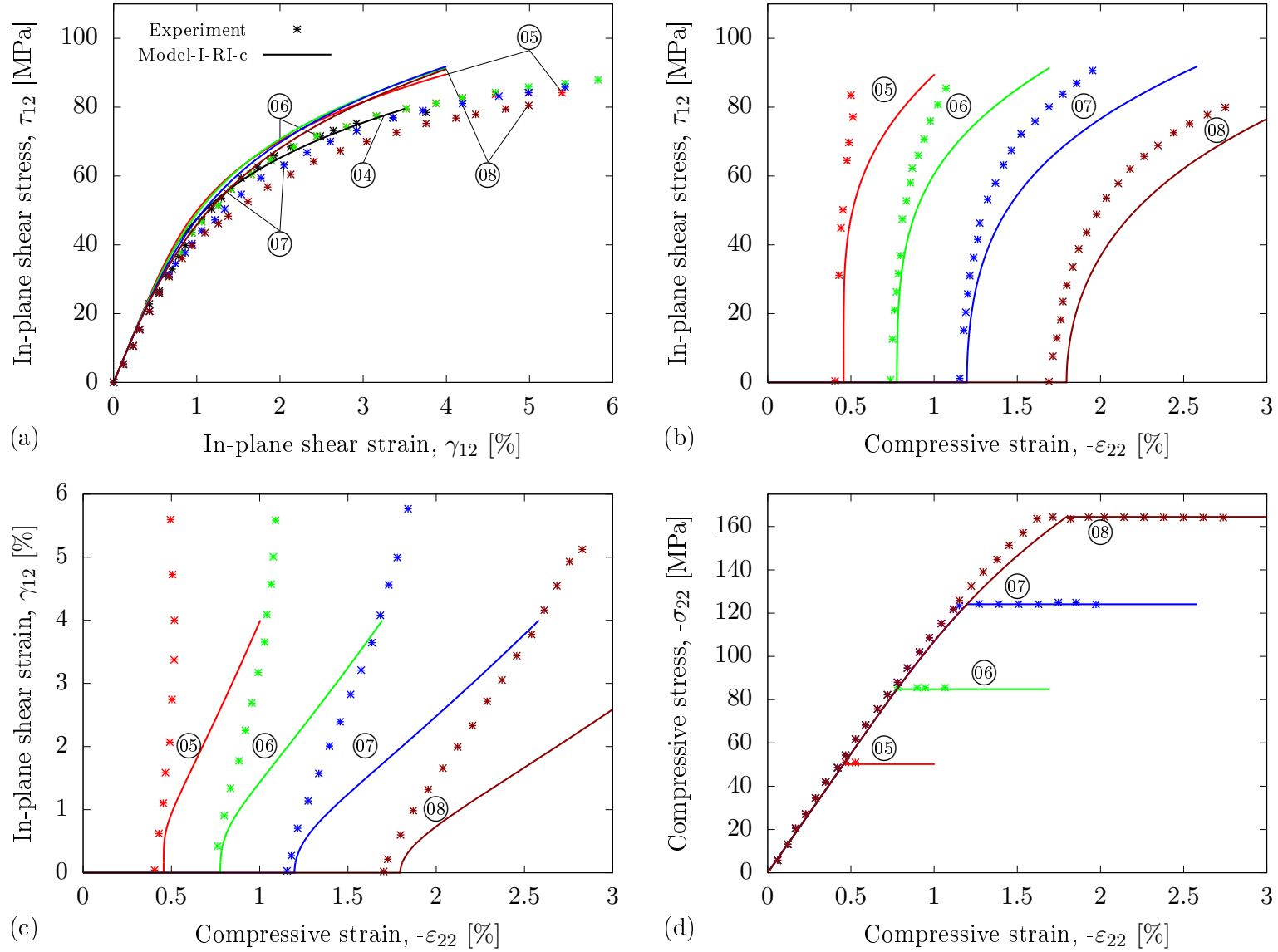
FIGURE 54: **Predictions for biaxial loads.** Comparison of experimental and Model-I-RI-c responses for the $-\sigma_{22} \rightarrow \gamma_{12}$ loading path.
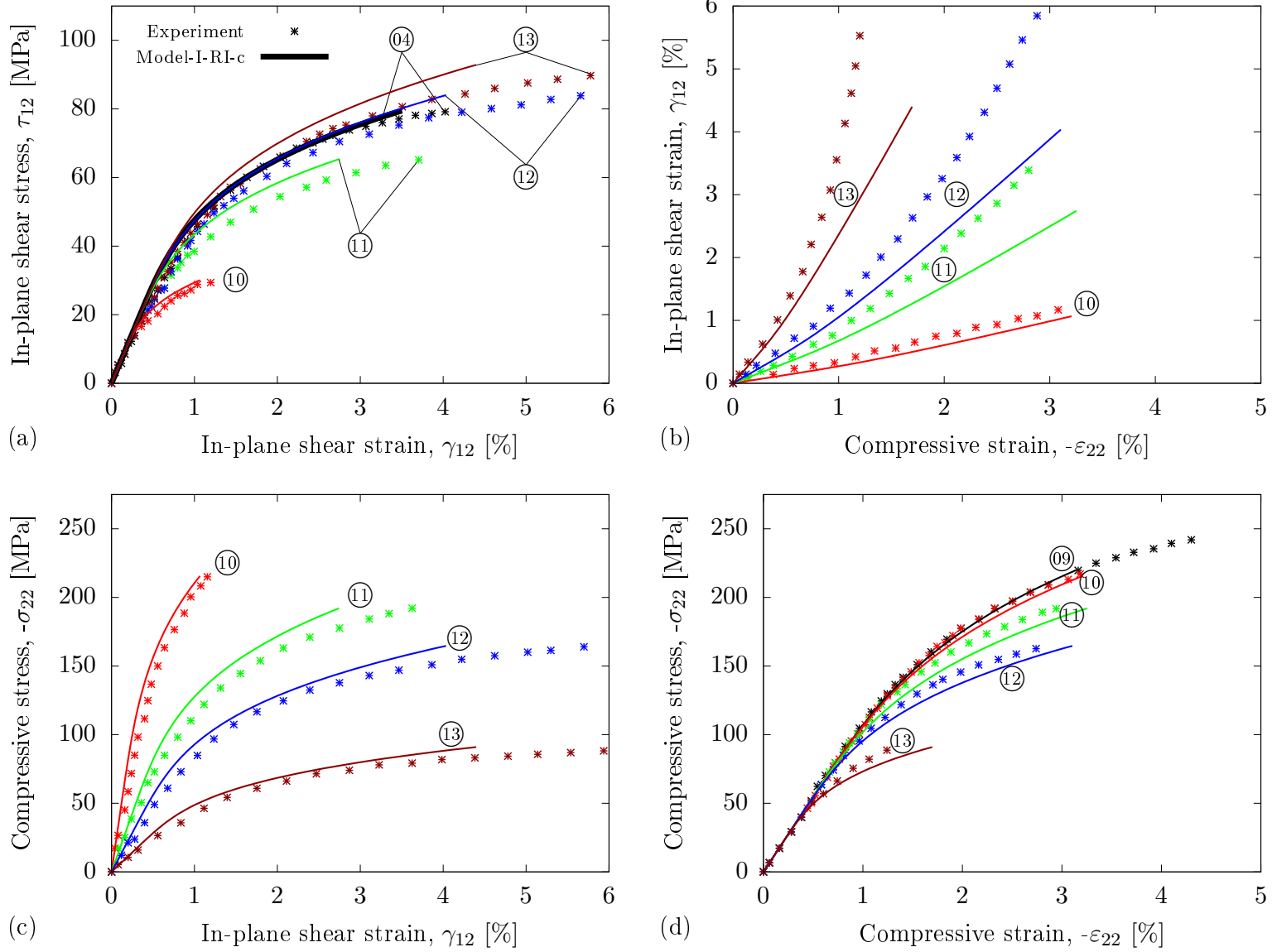
FIGURE 55: **Predictions for biaxial loads.** Comparison of experimental and Model-I-RI-c responses for the radial loading path.
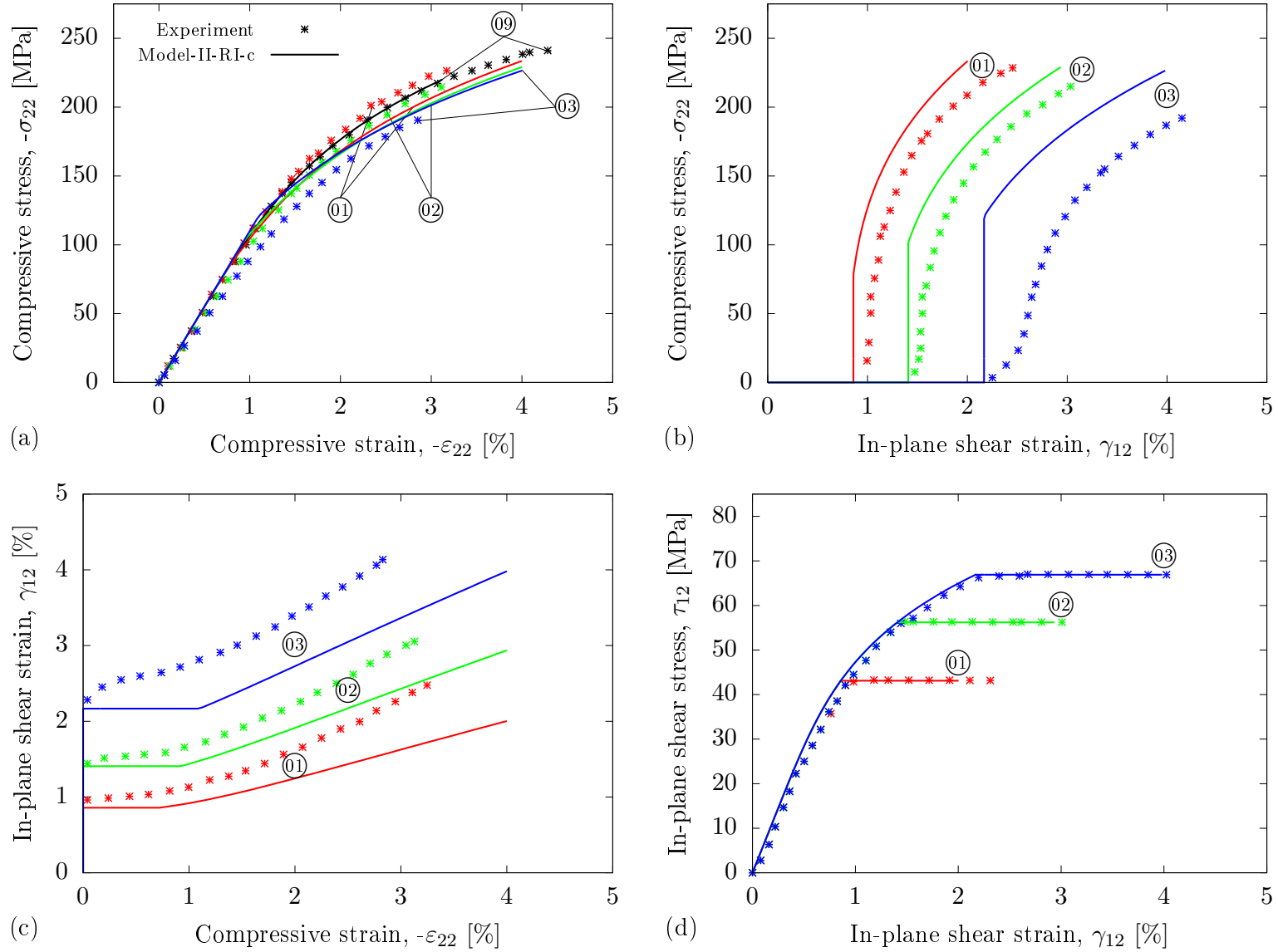
FIGURE 56: **Predictions for biaxial loads.** Comparison of experimental and Model-II-RI-c responses for the $\tau_{12} \rightarrow -\varepsilon_{22}$ loading path.
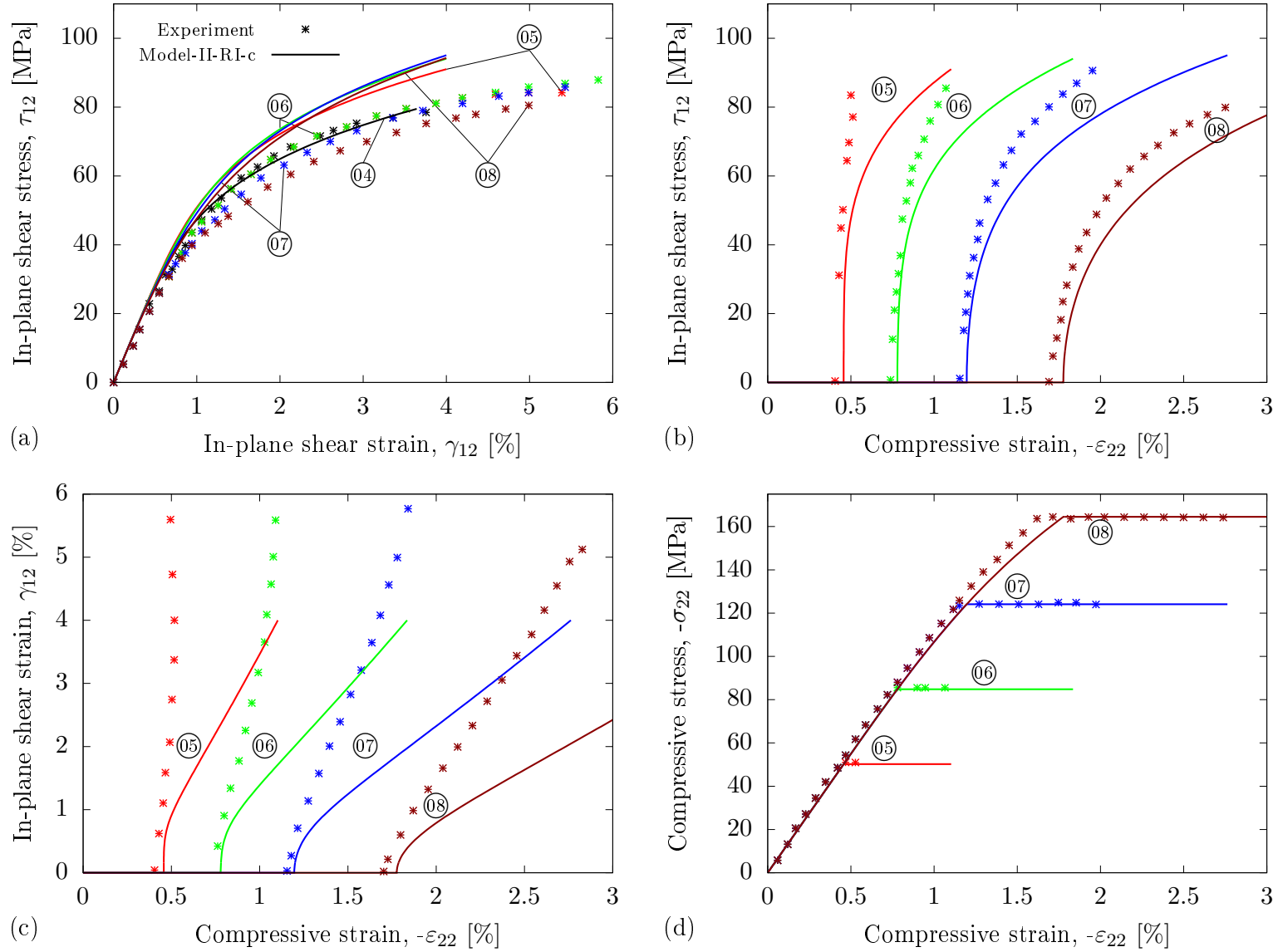
FIGURE 57: **Predictions for biaxial loads.** Comparison of experimental and Model-II-RI-c responses for the $-\sigma_{22} \to \gamma_{12}$ loading path.
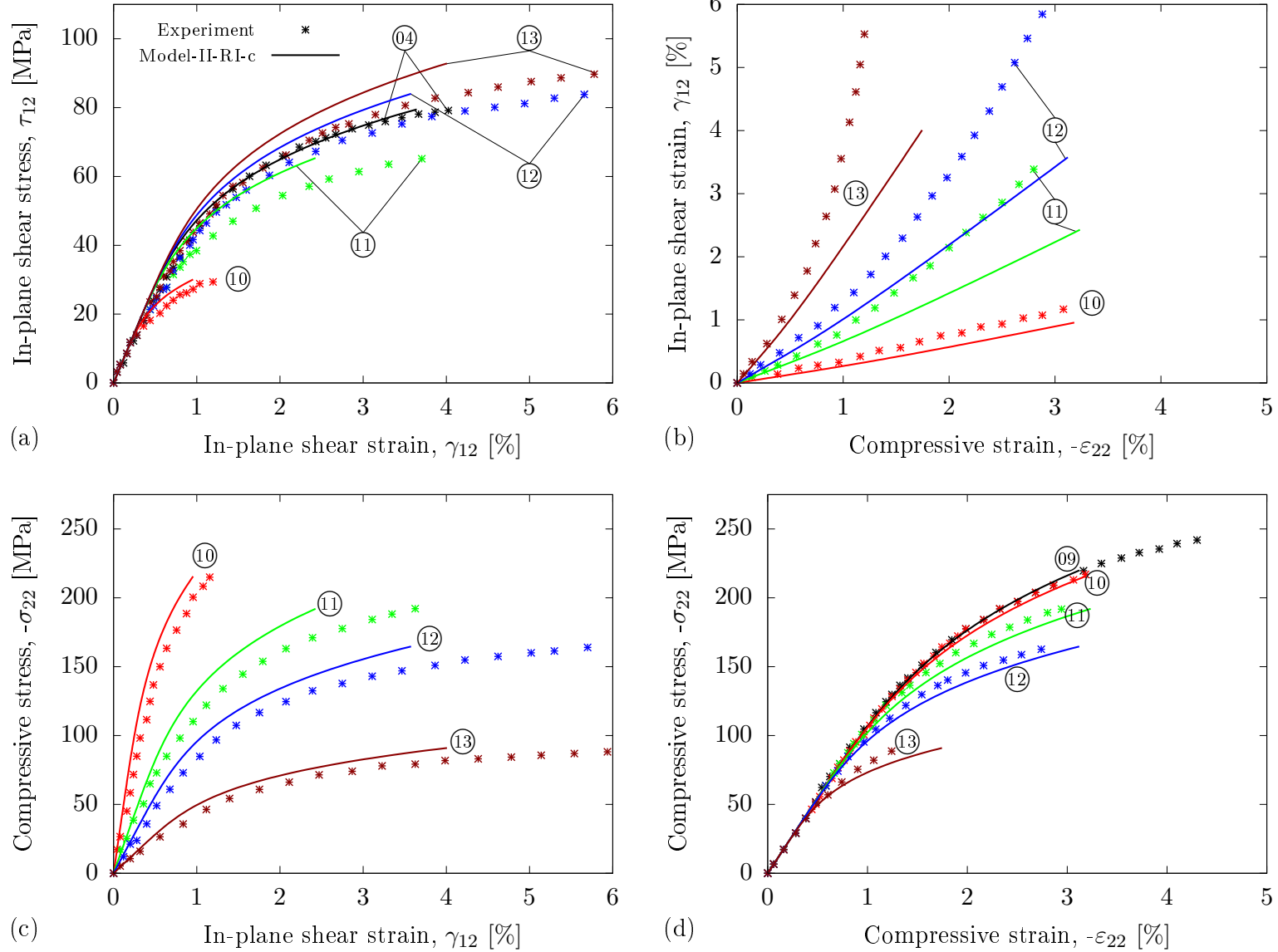
FIGURE 58: **Predictions for biaxial loads.** Comparison of experimental and Model-II-RI-c responses for the radial loading path.

### 7.3.4.  Tension of a plate with a hole

The last example is a benchmark test concerned with the uni-axial tension of a rectangular plate with a centrally located circular hole. The geometrical set up and boundary conditions are illustrated in Fig. 59. The radius of the hole is chosen to be 3.175 mm. With respect to the numerical implementation of the problem using the finite element method, the plate is discretised using 5218 C3D8 elements. At x = 0, the movement of the bottom surface of the plate is minimally constrained by imposing $u_x = 0$ (shaded area). At points A and B, $u_y = u_z = 0$ and $u_y = 0$, respectively, are imposed. The computation is performed in a deformation driven context where a prescribed deformation of $\bar{u}_x = 1.0$ mm is applied on the top surface of the plate as shown in Fig. 59. For the numerical simulations, Model-II-RI-c is used and the corresponding material parameters are listed in Table 6 and Table 10.
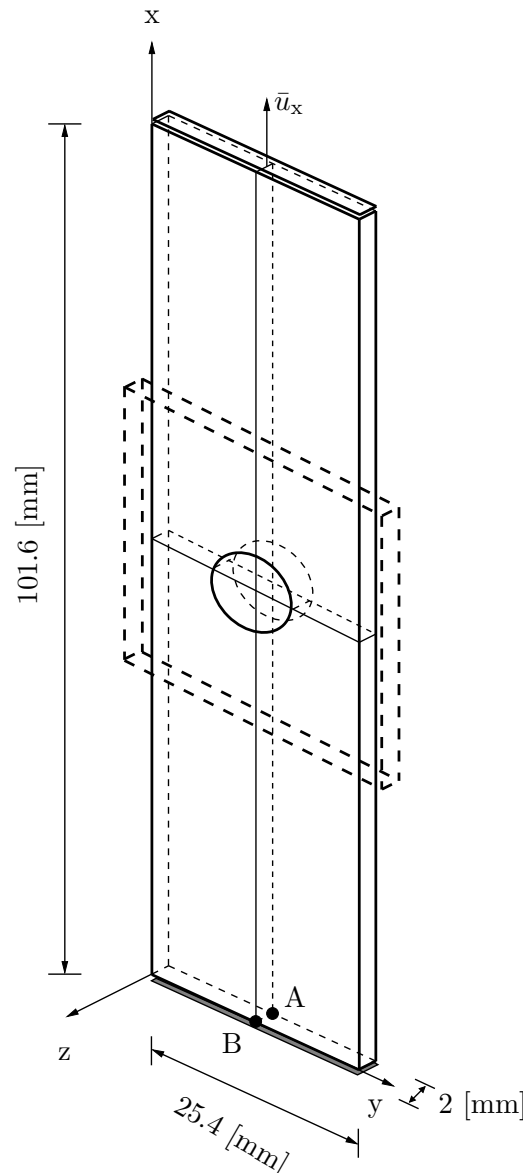


FIGURE 59: **Tension of a plate with a hole**. Geometrical set up and loading conditions.
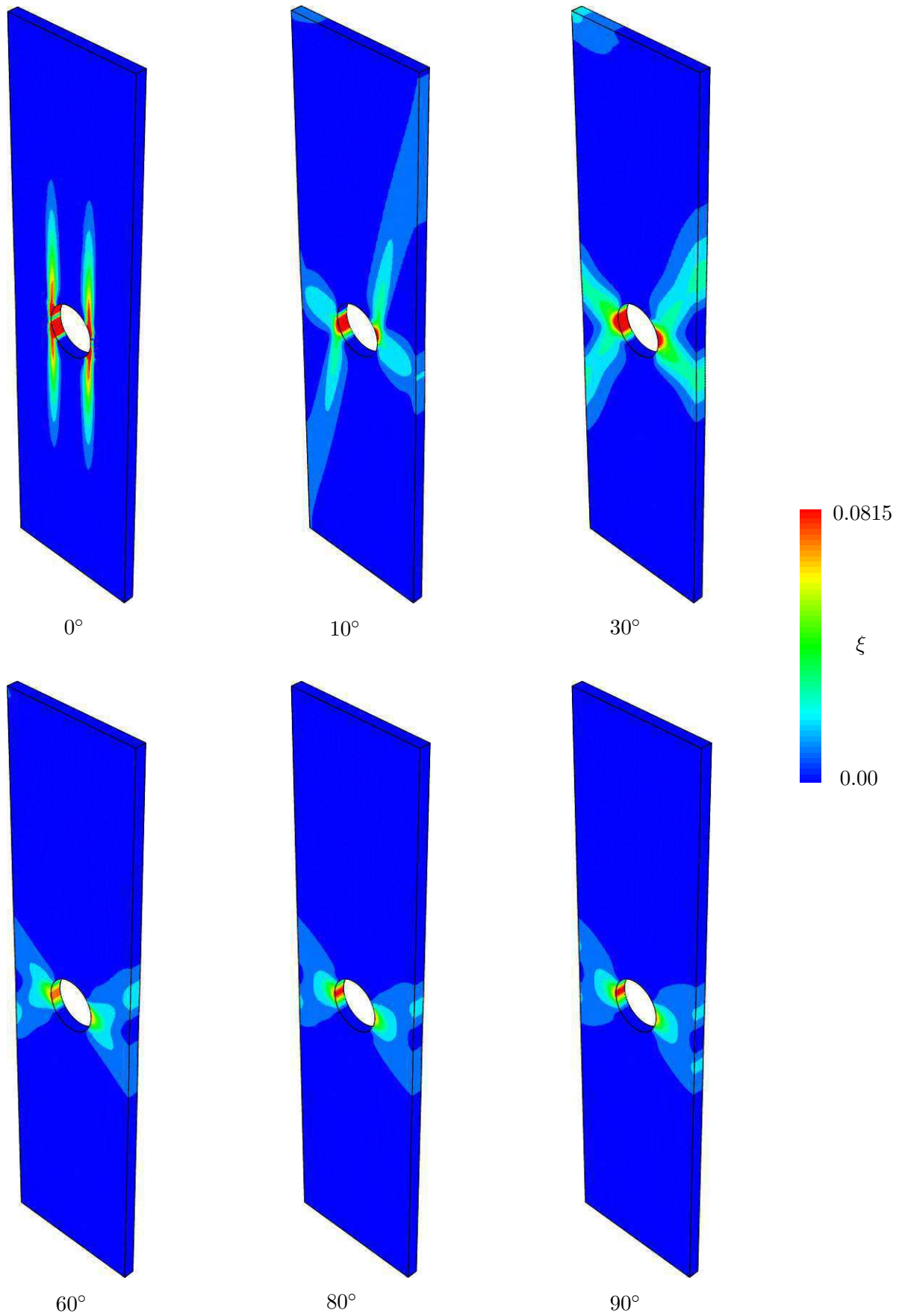
FIGURE 60: **Tension of a plate with a hole**. Distribution of equivalent plastic strain $\xi$ for various fibre orientations.

Figure 60 shows the contour plots of equivalent plastic strain $\xi$, at the final deformation state for various fibre orientations. As it is well known, the equivalent plastic strain localises in the shear band-type distribution along the fibre orientation. Similar to the observations in [78], it is seen that the plastic deformation spreads along the fibre direction and there is no localisation along the width of the specimen for $0°$ and $90°$ fibre orientations. However, inclined shear bands with slightly uneven branches can be seen for all the other fibre orientations. The anisotropic effect also makes the shear bands more diffuse which can be attributed to a change in the direction of the plastic flow.

# 8. Conclusion

## 8.1. Summary

This thesis is concerned with the formulation and numerical implementation of anisotropic elastoplasticity at infinitesimal strains, with application to fibre-reinforced composites. In this context, physically motivated and relatively general meso models are presented to simulate the non-linear plastic response of fibre-reinforced composites. From a continuum perspective, two symmetry groups (orthorhombic and transversely isotropic) are chosen and the governing constitutive equations of anisotropic elasticity applicable to these groups are first proposed with the aid of representation theorems. Next, two plasticity models that use isotropic plastic response functions to describe the plastic behaviour of composites are presented. The objective is to investigate the effect of using isotropic plastic response functions to capture the biaxial experimental responses, and understand the reasons for observed deficiencies and shortcomings of these models. Based on the foregoing observations, the main contribution of this work is the formulation of elastic-plastic constitutive equations which explicitly account for anisotropic behaviour in the stress response, yield condition, flow and hardening rules for the two symmetry groups. A point of departure from the previous chapter is the introduction of plasticity inducing stress tensors for the two symmetry groups, and the subsequent formulation of anisotropic plastic response functions using general representation theorems. The proposed plastic response functions are governed by only a few coefficients and the convexity conditions are rather simple to derive and impose. A set of canonical and non-conventional evolution equations are derived for the associative and non-associative plasticity theories, which result in a symmetric and non-symmetric constitutive structure, respectively. With respect to non-associative plasticity, a plastic flow potential which is purely deviatoric and stress free in the fibre direction is chosen to correct the physical inconsistencies by the associated flow rule under shear dominated loads. Further, a rate-dependent approximation of the rate-independent setting is outlined and implemented, apropos to the fact that a time regularisation of the rate-independent model always stabilises the algorithmic setting. From a theoretical standpoint, Model-I of the transversely isotropic symmetry group cannot be used in situations where the transverse shear response is stiffer than the in-plane shear response, owing to the restrictions imposed by the convexity requirement. This constraint is not applicable to Model-II. From a computational standpoint, the use of plasticity inducing stress in the formulation of plastic response functions results in a decoupled representation of the stress tensor, thus simplifying the problem of parameter identification.

The material parameters associated with the plastic response functions are identified by defining a non-linear optimisation problem with least-squares type functional, and evaluating the minimum of the functional using a simplex Nelder-Mead algorithm. Here, focus is restricted only to the transversely isotropic symmetry group due to a lack of experimental data for the orthorhombic system. The two models of the transversely isotropic system are first calibrated to reproduce the experimental shear response. The pressure-independent models reproduce the experimental shear response quite well, however, the predicted compressive response is notably less stiff. The associative and non-associative pressure-dependent models calibrated in a similar manner overcome this deficiency.

All the calibrated meso models are evaluated in detail by comparison to micro-mechanics simulations and experimental results, for a range of biaxial loads. Overall, the proposed models perform well in predicting the experimentally observed trends. In particular,

the predictions when combined with an associated flow rule are in excellent agreement with the experimental results. The asymmetric behaviour in the tension-compression regime is also well represented by these models. Besides the fact that the plastic flow is governed by fewer anisotropic coefficients, the findings are affirmative to state that the proposed plastic response functions are relatively general and can accurately describe the elastic-plastic response of fibre-reinforced composites. For the biaxial loads, the shear response in presence of compression is slightly over-predicted for some load paths, mainly by the pressure-dependent models when combined with a non-associative flow rule. Also, there is an observable deviation between the biaxial experimental response and the non-associative model predictions. This can purely be attributed to the respective model formulation, where it has been assumed that the plastic flow is traceless and stress-free in the fibre direction. In view of these characteristics, alternative formulations of non-associative plasticity are provided that account for dilatation during the course of plastic deformation. The proposed formulations still need to be validated with the experimental data. However, to the author's knowledge, this modification gives better results than the presented non-associative models where a purely pressure-independent flow response is assumed. The performance of the proposed models is also demonstrated by means of benchmark boundary value problems.

## 8.2. Outlook

Fundamentally, the development of constitutive relations for a homogenised composite is a challenging task where the formulation has to be simple, yet accurate for a wide range of loading scenarios. For instance, such formulations are applied in the failure analysis where an important partial ingredient is the modelling of non-linearity under shear dominated loads, i.e. plasticity. Plasticity prior to damage affects the onset of failure and therefore it is necessary to precisely model the elastic-plastic behaviour. In this context, necessary simplifications such as disregarding the influence of the stress in the fibre directions on plasticity under combined loads may lead to a loss of accuracy. Hence, the influence of fibre stress on plasticity under combined stress states, such as shear or compression load with tension/compression in the fibre direction should be quantified prior to the failure analysis. Furthermore, the effect of temperature on the elastic-plastic response could also be considered, see Appendix C for a general discussion, as polymeric composites are known to be temperature sensitive.

Moreover, the proposed framework can also be extended to include geometric non-linearities to account for the effects of the interface failure. A particularly interesting aspect in this extension would be to incorporate deformation-induced evolution of anisotropy, which demands the specification of additional constitutive (evolution) equations for the structural tensors, that allows for fibre rotations to be taken into account during the course of elastic/inelastic deformations.

# A. Isotropic functions of the symmetry groups

TABLE 11: List of invariants for scalar valued functions.

| Variables | Invariants |
|---|---|
| $\{\boldsymbol{A}\}$ | $\left\{\,\mathrm{tr}[\boldsymbol{A}],\,\mathrm{tr}[\boldsymbol{A}^2],\,\mathrm{tr}[\boldsymbol{A}^3]\right\}$ |
| $\{\boldsymbol{V}\}$ | $\left\{\,\mathrm{tr}[\boldsymbol{V}^2]\right\}$ |
| $\{\boldsymbol{A},\boldsymbol{U}\}$ | $\left\{\,\mathrm{tr}[\boldsymbol{A}\boldsymbol{U}],\,\mathrm{tr}[\boldsymbol{A}^2\boldsymbol{U}],\,\mathrm{tr}[\boldsymbol{A}\boldsymbol{U}^2],\,\mathrm{tr}[\boldsymbol{A}^2\boldsymbol{U}^2]\right\}$ |
| $\{\boldsymbol{A},\boldsymbol{V}\}$ | $\left\{\,\mathrm{tr}[\boldsymbol{A}\boldsymbol{V}^2],\,\mathrm{tr}[\boldsymbol{A}^2\boldsymbol{V}^2],\,\mathrm{tr}[\boldsymbol{A}^2\boldsymbol{V}^2\boldsymbol{A}\boldsymbol{V}]\right\}$ |
| $\{\boldsymbol{V}_1,\boldsymbol{V}_2\}$ | $\left\{\,\mathrm{tr}[\boldsymbol{V}_1\boldsymbol{V}_2]\right\}$ |
| $\{\boldsymbol{A},\boldsymbol{U},\boldsymbol{V}\}$ | $\left\{\,\mathrm{tr}[\boldsymbol{A}\boldsymbol{U}\boldsymbol{V}],\,\mathrm{tr}[\boldsymbol{A}^2\boldsymbol{U}\boldsymbol{V}],\,\mathrm{tr}[\boldsymbol{A}\boldsymbol{U}^2\boldsymbol{V}],\,\mathrm{tr}[\boldsymbol{A}\boldsymbol{V}^2\boldsymbol{U}\boldsymbol{V}]\right\}$ |
| $\{\boldsymbol{A},\boldsymbol{U}_1,\boldsymbol{U}_2\}$ | $\left\{\,\mathrm{tr}[\boldsymbol{A}\boldsymbol{U}_1\boldsymbol{U}_2]\right\}$ |
| $\{\boldsymbol{A},\boldsymbol{V}_1,\boldsymbol{V}_2\}$ | $\left\{\,\mathrm{tr}[\boldsymbol{A}\boldsymbol{V}_1\boldsymbol{V}_2],\,\mathrm{tr}[\boldsymbol{A}\boldsymbol{V}_1^2\boldsymbol{V}_2],\,\mathrm{tr}[\boldsymbol{A}\boldsymbol{V}_1\boldsymbol{V}_2^2]\right\}$ |
| $\{\boldsymbol{V}_1,\boldsymbol{V}_2,\boldsymbol{V}_3\}$ | $\left\{\,\mathrm{tr}[\boldsymbol{V}_1\boldsymbol{V}_2\boldsymbol{V}_3]\right\}$ |

In this appendix, explicit form of the scalar-valued potential (80) is derived for the symmetry groups listed in Table 2, following closely [75, 137]. Recall here that $\{\boldsymbol{a},\boldsymbol{b},\boldsymbol{c}\}$ is a vector triad representing an orthonormal preferred frame, as depicted in Fig. 61. For the sake of simplicity, focus is restricted to a *quadratic* form of Eqn. (80). At this stage, the functional bases for one, two and three tensor-valued arguments, introduced in [138], are listed in Table 11 which will play an important role in the derivation of the scalar-valued potential[12].

## A.1. Triclinic symmetry group $\mathscr{C}_1$

The *triclinic* symmetry group $\mathscr{C}_1$, generated by $\boldsymbol{1}$, has the lowest symmetry characterising a fully anisotropic material. The orientation of such a material is determined by two
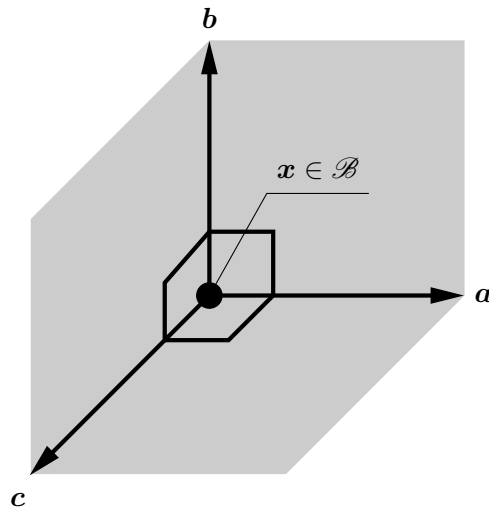


FIGURE 61: **Preferred directions.** Positively oriented orthonormal vector triad $\{\boldsymbol{a},\boldsymbol{b},\boldsymbol{c}\}$ attached to a material point $\boldsymbol{x}\in\mathscr{B}$.

---

[12]the invariants based on the vector-valued arguments in [138] are neglected as they are not of interest in the present work.

orthonormal vectors $\boldsymbol{a}$ and $\boldsymbol{b}$, such that the general form of the scalar-valued function $\mathfrak{F}$ is given by

$$\mathfrak{F} = \mathfrak{F}(\boldsymbol{A}, \boldsymbol{V}_1, \boldsymbol{V}_2) \quad \text{with} \quad \boldsymbol{V}_1 = \epsilon\boldsymbol{a} \quad \text{and} \quad \boldsymbol{V}_2 = \epsilon\boldsymbol{b} \,, \tag{401}$$

in terms of the argument tensor $\boldsymbol{A}$, and two skew-symmetric second-order tensors $\boldsymbol{V}_1$ and $\boldsymbol{V}_2$. It can be seen from Table 11 that the functional basis for the $\mathscr{C}_1$ group consists of the basic invariants of the arguments $\boldsymbol{A}$, $\boldsymbol{V}_1$ and $\boldsymbol{V}_2$, given by

$$\left\{ \operatorname{tr}[\boldsymbol{A}], \operatorname{tr}[\boldsymbol{A}^2], \operatorname{tr}[\boldsymbol{A}^3], \operatorname{tr}[\boldsymbol{V}_1^2], \operatorname{tr}[\boldsymbol{V}_2^2] \right\} \,, \tag{402}$$

the mixed invariants of every two arguments $\{\boldsymbol{A}, \boldsymbol{V}_1\}$, $\{\boldsymbol{A}, \boldsymbol{V}_2\}$ and $\{\boldsymbol{V}_1, \boldsymbol{V}_2\}$ such that

$$\left\{ \operatorname{tr}[\boldsymbol{A}\boldsymbol{V}_1^2], \operatorname{tr}[\boldsymbol{A}^2\boldsymbol{V}_1^2], \operatorname{tr}[\boldsymbol{A}^2\boldsymbol{V}_1^2\boldsymbol{A}\boldsymbol{V}_1], \operatorname{tr}[\boldsymbol{A}\boldsymbol{V}_2^2], \operatorname{tr}[\boldsymbol{A}^2\boldsymbol{V}_2^2], \operatorname{tr}[\boldsymbol{A}^2\boldsymbol{V}_2^2\boldsymbol{A}\boldsymbol{V}_2], \operatorname{tr}[\boldsymbol{V}_1\boldsymbol{V}_2] \right\} \,, \tag{403}$$

and the relative invariants of all the argument tensors $\{\boldsymbol{A}, \boldsymbol{V}_1, \boldsymbol{V}_2\}$, namely

$$\left\{ \operatorname{tr}[\boldsymbol{A}\boldsymbol{V}_1\boldsymbol{V}_2], \operatorname{tr}[\boldsymbol{A}\boldsymbol{V}_1^2\boldsymbol{V}_2], \operatorname{tr}[\boldsymbol{A}\boldsymbol{V}_1\boldsymbol{V}_2^2] \right\} \,, \tag{404}$$

see also [139]. The invariants in Eqns. (402)–(404) are multiplicatively combined to obtain quadratic terms in $\boldsymbol{A}$, which leads to the definition of an irreducible integrity basis as

$$\begin{aligned}
\mathcal{I}_{\mathscr{C}_1} = \big\{ \; & \operatorname{tr}^2[\boldsymbol{A}], \operatorname{tr}[\boldsymbol{A}^2], \operatorname{tr}^2[\boldsymbol{A}\boldsymbol{V}_1^2], \operatorname{tr}^2[\boldsymbol{A}\boldsymbol{V}_2^2], \operatorname{tr}^2[\boldsymbol{A}\boldsymbol{V}_1\boldsymbol{V}_2], \operatorname{tr}^2[\boldsymbol{A}\boldsymbol{V}_1^2\boldsymbol{V}_2], \\
& \operatorname{tr}^2[\boldsymbol{A}\boldsymbol{V}_1\boldsymbol{V}_2^2], \operatorname{tr}[\boldsymbol{A}^2\boldsymbol{V}_1^2], \operatorname{tr}[\boldsymbol{A}^2\boldsymbol{V}_2^2], \operatorname{tr}[\boldsymbol{A}]\operatorname{tr}[\boldsymbol{A}\boldsymbol{V}_1\boldsymbol{V}_2], \\
& \operatorname{tr}[\boldsymbol{A}]\operatorname{tr}[\boldsymbol{A}\boldsymbol{V}_1^2\boldsymbol{V}_2], \operatorname{tr}[\boldsymbol{A}]\operatorname{tr}[\boldsymbol{A}\boldsymbol{V}_1\boldsymbol{V}_2^2], \operatorname{tr}[\boldsymbol{A}\boldsymbol{V}_1^2]\operatorname{tr}[\boldsymbol{A}\boldsymbol{V}_1\boldsymbol{V}_2], \\
& \operatorname{tr}[\boldsymbol{A}\boldsymbol{V}_1^2]\operatorname{tr}[\boldsymbol{A}\boldsymbol{V}_1^2\boldsymbol{V}_2], \operatorname{tr}[\boldsymbol{A}\boldsymbol{V}_1^2]\operatorname{tr}[\boldsymbol{A}\boldsymbol{V}_1\boldsymbol{V}_2^2], \operatorname{tr}[\boldsymbol{A}\boldsymbol{V}_2^2]\operatorname{tr}[\boldsymbol{A}\boldsymbol{V}_1\boldsymbol{V}_2], \\
& \operatorname{tr}[\boldsymbol{A}\boldsymbol{V}_2^2]\operatorname{tr}[\boldsymbol{A}\boldsymbol{V}_1^2\boldsymbol{V}_2], \operatorname{tr}[\boldsymbol{A}\boldsymbol{V}_2^2]\operatorname{tr}[\boldsymbol{A}\boldsymbol{V}_1\boldsymbol{V}_2^2], \operatorname{tr}[\boldsymbol{A}\boldsymbol{V}_1\boldsymbol{V}_2]\operatorname{tr}[\boldsymbol{A}\boldsymbol{V}_1^2\boldsymbol{V}_2] \\
& \operatorname{tr}[\boldsymbol{A}\boldsymbol{V}_1\boldsymbol{V}_2]\operatorname{tr}[\boldsymbol{A}\boldsymbol{V}_1\boldsymbol{V}_2^2], \operatorname{tr}[\boldsymbol{A}\boldsymbol{V}_1^2\boldsymbol{V}_2]\operatorname{tr}[\boldsymbol{A}\boldsymbol{V}_1\boldsymbol{V}_2^2] \big\} \,,
\end{aligned} \tag{405}$$

where the invariants

$$\begin{aligned}
\operatorname{tr}[\boldsymbol{A}]\operatorname{tr}[\boldsymbol{A}\boldsymbol{V}_1^2] &= -\frac{1}{2}(\operatorname{tr}^2[\boldsymbol{A}] + \operatorname{tr}^2[\boldsymbol{A}\boldsymbol{V}_1^2] + \operatorname{tr}^2[\boldsymbol{A}\boldsymbol{V}_1\boldsymbol{V}_2] + \operatorname{tr}[\boldsymbol{A}\boldsymbol{V}_1^2\boldsymbol{V}_2] - \operatorname{tr}[\boldsymbol{A}^2] - \operatorname{tr}[\boldsymbol{A}^2\boldsymbol{V}_1^2]) \,, \\
\operatorname{tr}[\boldsymbol{A}]\operatorname{tr}[\boldsymbol{A}\boldsymbol{V}_2^2] &= -\frac{1}{2}(\operatorname{tr}^2[\boldsymbol{A}] + \operatorname{tr}^2[\boldsymbol{A}\boldsymbol{V}_2^2] + \operatorname{tr}^2[\boldsymbol{A}\boldsymbol{V}_1\boldsymbol{V}_2] + \operatorname{tr}[\boldsymbol{A}\boldsymbol{V}_1\boldsymbol{V}_2^2] - \operatorname{tr}[\boldsymbol{A}^2] - \operatorname{tr}[\boldsymbol{A}^2\boldsymbol{V}_2^2]) \,, \\
\operatorname{tr}[\boldsymbol{A}\boldsymbol{V}_1^2]\operatorname{tr}[\boldsymbol{A}\boldsymbol{V}_2^2] &= -\frac{1}{2}\operatorname{tr}^2[\boldsymbol{A}] + \operatorname{tr}^2[\boldsymbol{A}\boldsymbol{V}_1\boldsymbol{V}_2] - \frac{3}{2}\operatorname{tr}[\boldsymbol{A}^2] - \operatorname{tr}[\boldsymbol{A}\boldsymbol{V}_1^2] - \operatorname{tr}[\boldsymbol{A}^2\boldsymbol{V}_2^2] \,,
\end{aligned} \tag{406}$$

are dropped from Eqn. (405) since they can be expressed in terms of the other invariants. A *quadratic* form of Eqn. (80) can be readily written with the aid of Eqn. (405) as

$$\mathfrak{F} = \sum_{i=1}^{21} \mu_i I_i \,, \tag{407}$$

where $I_{1-21}$ are the elements of the integrity basis $\mathcal{I}_{\mathscr{C}_1}$, and $\mu_{1-21}$ are material constants. The second-order stress-like tensor $\boldsymbol{\mathsf{S}}$ associated with the potential is given by the deriva-

tive of Eqn. (407) with respect to the argument $\boldsymbol{A}$ as

$$\boldsymbol{\mathcal{S}} = \mathfrak{F}_{,\boldsymbol{A}} = \sum_{i=1}^{21} \mathfrak{F}_{,I_i} \, I_{i,\,\boldsymbol{A}}$$

$$\begin{aligned}
=&\, 2\mu_1 \, \mathrm{tr}[\boldsymbol{A}]\,\boldsymbol{1} + 2\mu_2 \boldsymbol{A} + 2\mu_3 \, \mathrm{tr}[\boldsymbol{A}\boldsymbol{V}_1^2]\boldsymbol{V}_1^2 + 2\mu_4 \, \mathrm{tr}[\boldsymbol{A}\boldsymbol{V}_2^2]\boldsymbol{V}_2^2 \\
&+ \mu_5 tr[\boldsymbol{A}\boldsymbol{V}_1\boldsymbol{V}_2](\boldsymbol{V}_1\boldsymbol{V}_2 + \boldsymbol{V}_2\boldsymbol{V}_1) + \mu_6 \, \mathrm{tr}[\boldsymbol{A}\boldsymbol{V}_1^2\boldsymbol{V}_2](\boldsymbol{V}_1^2\boldsymbol{V}_2 - \boldsymbol{V}_2\boldsymbol{V}_1^2) \\
&+ \mu_7 \, \mathrm{tr}[\boldsymbol{A}\boldsymbol{V}_1\boldsymbol{V}_2^2](\boldsymbol{V}_1\boldsymbol{V}_2^2 - \boldsymbol{V}_2^2\boldsymbol{V}_1) + \mu_8(\boldsymbol{A}\boldsymbol{V}_1^2 + \boldsymbol{V}_1^2\boldsymbol{A}) \\
&+ \mu_9(\boldsymbol{A}\boldsymbol{V}_2^2 + \boldsymbol{V}_2^2\boldsymbol{A}) + \mu_{10}\Big\{\mathrm{tr}[\boldsymbol{A}\boldsymbol{V}_1\boldsymbol{V}_2]\boldsymbol{1} + \frac{1}{2}\,\mathrm{tr}[\boldsymbol{A}](\boldsymbol{V}_2\boldsymbol{V}_1 + \boldsymbol{V}_1\boldsymbol{V}_2)\Big\} \\
&+ \mu_{11}\Big\{\mathrm{tr}[\boldsymbol{A}\boldsymbol{V}_1^2\boldsymbol{V}_2]\boldsymbol{1} + \frac{1}{2}\,\mathrm{tr}[\boldsymbol{A}](\boldsymbol{V}_1^2\boldsymbol{V}_2 - \boldsymbol{V}_2\boldsymbol{V}_1^2)\Big\} \\
&+ \mu_{12}\Big\{\mathrm{tr}[\boldsymbol{A}\boldsymbol{V}_1\boldsymbol{V}_2^2]\boldsymbol{1} + \frac{1}{2}\,\mathrm{tr}[\boldsymbol{A}](\boldsymbol{V}_1\boldsymbol{V}_2^2 - \boldsymbol{V}_2^2\boldsymbol{V}_1)\Big\} \\
&+ \mu_{13}\Big\{\mathrm{tr}[\boldsymbol{A}\boldsymbol{V}_1\boldsymbol{V}_2]\boldsymbol{V}_1^2 + \frac{1}{2}\,\mathrm{tr}[\boldsymbol{A}\boldsymbol{V}_1^2](\boldsymbol{V}_2\boldsymbol{V}_1 + \boldsymbol{V}_1\boldsymbol{V}_2)\Big\} \\
&+ \mu_{14}\Big\{\mathrm{tr}[\boldsymbol{A}\boldsymbol{V}_1^2\boldsymbol{V}_2]\boldsymbol{V}_1^2 + \frac{1}{2}\,\mathrm{tr}[\boldsymbol{A}\boldsymbol{V}_1^2](\boldsymbol{V}_1^2\boldsymbol{V}_2 - \boldsymbol{V}_2\boldsymbol{V}_1^2)\Big\} \\
&+ \mu_{15}\Big\{\mathrm{tr}[\boldsymbol{A}\boldsymbol{V}_1\boldsymbol{V}_2^2]\boldsymbol{V}_1^2 + \frac{1}{2}\,\mathrm{tr}[\boldsymbol{A}\boldsymbol{V}_1^2](\boldsymbol{V}_1\boldsymbol{V}_2^2 - \boldsymbol{V}_2^2\boldsymbol{V}_1)\Big\} \\
&+ \mu_{16}\Big\{\mathrm{tr}[\boldsymbol{A}\boldsymbol{V}_1\boldsymbol{V}_2]\boldsymbol{V}_2^2 + \frac{1}{2}\,\mathrm{tr}[\boldsymbol{A}\boldsymbol{V}_2^2](\boldsymbol{V}_2\boldsymbol{V}_1 + \boldsymbol{V}_1\boldsymbol{V}_2)\Big\} \\
&+ \mu_{17}\Big\{\mathrm{tr}[\boldsymbol{A}\boldsymbol{V}_1^2\boldsymbol{V}_2]\boldsymbol{V}_2^2 + \frac{1}{2}\,\mathrm{tr}[\boldsymbol{A}\boldsymbol{V}_2^2](\boldsymbol{V}_1^2\boldsymbol{V}_2 - \boldsymbol{V}_2\boldsymbol{V}_1^2)\Big\} \\
&+ \mu_{18}\Big\{\mathrm{tr}[\boldsymbol{A}\boldsymbol{V}_1\boldsymbol{V}_2^2]\boldsymbol{V}_2^2 + \frac{1}{2}\,\mathrm{tr}[\boldsymbol{A}\boldsymbol{V}_2^2](\boldsymbol{V}_1\boldsymbol{V}_2^2 - \boldsymbol{V}_2^2\boldsymbol{V}_1)\Big\} \\
&+ \frac{\mu_{19}}{2}\Big\{\mathrm{tr}[\boldsymbol{A}\boldsymbol{V}_1^2\boldsymbol{V}_2](\boldsymbol{V}_2\boldsymbol{V}_1 + \boldsymbol{V}_1\boldsymbol{V}_2) + \mathrm{tr}[\boldsymbol{A}\boldsymbol{V}_1\boldsymbol{V}_2](\boldsymbol{V}_1^2\boldsymbol{V}_2 - \boldsymbol{V}_2\boldsymbol{V}_1^2)\Big\} \\
&+ \frac{\mu_{20}}{2}\Big\{\mathrm{tr}[\boldsymbol{A}\boldsymbol{V}_1\boldsymbol{V}_2^2](\boldsymbol{V}_2\boldsymbol{V}_1 + \boldsymbol{V}_1\boldsymbol{V}_2) + \mathrm{tr}[\boldsymbol{A}\boldsymbol{V}_1\boldsymbol{V}_2](\boldsymbol{V}_1\boldsymbol{V}_2^2 - \boldsymbol{V}_2^2\boldsymbol{V}_1)\Big\} \\
&+ \frac{\mu_{21}}{2}\Big\{\mathrm{tr}[\boldsymbol{A}\boldsymbol{V}_1\boldsymbol{V}_2^2](\boldsymbol{V}_1^2\boldsymbol{V}_2 - \boldsymbol{V}_2\boldsymbol{V}_1^2) + \mathrm{tr}[\boldsymbol{A}\boldsymbol{V}_1^2\boldsymbol{V}_2](\boldsymbol{V}_1\boldsymbol{V}_2^2 - \boldsymbol{V}_2^2\boldsymbol{V}_1)\Big\}
\end{aligned} \tag{408}$$

The constant fourth-order Hessian $\mathbb{F}$ associated with the potential $\mathfrak{F}$ is obtained by the second derivative with respect to the argument $\boldsymbol{A}$ as

$$
\begin{aligned}
\mathbb{F} = \mathfrak{F}_{,\boldsymbol{AA}} = {}&\sum_{i=1}^{21}\sum_{j=1}^{21} \mathfrak{F}_{,I_i}\, I_{i,\boldsymbol{AA}} + \mathfrak{F}_{,I_iI_j}\, I_{i,\boldsymbol{A}} \otimes I_{j,\boldsymbol{A}} \\[2mm]
={}& 2\mu_1 \boldsymbol{1} \otimes \boldsymbol{1} + \mu_2\big\{(\boldsymbol{1} \oplus \boldsymbol{1}) + (\boldsymbol{1} \ominus \boldsymbol{1})\big\} + 2\mu_3 \boldsymbol{V}_1^2 \otimes \boldsymbol{V}_1^2 + 2\mu_4 \boldsymbol{V}_2^2 \otimes \boldsymbol{V}_2^2 \\[1mm]
&+ \frac{\mu_5}{2}\big\{(\boldsymbol{V}_2\boldsymbol{V}_1 + \boldsymbol{V}_1\boldsymbol{V}_2) \otimes (\boldsymbol{V}_2\boldsymbol{V}_1 + \boldsymbol{V}_1\boldsymbol{V}_2)\big\} \\[1mm]
&+ \frac{\mu_6}{2}\big\{(\boldsymbol{V}_1^2\boldsymbol{V}_2 - \boldsymbol{V}_2\boldsymbol{V}_1^2) \otimes (\boldsymbol{V}_1^2\boldsymbol{V}_2 - \boldsymbol{V}_2\boldsymbol{V}_1^2)\big\} \\[1mm]
&+ \frac{\mu_7}{2}\big\{(\boldsymbol{V}_1\boldsymbol{V}_2^2 - \boldsymbol{V}_2^2\boldsymbol{V}_1) \otimes (\boldsymbol{V}_1\boldsymbol{V}_2^2 - \boldsymbol{V}_2^2\boldsymbol{V}_1)\big\} \\[1mm]
&+ \frac{\mu_8}{2}\big\{(\boldsymbol{1} \oplus \boldsymbol{V}_1^2) + (\boldsymbol{V}_1^2 \oplus \boldsymbol{1}) + (\boldsymbol{1} \ominus \boldsymbol{V}_1^2) + (\boldsymbol{V}_1^2 \ominus \boldsymbol{1})\big\} \\[1mm]
&+ \frac{\mu_9}{2}\big\{(\boldsymbol{1} \oplus \boldsymbol{V}_2^2) + (\boldsymbol{V}_2^2 \oplus \boldsymbol{1}) + (\boldsymbol{1} \ominus \boldsymbol{V}_2^2) + (\boldsymbol{V}_2^2 \ominus \boldsymbol{1})\big\} \\[1mm]
&+ \frac{\mu_{10}}{2}\big\{[\boldsymbol{1} \otimes (\boldsymbol{V}_2\boldsymbol{V}_1 + \boldsymbol{V}_1\boldsymbol{V}_2)] + [(\boldsymbol{V}_2\boldsymbol{V}_1 + \boldsymbol{V}_1\boldsymbol{V}_2) \otimes \boldsymbol{1}]\big\} \\[1mm]
&+ \frac{\mu_{11}}{2}\big\{[\boldsymbol{1} \otimes (\boldsymbol{V}_1^2\boldsymbol{V}_2 - \boldsymbol{V}_2\boldsymbol{V}_1^2)] + [(\boldsymbol{V}_1^2\boldsymbol{V}_2 - \boldsymbol{V}_2\boldsymbol{V}_1^2) \otimes \boldsymbol{1}]\big\} \\[1mm]
&+ \frac{\mu_{12}}{2}\big\{[\boldsymbol{1} \otimes (\boldsymbol{V}_1\boldsymbol{V}_2^2 - \boldsymbol{V}_2^2\boldsymbol{V}_1)] + [(\boldsymbol{V}_1\boldsymbol{V}_2^2 - \boldsymbol{V}_2^2\boldsymbol{V}_1) \otimes \boldsymbol{1}]\big\} \\[1mm]
&+ \frac{\mu_{13}}{2}\big\{[\boldsymbol{V}_1^2 \otimes (\boldsymbol{V}_2\boldsymbol{V}_1 + \boldsymbol{V}_1\boldsymbol{V}_2)] + [(\boldsymbol{V}_2\boldsymbol{V}_1 + \boldsymbol{V}_1\boldsymbol{V}_2) \otimes \boldsymbol{V}_1^2]\big\} \\[1mm]
&+ \frac{\mu_{14}}{2}\big\{[\boldsymbol{V}_1^2 \otimes (\boldsymbol{V}_1^2\boldsymbol{V}_2 - \boldsymbol{V}_2\boldsymbol{V}_1^2)] + [(\boldsymbol{V}_1^2\boldsymbol{V}_2 - \boldsymbol{V}_2\boldsymbol{V}_1^2) \otimes \boldsymbol{V}_1^2]\big\} \\[1mm]
&+ \frac{\mu_{15}}{2}\big\{[\boldsymbol{V}_1^2 \otimes (\boldsymbol{V}_1\boldsymbol{V}_2^2 - \boldsymbol{V}_2^2\boldsymbol{V}_1)] + [(\boldsymbol{V}_1\boldsymbol{V}_2^2 - \boldsymbol{V}_2^2\boldsymbol{V}_1) \otimes \boldsymbol{V}_1^2]\big\} \\[1mm]
&+ \frac{\mu_{16}}{2}\big\{[\boldsymbol{V}_2^2 \otimes (\boldsymbol{V}_2\boldsymbol{V}_1 + \boldsymbol{V}_1\boldsymbol{V}_2)] + [(\boldsymbol{V}_2\boldsymbol{V}_1 + \boldsymbol{V}_1\boldsymbol{V}_2) \otimes \boldsymbol{V}_2^2]\big\} \\[1mm]
&+ \frac{\mu_{17}}{2}\big\{[\boldsymbol{V}_2^2 \otimes (\boldsymbol{V}_1^2\boldsymbol{V}_2 - \boldsymbol{V}_2\boldsymbol{V}_1^2)] + [(\boldsymbol{V}_1^2\boldsymbol{V}_2 - \boldsymbol{V}_2\boldsymbol{V}_1^2) \otimes \boldsymbol{V}_2^2]\big\} \\[1mm]
&+ \frac{\mu_{18}}{2}\big\{[\boldsymbol{V}_2^2 \otimes (\boldsymbol{V}_1\boldsymbol{V}_2^2 - \boldsymbol{V}_2^2\boldsymbol{V}_1)] + [(\boldsymbol{V}_1\boldsymbol{V}_2^2 - \boldsymbol{V}_2^2\boldsymbol{V}_1) \otimes \boldsymbol{V}_2^2]\big\} \\[1mm]
&+ \frac{\mu_{19}}{2}\big\{[(\boldsymbol{V}_2\boldsymbol{V}_1 + \boldsymbol{V}_1\boldsymbol{V}_2) \otimes (\boldsymbol{V}_1^2\boldsymbol{V}_2 - \boldsymbol{V}_2\boldsymbol{V}_1^2)] \\
&\qquad\quad + [(\boldsymbol{V}_1^2\boldsymbol{V}_2 - \boldsymbol{V}_2\boldsymbol{V}_1^2) \otimes (\boldsymbol{V}_2\boldsymbol{V}_1 + \boldsymbol{V}_1\boldsymbol{V}_2)]\big\} \\[1mm]
&+ \frac{\mu_{20}}{2}\big\{[(\boldsymbol{V}_2\boldsymbol{V}_1 + \boldsymbol{V}_1\boldsymbol{V}_2) \otimes (\boldsymbol{V}_1\boldsymbol{V}_2^2 - \boldsymbol{V}_2^2\boldsymbol{V}_1)] \\
&\qquad\quad + [(\boldsymbol{V}_1\boldsymbol{V}_2^2 - \boldsymbol{V}_2^2\boldsymbol{V}_1) \otimes (\boldsymbol{V}_2\boldsymbol{V}_1 + \boldsymbol{V}_1\boldsymbol{V}_2)]\big\} \\[1mm]
&+ \frac{\mu_{21}}{2}\big\{[(\boldsymbol{V}_1^2\boldsymbol{V}_2 - \boldsymbol{V}_2\boldsymbol{V}_1^2) \otimes (\boldsymbol{V}_1\boldsymbol{V}_2^2 - \boldsymbol{V}_2^2\boldsymbol{V}_1)] \\
&\qquad\quad + [(\boldsymbol{V}_1\boldsymbol{V}_2^2 - \boldsymbol{V}_2^2\boldsymbol{V}_1) \otimes (\boldsymbol{V}_1^2\boldsymbol{V}_2 - \boldsymbol{V}_2\boldsymbol{V}_1^2)]\big\}
\end{aligned}
$$

$$\tag{409}$$

with the identities

$$
\begin{aligned}
\big\{(\bullet) \otimes (\bullet)\big\}_{ijkl} &= (\bullet)_{ij}(\bullet)_{kl}\ , \\
\big\{(\bullet) \oplus (\bullet)\big\}_{ijkl} &= (\bullet)_{ik}(\bullet)_{jl}\ , \\
\big\{(\bullet) \ominus (\bullet)\big\}_{ijkl} &= (\bullet)_{il}(\bullet)_{jk}\ .
\end{aligned}
\tag{410}
$$

If the orthonormal vectors are chosen such that $\boldsymbol{a} = [1, 0, 0]^T$ and $\boldsymbol{b} = [0, 1, 0]^T$, the fourth-order tensor $\mathbb{F}$ appears in the coordinate form

$$[\mathbb{F}] = \begin{bmatrix} \mathbb{F}_{1111} & \mathbb{F}_{1122} & \mathbb{F}_{1133} & \mathbb{F}_{1112} & \mathbb{F}_{1113} & \mathbb{F}_{1123} \\ & \mathbb{F}_{2222} & \mathbb{F}_{2233} & \mathbb{F}_{2212} & \mathbb{F}_{2213} & \mathbb{F}_{2223} \\ & & \mathbb{F}_{3333} & \mathbb{F}_{3312} & \mathbb{F}_{3313} & \mathbb{F}_{3323} \\ & & & \mathbb{F}_{1212} & \mathbb{F}_{1213} & \mathbb{F}_{1223} \\ & \text{sym.} & & & \mathbb{F}_{1313} & \mathbb{F}_{1323} \\ & & & & & \mathbb{F}_{2323} \end{bmatrix} , \tag{411}$$

with the components

$$\mathbb{F}_{1111} = 2(\mu_1 + \mu_2 + \mu_4 - \mu_9), \quad \mathbb{F}_{1122} = 2\mu_1, \quad \mathbb{F}_{1133} = 2(\mu_1 + \mu_4),$$

$$\mathbb{F}_{1112} = \frac{1}{2}(\mu_{10} - \mu_{16}), \quad \mathbb{F}_{1113} = \frac{1}{2}(\mu_{17} - \mu_{11}), \quad \mathbb{F}_{1123} = \frac{1}{2}(\mu_{18} - \mu_{12}),$$

$$\mathbb{F}_{2222} = 2(\mu_1 + \mu_2 + \mu_3 - \mu_8 + \mu_{13}), \quad \mathbb{F}_{2233} = 2(\mu_1 + \mu_3) + \mu_{13},$$

$$\mathbb{F}_{2212} = \frac{1}{2}\mu_{10}, \quad \mathbb{F}_{2213} = \frac{1}{2}(\mu_{14} - \mu_{11}), \quad \mathbb{F}_{2223} = \frac{1}{2}(\mu_{15} - \mu_{12}),$$

$$\mathbb{F}_{3333} = 2(\mu_1 + \mu_2 + \mu_3 + \mu_4 - \mu_8 + \mu_9), \quad \mathbb{F}_{3312} = \frac{1}{2}(\mu_{10} - \mu_{16}),$$

$$\mathbb{F}_{3313} = \frac{1}{2}(\mu_{14} + \mu_{17} - \mu_{11}), \quad \mathbb{F}_{3323} = \frac{1}{2}(\mu_{15} + \mu_{18} - \mu_{12}), \tag{412}$$

$$\mathbb{F}_{1212} = \mu_2 + \frac{1}{2}(\mu_5 - \mu_8 - \mu_9), \quad \mathbb{F}_{1213} = -\frac{1}{4}\mu_{19}, \quad \mathbb{F}_{1223} = -\frac{1}{4}\mu_{20},$$

$$\mathbb{F}_{1313} = (\mu_2 - \mu_9) + \frac{1}{2}(\mu_6 - \mu_8), \quad \mathbb{F}_{1323} = -\frac{1}{4}\mu_{21},$$

$$\mathbb{F}_{2323} = (\mu_2 - \mu_8) + \frac{1}{2}(\mu_7 - \mu_9),$$

in terms of twenty one material constants $\mu_{1-21}$.

### A.2. Monoclinic symmetry group $\mathscr{C}_2$

The orientation of the materials belonging to the *monoclinic* symmetry group $\mathscr{C}_2$ is determined by two arbitrary orthonormal vectors $\boldsymbol{a}$ and $\boldsymbol{b}$, which are perpendicular to an unit normal vector $\tilde{\boldsymbol{n}}$. The scalar-valued potential $\mathfrak{F}$ which has a functional dependence on these vectors, can generally be specified as

$$\mathfrak{F} = \mathfrak{F}(\boldsymbol{A}, \boldsymbol{U}, \boldsymbol{V}) \quad \text{where} \quad \boldsymbol{U} = \boldsymbol{a} \otimes \boldsymbol{a} - \boldsymbol{b} \otimes \boldsymbol{b} \quad \text{and} \quad \boldsymbol{V} = \epsilon \tilde{\boldsymbol{n}}, \tag{413}$$

in terms of two symmetric second-order tensors $\boldsymbol{A}$ and $\boldsymbol{U}$, and a skew-symmetric second-order tensor $\boldsymbol{V}$. It follows from Table 11 that the functional basis of the $\mathscr{C}_2$ group consists of the basic invariants

$$\left\{ \text{tr}[\boldsymbol{A}], \text{tr}[\boldsymbol{A}^2], \text{tr}[\boldsymbol{A}^3], \text{tr}[\boldsymbol{U}], \text{tr}[\boldsymbol{U}^2], \text{tr}[\boldsymbol{U}^3], \text{tr}[\boldsymbol{V}^2] \right\}, \tag{414}$$

of the argument tensor $\boldsymbol{A}$ and the additional arguments tensors $\boldsymbol{U}$ and $\boldsymbol{V}$, the mixed invariants of every two arguments $\{\boldsymbol{A}, \boldsymbol{U}\}$, $\{\boldsymbol{A}, \boldsymbol{V}\}$ and $\{\boldsymbol{U}, \boldsymbol{V}\}$

$$\left\{ \begin{aligned} &\text{tr}[\boldsymbol{A}\boldsymbol{U}], \text{tr}[\boldsymbol{A}^2\boldsymbol{U}], \text{tr}[\boldsymbol{A}\boldsymbol{U}^2], \text{tr}[\boldsymbol{A}^2\boldsymbol{U}^2], \text{tr}[\boldsymbol{A}\boldsymbol{V}^2], \text{tr}[\boldsymbol{A}^2\boldsymbol{V}^2], \text{tr}[\boldsymbol{A}^2\boldsymbol{V}^2\boldsymbol{A}\boldsymbol{V}], \\ &\text{tr}[\boldsymbol{U}\boldsymbol{V}^2], \text{tr}[\boldsymbol{U}^2\boldsymbol{V}^2], \text{tr}[\boldsymbol{U}^2\boldsymbol{V}^2\boldsymbol{U}\boldsymbol{V}] \end{aligned} \right\} \tag{415}$$

and the relative invariants of all the argument tensors $\{\boldsymbol{A}, \boldsymbol{U}, \boldsymbol{V}\}$ such that

$$\left\{ \operatorname{tr}[\boldsymbol{AUV}], \operatorname{tr}[\boldsymbol{A}^2\boldsymbol{UV}], \operatorname{tr}[\boldsymbol{AU}^2\boldsymbol{V}], \operatorname{tr}[\boldsymbol{AV}^2\boldsymbol{UV}] \right\} . \tag{416}$$

With reference to Eqns. (415) and (416), the following linear dependencies can be trivially verified

$$\begin{aligned}
-\operatorname{tr}[\boldsymbol{AU}^2] &= \operatorname{tr}[\boldsymbol{AV}^2] \ , \\
-\operatorname{tr}[\boldsymbol{A}^2\boldsymbol{U}^2] &= \operatorname{tr}[\boldsymbol{A}^2\boldsymbol{V}^2] \ , \\
-\operatorname{tr}[\boldsymbol{AUV}] &= \operatorname{tr}[\boldsymbol{AV}^2\boldsymbol{UV}] \ , \\
\operatorname{tr}[\boldsymbol{AU}^2\boldsymbol{V}] &= 0 \ .
\end{aligned} \tag{417}$$

An irreducible integrity basis can be defined with the combination of invariants in Eqns. (414)–(416) to obtain quadratic terms in $\boldsymbol{A}$, taking into account Eqn. (417) as

$$\begin{aligned}
\mathcal{I}_{\mathscr{C}_2} = \big\{ \ &\operatorname{tr}^2[\boldsymbol{A}], \operatorname{tr}[\boldsymbol{A}^2], \operatorname{tr}^2[\boldsymbol{AU}], \operatorname{tr}^2[\boldsymbol{AU}^2], \operatorname{tr}^2[\boldsymbol{AUV}], \operatorname{tr}[\boldsymbol{A}^2\boldsymbol{U}], \operatorname{tr}[\boldsymbol{A}^2\boldsymbol{UV}], \\
&\operatorname{tr}[\boldsymbol{A}]\operatorname{tr}[\boldsymbol{AU}], \operatorname{tr}[\boldsymbol{A}]\operatorname{tr}[\boldsymbol{AU}^2], \operatorname{tr}[\boldsymbol{A}]\operatorname{tr}[\boldsymbol{AUV}], \operatorname{tr}[\boldsymbol{AU}]\operatorname{tr}[\boldsymbol{AU}^2] \\
&\operatorname{tr}[\boldsymbol{AU}]\operatorname{tr}[\boldsymbol{AUV}], \operatorname{tr}[\boldsymbol{AU}^2]\operatorname{tr}[\boldsymbol{AUV}] \big\}
\end{aligned} \tag{418}$$

where the invariant

$$\begin{aligned}
\operatorname{tr}[\boldsymbol{A}^2\boldsymbol{U}^2] &= \frac{1}{2}\big( \operatorname{tr}[\boldsymbol{A}^2] - \operatorname{tr}^2[\boldsymbol{A}] \big) \\
&+ \frac{1}{2}\big( \operatorname{tr}^2[\boldsymbol{AU}] - \operatorname{tr}^2[\boldsymbol{AU}^2] \big) \\
&+ \frac{1}{4}\operatorname{tr}^2[\boldsymbol{AUV}] + \operatorname{tr}[\boldsymbol{A}]\operatorname{tr}[\boldsymbol{AU}^2]
\end{aligned} \tag{419}$$

is dropped as it can be expressed in terms of other invariants. Equation (418) allows for the definition of a quadratic scalar-valued potential (80) as

$$\mathfrak{F} = \sum_{i=1}^{13} \mu_i I_i \ , \tag{420}$$

where $I_{1-13}$ are the elements of the integrity basis $\mathcal{I}_{\mathscr{C}_2}$, and $\mu_{1-13}$ are material constants. The second-order stress-like tensor $\boldsymbol{\mathsf{S}}$ associated with the potential is given by

$$\begin{aligned}
\boldsymbol{\mathsf{S}} = \mathfrak{F}_{,\boldsymbol{A}} = &\sum_{i=1}^{13} \mathfrak{F}_{,I_i} \, I_{i,\,\boldsymbol{A}} \\
= &\, 2\mu_1 \operatorname{tr}[\boldsymbol{A}]\boldsymbol{1} + 2\mu_2 \boldsymbol{A} + 2\mu_3 \operatorname{tr}[\boldsymbol{AU}]\boldsymbol{U} + 2\mu_4 \operatorname{tr}[\boldsymbol{AU}^2]\boldsymbol{U}^2 \\
&+ 2\mu_5 \operatorname{tr}[\boldsymbol{AUV}]\boldsymbol{UV} + \mu_6\{\boldsymbol{AU} + \boldsymbol{UA}\} + \mu_7\{\boldsymbol{AUV} + \boldsymbol{UVA}\} \\
&+ \mu_8\{\operatorname{tr}[\boldsymbol{AU}]\boldsymbol{1} + \operatorname{tr}[\boldsymbol{A}]\boldsymbol{U}\} + \mu_9\{\operatorname{tr}[\boldsymbol{AU}^2]\boldsymbol{1} + \operatorname{tr}[\boldsymbol{A}]\boldsymbol{U}^2\} \\
&+ \mu_{10}\{\operatorname{tr}[\boldsymbol{AUV}]\boldsymbol{1} + \operatorname{tr}[\boldsymbol{A}]\boldsymbol{UV}\} + \mu_{11}\{\operatorname{tr}[\boldsymbol{AU}^2]\boldsymbol{U} + \operatorname{tr}[\boldsymbol{AU}]\boldsymbol{U}^2\} \\
&+ \mu_{12}\{\operatorname{tr}[\boldsymbol{AUV}]\boldsymbol{U} + \operatorname{tr}[\boldsymbol{AU}]\boldsymbol{UV}\} \\
&+ \mu_{13}\{\operatorname{tr}[\boldsymbol{AUV}]\boldsymbol{U}^2 + \operatorname{tr}[\boldsymbol{AU}^2]\boldsymbol{UV}\}
\end{aligned} \tag{421}$$

Likewise, the constant fourth-order Hessian $\mathbb{F}$ associated with the potential $\mathfrak{F}$ is given by

$$
\begin{aligned}
\mathbb{F} = \mathfrak{F},_{\boldsymbol{AA}} = &\sum_{i=1}^{13}\sum_{j=1}^{13}\mathfrak{F},_{I_i}I_{i,\boldsymbol{AA}} + \mathfrak{F},_{I_iI_j}I_{i,\boldsymbol{A}}\otimes I_{j,\boldsymbol{A}} \\
= &2\mu_1\boldsymbol{1}\otimes\boldsymbol{1} + \mu_2\big\{(\boldsymbol{1}\oplus\boldsymbol{1})+(\boldsymbol{1}\ominus\boldsymbol{1})\big\} + 2\mu_3\boldsymbol{U}\otimes\boldsymbol{U} + 2\mu_4\boldsymbol{U}^2\otimes\boldsymbol{U}^2 \\
&+2\mu_5\boldsymbol{UV}\otimes\boldsymbol{UV} + \frac{\mu_6}{2}\big\{(\boldsymbol{1}\oplus\boldsymbol{U})+(\boldsymbol{U}\oplus\boldsymbol{1})+(\boldsymbol{1}\ominus\boldsymbol{U})+(\boldsymbol{U}\ominus\boldsymbol{1})\big\} \\
&+\frac{\mu_7}{2}\big\{(\boldsymbol{1}\oplus\boldsymbol{UV})+(\boldsymbol{UV}\oplus\boldsymbol{1})+(\boldsymbol{1}\ominus\boldsymbol{UV})+(\boldsymbol{UV}\ominus\boldsymbol{1})\big\} \\
&+\mu_8\big\{\boldsymbol{1}\otimes\boldsymbol{U}+\boldsymbol{U}\otimes\boldsymbol{1}\big\} + \mu_9\big\{\boldsymbol{1}\otimes\boldsymbol{U}^2+\boldsymbol{U}^2\otimes\boldsymbol{1}\big\} \\
&+\mu_{10}\big\{\boldsymbol{1}\otimes(\boldsymbol{UV})+(\boldsymbol{UV})\otimes\boldsymbol{1}\big\} + \mu_{11}\big\{\boldsymbol{U}\otimes\boldsymbol{U}^2+\boldsymbol{U}^2\otimes\boldsymbol{U}\big\} \\
&+\mu_{12}\big\{\boldsymbol{U}\otimes(\boldsymbol{UV})+(\boldsymbol{UV})\otimes\boldsymbol{U}\big\} + \mu_{13}\big\{\boldsymbol{U}^2\otimes(\boldsymbol{UV})+(\boldsymbol{UV})\otimes\boldsymbol{U}^2\big\}
\end{aligned}
\tag{422}
$$

For $\boldsymbol{a} = [1,0,0]^T$, $\boldsymbol{b} = [0,1,0]^T$ and $\tilde{\boldsymbol{n}} = [0,0,1]^T$, the fourth-order tensor $\mathbb{F}$ appears in the simple coordinate form

$$
[\mathbb{F}] =
\begin{bmatrix}
\mathbb{F}_{1111} & \mathbb{F}_{1122} & \mathbb{F}_{1133} & \mathbb{F}_{1112} & 0 & 0 \\
 & \mathbb{F}_{2222} & \mathbb{F}_{2233} & \mathbb{F}_{2212} & 0 & 0 \\
 & & \mathbb{F}_{3333} & \mathbb{F}_{3312} & 0 & 0 \\
 & & & \mathbb{F}_{1212} & 0 & 0 \\
 & \text{sym.} & & & \mathbb{F}_{1313} & \mathbb{F}_{1323} \\
 & & & & & \mathbb{F}_{2323}
\end{bmatrix},
\tag{423}
$$

with the definitions

$$
\begin{aligned}
&\mathbb{F}_{1111} = 2(\mu_1 + \mu_2 + \mu_3 + \mu_4 + \mu_6 + \mu_8 + \mu_9 + \mu_{11})\,, \\
&\mathbb{F}_{1122} = 2(\mu_1 - \mu_3 + \mu_4 + \mu_9)\,, \quad \mathbb{F}_{1133} = 2\mu_1 + \mu_8 + \mu_9\,, \\
&\mathbb{F}_{1112} = \mu_7 + \mu_{10} + \mu_{12} + \mu_{13}\,, \\[4pt]
&\mathbb{F}_{2222} = 2(\mu_1 + \mu_2 + \mu_3 + \mu_4 + \mu_6 - \mu_8 + \mu_9 - \mu_{11})\,, \\
&\mathbb{F}_{2233} = 2\mu_1 - \mu_8 + \mu_9\,, \quad \mathbb{F}_{2212} = \mu_7 + \mu_{10} - \mu_{12} + \mu_{13}\,, \\[4pt]
&\mathbb{F}_{3333} = 2(\mu_1 + \mu_2)\,, \quad \mathbb{F}_{3312} = \mu_{10}\,, \\[4pt]
&\mathbb{F}_{1212} = \mu_2 + 2\mu_5\,, \\[4pt]
&\mathbb{F}_{1313} = \mu_2 + \frac{1}{2}\mu_6\,, \quad \mathbb{F}_{1323} = \frac{1}{2}\mu_7\,, \\[4pt]
&\mathbb{F}_{2323} = \mu_2 - \frac{1}{2}\mu_6\,,
\end{aligned}
\tag{424}
$$

in terms of thirteen material constants $\mu_{1-13}$.

## A.3. Orthorhombic symmetry group $\mathscr{C}_3$

The *orthorhombic* symmetry group $\mathscr{C}_3$ is generated by orthogonal rotations $\boldsymbol{Q}_{\boldsymbol{a}}^\pi$ and $\boldsymbol{Q}_{\boldsymbol{b}}^\pi$, which correspond to 180° rotations around the orthonormal vectors $\boldsymbol{a}$ and $\boldsymbol{b}$, respectively. A general form of the scalar potential $\mathfrak{F}$ can be specified as

$$
\mathfrak{F} = \mathfrak{F}(\boldsymbol{A}, \boldsymbol{U}) \quad \text{where} \quad \boldsymbol{U} = \boldsymbol{a}\otimes\boldsymbol{a} - \boldsymbol{b}\otimes\boldsymbol{b}\,,
\tag{425}
$$

in terms of two symmetric second-order tensors $\boldsymbol{A}$ and $\boldsymbol{U}$. Analogous to the previous two symmetry groups, the functional basis for the $\mathscr{C}_3$ group consists of the basic invariants

$$\left\{ \operatorname{tr}[\boldsymbol{A}], \operatorname{tr}[\boldsymbol{A}^2], \operatorname{tr}[\boldsymbol{A}^3], \operatorname{tr}[\boldsymbol{U}], \operatorname{tr}[\boldsymbol{U}^2], \operatorname{tr}[\boldsymbol{U}^3] \right\} , \tag{426}$$

of the arguments $\boldsymbol{A}$ and $\boldsymbol{U}$, and the mixed invariants of the two arguments $\{\boldsymbol{A}, \boldsymbol{U}\}$

$$\left\{ \operatorname{tr}[\boldsymbol{A}\boldsymbol{U}], \operatorname{tr}[\boldsymbol{A}^2\boldsymbol{U}], \operatorname{tr}[\boldsymbol{A}\boldsymbol{U}^2], \operatorname{tr}[\boldsymbol{A}^2\boldsymbol{U}^2] \right\} , \tag{427}$$

see Table 11. An irreducible integrity basis can be specified by multiplicatively combining the invariants in Eqns. (426) and (427) to obtain quadratic terms in $\boldsymbol{A}$ as

$$\begin{aligned} \mathcal{I}_{\mathscr{C}_3} = \{ \quad & \operatorname{tr}^2[\boldsymbol{A}], \operatorname{tr}[\boldsymbol{A}^2], \operatorname{tr}^2[\boldsymbol{A}\boldsymbol{U}], \operatorname{tr}[\boldsymbol{A}^2\boldsymbol{U}], \operatorname{tr}^2[\boldsymbol{A}\boldsymbol{U}^2], \operatorname{tr}[\boldsymbol{A}^2\boldsymbol{U}^2] , \\ & \operatorname{tr}[\boldsymbol{A}] \operatorname{tr}[\boldsymbol{A}\boldsymbol{U}], \operatorname{tr}[\boldsymbol{A}] \operatorname{tr}[\boldsymbol{A}\boldsymbol{U}^2], \operatorname{tr}[\boldsymbol{A}\boldsymbol{U}] \operatorname{tr}[\boldsymbol{A}\boldsymbol{U}^2]\} \end{aligned} , \tag{428}$$

which allows for the definition of a quadratic scalar-valued function $\mathfrak{F}$ as

$$\mathfrak{F} = \sum_{i=1}^{9} \mu_i I_i , \tag{429}$$

where $I_{1-9}$ are the elements of the integrity basis $\mathcal{I}_{\mathscr{C}_3}$, and $\mu_{1-9}$ are the material constants. The second-order stress-like tensor $\boldsymbol{S}$ associated with the potential is given by

$$\begin{aligned} \boldsymbol{S} = \mathfrak{F}_{,\boldsymbol{A}} = & \sum_{i=1}^{9} \mathfrak{F}_{,I_i} I_{i,\boldsymbol{A}} \\ = & 2\mu_1 \operatorname{tr}[\boldsymbol{A}]\boldsymbol{1} + 2\mu_2 \boldsymbol{A} + 2\mu_3 \operatorname{tr}[\boldsymbol{A}\boldsymbol{U}]\boldsymbol{U} + 2\mu_4 \operatorname{tr}[\boldsymbol{A}\boldsymbol{U}^2]\boldsymbol{U}^2 \\ & + \mu_5 \{\boldsymbol{A}\boldsymbol{U} + \boldsymbol{U}\boldsymbol{A}\} + \mu_6 \{\boldsymbol{A}\boldsymbol{U}^2 + \boldsymbol{U}^2\boldsymbol{A}\} + \mu_7 \{\operatorname{tr}[\boldsymbol{A}\boldsymbol{U}]\boldsymbol{1} + \operatorname{tr}[\boldsymbol{A}]\boldsymbol{U}\} \\ & + \mu_8 \{\operatorname{tr}[\boldsymbol{A}\boldsymbol{U}^2]\boldsymbol{1} + \operatorname{tr}[\boldsymbol{A}]\boldsymbol{U}^2\} + \mu_9 \{\operatorname{tr}[\boldsymbol{A}\boldsymbol{U}^2]\boldsymbol{U} + \operatorname{tr}[\boldsymbol{A}\boldsymbol{U}]\boldsymbol{U}^2\} \end{aligned} . \tag{430}$$

It follows that the constant fourth-order Hessian $\mathbb{F}$ associated with the scalar-valued potential $\mathfrak{F}$ can be expressed as

$$\begin{aligned} \mathbb{F} = \mathfrak{F}_{,\boldsymbol{A}\boldsymbol{A}} = & \sum_{i=1}^{9} \sum_{j=1}^{9} \mathfrak{F}_{,I_i} I_{i,\boldsymbol{A}\boldsymbol{A}} + \mathfrak{F}_{,I_iI_j} I_{i,\boldsymbol{A}} \otimes I_{j,\boldsymbol{A}} \\ = & 2\mu_1 \boldsymbol{1} \otimes \boldsymbol{1} + \mu_2 \{(\boldsymbol{1} \oplus \boldsymbol{1}) + (\boldsymbol{1} \ominus \boldsymbol{1})\} + 2\mu_3 \boldsymbol{U} \otimes \boldsymbol{U} + 2\mu_4 \boldsymbol{U}^2 \otimes \boldsymbol{U}^2 \\ & + \frac{\mu_5}{2} \{(\boldsymbol{1} \oplus \boldsymbol{U}) + (\boldsymbol{U} \oplus \boldsymbol{1}) + (\boldsymbol{1} \ominus \boldsymbol{U}) + (\boldsymbol{U} \ominus \boldsymbol{1})\} \\ & + \frac{\mu_6}{2} \{(\boldsymbol{1} \oplus \boldsymbol{U}^2) + (\boldsymbol{U}^2 \oplus \boldsymbol{1}) + (\boldsymbol{1} \ominus \boldsymbol{U}^2) + (\boldsymbol{U}^2 \ominus \boldsymbol{1})\} \\ & + \mu_7 \{\boldsymbol{1} \otimes \boldsymbol{U} + \boldsymbol{U} \otimes \boldsymbol{1}\} + \mu_8 \{\boldsymbol{1} \otimes \boldsymbol{U}^2 + \boldsymbol{U}^2 \otimes \boldsymbol{1}\} \\ & + \mu_9 \{\boldsymbol{U} \otimes \boldsymbol{U}^2 + \boldsymbol{U}^2 \otimes \boldsymbol{U}\} \end{aligned} . \tag{431}$$

For the choice $\boldsymbol{a} = [1, 0, 0]^T$ and $\boldsymbol{b} = [0, 1, 0]^T$ of the orthonormal vectors, the fourth-order tensor $\mathbb{F}$ appears in the coordinate form

$$[\mathbb{F}] = \begin{bmatrix} \mathbb{F}_{1111} & \mathbb{F}_{1122} & \mathbb{F}_{1133} & 0 & 0 & 0 \\ & \mathbb{F}_{2222} & \mathbb{F}_{2233} & 0 & 0 & 0 \\ & & \mathbb{F}_{3333} & 0 & 0 & 0 \\ & & & \mathbb{F}_{1212} & 0 & 0 \\ & \text{sym.} & & & \mathbb{F}_{1313} & 0 \\ & & & & & \mathbb{F}_{2323} \end{bmatrix} , \tag{432}$$

along with the definitions

$$\mathbb{F}_{1111} = 2(\mu_1 + \mu_2 + \mu_3 + \mu_4 + \mu_5 + \mu_6 + \mu_7 + \mu_8 + \mu_9) \ ,$$

$$\mathbb{F}_{1122} = 2(\mu_1 - \mu_3 + \mu_4 + \mu_8) \ , \quad \mathbb{F}_{1133} = 2\mu_1 + \mu_7 + \mu_8 \ ,$$

$$\mathbb{F}_{2222} = 2(\mu_1 + \mu_2 + \mu_3 + \mu_4 - \mu_5 + \mu_6 - \mu_7 + \mu_8 - \mu_9) \ ,$$

$$\mathbb{F}_{2233} = 2\mu_1 - \mu_7 + \mu_8 \ , \tag{433}$$

$$\mathbb{F}_{3333} = 2(\mu_1 + \mu_2) \ ,$$

$$\mathbb{F}_{1212} = \mu_2 + \mu_6 \ , \quad \mathbb{F}_{1313} = \mu_2 + \frac{1}{2}\mu_5 + \frac{1}{2}\mu_6 \ , \quad \mathbb{F}_{2323} = \mu_2 - \frac{1}{2}\mu_5 + \frac{1}{2}\mu_6 \ ,$$

in terms of nine material constants $\mu_{1-9}$. Note that for special choices of the material constants $\mu_{1-9}$ in Eqn. (429) of the orthorhombic symmetry group, a number of other symmetry groups can be characterised [78].

### A.4. Tetragonal symmetry group $\mathscr{C}_4$

The *tetragonal* symmetry group $\mathscr{C}_4$ is generated by orthogonal rotation $\boldsymbol{Q}_{\boldsymbol{c}}^{\frac{\pi}{2}}$, which corresponds to 90° rotation around an orthonormal vector $\boldsymbol{c}$. The functional basis of the $\mathscr{C}_4$ symmetry group comprises of three symmetric second-order tensors $\boldsymbol{A}, \boldsymbol{U}_1, \boldsymbol{U}_2$, and a single skew-symmetric second-order tensor $\boldsymbol{V}$, based on which a general form of the scalar-valued potential can be specified as

$$\mathfrak{F} = \mathfrak{F}(\boldsymbol{A}, \boldsymbol{U}_1, \boldsymbol{U}_2, \boldsymbol{V}) \ , \tag{434}$$

where

$$\begin{aligned}
\boldsymbol{U}_1 &= (\boldsymbol{a} \otimes \boldsymbol{a} \otimes \boldsymbol{a} \otimes \boldsymbol{a} + \boldsymbol{b} \otimes \boldsymbol{b} \otimes \boldsymbol{b} \otimes \boldsymbol{b}) : \boldsymbol{A} \\
\boldsymbol{U}_2 &= (\boldsymbol{a} \otimes \boldsymbol{a} \otimes \boldsymbol{a} \otimes \boldsymbol{a} + \boldsymbol{b} \otimes \boldsymbol{b} \otimes \boldsymbol{b} \otimes \boldsymbol{b}) : \boldsymbol{A}^2 \quad , \\
\boldsymbol{V} &= \epsilon \tilde{\boldsymbol{n}}
\end{aligned} \tag{435}$$

see [75]. The vectors $\boldsymbol{a}$ and $\boldsymbol{b}$ are two orthonormal vectors perpendicular to the unit normal vector $\tilde{\boldsymbol{n}}$. It can be seen from Table 11 that the functional basis of the $\mathscr{C}_4$ group consists of the basic invariants of the arguments $\boldsymbol{A}$, $\boldsymbol{U}_1$, $\boldsymbol{U}_2$ and $\boldsymbol{V}$, namely that

$$\left\{ \operatorname{tr}[\boldsymbol{A}], \operatorname{tr}[\boldsymbol{A}^2], \operatorname{tr}[\boldsymbol{A}^3], \operatorname{tr}[\boldsymbol{U}_1], \operatorname{tr}[\boldsymbol{U}_1^2], \operatorname{tr}[\boldsymbol{U}_1^3], \operatorname{tr}[\boldsymbol{U}_2], \operatorname{tr}[\boldsymbol{U}_2^2], \operatorname{tr}[\boldsymbol{U}_2^3], \operatorname{tr}[\boldsymbol{V}^2] \right\} \ , \tag{436}$$

the mixed invariants of every two arguments $\{\boldsymbol{A}, \boldsymbol{U}_1\}$, $\{\boldsymbol{A}, \boldsymbol{U}_2\}$, $\{\boldsymbol{A}, \boldsymbol{V}\}$, $\{\boldsymbol{U}_1, \boldsymbol{U}_2\}$, $\{\boldsymbol{U}_1, \boldsymbol{V}\}$ and $\{\boldsymbol{U}_2, \boldsymbol{V}\}$ defined by

$$\begin{aligned}
\Big\{ &\operatorname{tr}[\boldsymbol{A}\boldsymbol{U}_1], \operatorname{tr}[\boldsymbol{A}^2\boldsymbol{U}_1], \operatorname{tr}[\boldsymbol{A}\boldsymbol{U}_1^2], \operatorname{tr}[\boldsymbol{A}^2\boldsymbol{U}_1^2], \operatorname{tr}[\boldsymbol{A}\boldsymbol{U}_2], \operatorname{tr}[\boldsymbol{A}^2\boldsymbol{U}_2], \operatorname{tr}[\boldsymbol{A}\boldsymbol{U}_2^2], \\
&\operatorname{tr}[\boldsymbol{A}^2\boldsymbol{U}_2^2], \operatorname{tr}[\boldsymbol{A}\boldsymbol{V}^2], \operatorname{tr}[\boldsymbol{A}^2\boldsymbol{V}^2], \operatorname{tr}[\boldsymbol{A}^2\boldsymbol{V}^2\boldsymbol{A}\boldsymbol{V}], \operatorname{tr}[\boldsymbol{U}_1\boldsymbol{U}_2], \operatorname{tr}[\boldsymbol{U}_1^2\boldsymbol{U}_2], \\
&\operatorname{tr}[\boldsymbol{U}_1\boldsymbol{U}_2^2], \operatorname{tr}[\boldsymbol{U}_1^2\boldsymbol{U}_2^2], \operatorname{tr}[\boldsymbol{U}_1\boldsymbol{V}^2], \operatorname{tr}[\boldsymbol{U}_1^2\boldsymbol{V}^2], \operatorname{tr}[\boldsymbol{U}_1^2\boldsymbol{V}^2\boldsymbol{U}_1\boldsymbol{V}], \\
&\operatorname{tr}[\boldsymbol{U}_2\boldsymbol{V}^2], \operatorname{tr}[\boldsymbol{U}_2^2\boldsymbol{V}^2], \operatorname{tr}[\boldsymbol{U}_2^2\boldsymbol{V}^2\boldsymbol{U}_2\boldsymbol{V}] \Big\}
\end{aligned} \tag{437}$$

and the relative invariants of each three argument tensors $\{\boldsymbol{A}, \boldsymbol{U}_1, \boldsymbol{U}_2\}$, $\{\boldsymbol{A}, \boldsymbol{U}_1, \boldsymbol{V}\}$, $\{\boldsymbol{A}, \boldsymbol{U}_2, \boldsymbol{V}\}$ and $\{\boldsymbol{U}_1, \boldsymbol{U}_2, \boldsymbol{V}\}$ such that

$$\begin{aligned}
\Big\{ &\operatorname{tr}[\boldsymbol{A}\boldsymbol{U}_1\boldsymbol{U}_2], \operatorname{tr}[\boldsymbol{A}\boldsymbol{U}_1\boldsymbol{V}], \operatorname{tr}[\boldsymbol{A}^2\boldsymbol{U}_1\boldsymbol{V}], \operatorname{tr}[\boldsymbol{A}\boldsymbol{U}_1\boldsymbol{V}^2], \operatorname{tr}[\boldsymbol{A}\boldsymbol{V}^2\boldsymbol{U}_1\boldsymbol{V}], \operatorname{tr}[\boldsymbol{A}\boldsymbol{U}_2\boldsymbol{V}], \\
&\operatorname{tr}[\boldsymbol{A}^2\boldsymbol{U}_2\boldsymbol{V}], \operatorname{tr}[\boldsymbol{A}\boldsymbol{U}_2\boldsymbol{V}^2], \operatorname{tr}[\boldsymbol{A}\boldsymbol{V}^2\boldsymbol{U}_2\boldsymbol{V}], \operatorname{tr}[\boldsymbol{U}_1\boldsymbol{U}_2\boldsymbol{V}], \\
&\operatorname{tr}[\boldsymbol{U}_1^2\boldsymbol{U}_2\boldsymbol{V}], \operatorname{tr}[\boldsymbol{U}_1\boldsymbol{U}_2\boldsymbol{V}^2], \operatorname{tr}[\boldsymbol{U}_1\boldsymbol{V}^2\boldsymbol{U}_2\boldsymbol{V}] \Big\}
\end{aligned} \tag{438}$$

Analogous to Eqn. (417), the following linear dependencies for the $\mathscr{C}_4$ symmetry group can also be trivially verified

$$
\begin{aligned}
\operatorname{tr}[\boldsymbol{U}_1] &= -\operatorname{tr}[\boldsymbol{A}\boldsymbol{V}^2] = -\operatorname{tr}[\boldsymbol{U}_1\boldsymbol{V}^2] \ , \\
\operatorname{tr}[\boldsymbol{U}_2] &= -\operatorname{tr}[\boldsymbol{A}^2\boldsymbol{V}^2] = -\operatorname{tr}[\boldsymbol{U}_2\boldsymbol{V}^2] \ , \\
\operatorname{tr}[\boldsymbol{U}_1^2] &= \operatorname{tr}[\boldsymbol{A}\boldsymbol{U}_1] = -\operatorname{tr}[\boldsymbol{A}^2\boldsymbol{V}^2] \ , \\
\operatorname{tr}[\boldsymbol{A}\boldsymbol{U}\boldsymbol{V}] &= -\operatorname{tr}[\boldsymbol{A}\boldsymbol{V}^2\boldsymbol{U}_1\boldsymbol{V}] \ .
\end{aligned}
\tag{439}
$$

An irreducible integrity basis can be defined by combining the invariants in Eqns. (436)–(438) to obtain quadratic terms in $\boldsymbol{A}$, and taking into account Eqn. (439) as

$$
\mathcal{I}_{\mathscr{C}_4} = \big\{ \operatorname{tr}^2[\boldsymbol{A}], \operatorname{tr}[\boldsymbol{A}^2], \operatorname{tr}^2[\boldsymbol{U}_1], \operatorname{tr}[\boldsymbol{U}_1^2], \operatorname{tr}[\boldsymbol{U}_2], \operatorname{tr}[\boldsymbol{A}]\operatorname{tr}[\boldsymbol{U}_1], \operatorname{tr}[\boldsymbol{A}\boldsymbol{U}_1\boldsymbol{V}] \big\} \ .
\tag{440}
$$

Equation (440) allows for the definition of a scalar-valued quadratic potential as

$$
\mathfrak{F} = \sum_{i=1}^{7} \mu_i I_i \ ,
\tag{441}
$$

where $I_{1-7}$ are the elements of the integrity basis $\mathcal{I}_{\mathscr{C}_4}$ defined in Eqn. (440), and $\mu_{1-7}$ are the material constants. Given the potential (441), the second-order stress-like tensor $\boldsymbol{S}$ takes the form

$$
\begin{aligned}
\boldsymbol{S} = \mathfrak{F}_{,\boldsymbol{A}} =& \sum_{i=1}^{7} \mathfrak{F}_{,I_i} I_{i,\boldsymbol{A}} \\
=& 2\mu_1 \operatorname{tr}[\boldsymbol{A}]\boldsymbol{1} + 2\mu_2\boldsymbol{A} + +2\mu_3 \operatorname{tr}[\boldsymbol{U}_1][(\boldsymbol{a}\cdot\boldsymbol{a})(\boldsymbol{a}\otimes\boldsymbol{a}) + (\boldsymbol{b}\cdot\boldsymbol{b})(\boldsymbol{b}\otimes\boldsymbol{b})] \\
&+ 2\mu_4\big\{(\boldsymbol{a}\otimes\boldsymbol{a}\otimes\boldsymbol{a}\otimes\boldsymbol{a} + \boldsymbol{b}\otimes\boldsymbol{b}\otimes\boldsymbol{b}\otimes\boldsymbol{b}) : \boldsymbol{U}_1\big\} \\
&+ 2\mu_5[(\boldsymbol{a}\cdot\boldsymbol{a})(\boldsymbol{a}\otimes\boldsymbol{a}) + (\boldsymbol{b}\cdot\boldsymbol{b})(\boldsymbol{b}\otimes\boldsymbol{b})]\boldsymbol{A} \\
&+ \mu_6\big\{ \operatorname{tr}[\boldsymbol{U}_1]\boldsymbol{1} + \operatorname{tr}[\boldsymbol{A}][(\boldsymbol{a}\cdot\boldsymbol{a})(\boldsymbol{a}\otimes\boldsymbol{a}) + (\boldsymbol{b}\cdot\boldsymbol{b})(\boldsymbol{b}\otimes\boldsymbol{b})]\big\} \\
&+ \mu_7\big\{\boldsymbol{U}\boldsymbol{V} + (\boldsymbol{a}\otimes\boldsymbol{a}\otimes\boldsymbol{a}\otimes\boldsymbol{a} + \boldsymbol{b}\otimes\boldsymbol{b}\otimes\boldsymbol{b}\otimes\boldsymbol{b}) : \boldsymbol{V}\boldsymbol{A}\big\}
\end{aligned} \qquad ,
\tag{442}
$$

and the fourth-order Hessian $\mathbb{F}$ can be expressed as

$$
\begin{aligned}
\mathbb{F} = \mathfrak{F}_{,\boldsymbol{A}\boldsymbol{A}} =& \sum_{i=1}^{7}\sum_{j=1}^{7} \mathfrak{F}_{,I_i} I_{i,\boldsymbol{A}\boldsymbol{A}} + \mathfrak{F}_{,I_iI_j} I_{i,\boldsymbol{A}}\otimes I_{j,\boldsymbol{A}} \\
=& 2\mu_1\boldsymbol{1}\otimes\boldsymbol{1} + \mu_2\big\{(\boldsymbol{1}\oplus\boldsymbol{1}) + (\boldsymbol{1}\ominus\boldsymbol{1})\big\} \\
&+ 2\mu_3\big\{[(\boldsymbol{a}\cdot\boldsymbol{a})(\boldsymbol{a}\otimes\boldsymbol{a}) + (\boldsymbol{b}\cdot\boldsymbol{b})(\boldsymbol{b}\otimes\boldsymbol{b})]\otimes[(\boldsymbol{a}\cdot\boldsymbol{a})(\boldsymbol{a}\otimes\boldsymbol{a}) + (\boldsymbol{b}\cdot\boldsymbol{b})(\boldsymbol{b}\otimes\boldsymbol{b})]\big\} \\
&+ 2\mu_4\big\{(\boldsymbol{a}\otimes\boldsymbol{a}\otimes\boldsymbol{a}\otimes\boldsymbol{a} + \boldsymbol{b}\otimes\boldsymbol{b}\otimes\boldsymbol{b}\otimes\boldsymbol{b}) : (\boldsymbol{a}\otimes\boldsymbol{a}\otimes\boldsymbol{a}\otimes\boldsymbol{a} + \boldsymbol{b}\otimes\boldsymbol{b}\otimes\boldsymbol{b}\otimes\boldsymbol{b})\big\} \\
&+ \frac{\mu_5}{2}\Big\{\big\{[(\boldsymbol{a}\cdot\boldsymbol{a})(\boldsymbol{a}\otimes\boldsymbol{a}) + (\boldsymbol{b}\cdot\boldsymbol{b})(\boldsymbol{b}\otimes\boldsymbol{b})]\oplus\boldsymbol{1}\big\} \\
&\qquad + \big\{[(\boldsymbol{a}\cdot\boldsymbol{a})(\boldsymbol{a}\otimes\boldsymbol{a}) + (\boldsymbol{b}\cdot\boldsymbol{b})(\boldsymbol{b}\otimes\boldsymbol{b})]\ominus\boldsymbol{1}\big\} \\
&\qquad + \big\{\boldsymbol{1}\oplus[(\boldsymbol{a}\cdot\boldsymbol{a})(\boldsymbol{a}\otimes\boldsymbol{a}) + (\boldsymbol{b}\cdot\boldsymbol{b})(\boldsymbol{b}\otimes\boldsymbol{b})]\big\} \\
&\qquad + \big\{\boldsymbol{1}\ominus[(\boldsymbol{a}\cdot\boldsymbol{a})(\boldsymbol{a}\otimes\boldsymbol{a}) + (\boldsymbol{b}\cdot\boldsymbol{b})(\boldsymbol{b}\otimes\boldsymbol{b})]\big\}\Big\} \\
&+ \mu_6\big\{\boldsymbol{1}\otimes[(\boldsymbol{a}\cdot\boldsymbol{a})(\boldsymbol{a}\otimes\boldsymbol{a}) + (\boldsymbol{b}\cdot\boldsymbol{b})(\boldsymbol{b}\otimes\boldsymbol{b})] + [(\boldsymbol{a}\cdot\boldsymbol{a})(\boldsymbol{a}\otimes\boldsymbol{a}) + (\boldsymbol{b}\cdot\boldsymbol{b})(\boldsymbol{b}\otimes\boldsymbol{b})]\otimes\boldsymbol{1}\big\} \\
&+ \mu_7\bar{\mathbb{F}}
\end{aligned} \qquad ,
$$

$$\tag{443}$$

where the term $\bar{\mathbb{F}}$ is expressed in the index notation as

$$\bar{\mathbb{F}}_{ijkl} = \frac{1}{2}\Big[(a_b a_l a_c a_d + b_b b_l b_c b_d)V_{la} + (a_a a_l a_c a_d + b_a b_l b_c b_d)V_{lb} \\ + (a_d a_l a_a a_b + b_d b_l b_a b_b)V_{lc} + (a_c a_l a_a a_b + b_c b_l b_a b_b)V_{ld}\Big] \tag{444}$$

If a coordinate system is chosen such that $\boldsymbol{a} = [1,0,0]^T$, $\boldsymbol{b} = [0,1,0]^T$ and $\tilde{\boldsymbol{n}} = [0,0,1]^T$, then the fourth-order tensor $\mathbb{F}$ in Eqn. (443) takes the coordinate-dependent form

$$[\mathbb{F}] = \begin{bmatrix} \mathbb{F}_{1111} & \mathbb{F}_{1122} & \mathbb{F}_{1133} & \mathbb{F}_{1112} & 0 & 0 \\ & \mathbb{F}_{2222} & \mathbb{F}_{1133} & -\mathbb{F}_{1112} & 0 & 0 \\ & & \mathbb{F}_{2222} & 0 & 0 & 0 \\ & & & \mathbb{F}_{1212} & 0 & 0 \\ & \text{sym.} & & & \mathbb{F}_{1313} & 0 \\ & & & & & \mathbb{F}_{1313} \end{bmatrix}, \tag{445}$$

along with the definitions

$$\mathbb{F}_{1111} = 2\sum_{i=1}^{6}\mu_i \,, \quad \mathbb{F}_{1122} = 2(\mu_1 + \mu_3 + \mu_6)\,, \quad \mathbb{F}_{1133} = 2\mu_1 + \mu_6\,,$$

$$\mathbb{F}_{1112} = \frac{\mu_7}{2}\,, \quad \mathbb{F}_{2222} = 2\sum_{i=1}^{6}\mu_i\,, \quad \mathbb{F}_{3333} = 2(\mu_1 + \mu_2)\,, \tag{446}$$

$$\mathbb{F}_{1212} = \mu_2 + \mu_5\,, \quad \mathbb{F}_{1313} = \mu_2 + \frac{\mu_5}{2}\,,$$

in terms of seven material constants $\mu_{1-7}$.

### A.5. Tetragonal symmetry group $\mathscr{C}_5$

The constitutive expressions of the $\mathscr{C}_5$ symmetry group, generated by $\boldsymbol{Q}_{\hat{c}}^{\frac{\pi}{2}}, \boldsymbol{Q}_{\boldsymbol{a}}^{\pi}$, are obtained from the $\mathscr{C}_4$ group by replacing the skew-symmetric tensor $\boldsymbol{V}$ with the symmetric tensor $\boldsymbol{U}_3$. Thus, the general form of the scalar-valued potential now reads

$$\mathfrak{F} = \mathfrak{F}(\boldsymbol{A}, \boldsymbol{U}_1, \boldsymbol{U}_2, \boldsymbol{U}_3)\,, \tag{447}$$

where

$$\begin{aligned} \boldsymbol{U}_1 &= (\boldsymbol{a}\otimes\boldsymbol{a}\otimes\boldsymbol{a}\otimes\boldsymbol{a} + \boldsymbol{b}\otimes\boldsymbol{b}\otimes\boldsymbol{b}\otimes\boldsymbol{b}):\boldsymbol{A} \\ \boldsymbol{U}_2 &= (\boldsymbol{a}\otimes\boldsymbol{a}\otimes\boldsymbol{a}\otimes\boldsymbol{a} + \boldsymbol{b}\otimes\boldsymbol{b}\otimes\boldsymbol{b}\otimes\boldsymbol{b}):\boldsymbol{A}^2 \\ \boldsymbol{U}_3 &= \tilde{\boldsymbol{n}}\otimes\tilde{\boldsymbol{n}} \end{aligned} \tag{448}$$

According to Table 11, the functional basis of the $\mathscr{C}_5$ group comprises of the basic invariants of the arguments $\boldsymbol{A}$, $\boldsymbol{U}_1$, $\boldsymbol{U}_2$ and $\boldsymbol{U}_3$ namely

$$\big\{\,\text{tr}[\boldsymbol{A}], \text{tr}[\boldsymbol{A}^2], \text{tr}[\boldsymbol{A}^3], \text{tr}[\boldsymbol{U}_1], \text{tr}[\boldsymbol{U}_1^2], \text{tr}[\boldsymbol{U}_1^3], \text{tr}[\boldsymbol{U}_2], \text{tr}[\boldsymbol{U}_2^2], \text{tr}[\boldsymbol{U}_2^3], \text{tr}[\boldsymbol{U}_3], \text{tr}[\boldsymbol{U}_3^2], \text{tr}[\boldsymbol{U}_3^3]\big\}\,, \tag{449}$$

the mixed invariants of every two arguments $\{\boldsymbol{A}, \boldsymbol{U}_1\}$, $\{\boldsymbol{A}, \boldsymbol{U}_2\}$, $\{\boldsymbol{A}, \boldsymbol{U}_3\}$, $\{\boldsymbol{U}_1, \boldsymbol{U}_2\}$, $\{\boldsymbol{U}_1, \boldsymbol{U}_3\}$ and $\{\boldsymbol{U}_2, \boldsymbol{U}_3\}$ defined by

$$\begin{aligned} \big\{\,&\text{tr}[\boldsymbol{A}\boldsymbol{U}_1], \text{tr}[\boldsymbol{A}^2\boldsymbol{U}_1], \text{tr}[\boldsymbol{A}\boldsymbol{U}_1^2], \text{tr}[\boldsymbol{A}^2\boldsymbol{U}_1^2], \text{tr}[\boldsymbol{A}\boldsymbol{U}_2], \text{tr}[\boldsymbol{A}^2\boldsymbol{U}_2], \text{tr}[\boldsymbol{A}\boldsymbol{U}_2^2], \\ &\text{tr}[\boldsymbol{A}^2\boldsymbol{U}_2^2], \text{tr}[\boldsymbol{A}\boldsymbol{U}_3], \text{tr}[\boldsymbol{A}\boldsymbol{U}_3^2], \text{tr}[\boldsymbol{A}^2\boldsymbol{U}_3^2], \text{tr}[\boldsymbol{U}_1\boldsymbol{U}_2], \text{tr}[\boldsymbol{U}_1^2\boldsymbol{U}_2], \text{tr}[\boldsymbol{U}_1\boldsymbol{U}_2^2], \\ &\text{tr}[\boldsymbol{U}_1^2\boldsymbol{U}_2^2], \text{tr}[\boldsymbol{U}_1\boldsymbol{U}_3], \text{tr}[\boldsymbol{U}_1^2\boldsymbol{U}_3], \text{tr}[\boldsymbol{U}_1\boldsymbol{U}_3^2], \text{tr}[\boldsymbol{U}_1^2\boldsymbol{U}_3^2], \\ &\text{tr}[\boldsymbol{U}_2\boldsymbol{U}_3], \text{tr}[\boldsymbol{U}_2^2\boldsymbol{U}_3], \text{tr}[\boldsymbol{U}_2\boldsymbol{U}_3^2], \text{tr}[\boldsymbol{U}_2^2\boldsymbol{U}_3^2]\big\} \end{aligned} \tag{450}$$

and the relative invariants of each three argument tensors $\{\boldsymbol{A}, \boldsymbol{U}_1, \boldsymbol{U}_2\}$, $\{\boldsymbol{A}, \boldsymbol{U}_1, \boldsymbol{U}_3\}$, $\{\boldsymbol{A}, \boldsymbol{U}_2, \boldsymbol{U}_3\}$ and $\{\boldsymbol{U}_1, \boldsymbol{U}_2, \boldsymbol{U}_3\}$ such that

$$\left\{\, \mathrm{tr}[\boldsymbol{A}\boldsymbol{U}_1\boldsymbol{U}_2], \mathrm{tr}[\boldsymbol{A}\boldsymbol{U}_1\boldsymbol{U}_3], \mathrm{tr}[\boldsymbol{A}\boldsymbol{U}_2\boldsymbol{U}_3], \mathrm{tr}[\boldsymbol{U}_1\boldsymbol{U}_2\boldsymbol{U}_3] \right\} \, . \tag{451}$$

Additionally, the following linear dependencies for the $\mathscr{C}_5$ symmetry group are valid

$$\begin{aligned}
&\mathrm{tr}[\boldsymbol{U}_1\boldsymbol{U}_3] = \mathrm{tr}[\boldsymbol{U}_1^2\boldsymbol{U}_3] = \mathrm{tr}[\boldsymbol{U}_2\boldsymbol{U}_3] = \mathrm{tr}[\boldsymbol{A}\boldsymbol{U}_1\boldsymbol{U}_3] = 0 \, , \\
&\mathrm{tr}[\boldsymbol{U}_1^2] = \mathrm{tr}[\boldsymbol{A}\boldsymbol{U}_1] \, , \\
&\mathrm{tr}[\boldsymbol{A}\boldsymbol{U}_3] = \mathrm{tr}[\boldsymbol{A}] - \mathrm{tr}[\boldsymbol{U}_1] \, , \\
&\mathrm{tr}[\boldsymbol{A}^2\boldsymbol{U}_3] = \mathrm{tr}[\boldsymbol{A}^2] - \mathrm{tr}[\boldsymbol{U}_2] \, , \\
&\boldsymbol{U}_3^2 = \boldsymbol{U}_3 \, .
\end{aligned} \tag{452}$$

An irreducible integrity basis can be defined by combining the invariants in Eqns. (449)–(451), and taking into account Eqn. (452) as

$$\mathcal{I}_{\mathscr{C}_5} = \left\{\, \mathrm{tr}^2[\boldsymbol{A}], \mathrm{tr}[\boldsymbol{A}^2], \mathrm{tr}^2[\boldsymbol{U}_1], \mathrm{tr}[\boldsymbol{U}_1^2], \mathrm{tr}[\boldsymbol{U}_2], \mathrm{tr}[\boldsymbol{A}]\,\mathrm{tr}[\boldsymbol{U}_1] \right\} \, , \tag{453}$$

appealing to which, a general form of the quadratic potential can be specified as

$$\mathfrak{F} = \sum_{i=1}^{6} \mu_i I_i \, , \tag{454}$$

where $I_{1-6}$ are the elements of the integrity basis $\mathcal{I}_{\mathscr{C}_5}$ defined in Eqn. (453) and $\mu_{1-6}$ are the material constants. The second-order stress-like tensor $\boldsymbol{S}$ is given by the expression

$$\begin{aligned}
\boldsymbol{S} = \mathfrak{F}_{,\boldsymbol{A}} =& \sum_{i=1}^{7} \mathfrak{F}_{,I_i}\, I_{i,\,\boldsymbol{A}} \\
=& 2\mu_1 \mathrm{tr}[\boldsymbol{A}]\boldsymbol{1} + 2\mu_2 \boldsymbol{A} + 2\mu_3 \mathrm{tr}[\boldsymbol{U}_1][(\boldsymbol{a}\cdot\boldsymbol{a})(\boldsymbol{a}\otimes\boldsymbol{a}) + (\boldsymbol{b}\cdot\boldsymbol{b})(\boldsymbol{b}\otimes\boldsymbol{b})] \\
&+ 2\mu_4\{(\boldsymbol{a}\otimes\boldsymbol{a}\otimes\boldsymbol{a}\otimes\boldsymbol{a} + \boldsymbol{b}\otimes\boldsymbol{b}\otimes\boldsymbol{b}\otimes\boldsymbol{b}) : \boldsymbol{U}_1\} \\
&+ 2\mu_5[(\boldsymbol{a}\cdot\boldsymbol{a})(\boldsymbol{a}\otimes\boldsymbol{a}) + (\boldsymbol{b}\cdot\boldsymbol{b})(\boldsymbol{b}\otimes\boldsymbol{b})]\boldsymbol{A} \\
&+ \mu_6\{\mathrm{tr}[\boldsymbol{U}_1]\boldsymbol{1} + \mathrm{tr}[\boldsymbol{A}][(\boldsymbol{a}\cdot\boldsymbol{a})(\boldsymbol{a}\otimes\boldsymbol{a}) + (\boldsymbol{b}\cdot\boldsymbol{b})(\boldsymbol{b}\otimes\boldsymbol{b})]\}
\end{aligned} \quad , \tag{455}$$

and the fourth-order Hessian $\mathbb{F}$ takes the form

$$\begin{aligned}
\mathbb{F} = \mathfrak{F}_{,\boldsymbol{A}\boldsymbol{A}} =& \sum_{i=1}^{6}\sum_{j=1}^{6} \mathfrak{F}_{,I_i}\, I_{i,\boldsymbol{A}\boldsymbol{A}} + \mathfrak{F}_{,I_i I_j}\, I_{i,\boldsymbol{A}} \otimes I_{j,\boldsymbol{A}} \\
=& 2\mu_1 \boldsymbol{1}\otimes\boldsymbol{1} + \mu_2\{(\boldsymbol{1}\oplus\boldsymbol{1}) + (\boldsymbol{1}\ominus\boldsymbol{1})\} \\
&+ 2\mu_3\{[(\boldsymbol{a}\cdot\boldsymbol{a})(\boldsymbol{a}\otimes\boldsymbol{a}) + (\boldsymbol{b}\cdot\boldsymbol{b})(\boldsymbol{b}\otimes\boldsymbol{b})]\otimes[(\boldsymbol{a}\cdot\boldsymbol{a})(\boldsymbol{a}\otimes\boldsymbol{a}) + (\boldsymbol{b}\cdot\boldsymbol{b})(\boldsymbol{b}\otimes\boldsymbol{b})]\} \\
&+ 2\mu_4\{(\boldsymbol{a}\otimes\boldsymbol{a}\otimes\boldsymbol{a}\otimes\boldsymbol{a} + \boldsymbol{b}\otimes\boldsymbol{b}\otimes\boldsymbol{b}\otimes\boldsymbol{b}) : (\boldsymbol{a}\otimes\boldsymbol{a}\otimes\boldsymbol{a}\otimes\boldsymbol{a} + \boldsymbol{b}\otimes\boldsymbol{b}\otimes\boldsymbol{b}\otimes\boldsymbol{b})\} \\
&+ \frac{\mu_5}{2}\Big\{\{[(\boldsymbol{a}\cdot\boldsymbol{a})(\boldsymbol{a}\otimes\boldsymbol{a}) + (\boldsymbol{b}\cdot\boldsymbol{b})(\boldsymbol{b}\otimes\boldsymbol{b})]\oplus\boldsymbol{1}\} \\
&\qquad + \{[(\boldsymbol{a}\cdot\boldsymbol{a})(\boldsymbol{a}\otimes\boldsymbol{a}) + (\boldsymbol{b}\cdot\boldsymbol{b})(\boldsymbol{b}\otimes\boldsymbol{b})]\ominus\boldsymbol{1}\} \\
&\qquad + \{\boldsymbol{1}\oplus[(\boldsymbol{a}\cdot\boldsymbol{a})(\boldsymbol{a}\otimes\boldsymbol{a}) + (\boldsymbol{b}\cdot\boldsymbol{b})(\boldsymbol{b}\otimes\boldsymbol{b})]\} \\
&\qquad + \{\boldsymbol{1}\ominus[(\boldsymbol{a}\cdot\boldsymbol{a})(\boldsymbol{a}\otimes\boldsymbol{a}) + (\boldsymbol{b}\cdot\boldsymbol{b})(\boldsymbol{b}\otimes\boldsymbol{b})]\}\Big\} \\
&+ \mu_6\{\boldsymbol{1}\otimes[(\boldsymbol{a}\cdot\boldsymbol{a})(\boldsymbol{a}\otimes\boldsymbol{a}) + (\boldsymbol{b}\cdot\boldsymbol{b})(\boldsymbol{b}\otimes\boldsymbol{b})] + [(\boldsymbol{a}\cdot\boldsymbol{a})(\boldsymbol{a}\otimes\boldsymbol{a}) + (\boldsymbol{b}\cdot\boldsymbol{b})(\boldsymbol{b}\otimes\boldsymbol{b})]\otimes\boldsymbol{1}\}
\end{aligned} \quad , \tag{456}$$

similar to the $\mathscr{C}_4$ group for $\mu_7 = 0$. If a coordinate system is chosen such that $\boldsymbol{a} = [1, 0, 0]^T$, $\boldsymbol{b} = [0, 1, 0]^T$ and $\tilde{\boldsymbol{n}} = [0, 0, 1]^T$, the fourth-order tensor $\mathbb{F}$ appears in the coordinate form

$$
[\mathbb{F}] = \begin{bmatrix} \mathbb{F}_{1111} & \mathbb{F}_{1122} & \mathbb{F}_{1133} & 0 & 0 & 0 \\ & \mathbb{F}_{2222} & \mathbb{F}_{1133} & 0 & 0 & 0 \\ & & \mathbb{F}_{2222} & 0 & 0 & 0 \\ & & & \mathbb{F}_{1212} & 0 & 0 \\ & \text{sym.} & & & \mathbb{F}_{1212} & 0 \\ & & & & & \mathbb{F}_{2323} \end{bmatrix} , \tag{457}
$$

along with the expressions

$$
\begin{aligned}
\mathbb{F}_{1111} &= 2\sum_{i=1}^{6} \mu_i , \quad \mathbb{F}_{1122} = 2(\mu_1 + \mu_3 + \mu_6) , \quad \mathbb{F}_{1133} = 2\mu_1 + \mu_6 , \\
\mathbb{F}_{2222} &= 2\sum_{i=1}^{6} \mu_i , \quad \mathbb{F}_{3333} = 2(\mu_1 + \mu_2) , \\
\mathbb{F}_{1212} &= \mu_2 + \mu_5 , \quad \mathbb{F}_{1313} = \mu_2 + \frac{\mu_5}{2} ,
\end{aligned} \tag{458}
$$

in terms of six material constants $\mu_{1-6}$.

## A.6. Trigonal symmetry group $\mathscr{C}_6$

The *trigonal* symmetry group $\mathscr{C}_6$ is generated by orthogonal rotation $\boldsymbol{Q}_{\boldsymbol{c}}^{\frac{2\pi}{3}}$, which corresponds to $120°$ rotation around an orthonormal vector $\boldsymbol{c}$. The functional basis of the $\mathscr{C}_6$ group is defined by a single symmetric second-order tensor $\boldsymbol{A}$ and three skew-symmetric tensors $\boldsymbol{V}_1, \boldsymbol{V}_2$ and $\boldsymbol{V}_3$, based on which the scalar-valued potential can generally be specified as

$$
\mathfrak{F} = \mathfrak{F}(\boldsymbol{A}, \boldsymbol{V}_1, \boldsymbol{V}_2, \boldsymbol{V}_3) , \tag{459}
$$

with

$$
\begin{aligned}
\boldsymbol{V}_1 &= \left( \sum_{i=1}^{3} \boldsymbol{\epsilon}\boldsymbol{a}_i \otimes \boldsymbol{a}_i \otimes \boldsymbol{a}_i \right) : \boldsymbol{A} \\
\boldsymbol{V}_2 &= \left( \sum_{i=1}^{3} \boldsymbol{\epsilon}\boldsymbol{a}_i \otimes \boldsymbol{a}_i \otimes \boldsymbol{a}_i \right) : \boldsymbol{A}^2 \\
\boldsymbol{V}_3 &= \boldsymbol{\epsilon}\tilde{\boldsymbol{n}}
\end{aligned} \tag{460}
$$

where $\tilde{\boldsymbol{n}}$ is the unit vector denoting the principle axis of the $\mathscr{C}_6$ group. The three vectors $\boldsymbol{a}_{1-3}$ are all orthogonal to $\tilde{\boldsymbol{n}}$, and are inclined at $120°$ to each other. From Table 11 it follows that the functional basis for the $\mathscr{C}_6$ group consists of the basic invariants of the arguments $\boldsymbol{A}, \boldsymbol{V}_1, \boldsymbol{V}_2$ and $\boldsymbol{V}_3$, given by

$$
\left\{ \mathrm{tr}[\boldsymbol{A}], \mathrm{tr}[\boldsymbol{A}^2], \mathrm{tr}[\boldsymbol{A}^3], \mathrm{tr}[\boldsymbol{V}_1^2], \mathrm{tr}[\boldsymbol{V}_2^2], \mathrm{tr}[\boldsymbol{V}_3^2] \right\} , \tag{461}
$$

the mixed invariants of every two arguments $\{\boldsymbol{A}, \boldsymbol{V}_1\}$, $\{\boldsymbol{A}, \boldsymbol{V}_2\}$, $\{\boldsymbol{A}, \boldsymbol{V}_3\}$, $\{\boldsymbol{V}_1, \boldsymbol{V}_2\}$, $\{\boldsymbol{V}_1, \boldsymbol{V}_3\}$ and $\{\boldsymbol{V}_2, \boldsymbol{V}_3\}$ such that

$$
\begin{aligned}
\big\{ &\mathrm{tr}[\boldsymbol{A}\boldsymbol{V}_1^2], \mathrm{tr}[\boldsymbol{A}^2\boldsymbol{V}_1^2], \mathrm{tr}[\boldsymbol{A}^2\boldsymbol{V}_1^2\boldsymbol{A}\boldsymbol{V}_1], \mathrm{tr}[\boldsymbol{A}\boldsymbol{V}_2^2], \mathrm{tr}[\boldsymbol{A}^2\boldsymbol{V}_2^2], \mathrm{tr}[\boldsymbol{A}^2\boldsymbol{V}_2^2\boldsymbol{A}\boldsymbol{V}_2], \\
&\mathrm{tr}[\boldsymbol{A}\boldsymbol{V}_3^2], \mathrm{tr}[\boldsymbol{A}^2\boldsymbol{V}_3^2], \mathrm{tr}[\boldsymbol{A}^2\boldsymbol{V}_3^2\boldsymbol{A}\boldsymbol{V}_3], \mathrm{tr}[\boldsymbol{V}_1\boldsymbol{V}_2], \mathrm{tr}[\boldsymbol{V}_1\boldsymbol{V}_3], \mathrm{tr}[\boldsymbol{V}_2\boldsymbol{V}_3] \big\} ,
\end{aligned} \tag{462}
$$

and the relative invariants of each three argument tensors $\{\boldsymbol{A}, \boldsymbol{V}_1, \boldsymbol{V}_2\}$, $\{\boldsymbol{A}, \boldsymbol{V}_1, \boldsymbol{V}_3\}$, $\{\boldsymbol{A}, \boldsymbol{V}_2, \boldsymbol{V}_3\}$ and $\{\boldsymbol{V}_1, \boldsymbol{V}_2, \boldsymbol{V}_3\}$ such that

$$
\begin{aligned}
\big\{\, &\mathrm{tr}[\boldsymbol{A}\boldsymbol{V}_1\boldsymbol{V}_2], \mathrm{tr}[\boldsymbol{A}\boldsymbol{V}_1^2\boldsymbol{V}_2], \mathrm{tr}[\boldsymbol{A}\boldsymbol{V}_1\boldsymbol{V}_2^2], \\
&\mathrm{tr}[\boldsymbol{A}\boldsymbol{V}_1\boldsymbol{V}_3], \mathrm{tr}[\boldsymbol{A}\boldsymbol{V}_1^2\boldsymbol{V}_3], \mathrm{tr}[\boldsymbol{A}\boldsymbol{V}_1\boldsymbol{V}_3^2], \\
&\mathrm{tr}[\boldsymbol{A}\boldsymbol{V}_2\boldsymbol{V}_3], \mathrm{tr}[\boldsymbol{A}\boldsymbol{V}_2^2\boldsymbol{V}_3], \mathrm{tr}[\boldsymbol{A}\boldsymbol{V}_2\boldsymbol{V}_3^2], \mathrm{tr}[\boldsymbol{V}_1\boldsymbol{V}_2\boldsymbol{V}_3] \big\}\,,
\end{aligned} \tag{463}
$$

An irreducible integrity basis can be defined by multiplicative combination of the invariants in Eqns. (461)– (463) to obtain quadratic terms in $\boldsymbol{A}$ as

$$
\mathcal{I}_{\mathscr{C}_6} = \big\{\, \mathrm{tr}^2[\boldsymbol{A}], \mathrm{tr}[\boldsymbol{A}^2], \mathrm{tr}^2[\boldsymbol{A}\boldsymbol{V}_3^2], \mathrm{tr}[\boldsymbol{V}_1^2], \mathrm{tr}[\boldsymbol{A}]\,\mathrm{tr}[\boldsymbol{A}\boldsymbol{V}_3^2], \mathrm{tr}[\boldsymbol{A}\boldsymbol{V}_1\boldsymbol{V}_3], \mathrm{tr}[\boldsymbol{A}\boldsymbol{V}_1\boldsymbol{V}_3^2] \big\}\,. \tag{464}
$$

The following linear dependencies can be trivially verified, and hence the invariants are dropped from Eqn. (464)

$$
\mathrm{tr}[\boldsymbol{V}_1\boldsymbol{V}_3] = \mathrm{tr}[\boldsymbol{V}_2\boldsymbol{V}_3] = 0
$$
$$
\mathrm{tr}[\boldsymbol{A}^2\boldsymbol{V}_3^2] = \frac{1}{2}\big(\mathrm{tr}[\boldsymbol{A}^2] + \mathrm{tr}^2[\boldsymbol{A}]\big) + \frac{1}{4}\mathrm{tr}^2[\boldsymbol{A}\boldsymbol{V}_3^2] + \mathrm{tr}[\boldsymbol{A}]\,\mathrm{tr}[\boldsymbol{A}\boldsymbol{V}_3^2] + \frac{2}{9}\mathrm{tr}[\boldsymbol{V}_1^2]\,. \tag{465}
$$

Scalar quadratic potential Eqn. (80) can be specified using Eqn. (465) as

$$
\mathfrak{F} = \sum_{i=1}^{7} \mu_i I_i\,, \tag{466}
$$

where $I_{1-7}$ are the elements of the integrity basis $\mathcal{I}_{\mathscr{C}_6}$ defined in Eqn. (464) and $\mu_{1-7}$ are material constants. The second-order stress-like tensor $\boldsymbol{\mathcal{S}}$ is given by

$$
\begin{aligned}
\boldsymbol{\mathcal{S}} = \mathfrak{F}_{,\boldsymbol{A}} = \sum_{i=1}^{7} \mathfrak{F}_{,I_i}\, I_{i,\boldsymbol{A}} = {}& 2\mu_1\,\mathrm{tr}[\boldsymbol{A}]\boldsymbol{1} + 2\mu_2\boldsymbol{A} + 2\mu_3\,\mathrm{tr}[\boldsymbol{A}\boldsymbol{V}_3^2]\boldsymbol{V}_3^2 + \mu_4\bar{\boldsymbol{\mathcal{S}}}_1 \\
&+ \mu_5\big\{\mathrm{tr}[\boldsymbol{A}\boldsymbol{V}_3^2]\boldsymbol{1} + \mathrm{tr}[\boldsymbol{A}]\boldsymbol{V}_3^2\big\} + \mu_6\bar{\boldsymbol{\mathcal{S}}}_2 + \mu_7\bar{\boldsymbol{\mathcal{S}}}_3
\end{aligned} \tag{467}
$$

where $\bar{\boldsymbol{\mathcal{S}}}_{1-3}$ are expressed in the index notation as

$$
\bar{\mathcal{S}}_{1_{ab}} = V_{1_{ij}}[\mathbb{D}_{ijab} + \mathbb{D}_{ijba}] \quad \text{with} \quad \mathbb{D}_{ijab} = e_{ijm}a_{1_m}a_{1_a}a_{1_b} + e_{ijm}a_{2_m}a_{2_a}a_{2_b} + e_{ijm}a_{3_m}a_{3_a}a_{3_b}\,,
$$
$$
\bar{\mathcal{S}}_{2_{ab}} = \frac{1}{2}\big\{[V_{1_{bn}}V_{3_{na}} + V_{1_{an}}V_{3_{nb}}] + [\mathbb{D}_{mnab} + \mathbb{D}_{mnba}]V_{3_{ni}}A_{im}\big\}\,,
$$
$$
\bar{\mathcal{S}}_{3_{ab}} = \frac{1}{2}\big\{[V_{1_{bn}}V_{3_{np}}V_{3_{pa}} + V_{1_{an}}V_{3_{np}}V_{3_{pb}}] + [\mathbb{D}_{mnab} + \mathbb{D}_{mnba}]V_{3_{np}}V_{3_{pi}}A_{im}\big\}\,.
\tag{468}
$$

The Hessian associated with the potential can be expressed as

$$
\begin{aligned}
\mathbb{F} = \mathfrak{F}_{,\boldsymbol{A}\boldsymbol{A}} = {}& \sum_{i=1}^{7}\sum_{j=1}^{7} \mathfrak{F}_{,I_i}\, I_{i,\boldsymbol{A}\boldsymbol{A}} + \mathfrak{F}_{,I_i I_j}\, I_{i,\boldsymbol{A}} \otimes I_{j,\boldsymbol{A}} \\
= {}& 2\mu_1\boldsymbol{1} \otimes \boldsymbol{1} + \mu_2\big\{(\boldsymbol{1} \oplus \boldsymbol{1}) + (\boldsymbol{1} \ominus \boldsymbol{1})\big\} \\
&+ \mu_3\boldsymbol{V}_3^2 \otimes \boldsymbol{V}_3^2 + \mu_4\bar{\mathbb{F}}_1 + \mu_5\big\{(\boldsymbol{1} \otimes \boldsymbol{V}_3^2) + (\boldsymbol{V}_3^2 \otimes \boldsymbol{1})\big\} \\
&+ \mu_6\bar{\mathbb{F}}_2 + \mu_7\bar{\mathbb{F}}_3
\end{aligned} \tag{469}
$$

along with the expressions

$$\bar{\mathbb{F}}_{1_{abcd}} = \frac{1}{2}[\mathbb{D}_{ijcd} + \mathbb{D}_{ijdc}][\mathbb{D}_{ijab} + \mathbb{D}_{ijba}] \,,$$

$$\bar{\mathbb{F}}_{2_{abcd}} = \frac{1}{4}\big\{[\mathbb{D}_{bncd} + \mathbb{D}_{bndc}]V_{3_{na}} + [\mathbb{D}_{ancd} + \mathbb{D}_{andc}]V_{3_{nb}}$$
$$+[\mathbb{D}_{dnab} + \mathbb{D}_{dnba}]V_{3_{nc}} + [\mathbb{D}_{cnab} + \mathbb{D}_{cnba}]V_{3_{nd}}\big\} \,, \tag{470}$$

$$\bar{\mathbb{F}}_{3_{abcd}} = \frac{1}{4}\big\{[\mathbb{D}_{bncd} + \mathbb{D}_{bndc}]V_{3_{np}}V_{3_{pa}} + [\mathbb{D}_{ancd} + \mathbb{D}_{andc}]V_{3_{np}}V_{3_{pb}}$$
$$+[\mathbb{D}_{dnab} + \mathbb{D}_{dnba}]V_{3_{np}}V_{3_{pc}} + [\mathbb{D}_{cnab} + \mathbb{D}_{cnba}]V_{3_{np}}V_{3_{pd}}\big\} \,.$$

For the choice $\tilde{\boldsymbol{n}} = [1,0,0]^T$, $\boldsymbol{a}_1 = [0,1,0]^T$, $\boldsymbol{a}_2 = [0,-1/2,\sqrt{3}/2]^T$ and $\boldsymbol{a}_3 = [0,-1/2,-\sqrt{3}/2]^T$, the fourth-order Hessian $\mathbb{F}$ appears in the coordinate form

$$[\mathbb{F}] = \begin{bmatrix} \mathbb{F}_{1111} & \mathbb{F}_{1122} & \mathbb{F}_{1122} & 0 & 0 & 0 \\ & \mathbb{F}_{2222} & \mathbb{F}_{2233} & \mathbb{F}_{2212} & \mathbb{F}_{2213} & 0 \\ & & \mathbb{F}_{2222} & -\mathbb{F}_{2212} & -\mathbb{F}_{2213} & 0 \\ & & & \mathbb{F}_{1212} & 0 & \mathbb{F}_{2213} \\ & \text{sym.} & & & \mathbb{F}_{1212} & -\mathbb{F}_{2212} \\ & & & & & \frac{1}{2}(\mathbb{F}_{2222} - \mathbb{F}_{2223}) \end{bmatrix} \,, \tag{471}$$

with the components

$$\mathbb{F}_{1111} = 2(\mu_1 + \mu_3) \,, \quad \mathbb{F}_{1122} = 2\mu_1 - \mu_5 \,,$$

$$\mathbb{F}_{2222} = 2(\mu_1 + \mu_2 + \mu_3 + \frac{9}{4}\mu_4 - \mu_5) \,, \quad \mathbb{F}_{2223} = 2(\mu_1 + \mu_2 - \frac{9}{4}\mu_4 - \mu_5) \,, \tag{472}$$

$$\mathbb{F}_{2212} = \frac{3}{8}\mu_6 \,, \quad \mathbb{F}_{2213} = \frac{3}{8}\mu_7 \,,$$

$$\mathbb{F}_{1212} = \mu_3 \,,$$

in terms of seven material constants $\mu_{1-7}$.

### A.7. Trigonal symmetry group $\mathscr{C}_7$

The constitutive expressions of the $\mathscr{C}_7$ symmetry group are obtained from the $\mathscr{C}_6$ group by replacing the skew-symmetric tensor $\boldsymbol{V}_3$ with a symmetric tensor $\boldsymbol{U}$. Thus, the scalar-valued potential now reads

$$\mathfrak{F} = \mathfrak{F}(\boldsymbol{A}, \boldsymbol{V}_1, \boldsymbol{V}_2, \boldsymbol{U}) \,, \tag{473}$$

with

$$\boldsymbol{V}_1 = \left(\sum_{i=1}^3 \boldsymbol{\epsilon}\boldsymbol{a}_i \otimes \boldsymbol{a}_i \otimes \boldsymbol{a}_i\right) : \boldsymbol{A}$$

$$\boldsymbol{V}_2 = \left(\sum_{i=1}^3 \boldsymbol{\epsilon}\boldsymbol{a}_i \otimes \boldsymbol{a}_i \otimes \boldsymbol{a}_i\right) : \boldsymbol{A}^2 \tag{474}$$

$$\boldsymbol{U} = \tilde{\boldsymbol{n}} \otimes \tilde{\boldsymbol{n}}$$

Analogous to the previous case, the three vectors $\boldsymbol{a}_{1-3}$ are all orthogonal to the unit vector $\tilde{\boldsymbol{n}}$, and aligned at 120° to each other. It can be seen from Table 11 that the functional

basis for the $\mathscr{C}_7$ group consists of the basic invariants of the arguments $\boldsymbol{A}, \boldsymbol{V}_1, \boldsymbol{V}_2$ and $\boldsymbol{U}$ such that

$$\left\{ \operatorname{tr}[\boldsymbol{A}], \operatorname{tr}[\boldsymbol{A}^2], \operatorname{tr}[\boldsymbol{A}^3], \operatorname{tr}[\boldsymbol{V}_1^2], \operatorname{tr}[\boldsymbol{V}_2^2], \operatorname{tr}[\boldsymbol{V}_3^2], \operatorname{tr}[\boldsymbol{U}], \operatorname{tr}[\boldsymbol{U}^2], \operatorname{tr}[\boldsymbol{U}^3] \right\} , \tag{475}$$

the mixed invariants of every two arguments $\{\boldsymbol{A}, \boldsymbol{V}_1\}$, $\{\boldsymbol{A}, \boldsymbol{V}_2\}$, $\{\boldsymbol{A}, \boldsymbol{U}\}$, $\{\boldsymbol{V}_1, \boldsymbol{V}_2\}$, $\{\boldsymbol{V}_1, \boldsymbol{U}\}$ and $\{\boldsymbol{V}_2, \boldsymbol{U}\}$ given by

$$\begin{aligned}
\big\{ &\operatorname{tr}[\boldsymbol{A}\boldsymbol{V}_1^2], \operatorname{tr}[\boldsymbol{A}^2\boldsymbol{V}_1^2], \operatorname{tr}[\boldsymbol{A}^2\boldsymbol{V}_1^2\boldsymbol{A}\boldsymbol{V}_1], \operatorname{tr}[\boldsymbol{A}\boldsymbol{V}_2^2], \operatorname{tr}[\boldsymbol{A}^2\boldsymbol{V}_2^2], \operatorname{tr}[\boldsymbol{A}^2\boldsymbol{V}_2^2\boldsymbol{A}\boldsymbol{V}_2], \\
&\operatorname{tr}[\boldsymbol{A}\boldsymbol{U}], \operatorname{tr}[\boldsymbol{A}^2\boldsymbol{U}], \operatorname{tr}[\boldsymbol{A}\boldsymbol{U}^2], \operatorname{tr}[\boldsymbol{A}^2\boldsymbol{U}^2], \operatorname{tr}[\boldsymbol{V}_1\boldsymbol{V}_2], \operatorname{tr}[\boldsymbol{V}_1^2\boldsymbol{U}], \operatorname{tr}[\boldsymbol{V}_1^2\boldsymbol{U}^2], \\
&\operatorname{tr}[\boldsymbol{V}_1^2\boldsymbol{U}^2\boldsymbol{V}_1\boldsymbol{U}], \operatorname{tr}[\boldsymbol{V}_2^2\boldsymbol{U}], \operatorname{tr}[\boldsymbol{V}_2^2\boldsymbol{U}^2], \operatorname{tr}[\boldsymbol{V}_2^2\boldsymbol{U}^2\boldsymbol{V}_2\boldsymbol{U}] \big\} ,
\end{aligned} \tag{476}$$

and the relative invariants of each three argument tensors $\{\boldsymbol{A}, \boldsymbol{V}_1, \boldsymbol{V}_2\}$, $\{\boldsymbol{A}, \boldsymbol{V}_1, \boldsymbol{U}\}$, $\{\boldsymbol{A}, \boldsymbol{V}_2, \boldsymbol{U}\}$ and $\{\boldsymbol{V}_1, \boldsymbol{V}_2, \boldsymbol{U}\}$ such that

$$\begin{aligned}
\big\{ &\operatorname{tr}[\boldsymbol{A}\boldsymbol{V}_1\boldsymbol{V}_2], \operatorname{tr}[\boldsymbol{A}\boldsymbol{V}_1^2\boldsymbol{V}_2], \operatorname{tr}[\boldsymbol{A}\boldsymbol{V}_1\boldsymbol{V}_2^2], \\
&\operatorname{tr}[\boldsymbol{A}\boldsymbol{V}_1\boldsymbol{U}], \operatorname{tr}[\boldsymbol{A}^2\boldsymbol{V}_1\boldsymbol{U}], \operatorname{tr}[\boldsymbol{A}\boldsymbol{V}_1\boldsymbol{U}^2], \operatorname{tr}[\boldsymbol{A}\boldsymbol{V}_1^2\boldsymbol{U}\boldsymbol{V}_1], \\
&\operatorname{tr}[\boldsymbol{A}\boldsymbol{V}_2\boldsymbol{U}], \operatorname{tr}[\boldsymbol{A}^2\boldsymbol{V}_2\boldsymbol{U}], \operatorname{tr}[\boldsymbol{A}\boldsymbol{V}_2\boldsymbol{U}^2], \operatorname{tr}[\boldsymbol{A}\boldsymbol{V}_2^2\boldsymbol{U}\boldsymbol{V}_2], \\
&\operatorname{tr}[\boldsymbol{V}_1\boldsymbol{V}_2\boldsymbol{U}], \operatorname{tr}[\boldsymbol{V}_1\boldsymbol{V}_2^2\boldsymbol{U}], \operatorname{tr}[\boldsymbol{V}_1^2\boldsymbol{V}_2\boldsymbol{U}] \big\} ,
\end{aligned} \tag{477}$$

A multiplicative combination of invariants in Eqns. (475)–(477) to obtain quadratic terms in $\boldsymbol{A}$ leads to the definition of an irreducible integrity basis for this symmetry group as

$$\mathcal{I}_{\mathscr{C}_7} = \left\{ \operatorname{tr}^2[\boldsymbol{A}], \operatorname{tr}[\boldsymbol{A}^2], \operatorname{tr}^2[\boldsymbol{A}\boldsymbol{U}], \operatorname{tr}[\boldsymbol{V}_1^2], \operatorname{tr}[\boldsymbol{A}] \operatorname{tr}[\boldsymbol{A}\boldsymbol{U}], \operatorname{tr}[\boldsymbol{A}\boldsymbol{V}_1\boldsymbol{U}] \right\} , \tag{478}$$

where the following invariants are not considered in Eqn. (478) as they can be expressed in terms of other invariants

$$\begin{aligned}
\operatorname{tr}[\boldsymbol{A}^2\boldsymbol{U}] &= \frac{1}{4}\big( \operatorname{tr}^2[\boldsymbol{A}\boldsymbol{U}] - \operatorname{tr}^2[\boldsymbol{A}] \big) + \frac{1}{2}\big( \operatorname{tr}[\boldsymbol{A}] \operatorname{tr}[\boldsymbol{A}\boldsymbol{U}] + \operatorname{tr}[\boldsymbol{A}^2] \big) + \frac{2}{9} \operatorname{tr}[\boldsymbol{V}_1^2] , \\
\operatorname{tr}[\boldsymbol{U}\boldsymbol{V}_1^2] &= \frac{1}{2} \operatorname{tr}[\boldsymbol{A}\boldsymbol{U}] , \\
\boldsymbol{U} &= \boldsymbol{U}^2 .
\end{aligned} \tag{479}$$

A scalar quadratic potential can be defined with the aid of Eqn. (478) as

$$\mathfrak{F} = \sum_{i=1}^{6} \mu_i I_i , \tag{480}$$

where $I_{1-6}$ are the elements of the integrity basis $\mathcal{I}_{\mathscr{C}_7}$ and $\mu_{1-6}$ are material constants. The second-order stress-like tensor $\boldsymbol{S}$ associated with the potential is given by

$$\begin{aligned}
\boldsymbol{S} = \mathfrak{F}_{,\boldsymbol{A}} = \sum_{i=1}^{6} \mathfrak{F}_{,I_i} I_{i,\,\boldsymbol{A}} = &2\mu_1 \operatorname{tr}[\boldsymbol{A}]\boldsymbol{1} + 2\mu_2 \boldsymbol{A} + 2\mu_3 \operatorname{tr}[\boldsymbol{A}\boldsymbol{U}]\boldsymbol{U} + \mu_4 \bar{\boldsymbol{S}}_1 \\
&+ \mu_5 \big\{ \operatorname{tr}[\boldsymbol{A}\boldsymbol{U}]\boldsymbol{1} + \operatorname{tr}[\boldsymbol{A}]\boldsymbol{U} \big\} + \mu_6 \bar{\boldsymbol{S}}_2
\end{aligned} , \tag{481}$$

where $\bar{\boldsymbol{S}}_1$ is defined in Eqn. (468), and

$$\bar{S}_{2_{ab}} = \frac{1}{2}\big\{ [V_{1_{bn}} U_{na} + V_{1_{an}} U_{nb}] + [\mathbb{D}_{mnab} + \mathbb{D}_{mnba}] U_{ni} A_{im} \big\} . \tag{482}$$

Likewise, the fourth-order Hessian matrix can be expressed as

$$
\begin{aligned}
\mathbb{F} = \mathfrak{F},_{\boldsymbol{AA}} &= \sum_{i=1}^{6} \sum_{j=1}^{6} \mathfrak{F},_{I_i} I_{i,\boldsymbol{AA}} + \mathfrak{F},_{I_i I_j} I_{i,\boldsymbol{A}} \otimes I_{j,\boldsymbol{A}} \\
&= 2\mu_1 \boldsymbol{1} \otimes \boldsymbol{1} + \mu_2 \big\{ (\boldsymbol{1} \oplus \boldsymbol{1}) + (\boldsymbol{1} \ominus \boldsymbol{1}) \big\} + \mu_3 \boldsymbol{U} \otimes \boldsymbol{U} \\
&\quad + \mu_4 \bar{\mathbb{F}}_1 + \mu_5 \big\{ (\boldsymbol{1} \otimes \boldsymbol{U}) + (\boldsymbol{U} \otimes \boldsymbol{1}) \big\} + \mu_6 \bar{\mathbb{F}}_2
\end{aligned}
\tag{483}
$$

where $\bar{\mathbb{F}}_1$ is defined in Eqn. (468), and

$$
\begin{aligned}
\bar{\mathbb{F}}_{2_{abcd}} = \frac{1}{4} \big\{ &[\mathbb{D}_{bncd} + \mathbb{D}_{bndc}]U_{na} + [\mathbb{D}_{ancd} + \mathbb{D}_{andc}]U_{nb} \\
&+ [\mathbb{D}_{dnab} + \mathbb{D}_{dnba}]U_{nc} + [\mathbb{D}_{cnab} + \mathbb{D}_{cnba}]U_{nd} \big\} \; .
\end{aligned}
\tag{484}
$$

If the vectors $\tilde{\boldsymbol{n}}, \boldsymbol{a}_{1-3}$ are chosen in complete analogy to the $\mathscr{C}_6$ group, the fourth-order tensor $\mathbb{F}$ appears in a coordinate form as

$$
[\mathbb{F}] =
\begin{bmatrix}
\mathbb{F}_{1111} & \mathbb{F}_{1122} & \mathbb{F}_{1122} & 0 & 0 & 0 \\
 & \mathbb{F}_{2222} & \mathbb{F}_{2233} & \mathbb{F}_{2212} & 0 & 0 \\
 & & \mathbb{F}_{2222} & -\mathbb{F}_{2212} & 0 & 0 \\
 & & & \mathbb{F}_{1212} & 0 & 0 \\
 & \text{sym.} & & & \mathbb{F}_{1212} & -\mathbb{F}_{2212} \\
 & & & & & \frac{1}{2}(\mathbb{F}_{2222} - \mathbb{F}_{2223})
\end{bmatrix}
,
\tag{485}
$$

with the components

$$
\mathbb{F}_{1111} = 2(\mu_1 + \mu_3) \; , \quad \mathbb{F}_{1122} = 2\mu_1 - \mu_5 \; ,
$$

$$
\mathbb{F}_{2222} = 2\left(\mu_1 + \mu_2 + \mu_3 + \frac{9}{4}\mu_4 - \mu_5\right) , \quad \mathbb{F}_{2223} = 2\left(\mu_1 + \mu_2 - \frac{9}{4}\mu_4 - \mu_5\right) , \tag{486}
$$

$$
\mathbb{F}_{2212} = \frac{3}{8}\mu_6 \; , \quad \mathbb{F}_{1212} = \mu_3 \; ,
$$

in terms of six material constants $\mu_{1-6}$.

### A.8. Hexagonal symmetry group $\mathscr{C}_8$

The *hexagonal* symmetry group $\mathscr{C}_8$ is characterised by the existence of three symmetric second order tensors $\boldsymbol{A}, \boldsymbol{U}_1, \boldsymbol{U}_2$ and a single skew-symmetric second-order tensor $\boldsymbol{V}$. Thus, one may specify a general form of the scalar-valued potential as

$$
\mathfrak{F} = \mathfrak{F}(\boldsymbol{A}, \boldsymbol{U}_1, \boldsymbol{U}_2, \boldsymbol{V}) \; , \tag{487}
$$

with

$$
\begin{aligned}
\boldsymbol{U}_1 &= \left\{ \left( \sum_{i=1}^{3} \boldsymbol{a}_i \otimes \boldsymbol{a}_i \otimes \boldsymbol{a}_i \otimes \boldsymbol{a}_i \otimes \boldsymbol{a}_i \otimes \boldsymbol{a}_i \right) : \boldsymbol{A} \right\} : \boldsymbol{A} \\
\boldsymbol{U}_2 &= \left\{ \left( \sum_{i=1}^{3} \boldsymbol{a}_i \otimes \boldsymbol{a}_i \otimes \boldsymbol{a}_i \otimes \boldsymbol{a}_i \otimes \boldsymbol{a}_i \otimes \boldsymbol{a}_i \right) : \boldsymbol{A}^2 \right\} : \boldsymbol{A}^2 \\
\boldsymbol{V} &= \boldsymbol{\epsilon} \tilde{\boldsymbol{n}}
\end{aligned}
\tag{488}
$$

where the three vectors $\boldsymbol{a}_{1-3}$ are aligned at $120°$ to each other, and are all orthogonal to a unit normal vector $\tilde{\boldsymbol{n}}$. The functional basis for the $\mathscr{C}_8$ group can be specified from

Table 11 for the arguments $\boldsymbol{A}, \boldsymbol{U}_1, \boldsymbol{U}_2$ and $\boldsymbol{V}$. The basis consists of the fundamental invariants of each argument such that

$$\big\{\, \mathrm{tr}[\boldsymbol{A}], \mathrm{tr}[\boldsymbol{A}^2], \mathrm{tr}[\boldsymbol{A}^3], \mathrm{tr}[\boldsymbol{U}_1], \mathrm{tr}[\boldsymbol{U}_1^2], \mathrm{tr}[\boldsymbol{U}_1^3], \mathrm{tr}[\boldsymbol{U}_2], \mathrm{tr}[\boldsymbol{U}_2^2], \mathrm{tr}[\boldsymbol{U}_2^3], \mathrm{tr}[\boldsymbol{V}^2] \big\}\,, \qquad (489)$$

together with the mixed invariants of each two arguments $\{\boldsymbol{A}, \boldsymbol{U}_1\}$, $\{\boldsymbol{A}, \boldsymbol{U}_2\}$, $\{\boldsymbol{A}, \boldsymbol{V}\}$, $\{\boldsymbol{U}_1, \boldsymbol{U}_2\}$, $\{\boldsymbol{U}_1, \boldsymbol{V}\}$ and $\{\boldsymbol{U}_2, \boldsymbol{V}\}$ given by

$$\begin{aligned} \big\{\, &\mathrm{tr}[\boldsymbol{A}\boldsymbol{U}_1], \mathrm{tr}[\boldsymbol{A}^2\boldsymbol{U}_1], \mathrm{tr}[\boldsymbol{A}\boldsymbol{U}_1^2], \mathrm{tr}[\boldsymbol{A}^2\boldsymbol{U}_1^2], \mathrm{tr}[\boldsymbol{A}\boldsymbol{U}_2], \mathrm{tr}[\boldsymbol{A}^2\boldsymbol{U}_2], \mathrm{tr}[\boldsymbol{A}\boldsymbol{U}_2^2], \mathrm{tr}[\boldsymbol{A}^2\boldsymbol{U}_2^2], \\ &\mathrm{tr}[\boldsymbol{A}\boldsymbol{V}^2], \mathrm{tr}[\boldsymbol{A}^2\boldsymbol{V}^2], \mathrm{tr}[\boldsymbol{A}^2\boldsymbol{V}^2\boldsymbol{A}\boldsymbol{V}], \mathrm{tr}[\boldsymbol{U}_1\boldsymbol{U}_2], \mathrm{tr}[\boldsymbol{U}_1^2\boldsymbol{U}_2], \mathrm{tr}[\boldsymbol{U}_1\boldsymbol{U}_2^2], \mathrm{tr}[\boldsymbol{U}_1^2\boldsymbol{U}_2^2], \qquad (490) \\ &\mathrm{tr}[\boldsymbol{U}_1\boldsymbol{V}^2], \mathrm{tr}[\boldsymbol{U}_1^2\boldsymbol{V}^2], \mathrm{tr}[\boldsymbol{U}_1^2\boldsymbol{V}^2\boldsymbol{U}_1\boldsymbol{V}], \mathrm{tr}[\boldsymbol{U}_2\boldsymbol{V}^2], \mathrm{tr}[\boldsymbol{U}_2^2\boldsymbol{V}^2], \mathrm{tr}[\boldsymbol{U}_2^2\boldsymbol{V}^2\boldsymbol{U}_2\boldsymbol{V}] \big\}\,, \end{aligned}$$

and the relative invariants of each three argument tensors $\{\boldsymbol{A}, \boldsymbol{V}_1, \boldsymbol{V}_2\}$, $\{\boldsymbol{A}, \boldsymbol{V}_1, \boldsymbol{U}\}$, $\{\boldsymbol{A}, \boldsymbol{V}_2, \boldsymbol{U}\}$ and $\{\boldsymbol{V}_1, \boldsymbol{V}_2, \boldsymbol{U}\}$ such that

$$\begin{aligned} \big\{\, &\mathrm{tr}[\boldsymbol{A}\boldsymbol{U}_1\boldsymbol{U}_2], \mathrm{tr}[\boldsymbol{A}\boldsymbol{U}_1\boldsymbol{V}], \mathrm{tr}[\boldsymbol{A}^2\boldsymbol{U}_1\boldsymbol{V}], \mathrm{tr}[\boldsymbol{A}\boldsymbol{U}_1^2\boldsymbol{V}], \mathrm{tr}[\boldsymbol{A}\boldsymbol{V}^2\boldsymbol{U}_1\boldsymbol{V}], \\ &\mathrm{tr}[\boldsymbol{A}\boldsymbol{U}_2\boldsymbol{V}], \mathrm{tr}[\boldsymbol{A}^2\boldsymbol{U}_2\boldsymbol{V}], \mathrm{tr}[\boldsymbol{A}\boldsymbol{U}_2^2\boldsymbol{V}], \mathrm{tr}[\boldsymbol{A}\boldsymbol{V}^2\boldsymbol{U}_2\boldsymbol{V}], \qquad (491) \\ &\mathrm{tr}[\boldsymbol{U}_1\boldsymbol{U}_2\boldsymbol{V}], \mathrm{tr}[\boldsymbol{U}_1^2\boldsymbol{U}_2\boldsymbol{V}], \mathrm{tr}[\boldsymbol{U}_1\boldsymbol{U}_2^2\boldsymbol{V}], \mathrm{tr}[\boldsymbol{U}_1\boldsymbol{V}^2\boldsymbol{U}_2\boldsymbol{V}] \big\}\,. \end{aligned}$$

With respect to the $\mathscr{C}_8$ symmetry group, the following linear dependencies of the invariants can be trivially verified

$$\mathrm{tr}[\boldsymbol{U}_1] = -\,\mathrm{tr}[\boldsymbol{U}_1\boldsymbol{V}^2]\,,$$

$$\mathrm{tr}[\boldsymbol{A}^2\boldsymbol{V}^2] = \frac{1}{2}\big(\,\mathrm{tr}^2[\boldsymbol{A}] - \mathrm{tr}[\boldsymbol{A}^2]\big) + \frac{3}{4}\,\mathrm{tr}^2[\boldsymbol{A}\boldsymbol{V}^2] + \mathrm{tr}[\boldsymbol{A}]\,\mathrm{tr}^2[\boldsymbol{A}\boldsymbol{V}^2] - \frac{2}{3}\,\mathrm{tr}[\boldsymbol{U}_1]\,, \qquad (492)$$

$$\boldsymbol{U} = \boldsymbol{U}^2\,.$$

An irreducible integrity basis for the $\mathscr{C}_8$ symmetry group can be obtained by multiplicatively combining the invariants in Eqns. (489)–(491) to obtain quadratic terms in $\boldsymbol{A}$, while taking into account Eqn. (492) as

$$\mathcal{I}_{\mathscr{C}_8} = \big\{\, \mathrm{tr}^2[\boldsymbol{A}], \mathrm{tr}[\boldsymbol{A}^2], \mathrm{tr}[\boldsymbol{A}\boldsymbol{V}^2], \mathrm{tr}[\boldsymbol{U}_1], \mathrm{tr}[\boldsymbol{A}]\,\mathrm{tr}[\boldsymbol{A}\boldsymbol{V}^2] \big\}\,, \qquad (493)$$

which allows for the definition a scalar-valued quadratic potential as

$$\mathfrak{F} = \sum_{i=1}^{5} \mu_i I_i\,, \qquad (494)$$

where $I_{1-5}$ are the elements of the integrity basis $\mathcal{I}_{\mathscr{C}_8}$ and $\mu_{1-5}$ are material constants. It follows that the second-order stress-like tensor $\boldsymbol{\mathsf{S}}$ can be expressed as

$$\begin{aligned} \boldsymbol{\mathsf{S}} = \mathfrak{F}_{,\boldsymbol{A}} = \sum_{i=1}^{5} \mathfrak{F}_{,I_i}\, I_{i,\,\boldsymbol{A}} = &\,2\mu_1\,\mathrm{tr}[\boldsymbol{A}]\boldsymbol{1} + 2\mu_2\boldsymbol{A} + 2\mu_3\,\mathrm{tr}[\boldsymbol{A}\boldsymbol{V}^2]\boldsymbol{V}^2 \\ &+ \mu_4\bar{\boldsymbol{\mathsf{S}}}_1 + \mu_5\big\{\,\mathrm{tr}[\boldsymbol{A}\boldsymbol{V}^2]\boldsymbol{1} + \mathrm{tr}[\boldsymbol{A}]\boldsymbol{V}^2\big\} \end{aligned}\,, \qquad (495)$$

where

$$\bar{\mathsf{S}}_{1_{ab}} = \frac{1}{2}\big\{[\mathbb{D}_{iiklab} + \mathbb{D}_{iiklba}]A_{kl} + [\mathbb{D}_{iiabmn} + \mathbb{D}_{iibamn}]A_{mn}\big\}\,. \qquad (496)$$

The fourth-order Hessian matrix takes the form

$$
\begin{aligned}
\mathbb{F} = \mathfrak{F},_{\boldsymbol{AA}} &= \sum_{i=1}^{5} \sum_{j=1}^{5} \mathfrak{F},_{I_i} I_{i,\boldsymbol{AA}} + \mathfrak{F},_{I_i I_j} I_{i,\boldsymbol{A}} \otimes I_{j,\boldsymbol{A}} \\
&= 2\mu_1 \boldsymbol{1} \otimes \boldsymbol{1} + \mu_2 \big\{ (\boldsymbol{1} \oplus \boldsymbol{1}) + (\boldsymbol{1} \ominus \boldsymbol{1}) \big\} + \mu_3 \boldsymbol{V}^2 \otimes \boldsymbol{V}^2 \\
&\quad + \mu_4 \bar{\mathbb{F}}_1 + \mu_5 \big\{ (\boldsymbol{1} \otimes \boldsymbol{V}^2) + (\boldsymbol{V}^2 \otimes \boldsymbol{1}) \big\}
\end{aligned}
\tag{497}
$$

where $\bar{\mathbb{F}}_1$ is expressed in the index notation as

$$
\bar{\mathbb{F}}_{1_{abcd}} = \frac{1}{4} \big\{ \mathbb{D}_{iicdab} + \mathbb{D}_{iicdba} + \mathbb{D}_{iidcab} + \mathbb{D}_{iidcba} + \mathbb{D}_{iiabcd} + \mathbb{D}_{iibacd} + \mathbb{D}_{iiabdc} + \mathbb{D}_{iibadc} \big\} \ .
\tag{498}
$$

Setting $\tilde{\boldsymbol{n}} = [1,0,0]^T$, $\boldsymbol{a}_1 = [0,1,0]^T$, $\boldsymbol{a}_2 = [0,-1/2,\sqrt{3}/2]^T$ and $\boldsymbol{a}_3 = [0,-1/2,-\sqrt{3}/2]^T$, a coordinate form of the Hessian matrix is obtained as

$$
[\mathbb{F}] =
\begin{bmatrix}
\mathbb{F}_{1111} & \mathbb{F}_{1122} & \mathbb{F}_{1122} & 0 & 0 & 0 \\
 & \mathbb{F}_{2222} & \mathbb{F}_{2233} & 0 & 0 & 0 \\
 & & \mathbb{F}_{2222} & 0 & 0 & 0 \\
 & & & \mathbb{F}_{1212} & 0 & 0 \\
 & \text{sym.} & & & \mathbb{F}_{1212} & 0 \\
 & & & & & \frac{1}{2}(\mathbb{F}_{2222} - \mathbb{F}_{2223})
\end{bmatrix} ,
\tag{499}
$$

where

$$
\mathbb{F}_{1111} = 2(\mu_1 + \mu_3) \ , \quad \mathbb{F}_{1122} = 2\mu_1 - \mu_5 \ ,
$$

$$
\mathbb{F}_{2222} = 2\Big(\mu_1 + \mu_2 + \mu_3 + \frac{9}{8}\mu_4 - \mu_5\Big) \ , \quad \mathbb{F}_{2223} = 2\Big(\mu_1 + \mu_2 - \frac{3}{8}\mu_4 - \mu_5\Big) \ ,
\tag{500}
$$

$$
\mathbb{F}_{1212} = \mu_3 \ ,
$$

in terms of five material constants $\mu_{1-5}$.

## A.9. Hexagonal symmetry group $\mathscr{C}_9$

Analogous to the $\mathscr{C}_7$ group, the constitutive expressions of the $\mathscr{C}_9$ symmetry group are obtained from those of the $\mathscr{C}_8$ group by replacing the skew-symmetric tensor $\boldsymbol{V}$ with a symmetric tensor $\boldsymbol{U}_3$. The scalar-valued potential now reads

$$
\mathfrak{F} = \mathfrak{F}(\boldsymbol{A}, \boldsymbol{U}_1, \boldsymbol{U}_2, \boldsymbol{U}_3) \ ,
\tag{501}
$$

with

$$
\begin{aligned}
\boldsymbol{U}_1 &= \left\{ \left( \sum_{i=1}^{3} \boldsymbol{a}_i \otimes \boldsymbol{a}_i \otimes \boldsymbol{a}_i \otimes \boldsymbol{a}_i \otimes \boldsymbol{a}_i \otimes \boldsymbol{a}_i \right) : \boldsymbol{A} \right\} : \boldsymbol{A} \\
\boldsymbol{U}_2 &= \left\{ \left( \sum_{i=1}^{3} \boldsymbol{a}_i \otimes \boldsymbol{a}_i \otimes \boldsymbol{a}_i \otimes \boldsymbol{a}_i \otimes \boldsymbol{a}_i \otimes \boldsymbol{a}_i \right) : \boldsymbol{A}^2 \right\} : \boldsymbol{A}^2 \\
\boldsymbol{U}_3 &= \tilde{\boldsymbol{n}} \otimes \tilde{\boldsymbol{n}}
\end{aligned}
\tag{502}
$$

Again, it follows from Table 11 that the functional basis for the $\mathscr{C}_9$ group consists of the basic invariants of $\boldsymbol{A}, \boldsymbol{U}_1, \boldsymbol{U}_2$ and $\boldsymbol{U}_3$ such that

$$
\big\{ \mathrm{tr}[\boldsymbol{A}], \mathrm{tr}[\boldsymbol{A}^2], \mathrm{tr}[\boldsymbol{A}^3], \mathrm{tr}[\boldsymbol{U}_1], \mathrm{tr}[\boldsymbol{U}_1^2], \mathrm{tr}[\boldsymbol{U}_1^3], \mathrm{tr}[\boldsymbol{U}_2], \mathrm{tr}[\boldsymbol{U}_2^2], \mathrm{tr}[\boldsymbol{U}_2^3], \mathrm{tr}[\boldsymbol{U}_3], \mathrm{tr}[\boldsymbol{U}_3^2], \mathrm{tr}[\boldsymbol{U}_3^3] \big\} \ ,
\tag{503}
$$

along with the mixed invariants of $\{\boldsymbol{A}, \boldsymbol{U}_1\}$, $\{\boldsymbol{A}, \boldsymbol{U}_2\}$, $\{\boldsymbol{A}, \boldsymbol{U}_3\}$, $\{\boldsymbol{U}_1, \boldsymbol{U}_2\}$, $\{\boldsymbol{U}_1, \boldsymbol{U}_3\}$ and $\{\boldsymbol{U}_2, \boldsymbol{U}_3\}$ given by

$$\begin{aligned} \big\{\, &\mathrm{tr}[\boldsymbol{A}\boldsymbol{U}_1], \mathrm{tr}[\boldsymbol{A}^2\boldsymbol{U}_1], \mathrm{tr}[\boldsymbol{A}\boldsymbol{U}_1^2], \mathrm{tr}[\boldsymbol{A}^2\boldsymbol{U}_1^2], \mathrm{tr}[\boldsymbol{A}\boldsymbol{U}_2], \mathrm{tr}[\boldsymbol{A}^2\boldsymbol{U}_2], \mathrm{tr}[\boldsymbol{A}\boldsymbol{U}_2^2], \mathrm{tr}[\boldsymbol{A}^2\boldsymbol{U}_2^2], \\ &\mathrm{tr}[\boldsymbol{A}\boldsymbol{U}_3], \mathrm{tr}[\boldsymbol{A}^2\boldsymbol{U}_3], \mathrm{tr}[\boldsymbol{A}\boldsymbol{U}_3^2], \mathrm{tr}[\boldsymbol{A}^2\boldsymbol{U}_3^2], \mathrm{tr}[\boldsymbol{U}_1\boldsymbol{U}_2], \mathrm{tr}[\boldsymbol{U}_1^2\boldsymbol{U}_2], \mathrm{tr}[\boldsymbol{U}_1\boldsymbol{U}_2^2], \mathrm{tr}[\boldsymbol{U}_1^2\boldsymbol{U}_2^2], \\ &\mathrm{tr}[\boldsymbol{U}_1\boldsymbol{U}_3], \mathrm{tr}[\boldsymbol{U}_1^2\boldsymbol{U}_3], \mathrm{tr}[\boldsymbol{U}_1\boldsymbol{U}_3^2], \mathrm{tr}[\boldsymbol{U}_1^2\boldsymbol{U}_3^2], \mathrm{tr}[\boldsymbol{U}_2\boldsymbol{U}_3], \mathrm{tr}[\boldsymbol{U}_2^2\boldsymbol{U}_3], \mathrm{tr}[\boldsymbol{U}_2\boldsymbol{U}_3^2], \mathrm{tr}[\boldsymbol{U}_2^2\boldsymbol{U}_3^2] \,\big\} \,, \end{aligned} \tag{504}$$

and the relative invariants of each three argument tensors $\{\boldsymbol{A}, \boldsymbol{U}_1, \boldsymbol{U}_2\}$, $\{\boldsymbol{A}, \boldsymbol{U}_1, \boldsymbol{U}_3\}$, $\{\boldsymbol{A}, \boldsymbol{U}_2, \boldsymbol{U}_3\}$ and $\{\boldsymbol{U}_1, \boldsymbol{U}_2, \boldsymbol{U}_3\}$ such that

$$\big\{\, \mathrm{tr}[\boldsymbol{A}\boldsymbol{U}_1\boldsymbol{U}_2], \mathrm{tr}[\boldsymbol{A}\boldsymbol{U}_1\boldsymbol{U}_3], \mathrm{tr}[\boldsymbol{A}\boldsymbol{U}_2\boldsymbol{U}_3], \mathrm{tr}[\boldsymbol{U}_1\boldsymbol{U}_2\boldsymbol{U}_3] \,\big\} \,. \tag{505}$$

The invariants in Eqns. (503)–(505) are multiplicatively combined to obtained quadratic terms in $\boldsymbol{A}$, leading to the definition of an irreducible integrity basis as

$$\mathcal{I}_{\mathscr{C}_9} = \big\{\, \mathrm{tr}^2[\boldsymbol{A}], \mathrm{tr}[\boldsymbol{A}^2], \mathrm{tr}^2[\boldsymbol{A}\boldsymbol{U}_3^2], \mathrm{tr}[\boldsymbol{U}_1], \mathrm{tr}[\boldsymbol{A}]\,\mathrm{tr}[\boldsymbol{A}\boldsymbol{U}_3^2] \,\big\} \,, \tag{506}$$

where the following invariants are dropped as they can be expressed in terms of other invariants

$$\begin{aligned} &\mathrm{tr}[\boldsymbol{U}_1\boldsymbol{U}_3] = 0 \,, \\ &\mathrm{tr}[\boldsymbol{A}^2\boldsymbol{U}_3] = \frac{1}{2}\left(\frac{1}{2}\,\mathrm{tr}^2[\boldsymbol{A}] + \mathrm{tr}[\boldsymbol{A}^2]\right) + \frac{3}{4}\,\mathrm{tr}^2[\boldsymbol{A}\boldsymbol{U}_3] - \frac{1}{2}\,\mathrm{tr}[\boldsymbol{A}]\,\mathrm{tr}[\boldsymbol{A}\boldsymbol{U}_3] - \frac{2}{3}\,\mathrm{tr}[\boldsymbol{U}_1] \,, \\ &\boldsymbol{U}_3 = \boldsymbol{U}_3^2 \,. \end{aligned} \tag{507}$$

A scalar-valued potential can readily be written with the aid of Eqn. (506) as

$$\mathfrak{F} = \sum_{i=1}^{5} \mu_i I_i \,, \tag{508}$$

where $I_{1-5}$ are the elements of the integrity basis $\mathcal{I}_{\mathscr{C}_9}$ and $\mu_{1-5}$ are material constants. The second-order stress-like tensor $\boldsymbol{\mathcal{S}}$ can be expressed as

$$\begin{aligned} \boldsymbol{\mathcal{S}} = \mathfrak{F},_{\boldsymbol{A}} = \sum_{i=1}^{5} \mathfrak{F},_{I_i} I_{i,\,\boldsymbol{A}} = {} & 2\mu_1\,\mathrm{tr}[\boldsymbol{A}]\,\boldsymbol{1} + 2\mu_2\boldsymbol{A} + 2\mu_3\,\mathrm{tr}[\boldsymbol{A}\boldsymbol{U}_3]\boldsymbol{U}_3 \\ & + \mu_4\bar{\boldsymbol{\mathcal{S}}}_1 + \mu_5\big\{\,\mathrm{tr}[\boldsymbol{A}\boldsymbol{U}_3]\boldsymbol{1} + \mathrm{tr}[\boldsymbol{A}]\boldsymbol{U}_3\,\big\} \end{aligned} \,, \tag{509}$$

with $\bar{\boldsymbol{\mathcal{S}}}_1$ defined in Eqn. (496). Likewise, the fourth-order Hessian associated with the potential (508) is given by

$$\begin{aligned} \mathbb{F} = \mathfrak{F},_{\boldsymbol{A}\boldsymbol{A}} = {} & \sum_{i=1}^{5}\sum_{j=1}^{5} \mathfrak{F},_{I_i} I_{i,\boldsymbol{A}\boldsymbol{A}} + \mathfrak{F},_{I_i I_j} I_{i,\boldsymbol{A}} \otimes I_{j,\boldsymbol{A}} \\ = {} & 2\mu_1 \boldsymbol{1} \otimes \boldsymbol{1} + \mu_2\big\{(\boldsymbol{1} \oplus \boldsymbol{1}) + (\boldsymbol{1} \ominus \boldsymbol{1})\big\} + \mu_3 \boldsymbol{U}_3^2 \otimes \boldsymbol{U}_3^2 \\ & + \mu_4\bar{\mathbb{F}}_1 + \mu_5\big\{(\boldsymbol{1} \otimes \boldsymbol{U}_3) + (\boldsymbol{U}_3 \otimes \boldsymbol{1})\big\} \end{aligned} \,, \tag{510}$$

where $\bar{\mathbb{F}}_1$ is defined in Eqn. (498). For the choice of $\tilde{\boldsymbol{n}}, \boldsymbol{a}_{1-3}$ same as that of the $\mathscr{C}_8$ group, the coordinate form of the Hessian matrix looks

$$[\mathbb{F}] = \begin{bmatrix} \mathbb{F}_{1111} & \mathbb{F}_{1122} & \mathbb{F}_{1122} & 0 & 0 & 0 \\ & \mathbb{F}_{2222} & \mathbb{F}_{2233} & 0 & 0 & 0 \\ & & \mathbb{F}_{2222} & 0 & 0 & 0 \\ & & & \mathbb{F}_{1212} & 0 & 0 \\ & \text{sym.} & & & \mathbb{F}_{1212} & 0 \\ & & & & & \frac{1}{2}(\mathbb{F}_{2222} - \mathbb{F}_{2223}) \end{bmatrix} , \tag{511}$$

where

$$\mathbb{F}_{1111} = 2(\mu_1 + \mu_2 + \mu_3 + \mu_5) , \quad \mathbb{F}_{1122} = 2\mu_1 + \mu_5 ,$$

$$\mathbb{F}_{2222} = 2(\mu_1 + \mu_3 + \frac{9}{8}\mu_4) , \quad \mathbb{F}_{2223} = 2(\mu_1 + \frac{3}{8}\mu_4) , \tag{512}$$

$$\mathbb{F}_{1212} = \mu_3 ,$$

in terms of five material constants $\mu_{1-5}$.

## A.10. Cubic symmetry group $\mathscr{C}_{10}$

The *cubic* symmetry group $\mathscr{C}_{10}$ is characterised by the existence of three symmetric second-order tensors $\boldsymbol{A}, \boldsymbol{U}_1$ and $\boldsymbol{U}_2$, such that a general form of the scalar-valued potential can be specified as

$$\mathfrak{F} = \mathfrak{F}(\boldsymbol{A}, \boldsymbol{U}_1, \boldsymbol{U}_2) , \tag{513}$$

with

$$\boldsymbol{U}_1 = \left( \sum_{i=1}^{3} \boldsymbol{a}_i \otimes \boldsymbol{a}_i \otimes \boldsymbol{a}_i \otimes \boldsymbol{a}_i \right) : \boldsymbol{A}$$

$$\boldsymbol{U}_2 = \left( \sum_{i=1}^{3} \boldsymbol{a}_i \otimes \boldsymbol{a}_i \otimes \boldsymbol{a}_i \otimes \boldsymbol{a}_i \right) : \boldsymbol{A}^2 \tag{514}$$

where $\boldsymbol{a}_{1-3}$ denote three unit vectors which are orthogonal to each other. With reference to Table 11, the functional basis for the $\mathscr{C}_{10}$ group comprises of the basic invariants of the arguments $\boldsymbol{A}, \boldsymbol{U}_1$ and $\boldsymbol{U}_2$, namely

$$\left\{ \text{tr}[\boldsymbol{A}], \text{tr}[\boldsymbol{A}^2], \text{tr}[\boldsymbol{A}^3], \text{tr}[\boldsymbol{U}_1], \text{tr}[\boldsymbol{U}_1^2], \text{tr}[\boldsymbol{U}_1^3], \text{tr}[\boldsymbol{U}_2], \text{tr}[\boldsymbol{U}_2^2], \text{tr}[\boldsymbol{U}_2^3] \right\} , \tag{515}$$

together with the mixed invariants of $\{\boldsymbol{A}, \boldsymbol{U}_1\}$, $\{\boldsymbol{A}, \boldsymbol{U}_2\}$ and $\{\boldsymbol{U}_1, \boldsymbol{U}_2\}$ given by

$$\left\{ \text{tr}[\boldsymbol{A}\boldsymbol{U}_1], \text{tr}[\boldsymbol{A}^2\boldsymbol{U}_1], \text{tr}[\boldsymbol{A}\boldsymbol{U}_1^2], \text{tr}[\boldsymbol{A}^2\boldsymbol{U}_1^2], \text{tr}[\boldsymbol{A}\boldsymbol{U}_2], \text{tr}[\boldsymbol{A}^2\boldsymbol{U}_2], \right.$$

$$\left. \text{tr}[\boldsymbol{A}\boldsymbol{U}_2^2], \text{tr}[\boldsymbol{A}^2\boldsymbol{U}_2^2], \text{tr}[\boldsymbol{U}_1\boldsymbol{U}_2], \text{tr}[\boldsymbol{U}_1^2\boldsymbol{U}_2], \text{tr}[\boldsymbol{U}_1\boldsymbol{U}_2^2], \text{tr}[\boldsymbol{U}_1^2\boldsymbol{U}_2^2] \right\} , \tag{516}$$

and the relative invariants of all the three argument tensors $\{\boldsymbol{A}, \boldsymbol{U}_1, \boldsymbol{U}_2\}$ such that

$$\left\{ \text{tr}[\boldsymbol{A}\boldsymbol{U}_1\boldsymbol{U}_2] \right\} . \tag{517}$$

A possible complete and irreducible integrity basis can be defined by multiplicatively combining the invariants in Eqns. (515)–(517) as

$$\mathcal{I}_{\mathscr{C}_{10}} = \left\{ \text{tr}^2[\boldsymbol{A}], \text{tr}[\boldsymbol{A}^2], \text{tr}[\boldsymbol{U}_1^2] \right\} , \tag{518}$$

where the following equalities are already taken into account

$$
\begin{aligned}
\text{tr}[\boldsymbol{A}] &= \text{tr}[\boldsymbol{U}_1] \ , \\
\text{tr}[\boldsymbol{A}^2] &= \text{tr}[\boldsymbol{U}_2] \ , \\
\text{tr}[\boldsymbol{U}_1^2] &= \text{tr}[\boldsymbol{A}\boldsymbol{U}_1] \ .
\end{aligned} \tag{519}
$$

Equation (518) allows for the definition of a scalar-valued potential as

$$
\mathfrak{F} = \sum_{i=1}^{3} \mu_i I_i \ , \tag{520}
$$

where $I_{1-3}$ are the elements of the integrity basis $\mathcal{I}_{\mathscr{C}_{10}}$ and $\mu_{1-3}$ are material constants. The second-order stress-like tensor $\boldsymbol{S}$ is given by

$$
\boldsymbol{S} = \mathfrak{F},_{\boldsymbol{A}} = \sum_{i=1}^{3} \mathfrak{F},_{I_i} I_{i,\,\boldsymbol{A}} = 2\mu_1 \,\text{tr}[\boldsymbol{A}]\boldsymbol{1} + 2\mu_2 \boldsymbol{A} + 2\mu_3 \bar{\boldsymbol{S}}_1 \quad , \tag{521}
$$

with $\bar{\boldsymbol{S}}_1$ defined analogous to Eqn. $(468)_1$. Likewise, the fourth-order Hessian is given by

$$
\begin{aligned}
\mathbb{F} = \mathfrak{F},_{\boldsymbol{A}\boldsymbol{A}} &= \sum_{i=1}^{3}\sum_{j=1}^{3} \mathfrak{F},_{I_i} I_{i,\boldsymbol{A}\boldsymbol{A}} + \mathfrak{F},_{I_i I_j} I_{i,\boldsymbol{A}} \otimes I_{j,\boldsymbol{A}} \\
&= 2\mu_1 \boldsymbol{1} \otimes \boldsymbol{1} + \mu_2\big\{(\boldsymbol{1} \oplus \boldsymbol{1}) + (\boldsymbol{1} \ominus \boldsymbol{1})\big\} + \mu_3 \bar{\mathbb{F}}_1
\end{aligned} \tag{522}
$$

where $\bar{\mathbb{F}}_1$ is defined similar to Eqn. $(470)_1$. For the choice $\boldsymbol{a}_1 = [1,0,0]^T$, $\boldsymbol{a}_2 = [0,1,0]^T$ and $\boldsymbol{a}_3 = [0,0,1]^T$, the fourth-order Hessian $\mathbb{F}$ appears in the coordinate form

$$
[\mathbb{F}] = \begin{bmatrix}
\mathbb{F}_{1111} & \mathbb{F}_{1122} & \mathbb{F}_{1122} & 0 & 0 & 0 \\
 & \mathbb{F}_{1111} & \mathbb{F}_{1122} & 0 & 0 & 0 \\
 & & \mathbb{F}_{1111} & 0 & 0 & 0 \\
 & & & \mathbb{F}_{1212} & 0 & 0 \\
 & \text{sym.} & & & \mathbb{F}_{1212} & 0 \\
 & & & & & \mathbb{F}_{1212}
\end{bmatrix} \ , \tag{523}
$$

with the individual components

$$
\mathbb{F}_{1111} = 2(\mu_1 + \mu_2 + \mu_3) \ , \quad \mathbb{F}_{1122} = 2\mu_1 \ , \quad \mathbb{F}_{1212} = \mu_2 \ , \tag{524}
$$

in terms of three material constants $\mu_{1-3}$.

## A.11.  Cubic symmetry group $\mathscr{C}_{11}$

The second *cubic* symmetry group $\mathscr{C}_{11}$ is characterised by the existence of two symmetric second-order tensors $\boldsymbol{A},\boldsymbol{U}$ and a single skew-symmetric second-order tensor $\boldsymbol{V}$, which allow to specify a general form of the scalar-valued potential as

$$
\mathfrak{F} = \mathfrak{F}(\boldsymbol{A},\boldsymbol{U},\boldsymbol{V}) \ , \tag{525}
$$

with

$$
\begin{aligned}
\boldsymbol{U} = \Big\{ &(\boldsymbol{a}_1 \otimes \boldsymbol{a}_1 \otimes \boldsymbol{a}_2 \otimes \boldsymbol{a}_2 - \boldsymbol{a}_2 \otimes \boldsymbol{a}_2 \otimes \boldsymbol{a}_1 \otimes \boldsymbol{a}_1) \\
&-(\boldsymbol{a}_1 \otimes \boldsymbol{a}_1 \otimes \boldsymbol{a}_3 \otimes \boldsymbol{a}_3 - \boldsymbol{a}_3 \otimes \boldsymbol{a}_3 \otimes \boldsymbol{a}_1 \otimes \boldsymbol{a}_1) \\
&-(\boldsymbol{a}_2 \otimes \boldsymbol{a}_2 \otimes \boldsymbol{a}_3 \otimes \boldsymbol{a}_3 - \boldsymbol{a}_3 \otimes \boldsymbol{a}_3 \otimes \boldsymbol{a}_2 \otimes \boldsymbol{a}_2) \Big\} : \boldsymbol{A}
\end{aligned}
$$

$$
\begin{aligned}
\boldsymbol{V} = \Big\{ &\epsilon \boldsymbol{a}_1 \otimes (\boldsymbol{a}_2 \otimes \boldsymbol{a}_3 + \boldsymbol{a}_3 \otimes \boldsymbol{a}_2) \\
&+\epsilon \boldsymbol{a}_2 \otimes (\boldsymbol{a}_1 \otimes \boldsymbol{a}_3 + \boldsymbol{a}_3 \otimes \boldsymbol{a}_1) \\
&+\epsilon \boldsymbol{a}_3 \otimes (\boldsymbol{a}_1 \otimes \boldsymbol{a}_2 + \boldsymbol{a}_2 \otimes \boldsymbol{a}_1) \Big\} : \boldsymbol{A}
\end{aligned}
\tag{526}
$$

The functional basis for the $\mathscr{C}_{11}$ group comprises of the basic invariants of the arguments $\boldsymbol{A}, \boldsymbol{U}$ and $\boldsymbol{V}$, namely

$$
\big\{ \operatorname{tr}[\boldsymbol{A}], \operatorname{tr}[\boldsymbol{A}^2], \operatorname{tr}[\boldsymbol{A}^3], \operatorname{tr}[\boldsymbol{U}], \operatorname{tr}[\boldsymbol{U}^2], \operatorname{tr}[\boldsymbol{U}^3], \operatorname{tr}[\boldsymbol{V}^2] \big\} \; .
\tag{527}
$$

Additionally, the mixed invariants of $\{\boldsymbol{A}, \boldsymbol{U}\}$, $\{\boldsymbol{A}, \boldsymbol{V}\}$ and $\{\boldsymbol{U}, \boldsymbol{V}\}$ are given by

$$
\begin{aligned}
\big\{ &\operatorname{tr}[\boldsymbol{AU}], \operatorname{tr}[\boldsymbol{A}^2\boldsymbol{U}], \operatorname{tr}[\boldsymbol{AU}^2], \operatorname{tr}[\boldsymbol{A}^2\boldsymbol{U}^2], \operatorname{tr}[\boldsymbol{AV}^2], \operatorname{tr}[\boldsymbol{A}^2\boldsymbol{V}^2], \operatorname{tr}[\boldsymbol{A}^2\boldsymbol{V}^2\boldsymbol{AV}], \\
&\operatorname{tr}[\boldsymbol{UV}^2], \operatorname{tr}[\boldsymbol{U}^2\boldsymbol{V}^2], \operatorname{tr}[\boldsymbol{U}^2\boldsymbol{V}^2\boldsymbol{UV}] \big\} \; ,
\end{aligned}
\tag{528}
$$

and the relative invariants of each three argument tensors $\{\boldsymbol{A}, \boldsymbol{U}, \boldsymbol{V}\}$ are given by

$$
\big\{ \operatorname{tr}[\boldsymbol{AUV}], \operatorname{tr}[\boldsymbol{A}^2\boldsymbol{UV}], \operatorname{tr}[\boldsymbol{AU}^2\boldsymbol{V}], \operatorname{tr}[\boldsymbol{AV}^2\boldsymbol{UV}], \big\} \; .
\tag{529}
$$

It can be easily verified that the following linear dependencies are valid for the $\mathscr{C}_{11}$ group

$$
\operatorname{tr}[\boldsymbol{V}^2] = \frac{4}{3} \big( \operatorname{tr}^2[\boldsymbol{A}] + \operatorname{tr}[\boldsymbol{U}^2] \big) - 4 \operatorname{tr}[\boldsymbol{A}^2] \; ,
$$

$$
\operatorname{tr}[\boldsymbol{U}] = 0 \quad \text{and} \quad \operatorname{tr}^2[\boldsymbol{AU}] = 0 \; .
\tag{530}
$$

An irreducible integrity basis for the $\mathscr{C}_8$ symmetry group can be defined as

$$
\mathcal{I}_{\mathscr{C}_{11}} = \big\{ \operatorname{tr}^2[\boldsymbol{A}], \operatorname{tr}[\boldsymbol{A}^2], \operatorname{tr}[\boldsymbol{U}^2] \big\} \; ,
\tag{531}
$$

which allows for the the definition of a scalar-valued potential as

$$
\mathfrak{F} = \sum_{i=1}^{3} \mu_i I_i \; ,
\tag{532}
$$

where $I_{1-3}$ are the elements of the integrity basis $\mathcal{I}_{\mathscr{C}_{11}}$ and $\mu_{1-3}$ are material constants. The second-order stress-like tensor $\boldsymbol{S}$ is given by

$$
\boldsymbol{S} = \mathfrak{F},_{\boldsymbol{A}} = \sum_{i=1}^{3} \mathfrak{F},_{I_i} I_i,_{\boldsymbol{A}} = 2\mu_1 \operatorname{tr}[\boldsymbol{A}]\boldsymbol{1} + 2\mu_2 \boldsymbol{A} + 2\mu_3 \bar{\boldsymbol{S}}_1 \; ,
\tag{533}
$$

with $\bar{\boldsymbol{S}}_1$ defined analogous to Eqn. $(468)_1$. Likewise, the fourth-order Hessian is given by

$$
\begin{aligned}
\mathbb{F} = \mathfrak{F},_{\boldsymbol{AA}} &= \sum_{i=1}^{3} \sum_{j=1}^{3} \mathfrak{F},_{I_i} I_{i,\boldsymbol{AA}} + \mathfrak{F},_{I_i I_j} I_{i,\boldsymbol{A}} \otimes I_{j,\boldsymbol{A}} \\
&= 2\mu_1 \boldsymbol{1} \otimes \boldsymbol{1} + \mu_2 \big\{ (\boldsymbol{1} \oplus \boldsymbol{1}) + (\boldsymbol{1} \ominus \boldsymbol{1}) \big\} + \mu_3 \bar{\mathbb{F}}_1
\end{aligned}
\tag{534}
$$

where $\bar{\mathbb{F}}_1$ is defined similar to Eqn. $(470)_1$. For the choice $\boldsymbol{a}_1 = [1,0,0]^T$, $\boldsymbol{a}_2 = [0,1,0]^T$ and $\boldsymbol{a}_3 = [0,0,1]^T$, the fourth-order Hessian $\mathbb{F}$ appears in the coordinate form

$$[\mathbb{F}] = \begin{bmatrix} \mathbb{F}_{1111} & \mathbb{F}_{1122} & \mathbb{F}_{1122} & 0 & 0 & 0 \\ & \mathbb{F}_{1111} & \mathbb{F}_{1122} & 0 & 0 & 0 \\ & & \mathbb{F}_{1111} & 0 & 0 & 0 \\ & & & \mathbb{F}_{1212} & 0 & 0 \\ & \text{sym.} & & & \mathbb{F}_{1212} & 0 \\ & & & & & \mathbb{F}_{1212} \end{bmatrix}, \tag{535}$$

with the individual components

$$\mathbb{F}_{1111} = 2(\mu_1 + \mu_2 + 2\mu_3)\,, \quad \mathbb{F}_{1122} = 2(\mu_1 - \mu_2 + \mu_3)\,, \quad \mathbb{F}_{1212} = \mu_2\,, \tag{536}$$

in terms of three material constants $\mu_{1-3}$.

## A.12. Transversely isotropic symmetry group $\mathscr{C}_{12}$

The *transversely isotropic* symmetry group $\mathscr{C}_{12}$ is characterised by the existence of two skew-symmetric second-order tensors $\boldsymbol{A}$ and $\boldsymbol{V}$, based on which a general form of the scalar-valued potential can be specified as

$$\mathfrak{F} = \mathfrak{F}(\boldsymbol{A}, \boldsymbol{V}) \quad \text{with} \quad \boldsymbol{V} = \boldsymbol{\epsilon}\tilde{\boldsymbol{n}}\,, \tag{537}$$

where $\tilde{\boldsymbol{n}}$ denotes a unit normal vector. The functional basis for the $\mathscr{C}_{12}$ symmetry group, with reference to Table 11, consists of the basic invariants of the two arguments $\boldsymbol{A}$ and $\boldsymbol{V}$ such that

$$\left\{ \mathrm{tr}[\boldsymbol{A}], \mathrm{tr}[\boldsymbol{A}^2], \mathrm{tr}[\boldsymbol{A}^3], \mathrm{tr}[\boldsymbol{V}^2] \right\}\,, \tag{538}$$

the mixed invariants of $\{\boldsymbol{A}, \boldsymbol{V}\}$ given by

$$\left\{ \mathrm{tr}[\boldsymbol{A}\boldsymbol{V}^2], \mathrm{tr}[\boldsymbol{A}^2\boldsymbol{V}^2] \right\}\,. \tag{539}$$

With no linear dependencies, an irreducible integrity basis for this symmetry group can be specified by multiplicatively combining the invariants in Eqns. (538)–(539) as

$$\mathcal{I}_{\mathscr{C}_{12}} = \left\{ \mathrm{tr}^2[\boldsymbol{A}], \mathrm{tr}[\boldsymbol{A}^2], \mathrm{tr}^2[\boldsymbol{A}\boldsymbol{V}^2], \mathrm{tr}[\boldsymbol{A}]\,\mathrm{tr}[\boldsymbol{A}\boldsymbol{V}^2], \mathrm{tr}[\boldsymbol{A}^2\boldsymbol{V}^2] \right\}\,, \tag{540}$$

which allows for the definition of a scalar-valued potential as

$$\mathfrak{F} = \sum_{i=1}^{5} \mu_i I_i\,, \tag{541}$$

where $I_{1-5}$ are the elements of the integrity basis $\mathcal{I}_{\mathscr{C}_{12}}$ and $\mu_{1-5}$ are material constants. Given the potential (541), the second-order stress-like tensor $\boldsymbol{\mathsf{S}}$ can be expressed as

$$\boldsymbol{\mathsf{S}} = \mathfrak{F}_{,\boldsymbol{A}} = \sum_{i=1}^{5} \mathfrak{F}_{,I_i} I_{i,\boldsymbol{A}} = 2\mu_1 \mathrm{tr}[\boldsymbol{A}]\boldsymbol{1} + 2\mu_2 \boldsymbol{A} + 2\mu_3 \mathrm{tr}[\boldsymbol{A}\boldsymbol{V}^2]\boldsymbol{V}^2$$
$$+ \mu_4\{\boldsymbol{A}\boldsymbol{V}^2 + \boldsymbol{V}^2\boldsymbol{A}\} + \mu_5\{\mathrm{tr}[\boldsymbol{A}]\boldsymbol{V}^2 + \mathrm{tr}[\boldsymbol{A}\boldsymbol{V}^2]\boldsymbol{1}\} \tag{542}$$

Likewise, the constant fourth-order Hessian can be expressed as

$$
\begin{aligned}
\mathbb{F} = \mathfrak{F},_{\boldsymbol{A}\boldsymbol{A}} =& \sum_{i=1}^{5}\sum_{j=1}^{5} \mathfrak{F},_{I_i} I_{i,\boldsymbol{A}\boldsymbol{A}} + \mathfrak{F},_{I_i I_j} I_{i,\boldsymbol{A}} \otimes I_{j,\boldsymbol{A}} \\
=& 2\mu_1 \boldsymbol{1} \otimes \boldsymbol{1} + \mu_2\{(\boldsymbol{1} \oplus \boldsymbol{1}) + (\boldsymbol{1} \ominus \boldsymbol{1})\} + \mu_3 \boldsymbol{V}^2 \otimes \boldsymbol{V}^2 \\
&+ \mu_4\{(\boldsymbol{1} \otimes \boldsymbol{V}^2) + (\boldsymbol{V}^2 \otimes \boldsymbol{1})\} \\
&+ \frac{\mu_5}{2}\{(\boldsymbol{1} \oplus \boldsymbol{V}^2) + (\boldsymbol{1} \ominus \boldsymbol{V}^2) + (\boldsymbol{V}^2 \oplus \boldsymbol{1}) + (\boldsymbol{V}^2 \ominus \boldsymbol{1})\}
\end{aligned} \quad , \tag{543}
$$

which for the choice of $\tilde{\boldsymbol{n}} = [1,0,0]^T$ appears in the coordinate form

$$
[\mathbb{F}] = \begin{bmatrix}
\mathbb{F}_{1111} & \mathbb{F}_{1122} & \mathbb{F}_{1122} & 0 & 0 & 0 \\
 & \mathbb{F}_{2222} & \mathbb{F}_{2233} & 0 & 0 & 0 \\
 & & \mathbb{F}_{2222} & 0 & 0 & 0 \\
 & & & \mathbb{F}_{1212} & 0 & 0 \\
 & \text{sym.} & & & \mathbb{F}_{1212} & 0 \\
 & & & & & \frac{1}{2}(\mathbb{F}_{2222} - \mathbb{F}_{2223})
\end{bmatrix} , \tag{544}
$$

with the individual components

$$
\mathbb{F}_{1111} = 2(\mu_1 + \mu_4) , \quad \mathbb{F}_{1122} = 2\mu_1 - \mu_3 ,
$$

$$
\mathbb{F}_{2222} = 2(\mu_1 + \mu_2 - \mu_3 + \mu_4 - \mu_5) , \quad \mathbb{F}_{2233} = 2(\mu_1 + \mu_2 - \mu_3) , \tag{545}
$$

$$
\mathbb{F}_{1212} = \mu_4 - \frac{\mu_5}{2}
$$

in terms of five material constants $\mu_{1-5}$.

### A.13. Transversely isotropic symmetry group $\mathscr{C}_{13}$

The constitutive expressions of the second *transversely isotropic* symmetry group $\mathscr{C}_{13}$ are obtained from those of $\mathscr{C}_{12}$ by replacing the skew-symmetric tensor $\boldsymbol{V}$ with a symmetric tensor $\boldsymbol{U}$, such that the scalar-valued potential takes the form

$$
\mathfrak{F} = \mathfrak{F}(\boldsymbol{A}, \boldsymbol{U}) \quad \text{with} \quad \boldsymbol{U} = \tilde{\boldsymbol{n}} \otimes \tilde{\boldsymbol{n}} , \tag{546}
$$

where $\tilde{\boldsymbol{n}}$ denotes a unit normal vector. The functional basis for the $\mathscr{C}_{13}$ symmetry group, with reference to Table 11, consists of the basic invariants of the two arguments $\boldsymbol{A}$ and $\boldsymbol{U}$ such that

$$
\{\operatorname{tr}[\boldsymbol{A}], \operatorname{tr}[\boldsymbol{A}^2], \operatorname{tr}[\boldsymbol{A}^3], \operatorname{tr}[\boldsymbol{U}], \operatorname{tr}[\boldsymbol{U}^2], \operatorname{tr}[\boldsymbol{U}^3], \} , \tag{547}
$$

the mixed invariants of $\{\boldsymbol{A}, \boldsymbol{U}\}$ given by

$$
\{\operatorname{tr}[\boldsymbol{A}\boldsymbol{U}], \operatorname{tr}[\boldsymbol{A}^2\boldsymbol{U}], \operatorname{tr}[\boldsymbol{A}\boldsymbol{U}^2], \operatorname{tr}[\boldsymbol{A}^2\boldsymbol{U}^2]\} . \tag{548}
$$

An irreducible integrity basis for the $\mathscr{C}_{13}$ symmetry group can be specified by multiplicatively combining the invariants in Eqns. (547)–(548) as

$$
\mathcal{I}_{\mathscr{C}_{13}} = \{\operatorname{tr}^2[\boldsymbol{A}], \operatorname{tr}[\boldsymbol{A}^2], \operatorname{tr}^2[\boldsymbol{A}\boldsymbol{U}], \operatorname{tr}[\boldsymbol{A}^2\boldsymbol{U}], \operatorname{tr}[\boldsymbol{A}] \operatorname{tr}[\boldsymbol{A}\boldsymbol{U}]\} , \tag{549}
$$

where the following linear dependencies are already taken into account

$$\text{tr}[\boldsymbol{AU}] = \text{tr}[\boldsymbol{AU}^2] \quad \text{and} \quad \text{tr}[\boldsymbol{A}^2\boldsymbol{U}] = \text{tr}[\boldsymbol{A}^2\boldsymbol{U}^2] \ . \tag{550}$$

The explicit form of the scalar-valued potential is given by

$$\mathfrak{F} = \sum_{i=1}^{5} \mu_i I_i \ , \tag{551}$$

where $I_{1-5}$ are the elements of the integrity basis $\mathcal{I}_{\mathscr{C}_{13}}$ and $\mu_{1-5}$ are material constants. The second-order stress-like tensor $\boldsymbol{S}$ is expressed as

$$\boldsymbol{S} = \mathfrak{F}_{,\boldsymbol{A}} = \sum_{i=1}^{5} \mathfrak{F}_{,I_i} I_{i,\boldsymbol{A}} = 2\mu_1 \text{tr}[\boldsymbol{A}]\boldsymbol{1} + 2\mu_2\boldsymbol{A} + 2\mu_3 \text{tr}[\boldsymbol{AU}]\boldsymbol{U} \\ + \mu_4\{\boldsymbol{AU} + \boldsymbol{UA}\} + \mu_5\{\text{tr}[\boldsymbol{A}]\boldsymbol{U} + \text{tr}[\boldsymbol{AU}]\boldsymbol{1}\} \ . \tag{552}$$

Likewise, the constant fourth-order Hessian is given by

$$\begin{aligned} \mathbb{F} = \mathfrak{F}_{,\boldsymbol{AA}} &= \sum_{i=1}^{5}\sum_{j=1}^{5} \mathfrak{F}_{,I_i} I_{i,\boldsymbol{AA}} + \mathfrak{F}_{,I_iI_j} I_{i,\boldsymbol{A}} \otimes I_{j,\boldsymbol{A}} \\ &= 2\mu_1\boldsymbol{1}\otimes\boldsymbol{1} + \mu_2\{(\boldsymbol{1}\oplus\boldsymbol{1}) + (\boldsymbol{1}\ominus\boldsymbol{1})\} + \mu_3\boldsymbol{U}\otimes\boldsymbol{U} \\ &+ \mu_4\{(\boldsymbol{1}\otimes\boldsymbol{U}) + (\boldsymbol{U}\otimes\boldsymbol{1})\} \\ &+ \frac{\mu_5}{2}\{(\boldsymbol{1}\oplus\boldsymbol{U}) + (\boldsymbol{1}\ominus\boldsymbol{U}) + (\boldsymbol{U}\oplus\boldsymbol{1}) + (\boldsymbol{U}\ominus\boldsymbol{1})\} \end{aligned} \ , \tag{553}$$

which appears in the coordinate form for the choice of $\tilde{\boldsymbol{n}} = [1,0,0]^T$ as

$$[\mathbb{F}] = \begin{bmatrix} \mathbb{F}_{1111} & \mathbb{F}_{1122} & \mathbb{F}_{1122} & 0 & 0 & 0 \\ & \mathbb{F}_{2222} & \mathbb{F}_{2233} & 0 & 0 & 0 \\ & & \mathbb{F}_{2222} & 0 & 0 & 0 \\ & & & \mathbb{F}_{1212} & 0 & 0 \\ & \text{sym.} & & & \mathbb{F}_{1212} & 0 \\ & & & & & \frac{1}{2}(\mathbb{F}_{2222} - \mathbb{F}_{2223}) \end{bmatrix} \ , \tag{554}$$

with the individual components

$$\begin{aligned} \mathbb{F}_{1111} &= 2\sum_{i=1}^{5}\mu_i \ , & \mathbb{F}_{1122} &= 2\mu_1 + \mu_3 \ , \\ \mathbb{F}_{2222} &= 2(\mu_1 + \mu_4) \ , & \mathbb{F}_{2233} &= 2\mu_1 \ , \\ \mathbb{F}_{1212} &= \mu_4 + \frac{\mu_5}{2} \end{aligned} \tag{555}$$

in terms of five material constants $\mu_{1-5}$.

### A.14. Isotropic symmetry group $\mathscr{C}_{14}$

The *isotropic* symmetry group $\mathscr{C}_{14}$, generated by $\mathcal{O}(3)$, is characterised by the existence of a single symmetric second-order argument tensor $\boldsymbol{A}$ such that

$$\mathfrak{F} = \mathfrak{F}(\boldsymbol{A}) \ . \tag{556}$$

With reference to Table 11, the functional basis for the isotropic symmetry group comprises only of the basic invariants of the argument $\boldsymbol{A}$ namely

$$\left\{ \operatorname{tr}[\boldsymbol{A}], \operatorname{tr}[\boldsymbol{A}^2], \operatorname{tr}[\boldsymbol{A}^3] \right\} \ , \tag{557}$$

which allows to specify an irreducible integrity basis for the $\mathscr{C}_{14}$ symmetry group as

$$\mathcal{I}_{\mathscr{C}_{14}} = \left\{ \operatorname{tr}^2[\boldsymbol{A}], \operatorname{tr}[\boldsymbol{A}^2] \right\} \ , \tag{558}$$

based on which the explicit form of the scalar-valued potential is given by

$$\mathfrak{F} = \sum_{i=1}^{2} \mu_i I_i \ , \tag{559}$$

where $I_{1-2}$ are the elements of the integrity basis $\mathcal{I}_{\mathscr{C}_{14}}$ and $\mu_{1-2}$ are material constants. The second-order stress-like tensor $\boldsymbol{S}$ is expressed as

$$\boldsymbol{S} = \mathfrak{F},_{\boldsymbol{A}} = \sum_{i=1}^{2} \mathfrak{F},_{I_i} I_i,_{\boldsymbol{A}} = 2\mu_1 \operatorname{tr}[\boldsymbol{A}]\boldsymbol{1} + 2\mu_2 \boldsymbol{A} \ , \tag{560}$$

and the constant fourth-order Hessian is given by

$$\begin{aligned} \mathbb{F} = \mathfrak{F},_{\boldsymbol{AA}} &= \sum_{i=1}^{2}\sum_{j=1}^{2} \mathfrak{F},_{I_i} I_{i,\boldsymbol{AA}} + \mathfrak{F},_{I_i I_j} I_{i,\boldsymbol{A}} \otimes I_{j,\boldsymbol{A}} \\ &= 2\mu_1 \boldsymbol{1} \otimes \boldsymbol{1} + \mu_2 \left\{ (\boldsymbol{1} \oplus \boldsymbol{1}) + (\boldsymbol{1} \ominus \boldsymbol{1}) \right\} \end{aligned} \ , \tag{561}$$

which can be equivalently expressed in the coordinate form as

$$[\mathbb{F}] = \begin{bmatrix} \mathbb{F}_{1111} & \mathbb{F}_{1111} - 2\mathbb{F}_{2222} & \mathbb{F}_{1111} - 2\mathbb{F}_{2222} & 0 & 0 & 0 \\ & \mathbb{F}_{1111} & \mathbb{F}_{1111} - 2\mathbb{F}_{2222} & 0 & 0 & 0 \\ & & \mathbb{F}_{1111} & 0 & 0 & 0 \\ & & & \mathbb{F}_{2222} & 0 & 0 \\ & \text{sym.} & & & \mathbb{F}_{2222} & 0 \\ & & & & & \mathbb{F}_{2222} \end{bmatrix} \ , \tag{562}$$

with the individual components

$$\mathbb{F}_{1111} = 2(\mu_1 + \mu_2) \quad \text{and} \quad \mathbb{F}_{2222} = \mu_2 \ , \tag{563}$$

in terms of two material constants $\mu_{1-2}$.

# B. Comparison to Hill's orthotropic yield criterion

In this appendix, the orthotropic yield function proposed by Hill [25] within the framework of infinitesimal deformations is compared with the yield function in Eqn. (279). Setting $\varkappa_1 = 0$, $\kappa = 0$, $\boldsymbol{\beta} = \boldsymbol{0}$, and choosing $\boldsymbol{a}_1 = [1,0,0]^T$ and $\boldsymbol{a}_2 = [0,1,0]^T$, the latter reformulates to the component form

$$\chi = \left[ \frac{9\varkappa_2}{4} \frac{(2\sigma_{33} - \sigma_{11} - \sigma_{22})^2}{9} + 2\varkappa_3 \tau_{12}^2 + 2\varkappa_4 \tau_{13}^2 + 2\varkappa_5 \tau_{23}^2 \right]^{1/2} - 1 \ . \tag{564}$$

Now, it can be trivially verified that

$$\frac{(2\sigma_{33} - \sigma_{11} - \sigma_{22})^2}{9} = \frac{2}{9}(\sigma_{22} - \sigma_{33})^2 + \frac{2}{9}(\sigma_{33} - \sigma_{11})^2 - \frac{1}{9}(\sigma_{11} - \sigma_{22})^2 \ . \tag{565}$$

Inserting the above identity into Eqn. (564) yields

$$\chi = \left[ \frac{\varkappa_2}{2}(\sigma_{22} - \sigma_{33})^2 + \frac{\varkappa_2}{2}(\sigma_{33} - \sigma_{11})^2 - \frac{\varkappa_2}{4}(\sigma_{11} - \sigma_{22})^2 + 2\varkappa_3 \tau_{12}^2 + 2\varkappa_4 \tau_{13}^2 + 2\varkappa_5 \tau_{23}^2 \right]^{1/2} - 1 \ . \tag{566}$$

The yield function proposed by Hill [25, Chapter XII] reads

$$\chi = \left[ F(\sigma_{22} - \sigma_{33})^2 + G(\sigma_{33} - \sigma_{11})^2 + H(\sigma_{11} - \sigma_{22})^2 + 2L\tau_{23}^2 + 2M\tau_{13}^2 + 2N\tau_{12}^2 \right]^{1/2} - 1 \ , \tag{567}$$

where $F, G, H, L, M$ and $N$ are the six parameters governing the orthotropic plastic yielding. A direct comparison of Eqns. (566) and (567) gives the equalities

$$F = G = \frac{\varkappa_2}{2}, \ H = -\frac{\varkappa_2}{4}, \ L = \varkappa_5, \ M = \varkappa_4 \quad \text{and} \quad N = \varkappa_3 \ , \tag{568}$$

see also [77] for a higher-order generalisation of the yield function.

## C. Extension to coupled thermoplasticity

In this appendix, a general framework for the analysis of coupled thermo-mechanical boundary value problems of anisotropic thermoplasticity is discussed. An infinitesimal anisotropic thermoplasticity model is presented to describe the temperature-dependent elastic and plastic response at the continuum level. The constitutive response functions of the presented model are straightforward extensions of those described in **Chapter 5**. Additionally, the algorithmic treatment of the model is provided which is slightly complicated than that discussed in **Chapter 5**, but yields a structure that is very useful for coupled problems. Non-local constitutive formulation of this problem has been recently explored in [73], with an emphasis on the isotropic response. In this work, anisotropic effects are incorporated while restricting to the local theory.

Following [73], a decoupled scalar energetic potential reads

$$\psi(\boldsymbol{\varepsilon} - \boldsymbol{\varepsilon}^p, \xi, \boldsymbol{\alpha}, \Theta) = \psi^e(\boldsymbol{\varepsilon} - \boldsymbol{\varepsilon}^p) + \psi^{th-e}(\boldsymbol{\varepsilon} - \boldsymbol{\varepsilon}^p, \Theta) + \psi^{th-p}(\xi, \boldsymbol{\alpha}, \Theta) + \psi^{th}(\Theta) , \quad (569)$$

in terms of an elastic, thermo-elastic, thermo-plastic and a purely thermal part. The individual contributions can be expressed as

$$\psi^e(\boldsymbol{\varepsilon} - \boldsymbol{\varepsilon}^p) = \frac{1}{2} \|\boldsymbol{\varepsilon} - \boldsymbol{\varepsilon}^p\|_{\mathbb{E}}^2 ,$$

$$\psi^{th-e}(\boldsymbol{\varepsilon} - \boldsymbol{\varepsilon}^p, \Theta) = -(\boldsymbol{\varepsilon} - \boldsymbol{\varepsilon}^p) : \mathbb{E} : \boldsymbol{\alpha}_t(\Theta - \Theta_0) ,$$

$$\psi^{th-p}(\xi, \boldsymbol{\alpha}, \Theta) = \frac{h(\Theta)}{n+1}(\bar{\xi} + \xi)^{n+1} + \frac{1}{2} \|\boldsymbol{\alpha}\|_{\mathsf{H}(\Theta)}^2 ,$$

$$\psi^{th}(\Theta) = \mathfrak{c}\Big[(\Theta - \Theta_0) - \Theta \ln[\Theta/\Theta_0]\Big] ,$$

(570)

where $\mathbb{E}$ is of the form in Eqn. (202), $\boldsymbol{\alpha}_t$ is a second-order tensor that contains the coefficients of thermal expansion and $\Theta_0$ is the reference temperature of the body. The temperature dependent isotropic hardening modulus $h(\Theta)$ is defined following [72] as

$$h(\Theta) = h[1 - w_h(\Theta - \Theta_0)] . \quad (571)$$

To express the temperature dependent anisotropic kinematic hardening modulus $\mathsf{H}(\Theta)$, a second-order anisotropy tensor is defined following [140] as

$$\mathbf{T} = w_{h_1}(\boldsymbol{a}_1 \otimes \boldsymbol{a}_1) + w_{h_2}(\boldsymbol{a}_2 \otimes \boldsymbol{a}_2) + w_{h_3}(\boldsymbol{a}_3 \otimes \boldsymbol{a}_3) , \quad (572)$$

based on which a fourth-order anisotropy tensor is given by

$$\mathbb{T} = (\boldsymbol{1} \oplus \boldsymbol{1}) - \frac{1}{2}\{(\mathbf{T} \oplus \mathbf{T}) + (\mathbf{T} \ominus \mathbf{T})\}(\Theta - \Theta_0) . \quad (573)$$

With Eqns. (572) and (573), the modulus $\mathsf{H}(\Theta)$ is proposed to have the following form

$$\mathsf{H}(\Theta) = \mathbb{H} : \mathbb{T} , \quad (574)$$

where $\mathbb{H}$ is defined in Eqn. $(264)_3$. Note that Eqns. (572) and (573) are formulated for the $\mathscr{C}_3$ symmetry group, and they represent the $\mathscr{C}_{13}$ symmetry group for the choice $w_{h_1} = w_{h_2}$. Further, for $w_{h_1} = w_{h_2} = w_{h_3}$, the $\mathscr{C}_{14}$ symmetry group is characterised.

Given the potential in Eqn. (570), the closed-form expressions of the stress tensor, entropy and the driving forces are obtained with the aid of Eqns. (51) and (96), respectively, as

$$\boldsymbol{\sigma} = \mathbb{E} : \left[ (\boldsymbol{\varepsilon} - \boldsymbol{\varepsilon}^p) - \boldsymbol{\alpha}_t (\Theta - \Theta_0) \right] ,$$

$$\varrho = (\boldsymbol{\varepsilon} - \boldsymbol{\varepsilon}^p) : \mathbb{E} : \boldsymbol{\alpha}_t - \frac{h w_h}{n+1} (\bar{\xi} + \xi)^{n+1} - \frac{1}{2} \|\boldsymbol{\alpha}\|_{\overline{\mathbb{H}}}^2 + \mathfrak{c} \ln[\Theta/\Theta_0] ,$$

$$\kappa = -h(\Theta)(\bar{\xi} + \xi)^n ,$$

$$\boldsymbol{\beta} = -\overline{\mathbb{H}}(\Theta) : \boldsymbol{\alpha} ,$$

(575)

where

$$\overline{\mathbb{H}} = \mathbb{H} : \overline{\mathbb{T}} \quad \text{with} \quad \overline{\mathbb{T}} = -\frac{1}{2} \{ (\mathbf{T} \oplus \mathbf{T}) + (\mathbf{T} \ominus \mathbf{T}) \} . \tag{576}$$

As outlined in **Chapter 2**, Section 2.1, the heat flux can be constitutively prescribed as

$$\mathfrak{q} = -\mathbf{K} \cdot \nabla \Theta , \tag{577}$$

where $\mathbf{K}$ is a second-order tensor containing the thermal conductivities. With the preceding definitions at hand, the thermodynamic restriction can be evaluated in line with Eqns. (53) and (54) as

$$\mathscr{D}^{\text{red}} = \underbrace{\boldsymbol{\sigma} : \dot{\boldsymbol{\varepsilon}}^p + \kappa \dot{\xi} + \boldsymbol{\beta} : \dot{\boldsymbol{\alpha}}}_{\mathscr{D}_{\text{loc}}^{\text{red}}} \underbrace{- \frac{1}{\Theta} \nabla \Theta \cdot \mathfrak{q}}_{\mathscr{D}_{\text{con}}^{\text{red}}} \geq 0 , \tag{578}$$

from which it is clear that the evolution of plastic variables $\{\dot{\boldsymbol{\varepsilon}}^p, \dot{\xi}, \dot{\boldsymbol{\alpha}}\}$ has to be prescribed along with the heat flux $\mathfrak{q}$. To formally prescribe the evolution of plastic variables, a yield function is defined in the space of admissible thermodynamic forces as

$$\chi = \varkappa p + \|\boldsymbol{\Sigma}\|_{\mathbb{X}} - \sqrt{\frac{2}{3}} [y_0(\Theta) - \kappa] + \frac{1}{2} \|\boldsymbol{\beta}\|_{\mathbb{Y}}^2 \quad \text{with} \quad \boldsymbol{\Sigma} = \boldsymbol{\sigma} + \boldsymbol{\beta} , \tag{579}$$

where $\varkappa$ is the coefficient of the hydrostatic pressure, $p$ is the hydrostatic pressure of the form in Eqn. $(277)_1$ and $y_0(\Theta)$ is temperature dependent initial threshold yield stress defined analogous to Eqn. (571). The fourth-order Hill-type tensors $\mathbb{X}$ and $\mathbb{Y}$ can be defined based on appropriate considerations, see for example [141]. In the present work, they are defined as follows. Firstly, set $\mathbb{X} = \mathbb{E}$ in Eqn. (202) with temperature dependent yield surface parameters instead of the elastic constants, i.e.

$$[\mathbb{X}] = \begin{bmatrix} \varkappa_1(\Theta) & \varkappa_4(\Theta) & \varkappa_5(\Theta) & 0 & 0 & 0 \\ & \varkappa_2(\Theta) & \varkappa_6(\Theta) & 0 & 0 & 0 \\ & & \varkappa_3(\Theta) & 0 & 0 & 0 \\ & & & \varkappa_7(\Theta) & 0 & 0 \\ & \text{sym}. & & & \varkappa_8(\Theta) & 0 \\ & & & & & \varkappa_9(\Theta) \end{bmatrix} , \tag{580}$$

where $\varkappa_1(\Theta) - \varkappa_9(\Theta)$ are the nine temperature dependent yield parameters. The deviatoric property of $\mathbb{X}$ is satisfied for

$$\mathbb{X} : \boldsymbol{1} = \boldsymbol{0} , \tag{581}$$

which yields the relations

$$\varkappa_4(\Theta) = \frac{\varkappa_3(\Theta) - \varkappa_1(\Theta) - \varkappa_2(\Theta)}{2} \ ,$$

$$\varkappa_5(\Theta) = \frac{\varkappa_1(\Theta) - \varkappa_2(\Theta) - \varkappa_3(\Theta)}{2} \ , \tag{582}$$

$$\varkappa_6(\Theta) = \frac{\varkappa_2(\Theta) - \varkappa_1(\Theta) - \varkappa_3(\Theta)}{2} \ ,$$

see also [84]. Thus, Eqn. (580) reformulates to

$$[\text{dev}[\mathbb{X}]] = \begin{bmatrix} \varkappa_1(\Theta) & \dfrac{\varkappa_3(\Theta) - \varkappa_1(\Theta) - \varkappa_2(\Theta)}{2} & \dfrac{\varkappa_1(\Theta) - \varkappa_2(\Theta) - \varkappa_3(\Theta)}{2} & 0 & 0 & 0 \\[2ex] & \varkappa_2(\Theta) & \dfrac{\varkappa_2(\Theta) - \varkappa_1(\Theta) - \varkappa_3(\Theta)}{2} & 0 & 0 & 0 \\[2ex] & & \varkappa_3(\Theta) & 0 & 0 & 0 \\[1ex] & & & \varkappa_7(\Theta) & 0 & 0 \\[1ex] & \text{sym.} & & & \varkappa_8(\Theta) & 0 \\[1ex] & & & & & \varkappa_9(\Theta) \end{bmatrix} . \tag{583}$$

Next, it is presumed that the deviatoric stress in the two preferred directions does not contribute to the plastic yielding. This property is satisfied by the equalities

$$\text{dev}[\mathbb{X}] : \boldsymbol{m}_1 = \boldsymbol{0} \quad \text{and} \quad \text{dev}[\mathbb{X}] : \boldsymbol{m}_2 = \boldsymbol{0} \ , \tag{584}$$

which yields

$$\varkappa_1(\Theta) = 0 \ , \varkappa_2(\Theta) = 0 \quad \text{and} \quad \varkappa_3(\Theta) = 0 \ . \tag{585}$$

Substituting Eqn. (585) into Eqn. (583), and taking into account the contribution of deviatoric stress in the third preferred direction to plastic yielding, the fourth-order tensor $\mathbb{X}$ finally reads

$$\mathbb{X} = [\text{dev}[\mathbb{X}]]|_{(\varkappa_1(\Theta) = \varkappa_2(\Theta) = \varkappa_3(\Theta) = 0)} + \frac{9}{4}\varkappa_{10}(\Theta)(\boldsymbol{m}'_3 \otimes \boldsymbol{m}'_3) \ , \tag{586}$$

which can be expressed in the coordinate form as

$$[\mathbb{X}] = \begin{bmatrix} \dfrac{\varkappa_{10}(\Theta)}{4} & \dfrac{\varkappa_{10}(\Theta)}{4} & -\dfrac{\varkappa_{10}(\Theta)}{2} & 0 & 0 & 0 \\[2ex] & \dfrac{\varkappa_{10}(\Theta)}{4} & -\dfrac{\varkappa_{10}(\Theta)}{2} & 0 & 0 & 0 \\[2ex] & & \varkappa_{10}(\Theta) & 0 & 0 & 0 \\[1ex] & & & \varkappa_7(\Theta) & 0 & 0 \\[1ex] & \text{sym.} & & & \varkappa_8(\Theta) & 0 \\[1ex] & & & & & \varkappa_9(\Theta) \end{bmatrix} . \tag{587}$$

The three temperature dependent parameters $\varkappa_7(\Theta) - \varkappa_{10}(\Theta)$ in Eqn. (587) can be determined by evaluating Eqn. (579) for three shear modes and one simple tension mode

as

$$\varkappa_7(\Theta) = \frac{2}{3}\frac{y_0^2(\Theta)}{y_{12}^2(\Theta)}\,, \quad \varkappa_8(\Theta) = \frac{2}{3}\frac{y_0^2(\Theta)}{y_{13}^2(\Theta)}\,, \quad \varkappa_9(\Theta) = \frac{2}{3}\frac{y_0^2(\Theta)}{y_{23}^2(\Theta)} \quad \text{and} \quad \varkappa_{10}(\Theta) = \frac{2}{3}\frac{y_0^2(\Theta)}{y_{33}^2(\Theta)}\,.$$
(588)

The fourth-order tensor $\mathbb{Y}$ that governs the non-linearity of kinematic hardening can be expressed analogously as

$$[\mathbb{Y}] = \begin{bmatrix} \dfrac{\zeta_{10}(\Theta)}{4} & \dfrac{\zeta_{10}(\Theta)}{4} & -\dfrac{\zeta_{10}(\Theta)}{2} & 0 & 0 & 0 \\[2mm] & \dfrac{\zeta_{10}(\Theta)}{4} & -\dfrac{\zeta_{10}(\Theta)}{2} & 0 & 0 & 0 \\[2mm] & & \zeta_{10}(\Theta) & 0 & 0 & 0 \\[2mm] & & & \zeta_7(\Theta) & 0 & 0 \\[2mm] & \text{sym}. & & & \zeta_8(\Theta) & 0 \\[2mm] & & & & & \zeta_9(\Theta) \end{bmatrix}\,,$$
(589)

in terms of four material parameters. Note that the parameter $\varkappa$ governing the hydrostatic pressure can be determined similar to Eqn. $(285)_1$.

A canonical form of the evolution equations for plastic variables is determined by invoking the principle of maximum dissipation, which yields the normality rules as

$$\begin{aligned} \dot{\boldsymbol{\varepsilon}}^p &= \lambda\chi_{,\boldsymbol{\sigma}} = \lambda\{\varkappa\boldsymbol{m}_3 + \bar{\mathbf{n}}\}\,, \\ \dot{\xi} &= \lambda\chi_{,\kappa} = \lambda\sqrt{2/3}\,, \\ \dot{\boldsymbol{\alpha}} &= \lambda\chi_{,\boldsymbol{\beta}} = \lambda\{\varkappa\boldsymbol{m}_3 + \bar{\mathbf{n}} + \mathbb{Y}:\boldsymbol{\beta}\}\,, \end{aligned}$$
(590)

along with the plastic loading/unloading conditions

$$\lambda \geq 0, \quad \chi \leq 0 \quad \text{and} \quad \lambda\chi \equiv 0\,,$$
(591)

where $\lambda$ and $\bar{\mathbf{n}}$ denote the amount and direction of the plastic flow respectively, with a closed-form expression of the latter reading

$$\bar{\mathbf{n}} = \frac{\mathbb{X}:\boldsymbol{\Sigma}}{\|\boldsymbol{\Sigma}\|_{\mathbb{X}}}\,.$$
(592)

The framework of non-associative thermoplasticity can be derived by relaxing the principle of maximum dissipation, i.e. using a separate flow potential to derive the evolution equations. This aspect is precluded in the present appendix as the framework is entirely similar to that in **Chapter 5**.

The next computational aspect is to express the governing balance and evolution equations of coupled thermoplasticity in a time discrete setting, which is the first step of the algorithmic implementation. To do so, it can be seen from Eqn. (60) that the latent heat $\mathcal{H}$ needs to be defined for the present model. Appealing to Eqn. (61), it follows that $\mathcal{H}$ can be expressed with the aid of Eqn. (570) as

$$\mathcal{H} = -\Theta\{\boldsymbol{\alpha}_t : \mathbb{E} : (\dot{\boldsymbol{\varepsilon}} - \dot{\boldsymbol{\varepsilon}}^p) - hw_h(\bar{\xi} + \xi)^n\dot{\xi} - \boldsymbol{\alpha} : \overline{\mathbb{H}} : \dot{\boldsymbol{\alpha}}\}\,.$$
(593)

Employing a fully implicit backward Euler time integration scheme, the associated equations (16), (60) and (590) can be integrated while taking into account Eqns. $(575)_1$, (578) and (593) as

$$\text{div}[\boldsymbol{\sigma}_{n+1}] + \boldsymbol{\Upsilon}_{n+1} = \boldsymbol{0} \ ,$$

$$
\begin{aligned}
\frac{\mathfrak{c}}{\Delta t}(\Theta_{n+1} - \Theta_n) = & -\text{div}[\mathfrak{q}_{n+1}] + \mathscr{R}_{n+1} \\
& + \boldsymbol{\sigma}_{n+1} : (\boldsymbol{\varepsilon}^p_{n+1} - \boldsymbol{\varepsilon}^p_n)/\Delta t \\
& + \kappa_{n+1}(\xi_{n+1} - \xi_n)/\Delta t \\
& + \boldsymbol{\beta}_{n+1} : (\boldsymbol{\alpha}_{n+1} - \boldsymbol{\alpha}_n)/\Delta t \\
& - \Theta_{n+1}\Bigg[\boldsymbol{\alpha}_t : \mathbb{E} : \left\{ \frac{(\boldsymbol{\varepsilon}_{n+1} - \boldsymbol{\varepsilon}_n)}{\Delta t} - \frac{(\boldsymbol{\varepsilon}^p_{n+1} - \boldsymbol{\varepsilon}^p_n)}{\Delta t} \right\} \\
& \qquad + hw_h(\bar{\xi} + \xi)^n \frac{(\xi_{n+1} - \xi_n)}{\Delta t} \\
& \qquad + \boldsymbol{\alpha}_{n+1} : \overline{\mathbb{H}} : \frac{(\boldsymbol{\alpha}_{n+1} - \boldsymbol{\alpha}_n)}{\Delta t} \Bigg] \ ,
\end{aligned}
\tag{594}
$$

$$\boldsymbol{\varepsilon}^p_{n+1} = \boldsymbol{\varepsilon}^p_n + \Delta\lambda_{n+1}\{\varkappa\boldsymbol{m}_3 + \bar{\mathbf{n}}_{n+1}\} \ ,$$

$$\xi_{n+1} = \xi_n + \Delta\lambda_{n+1}\sqrt{2/3} \ ,$$

$$\boldsymbol{\alpha}_{n+1} = \boldsymbol{\alpha}_n + \Delta\lambda_{n+1}\{\varkappa\boldsymbol{m}_3 + \bar{\mathbf{n}}_{n+1} + \mathbb{Y} : \boldsymbol{\beta}_{n+1}\} \ .$$

where $\Delta\lambda_{n+1} = \Delta t \lambda_{n+1}$ is the time discrete plastic increment. Before proceeding to the next steps, the internal variables are locally updated using a Newton-Raphson iteration scheme in line with **Chapter 5**. To do so, recall the time discrete conjugate driving forces dual to $\{\boldsymbol{\varepsilon}^p, \xi, \boldsymbol{\alpha}\}$

$$\boldsymbol{\sigma}_{n+1} = \mathbb{E} : [(\boldsymbol{\varepsilon}_{n+1} - \boldsymbol{\varepsilon}^p_{n+1}) - \boldsymbol{\alpha}_t(\Theta_{n+1} - \Theta_0)] \ ,$$

$$\kappa_{n+1} = -h(\Theta)(\bar{\xi} + \xi_{n+1})^n \ , \tag{595}$$

$$\boldsymbol{\beta}_{n+1} = -\mathbb{H}(\Theta) : \boldsymbol{\alpha}_{n+1} \ ,$$

and define the thermoelastic trial values by setting $\Delta\lambda_{n+1} = 0$ in Eqns. $(594)_{3-5}$ and substituting the resulting expressions in Eqn. (595) as

$$\boldsymbol{\sigma}^{\text{trial}}_{n+1} = \mathbb{E} : [(\boldsymbol{\varepsilon}_{n+1} - \boldsymbol{\varepsilon}^p_n - \boldsymbol{\alpha}_t(\Theta_{n+1} - \Theta_0)] \ ,$$

$$\kappa^{\text{trial}}_{n+1} = -h(\Theta)(\bar{\xi} + \xi_n)^n \ , \tag{596}$$

$$\boldsymbol{\beta}^{\text{trial}}_{n+1} = -\mathbb{H}(\Theta) : \boldsymbol{\alpha}_n \ ,$$

which allows to compute the trial value of the yield function as

$$\chi^{\text{trial}} = \chi(\boldsymbol{\sigma}^{\text{trial}}_{n+1}, \kappa^{\text{trial}}_{n+1}, \boldsymbol{\beta}^{\text{trial}}_{n+1}) \ , \tag{597}$$

based on which loading cases can be identified. For a thermoelastic step characterised by $\chi^{\text{trial}} \leq 0$, Eqn. (374) is recovered, whereas for a thermoplastic step ($\chi^{\text{trial}} > 0$),

Eqns. (594) and the consistency condition lead to a system of non-linear equations as

$$\mathfrak{R} = \begin{bmatrix} \mathfrak{R}_{\varepsilon^p} \\ \mathfrak{R}_{\xi} \\ \mathfrak{R}_{\alpha} \\ \mathfrak{R}_{\chi} \end{bmatrix} = \begin{bmatrix} \varepsilon_{n+1}^p - \varepsilon^p - \Delta\lambda_{n+1}\{\varkappa m_3 + \bar{\mathfrak{n}}_{n+1}\} \\ \xi_{n+1} - \xi_n - \Delta\lambda_{n+1}\sqrt{2/3} \\ \alpha_{n+1} - \alpha_n - \Delta\lambda_{n+1}\{\varkappa m_3 + \bar{\mathfrak{n}}_{n+1} + \mathbb{Y} : \beta_{n+1}\} \\ \chi \end{bmatrix} = \mathbf{0} \quad , \qquad (598)$$

in terms of the unknowns $\mathfrak{P}_{n+1} = \{\varepsilon_{n+1}^p, \xi_{n+1}, \alpha_{n+1}, \Delta\lambda_{n+1}\}$. Following Eqns. (377)–(378), the necessary iteration tangent $\mathfrak{R}(\mathfrak{P}_{n+1}),_{\mathfrak{P}}$ reads

$$\mathfrak{R}(\mathfrak{P}_{n+1}^i),_{\mathfrak{P}} = \begin{bmatrix} \mathfrak{R}_{\varepsilon^p, \varepsilon_{n+1}^p} & \mathfrak{R}_{\varepsilon^p, \xi_{n+1}} & \mathfrak{R}_{\varepsilon^p, \alpha_{n+1}} & \mathfrak{R}_{\varepsilon^p, \Delta\lambda_{n+1}} \\ \mathfrak{R}_{\xi, \varepsilon_{n+1}^p} & \mathfrak{R}_{\xi, \xi_{n+1}} & \mathfrak{R}_{\xi, \alpha_{n+1}} & \mathfrak{R}_{\xi, \Delta\lambda_{n+1}} \\ \mathfrak{R}_{\alpha, \varepsilon_{n+1}^p} & \mathfrak{R}_{\alpha, \xi_{n+1}} & \mathfrak{R}_{\alpha, \alpha_{n+1}} & \mathfrak{R}_{\alpha, \Delta\lambda_{n+1}} \\ \mathfrak{R}_{\chi, \varepsilon_{n+1}^p} & \mathfrak{R}_{\chi, \xi_{n+1}} & \mathfrak{R}_{\chi, \alpha_{n+1}} & \mathfrak{R}_{\chi, \Delta\lambda_{n+1}} \end{bmatrix} \quad , \qquad (599)$$

where

$$\begin{aligned} \mathfrak{R}_{\varepsilon^p, \varepsilon_{n+1}^p} &= (\mathbf{1} \oplus \mathbf{1}) - \Delta\lambda_{n+1}\{\varkappa m_3 + \bar{\mathfrak{n}}_{n+1}\},_{\sigma_{n+1}} : \sigma_{n+1},_{\varepsilon_{n+1}^p} \quad, \\ \mathfrak{R}_{\varepsilon^p, \kappa_{n+1}} &= 0 \quad, \\ \mathfrak{R}_{\varepsilon^p, \alpha_{n+1}} &= -\Delta\lambda_{n+1}\{\varkappa m_3 + \bar{\mathfrak{n}}_{n+1}\},_{\beta_{n+1}} : \beta_{n+1},_{\alpha_{n+1}} \quad, \\ \mathfrak{R}_{\varepsilon^p, \Delta\lambda_{n+1}} &= -\{\varkappa m_3 + \bar{\mathfrak{n}}_{n+1}\} \quad, \\[4pt] \mathfrak{R}_{\xi, \varepsilon_{n+1}^p} &= \mathbf{0} \quad, \\ \mathfrak{R}_{\xi, \kappa_{n+1}} &= 1 \quad, \\ \mathfrak{R}_{\xi, \alpha_{n+1}} &= \mathbf{0} \quad, \\ \mathfrak{R}_{\xi, \Delta\lambda_{n+1}} &= -\sqrt{2/3} \quad, \\[4pt] \mathfrak{R}_{\alpha, \varepsilon_{n+1}^p} &= -\Delta\lambda_{n+1}\{\varkappa m_3 + \bar{\mathfrak{n}}_{n+1} + \mathbb{Y} : \beta_{n+1}\},_{\sigma_{n+1}} : \sigma_{n+1},_{\varepsilon_{n+1}^p} \quad, \\ \mathfrak{R}_{\alpha, \kappa_{n+1}} &= 0 \quad, \\ \mathfrak{R}_{\alpha, \alpha_{n+1}} &= (\mathbf{1} \oplus \mathbf{1}) - \Delta\lambda_{n+1}\{\varkappa m_3 + \bar{\mathfrak{n}}_{n+1} + \mathbb{Y} : \beta_{n+1}\},_{\beta_{n+1}} : \beta_{n+1},_{\alpha_{n+1}} \quad, \\ \mathfrak{R}_{\alpha, \Delta\lambda_{n+1}} &= -\{\varkappa m_3 + \bar{\mathfrak{n}}_{n+1} + \mathbb{Y} : \beta_{n+1}\} \quad, \\[4pt] \mathfrak{R}_{\chi, \varepsilon_{n+1}^p} &= \chi,_{\sigma_{n+1}} : \sigma_{n+1},_{\varepsilon_{n+1}^p} \quad, \\ \mathfrak{R}_{\chi, \kappa_{n+1}} &= \chi,_{\kappa_{n+1}} : \kappa_{n+1},_{\xi_{n+1}} \quad, \\ \mathfrak{R}_{\chi, \alpha_{n+1}} &= \chi,_{\beta_{n+1}} : \beta_{n+1},_{\alpha_{n+1}} \quad, \\ \mathfrak{R}_{\chi, \Delta\lambda_{n+1}} &= 0 \quad. \end{aligned} \qquad (600)$$

The closed-form expressions of the partial derivatives appearing in the equation above are

given by

$$\{\varkappa m_3 + \bar{\mathbf{n}}_{n+1}\}_{,\boldsymbol{\sigma}_{n+1}} = \bar{\mathbf{n}}_{n+1,\boldsymbol{\sigma}_{n+1}} = \frac{1}{\|\boldsymbol{\Sigma}_{n+1}\|_{\mathbb{X}}}\{\mathbb{X} - \bar{\mathbf{n}}_{n+1} \otimes \bar{\mathbf{n}}_{n+1}\} \ ,$$

$$\{\varkappa m_3 + \bar{\mathbf{n}}_{n+1}\}_{,\boldsymbol{\beta}_{n+1}} = \bar{\mathbf{n}}_{n+1,\boldsymbol{\beta}_{n+1}} = \frac{1}{\|\boldsymbol{\Sigma}_{n+1}\|_{\mathbb{X}}}\{\mathbb{X} - \bar{\mathbf{n}}_{n+1} \otimes \bar{\mathbf{n}}_{n+1}\} \ ,$$

$$\{\varkappa m_3 + \bar{\mathbf{n}}_{n+1} + \mathbb{Y} : \boldsymbol{\beta}_{n+1}\}_{,\boldsymbol{\sigma}_{n+1}} = \bar{\mathbf{n}}_{n+1,\boldsymbol{\sigma}_{n+1}} = \frac{1}{\|\boldsymbol{\Sigma}_{n+1}\|_{\mathbb{X}}}\{\mathbb{X} - \bar{\mathbf{n}}_{n+1} \otimes \bar{\mathbf{n}}_{n+1}\} \ ,$$

$$\{\varkappa m_3 + \bar{\mathbf{n}}_{n+1} + \mathbb{Y} : \boldsymbol{\beta}_{n+1}\}_{,\boldsymbol{\beta}_{n+1}} = \{\bar{\mathbf{n}}_{n+1} + \mathbb{Y} : \boldsymbol{\beta}_{n+1}\}_{,\boldsymbol{\beta}_{n+1}} = \frac{1}{\|\boldsymbol{\Sigma}_{n+1}\|_{\mathbb{X}}}\{\mathbb{X} - \bar{\mathbf{n}}_{n+1} \otimes \bar{\mathbf{n}}_{n+1} + \mathbb{Y}\} \ ,$$

$$(601)$$

and

$$\boldsymbol{\sigma}_{n+1,\boldsymbol{\varepsilon}_{n+1}^p} = -\mathbb{E} \ , \quad \kappa_{n+1,\xi_{n+1}} = -\mathsf{H} = -nh(\Theta)(\bar{\xi} + \xi)^n \quad \text{and} \quad \boldsymbol{\beta}_{n+1,\boldsymbol{\alpha}_{n+1}} = -\mathbb{H} \ . \quad (602)$$

Having locally updated the internal variables, the next step of algorithmic implementation is to recast the time discrete strong form of equations, namely Eqns. $(594)_{1,2}$, into a time discrete weak form using the standard Galerkin procedure. Accordingly, one can write

$$\int_{\mathscr{B}} \delta\boldsymbol{u} \cdot \big\{ -\operatorname{div}[\boldsymbol{\sigma}_{n+1} - \boldsymbol{\Upsilon}_{n+1}] \big\} \, dV \\ + \int_{\mathscr{B}} \delta\Theta \big\{ \operatorname{div}[\mathbf{q}_{n+1} - \mathscr{R}_{n+1} + \frac{\mathfrak{c}}{\Delta t}(\Theta_{n+1} - \Theta_n) - \mathscr{D}_{\operatorname{loc} n+1}^{\operatorname{red}} - \mathcal{H}_{n+1} \big\} \, dV = \boldsymbol{0} \quad , \quad (603)$$

where $\delta\boldsymbol{u}$ and $\delta\Theta$ are virtual displacement and temperature fields defined on the body $\mathscr{B}$, respectively. Appealing to Eqns. (154)–(157), Eqn. (603) reformulates to

$$-\int_{\partial\mathscr{B}} \delta\boldsymbol{u} \cdot \boldsymbol{t}_{n+1} \, dA - \int_{\mathscr{B}} \delta\boldsymbol{u} \cdot \boldsymbol{\Upsilon}_{n+1} \, dV + \int_{\mathscr{B}} \delta\boldsymbol{\varepsilon} : \boldsymbol{\sigma}_{n+1} \, dV \\ + \int_{\partial\mathscr{B}} \delta\Theta \mathfrak{h}_{n+1} \, dA - \int_{\mathscr{B}} \delta\Theta \mathscr{R}_{n+1} \, dV - \int_{\mathscr{B}} \nabla\delta\Theta \cdot \mathbf{q}_{n+1} \, dV \quad , \quad (604) \\ + \int_{\partial\mathscr{B}} \delta\Theta \left[ \frac{\mathfrak{c}}{\Delta t}(\Theta_{n+1} - \Theta_n) - \mathscr{D}_{\operatorname{loc} n+1}^{\operatorname{red}} - \mathcal{H}_{n+1} \right] dV = \boldsymbol{0}$$

where $\boldsymbol{t}_{n+1}$ and $\mathfrak{h}_{n+1}$ are used from Eqn. (5). Equation (604) denotes the time discrete weak form of Eqn. (594).

In the final step of algorithmic implementation, the unknowns $\boldsymbol{u}_{n+1}$ and $\Theta_{n+1}$ in Eqn. (604) are solved using the finite element method. Following the same procedure as outlined in **Chapter 2**, the vector of internal and external forces respectively read

$$\mathfrak{R}_{\operatorname{int}}(\mathfrak{D}_{n+1}) = \int_{\mathscr{B}} \{\mathfrak{B}_{\boldsymbol{\varepsilon}}^T \cdot \boldsymbol{\sigma}_{n+1} + \mathfrak{N}_{\Theta}^T \cdot \mathcal{Q}_{n+1} - \mathfrak{B}_{\nabla\Theta}^T \cdot \mathbf{q}_{n+1}\} \, dV \quad (605)$$

and

$$\mathfrak{R}_{\operatorname{ext}} = \int_{\partial\mathscr{B}} (\mathfrak{N}_u^T \cdot \boldsymbol{t}_{n+1} - \mathfrak{N}_{\Theta}^T \cdot \mathfrak{h}_{n+1}) \, dA + \int_{\mathscr{B}} (\mathfrak{N}_u^T \cdot \boldsymbol{\Upsilon}_{n+1} + \mathfrak{N}_{\Theta}^T \cdot \mathscr{R}_{n+1}) \, dV \ , \quad (606)$$

where $\boldsymbol{\mathfrak{D}}_{n+1} = \{\boldsymbol{\varepsilon}_{n+1}, \Theta_{n+1}, \nabla\Theta_{n+1}\}$ denotes the nodal displacements and temperatures analogous to Eqn. (163), and

$$\mathcal{Q}_{n+1} = \frac{\mathfrak{c}}{\Delta t}(\Theta_{n+1} - \Theta_n) - \mathscr{D}_{\mathrm{loc}\ n+1}^{\mathrm{red}} - \mathcal{H}_{n+1} \ . \tag{607}$$

To this end, Eqn. (605) can be generalised to

$$\boldsymbol{\mathfrak{R}}_{\mathrm{int}}(\boldsymbol{\mathfrak{D}}_{n+1}) = \int_{\mathscr{B}} \boldsymbol{\mathfrak{B}}_{\boldsymbol{\mathfrak{D}}}^T \cdot \boldsymbol{\mathcal{S}}_{n+1}\, dV \ , \tag{608}$$

where $\boldsymbol{\mathcal{S}}_{n+1}$ is the generalised stress tensor of the form

$$\boldsymbol{\mathcal{S}}_{n+1} = \begin{bmatrix} \boldsymbol{\sigma}_{n+1} \\ \mathcal{Q}_{n+1} \\ -\mathbf{q}_{n+1} \end{bmatrix} = \begin{bmatrix} \mathbb{E} : [(\boldsymbol{\varepsilon}_{n+1} - \boldsymbol{\varepsilon}_{n+1}^p) - \boldsymbol{\alpha}_t(\Theta_{n+1} - \Theta_0)] \\ \dfrac{\mathfrak{c}}{\Delta t}(\Theta_{n+1} - \Theta_n) - \mathscr{D}_{\mathrm{loc}\ n+1}^{\mathrm{red}} - \mathcal{H}_{n+1} \\ \mathbf{K} \cdot \nabla\Theta_{n+1} \end{bmatrix} \ . \tag{609}$$

Furthermore, it follows from Eqn. (177) that the material dependent term $\boldsymbol{\mathfrak{R}}_{\mathrm{int}}(\boldsymbol{\mathfrak{D}}_{n+1})_{,\boldsymbol{\mathfrak{D}}}$ can be expressed as

$$\boldsymbol{\mathfrak{R}}_{\mathrm{int}}(\boldsymbol{\mathfrak{D}}_{n+1})_{,\boldsymbol{\mathfrak{D}}} = \int_{\mathscr{B}} \boldsymbol{\mathfrak{B}}_{\boldsymbol{\mathfrak{D}}}^T \cdot \boldsymbol{\mathcal{S}}_{n+1,\boldsymbol{\mathfrak{D}}}\, dV = \int_{\mathscr{B}} \boldsymbol{\mathfrak{B}}_{\boldsymbol{\mathfrak{D}}}^T \cdot \mathbb{F}_{n+1} \cdot \boldsymbol{\mathfrak{B}}_{\boldsymbol{\mathfrak{D}}}\, dV \ , \tag{610}$$

where $\mathbb{F}_{n+1}$ denotes the generalised modulus tensor. For the present model, it is defined by

$$\mathbb{F}_{n+1} = \boldsymbol{\mathcal{S}}_{n+1,\boldsymbol{\mathfrak{D}}} = \begin{bmatrix} \dfrac{d\boldsymbol{\sigma}_{n+1}}{d\boldsymbol{\varepsilon}_{n+1}} & \dfrac{d\boldsymbol{\sigma}_{n+1}}{d\Theta_{n+1}} & \dfrac{d\boldsymbol{\sigma}_{n+1}}{d\nabla\Theta_{n+1}} \\[2mm] \dfrac{d\mathcal{Q}_{n+1}}{d\boldsymbol{\varepsilon}_{n+1}} & \dfrac{d\mathcal{Q}_{n+1}}{d\Theta_{n+1}} & \dfrac{d\mathcal{Q}_{n+1}}{d\nabla\Theta_{n+1}} \\[2mm] \dfrac{d\mathbf{q}_{n+1}}{d\boldsymbol{\varepsilon}_{n+1}} & \dfrac{d\mathbf{q}_{n+1}}{d\Theta_{n+1}} & \dfrac{d\mathbf{q}_{n+1}}{d\nabla\Theta_{n+1}} \end{bmatrix} \ . \tag{611}$$

It can be seen from Eqn. (611) that the sensitivities $\boldsymbol{\varepsilon}_{n+1,\boldsymbol{\varepsilon}_{n+1}}^p, \xi_{n+1,\boldsymbol{\varepsilon}_{n+1}}, \boldsymbol{\alpha}_{n+1,\boldsymbol{\varepsilon}_{n+1}}$ as well as $\boldsymbol{\varepsilon}_{n+1,\Theta_{n+1}}^p, \xi_{n+1,\Theta_{n+1}}$ and $\boldsymbol{\alpha}_{n+1,\Theta_{n+1}}$ need to be computed to correctly define the modulus tensor. The sensitivities can be computed by first defining a residuum vector as

$$\boldsymbol{\mathfrak{R}} = \boldsymbol{\mathfrak{R}}(\boldsymbol{\varepsilon}_{n+1}, \Theta_{n+1}, \boldsymbol{\mathfrak{P}}_{n+1}) \ , \tag{612}$$

in terms of the unknowns $\boldsymbol{\mathfrak{P}}_{n+1} = \{\boldsymbol{\varepsilon}_{n+1}^p, \xi_{n+1}, \boldsymbol{\alpha}_{n+1}, \Delta\lambda_{n+1}\}$. For infinitesimal perturbations, it follows that Eqn. (612) can be expressed as

$$d\boldsymbol{\mathfrak{R}} = \boldsymbol{\mathfrak{R}}_{,\boldsymbol{\varepsilon}_{n+1}} : d\boldsymbol{\varepsilon}_{n+1} + \boldsymbol{\mathfrak{R}}_{,\Theta_{n+1}} : d\Theta_{n+1} + \boldsymbol{\mathfrak{R}}_{,\boldsymbol{\mathfrak{P}}_{n+1}} : d\boldsymbol{\mathfrak{P}}_{n+1} \ . \tag{613}$$

Setting $d\boldsymbol{\mathfrak{R}} = \boldsymbol{0}$, the sensitivities can be evaluated as

$$d\boldsymbol{\mathfrak{P}}_{n+1} = \underbrace{-\left[\boldsymbol{\mathfrak{R}}_{,\boldsymbol{\mathfrak{P}}_{n+1}}\right]^{-1}\boldsymbol{\mathfrak{R}}_{,\boldsymbol{\varepsilon}_{n+1}}}_{\boldsymbol{\mathfrak{P}}_{n+1,\boldsymbol{\varepsilon}_{n+1}}} : d\boldsymbol{\varepsilon}_{n+1} \underbrace{-\left[\boldsymbol{\mathfrak{R}}_{,\boldsymbol{\mathfrak{P}}_{n+1}}\right]^{-1}\boldsymbol{\mathfrak{R}}_{,\Theta_{n+1}}}_{\boldsymbol{\mathfrak{P}}_{n+1,\Theta_{n+1}}} d\Theta_{n+1} \ . \tag{614}$$

With the aid of Eqns. (598)–(602), the sensitivities can be reformulated as

$$\boldsymbol{\mathfrak{P}}_{n+1,\boldsymbol{\varepsilon}_{n+1}} = \begin{bmatrix} \boldsymbol{\varepsilon}_{n+1,\boldsymbol{\varepsilon}_{n+1}}^p \\ \xi_{n+1,\boldsymbol{\varepsilon}_{n+1}} \\ \boldsymbol{\alpha}_{n+1,\boldsymbol{\varepsilon}_{n+1}} \\ \Delta\lambda_{n+1,\boldsymbol{\varepsilon}_{n+1}} \end{bmatrix} = -\left[\boldsymbol{\mathfrak{R}}_{,\boldsymbol{\mathfrak{P}}_{n+1}}\right]^{-1} \begin{bmatrix} -\Delta\lambda_{n+1}\{\varkappa\boldsymbol{m}_3 + \bar{\mathbf{n}}_{n+1}\}_{,\boldsymbol{\sigma}_{n+1}} : \boldsymbol{\sigma}_{n+1,\boldsymbol{\varepsilon}_{n+1}} \\ 0 \\ \{\varkappa\boldsymbol{m}_3 + \bar{\mathbf{n}}_{n+1} + \mathbb{Y} : \boldsymbol{\beta}_{n+1}\}_{,\boldsymbol{\sigma}_{n+1}} : \boldsymbol{\sigma}_{n+1,\boldsymbol{\varepsilon}_{n+1}} \\ \{\varkappa\boldsymbol{m}_3 + \bar{\mathbf{n}}_{n+1}\}_{,\boldsymbol{\sigma}_{n+1}} : \boldsymbol{\sigma}_{n+1,\boldsymbol{\varepsilon}_{n+1}} \end{bmatrix} \ , \tag{615}$$

and similarly

$$\mathfrak{P}_{n+1,\Theta_{n+1}} = \begin{bmatrix} \boldsymbol{\varepsilon}^p_{n+1,\Theta_{n+1}} \\ \xi_{n+1,\Theta_{n+1}} \\ \boldsymbol{\alpha}_{n+1,\Theta_{n+1}} \\ \Delta\lambda_{n+1,\Theta_{n+1}} \end{bmatrix} = -\left[\mathfrak{R},_{\mathfrak{P}_{n+1}}\right]^{-1} \begin{bmatrix} -\Delta\lambda_{n+1}\{\varkappa\boldsymbol{m}_3 + \bar{\mathbf{n}}_{n+1}\},_{\boldsymbol{\sigma}_{n+1}} : \boldsymbol{\sigma}_{n+1,\Theta_{n+1}} \\ 0 \\ \{\varkappa\boldsymbol{m}_3 + \bar{\mathbf{n}}_{n+1} + \mathbb{Y} : \boldsymbol{\beta}_{n+1}\},_{\boldsymbol{\sigma}_{n+1}} : \boldsymbol{\sigma}_{n+1,\Theta_{n+1}} \\ \{\varkappa\boldsymbol{m}_3 + \bar{\mathbf{n}}_{n+1}\},_{\boldsymbol{\sigma}_{n+1}} : \boldsymbol{\sigma}_{n+1,\Theta_{n+1}} \end{bmatrix} , \tag{616}$$

where

$$\boldsymbol{\sigma}_{n+1,\Theta_{n+1}} = -\mathbb{E} : \boldsymbol{\alpha}_t . \tag{617}$$

The remaining partial derivatives appearing in Eqns. (615) and (616) are defined in Eqns. (601) and (602). In the system of equations (614)–(616), the term $\mathfrak{R},_{\mathfrak{P}_{n+1}}$ is the necessary iteration tangent defined in Eqn. (599). With the expressions (615) and (616) at hand, the generalised modulus tensor (611) for the present model can be evaluated as

$$\mathbb{F}_{n+1} = \begin{bmatrix} \dfrac{d\boldsymbol{\sigma}_{n+1}}{d\boldsymbol{\varepsilon}_{n+1}} & \dfrac{d\boldsymbol{\sigma}_{n+1}}{d\Theta_{n+1}} & \boldsymbol{0} \\ \dfrac{d\mathcal{Q}_{n+1}}{d\boldsymbol{\varepsilon}_{n+1}} & \dfrac{d\mathcal{Q}_{n+1}}{d\Theta_{n+1}} & \boldsymbol{0} \\ \boldsymbol{0} & \boldsymbol{0} & \mathbf{K} \end{bmatrix} , \tag{618}$$

where

$$\begin{aligned} \frac{d\boldsymbol{\sigma}_{n+1}}{d\boldsymbol{\varepsilon}_{n+1}} &= \boldsymbol{\sigma}_{n+1,\varepsilon_{n+1}} + \boldsymbol{\sigma}_{n+1,\varepsilon^p_{n+1}} : \boldsymbol{\varepsilon}^p_{n+1,\varepsilon_{n+1}} = \mathbb{E} - \mathbb{E} : \boldsymbol{\varepsilon}^p_{n+1,\varepsilon_{n+1}} , \\ \frac{d\boldsymbol{\sigma}_{n+1}}{d\Theta_{n+1}} &= \boldsymbol{\sigma}_{n+1,\Theta_{n+1}} + \boldsymbol{\sigma}_{n+1,\varepsilon^p_{n+1}} : \boldsymbol{\varepsilon}^p_{n+1,\Theta_{n+1}} = -\boldsymbol{\alpha}_t : \mathbb{E} - \mathbb{E} : \boldsymbol{\varepsilon}^p_{n+1,\Theta_{n+1}} , \end{aligned} \tag{619}$$

and similarly, albeit cumbersome

$$\frac{d\mathcal{Q}_{n+1}}{d\boldsymbol{\varepsilon}_{n+1}} = \mathcal{Q}_{n+1,\varepsilon_{n+1}} + \mathcal{Q}_{n+1,\varepsilon^p_{n+1}} : \boldsymbol{\varepsilon}^p_{n+1,\varepsilon_{n+1}} + \mathcal{Q}_{n+1,\xi_{n+1}}\,\xi_{n+1,\varepsilon_{n+1}} + \mathcal{Q}_{n+1,\alpha_{n+1}} : \boldsymbol{\alpha}_{n+1,\varepsilon_{n+1}} ,$$

$$\frac{d\mathcal{Q}_{n+1}}{d\Theta_{n+1}} = \mathcal{Q}_{n+1,\Theta_{n+1}} + \mathcal{Q}_{n+1,\varepsilon^p_{n+1}} : \boldsymbol{\varepsilon}^p_{n+1,\Theta_{n+1}} + \mathcal{Q}_{n+1,\xi_{n+1}}\,\xi_{n+1,\Theta_{n+1}} + \mathcal{Q}_{n+1,\alpha_{n+1}} : \boldsymbol{\alpha}_{n+1,\Theta_{n+1}} . \tag{620}$$

# References

[1] https://www.unsw.adfa.edu.au/school-of-engineering-and-information-technology/school-research-themes/civil-engineering.

[2] Schuecker, C. [2017]: "Verbundwerkstoffe-I". Lecture Notes, Montanuniversität Leoben.

[3] Schuecker, C., Davillá, C.G. and Pettermann, H.E. [2008]: "Modeling the non-linear response of fiber-reinforced laminates using a combined damage/plasticity model". Technical report, TM-2008-215314, NASA Langley Research Center.

[4] Germain, N., Besson, J. and Feyel, F. [2007]: "Composite layered materials: Anisotropic nonlocal damage models". *Computer methods in applied mechanics and engineering*, 196: 4272–4282.

[5] Smith, P.A. [2000]: "Carbon Fiber Reinforced Plastics–Properties". In Kelly, Anthony and Zweben, Carl (Editors): *Comprehensive Composite Materials*, Chapter 2.04, pp. 107–150. Pergamon, Oxford.

[6] Vogler, T.J. and Kyriakides, S. [1998]: "On the effect of loading rate on the compressive strength of an AS4/PEEK composite". *Journal of Applied Mechanics, ASME*, 65: 1056–1058.

[7] Vogler, T.J. and Kyriakides, S. [1999]: "Inelastic behavior of an AS4/PEEK composite under combined transverse compression and shear. Part I: experiments". *International Journal of Plasticity*, 15: 783–806.

[8] Weeks, C.A. and Sun, C.T. [1995]: "Nonlinear Rate Dependence of Thick-Section Composite Laminates. High Strain Rate Effects on Polymer, Metal and Ceramic Matrix Composites and Other Advanced Materials". *Y.D.S. Rajapakse and J.R. Vinson, eds., ASME*, 48: 81–95.

[9] Rabotnov, J.N. [1969]: "Creep problems in Structural members". North-Holland series in Applied Mathematics and Mechanics, North-Holland, Amsterdam, Netherlands.

[10] Lemaitre, J. [1992]: "A course on Damage mechanics". Springer-Verlag, Berlin, Heidelberg, Germany.

[11] Gilat, A., Goldberg, R.K. and Roberts, G.D. [2005]: "Strain rate sensitivity of epoxy resin in tensile and shear loading". Technical report, TM-2005-213595.

[12] G'sell, C., Jacques, D. and Favre, J.P. [1990]: "Plastic behavior under simple shear of thermosetting resins for fiber composite matrices". *Journal of material sciences*, 25: 2004–2010.

[13] Schuecker, C. and Pettermann, H.E. [2008]: "Combining elastic brittle damage with plasticity to model the non-linear behavior of fiber reinforced laminates". *Computer methods in applied sciences*, 10: 99–117.

[14] Chang, F.K. and Chang, K.-Y. [1987]: "A progressive damage model for laminated composites containing stress concentrations". *Journal of Composite Materials*, 21(9): 834–855.

[15] Yang, L., Wu, Z., Cao, Y. and Ye, Y. [2015]: "Micromechanical modelling and simulation of unidirectional fibre-reinforced composite under shear loading". *Journal of Reinforced Plastics and Composites*, 34: 72–83.

[16] https://element6composites.com/.

[17] Pettermann, H.E., Plansensteiner, A.F., Böhm, H.J. and Rammerstorfer, F.J. [1993]: "A thermo-elasto-plastic constitutive material law based on an incremental Mori-Tanaka approach". *Computers and Structures*, 71: 197–214.

[18] Hsu, S.-Y., Vogler, T.J. and Kyriakides, S. [1999]: "Inelastic behavior of an AS4/PEEK composite under combined transverse compression and shear. Part II: modeling". *International Journal of Plasticity*, 15: 807–836.

[19] Doghri, I. and Ouaar, A. [2003]: "Homogenization of two-phase elasto-plastic composite materials and structures. Study of tangent operators, cyclic plasticity and numerical algorithms". *International Journal of Solids and Structures*, 40: 1681–1712.

[20] Doghri, I., Adam, L. and Bilger, N. [2010]: "Mean-field homogenization of elasto-viscoplastic composites based on a general incrementally affine linearization method". *International Journal of Plasticity*, 26(2): 219–238.

[21] Mori, T. and Tanaka, K. [1973]: "Average Stress in the matrix and average Elastic Energy of Materials with Misfitting Inclusions". *Acta Metalurgica*, 21: 571–574.

[22] Gavazzi, A.C. and Lagoudas, D.C. [1990]: "On the numerical evaluation of Eshelby's tensor and its application to elastoplastic fibrous composites". *Computational Mechanics*, 7: 13–19.

[23] Car, E., Oller, S. and E, Oñate. [2000]: "An anisotropic elastoplastic constitutive model for large strain analysis of fiber reinforced composite materials". *International Journal of Plasticity*, 185: 11–21.

[24] Car, E., Oller, S. and E, Oñate. [2001]: "A large strain plasticity model for anisotropic materials-composite material application". *International Journal of Plasticity*, 17: 1437–1463.

[25] Hill, R. [1950]: "The mathematical theory of plasticity". Oxford: clarendon press.

[26] Mises, R.v. [1928]: "Mechanik der plastischen Formänderung von Kristallen". *ZAMM*, 8: 161–185.

[27] Xie, M. and Adams, D.F. [1995]: "A plasticity model for unidirectional composite materials and its applications in modeling composites testing". *Composite Science and Technology*, 27: 11–21.

[28] Sun, C.T. and Chen, J.L. [1989]: "A simple flow rule for characterizing nonlinear behavior of fiber composite". *Journal of Composite Materials*, 23: 1009–1020.

[29] Chen, J.L. and Sun, C.T. [1993]: "A plastic potential function suitable for anisotropic fiber composites". *Journal of Composite Materials*, 27: 1379–1390.

[30] Dvorak, G.J. and Bahei-El-Din, Y.A. [1987]: "A bimodal plasticity theory of fibrous composite materials". *Acta Mechanica*, 69: 219–241.

[31] Rogers, T. [1987]: "Yield criteria, flow rules and hardening in anisotropic plasticity". *Boehler, Yielding, damage and failure of anisotropic solids, EGF publication*, 5: 53–79.

[32] Spencer, A.J.M. [1992]: "Plasticity theory for fibre-reinforced composites". *Journal of Engineering Mathematics*, 26: 107–118.

[33] Voyiadjis, G.Z. and Thiagarajan, G. [1995]: "An anisotropic yield surface model for directionally reinforced metal-matrix composites". *International Journal of Plasticity*, 11: 867–894.

[34] Voyiadjis, G.Z. and Thiagarajan, G. [1996]: "A cyclic anisotropic-plasticity model for metal matrix composites". *International Journal of Plasticity*, 12-1: 69–91.

[35] Smith, J., Liu, W.K. and Cao, J. [2015]: "A general anisotropic yield criterion for pressure-dependent materials". *International Journal of Plasticity*, 75: 2–21.

[36] Chaboche, J.L. [2008]: "A review of some plasticity and viscoplasticity constitutive theories". *International Journal of Plasticity*, 24: 1642–1693.

[37] Flatscher, T., Schuecker, C. and Pettermann, H.E. [2013]: "A constitutive ply model for stiffness degradation and plastic strain accumulation: Its application to the Third World Wide Failure Exercise (Part A)". *Journal of Composite Materials*, 47: 2575–2593.

[38] Maimí, P., Camanho, P.P., Mayugo, J.A. and Turon, A. [2011]: "Matrix cracking and delamination in laminated composites. Part I: Ply constitutive law, first ply failure and onset of delamination". *Mechanics of Materials*, 43(4): 169–185.

[39] Al-Haik, M.S., Garmestani, H. and Savran, A. [2004]: "Explicit and implicit viscoplastic models for polymeric composite". *International Journal of Plasticity*, 20(10): 1875–1907.

[40] Tsai, J. and Sun, C.T. [2002]: "Constitutive model for high strain rate response of polymeric composites". *Composites Science and Technology*, 62(10): 1289–1297.

[41] Kontou, E. and Spathis, G. [2006]: "Application of finite strain viscoplasticity to polymeric fiber composites". *International Journal of Plasticity*, 22(7): 1287–1303.

[42] Vyas, G.M., Pinho, S.T. and Robinson, P. [2011]: "Constitutive modeling of unidirectional composites at the ply level using a plasticity-based approach". *Composite Science and Technology*, 78: 1068–1074.

[43] Vogler, M., Rolfes, R. and Camanho, P.P. [2013]: "Modeling the inelastic deformation and fracture of polymer composites - Part I: Plasticity model". *Mechanics of Materials*, 59: 50–6459.

[44] Nagaraja, S.G., Pletz, M. and Schuecker, C. [2019]: "Constitutive modeling of anisotropic plasticity with application to fiber-reinforced composites". *International Journal of Solids and Structures*, 180-181C: 84–96.

[45] Boehler, J.-P. [1979]: "A simple derivation of representations for non-polynomial constitutive equations in some case of anisotropy". *Zeitschrift für Angewandte Mechanik und Mathematik*, 59: 157–167.

[46] Liu, I.-S. [1982]: "On representations of anisotropic invariants". *International Journal of Engineering Science*, 31: 1099–1109.

[47] Zheng, Q.S. and Spencer, A.J.M. [1993]: "On the canonical representations for Kronecker powers of orthogonal tensors with application to material symmetry problems". *International Journal of Engineering Science*, 31: 619–635.

[48] Miehe, C. [1998]: "A constitutive frame of elastoplasticity at large strains based on the notion of a plastic metric". *International Journal of Solids and Structures*, 35: 3859–3897.

[49] Totry, E., González, C. and LLorca, J. [2008]: "Prediction of the failure locus of C/PEEK composites under transverse compression and longitudinal shear through computational micromechanics". *Composites Science and Technology*, 68(15): 3128–3136.

[50] Totry, E., Molina-Aldareguía, J.M., González, C. and LLorca, J. [2010]: "Effect of fiber, matrix and interface properties on the in-plane shear deformation of carbon-fiber reinforced composites". *Composites Science and Technology*, 70(6): 970–980.

[51] Truesdell, C. and Noll, W. [1965]: "The non-linear field theories of mechanics". Handbuch der Physik Bd.III/3, Edited by S. Flügge, Springer.

[52] Chadwick, P. [2000]: "Continuum Mechanics. Concise Theory and Problems". Dover Publications, New York.

[53] Holzapfel, G. [2000]: "Nonlinear Solid Mechanics". John Wiley and Sons.

[54] Šilhavý, M. [1999]: "The Mechanics and Thermodynamics of Continuous Media". Springer.

[55] Haupt, P. [2000]: "Continuum Mechanics and Theory of Materials". Springer.

[56] Jog, C.S. [2015]: "Continuum Mechanics: Foundation and Application of Mechanics", Vol. 1, Third edition. Cambridge University Press.

[57] Hammermesh, M. [1964]: "Group theory and its application to physical problems". Addison-Wesley.

[58] Kennon, N.F. [1978]: "Patterns in crystals". John Wiley and Sons.

[59] Whittaker, E. [1981]: "Crystallography". Pergamon Press.

[60] Powell, R.C. [2010]: "Symmetry, group theory and the physical properties of the crystals". Springer.

[61] Boehler, J.-P. (Editor) [1965]: "Applications of tensor functions in solid Mechanics", Vol. 292 of *CISM courses and lectures*. Springer Verlag, Wien.

[62] Spencer, A.J.M. [1971]: "Theory of Invariants". In *Eringen, Continuum Physics*, Vol. 1. Academic Press, New York.

[63] Spencer, A.J.M. [1987]: "Isotropic polynomial invariants and tensor functions". In Boehler, J.-P. (Editor): *Applications of Tensor functions in Solid Mechanics*, Vol. 292 of *CISM courses and lectures*. Springer Verlag, Wien.

[64] Zheng, Q.S. [1994]: "Theory of representations for tensor functions-a unified invariant approach to constitutive equations". *Applied mechanics review*, 47 (11): 545–586.

[65] Miehe, C. [2012]: "Micromechanics of Materials and Homogenization Methods". Lecture Notes, Universität Stuttgart.

[66] Simo, J.C. and Hughes, T.J.R. [2000]: "Computational Inelasticity". Mechanics and Materials, Springer.

[67] Coleman, B.D. and Gurtin, M.E. [1967]: "Thermodynamics with Internal State Variables". *The Journal of Chemical Physics*, 47(2): 597–613.

[68] Khan, A.S. and Huang, S. [1995]: "Continuum Theory of Plasticity". A Wiley-Interscience Publication, John Wiley and Sons, New York.

[69] Lubliner, J. [1997]: "Plasticity theory". Maxwell Macmillan International Edition.

[70] Aldakheel, F. [2016]: "Mechanics of Nonlocal Dissipative Solids: Gradient Plasticity and Phase Field Modeling of Ductile Fracture". Ph.D. Thesis, Universität Stuttgart.

[71] Coleman, B.D. and Noll, W. [1963]: "The thermodynamics of elastic materials with heat conduction and viscosity". *Archive for Rational Mechanics and Analysis*, 13: 167–178.

[72] Simo, J.C. and Miehe, C. [1992]: "Associative coupled thermoplasticity at finite strains: Formulation, numerical analysis and implementation". *Computer Methods in Applied Mechanics and Engineering*, 98: 41–104.

[73] Aldakheel, F. and Miehe, C. [2017]: "Coupled Thermomechanical response of gradient plasticity". *International Journal of Plasticity*, 91: 1–24.

[74] Hahn, T. (Editor) [1983]: "International tables for crystallography", Vol. A. D. Reidel Publishing Company.

[75] Apel, N. [2004]: "Approaches to the Description of Anisotropic Material Behavior at Finite Elastic and Plastic Deformations, Theory and Numerics". Ph.D. Thesis, Universität Stuttgart.

[76] Miehe, C. [2013]: "Selected Topics in the Theories of Plasticity and Viscoelasticity". Lecture Notes, Universität Stuttgart.

[77] Schröder, J. [1996]: "Theoretische und algorithmische Konzepte zur phänomenologischen Beschreibung anisotropen Materialverhaltens". Ph.D. Thesis, Universität Hannover.

[78] Papadopoulos, P. and Lu, J. [2001]: "On the formulation and numerical solution of problems in anisotropic finite plasticity". *Computer Methods in Applied Mechanics and Engineering*, 190: 4889–4910.

[79] Zheng, Q.S. and Spencer, A.J.M. [1993]: "Tensors which characterize anisotropies". *International Journal of Engineering Science*, 31: 679–693.

[80] Olive, M., Kolev, B. and Auffray, N. [2017]: "A minimal Integrity Basis for the Elasticity Tensor". *Archive for Rational Mechanics and Analysis*, 226: 1–31.

[81] Xiao, H. [1996]: "On anisotropic scalar functions of a single symmetric tensor". *Proceedings: Mathematical, Physical and Engineering Sciences*, 452: 1545–1561.

[82] Drucker, D.C. [1964]: "On the postulate of stability of materials in mechanics of continua". *Journal de Mécanique*, 3: 235–249.

[83] Mandel, J. [1964]: "Contribution Theorique a l'Etude de l'Ecrouissage et des Lois de l'Ecoulement Plastique". In *Proceedings on the 11th International Congress on Applied Mechanics*, pp. 502–209.

[84] Miehe, C., Apel, N. and Lambrecht, M. [2002]: "Anisotropic additive plasticity in the logarithmic strain space: modular kinematic formulation and implementation based on incremental minimization principles for standard materials". *Computer methods in applied mechanics and engineering*, 191: 5383–5425.

[85] Bennett, K.C., Regueiro, R.A. and Borja, R.I. [2016]: "Finite strain elastoplasticity considering the Eshelby stress for materials undergoing plastic volume change". *International Journal of Plasticity*, 77: 214–245.

[86] Perzyna, P. [1971]: "Thermodynamics of rheological materials with internal changes". *Journal de Mécanique*, 10: 391–408.

[87] Lubliner, J. [1972]: "On the thermodynamic formulations of non-linear solid mechanics". *International Journal of Non-linear Mechanics*, 7: 237–254.

[88] Simo, J.C. and Ortiz, M. [1985]: "A unified approach to finite deformation elastoplasticity based on the use of hyperelastic constitutive equations". *Computer Methods in Applied Mechanics and Engineering*, 49: 221–245.

[89] Perzyna, P. [1966]: "Fundamental problems in viscoplasticity". *Advances in Applied Mechanics*, 9: 1–18.

[90] Simo, J.C. and Taylor, R.L. [1985]: "Consistent Tangent Operators for Rate-Independent Elastoplasticity". *Computer Methods in Applied Mechanics and Engineering*, 48: 101–118.

[91] Govindjee, S. and Miehe, C. [2001]: "A multi-variant martensitic phase transformation model:formulation and numerical implementation". *Computer Methods in Applied Mechanics and Engineering*, 191: 215–238.

[92] Schröder, J., Gruttmann, F. and Löblein, J. [2002]: "A simple orthotropic finite elasto-plasticity model based on generalized stress-strain measures". *Computational Mechanics*, 30: 48–64.

[93] Zienkiewicz, O.C., Taylor, R. and Zhu, J.Z. [2005]: "The Finite Element Method: Its Basics and Fundamentals". Elsevier: Oxford.

[94] Hughes, T.J.R. [2000]: "The Finite element method". Dover Publications.

[95] Ma, R., Pilchak, A.L., Semiatin, S.L. and Truster, T.J. [2018]: "Modeling the evolution of microtextured regions during $\alpha/\beta$ processing using the crystal plasticity finite element method". *International Journal of Plasticity*, 107: 189–206.

[96] Beiermann, B.B. and Bruhns, O. [1994]: "A physically motivated set of invariants and tensor generators in the case of transverse isotropy". *International Journal of Solids and Structures*, 32: 1531–1552.

[97] Zheng, Q.S., Betten, J. and Spencer, A.J.M. [1992]: "The formulation of constitutive equations for fibre-reinforced composites in plane problems: Part I". *Archive of Applied Mechanics*, 65: 530–543.

[98] Zheng, Q.S., Betten, J. and Spencer, A.J.M. [1995]: "The formulation of constitutive equations for fibre-reinforced composites in plane problems: Part II". *Archive of Applied Mechanics*, 65: 161–177.

[99] Kaliske, M. [2000]: "A formulation of elasticity and viscoelasticity for fiber-reinforced material at small and finite strains". *Computer Methods in Applied Mechanics and Engineering*, 185: 225–243.

[100] Holzapfel, G. and Gasser, T. [2001]: "A viscoelastic model for fiber-reinforced composites at finite strains: Continuum basis, computational aspects and applications". *Computer Methods in Applied Mechanics and Engineering*, 190: 4379–4403.

[101] Miehe, C. [1994]: "Aspects of the formulation and finite element implementation of large strain isotropic elasticity". *International Journal of Numerical Methods in Engineering*, 37: 1981–2004.

[102] Menzel, A. and Steinmann, P. [2001]: "On the comparison of two strategies to formulate orthotropic hyperelasticity". *Journal of Elasticity*, 62: 172–201.

[103] Menzel, A. [2002]: "Modelling and Computation of Geometrically Nonlinear Inelasticity". Ph.D. Thesis, Universität Kaiserslautern.

[104] Spencer, A.J.M. [1984]: "Continuum theory of the mechanics of fiber-reinforced composites". Springer Verlag, Wien.

[105] Jones, R.M. [2000]: "Mechanics of Composite Materials". Taylor and Francis.

[106] Daniel, I.M. and Ishai, O. [1994]: "Engineering Mechanics of Composite Materials". Oxford University Press.

[107] Herakovich, C.T. [1998]: "Mechanics of Fibrous Composites". John Wiley and Sons.

[108] Lu, J. and Zhang, L. [2005]: "Physically motivated invariant formulation for transversely isotropic hyperelasticity". *International Journal of Solids and Structures*, 42: 6015–6031.

[109] Mosler, J. and Bruhns, O.T. [2009]: "Towards variational constitutive updates for non-associative plasticity models at finite strain: Models based on a volumetric-deviatoric split". *International Journal of Solids and Structures*, 46: 1676–1684.

[110] Raghava, R., Caddell, R.M. and Yeh, G.S.Y [1973]: "The macroscopic yield behaviour of polymers". *Journal of Materials Science*, 8(2): 225–232.

[111] Zhang, J., Kikuchi, V., Li, V., Yee, A. and Nusholtz, G. [1998]: "Constitutive modeling of polymeric foam material subjected to dynamic crash loading". *International Journal of Impact Engineering*, 21(5): 369–386.

[112] Laux, T., Gan, K.W., Dulieu-Barton, J.M. and Thomsen, O.T. [2019]: "A simple nonlinear constitutive model based on non-associative plasticity for UD composites: Development and calibration using a Modified Arcan Fixture". *International Journal of Solids and Structures*, 162: 135–147.

[113] Li, W., Gazonas, G., Brown, E.N., Rae, P.J. and Negahban, M. [2019]: "Thermomechanical model for monotonic and cyclic loading of PEEK". *Mechanics of Materials*, 129: 113–138.

[114] Schröder, J. and Miehe, C. [1997]: "Aspects of rate-independent crystal plasticity". *Computational Material Science*, 9: 168–176.

[115] Mulhern, T.J., Rogers, T.G. and Spencer, A.J.M. [1967]: "A Continuum Model for Fibre-Reinforced Plastic Materials". *Proceedings of the Royal Society of London. Series A, Mathematics and Physical Sciences*, 301: 473–492.

[116] Colak, O.U. [2005]: "Modeling deformation behavior of polymers with viscoplasticity theory based on overstress". *International Journal of Plasticity*, 21: 145–160.

[117] Cordoso, R.P.R and Adetoro, O.B. [2017]: "A generalisation of the Hill's quadratic yield function for planar plastic anisotropy to consider loading direction". *International Journal of Mechanical Sciences*, 128–129: 253–268.

[118] Barlat, F., Lege, D.J. and Brem, J.C. [1991]: "A six-component yield function for anisotropic materials". *International Journal of Plasticity*, 7: 693–712.

[119] Boyd, S. and Vandenberghe, L. [2004]: "Convex Optimization". Cambridge University Press.

[120] Armstrong, P.J. and Frederick, C.O. [1996]: "A mathematical representation of multiaxial Bauschinger effect". CEGB Report, RD/B/N/731, Berkeley Laboratories, R and D Department, CA.

[121] Prager, W. [1956]: "A new method of analyzing stresses and strains in workhardening plastic solids". *Journal of Applied Mechanics, ASME*, 23: 493–496.

[122] Nagaraja, S.G. and Schuecker, C. [2019]: "On the formulation of anisotropic plasticity for polymeric composites – rate-dependent models with non-linear isotropic/kinematic hardening". In *Proceedings in Applied Mathematics and Mechanics*.

[123] Naghdi, P.M. and Trapp, J.A. [1975]: "The significance of formulating plasticity theory with reference to loading surfaces in strain space". *International Journal of Engineering Sciences*, 13: 785–797.

[124] Naghdi, P.M. and Trapp, J.A. [1975]: "Restrictions on constitutive equations of finitely deformed elastic-plastic materials". *Quarterly Journal of Mechanics and Applied Mathematics*, 28: 25–46.

[125] Casey, J. [1984]: "A simple proof of a result in finite plasticity". *Quarterly Applied Mathematics*, 42: 61–71.

[126] Belytschko, T., Liu, W.K. and Moran, B. [2000]: "Nonlinear finite elements for continua and structures". John Wiley and Sons Ltd, New York.

[127] Ehlers, W., Zinatbaksh, S. and Markert, B. [2013]: "Stability analysis of finite difference schemes revisited: A study of decoupled solution strategies for coupled multifield problems". *International Journal of Numerical Methods in Engineering*, 94: 758–786.

[128] Ethiraj, G. [2005]: "Implementation of a Paramter Identification Algorithm for Finite Magnetostriction Models". Internship report, Universität Stuttgart.

[129] Press, W.H., Teukolsky, S.A., Vetterling, W.T. and Flannery, B.P [1992]: "Numerical Recipes in Fortran". Cambridge University Press, Cambridge.

[130] Yun, G.J. and Shang, S. [2011]: "A self-optimizing inverse analysis method for estimation of cyclic elasto-plasticity model parameters". *International Journal of Plasticity*, 27(4): 576–595.

[131] Li, H., Hu, X., Yang, H. and Li, L. [2016]: "Anisotropic and asymmetrical yielding and its distorted evolution: Modeling and applications". *International Journal of Plasticity*, 82: 127–158.

[132] Steinschneider, S. [2018]: "Entwicklung eines Tools zur inversen Kalibrierung von Modellparametern in Finite Elemente Modellen". Bachelorarbeit, Montanuniversität Leoben.

[133] "DIGIMAT User's Manual". e-Xstream engineering, MSC Software Corporation.

[134] "ABAQUS/Standard User's Manual, Version 6.13-2". Dassault Systemès Simulia Corp., Providence, RI, USA.

[135] Mahnken, R., Schneidt, A. and Antretter, T. [2009]: "Macro modelling and homogenization for transformation induced plasticity of a low alloy steel". *International Journal of Plasticity*, 25: 183–204.

[136] Wang, H.W., Zhou, H.W., Gui, L.L and Ji, H.W. Zhang, X.C [2014]: "Analysis of effect of fiber orientation on Young's modulus for unidirectional fiber reinforced composites". *Composites: Part B*, 56: 733–739.

[137] Ebbing, V. [2010]: "Design of Polyconvex Energy Functions for All Anisotropy Classes". Ph.D. Thesis, Universität Duisburg-Essen.

[138] Boehler, J.-P. [1977]: "On irreducible representations for isotropic scalar functions". *Zeitschrift für Angewandte Mechanik und Mathematik*, 57: 323–327.

[139] Xiao, H. [1996]: "On isotropic extension of anisotropic tensor functions". *Zeitschrift für Angewandte Mechanik und Mathematik*, 76(4): 205–214.

[140] Raina, A. and Miehe, C. [2016]: "A phase-field model for fracture in biological tissues". *Biomechanics and Modeling in Mechanobiology*, 15: 479–496.

[141] Dean, A., Reinoso, J., Sahraee, S. and Rolfes, R. [2016]: "An invariant-based anisotropic material model for short fiber-reinforced thermoplastics: Coupled thermo-plastic formulation". *Composites: Part A*, 90: 186–199.